SOLID STATE AND MECHANISTIC STUDY ON PYRONE BASED COMPLEXES OF EARLY, MIDDLE AND PLATINUM GROUP TRANSITION METAL ELEMENTS

by

Pule Petrus Molokoane

A thesis submitted to meet the requirements for the degree of

PHILOSOPHIAE DOCTOR

in the

Department Of Chemistry
Faculty of Natural- and Agricultural Sciences

at the

University of the Free State

Supervisor: Prof. Andreas Roodt
Co-Supervisor: Dr. Marietjie Schutte-Smith

February 2018

Acknowledgements

There is good and evil in all of us, growing up as a child I was inclined to think that all people genuinely wanted to do good. That it came naturally to do good than evil. However, as I grew up and being a native in a colonized African country this distorted perspective began to change. But none so like it did in my ten years in higher education and training as these were my first experiences of racism. To give context I relate both the past including our history as South Africans and the present including my personal experiences and my reality as I perceived it. My experiences for the most part are thus the authoritative point of reference for these acknowledgements and the authoritative rationale from which the views expressed here are constructed.

Being a native of Africa does not mean that I am a lesser being or sub-human, that I am incapable in any way including a lack of capacity to do mathematics and science, or to successfully engage in anything advanced like the former prime minister Verwoed once said. Let this contribution affirm this notion as the evil it really was, the injustice and human rights violation it perpetuated. As ancient as these derogatory statements may be they are still somewhat relevant as many of our public institutions are still largely colonized with their departments operating in a semi-military modus operandi laced with racial prejudice and discrimination against natives. Surprisingly and interesting to note, those that claim to be Africans still detest everything about us the natives of this continent. This hatred manifesting in various ways including subjugation, victimization and discrimination in these so called parallel medium instruction institutions. This is perpetuated largely by conscripts posing as academics, tyrants out to enforce the old status quo by the old regime that there's no place for natives in higher education. Hell bent in their cause for domination, reserving occupation for a minority elite based purely on race, preserving bigotry and the imperial force that reigns supreme in these institutions at the expense of transformation and decolonized public institutions and spaces. Of course they would never publicly admit this, such that we the natives, continue to fight a rampant faceless beast. I will however, categorically acknowledge this regardless.

The essence of education is not the validation of one race by another as perpetuated by some South African universities on the misguided notion that one is superior then the other or the dominance of one race by another. I whole heartedly reject these sentiments, in my view the call for decolonized and transformed institutions and public spaces is ever more urgent and an inevitable matter. My entire tertiary education despite what some would say and this which some history books would eloquently articulate, was under the frameworks of a racially segregated institutionalized development with the pretext of a parallel medium instruction institution (still colonized and racism deeply entrenched). This was designed to protect the privilege of the so-called Africans and to ensure segregation as envisioned by those who designed the system. In my view this was always a deliberate attempt to firmly entrench imperialism at the expense of transformation and progress in higher learning institutions and not some failed policy as some rulings have declared. Some of the finest legacies of these kinds of policies translates directly to the hostility, vile prejudices and subsequent victimization of natives in these environments by those claiming exclusive rights on intelligence, progress and advancement. To be honest I don't

think I've ever witnessed or heard anything more absurd, in my view the essence of these absurd views is only as a result of the evil that once presided on this continent. These so-called academics or professors, barbaric buffoons really, referring to us natives as 'hungry masses' when it pleased them. With the same breath though failing to acknowledge their inherited privileges passed down for generations from the total marginalization and exploitation of natives. Even those distinct as they are and tasked with protecting and mentoring us saw nothing wrong with such transgressions thus undermining our dignity and decency (an indication of how distorted their sense of ethics, professionalism, reason, and justice is) or pretending to be powerless despite being university officials. I was never phased by any of this, because from the onset I saw it for what it really was (bigotry and imperialism). This did not come as a surprise because all this (the contemptuous treatment, denigration and derision of natives) was instituted by conscripts of the previous regime and the previous criminal state had institutionalized and legalized this kind of conduct. I considered giving in to these imperial forces and their directives as many around me did to survive, but my conscience and black consciousness alike could not allow for this. Consistent with these virtues I remained insurgent as a rebellion to what I was witnessing. I have no doubt that these views expressed here will be met with some form of retaliation by tyrants. To that, I would like to categorically state that; as I was before and have always been, I am un-phased.

Due to these injustices (victimization, discrimination, prejudice) I saw three long years of my life go down the drain, because I was a native with a voice and various views, something you would think would be valued in these public institutions. To the NRF for its intervention when victimization manifested in my funding being withdrawn in an attempt to 'shut me up', I will eternally be grateful and thankful. The perpetrators, in their blissful ignorance (the essence of their stupidity) or maybe sheer ruthlessness, I could never really tell with absolute certainty which was which, are unapologetic. (Un)Aware that by robbing people off their right to education or seeking to undermine this process, is not only to rob them of their right to dignity and decency (essential human rights) but to rob their families hope, justice, restitution and the will to live and thrive. My mother and father never had these rights, this is why this will always resonate deeply with me. I have finished this course on my own terms as it should be, a proud native African and an integral citizen of this country (not a brainwashed colonial product that has conformed to the prevailing circumstances as many have done for favour and to survive) as it should be. I am a descendant of slaves, peasants and the dehumanized formerly condemned to subservient roles. I am an embodiment of the aspirations, hopes and dreams of the once oppressed natives, insurgent to the notion that my so-called black skin or non-straight hair is synonymous with a lack of capacity to do science or think rationally, logically or even with superior reason, and through me and many the evil is exposed.

To die in silence amidst injustice is cowardly and it's a form of repression reducing one to a lesser being. For this reason I felt not only compelled, but I felt that it would be to betray both my conscience and black consciousness alike, not to speak out. I have learned that as a native in this country sometimes my voice is the only thing that I have. I will take this victory in defeat with a clear conscience and view it as signals of the native renaissance, a once completely marginalized nation with little to no hope.

'No nation can win a battle without faith'……………………….………….Bantu Stephen Biko

On a much lighter note, and to my lovely mother, Nthabiseng Julia Molokoane all your sacrifices were not in vain and I am grateful for your presence in my life and all that you have done for me. I would not have made it this far without your love, support and prayers. Thank you for always believing in me and trusting me. I couldn't have asked for a better parent. I would like to thank my two sisters Montlai Agnes Molokoane and Mmangwale Victoria Molokoane for all their love and support which for the most part proved to be the difference between success and failure. I'd like to thank all family and friends for all the love and support, the great council, many rich memories and the faith which they bestowed on me. To Sandiswa Sheildah Ndyumbu thank you for all the love, support, sacrifices, belief, our son (Moabi Kaone Molokoane) and everything that you selflessly do for us.

'Never give in. Never give in. Never, never, never, never—in nothing, great or small, large or petty—never give in, except to convictions of honour and good sense. Never yield to force. Never yield to the apparently overwhelming might of the enemy.'……………………………………………………………………..…..Winston S. Churchill

Table of Contents

ABBREVIATIONS

Abbreviation	Meaning
A_{obs}	Observed absorbance
ATR	Attenuated total reflectance
Å	Angstrom
cm	Centimeter
3-ClPy	3-chloropyridine
DMAP	4-dimethylaminopyridine
Ethyl Maltol	3-hydroxy-2-ethylpyran-4-one
E(maltol)H	3-hydroxy-2-ethylpyran-4-one
EE(naltol)H	1,2-diethyl-3-hydroxy-4-pyridinone
EM(naltol)H	2-ethyl-3-hydroxy-1-methyl-4-pyridinone
EI(naltol)H	2-ethyl-3-hydroxy-1-isopropyl-4-pyridinone
Eq.	Equation
IR	Infra-red
Im	Imidazole
K_x	Equilibrium constant for an equilibrium reaction
k_{obs}	Observed rate constant
k_1	rate constant for the forward reaction
k_{-1}	rate constant for the reverse reaction
M	$mol.dm^{-3}$
mg	Milligram
mmol	Millimol

Maltol	3-hydroxy-2-methylpyran-4-one
ME(naltol)H	1-ethyl-3-hydroxy-2-methyl-4-pyridinone
MM(naltol)H	3-hydroxy-1,2-dimethyl-4-pyridinone
MI(naltol)H	3-hydroxy-2-methyl-1-isopropyl-4-pyridinone
nm	Nanometer
NMR	Nuclear Magnetic Resonance Spectroscopy
TON	Turn over number
PET	Positron Emission Tomography
ppm	(Unit of chemical shift) parts per million
Py	Pyridine
ν_{CO}	C=O IR stretching frequency
λ	UV/Vis wavelength
RMS	Root Mean Square
ReAA	$[NEt_4]_2[Re(CO)_3(Br)_3]$
SPECT	Single Photon Emission Computed Tomography
$t_{1/2}$	Half-life
XRD	X-ray diffraction
$\Delta H^{\ddagger}$	Enthalpy activation energy
$\Delta S^{\ddagger}$	Entropy activation energy
°	Degrees

Abstract

3-Hydroxypyrones and their corresponding analogues 3-hydroxypyridinones are a versatile class of chelators. The commercially available pyrones: 3-hydroxy-2-methylpyran-4-one (**1**) and 3-hydroxy-2-ethylpyran-4-one (**2**) were functionalised to yield the respective 3-hydroxy-2-methylpyrid-4-one (**3**) and 3-hydroxy-2-ethylpyrid-4-one (**4**) derivatives. These ligands were coordinated to an array of metals, divided broadly into three groups: early, middle and platinum group transition metals, to form the corresponding metal complexes. A total of eight bidentate ligands with different electronic and steric properties were used in this study. These ligands and the corresponding complexes are explored as models for: *(i)* the potential beneficiation of hafnium and zirconium for the nuclear industry, *(ii)* the application as model complexes for diagnostic and therapeutic radiopharmaceuticals in studies using the *fac*-[Re^I(CO)$_3$]$^+$ core and *(iii)* rhodium(I) homogeneous catalysts for oxidative addition reactions. In all of the respective sub-sections of this study, the structural characterisation of crystalline products of the above mentioned compounds were extensively evaluated by means of single crystal X-Ray Diffraction (XRD). This study therefore covers a detailed structural discussion of the analysis and comparison with similar Zr(IV), Hf(IV), Re(I) and Rh(I) compounds which could yield valuable insights into physical and/or chemical state differences to be exploited for purification/separation techniques, diagnostic and therapeutic endeavours and catalytic processes respectively. Finally, structure/ reactivity relationships were attempted to assist in the future prediction of relevant characteristics of these compounds. A kinetic evaluation on *fac*-[Re^I(O,O'-bid)(CO)$_3$(Y)] (O,O'-bid = O,O'-bidentate ligand and Y = monodentate ligand) substitution reactions with monodentate chelators in methanol, indicated a possible dissociative activated methanol substitution mechanism in these types of complexes and that these substitutions are solvolytic in nature.

Keywords; 3-Hydroxypyrones, 3-hydroxypyridinones, 3-hydroxy-2-methylpyran-4-one, 3-hydroxy-2-ethylpyran-4-one, 3-hydroxy-2-methylpyrid-4-one, 3-hydroxy-2-ethylpyrid-4-one, beneficiation, diagnostic, therapeutic, radiopharmaceuticals, rhodium(I) homogeneous catalysts, XRD and kinetics.

1 Introduction

1.1 Introduction

From an inorganic chemistry perspective, coordination chemistry has played a vital role in much advancement in science ranging from medicinal applications to catalytic industrial processes.[1-6]

The study of different aspects of coordination compounds were more formalized some 125 years ago by Alfred Werner.[7] The two integral and connecting aspects of coordination chemistry focus on the central metal atom and the ligands around it, which is the simple yet vast overarching and integrated chemistry discipline. There is still after all this time a continuous search for ligand systems which has the ability to introduce *just* the correct properties to the complex as required by the defined application.

Thus, adding to this thrust, pyrones and their derivatized *N*-functionalized analogues provide a new avenue as simple yet versatile ligands and are thus the focus of this PhD study, and they are introduced and evaluated herein as 'proof-of-concept-ligands' for three main applications.

In the early transition metals, focus is drawn to the beneficiation of zirconium and hafnium utilizing these chelator systems to evaluate any preferential affinity or selectivity to either metal. Zirconium is an ideal cladding material for nuclear reactors due to its low absorption cross-section for thermal neutrons. However, the small amount of hafnium contained within its mineral ores (mainly zircon, significant resources in South Africa; Hf around 5 % m/m), which has a

[1] D. C. Crans, *J. Org. Chem*., **2015**, *80*, 11899.
[2] L. E. Scott, C. Orvig, *Chem. Rev.,* **2009,** *109,* 4885.
[3] K. H. Thompson, C. A. Barta, C. Orvig, *Chem. Soc. Rev*., **2006**, *35*, 545.
[4] M. A. Santos, S. M. Marques, S. Chaves, *Coord. Chem. Rev.*, **2012**, *256*, 240.
[5] A. Brink, A. Roodt, G. Steyl, H. G. Visser, *J. Chem. Soc., Dalton Trans*., **2010**, *39*, 5572.
[6] M. M. Conradie, J. J. C. Erasmus, J. Conradie, *Polyhedron*, **2011**, *30*, 2345.
[7] "The Nobel Prize in Chemistry 1913". *Nobelprize.org*. Nobel Media AB 2014. Web. 11 Feb 2018.
<http://www.nobelprize.org/nobel_prizes/chemistry/laureates/1913/>

high thermal neutron absorption cross section is very harmful for zirconium as a fuel cladding material.[8,9] Hafnium with its very high affinity for thermal neutrons is used in nuclear reactors as control rods for shielding to control the flux (rate of fission). Due to these different applications of hafnium and zirconium, it is important to produce nuclear grade zirconium and hafnium.[9-11] The separation processes are categorized into hydro- and pyrometallurgical approaches and new and more energy efficient separation processes are a constant requirement nowadays.

Rhenium, as a middle transition metal, draws attention to the non-radioactive modelling of theranostics based on non-radioactive rhenium complexes, mainly due to the similar chemistry of rhenium and technetium.[12] Moving from the synthesis of zirconium and hafnium complexes to the evaluation of the ligand behavior in the corresponding radioactive precursor and model metallodrugs based on the radioactive isotopes $^{186/188}$Re, ^{99m}Tc and ^{105}Rh thus makes perfect sense. These isotopes have potential imaging and therapeutic applications with the corresponding radioactive ^{89}Zr complexes, strictly having potential PET applications, focused on to a lesser extent.[12,13]

Finally, in the late transition metal group, much international research is still focused on homogenous models of the rhodium phosphine based type catalysts and the potential utilization of new chelator systems therein.[14-16] Modifications are done on the original Monsanto catalyst and analogs to improve the propensity within this system by using new chelator systems and triphenylphosphine. A prime aim and drive naturally is to manipulate the electron density on the rhodium metal which will subsequently influence different steps in the catalytic cycle, including

---

[8] R. Callaghan, USGS Minerals Information, **2008**. Available:
http://minerals.usgs.gov/minerals/pubs/commodity/zirconium.

[9] L. Xu, Y. Xiao, A. van Sandwijk, Q. Xu, Y. Yang, *J. Nucl. Mater.,* **2015**, *466*, 21.

[10] C. Ganguly, Advances in zirconium technology for nuclear application, in: Proceedings of the Symposium Zirconium, Mumbai, India, **2002**,11.

[11] D. R. Lide, ed.; CRC Handbook of Chemistry and Physics, Section 4: Properties of the Elements and Inorganic Compounds, Int.Vers., CRC Press, Boca Raton (FL), **2005**, 4.

[12] C. S. Cutler, H. M. Hennkens, N. Sisay, S. Huclier-Markai, S. S. Jurisson, *Chem. Rev.*, **2013**, *113*, 858.

[13] B. M. Zeglis, J. L. Houghton, M. J. Evans, N. Viola-Villegas, J. S. Lewis, *Inorg. Chem.*, **2014**, *53*, 1880.

[14] A. Roodt, S. Otto, G. Steyl, *Coord. Chem. Rev.,* **2003**, *245*, 121.

[15] S. Warsink, F. G. Fessha, W. Purcell, J. A. Venter, *J. Organomet. Chem.*, **2013**, *726*, 14.

[16] C. M. Thomas, G. Süss-Fink, *Coord. Chem. Rev.*, **2003**, *243*, 125.

potentially the rate-determining step (often oxidative addition), thus affecting (and potentially controlling) the overall rate and efficiency of the process.

1.2   3-Hydroxy-4-pyranones

The pyrones maltol and ethyl maltol occur naturally in the bark and needles of certain conifers e.g. *Abies sibirica* (Siberian Fir) while they are also naturally obtained from malt, coffee, cocoa, milk, soya, etc. and even in passion fruit hybrids.[17] Pyrones are also formed during the pyrolysis of materials like cellulose, starch, and wood. Maltol and ethyl maltol are both low-toxic compounds (LD_{50} 1400 mg/kg) and for this reason find good application in the food and cosmetic industry.[17] However, it has been reported that maltol is a growth inhibitor.[18] These substances have a caramel-like taste and induce the distinct scent of baking and roasting.[19] They also act as synergistic agents in flavour and sweetness enhancement of beverages, confections and chocolate products.

Of interest to this study is that these compounds are relatively cheap, readily functionalized and the fact that these compounds and their derivatives are biologically active compounds (especially 3-hydroxy-4-pyridones (3,4-HPs)).[20] Furthermore, these easy-to-functionalize heteroatomic rings are strong chelating ligands towards hard metal ions (e.g. Cu, Fe, Al, etc.).[21] This implies that using these compounds as basis, structural modifications can be performed strategically to investigate the influence of chemical properties such as the effect of electron withdrawing and donating groups and the effect of steric bulk while employing different metals, including relatively hard ones. For this reason 3-hydroxypyranones were functionalized to the corresponding 3-hydroxy-4-pyridinones (3,4-HPs) by substituting the cyclic oxygen with primary amines (methyl amine, ethyl amine and *iso*-propyl amine). From this series the electron

[17] S. A. Mukha, I. A. Antipova, S. A. Medvedva, V. V. Saraev, L. I. Larina, A. V. Tsyrenzhapov, B. G. Sukhov, *Chemistry for Sustainable Development,* **2007**, *15,* 448.
[18] S. Patton, *J. Biol. Chem.,* **1950**, *184,* 131.
[19] A. O. Pittet, P. Rittersbacher, R. Muralidhara, *J. Agr. Food Chem.,* **1970**, *18*, 929.
[20] M. A. Santos, S. M. Marques, S. Chaves, *Coord. Chem. Rev.* **2012**, *256,* 240.
[21] M. A. Barrand, B. A. Callingham, R. C. Hider, *J. Pharm. Pharmacol.,* **1987**, *39,* 203.

donating ability of the alkyl groups is in the order: methyl > ethyl > *iso*-propyl. The effects of these substituents can be investigated in the resulting 3-hydroxypyridinone compounds.

1.3 3-hydroxy-4-pyridinones (3,4-HPs)

The 3-hydroxy-4-pyridinones belong to a group of *N*-heterocyclic chelators. These compounds are easily functionalized and derivatized to form a variety of compounds. This family of compounds is an important class of metal-related pharmaceutical drugs as they abstract/transfer hard metal ions (Fe^{3+}, Al^{3+}, etc.) from/into the human body.[21] These compounds are clinically used as iron chelating agents in patients suffering from metal overload related illnesses (*β*-Thalassemia, Alzheimer, etc.).[22] Biometals (Fe, Zn, Cu, Mo etc.) although important trace elements, can accumulate in the body as non-essential metal ions.[20] This can be attributed to either environmental exposure or the administration of metallodrugs to the human body.[22] This may result in the disruption of several homeostatic mechanisms and buffering systems which regulate the low concentration of free metal ions.[20] 3,4-HPs are then administered orally to sequester dysfunctional metal ions in the body.[23] Because the resulting complexes are neutral they are readily partitioned across the cell membrane and in this way can facilitate the transportation of metals across the intestinal walls.

1.4 Aim of the study

The primary broad objective of this study is thus to successfully synthesize and characterize 3-hydroxypyridinones from the corresponding pyrones as ligand systems and utilise appropriate examples of both herein. This will then be followed by the evaluation of the early, middle and late transition metal elements within the context of their respective applications, as summarized below.

[22] G. Crisponi, M. Remelli, *Coord. Chem. Rev.,* **2008**, *252,* 1225.
[23] Z. D. Liu, R. C. Hider, *Coord. Chem. Rev.,* **2002**, *232,* 151.

The current techniques of Zr and Hf separation is mainly by exploiting the physical properties of the coordination compounds of these metals (mainly chlorides, iodides, thiocyanates and fluorides) by hydrometallurgical or pyrometallurgical approaches.[24] In this study two ligand systems (pyrones and pyridinones) with varying steric demands and electronic properties will be evaluated as a basis for separation. Any difference in chemical and physical properties of the compounds will potentially aid in the separation *via* either sustainable hydrometallurgical or pyrometallurgical routes or a combination thereof.

Technetium complexes have successfully been employed as radiopharmaceuticals.[25] Due to the similarity in chemistry between technetium and rhenium, and the fact that all technetium isotopes are radioactive, non-radioactive rhenium was used as a model to develop potential theranostic drugs and to do some kinetic evaluations of these compounds. In the broader sense the radioactive counterparts of the zirconium and rhodium complexes synthesized in this study also has potential imaging (^{89}Zr and ^{105}Rh) and therapeutic (^{105}Rh) applications.[26]

Platinum group metals are known for their various catalytic properties.[27,28] The aim is to develop rhodium(I) phosphine catalysts based on the two chelator systems and to evaluate the effect of the respective electronic and steric parameters on the efficiency of the catalyst.[29]

A summary of the four more detailed objectives of the PhD study is given below:

[24] l. Xu, Y. Xiao, A. van Sandwijk, Q. Xu, Y. Yang, *J. Nucl. Mater.*, **2015**, *466*, 21.

[25] U. Abram, R. Alberto, *J. Braz. Chem. Soc.,* **2006**, *17*, 1486.

[26] C. S. Cutler, H. M. Hennkens, N. Sisay, S. Huclier-Markai, S. S. Jurisson, *Chem. Rev*., **2013**, *113*, 858.

[27] R. T. Eby, T. C. Singleton, Applied Industrial Catalysts, B. E. Leach (Ed.), Academic Press, **1983**, *1*, 275.

[28] N. von Kutepow, W. Himmele, H. Hohenschutz, *Chem. Ing. Technol*., **1965**, *37*, 297.

[29] C. M. Thomas, G. Süss-Fink, *Coord. Chem. Rev*., **2003**, *243*, 125.

➢ Synthesis of novel zirconium(IV), hafnium(IV), rhenium(I) and rhodium(I) coordination compounds with the two chelator systems, two pyrones and six pyridinones (*i.e.* 3-hydroxy-2-methylpyran-4-one, 3-hydroxy-1,2-dimethyl-4-pyridone, 1-ethyl-3-hydroxy-2-methyl-4-pyridone, 3-hydroxy-2-methyl-1-isopropyl-4-pyridone, 3-hydroxy-2-ethylpyran-4-one, 2-ethyl-3-hydroxy-1-methyl-4-pyridone, 1,2-diethyl-3-hydroxy-4-pyridone and 2-ethyl-3-hydroxy-1-isopropyl-4-pyridone). This will then be accompanied by subsequent characterisation thereof by means of analytical techniques, such as IR- and NMR spectroscopies. The various applications of these chelators are discussed in detail in Chapter 2.

➢ Solid state structural characterisation of the crystalline products of the above mentioned complexes, intended to elucidate the three dimensional structures of these complexes. To evaluate coordination modes, coordination geometries, intra- and intermolecular interactions and to evaluate structural distortions due to either steric or electronic demands, as well as to confirm and characterise products of substitution processes with appropriate entering nucleophiles.

➢ A comparison with similar compounds to evaluate the physical and/or chemical state differences that can be exploited in the three different domains of this research (beneficiation, development of theranostic drugs and homogeneous catalysis).

➢ Mechanistic study of the methanol substitution kinetics of two rhenium(I) complexes by appropriate entering nucleophiles, to obtain insights with regards to the reactivity, stability and processes related to selectivity and targeting. This will be achieved by means of detailed UV/Vis kinetic studies and reaction rate modelling with the intention of shedding light on the inherent reactivity manipulation and equilibrium influences, induced by the chosen bidentate ligands in these types of compounds that could be exploited for radiopharmaceutical applications.

In the following chapter, a brief insight into the various applications of pyrones and pyridinones as ligand systems and theoretical considerations regarding the known techniques of zirconium-hafnium separation, theranostic drug development and modelling and homogeneous catalytic oxidative addition is presented.

2 Pyrones and Related Analogues in Applied Inorganic Chemistry

2.1 Introduction

3-Hydroxypyrones and their corresponding analogues 3-hydroxypyridinones are a versatile class of chelators.[1,2] Both groups of compounds contain several classes of compounds. In both cases the compounds are heterocycles with a hydroxyl group *ortho* to a ketone (Scheme 2.1). This presents two oxygen donors in close proximity, which upon deprotonation electron density is then delocalized between the two oxygens and the two cyclic carbons.[3] This generally represents the binding site for metals, depending on whether the ligand is protonated or not. The ligand coordinates in a bidentate or monodentate fashion (evidence of this is presented in the crystallography chapters that follow). The hydroxyl group of these six membered heterocycles is easily ionizable and therefore produces a mono-anionic structure or the corresponding partially aromatic zwitterionic structure.[4] These compounds form neutral complexes with charged metal ions, with the ratio of coordinated ligand to metal dependent on the charge on the metal ion at neutral pH.[5,6] In general terms pyrones have lesser bidentate binding strength compared to pyridinones, primarily because of the aromaticity of pyridinones.[7-10]

[1] Y. Ma, W. Luo, P. J. Quinn, Z. Liu, R. C. Hider, *J. Med. Chem.,* **2004,** *47,* 6349.

[2] J. J. Molenda, M. M. Jones, K. M. Cecil, M. A. Basinger, *Chem. Res. Toxicol.,* **1994**, *7,* 815.

[3] M. A. Santos, *Coord. Chem. Rev.*, **2002**, *228*, 187.

[4] M. M. Finnegan, T. G. Lutz, W. O. Nelson, A. Smith, C. Orvig, *Inorg. Chem*., **1987**, *26*, 2171.

[5] R. D. Hancock, A. E. Martell, *Chem. Rev.*, **1989**, *89*, 1875.

[6] E. Kiss, I. Fabian, T. Kiss, *Inorg. Chim. Acta*, **2002**, *340*, 114.

[7] R. A. Yokel, *Coord. Chem. Rev*., **2002**, *228*, 97.

[8] M. M. Finnegan, S. J. Rettig, C. Orvig, *J. Am. Chem. Soc*., **1986**, *108*, 5033.

[9] H. Sakurai, Y. Kojima, Y. Yoshikawa, K. Kawabe, H. Yasui, *Coord. Chem. Rev*., **2002**, *226*, 187.

[10] D. C. Kennedy, A. Wu, B. O. Patrick, B. R. James, *Inorg. Chem*., **2005**, *44*, 6529.
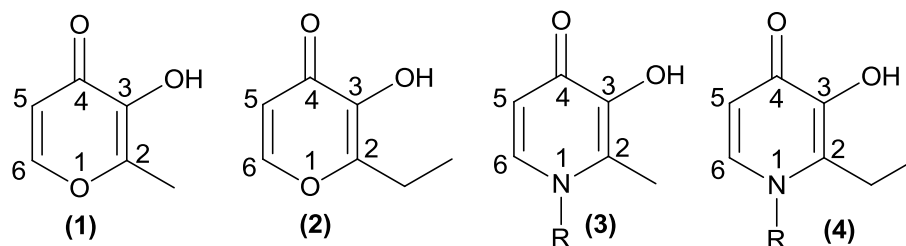
R = Me/Et/*iso*-propyl

Scheme 2.1: 3-Hydroxy-4-pyranones (1 and 2) and the corresponding 3-hydroxy-4-pyridones (3 and 4) used as chelator systems in this study.

In terms of Fe^{3+} these variations see hydroxypyridinones take precedence in iron removal whereas the corresponding pyrones are more effective for delivery.[11] High affinity for a range of metal ions and synthetic versatility render these ligands as excellent agents for various applications. Applications as diverse as iron removal and supplementation, contrast agents in imaging applications, chemotherapy and mobilization of undesirable excess metal ions are covered by these compounds.[3,7,11-14] In all these domains functionalization is imperative for optimizing metal binding, linking units and/or target tissue specificity.

2.2   The contrasting restoration of iron in anaemia and overload

2.2.1   Hydroxypyrones in iron deficiency anaemia

Anaemia, a metabolic disorder and a consequence of iron deficiency is common in humans.[15] This happens when the balance of iron intake, iron reserves, and the body's loss of iron is inadequate to fully support the production of erythrocytes.[16] This condition is rarely fatal but has a significant impact on human health. Haemoglobin is the most abundant iron-containing protein in humans, wherein over a half of the total body iron is contained within. To fully comprehend anaemia, attention is directed towards concepts of iron supply, demand and erythropoiesis. These

[11] Z. D. Liu, R. C. Hider, *Med. Res. Rev.*, **2002**, *22*, 26.

[12] R. C. Hider, T. Zhou, *Ann. N. Y. Acad. Sci.*, **2005**, *141*, 1054.

[13] K. H. Thompson, B. D. Liboiron, G. R. Hanson, C. Orvig, in Medicinal Inorganic Chemistry, ed. J. L. Sessler, S. R. Doctrow, T. J. McMurry, and S. J. Lippard, ACS, Washington (DC), **2005**.

[14] K. N. Raymond, V. C. Pierre, *Bioconjugate Chem.*, **2005**, *16*, 3.

[15] N. C. Andrews, *N. Engl. J. Med.*, **1999**, *341*, 1986.

[16] *Cold Spring Harb Perspect Med* doi: 10.1101/cshperspect.a011866.

requirements are created by three variables; tissue oxygenation, erythrocyte turn-over, and erythrocyte loss from haemorrhage. Senescent erythrocytes are cleared daily, and the iron in those cells is recycled for erythropoiesis related processes. These processes require iron for the production of heme (Figure 2.1) and haemoglobin.
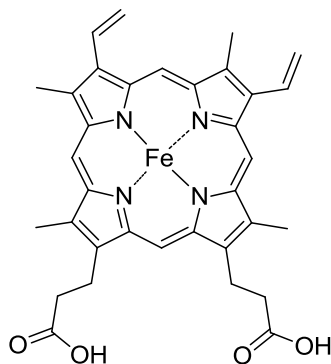
Figure 2.1: An illustration of the heme B molecule which forms the non-protein part of haemoglobin.[16]

If this is not the case, the newly formed erythrocytes will have reduced haemoglobin. Unlike thalassemia (iron overload), increased amounts of erythrocytes are not formed in the iron-deficient state to compensate for the depletion in intracellular haemoglobin content. The major causes of iron deficiency, anaemia, revolve around blood loss which can be due to menstruation, hookworm infection or severe malnourishment.

The elementary prevention of iron deficiency is *via* proper dietary iron intake.[17,18] Lean meats (particularly beef) are rich in highly bioavailable iron. Other foods that have high iron content include nuts, seeds, legumes, bean products, raisins, dark green leafy vegetables, whole grain and iron fortified cereals.[19,20] Heme iron found in meat, poultry and fish has a bioavailability of approximately 30 %.[21]

Oral iron supplements contain ferrous iron which is soluble even at pH of 7 to 8 and is more easily absorbed.[21] Iron supplementation therapy can be done orally, intramuscularly and

---

[17] Institute of Medicine. Dietary reference intakes (DRIs) for vitamin A, vitamin K, arsenic, boron, chromium, copper, iodine, iron, manganese, molybdenum, nickel, silicon, vanadium, and zinc. Washington (DC): National Academy Press, **2002**, *351*, 18.

[18] US Department of Agriculture and US Department of Health and Human Services. Nutrition and your health: dietary guidelines for Americans. (Home and Garden Bulletin No. 232). Washington (DC): US Department of Agriculture and US Department of Health and Human Services, **1995**.

[19] E. M. Ross, *Nutr Clin Care*, **2002**, *5*, 220.

[20] C.A. Venti, C. S. Johnston, *J Nutr*, **2002**, *132*, 1050.

[21] L. B. Trost, W. F. Bergfeld, E. Calogeras, *J Am Acad Dermatol*, **2006,** *54,* 824.

intravenously, and blood transfusions can also be performed in severe cases.[21] Oral supplementations include ferrous sulphate, ferrous fumarate and ferrous gluconate, while slow release iron coordination complex formulations are also widely used.[22]

To increase the effectiveness of iron supplementation the following requirements need to be met: high bioavailability, thermodynamic stability of the complex and the complex must be ferrous.[23] The ferrous complex on the other hand must have the following properties;

> The ligand must have a high affinity for Fe^{3+} to prevent catalytic formation of reactive oxidative species (ROS);

> High aqueous solubility;

> It must be neutral for passive diffusion through cell membranes;

> The ligand must be non-toxic;

> It must have a stable intermediate, such that the iron in the complex subsequent to gastrointestinal (GI) uptake would be given over to transferrin for entry into iron's pathways in the body.[24]

All these properties are met by 3-hydroxypyrones; maltol and ethyl maltol (see Scheme 2.1), which form *tris*-octrahedral distorted coordination complexes with Fe^{3+}.[24-29]

2.2.2   Hydroxypyridinones in iron overload disorders

The contrary condition to iron-deficiency anaemia is iron overload, these are disorders in which the metabolic problem is an excess of iron instead of a deficiency.[15] Two of these conditions that are well known are haemochromatosis and thalassemia major (*β*-thalassemia).[15,30] In both these cases excess iron accumulates in the liver, heart, pancreas and other organs. This can result in fibrosis, cirrhosis, hepatocellular carcinoma, diabetes and heart diseases.[31] To circumvent this

[22] T. McDiarmid, E. D. Johnson. *J Fam Pract*, **2002**, *51*, 576.

[23] J. A. Levey, M. A. Barrand, B. A. Callingham, R. C. Hider, *Biochem. Pharmacol*., **1988**, *37*, 2051.

[24] M. T. Ahmet, C. S. Frampton, J. Silver, *J. Chem. Soc., Dalton Trans.*, **1988**, 1159.

[25] R. C. Hider, G. Kontoghiorghes, M. A. Stockham, UK patent 2128998, **1984**.

[26] T. Hedlund, L.-O. Öhman, *Acta Chem. Scand. Ser. A*, **1988**, *A42*, 702.

[27] M. A. Barrand, B. A. Callingham, R. C. Hider, *J. Pharm. Pharmacol*., **1987**, *39*, 203.

[28] M. A. Barrand, R. C. Hider, B. A. Callingham, *J. Pharm. Pharmacol.*, **1990**, *42*, 279.

[29] M. A. Barrand, B. A. Callingham, *Br. J. Pharmacol*., **1991**, *102*, 408.

[30] N. Olivieri, G. Brittenham, D. Matsui, M. Berkovitch, L. Blendis, R. Cameron, R. McClelland, P. Liu, D. Templeton, G. Koren, *N. Engl. J. Med.*, **1995**, *332*, 918.

[31] C. Hershko, A. M. Konijn, G. Link, *Br. J. Haematol.*, **1998**, *101*, 399.

progressive deterioration, iron must be removed or passivated by appropriate chelators.[32] The pivotal feature of Fe^{3+} coordination that distinguishes its decorporation in a biological environment is the low solubility of ferric hydroxide ($K_{sp} \cong 10^{-38}$) at physiological pH.[33,34] This imposes tight binding to a sequestering agent to prevent hydrolysis and precipitation. Numerous naturally occurring hydroxamates and catecholates are known to act as strong multi-dentate chelating agents for Fe^{3+}. Desferrioxame-B (DFO) a siderophore, is a trihydroxamic acid that efficiently binds Fe^{3+} (Figure 2.2).

Desferrioxamine-B
(DFO)

Mimosine

1-(2'-trimethylacetoxyethyl)-
2-ethyl-3-hydroxypyridin-4-one
(CP117)

Deferiprone
(L1 or CP20)

1,6-dimethyl-3-hydroxypyridin-4-
one-2-carboxy-(N-alkyl)-amido
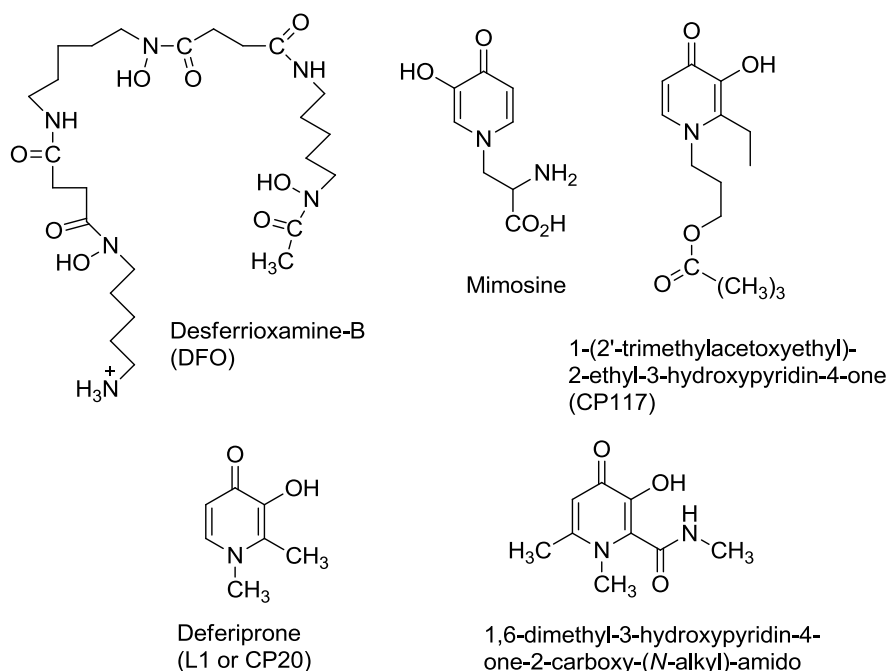
Figure 2.2: An Illustration of Desferrioxame-B (DFO) and 3-hydroxypiridinones with an affinity for Fe^{3+}.[35]

DFO is the most frequently utilized chelating agent for iron-overload disorders, however it is expensive and administered parenterally (by injection) as an infusion over several hours.[36] The work done by Raymond, Kontoghiorghes, Hider and coworkers has shown that the bidentate 3,4-hydroxypyridinones are promising alternatives to DFO as they can be administered orally.[37-47]

[32] J. J. Molenda, M. A. Basinger, T. P. Hanusa, M. M. Jones, *J. Inorg. Biochem.*, **1994**, *55*, 131.
[33] R. C. Scarrow, D. L. White, K. N. Raymond, *J. Am. Chem. Soc.*, **1985**, *107*, 6540.
[34] R. C. Scarrow, P. E. Riley, K. Abu-Dari, D. L. White, K. N. Raymond, *Inorg. Chem.*, **1985**, *24*, 954.
[35] K. H. Thompson, C. A. Barta, C. Orvig, *Chem. Soc. Rev.,* **2006**, *35*, 545.
[36] M. Summers, A. Jacobs, D. Tudway, P. Perera, C. Ricketts, *Br. J. Haematol.*, **1979**, *42*, 547.
[37] S. M. Cohen, B. O'Sullivan, K. N. Raymond, *Inorg. Chem.*, **2000**, *39*, 4339.
[38] A. C. G. Chua, H. A. Ingram, K. N. Raymond, E. Baker, *Eur. J. Biochem.*, **2003**, *270*, 1689.
[39] K. M. C. Jurchen, K. N. Raymond, *J. Coord. Chem.*, **2005**, *58*, 55.

The metal hydroxypyridinone complexes are more stable than their corresponding hydroxypyrone congeners.[48,49] The delocalization and tautomeric nature of the lone pair from the cyclic nitrogen atom renders the carbonyl functionality more basic. Furthermore, the formation constants for $Fe(III)(3\text{-hydroxypiridinone})_3$ complexes increase as the coordination site moves away from the ring nitrogen making 3-hydroxypyridinones iron complexes the most stable in this class. The need for Fe^{3+} selectivity and oral availability in iron overload therapy led to the choice of 3-hydroxy-1,2-dimethyl-4-pyridone (deferiprone, CP20 or L1) and 1,2-diethyl-3-hydroxy-4-pyridone analogues (Mimosine, CP117 etc.), which are considered 'first generation DFO alternatives' (Figure 2.2).[45,47]

2.3   Group 13 Metal Ions (Al, Ga, In)

The trivalent group 13 elements, contrary to iron are redox inactive and non-essential in the human body. Apart from these differences between these elements (Fe and M = Al, Ga, In) their cations are regarded as hard metal ions, showing similar chemical behavior in aqueous solution and coordinating to transferrin (Tf) which plays a key role in the transportation of ferric ions between sites of uptake, usage and storage.[50] In this context these group 13 metal ions are of biological interest.

[40] M. Meyer, J. R. Telford, S. M. Cohen, D. J. White, J. Xu, K. N. Raymond, *J. Am. Chem. Soc.*, **1997**, *119*, 10093.
[41] G. J. Kontoghiorghes, *Inorg. Chim. Acta*, **1987**, *135*, 145.
[42] G. J. Kontoghiorghes, L. Sheppard, *Inorg. Chim. Acta*, **1987**, *136*, L11.
[43] G. J. Kontoghiorghes, A. V. Hoffbrand, *Br. J. Haematol.*, **1986**, *62*, 607.
[44] J. B. Porter, M. Gyparki, L. C. Burke, E. R. Huehns, P. Sarpong, V. Saez, R. C. Hider, *Blood*, **1988**, *72*, 1497.
[45] R. Choudhury, R. O. Epemolu, B. L. Rai, R. C. Hider, S. Singh, *Drug Metab. Dispos.*, **1997**, *25*, 332.
[46] Z. D. Liu, H. H. Khodr, D. Y. Liu, S. L. Lu, R. C. Hider, *J. Med. Chem.*, **1999**, *42*, 4814.
[47] R. C. Hider, G. Kontoghiorghes, J. Silver, M. A. Stockham, UK Patent 2117766, **1982**.
[48] R. C. Hider, Z. D. Liu, *Curr. Med. Chem.*, **2003**, *10*, 1051.
[49] Z. D. Liu, R. C. Hider, *Med. Res. Rev.*, **2002**, *22*, 26.
[50] R. G. Pearson, *J. Am. Chem. Soc.*, **1963**, *85*, 3535.

2.3.1   Aluminium passivation

Aluminium in the body becomes toxic when accumulated.[51] It has a low bioavailability under normal environmental conditions. It can generally become bio-accessible through diet, underarm antiperspirants, vaccines, antacids, parenteral fluids, inhaled fumes or environmental exposure.[52,53] Due to its abundance in the earth's crust, acid rain can cause its bioavailability in drinking water and the food chain.[54] Because of a lack of an efficient excretory mechanism the element can accumulate in certain tissues. Aluminium toxicity is commonly associated with bone disorders, neurological diseases and eventually Alzheimer's disease and or renal failure as the kidney is the primary organ of aluminium elimination.[55,56] Aluminium can also aid the iron-induced oxidative damage of neurons.[57,58] This is because of the competing capacity of Al^{3+} over Fe^{3+} for the same bio-ligands, and consequently influencing the iron availability, its redox cycling and its respective homeostatic mechanisms.[59]

Transferrin is the main aluminium-binding protein in plasma and is 30 % saturated with iron in normal serum.[60] Therefore it still possesses a significant chelating capacity for other trivalent metal ions like Al^{3+}. 91 % of plasma aluminium is bound to transferrin and 7 - 8 % to citrate, thus an aluminium chelator that does not distribute out of the vascular chambers would have to compete successfully with transferrin and citrate for aluminium complexation.[55] Desferrioxamine (DFO) is currently the drug of choice for aluminium intoxication, however some 3,4-hydroxypyridinones have proven to be more effective than DFO with efficiencies ranging from 2.8 to 11.7 % compared to the efficiency of DFO which is only 2.1 %.[3,61] Biological essays were performed by Yorkel *et al*. with bidentate 3,4-hydroxypyridinones *in vivo* which based efficiency of these chelators on calculated urinary plus biliary aluminium excretion.[62] The results indicate that the correlation between the lipophilicity of chelators and total aluminium output is

[51] M. Nicolini, P. F. Zatta, B. Corain (Eds.), Aluminium in Chemistry, Biology and Medicine, Cortina International, Verona, Raven Press, New York, **1991**.

[52] P. Rubini, A. Lakatos, D. Champmartin, T. Kiss, *Coord. Chem. Rev*., **2002**, *228*, 1375.

[53] R. A. Yokel, A. K. Datta, E. G. Jackson, *J. Pharmacol. Exp. Ther*., **1991**, *257*, 100.

[54] C. Exley, *J. Inorg. Biochem*., **2003**, *97*, 1.

[55] R. A. Yokel, P. J. McNamara, *Pharmacol. Toxicol*., **2001**, *88*, 159.

[56] W. R. Harris, J. Sheldon, *Inorg. Chem*., **1990**, *29*, 119.

[57] G. Berthon, *Coord. Chem. Rev*., **2002**, *228*, 319.

[58] A. Khan, J. P. Dobson, C. Exley, *Free Radic. Biol. Med*., **2006**, *40*, 557.

[59] M. A. Santos, *Coord. Chem. Rev.*, **2008**, *252*, 1213.

[60] K. R. Phelps, K. Naylor, T. P. Brien, H. Wilbur, S. S. Haqqie, *Am. J. Med. Sci*., **1999**, *318*, 181.

[61] S. T. Wang, S. Pizzolato, H. P. Demshar, *J. Anal. Toxicol*., **1991**, *15*, 66.

[62] R. A. Yokel, K. A. Meurier, T. L. Skinner, A. M. Fredenburg, *Drug Metab. Dispos*., **1996**, *24*, 105.

insignificant, although the higher lipophilic complexes however correlate with higher biliary aluminium excretion. Based on these results the recommendation was that less lipophilic and orally active chelators can be utilized for aluminium passivation of patients with normal renal functions, while the more lipophilic chelators may be more effective for patients with lack of those functions (dialysed patients). Dialysis does not effectively passivate significant amounts of aluminium: this is due to the extensive coordination of aluminium to transferrin.[63]

Florence *et al.* also performed *in vivo* studies on aluminium-loaded rats to investigate the effects of lipophilicity on the mobilization of aluminium from the liver and brain.[64] Upon intra-peritoneal administration, DFO was the most effective chelator (74 %) followed by 1,2-diethyl-3-hydroxy-4-pyridone (44 %) and 3-hydroxy-1,2-dimethyl-4-pyridone (14 %) in mobilization liver aluminium. The most lipophilic chelator in the study 1,2-diethyl-3-hydroxy-4-pyridone was the most efficient in mobilizing brain aluminium. On the basis of the relatively low efficacy of these chelators used in this study to mobilize iron from the brain compared to aluminium it was proposed that administration of the more lipophilic chelator in patients with excessive aluminium might not interfere with iron homeostasis.[65]

2.3.2 Imaging probes (Ga) and therapeutic agents (In)

Hydroxypyrones and hydroxypyridinones can also coordinate other group 13 metals such as Ga^{3+} and In^{3+} for potential diagnostic and radionuclear therapeutic medicinal applications. Secure binding and rapid systemic clearance is important for both gallium imaging agents and for indium diagnostic and therapeutic agents. For medicinal interest there are two important gallium isotopes; ^{67}Ga and ^{68}Ga, the former a gamma emitter ($t_{1/2} = 78$ h, $\gamma = 93, 185, 300$ keV) predisposed for use in single photon emission computed tomography (SPECT) and the latter a positron emitter ($t_{1/2} = 68$ min) produced from the $^{68}Ge/^{68}Ga$ radionuclide generators or *via* direct production from cyclotrons, suitable for use in positron emission tomography (PET).[66-69] Indium

[63] R. B. Martin, J. Savory, S. Brown, R. L. Bertholf, M. R. Wills, *Clin. Chem.*, **1987**, *33*, 405.
[64] M. Gómez, J. L. Domingo, D. del Castillo, J. M. Llobet, J. Corbella, *Hum. Exp. Toxicol.*, **1994**, *13*, 135.
[65] J. P. Day, P. Ackrill, F. M. Garstang, K. C. Hodge, P. J. Metcalfe, M. O'Hara, Z. Benzo, R. A. Romero-Martinez, in: S. S. Brown, J. Savory (Eds.), Chemical Toxicology and Clinical Chemistry of Metals, Academic Press, New York, **1983**, 353.
[66] C. J. Anderson, M. J. Welch, *Chem. Rev.*, **1999**, *99*, 2219.
[67] Z. Zhang, D. M. Lyster, G. A. Webb, C. Orvig, *Nucl. Med. Biol.*, **1992**, *19*, 327.

has one isotope, ^{111}In ($t_{1/2}$ = 68 h, γ = 245, 172 keV) and is of interest for both SPECT diagnostic imaging and radiotherapy.[68]

In 1960 Edwards and Hayes discovered that ^{67}Ga citrate localized in soft tumor tissue, and since then there has been much interest in gallium chelators.[69,70] ^{67}Ga-citrate has been used for decades as a soft tumor imaging agent, imaging of skeletal disorders and the diagnosis of inflammatory processes.[71] The utility of the citrate ligand is however limited due to the fact that upon administration it is readily displaced by transferrin. Therefore a ligand that is thermodynamically stable and resists transferrin substitution will be more efficient.[72] Evaluation of a series of 3-hydroxypyridinones as chelators for ^{67}Ga compared to citrate, monitoring percentage uptake per gram tissue for 24 hrs after injection indicated that various *N*-substitutions changed the bio-distribution of the complexes without altering their stability.[73] Mimosine and 3-hydroxy-2-methyl-1-ethyl-4-pyridinone complexes had greater tissue uptake compared to 3-hydroxy-2-methyl-4-pyridinone or 3-hydroxy-1,2-dimethyl-4-pyridinone complexes in accordance with the respective differences in lipophilicity (Figure 2.3).[74] The highest tissue levels of ^{67}Ga resulted from injection with accompanied citrate, which gave significantly higher levels than all other tested ligands. Mimosine and 3-hydroxy-2-methyl-1-ethyl-4-pyridinone were moderately similar, with generally greater ^{67}Ga uptake compared to either 3-hydroxy-2-methyl-4-pyridinone or 3-hydroxy-1,2-dimethyl-4-pyridinone.
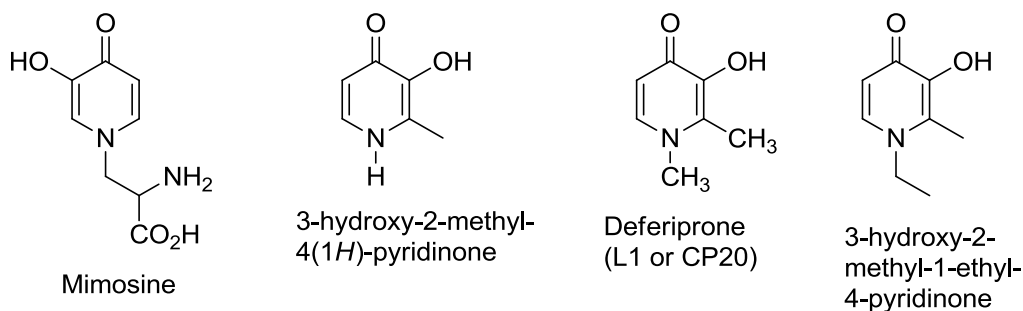
Figure 2.3: 3-Hydroxypyridinones evaluated for imaging and therapeutic applications.[73]

---

[68] G. J. Kontoghiorghes, *Int. J. Haematol.*, **1992**, *55*, 27.
[69] C. L. Edwards, R. L. Hayes, *J. Nucl. Med.*, **1969**, *10*, 103.
[70] M. M. Finnegan, T. G. Lutz, W. O. Nelson, A. Smith, C. Orvig, *Inorg. Chem.*, **1987**, *26*, 2171.
[71] R. E. Coleman, *Cancer*, **1991**, *67*, 1261.
[72] D. J. Clevette, W. O. Nelson, A. Nordin, C. Orvig, S. Sjoberg, *Inorg. Chem.*, **1989**, *28*, 2079.
[73] D. J. Clevette, C. Orvig, *Polyhedron*, **1990**, *9*, 151.
[74] D. J. Clevette, D. M. Lyster, W. O. Nelson, T. Rihela, G. A. Webb, C. Orvig, *Inorg. Chem.*, **1990**, *29*, 667.

Bio-distribution studies of 3-hydroxypyridinones in rabbits and a dog indicated high heart uptake showing potential for use in heart imaging.[67] For most *in vivo* applications of gallium and indium complexes, high stability of the complexes with a ligand: metal ratio of 1: 1 is crucial for minimizing toxicity. By improving the denticity of the ligand and subsequent chelation to [67,68]Ga or ^{111}In, complexes with highly favourable bio-distribution profiles *i.e.* high rate of excretion after bio-localization and no metal ion release can be obtained.[75]

The bifunctional chelate approach has also been utilized for designing imaging agents using ^{67}Ga and ^{111}In nuclides. This model includes a chelator to chelate the metal ion and another substituent directs the metal complex to tissues of interest.[76] Carbohydrate-bearing 3-hydroxypyridinones complexes of Ga and In (Figure 2.4) have been synthesized using the bifunctional chelate approach in which the pendant sugar is intended for targeting *in vivo*.[77]

1-[4-(*B*-D-glucopyranosyloxy)carbamoyl]-3-hydroxy-2-alkyl-4(1*H*)-pyridinone

N-carboxy-*n*-butyl-3-hydroxy-4-pyridinone

imino-bis(acetyl(1-(3'-aminopropyl)-3-hydroxy-2-methyl-4-pyridinone)
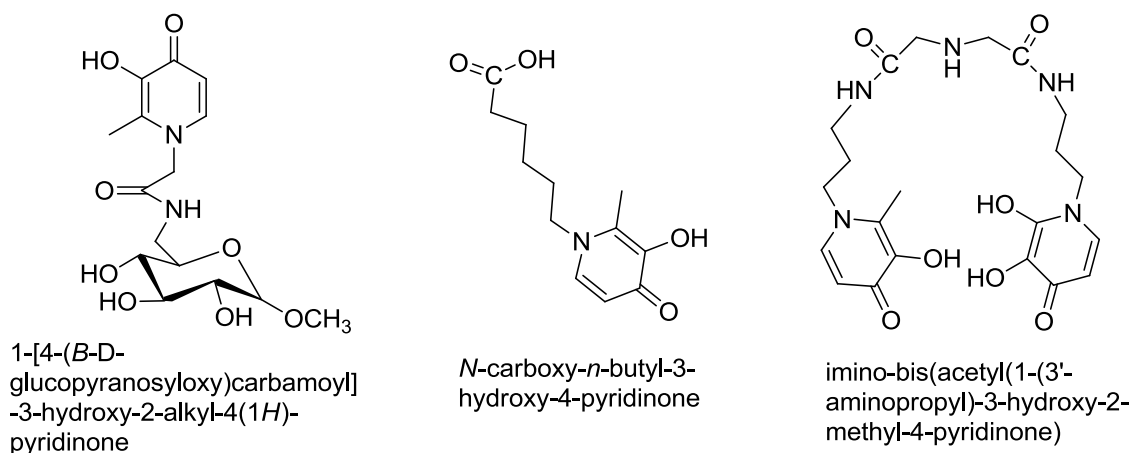
Figure 2.4: 3-Hydroxypyridinone derivatives for improved tissue targeting for potential diagnostic and radionuclear therapeutic applications.[77-79]

Studies by Santos *et al.* indicated that shorter chain lengths in *N*-carboxyalkyl substituents on 3-hydroxypyridinones were associated with elevated gallium complex stability and increased bone targeting along with a moderate decrease in blood clearance.[78,79]

---

[75] M. A. Santos, M. Gil, L. Gano, S. Chaves, *J. Biol. Inorg. Chem.*, **2005**, *10*, 564.

[76] T. Storr, K. H. Thompson, C. Orvig, *Chem. Soc. Rev.*, **2006**, *35*, 534.

[77] D. E. Green, C. L. Ferreira, R. V. Stick, B. O. Patrick, M. J. Adam, C. Orvig, *Bioconjugate Chem.*, **2005**, *16*, 1597.

[78] M. A. Santos, M. Gil, S. Marques, L. Gano, G. Cantinho, S. Chaves, *J. Inorg. Biochem.*, **2002**, *92*, 43.

[79] M. A. Santos, S. Gama, L. Gano, G. Cantinho, E. Farkas, *Dalton Trans.*, **2004**, 3772.

2.4 Contrast agents for MRI

Magnetic resonance imaging (MRI) is one of the most powerful techniques in diagnostic clinical medicine and biomedical research. This is because of its high depth penetration (1 mm to 1 m) and its ability to resolve different soft tissues.[80-82] The MRI signal is generated by the relaxation of *in vivo* water molecules' protons by acquiring high resolution, three-dimensional images of the distribution of water *in vivo*.[83] Thus to improve the MRI signal these relaxations have to be improved by developing pharmacological contrast agents. Ideally such a compound will catalytically reduce the relaxation times of nearby water molecules and in the process increase the contrast with background tissues. MRI images or signals can be improved by administering gadolinium-based paramagnetic agents due to its favourable electronic properties since it has seven unpaired electrons and a long relaxation time.[83] However $[Gd(H_2O)_8]^{3+}$ is very toxic *in vivo* which necessitates strong coordination to suitable ligands for sequestration from when the contrasting agent is administered until its clearance.[84] Ideally contrast agents should be site-specific to avoid the use of large doses required for reasonable image enhancements, this implies that higher relaxivities are required to account for the decrease in concentration that accompanies the increased tissue specificity.[85]

The image-enhancement capacity of these compounds is directly proportional to its relaxation of neighbouring water molecules by the paramagnetic ion and for this reason and although Gd^{3+} favours eight or nine coordination, some highly effective designs provide three or two coordination sites for inner-sphere water molecules.[86] Water molecules then rapidly exchange with the bulk solution and thus affect the relaxation rates of the bulk of the water molecules. These complexes increase both the longitudinal ($1/T_1$) and transverse relaxation rates ($1/T_2$) of nearby water molecules. However longitudinal relaxation *via* dipolar interactions is much significantly increased making gadolinium-based agents more effective for contrast enhancement in T_1-weighted images than in T_2-weighted images.[83]

---

[80] R. B. Lauffer, *Chem. Rev*., **1987**, *87*, 901.
[81] A. E. Merbach, E. Tóth, editors. The Chemistry of Contrast Agents in Medical Magnetic Resonance Imaging. Wiley; Chichester, **2001**.
[82] E. Tóth, L. Helm, A. E. Merbach, *Top. Curr. Chem.*, **2002**, *221*, 61.
[83] P. Caravan, J. J. Ellison, T. J. McMurry, R. B. Lauffer, *Chem. Rev.*, **1999**, *99*, 2293.
[84] R. Ranganathan, N. Raju, H. Fan, X. Zhang, M. Tweedle, J. Desreux, V. Jacques, *Inorg. Chem*., **2002**, *41*, 6856.
[85] K. N. Raymond, V. C. Pierre, *Bioconjugate Chem*., **2005,** *16*, 3.
[86] A. Datta, K. N. Raymond, *Acc Chem Res*., **2010**, *42*, 938.

Commercially available formulations are based on polyaminocarboxylate chelators, which are N,O'-donors.[83] These ligands are octadentate and leave one coordination site vacant for coordinating water molecules. High chelate denticity is required to maintain complex stability, however a low number of inner-sphere water molecules compromises relaxivity. Gd^{3+} like all the lanthanides are hard metals therefore hydroxypyridinones being hard ligands with low denticity offers high stability with low coordination numbers. However, their capacity to increase relaxivities is improved by grafting them on macromolecules to incorporate six oxygen donors (e.g. three bidentate hydroxypyridinone moieties attached *via* a tris(2-aminoethyl)amine (TREN)) for Gd^{3+} binding, leaving two to three coordination sites open for binding inner sphere water molecules (Figure 2.5).[83,87-89] This slows down the tumbling rate and increases the contrast. The Gd-TREN-1-Me-3,2-HOPO (HOPO = hydroxypiridinone) complex has a relaxivity value of 10.5 $mM^{-1}s^{-1}$ (at 20 MHz), which is almost twice that of commercial contrast agents.[86] This is likely due to the higher number of inner sphere water molecules.[87] This class of compounds (Gd-TREN-1-Me-3,2-HOPO) shows fast near-optimal water exchange rates which are more than twice that of commercially available contrast agents.

Gd-TREN-1-Me-3,2-HOPO   Gd-TREN-1,2-HOPO   Gd-Ser-TREN-1-Me-3,2-HOPO

Gd-TREN-bis-1-Me-3,2-HOPO-TAM-Me   Gd-TREN-bis-1-Me-3,2-HOPO-SAM   Gd-TREN-bis-1-Me-3,2-HOPO-IAM
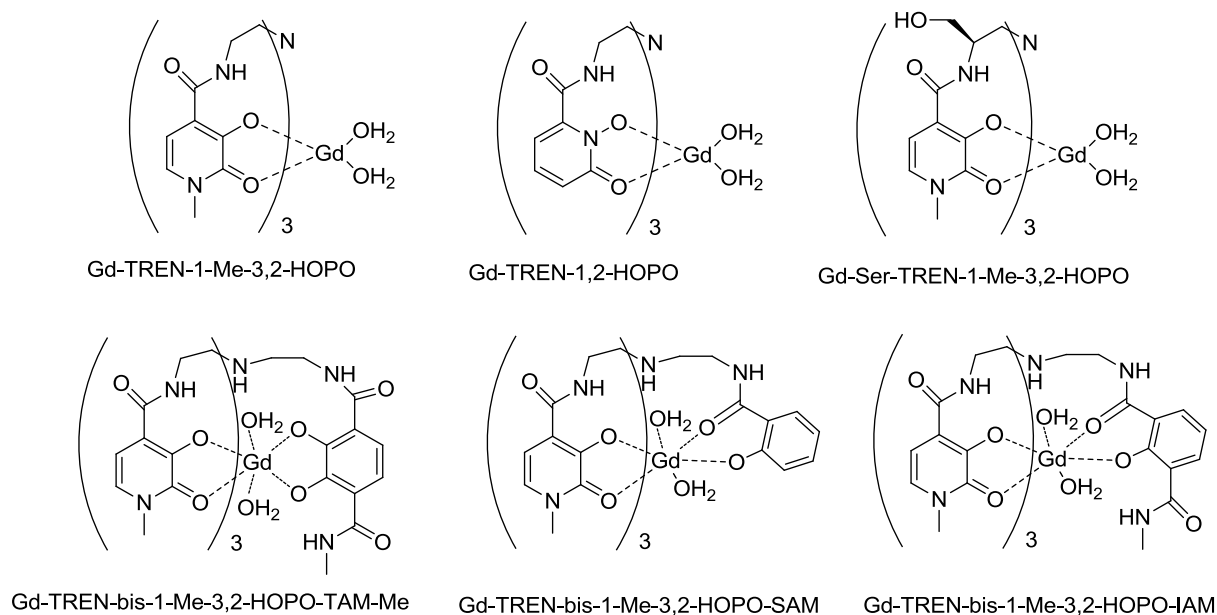
Figure 2.5: Gadolinium-TREN-hydroxypyridinonate based MRI contrast agents with high relaxativity.[35,86]

[87] J. Xu, S. J. Franklin, D. W. Whisenhunt, K. N. Raymond, *J. Am. Chem. Soc.*, **1995**, *117*, 7245.
[88] T. H. Cheng, Y. M. Wang, K. T. Lin, G. C. Liu, *J. Chem. Soc., Dalton Trans.*, **2001**, 3357.
[89] S. Laus, R. Ruloff, E. Toth, A. E. Merbach, *Chem. Eur. J.*, **2003**, *9*, 3555.

2.5 Insulin enhancing agents for diabetes mellitus

Vanadium compounds can be utilized to diminish insufficient insulin response in diabetes mellitus. These compounds are not functionally insulin mimetic as they cannot replace insulin (as in type 1 diabetes) but rather insulin enhancing as they require small amounts of insulin to be effective (as in type 2 diabetes).[90] They can reduce reliance on exogenous insulin, or possibly substitute for other oral hypoglycemic agents.[91] Both 3-hydroxy-2-methylpyrone (maltol) and 2-ethyl-3-hydroxypyrone (ethyl maltol) form bis(ligand) oxovanadium(IV) complexes that are orally available insulin enhancing drugs.[92-94] Both bis(maltolato)oxovanadium(IV) (BMOV), and the ethylmaltol analog, bis(ethylmaltolato)oxovanadium(IV) (BEOV) were developed to overcome the absorption and tolerability challenges observed with oral administration of inorganic vanadium salts such as vanadyl sulphate or ammonium tartarovanadate (Figure 2.6).[95,96] BMOV and BEOV are two to three times as bioavailable as vanadyl sulphate.[97] Additionally the biodistribution of these compounds indicates enhanced gastrointestinal uptake compared to vanadyl sulphate, which is followed by strong complex formation primarily with transferrin and subsequent distribution to tissues with the most accumulating in the bone.[91]

The ability of vanadium to lower elevated blood glucose and lipid levels is distinct among antidiabetic agents: both vanadium salts and complexes lower only elevated blood glucose levels of diabetic animals rather than normal blood glucose levels. This makes vanadium compounds as antidiabetic agents notably safe for treated subjects as the problem of hypoglycemia is minimal.[98] Transferrin has been associated with circulatory transport of absorbed vanadium ions. BEOV has undergone pharmacokinetic assessments and Phase I & IIa human clinical trials.[94,99-101]

[90] D. C. Crans, *J. Org. Chem.*, **2015**, *80*, 11899.
[91] K. H. Thompson, J. Lichter, C. LeBel, M. C. Scaife, J. H. McNeill, C. Orvig, *J. Inorg. Biochem.*, **2009**, *103*, 554.
[92] J. H. McNeill, V. G. Yuen, H. R. Hoveyda, C. Orvig, J. *Med. Chem.*, **1992**, *35*, 1489.
[93] C. Orvig, K. H. Thompson, M. Battell, J. H. McNeill, *Met. Ions Biol. Syst.*, **1995**, *31*, 575.
[94] K. H. Thompson, C. Orvig, *Met. Ions Biol. Syst.*, **2004**, *41*, 221.
[95] G. R. Willsky, A. B. Goldfine, P. J. Kostyniak, in: A. S. Tracey, D. C. Crans (Eds.), Vanadium Compounds: Chemistry, Biochemistry and Therapeutic Applications, ACS Symposium Series 711, Washington, DC, **1998**, 278.
[96] J. Somerville, B. Davies, *Amer. Heart J*., **1962**, *64*, 54.
[97] K. H. Thompson, C. Orvig, *J. Inorg. Biochem*., **2006**, *100*, 1925.
[98] G. R. Willsky, L.-H. Chi, M.(III) Godzala, P. J. Kostyniak, J. J. Smee, A. M. Trujillo, J. A. Alfano, W. Ding, Z. Hu, D. C. Crans, *Coord. Chem. Rev*., **2011**, *255*, 2258.
[99] K. J. Barnham, C. L. Masters, *Nat. Rev. Drug Discov.,* **2004**, *3*, 205.
[100] G. R. Willsky, A. B. Goldfine, P. J. Kostyniak, in: A. S. Tracey, D. C. Crans (Eds.), Vanadium Compounds: Chemistry, Biochemistry and Therapeutic Applications, ACS Symposium Series 711, Washington, DC, **1998**, 278.
[101] M. Melchior, S. Rettig, B. Liboiron, K. Thompson, V. Yuen, J. McNeill, C. Orvig, *Inorg. Chem*., **2001**, *40*, 4686.

R = CH$_3$ BMOV, C$_2$H$_5$ BEOV
R' = CH$_3$ or C$_2$H$_5$
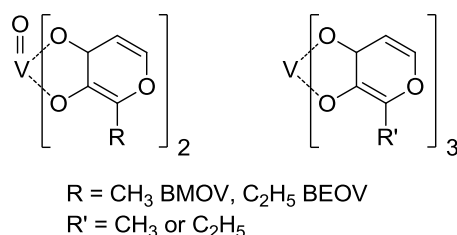
Figure 2.6: 3,4-Hydroxypyronato oxovanadium(IV) and 3,4-hydroxypyronato vanadium(III) insulin enhancing compounds.[35]

2.6 Neurodegenerative diseases: Alzheimer's disease

Alzheimer's disease (AD) is a neurological disease of the cerebral cortex which can be fatal and not a natural part of the aging process that affects the elderly.[102,103] There are two types of AD currently recognized: early onset (symptoms appear before the age of 65) and late onset (which is apparent after the age of 65) with the latter constituting 95 % of all diagnoses. Genetic factors have been identified in the development of early-onset AD, however increased age is a major risk factor for the late-onset AD.[104]

Current AD treatments are unable to stop disease progression, however they can offer symptomatic relief and even slow cognitive decline in some cases. These therapies target only the symptoms and new treatments are needed to target the underlying pathology of AD.

Advanced age is the major risk factor for neurodegenerative diseases, it is also known that the brain metal concentration increases as a result of aging.[105-107] It is also clear that the oxidative stress mechanism of Aβ toxicity is mediated by metal ions.[108,109] Copper in the AD brain appears to be mis-compartmentalized rather than elevated in every case, it is concentrated within Aβ plaques.

[102] A. Alzheimer, R. A. Stelzmann, H. N. Schnitzlein, F. R. Murtagh, *Clin. Anat.*, **1995**, *8*, 429.

[103] C. P. Ferri, M. Prince, C. Brayne, H. Brodaty, L. Fratiglioni, M. Ganguli, K. Hall, K. Hasegawa, H. Hendrie, Y. Huang, A. Jorm, C. Mathers, P. R. Menezes, E. Rimmer, M. Scazufca, *Lancet*, **2005**, *366*, 2112.

[104] D. M. Walsh, D. J. Selkoe, *J. Neurochem.*, **2007**, *101*, 1172.

[105] A. Morita, M. Kimura, Y. Itokawa, *Biol. Trace Elem. Res.*, **1994**, *42*, 165.

[106] S. Takahashi, I. Takahashi, H. Sato, Y. Kubota, S. Yoshida, Y. Muramatsu, *Biol. Trace Elem. Res.*, **2001**, *80*, 145.

[107] C. J. Maynard, R. Cappai, I. Volitakis, R. A. Cherny, A. R. White, K. Beyreuther, C. L. Masters, A. I. Bush, Q.-X. Li, *J. Biol. Chem.*, **2002**, *277*, 44670.

[108] K. J. Barnham, A. I. Bush, *Curr. Opin. Chem. Biol.*, **2008**, *12*, 222.

[109] D. G. Smith, R. Cappai, K. J. Barnham, *Biochim. Biophys. Acta, Biomembr.*, **2007**, *1768*, 1976.

Due to the harmful interactions of metal ions with Alzheimer's Aβ peptide, therapeutic approaches have been developed to modulate the metal-protein interactions.[110,111] The acronym 'metal-protein attenuating compound' (MPAC) was formulated to illustrate the chelatotherapeutic approach to disrupt specific, abnormal metal-protein interactions.[112] This approach is different from passivation and excretion of bulk metal ions as it is not systemic excretion but targeted repartitioning and normalization of metal ion distribution. Conventional chelation therapy sequesters and clears metal ions from the body using agents initially developed for treatment of heavy metal poisoning. In AD treatment the target site for action is the brain tissue. The blood brain barrier (BBB) permeation of the targeting chelator must be considered as diffusion through the BBB requires a high level of hydrophobicity. Glycosylation strategies have been applied to many chelators to improve their CNS uptake and to exploit the GLUT1 hexose transporter proteins localized within the BBB (Figure 2.7).[113,114]
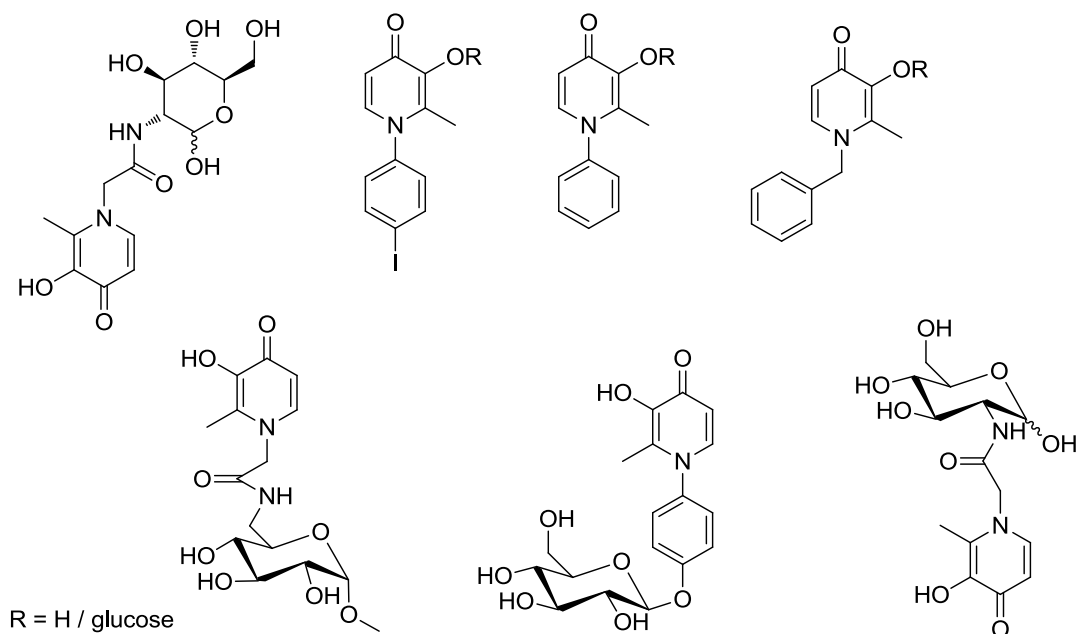
Figure 2.7: Selected 3-hydroxy-4-pyridinone derivatives developed for therapeutic metal ion manipulation.[115]

[110] A. I. Bush, R. E. Tanzi, *Neurotherapeutics*, **2008**, *5*, 421.

[111] M. P. Cuajungco, K. Y. Faget, X. Huang, R. E. Tanzi, A. I. Bush, *Ann. N.Y. Acad. Sci.*, **2000**, *920*, 292.

[112] K. J. Barnham, C. L. Masters, *Nat. Rev. Drug Discov.,* **2004**, *3*, 205.

[113] H. Schugar, D. E. Green, M. L. Bowen, L. E. Scott, T. Storr, K. Böhmerle, F. Thomas, D. D. Allen, P. R. Lockman, M. Merkel, K. H. Thompson, C. Orvig, *Angew. Chem., Int. Ed.* **2007**, *46*, 1716.

[114] C. Fernandez, O. Nieto, J. A. Fontenla, E. Rivas, M. L. de Ceballos, A. Fernandez-Mayoralas, *Org. Biomol. Chem.,* **2003**, *5*, 767.

[115] L. E. Scott, C. Orvig, *Chem. Rev.*, **2009**, *109*, 4885.

Due to the brain's high energy consumption, most glucose moiety bearing molecules are transported to the brain (Figure 2.7).[116] Glycosylation has been used to enhance brain uptake transporters of compounds like dopamine for Parkinson's disease treatment and opiate analgesics.[117-119] Glycosylation of the hydroxyl functional group in 3-hydroxypyridinones gives them dual purpose. It enables permeation of the BBB through GLUT1 transporters, and it also deactivates the binding site and antioxidant activity creating a precursor of the active drug preventing undesired systematic metal chelation before reaching the brain tissue. Glycosylation can also increase solubility of the precursor improving its pharmacokinetic properties.[120]

2.7 Beneficiation of zirconium and hafnium

In the first main focus of this study the evaluation of these chelators will be directed to determining any chemical affinity or selectivity of a given chelator to either hafnium or zirconium. The most common zirconium ore commonly referred to as zircon always contains hafnium. The composition of this zirconium ore varies but it mainly consists of zirconium silicate, often with some hafnium and occasionally with some uranium, thorium, and yttrium.[121] It can contain up to 5 % of hafnium in its structure. If the hafnium content exceeds 20 % then it is no longer Zircon but Hafnon. The separation of hafnium and zirconium is very difficult due to the similarities in chemical behaviour.

The zirconium metal has a wide range of applications, in many diverse industrial technologies. It is comprehensively employed as a catalyst for the synthesis of organic compounds but also in ceramics, the development of surgical equipment and applied in semi-conductors.[122-124]

---

[116] A. A. Qutub, C. A. Hunt, *Brain Res. Rev.*, **2005**, *49*, 595.

[117] C. Fernández, O. Nieto, J. A. Fontenla, E. Rivas, M. L. de Ceballos, A. Fernández-Mayoralas, *Org. Biomol. Chem.*, **2003**, *1*, 767.

[118] G. Battaglia, M. La Russa, V. Bruno, L. Arenare, R. Ippolito, A. Copani, F. Bonina, F. Nicoletti, *Brain Res.*, **2000**, *860*, 149.

[119] E. J. Bilsky, R. D. Egleton, S. A. Mitchell, M. M. Palian, P. Davis, J. D. Huber, H. Jones, H. I. Yamamura, J. Janders, T. P. Davis, F. Porreca, V. J. Hruby, R. Polt, *J. Med. Chem.*, **2000**, *43*, 2586.

[120] B. Gyurcsik, L. Nagy, *Coord. Chem. Rev.*, **2000**, *203*, 81.

[121] R. Callaghan, USGS Minerals Information, **2008**. Available: http://minerals.usgs.gov/minerals/pubs/commodity/zirconium.

[122] D. W. Hart, J. Schwartz, *J. Am. Chem. Soc.*, **1974**, *96*, 8115.

[123] J. Schwartz, J. A. Labinger, *Angew. Chem. Int. Ed.*, **2003**, *15*, 330.

[124] D. W. Hart, T. F. Blackburn, J. Schwartz, *J. Am. Chem. Soc.*, **1975**, *97*, 679.

Furthermore, its alloys have anti-corrosive properties and high thermal stability which makes them ideal for the use in refractory material in furnaces and crucibles.[121]

However, the most noteworthy application of this metal is found in the nuclear industry, as cladding material for fuel rods.[121] The nuclear grade zirconium is required to be hafnium free (< 100 ppm) because of hafnium's high thermal neutron absorption cross section (Hf = 104 barns *vs.* Zr = 0.184 barns). The separation of these two metals is of utmost importance, since impurities can compromise the metal's application in this field. The zirconium metal is applied in the form of an alloy cladding material, commonly referred to as zircaloy. These alloys contain other metals with similarly low thermal neutron absorption cross sections, but in very low quantities. Metals with high neutron capture cross-sections are capable of absorbing many neutrons without fissioning themselves. These metals (hafnium) are used in nuclear reactors to control the flux (rate of fission) in nuclear reactors.

Current industrial methods of separation for Zr and Hf are liquid-liquid extraction, extractive distillation and the Kroll process.[125-130] The application envisaged in this PhD study is to employ these chelators which display different electronic and steric properties to extract Hf/ Zr or both. This implies that in a systematic manner the influence of these properties can be investigated to determine selectivity or affinity which can aid in separation. Furthermore the resulting compounds should have different properties which could also be exploited for separation techniques e.g. solubility, boiling points etc. or the formation of these compounds might occur in different mechanisms which would allow for the manipulation of their respective equilibria based on their reaction rates. Mechanistic studies might also provide insights that will assist in the development of a beneficiation technique. A possible key factor might be the atomic mass and sizes of the metal centres, hafnium is slightly smaller and significantly heavier than zirconium although they possess the same valency of electrons. It is possible that certain chelators will be more selective to either of the metals just based strictly on the difference in size

[125] G. Roza, Zirconium, 1st Ed., Rosen Publishing Group, **2009**.

[126] W. Kroll, Method for Manufacturing Titanium, US Patent 2205854, **1940**.

[127] A. L. Lowe, G. W. Parry, Zirconium in the Nuclear Industry: Proceedings of the Third International Conference, **1976**, *633,* 7.

[128] R. H. Nielsen, J. H. Schlewitz, H. Nielsen, Zirconium and Zirconium Compounds, Kirk-Othmer Encyclopedia of Chemical Technology, John Wiley & Sons, Inc., **2000**, *26*, 630.

[129] R. H. Nielsen, Hafnium and Hafnium Compounds, Kirk-Othmer Encyclopedia of Chemical Technology, John Wiley & Sons, Inc., **2000**, *13*, 82.

[130] J. G. Speight, The Refinery of the Future, London: William Andrew, **2010**, 134.

as coordination might be easier or more difficult due to sterics around the respective metal centres.

2.7.1   Industrial production processes for zirconium

The presence of oxygen, nitrogen and carbon in zirconium reduces its ductility significantly and consequently compromises its mechanical properties. To prevent contamination by these elements, the ductile form of the metal is produced under a vacuum or an inert atmosphere. The two conventional industrial processes for zirconium production are the Van Arkel-de Boer process and the Kroll process.[131,132] The former was the first industrialized nuclear grade zirconium production process, it proceed *via* two primary reactions, the formation of zirconium(IV) tetraiodide (**1**) (Scheme 2.2). This is then succeeded by the decay of zirconium(IV) tetraiodide and subsequent formation of pure zirconium metal and iodine gas (**2**).[133]

$$Zr + 2I_2 = ZrI_4 \qquad (\text{ at 525 - 575 K or 745 - 825 K}) \qquad (\mathbf{1})$$

$$ZrI_4 = Zr + 2I_2 \qquad (\text{at 1475 - 1675 K}) \qquad (\mathbf{2})$$

$$3ZrI_4 + Zr = 4ZrI_3 \qquad (\text{ at 575 - 745 K}) \qquad (\mathbf{3})$$
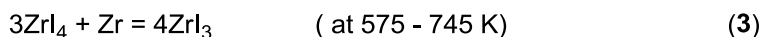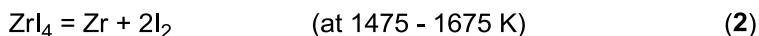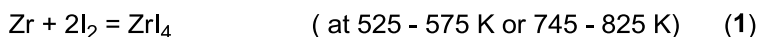
Scheme 2.2: A schematic representation of the Van Arkel-de Boer process.[134]

At temperatures between 575 and 745 K the formation of low volatility tri-iodide is prevalent which is undesirable as it subsequently decays into the tetraiodide and zirconium metal, significantly reducing the efficiency of the process (**3**). In this process nonmetals that do not form iodides (*i.e*. C, N and O) are successfully removed and metals that form stable iodides like copper, chromium, cobalt and magnesium can also be separated.[133,135] The inherent disadvantage of the Van Arkel-de Boer process despite producing high purity zirconium metal is the low yields and long production cycle.

[131] A. E. van Arkel, J. H. de Boer, *Z. Anorg, Allg. Chem*., **1925**, *148*, 345.
[132] W. J. Kroll, *J. Frankl. Inst.*, **1955**, *260*, 169.
[133] J. C. Haygarth, R. A. Graham, TMS Annual Meeting, San Diego, CA, **1999**.
[134] l. Xu, Y. Xiao, A. van Sandwijk, Q. Xu, Y. Yang, *J. Nucl. Mater.*, **2015**, *466*, 21.
[135] R. J. H. Clark, D. C. Bradley, P. C. Thornton, The Chemistry of Titanium, Zirconium and Hafnium, Pergamon Press, Oxford, **1975**.

The Kroll process on the other hand is commonly used on industrial scale to produce metals from the corresponding metal chlorides. It is currently used for the production of nearly all commercial titanium, zirconium and hafnium metals. In this process zirconium(IV) tetrachloride is reduced by molten magnesium in an inert atmosphere (**4**) (Scheme 2.3).

$$2Mg + ZrCl_4 = Zr + 2MgCl_2 \qquad\qquad (4)$$

Scheme 2.3: A schematic representation of the reduction of zirconium tetrachloride with molten magnesium.[134]

After the reduction, the formed magnesium chloride and the excess magnesium reductant are removed mechanically with further purification accomplished through distillation. The inherent disadvantage of the Kroll process is that each of its individual multi-steps is a batch process, and the required equipment is complex and expensive leading to high production costs.

2.7.2 Hydrometallurgical routes of Zr and Hf separation

The two conventional hydrometallurgical industrial technologies for the separation of zirconium and hafnium are fractional crystallization and solvent extraction. Fractional crystallization is a multi-step batch recrystallization process that exploits the difference in solubility between K_2ZrF_6 and K_2HfF_6 for separation.[136,137] The inherent disadvantage of this process is its batch property, numerous crystallization stages of separation and low efficiency.

Methyl isobutyl ketone (MIBK) and tributyl phosphate (TBP) are the two traditional solvents used in solvent extraction. In the MIBK extraction process the Zr(IV) and Hf(IV) tetrachlorides are hydrolyzed in HCl solution to form zirconium and hafnium dihydroxide chloride. Ammonium thiocyanate is then added to form thiocyanate compounds of the respective metals, subsequent to which a thiocyanic acid-containing MIBK solution is introduced. Hafnium is preferentially extracted into the MIBK solvent due to the difference in solubility of zirconium and hafnium thiocyanate complexes in this solvent.[133] The inherent disadvantage of this process

---

[136] A. N. Zelikman, O. E. Krein, G. V. Samsonov, Metallurgy of Rare Metals, Translated from Russian, Chapter V, Zirconium, **1964**.

[137] I. V. Vinarov, *Russ. Chem. Rev*., **1967**, *36*, 522.

is the large chemical volumes required and the low flash point of the solvent, high vapour pressures and the solubility of MIBK in water.[138] In the TBP extraction process, the hafnium-containing zirconium oxide is dissolved in nitric acid followed by the introduction of TBP in kerosene. Zirconium is then preferentially extracted into the organic solvent, leaving hafnium and all metallic impurities in the aqueous medium.[136,139] The TBP solvent has a high affinity for selective extraction of zirconium, however it is highly corrosive.[138]

2.7.3   Pyrometallurgical routes of Zr and Hf separation

There are three important approaches in pyrometallurgical technologies for the separation of zirconium and hafnium, these are based on: redox characteristics, volatility and on molten salt-metal equilibrium. Only the first two of these approaches are discussed here. Generally, hafnium compounds are slightly more stable than the corresponding zirconium compounds. A number of separation processes have been developed based on this notion, the most noteworthy being the Newnham process.[140] By exploiting differences in chemical reducibility between Zr and Hf the process achieves the separation of the two metals. Crude zirconium and hafnium tetrachlorides are heated with either zirconium metal (**1**) or zirconium dichloride (**2**) as reducing agent (Scheme 2.4). Zirconium tetrachloride is favourably reduced to the nonvolatile trichloride, while hafnium tetrachloride remains unchanged. The solid zirconium trichloride is retrieved *via* sublimation, and is disproportionated to produce pure $ZrCl_4$ (**3**). The by-product ($ZrCl_2$) is recovered and recycled for the reduction stage.

$$3ZrCl_4 + Zr = 4ZrCl_3 \qquad (\mathbf{1})$$

$$ZrCl_4 + ZrCl_2 = 2ZrCl_3 \qquad (\mathbf{2})$$

$$2ZrCl_3 = ZrCl_4 + ZrCl_2 \qquad (\mathbf{3})$$
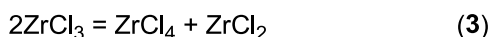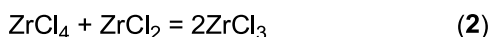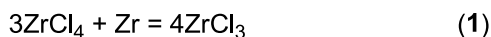
Scheme 2.4: A schematic representation of the reduction of zirconium tetrachloride.[134]

Extractive distillation utilizes a low-melting solvent at atmospheric pressure to directly separate crude zirconium and hafnium tetrachlorides. The crude tetrachlorides are added to a molten salt

[138] Z. Xu, Y. Wu, J. Zhang, *Trans. Nonferrous Met. Soc. China*, **2010**, *20*, 1527.
[139] R. Nielsen, T. W. Chang, Zirconium and Zirconium Compounds, United States, **2005**.
[140] I. E. Newnham, US Patent No. 2 791 485, **1957**.

bath to form a solution. This reduces the volatility of the tetrachlorides enabling separation at ambient pressure and low temperatures.[141] After several stages of separation, nuclear grade zirconium tetrachloride and commercially pure quality hafnium tetrachloride are produced. The fused salt solvent can be recycled and purified zirconium tetrachloride *via* the Kroll process can be reduced to zirconium metal.

2.8 Modelling of theranostics with non-radioactive rhenium

In the second main focus of the study, since these ligand systems have shown proven biological activity it is imperative that they be evaluated as potential diagnostic and therapeutic radiopharmaceuticals. Over the past few years, significant interest has been shown in rhenium and technetium tricarbonyl complexes of the form fac-$[M(L,L'\text{-bid})(CO)_3(X)]^n$ (M = Tc(I) and Re(I), (L,L'-bid) = different donor atom bidentate ligands, X = range of monodentate ligands), as potential diagnostic and therapeutic radiopharmaceutical models. This is mainly due to the discovery of the fac-$[M(CO)_3(H_2O)_3]^+$ synthon with the inert fac-$[M(CO)_3]^+$ core and the labile water molecules.[142-145] These properties make the synthons very appealing for application in nuclear medicine. The purpose of this exploration is to not only try and improve selectivity by creating a better targeting compound but to gain further insights into the chemistry, geometry, coordination and kinetic behaviour of complexes containing the fac-$[M(CO)_3]^+$ core.

2.8.1 Nuclear imaging with radiometals

Radiometals can be produced in three different ways: nuclear bombardment reactions in a cyclotron, or nuclear bombardment reactions in a nuclear reactor and decay of longer-lived radionuclides in a generator. Positron emission tomography (PET) imaging is mainly dominated by a radiohalogen, fluorine-18 (^{18}F, $t_{1/2} \sim 109.8$ min). Radiometal imaging on the other hand provides flexibility, modularity, and facilitation unmatched by non-metallic imaging isotopes.

[141] R. P. Tangri, D. K. Bose, C. K. Gupta, *J. Chem. Eng. Data*, **1995**, *40*, 823.
[142] M. Salmain, M. Gunn, A. Gorfi, S. Top, G. Jaouen, *Bioconjug. Chem.*, **1993**, *4*, 425.
[143] S. Top, E. H. Hafa, A. Vessières, J. Quivy, J. Vaissermann, D. W. Hughes, M. J. McGlinchey, J. -P. Mornan, E. Thoreau, G. Jaouen, *J. Am. Chem. Soc.*, **1995**, *117*, 8372.
[144] T. W. Spradau, J. A. Katzenellenbogen, *Organometallics*, **1998**, *17*, 2009.
[145] R. Alberto, R. Schibli, A. Egli, Patent no 97201232.2, **1997**.

The wide range of metallic radionuclides enables accurate matching of the physical half-life of the radioisotope to the biological half-life of the targeting vector. For instance, agents with short *in vivo* residence times can be labelled with gallium-68 (^{68}Ga; $t_{1/2} \sim 68$ min) or technetium-99m (^{99m}Tc; $t_{1/2} \sim 6$ h), while vectors that take longer to reach their targets can be labeled with copper-64 (^{64}Cu; $t_{1/2} \sim 12.7$ h), yttrium-86 (^{86}Y; $t_{1/2} \sim 14.7$ h), indium-111 (^{111}In; $t_{1/2} \sim 2.8$ days), or zirconium-89 (^{89}Zr; $t_{1/2} \sim 3.2$ days).[146-150]

The aspect of simplicity and modularity in using bifunctional chelators and radiometals allows for the creation of a wide variety of imaging agents. For example, the same antibody can be conjugated to a variety of chelators for labelling with ^{89}Zr for PET imaging, ^{111}In for single-photon emission computed tomography (SPECT) imaging, or lutetium-177 (^{177}Lu) for radioimmunotherapy. In some instances, the radiometal may be exchanged without changing the chelator. This modularity is clinically convenient when an imaging agent labeled with one isotope is utilized as a companion diagnostic tool for a therapeutic agent bearing another isotope.[151]

Radiometalation reactions are generally rapid and can be accomplished under mild conditions. Purification techniques are usually by cation exchange chromatography or reverse-phase C18 cartridges. The advantage of radiometals over radiohalogens is that probes bearing the latter often require multistep synthesis, harsh reaction conditions and complicated purifications.

Many radiometals (e.g. ^{86}Y, ^{89}Zr, and ^{111}In) are known to residualize in cells after the uptake of their vector. This results in retention enhancement of the radioactivity at target sites (tissues or organs) and higher tumor to background activity ratios compared to non-residualizing radiohalogens such as ^{18}F, iodine-124 (^{124}I), and bromine-76 (^{76}Br).[152]

---

[146] T. J. Wadas, E. H. Wong, G. R. Weisman, C. J. Anderson, *Curr. Pharm. Des.*, **2007**, *13*, 3.
[147] T. J. Wadas, E. H. Wong, G. R. Weisman, C. J. Anderson, *Chem. Rev.*, **2010**, *110*, 2858.
[148] B. M. Zeglis, J. S. Lewis, *Dalton Trans.*, **2011**, *40*, 6168.
[149] D. E. Reichert, J. Lewis, C. J. Anderson, *Coord. Chem. Rev.*, **1999**, *184*, 3.
[150] S. Liu, D. S. Edwards, *Chem. Rev.*, **1999**, *99*, 2235.
[151] S. S. Kelkar, T. M. Reineke, *Bioconjugate Chem.*, **2011**, *22*, 1879.
[152] E. M. Jagoda, L. Lang, V. Bhadrasetty, S. Histed, M. Williams, G. Kramer-Marek, E. Mena, L. Rosenblum, J. Marik, J. N. Tinianow, M. Merchant, L. Szajek, C. Paik, F. Cecchi, K. Raffensperger, J. M. Jose-Dizon, D. P. Bottaro, P. Choyke, *J. Nucl. Med.*, **2012**, *53*, 1592.

Lastly metallic radioisotopes due to their vast half-lifes are readily available as imaging agents. Thus hospitals and research labs don't need cyclotron facilities as they can be produced by portable generator systems (e.g. ^{68}Ga and ^{99m}Tc) or they have physical half-lifes long enough to be transported without excessive decay (e.g. ^{64}Cu, ^{111}In, and ^{89}Zr).

2.8.2   The architecture of radiometal-based imaging agents

From a structure point of view, radiometal-based imaging agents can be classified into three classes: small metal complexes, chelator-based conjugates, and colloids. Small metal complexes are the simplest radiotracers, there's two essential parts to their structure: a radiometal centre and a set of coordinating chelators. These coordination compounds carry out *in vivo* targeting, uptake, and retention. Many such complexes for PET and SPECT imaging have had a significant impact in clinical applications; this includes ^{99m}Tc-bisphosphonates (**A**) for bone imaging, ^{99m}Tc-sestamibi (**B**) for myocardial perfusion imaging, and ^{64}Cu-PTSM (**C**) for blood perfusion imaging (Figure 2.8).[149]
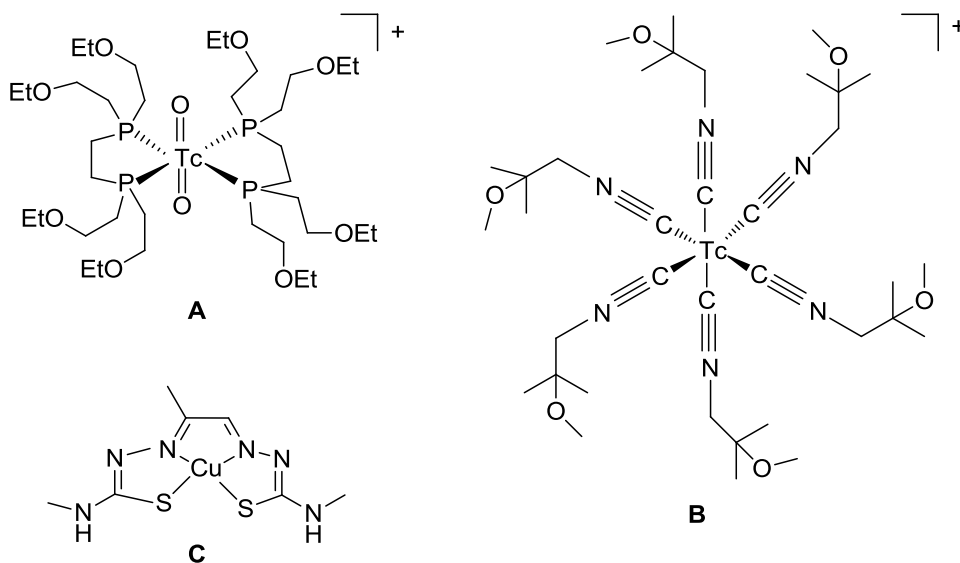
Figure 2.8: Radiometal complexes for imaging applications.[153,154]

Chelator-based conjugates have four essential parts to their structure; a radiometal centre, a ligand, a targeting vector and a linker joining the ligand and the targeting vector.[147-150] The

[153] U. Abram, R. Alberto, *J. Braz. Chem. Soc.,* **2006**, *17*, 1486.
[154] B. M. Zeglis, J. L. Houghton, M. J. Evans, N. Viola-Villegas, J. S. Lewis, *Inorg. Chem.*, **2014**, *53*, 1880.

targeting vector is normally a biomolecule (either a protein, an antibody or a peptide). The choice of a radiometal is guided by the biological half-life of the targeting vector and the imaging modality. The most common radiometals for SPECT and PET imaging are ^{111}In, ^{99m}Tc and ^{68}Ga, ^{64}Cu, ^{86}Y, ^{89}Zr respectively. Upon choosing an imaging modality the next crucial step is matching the radioactive half-life of the isotope to the biological half-life of the targeting vector. The half-lifes of the radiometals should be such that when labeled with these radiometals the targeting vectors reach optimal concentrations within target sites before significant decay of the isotope. The role of the chelator is to form a kinetically inert and thermodynamically stable coordination compound with the radiometal to prevent undesirable release *in vivo*. The choice of chelator is dictated by the identity of the radiometal and desired objectives (acyclic ligands have fast metal binding rates and less thermodynamic stability while the opposite is true for macrocyclic ligands).[155] The desired features of the linker other than linking are stability under physiological conditions and non-interference with the specificity and binding strength of the vector.

The ^{99m}Tc-radiocolloids are the oldest class of radiometal-based imaging agents and have had an enormous impact on the clinical imaging of the reticuloendothelial system (RES).[156-158] Colloids are removed from circulation in the body by phagocytosis, a process primarily active in macrophages. As a result, radiolabeled colloids can be employed to image tissues with high concentrations of macrophages, like the bone marrow, spleen, liver and lymph nodes. Consequently ^{99m}Tc-radiocolloids are vital for the imaging of the lymphatic system in oncology.

2.8.3   Radionuclides for imaging and therapy (Theranostics)

Diagnostic drugs decay by releasing photons with enough energy to be detected externally and collimated by a camera resulting in the intended non-invasive imaging. Therapeutic drugs decay by a particle, such as a β^- or α particle that can cause ionization and break bonds resulting in the

---

[155] R. E. Mewis, S. J. Archibald, *Coord. Chem. Rev*., **2010**, *254*, 1686.

[156] J. J. Albertini, G. H. Lyman, C. Cox, T. Yeatman, L. Balducci, N. N. Ku, S. Shivers, C. Berman, K. Wells, D. Rapaport, A. Shons, J. Horton, H. Greenberg, S. Nicosia, R. Clark, A. Cantor, D. S. Reintgen, *J. Am. Med. Assoc*., **1996**, *276*, 1818.

[157] D. Krag, D. Weaver, T. Ashikaga, F. Moffat, V. S. Klimberg, C. Shriver, S. Feldman, R. Kusminsky, M. Gadd, J. Kuhn, S. Harlow, P. Beitsch, *N. Engl. J. Med*., **1998**, *339*, 941.

[158] A. J. Wilhelm, G. S. Mijnhout, E. J. F. Franssen, *Eur. J. Nucl. Med.*, **1999**, *26*, S36.

intended non-invasive removal/ destruction. Until recently most radio-drugs were developed for use either as diagnostics or as therapeutics. The issue with this was the fact that different radionuclides used for either diagnosis or therapy had different chemistries which affected the distribution and the mechanism of localization resulting in issues related to dosage and efficacy. Current drugs being developed use radionuclides that emit photons that can be imaged as well as particles that can be used for therapy. The conceptual objective in this field is developing diagnostic tests related to therapy, to improve efficacy and costs by screening a disease state. This process entails initial minimal dose imaging to assess bio-distribution, dosimetry, dose-limiting organ or tissue, maximum tolerated dose (MTD), receptor expression, capacity and clearance.[159] Appropriate molecular targets are then determined in diseased organs or tissues that can be non-invasively targeted with the most effective dose of the radiopharmaceutical.[160] Many radionuclides have nuclear properties suitable for imaging and therapy these are among others: ^{99m}Tc, ^{111}In, ^{90}Y, ^{177}Lu, $^{186/188}$Re, ^{105}Rh). Thus in the broader sense the rhenium and rhodium compounds reported in this thesis have the potential to be employed as theranostics with their corresponding radioactive counterparts, with zirconium compounds strictly having potential PET applications with the corresponding radioactive nuclide ^{89}Zr. Although non-radioactive Re is conventionally used to model ^{99m}Tc, the radionuclides ^{186}Re and ^{188}Re have potential to be distinct theranostic drugs due to their decay *via* both particle and γ emissions.[161]

2.8.4 Substitution reactions as models for receptor specificity

The Re(I) tricarbonyl monocationic core has a low-spin d^6 electronic configuration, making it more kinetically inert than Re(V); this makes it more appealing for nuclear medical applications.[162] This stable core can be obtained as the tricarbonyl triaqua form *fac*-$[Re(CO)_3(H_2O)_3]^+$. In this study two of the facile aqua molecules are substituted with O,O'-bidentate ligands. Additionally, a unique coordination mode is observed that will assist in determining the nature of the substitution on the sixth position.

[159] S. C. Srivastava, *Semin. Nucl. Med.*, **2012**, *42*, 151.

[160] R. P. Baum, H. R. Kulkarni, C. Carreras, *Semin. Nucl. Med.*, **2012**, *42*, 190.

[161] C. S. Cutler, H. M. Hennkens, N. Sisay, S. Huclier-Markai, S. S. Jurisson, *Chem. Rev.*, **2013**, *113*, 858.

[162] R. Schibli, R. Schwarzbach, R. Alberto, K. Ortner, H. Schmalle, C. Dumas, A. Egli, P. A. Schubiger, *Bioconjugate Chem.*, **2002**, *13*, 750.

Substitution reactions in these types of complexes are reported to be preceded by solvolysis and the monodentate substitution on the sixth position in these types of complexes is said to be a solvent substitution.[163-167] With the unique set of complexes obtained in this study solution studies will be reported to investigate and to report on the reaction rates of the *fac*-[Re(CO)$_3$]$^+$ core activated by 3-hydroxypyridinones as a ligand system.

Some receptors are abundantly found in some organs or are overexpressed in tumor cells, making them appropriate target molecules for tumor imaging or organ imaging agents. For theranostic applications, antibodies or biomolecules can be attached either on the bifunctional bidentate ligand or on the monodentate ligand that are selective for receptors that are overexpressed on certain disease sites such as tumors. Additionally, some receptors can in principle be targeted directly by the nucleophilic Re centre as some receptors are nucleophiles (e.g. glutamine a tumor nutrient with a nucleophilic *N*-functional group).

Previous studies have shown that tropolone, tribromotropolone and 3-hydroxyflavone (all of which O,O′-bidentate ligands), can significantly activate the inert rhenium(I) metal center.[165,168] The results of the methanol substitution reactions by various entering ligands (pyridine, 4-dimethylaminopyridine (DMAP) and bromide ions) in methanol as solvent at 25.0 °C for the following complexes; *fac*-[Re(Trop)(CO)$_3$(MeOH)], *fac*-[Re(TropBr$_3$)(CO)$_3$(MeOH)] and *fac*-[Re(Flav)(CO)$_3$(MeOH)] (where TropH = tropolone, TropBr$_3$H = tribromotropolone and FlavH = Flavone) indicated an increase in rate of a factor of 10 for the substitution reactions of *fac*-[Re(Trop)(CO)$_3$(MeOH)] compared to that of *fac*-[Re(TropBr$_3$)(CO)$_3$(MeOH)]. For the complex with 3-hydroxyflavone as bidentate ligand, *fac*-[Re(Flav)(CO)$_3$(MeOH)], the methanol substitution reactions were ∼ 2 - 5 times faster than those of *fac*-[Re(Trop)(CO)$_3$(MeOH)].

[163] A. Brink, H. G. Visser, A. Roodt, *Inorg. Chem.,* **2014**, *53*, 12480.

[164] A. Brink, H. G. Visser, A. Roodt, *Inorg. Chem.,* **2013**, *52*, 8950.

[165] M. Schutte, A. Roodt, H. G. Visser, *Inorg. Chem.,* **2012**, *51*, 11996.

[166] M. Schutte, G. Kemp, H. G. Visser, A. Roodt, *Inorg. Chem.,* **2011**, *50*, 12486.

[167] M. Schutte, H. G. Visser, *Polyhedron,* **2015**, *89*, 122.

[168] M. Schutte, G. Kemp, H. G. Visser, A. Roodt, *Inorg. Chem.,* **2011**, *50*, 12486.

2.9 Rhodium-catalyzed carbonylation of methanol

The carbonylation of methanol is catalyzed by Group VIII transition metal compounds, mainly rhodium (Monsanto process), iridium (Cativa process), cobalt (BASF process), and nickel.[169,170] All catalytic methanol carbonylation processes need iodine compounds as vital co-catalysts. The reaction proceeds *via* methyl iodide, which alkylates the respective transition metal complex concerned. Acetic acid is an important industrial chemical commodity, with a world demand of about 6 million tons per annum (2003).[171]

The commercial Monsanto process for the production of acetic acid is based on a rhodium catalyst and it operates at 30-60 bar pressure and at 150-200 °C. This homogeneous catalytic cycle gives selectivity of over 99 % based on methanol and it includes oxidative addition, migratory insertion and reductive elimination steps.[172,173] The active catalytic species is the anion *cis*-$[Rh(CO)_2I_2]^-$ (**1**), and interaction thereof with the substrate CH_3I results in the formation of the hexa-coordinated Rh^{III} complex $[(CH_3)Rh(CO)_2I_3]^-$ (**2**) (Scheme 2.5).[172] This complex (**2**) is kinetically unstable and undergoes a migratory insertion of a CO into the $Rh-CH_3$ bond forming the isomeric penta-coordinated acetyl complex $[(CH_3CO)Rh(CO)I_3]^-$ (**3**) as a result of the migration of the methyl group to the CO ligand.[174,175] The penta-coordinated rhodium acetyl anion (**3**) reacts rapidly with CO to form the six coordinated dicarbonyl complex (**4**) with a terminal CO (*mer* isomer).[176,177] The subsequent reductive elimination of CH_3COI was proposed to be facilitated by a *fac* isomerization, the *fac* isomer decomposes at room temperature to yield acetyl iodide CH_3COI and $[Rh(CO)_2I_2]^-$, the latter species initiating the next catalytic cycle.[177] Finally, acetic acid is formed by acetyl iodide hydrolysis.

[169] R. T. Eby, T. C. Singleton, Applied Industrial Catalysts, B. E. Leach (Ed.), Academic Press, **1983**, *1*, 275.
[170] N. von Kutepow, W. Himmele, H. Hohenschutz, *Chem. Ing. Technol*., **1965**, *37*, 297.
[171] M. J. Howard, M. D. Jones, M. S. Roberts, S. A. Taylor, *Catal. Today*, **1993**, *18*, 325.
[172] D. Forster, *J. Am. Chem. Soc*., **1976**, *98*, 846.
[173] B. C. Gates, Catalytic Chemistry, Wiley, New York, **1992**.
[174] A. Haynes, B. E. Mann, G. E. Morris, P. M. Maitlis, *J. Am. Chem. Soc*., **1993**, *115*, 4093.
[175] M. Bassetti, D. Monti, A. Haynes, J. M. Pearson, I. A. Stanbridge, P. M. Maitlis, *Gaz. Chim. Ital*., **1992**, *122*, 391.
[176] H. Adams, N. A. Bailey, B. E. Mann, C. P. Manuel, C. M. Spencer, A. G. Kent, *J. Chem. Soc. Dalton Trans*., **1988**, 489.
[177] L. A. Howe, E. E. Bunel, *Polyhedron*, **1995**, *14*, 167.
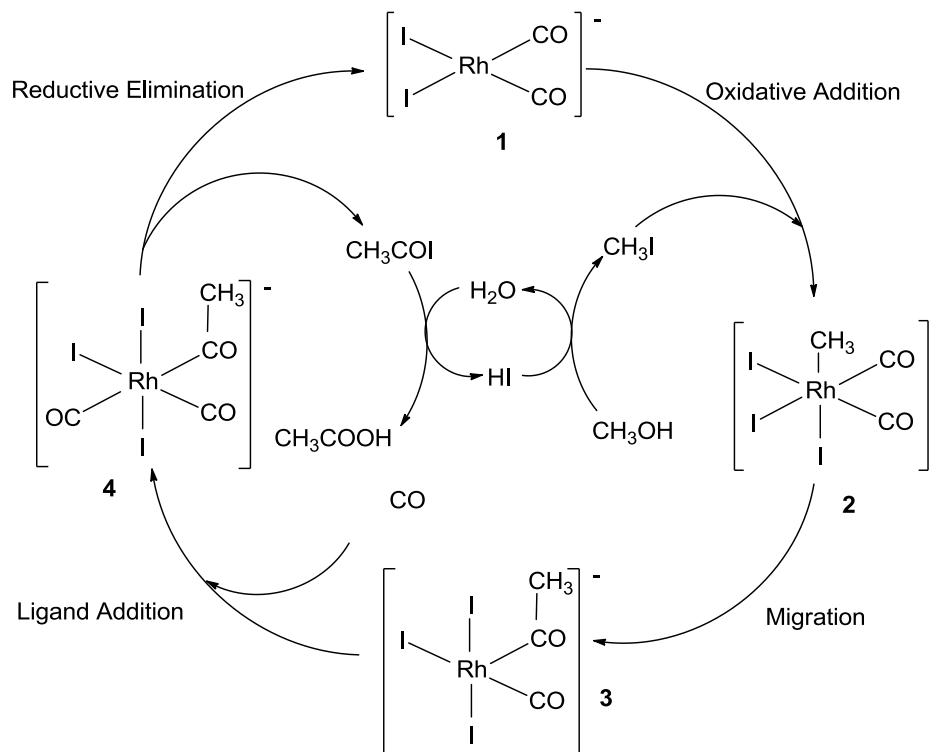
Scheme 2.5: A schemetic representation of the catalytic cycle of the rhodium-catalyzed methanol carbonylation.[178]

The rate of methanol carbonylation depends on both the rhodium complex and methyl iodide concentrations.[179] The reaction rate is independent of the methanol concentration and the carbon monoxide pressure. The iodomethane oxidative addition reaction is the rate-determining step of the catalytic cycle, and in an attempt to increase the rate of this step several modifications have been done to the conventional catalyst $[Rh(CO)_2I_2]^-$. This led to the development of $[Rh(Bid)(CO)(PR_3)]$ type complexes (Bid = different monocharged O,O'; N,O'; O,S' and N,S' donor atom bidentate chelators, PR_3 = different monodentate tertiary phosphine chelators) with more electron-donating ligands coordinated to the metal centre to increase the electron density on the Rh(I) centre, and to enhance the oxidative addition process.[180] In this study the catalyst design is similar with the bidentate ligand system being pyrones and pyridinones and the monodentate ligand being triphenylphosphine.

[178] C. M. Thomas, G. Süss-Fink, *Coord. Chem. Rev.*, **2003**, *243*, 125.
[179] J. F. Roth, J. H. Craddock, A. Hershman, F. E. Paulik, *Chem. Technol.*, **1971**, 600.
[180] A. Roodt, S. Otto, G. Steyl, *Coord. Chem. Rev.*, **2003**, *245*, 121.

2.10 Conclusion

There has been much advancement in the field of medicinal inorganic chemistry with specific focus revolving around the removal and introduction of metal ions in biological systems, and manoeuvring of metal ions within the biological system. Metal ions play a crucial role in the development and pathology of many medical conditions some of which can be treated by either pyrones or their corresponding analogues pyridinones. Additional applications of pyridinones not mentioned here include matrix metalloproteinases inhibitors (MPIs), organometallic Ru- and Os-arene complexes as anticancer agents and these compounds also have antimicrobial and antiviral properties.[181]

As far as beneficiation is concerned and from a chemical point of view, chemical properties can be exploited for separation purposes, this is evident from both hydrometallurgical and pyrometallurgical processes. However, these technologies need to be employed in a sustainable way to reduce or eliminate toxic byproducts which are normally generated by such processes and to increase the respective efficiencies of these processes. Some complex procedures from both hydrometallurgical and pyrometallurgical approaches need to be taken into account to develop advanced, cost effective and environmentally friendly approaches to separation. This makes the approach of pyrones and their derivatives as ligand systems for separation very relevant, as pyrones are naturally occurring and non-toxic compounds.

Radiometals enable a wide variety of structural and functional diversity due to their diverse nuclear properties. An increased application of these radiopharmaceuticals is inevitable with growing utilization of both diagnostic and therapeutic applications. Due to a large variability of diseases in patients which leads to personalized patient diagnosis and therapy, the need for highly selective drugs will increase which necessitates research and development in this field. With regards to homogeneous catalytic applications, the need for efficient and environmentally friendly systems is always an imperative which makes this research relevant.

---

[181] M. A. Santos, S. M. Marques, S. Chaves, *Coord. Chem. Rev.*, **2012**, *256*, 240.

3 Synthesis and Spectroscopic Characterization

3.1 Introduction

The synthesis of 3-hydroxypiridinones from their corresponding pyrone precursors (maltol and ethyl maltol) by substituting the cyclic oxygen atom with primary amines is a fundamental part of this study. The variation in electronic and steric properties brought about due to this functionalization will allow the capacity to systematically explore the different domains which constitute the focus of this study (beneficiation, modelling of theranostic drugs and homogeneous catalysis). One of the primary objectives of this study was characterization of these compounds using spectroscopic techniques and X-ray diffraction, which would not be successful without successful synthesis. However UV/Vis characterization was only done for complexes employed in the kinetic substitution studies with different monodentate ligands to identify appropriate wavelengths of maximum absorption to monitor reactions. This was also for practicality purposes as approximately 72 possible compounds were attempted in this study. Additionally, due to solubility issues not all the compounds are characterized by NMR spectroscopy or have ^{13}C NMR spectra reported. In some cases the proton peaks are overlapped by significantly larger solvent peaks depending on the respective deuterated solvent used. The two ligand systems that were investigated which are comprised of a total of eight chelators for coordination to zirconium(V), hafnium(V), rhenium(I) and rhodium(I) are illustrated in Scheme 3.1 with the detailed synthesis of the respective complexes given in Sections 3.4 – 3.8.
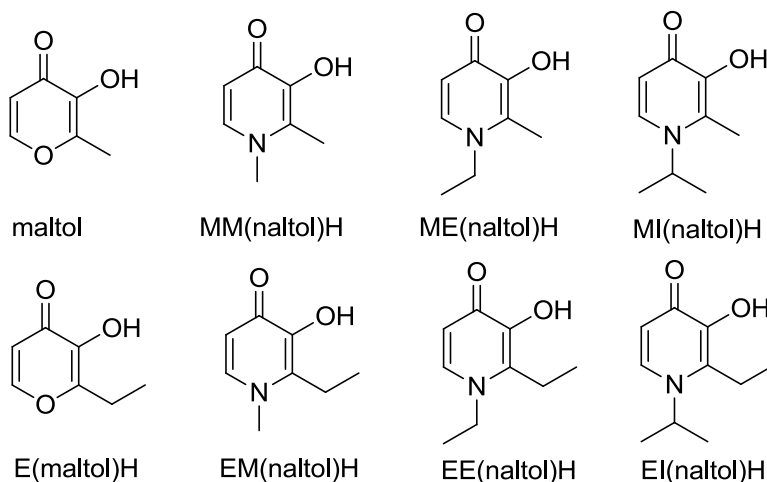
Scheme 3.1: A schematic representation of the two pyrone ligands and their respective *N*-derivatized pyridinone ligands employed in the synthesis of the respective complexes.

3.2 Chemical characterization and instrumentation

All reagents used for the synthesis and characterization were of analytical grade. Unless otherwise stated, all commercially available reagents were used as received from Sigma-Aldrich South Africa. All solvents were analytical grade and along with the reagents were used without further purification. All infrared spectra of the synthesized compounds were recorded as neat samples on a Bruker Digilab FTS 2000 Fourier transform spectrometer (ATR) using a He-Ne laser at 632.6 nm, in the range of 3000 to 600 cm^{-1}. The ^{1}H and ^{13}C NMR spectra were recorded on a Bruker 300 MHz nuclear magnetic resonance spectrometer unless otherwise stated. Different deuterated solvents were used and are indicated in each case. Chemical shifts (δ) are reported in ppm and given relative to tetramethylsilane (TMS) and coupling constants (*J*) are reported in Hz.

3.3 Synthesis of 3-hydroxy-4-pyridones derivatives

R' = Methyl/ Ethyl
R" = Methyl/ Ethyl/ *iso*-Propyl
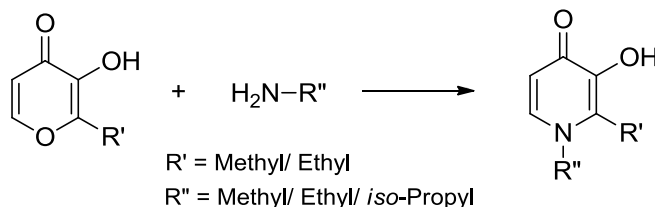
Scheme 3.2: A schematic representation of the synthetic procedure of the 3-hyroxypyridinone bidentate ligands.

3.3.1 3-Hydroxy-1,2-dimethyl-4-pyridone (MM(naltol)H)

3-Hydroxy-1,2-dimethyl-4-pyridone was prepared by refluxing 3-hydroxy-2-methyl-pyran-4-one (methyl maltol) (5.00 g, 39.65 mmol) with 3 equivalents of 40 % aqueous methylamine (4.10 ml, 119.00 mmol) in 100 ml of water overnight. The mixture turned dark brown. Decolourizing charcoal was added and the mixture was left to stand for 30 min. The mixture was filtered and the dark brown filtrate was evaporated *in vacuo* to yield a dark brown solid. Precipitation from cold acetone gave a white crystalline precipitate of 3-hydroxy-1,2-dimethyl-4-pyridone.

Yield: 3.50 g, 25.15 mmol, 63.4 %. IR (ATR) $v_{C=O}$ (cm^{-1}): 1567, 1631. ^{1}H NMR (300 MHz, DMSO) δ: 7.55 (d, $J = 7.2$ Hz, 1H), 6.07 (d, $J = 7.2$ Hz, 1H), 3.62 (s, 3H), 2.25 (s, 3H).

3.3.2 1-Ethyl-3-hydroxy-2-methyl-4-pyridone (ME(naltol)H)

1-Ethyl-3-hydroxy-2-methyl-4-pyridone was prepared by refluxing 3-hydroxy-2-methyl-pyran-4-one (methyl maltol) (10.03 g, 79.54 mmol) with 3 equivalents of 70 % aqueous ethylamine (12.64 ml, 240 mmol) in 200 ml of water overnight. The mixture turned dark brown. Decolourizing charcoal was added and the mixture was left to stand for 30 min. It was then filtered and the dark brown filtrate was evaporated *in vacuo* to yield a dark brown solid. After washing with acetone a brown precipitate of 1-ethyl-3-hydroxy-2-methyl-4-pyridone was obtained.

Yield: 8.01 g, 65.7 mmol, 79.7%. IR (ATR) $v_{C=O}$ (cm^{-1}): 1565, 1625. ^{1}H NMR (300 MHz, DMSO) δ: 7.58 (d, $J = 7.3$ Hz, 1H), 6.12 (d, $J = 7.3$ Hz, 1H), 3.96 (q, $J = 7.2$ Hz, 2H), 2.29 (s,

3H), 1.25 (t, J = 7.2 Hz, 3H). ^{13}C NMR (300 MHz, DMSO) δ: 169.27, 145.98, 137.42, 128.92, 111.37, 48.33, 16.46, 11.61.

3.3.3   3-Hydroxy-2-methyl-1-isopropyl-4-pyridone (MI(naltol)H)

3-Hydroxy-2-methyl-1-isopropyl-4-pyridinone was prepared by refluxing 3-hydroxy-2-methyl-pyran-4-one (methyl maltol) (5.01 g, 39.73 mmol) with 3.3 equivalents of aqueous isopropylamine (14.06 ml, 130.8 mmol, 99.0 %) in 100 ml of water overnight. The mixture turned dark brown. Decolourizing charcoal was added and the mixture was left to stand for 30 min. This was then filtered and the dark brown filtrate was evaporated *in vacuo* to yield a dark brown solid. Precipitation from cold acetone gave a pink precipitate of 3-hydroxy-2-methyl-1-isopropyl-4-pyridinone.

Yield: 4.10 g, 24.37 mmol, 61.3 %. IR (ATR) v $_{C=O}$ (cm^{-1}): 1568, 1624. ^{1}H NMR (300 MHz, DMSO) δ: 7.68 (d, J = 7.5 Hz, 1H), 6.17 (d, J = 7.5 Hz, 1H), 4.49 (dt, J = 13.3, 6.6 Hz, 1H), 1.35 (d, J = 6.6 Hz, 6H). ^{13}C NMR (300 MHz, DMSO) δ: 169.05, 145.61, 133.12, 128.97, 111.47, 51.72, 39.11, 22.76, 11.71.

3.3.4   2-Ethyl-3-hydroxy-1-methyl-4-pyridone (EM(naltol)H)

2-Ethyl-3-hydroxy-1-methyl-4-pyridone was prepared by refluxing 2-ethyl-3-hydroxy-pyran-4-one (ethyl maltol) (5.01 g, 35.75 mmol) with 3.3 equivalents of 40 % aqueous methylamine (18.29 ml, 117.70 mmol) in 100 ml of water overnight. The mixture turned dark brown. Decolourizing charcoal was added and the mixture was left to stand for 30 min. This was then filtered and the dark brown filtrate was evaporated *in vacuo* to yield a dark brown solid. After washing with cold acetone, a white crystalline precipitate of 2-ethyl-3-hydroxy-1-methyl-4-pyridone was obtained.

Yield: 3.92 g, 25.59 mmol, 71.6 %. IR (ATR) v $_{C=O}$ (cm^{-1}): 1569, 1624. ^{1}H NMR (300 MHz, DMSO) δ: 7.53 (d, J = 7.1 Hz, 1H), 6.09 (d, J = 7.2 Hz, 1H), 3.67 (s, 3H), 2.70 (dd, J = 14.5, 7.1 Hz, 2H), 1.11 (t, J = 7.3 Hz, 3H). ^{13}C NMR (300 MHz, DMSO) δ: 169.59, 145.62, 138.71, 135.03, 111.08, 40.85, 19.30, 12.53.

3.3.5   1,2-Diethyl-3-hydroxy-4-pyridone (EE(naltol)H)

1,2-Diethyl-3-hydroxy-4-pyridone was prepared by refluxing 2-ethyl-3-hydroxy-pyran-4-one (ethyl maltol) (5.00 g, 35.68 mmol) with 3.3 equivalents of 40 % aqueous methylamine (6.18 ml, 117.50 mmol) in 100 ml of water overnight. The mixture turned dark brown. Decolourizing charcoal was added and the mixture was left to stand for 30 min. This was then filtered and the dark brown filtrate was evaporated *in vacuo* to yield a dark brown solid. After washing with cold acetone, a white crystalline precipitate of 1,2-diethyl-3-hydroxy-4-pyridone was obtained.

Yield: 4.80 g, 28.70 mmol, 80.5 %. IR (ATR) $v_{C=O}$ (cm^{-1}): 1574, 1618. ^{1}H NMR (300 MHz, DMSO) δ: 7.58 (d, J = 7.3 Hz, 1H), 6.14 (d, J = 7.3 Hz, 1H), 3.95 (q, J = 7.1 Hz, 2H), 2.68 (q, J = 7.4 Hz, 2H), 1.26 (t, J = 7.1 Hz, 3H), 1.12 (t, J = 7.4 Hz, 3H). ^{13}C NMR (300 MHz, DMSO) δ: 169.51, 145.68, 137.48, 134.17, 111.69, 47.85, 18.98, 17.20, 13.20.

3.3.6   2-Ethyl-3-hydroxy-1-isopropyl-4-pyridone (EI(naltol)H)

2-Ethyl-3-hydroxy-1-isopropyl-4-pyridinone was prepared by refluxing 2-ethyl-3-hydroxypyran-4-one (ethyl maltol) (5.02 g, 35.82 mmol) with 6 equivalents of aqueous isopropylamine (12.65 ml, 214.10 mmol, 99 %) in 100 ml of water overnight. The mixture turned dark brown. Decolourizing charcoal was added and the mixture was left to stand for 30 min. This was then filtered and the dark brown filtrate was evaporated *in vacuo* to yield a dark brown solid. Crystallization from cold acetone gave pink crystals of 2-ethyl-3-hydroxy-1-isopropyl-4-pyridinone.

Yield: 2.5 g, 13.79 mmol, 38.5 %. IR (ATR) $v_{C=O}$ (cm^{-1}): 1571, 1619. ^{1}H NMR (300 MHz, DMSO) δ: 7.70 (d, J = 7.5 Hz, 1H), 6.18 (d, J = 7.5 Hz, 1H), 4.56 – 4.38 (m, 1H), 2.77 (q, J = 7.5 Hz, 2H), 1.37 (d, J = 6.6 Hz, 6H), 1.11 (t, J = 7.5 Hz, 3H). ^{13}C NMR (300 MHz, DMSO) δ: 169.23, 145.17, 134.32, 133.40, 111.91, 51.34, 23.09, 18.65, 13.38.

3.4 Attempted synthesis of *tetrakis*(pyronato)- and *tetrakis*(pyridinonato)- zirconium(V) complexes

In this section the attempted synthesis of *tetrakis*(O,O'-bid)zirconium(IV) complexes are reported by reacting four equivalents of the respective chelator in each case with one equivalent of ZrCl$_4$ (Scheme 3.3). However elemental analysis results were not yet available at the time of thesis submission and only one hafnium crystal structure was obtained (Chapter 4) which potentially indicates that all the hafnium complexes are chlorido-*tris*(O,O'-bid)hafnium(IV). Due to similarities in chemistry between Zr and Hf it is highly probable that the zirconium complexes are also chlorido-*tris*(O,O'-bid)zirconium(IV), for this reason, due to the lack of zirconium crystal structures and the lack of elemental analysis data, this work is presented as an attempted synthesis despite the reported NMR data which basically confirm the respective structures.
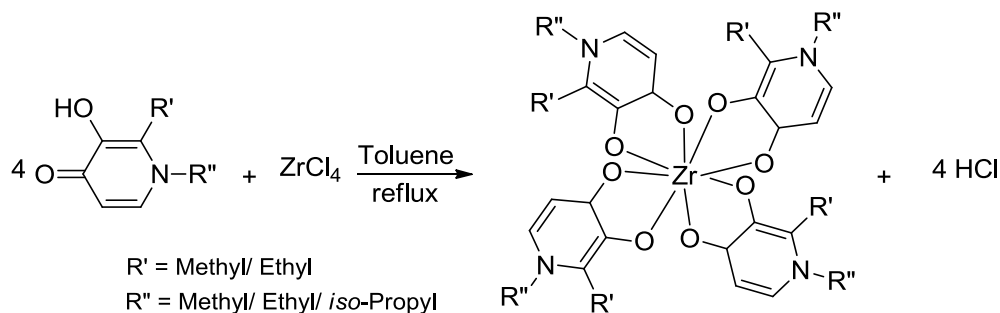
Scheme 3.3: A schematic representation of the synthesized zirconium complexes.

3.4.1 [Zr(maltol)$_4$]

Commercially available 3-hydroxy-2-methyl-pyran-4-one (2.165 g, 17.17 mmol) was added to a suspension of ZrCl$_4$ (1 g, 4.29 mmol) in toluene (150 ml). The mixture was refluxed overnight; the crude product was filtered and dried.

Yield: 2.2 g, 3.72 mmol, 86.7 %. ^{1}H NMR (300 MHz, DMSO) δ: 8.01 (d, J = 5.5 Hz, 1H), 6.33 (d, J = 5.5 Hz, 1H), 2.23 (s, 3H). ^{13}C NMR (300 MHz, DMSO) δ: 172.98, 155.08, 149.68, 143.46, 114.00, 14.40.

3.4.2 [Zr(MM(naltol))₄]

3-Hydroxy-1,2-dimethyl-4-pyridone (2.39 g, 17.17 mmol) was added to a suspension of $ZrCl_4$ (1 g, 4.29 mmol) in toluene (150 ml). The mixture was refluxed overnight; the crude product was filtered and dried.

Yield: 2.019 g, 3.14 mmol, 73.1 %. ^{1}H NMR (300 MHz, DMSO) δ: 8.18 (d, 1H), 7.21 (d, 1H), 3.95 (s, 3H), 2.47 (s, 3H). ^{13}C NMR (300 MHz, DMSO) δ: 158.92, 142.70, 138.58, 137.71, 129.35, 128.67, 125.73, 110.44, 12.98.

3.4.3 [Zr(ME(naltol))₄]

1-Ethyl-3-hydroxy-2-methyl-4-pyridone (2.64 g, 17.23 mmol) was added to a suspension of $ZrCl_4$ (1 g, 4.29 mmol) in toluene (150 ml). The mixture was refluxed overnight; the crude product was filtered and dried.

Yield: 1.840 g, 2.63 mmol, 61.3 %. ^{1}H NMR (300 MHz, DMSO) δ: 8.12 (d, J = 3.5 Hz, 1H), 7.16 (d, J = 9.6 Hz, 1H), 4.00 (s, 3H), 2.84 (q, 2H), 1.09 (t, 3H). ^{13}C NMR (300 MHz, DMSO) δ: 158.69, 156.73, 143.30, 141.89, 137.80, 129.36, 128.67, 125.78, 111.33, 108.37, 15.98, 12.65, 11.95.

3.4.4 [Zr(MI(naltol))₄]

3-Hydroxy-2-methyl-1-isopropyl-4-pyridone (3.00 g, 17.83 mmol) was added to a suspension of $ZrCl_4$ (1 g, 4.29 mmol) in toluene (150 ml). The mixture was refluxed overnight; the crude product was filtered and dried.

Yield: 2.30 g, 3.03 mmol, 70.5 %. ^{1}H NMR (300 MHz, D₂O) δ: 7.90 (d, J = 4.9 Hz, 1H), 6.83 (d, J = 2.7 Hz, 1H), 2.42 (s, 3H), 1.37 (d, J = 6.5 Hz, 6H).

3.4.5   [Zr(E(maltol))₄]

2-ethyl-3-hydroxy-pyran-4-one (2.41 g, 17.20 mmol) was added to a suspension of ZrCl₄ (1 g, 4.29 mmol) in toluene (150 ml). The mixture was refluxed overnight; the crude product was filtered and dried. Yield: 2.46 g, 3.80 mmol, 88.5 %. This compound was insoluble in many solvents and NMR characterization was not obtained.

3.4.6   [Zr(EM(naltol))₄]

2-Ethyl-3-hydroxy-1-methyl-4-pyridone (2.64 g, 17.23 mmol) was added to a suspension of ZrCl₄ (1 g, 4.29 mmol) in toluene (150 ml). The mixture was refluxed overnight; the crude product was filtered and dried.

Yield: 2.95 g, 4.21 mmol, 98.2 %. ^{1}H NMR (300 MHz, DMSO) δ: 8.12 (d, $J = 3.5$ Hz, 1H), 7.16 (d, $J = 9.6$ Hz, 1H), 4.00 (s, 3H), 2.84 (q, 2H), 1.09 (s, 3H). ^{13}C NMR (300 MHz, DMSO) δ: 139.49 – 138.72, 138.18, 129.33, 128.64, 125.75, 110.48, 19.86, 11.90.

3.4.7   [Zr(EE(naltol))₄]

1,2-Diethyl-3-hydroxy-4-pyridone (2.88 g, 17.22 mmol) was added to a suspension of ZrCl₄ (1 g, 4.29 mmol) in toluene (150 ml). The mixture was refluxed overnight; the crude product was filtered and dried.

Yield: 3.0 g, 3.97 mmol, 92.5 %. ^{1}H NMR (300 MHz, DMSO) δ: 8.13 (d, $J = 0.5$ Hz, 1H), 6.92 (d, 1H), 4.32 (q, $J = 5.7$ Hz, 2H), 2.86 (q, $J = 5.5$ Hz, 2H), 1.41 (t, $J = 6.8$ Hz, 3H), 1.13 (t, $J = 6.6$ Hz, 3H). ^{13}C NMR (300 MHz, DMSO) δ: 137.76, 136.47, 129.32, 128.64, 125.74, 110.03, 19.44, 17.20, 12.75.

3.4.8   [Zr(EI(naltol))₄]

2-Ethyl-3-hydroxy-1-isopropyl-4-pyridone (3.12 g, 17.21 mmol) was added to a suspension of ZrCl₄ (1 g, 4.29 mmol) in toluene (150 ml). The mixture was refluxed overnight; the crude product was filtered and dried.

Yield: 3.2 g, 3.94 mmol, 91.8 %. ^{1}H NMR (300 MHz, DMSO) δ: 8.44 (d, J = 12.2 Hz, 1H), 7.17 (d, J = 1.8 Hz, 1H), 4.85 (m, J = 1.5 Hz, 1H), 2.96 (q, 2H), 1.47 (d, 6H), 1.23 – 0.93 (t, 3H). ^{13}C NMR (300 MHz, DMSO) δ: 137.74, 134.61, 129.31, 128.62, 125.73, 111.77, 23.26, 19.35, 12.92.

3.5   Attempted synthesis of *tetrakis*(pyronato)- and *tetrakis*(pyridinonato)- hafnium(V) complexes

In this section the attempted synthesis of *tetrakis*(O,O'-bid)hafnium(IV) complexes are reported by reacting four equivalents of the respective chelator in each case with one equivalent of HfCl₄ (Scheme 3.4). However elemental analysis results were not yet available at the time of thesis submission and only one hafnium crystal structure was obtained (Chapter 4) which potentially indicates that all the hafnium complexes are chlorido-*tris*(O,O'-bid)hafnium(IV). Due to the lack of more hafnium crystal structures and the lack of elemental analysis data, this work is presented as an attempted synthesis despite the reported NMR data which basically confirm the respective structures.
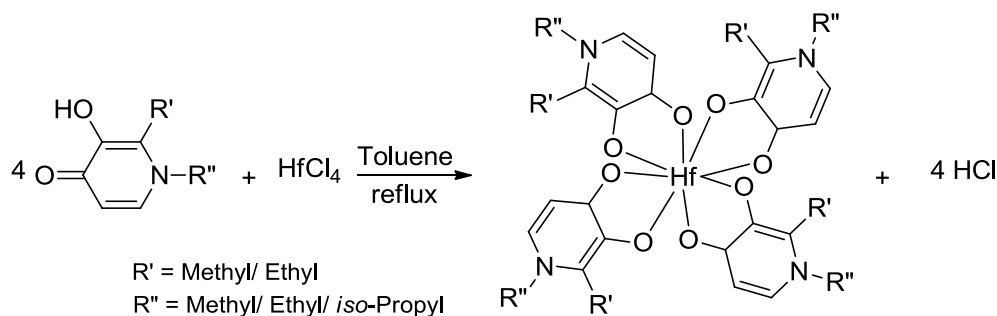
Scheme 3.4: A schematic representation of the synthesized hafnium complexes.

3.5.1 [Hf(maltol)$_4$]

3-hydroxy-2-methyl-pyran-4-one (1.575 g, 12.49 mmol) was added to a suspension of HfCl$_4$ (1 g, 3.12 mmol) in toluene (150 ml). The mixture was refluxed overnight; the crude product was filtered and dried.

Yield: 1.85 g, 2.73 mmol, 87.3 %. This compound was insoluble in many solvents and NMR characterization was not obtained.

3.5.2 [Hf(MM(naltol))$_4$]

3-Hydroxy-1,2-dimethyl-4-pyridone (1.74 g, 12.50 mmol) was added to a suspension of HfCl$_4$ (1 g, 3.12 mmol) in toluene (150 ml). The mixture was refluxed overnight; the crude product was filtered and dried.

Yield: 1.92 g, 2.63 mmol, 84.2 %. ^{1}H NMR (300 MHz, D$_2$O) δ: 7.68 (d, J = 5.3 Hz, 1H), 6.65 (d, 1H), 3.78 (s, 3H), 2.32 (s, 3H). ^{13}C NMR (300 MHz, DMSO) δ: 171.25, 158.82, 156.23, 155.81, 142.96, 138.73, 137.82, 137.05, 134.44, 129.34, 128.66, 110.56, 108.89, 12.98.

3.5.3 [Hf(ME(naltol))$_4$]

1-Ethyl-3-hydroxy-2-methyl-4-pyridone (1.91 g, 12.47 mmol) was added to a suspension of HfCl$_4$ (1 g, 3.12 mmol) in toluene (150 ml). The mixture was refluxed overnight; the crude product was filtered and dried.

Yield: 2.09 g, 2.65 mmol, 85 %. ^{1}H NMR (300 MHz, DMSO) δ: 8.50 − 7.82 (m, 1H), 7.31 (m, 1H), 4.31 (q, 2H), 1.34 (s, 3H). ^{13}C NMR (300 MHz, DMSO) δ: 158.71, 156.67, 143.27, 141.86, 137.77, 129.32, 128.64, 125.75, 111.05, 109.12, 16.15, 11.89.

3.5.4   [Hf(MI(naltol))$_4$]

3-Hydroxy-2-methyl-1-isopropyl-4-pyridone (2.10 g, 12.48 mmol) was added to a suspension of HfCl$_4$ (1 g, 3.12 mmol) in toluene (150 ml). The mixture was refluxed overnight; the crude product was filtered and dried.

Yield: 2.19 g, 2.58 mmol, 82.8 %. ^{1}H NMR (300 MHz, D$_2$O) δ: 7.86 (d, J = 5.4 Hz, 1H), 6.77 (d, J = 1.3 Hz, 1H), 2.40 (s, 3H), 1.35 (d, J = 6.5 Hz, 6H). ^{13}C NMR (300 MHz, D$_2$O) δ: 178.59, 156.72, 155.73, 132.81, 110.69, 55.43, 21.80, 13.97, 11.46.

3.5.5   [Hf(E(maltol))$_4$]

2-Ethyl-3-hydroxy-pyran-4-one (1.75 g, 12.49 mmol) was added to a suspension of HfCl$_4$ (1 g, 3.12 mmol) in toluene (150 ml). The mixture was refluxed overnight; the crude product was filtered and dried.

Yield: 1.92 g, 2.61 mmol, 83.7 %. ^{1}H NMR (300 MHz, CDCl$_3$) δ: 7.85 (d, J = 1.9 Hz, 1H), 6.62 (d, J = 2.6 Hz, 1H), 2.84 (q, J = 7.3 Hz, 2H), 1.15 (t, J = 8.5 Hz, 3H).

3.5.6   [Hf(EM(naltol))$_4$]

2-Ethyl-3-hydroxy-1-methyl-4-pyridone (1.91 g, 12.47 mmol) was added to a suspension of HfCl$_4$ (1 g, 3.12 mmol) in toluene (150 ml). The mixture was refluxed overnight; the crude product was filtered and dried.

Yield: 2.03 g, 2.58 mmol, 82.5 %. ^{1}H NMR (300 MHz, D$_2$O) δ: 7.70 (d, J = 2.3 Hz, 1H), 6.74 (d, J = 3.8 Hz, 1H), 3.86 (s, 3H), 2.78 (q, J = 6.4 Hz, 2H), 0.98 (t, 3H). ^{13}C NMR (300 MHz, DMSO) δ: 171.56, 159.27, 156.19, 146.81, 143.02, 139.17, 137.79, 129.34, 128.65, 125.76, 110.89, 108.76, 20.10, 11.65.

3.5.7 [Hf(EE(naltol))$_4$]

1,2-Diethyl-3-hydroxy-4-pyridone (2.09 g, 12.50 mmol) was added to a suspension of HfCl$_4$ (1 g, 3.12 mmol) in toluene (150 ml). The mixture was refluxed overnight; the crude product was filtered and dried.

Yield: 1.98 g, 2.98 mmol, 95.5 %. ^{1}H NMR (300 MHz, D$_2$O) δ: 7.47 (d, J = 3.8 Hz, 1H), 6.51 (d, J = 6.3 Hz, 1H), 3.81 (dd, J = 13.7, 6.6 Hz, 2H), 2.41 (dd, J = 14.1, 6.7 Hz, 2H), 0.95 (t, J = 7.2 Hz, 3H), 0.63 (t, J = 6.0 Hz, 3H). ^{13}C NMR (300 MHz, D$_2$O) δ: 136.94, 128.58, 128.01, 110.61, 50.92, 19.20, 17.09 – 15.73, 15.73 – 15.53, 11.24.

3.5.8 [Hf(EI(naltol))$_4$]

2-Ethyl-3-hydroxy-1-isopropyl-4-pyridone (2.26 g, 12.47 mmol) was added to a suspension of HfCl$_4$ (1 g, 3.12 mmol) in toluene (150 ml). The mixture was refluxed overnight; the crude product was filtered and dried.

Yield: 2.58 g, 2.87 mmol, 91.8 %. ^{1}H NMR (300 MHz, D$_2$O) δ: 7.87 (d, J = 1.3 Hz, 1H), 6.86 (d, J = 4.8 Hz, 1H), 2.83 (q, J = 6.3 Hz, 2H), 1.34 (d, J = 6.4 Hz, 6H), 0.96 (t, 3H). ^{13}C NMR (300 MHz, D$_2$O) δ: 164.57, 153.87, 143.61, 134.92 – 131.15, 128.26, 127.71, 110.59, 56.70 – 52.35, 22.31, 18.66, 11.70.

3.6 Synthesis of *fac*-[NEt$_4$]$_2$[Re(CO)$_3$(Br)$_3$] (ReAA)

The starting synthon *fac*-[NEt$_4$]$_2$[Re(CO)$_3$(Br)$_3$] which will now be referred to as ReAA was prepared under strict Schlenk conditions for maximum yields.

$$[Re(CO)_5(Br)] \quad + \quad 2(NEt_4)Br \quad \longrightarrow \quad fac\text{-}[NEt_4]_2[Re(CO)_3(Br)_3] \quad + \quad 2CO$$
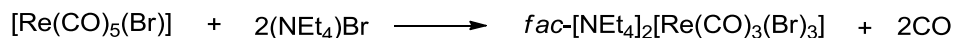
The (NEt$_4$)Br (5.25 g, 0.025 mol) was grounded to a powder and dried. 2,5,8-Trioxanone diglyme (150 ml) was added to the (NEt$_4$)Br under dry nitrogen and slurried on an oil bath at 180 °C for 30 minutes. During this time, the system was evacuated and purged with N$_2$ several times. The solid Re(CO)$_5$Br (5 g, 0.0123 mol) was added to the mixture and stirred for 15 hours at 115

°C. The whole system needs good stirring and ventilation because of the continuous evolution of CO gas. The reaction mixture was cooled to room temperature, filtered and dried. The colourless solid was stirred in a small amount of cold ethanol for 5 minutes, filtered, washed with cold DCM and dried. Yield: 8.78 g, 11.4 mmol, 91 %. IR (ATR) $v_{C≡O}$ (cm^{-1}): 1996, 1847.
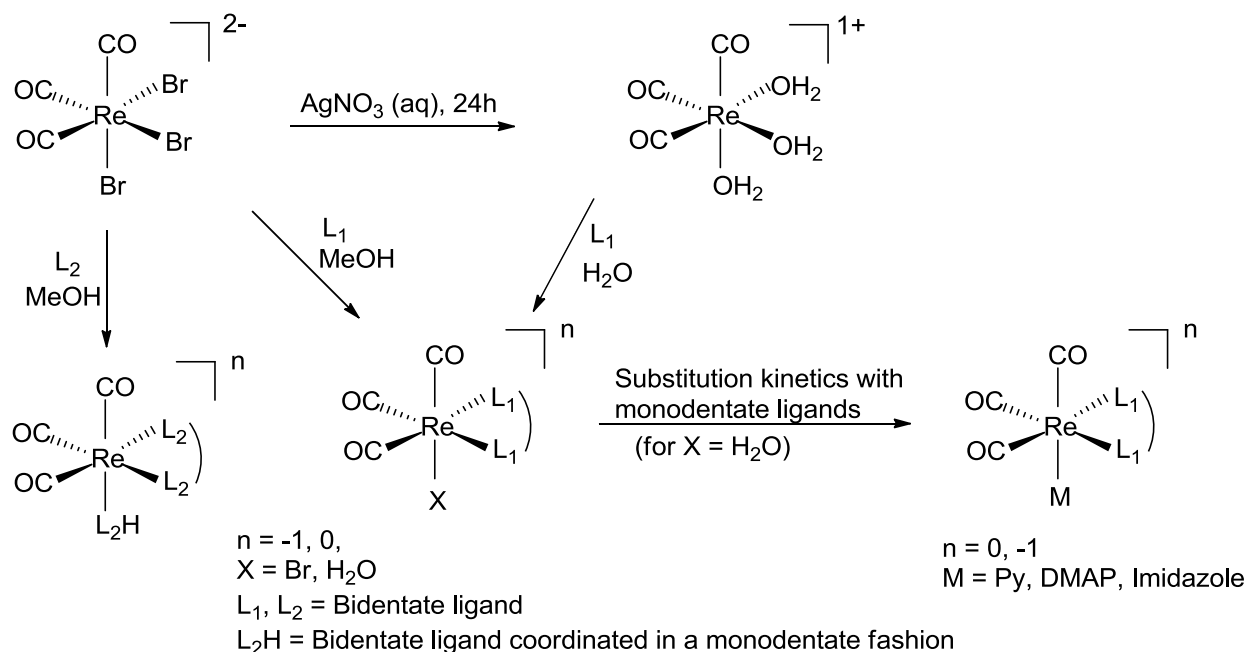
Scheme 3.5: A schematic representation of the synthesized rhenium complexes also illustrating the [2+1] approach.

In the [2+1] mixed ligand approach for fac-[Re(CO)$_3$(H$_2$O)$_3$]$^+$ or fac-[Re(CO)$_3$Br$_3$]$^{2-}$ complexes, the three aqua/ bromide ligands are substituted by one bidentate ligand and one monodentate ligand. The biomolecule can be attached either on the bidentate ligand ([2B+1] approach) or on the monodentate ligand ([2+1B] approach). Direct substitution of the two bromido ligands in fac-[Re(CO)$_3$Br$_3$]$^{2-}$ occurs at room temperature by a bidentate ligand in methanol as solvent. The corresponding aqua synthon (fac-[Re(CO)$_3$(H$_2$O)$_3$]$^+$) is obtained from fac-[Re(CO)$_3$Br$_3$]$^{2-}$ by removing the bromido ligands with silver nitrate in an acidic aqueous medium from the aqua complex, the bidentate ligand is added in water as solvent and coordinates in a bidentate fashion with H$_2$O still in the sixth position. However for five of the ligands L$_2$ (*i.e.* MM(naltol)H, EM(naltol)H, ME(naltol)H, EE(naltol)H and MI(naltol)H) in the bromido synthesis (attempted complex: fac-[Re(O,O'-bid)(CO)$_3$Br]), all three bromides were substituted by the bidentate

48

ligand L_2, coordinating in two different modes (see Scheme 3.5). Substitution kinetics were then evaluated on one of these types of complexes (*fac*-[Re(EM(naltol))(CO)$_3$(EM(naltol)H)]) and the corresponding aqua complex (*fac*-[Re(EM(naltol))(CO)$_3$(H$_2$O)]) to evaluate the reactivity, the reaction mechanism, the thermodynamic parameters and the rate constants by using monodentate pyridine-type ligands as entering ligands.

3.6.1 *fac*-[NEt$_4$]$_2$[Re(maltol)(CO)$_3$(Br)]

ReAA (1.00 g, 1.30 mmol) was dissolved in 150 ml MeOH. 3-hydroxy-2-methyl-pyran-4-one (0.17 g, 1.35 mmol) was added as a solid and the mixture was stirred at room temperature for 24 hours. The reaction mixture was dried *in vacuo*. A white precipitate was obtained.

Yield: 0.75 g, 1.02 mmol, 78.3 %. IR (ATR) v $_{C=O}$ (cm^{-1}): 1847, 1996. ^{1}H NMR (300 MHz, CDCl$_3$) δ: 7.64 (d, J = 5.5 Hz, 1H), 6.35 (d, J = 5.6 Hz, 1H), 3.36 (q, J = 7.0 Hz, 8H), 2.30 (s, 3H), 1.32 (t, J = 6.1 Hz, 12H). ^{13}C NMR (300 MHz, CDCl$_3$) δ: 172.62, 154.29, 148.76, 143.09, 112.89, 14.29, 8.08.

3.6.2 *fac*-[Re(MM(naltol))(MM(naltol)H)(CO)$_3$]

ReAA (1.00 g, 1.30 mmol) was dissolved in 150 ml MeOH. 3-Hydroxy-1,2-dimethyl-4-pyridone (0.37 g, 2.66 mmol) was added as a solid and the mixture was stirred at room temperature for 24 hours. The reaction mixture was dried *in vacuo*. A brown oil was obtained, colourless cuboidal crystals were grown from the acetone solution of the product.

Yield: 0.350 g, 0.64 mmol, 49.2 %. IR (ATR) v $_{C=O}$ (cm^{-1}): 1848, 1997. ^{1}H NMR (300 MHz, MeOD) δ: 8.19 (d, J = 6.9 Hz, 1H), 7.62 (d, J = 6.8 Hz, 1H), 7.12 (d, J = 6.9 Hz, 1H), 6.58 (d, J = 6.7 Hz, 1H), 4.10 (s, 3H), 3.91 (s, 3H), 2.63 (s, 3H), 2.51 (s, 3H). ^{13}C NMR (300 MHz, MeOD) δ: 198.21, 172.82, 158.16, 157.85, 143.35, 142.58, 138.51, 136.88, 136.59, 134.26, 134.18, 110.06, 109.70, 43.78, 42.09, 11.77, 11.00, 6.39.

3.6.3   *fac*-[Re(ME(naltol))(CO)$_3$(ME(naltol)H)]

ReAA (1.00 g, 1.30 mmol) was dissolved in 150 ml MeOH. 1-Ethyl-3-hydroxy-2-methyl-4-pyridone (0.40 g, 2.61 mmol) was added as a solid and the mixture was stirred at room temperature for 24 hours. The reaction mixture was dried *in vacuo*. A brown oil was obtained, colourless cuboidal crystals were grown from the acetone solution of the product.

Yield: 0.399 g, 0.69 mmol, 53.3 %. IR (ATR) v $_{C=O}$ (cm^{-1}): 1860, 1998. ^{1}H NMR (300 MHz, MeOD) δ: 8.16 (d, J = 6.7 Hz, 1H), 7.59 (d, J = 6.5 Hz, 1H), 7.08 (d, J = 6.8 Hz, 1H), 6.51 (d, J = 6.6 Hz, 1H), 4.37 (q, J = 7.3 Hz, 2H), 4.16 (dd, J = 14.1, 6.9 Hz, 2H), 2.56 (s, 3H), 2.42 (s, 3H), 1.41 (t, J = 7.2 Hz, 3H), 1.32 (t, J = 7.2 Hz, 3H). ^{13}C NMR (300 MHz, MeOD) δ: 198.35, 172.67, 158.25, 143.70, 141.44, 137.46, 110.54, 110.12, 52.13, 52.09, 52.05, 51.94, 50.06, 15.20, 14.98, 11.40, 10.71, 6.56.

3.6.4   *fac*-[Re(MI(naltol))(CO)$_3$(MI(naltol)H)]

ReAA (1.00 g, 1.30 mmol) was dissolved in 150 ml MeOH. 3-Hydroxy-2-methyl-1-isopropyl-4-pyridone (0.44 g, 2.62 mmol) was added as a solid and the mixture was stirred at room temperature for 24 hours. The reaction mixture was dried *in vacuo*. A white crystalline precipitate was obtained, colourless cuboidal crystals were grown from the acetone solution of the product.

Yield: 0.453 g, 0.75 mmol, 57.5 %. IR (ATR) v $_{C=O}$ (cm^{-1}): 1843, 1996. ^{1}H NMR (300 MHz, MeOD) δ: 8.36 (d, J = 7.2 Hz, 1H), 7.78 (d, J = 7.0 Hz, 1H), 7.25 (d, J = 7.1 Hz, 1H), 6.69 (d, J = 7.0 Hz, 1H), 5.11 − 5.00 (m, 1H), 3.59 (q, J = 7.3 Hz, 1H), 3.11 (dd, J = 14.6, 7.3 Hz, 1H), 2.72 (s, 3H), 2.58 (s, 3H), 1.60 (d, J = 6.6 Hz, 6H), 1.52 (d, J = 6.7 Hz, 6H). ^{13}C NMR (300 MHz, MeOD) δ: 198.57, 198.39, 172.53, 172.37, 157.82, 143.24, 141.61, 135.66, 133.75, 129.01, 110.88, 110.40, 56.46, 53.84, 21.79, 21.55, 11.34, 11.16, 10.72, 10.62.

3.6.5   *fac*-[NEt₄]₂[Re(E(maltol))(CO)₃(Br)]

ReAA (1.00 g, 1.30 mmol) was dissolved in 150 ml MeOH. 2-Ethyl-3-hydroxy-pyran-4-one (0.16 g, 1.30 mmol) was added as a solid and the mixture was stirred at room temperature for 24 hours. The reaction mixture was dried *in vacuo*. A white precipitate was obtained.

Yield: 0.783 g, 1.04 mmol, 80.3 %. IR (ATR) $v_{C=O}$ (cm⁻¹): 1847, 1996. ¹H NMR (300 MHz, CDCl₃) δ: 7.67 (d, *J* = 5.5 Hz, 1H), 6.35 (d, *J* = 5.5 Hz, 1H), 3.38 (q, *J* = 7.2 Hz, 8H), 2.69 (q, *J* = 7.6 Hz, 2H), 1.32 (q, *J* = 6.9 Hz, 12H), 1.19 (t, *J* = 7.6 Hz, 3H). ¹³C NMR (300 MHz, CDCl₃) δ: 173.18, 154.38, 153.15, 142.34, 112.81, 21.67, 10.82, 8.00.

3.6.6   *fac*-[Re(EM(naltol))(EM(naltol)H)(CO)₃]

ReAA (1.00 g, 1.30 mmol) was dissolved in 150 ml MeOH. 2-Ethyl-3-hydroxy-1-methyl-4-pyridone (0.40 g, 2.61 mmol) was added as a solid and the mixture was stirred at room temperature for 24 hours. The reaction mixture was dried *in vacuo*. A brown oil was obtained, colourless cuboidal crystals were grown from the acetone solution of the product.

Yield: 0.520 g, 0.90 mmol, 69.5 %. IR (ATR) $v_{C=O}$ (cm⁻¹): 1841, 1983, 2001. ¹H NMR (300 MHz, DMSO) δ: 7.91 (d, *J* = 7.0 Hz, 1H), 7.63 (d, *J* = 6.8 Hz, 1H), 6.62 (d, *J* = 6.9 Hz, 1H), 6.48 (d, *J* = 6.7 Hz, 1H), 3.88 (s, 3H), 3.24 (q, *J* = 7.2 Hz, 2H), 2.83 (dd, *J* = 15.1, 7.5 Hz, 2H), 2.09 (s, 3H). ¹³C NMR (300 MHz, DMSO) δ: 174.30, 169.41, 159.22, 145.49, 139.83, 138.77, 134.83, 134.39, 110.91, 109.70, 42.08, 31.15, 19.30, 19.15, 12.55, 12.52.

3.6.7   *fac*-[Re(EE(naltol))(EE(naltol)H)(CO)₃]

ReAA (1.00 g, 1.30 mmol) was dissolved in 150 ml MeOH. 1,2-Diethyl-3-hydroxy-4-pyridone (0.44 g, 2.63 mmol) was added as a solid and the mixture was stirred at room temperature for 24 hours. The reaction mixture was dried *in vacuo*. A white precipitate was obtained.

Yield: 0.396 g, 0.66 mmol, 50.5 %. IR (ATR) $v_{C=O}$ (cm⁻¹): 1843, 1867,1997. ¹H NMR (300 MHz, MeOD) δ: 8.23 (d, *J* = 7.0 Hz, 1H), 7.63 (d, *J* = 6.9 Hz, 1H), 7.16 (d, *J* = 7.0 Hz, 1H), 6.62

(d, J = 6.9 Hz, 1H), 4.47 (q, J = 7.3 Hz, 2H), 4.25 (q, J = 7.2 Hz, 2H), 3.58 (dd, J = 14.5, 7.2 Hz, 2H), 3.10 (q, J = 7.4 Hz, 2H), 1.13 – 1.07 (m, 6H).

3.6.8   *fac*-[NEt$_4$]$_2$[Re(El(naltol))(CO)$_3$(Br)]

ReAA (1.00 g, 1.30 mmol) was dissolved in 150 ml MeOH. 2-Ethyl-3-hydroxy-1-isopropyl-4-pyridone (0.24 g, 1.32 mmol) was added as a solid and the mixture was stirred at room temperature for 24 hours. The reaction mixture was dried *in vacuo*. A white crystalline precipitate was obtained, colourless cuboidal crystals were grown from the acetone solution of the product.

Yield: 0.358 g, 0.453 mmol, 34.8 %. IR (ATR) v $_{C=O}$ (cm^{-1}): 1882, 2004. ^{1}H NMR (300 MHz, DMSO) δ: 7.74 (d, J = 7.0 Hz, 1H), 6.55 (d, J = 7.0 Hz, 1H), 4.68 (m, J = 13.2, 6.6 Hz, 1H), 4.13 (dd, J = 9.5, 4.5 Hz, 8H), 3.08 – 2.75 (m, 12H), 1.43 (d, J = 6.6 Hz, 6H), 1.12 (t, J = 7.4 Hz, 3H).

3.6.9   *fac*-[Re(maltol)(CO)$_3$(H$_2$O)]

ReAA (1.00 g, 1.30 mmol) was dissolved in 80 ml water at pH 2.2 (adjusted with HNO$_3$). Silver nitrate (0.66 g, 3.89 mmol) was added and the mixture was stirred at room temperature for 24 hours. After the mixture was filtered, 3-hydroxy-2-methyl-pyran-4-one (0.16 g, 1.30 mmol) was added and then it was stirred at room temperature for 24 hours. A black mass which could not be purified was obtained. Unsuccessful.

3.6.10   *fac*-[Re(MM(naltol))(CO)$_3$(H$_2$O)]

ReAA (1.00 g, 1.30 mmol) was dissolved in 80 ml water at pH 2.2 (adjusted with HNO$_3$). Silver nitrate (0.66 g, 3.89 mmol) was added and the mixture was stirred at room temperature for 24 hours. After the mixture was filtered, 3-hydroxy-1,2-dimethyl-4-pyridone (0.18 g, 1.30 mmol) was added and then it was stirred at room temperature for 24 hours. A white precipitate was formed, filtered and dried at room temperature.

Yield: 0.218 g, 0.51 mmol, 39.3 %. IR (ATR) $v_{C=O}$ (cm^{-1}): 1870, 2014. ^{1}H NMR (300 MHz, DMSO) δ: 7.61 (d, 1H), 6.47 (d, J = 6.7 Hz, 1H), 3.80 (s, 3H), 2.37 (s, 3H). ^{13}C NMR (300 MHz, DMSO) δ: 207.06, 173.79, 159.25, 135.10, 134.20, 109.56, 42.67, 31.15.

3.6.11   *fac*-[Re(ME(naltol))(CO)$_3$(H$_2$O)]

ReAA (1.00 g, 1.30 mmol) was dissolved in 80 ml water at pH 2.2 (adjusted with HNO$_3$). Silver nitrate (0.66 g, 3.89 mmol) was added and the mixture was stirred at room temperature for 24 hours. After the mixture was filtered, 1-ethyl-3-hydroxy-2-methyl-4-pyridone (0.20 g, 1.30 mmol) was added and then it was stirred at room temperature for 24 hours. A white precipitate was formed, filtered and dried at room temperature.

Yield: 0.370 g, 0.84 mmol, 64.6 %. IR (ATR) $v_{C=O}$ (cm^{-1}): 1882, 2015. ^{1}H NMR (300 MHz, MeOD) δ: 7.61 (d, J = 6.9 Hz, 1H), 6.62 (d, J = 6.8 Hz, 1H), 4.23 (q, J = 7.2 Hz, 2H), 2.53 (s, 3H), 1.43 (t, J = 7.2 Hz, 3H). ^{13}C NMR (300 MHz, MeOD) δ: 173.05, 135.63, 133.10, 110.23, 49.91, 29.19, 14.82, 10.44.

3.6.12   *fac*-[Re(MI(naltol))(CO)$_3$(H$_2$O)]

ReAA (1.00 g, 1.30 mmol) was dissolved in 80 ml water at pH 2.2 (adjusted with HNO$_3$). Silver nitrate (0.66 g, 3.89 mmol) was added and the mixture was stirred at room temperature for 24 hours. After the mixture was filtered, 3-hydroxy-2-methyl-1-isopropyl-4-pyridone (0.22 g, 1.30 mmol) was added and then it was stirred at room temperature for 24 hours. A white precipitate was formed, filtered and dried at room temperature.

Yield: 0.305 g, 0.67 mmol, 51.5 %. IR (ATR) $v_{C=O}$ (cm^{-1}): 1882, 2015. ^{1}H NMR (300 MHz, MeOD) δ: 7.73 (d, J = 7.1 Hz, 1H), 6.68 (d, J = 7.0 Hz, 1H), 2.56 (s, 3H), 1.50 (d, J = 6.7 Hz, 6H). ^{13}C NMR (300 MHz, MeOD) δ: 172.38, 157.95, 129.01, 110.35, 53.73, 21.86, 10.42.

3.6.13 *fac*-[Re(E(maltol))(CO)₃(H₂O)]

ReAA (1.00 g, 1.30 mmol) was dissolved in 80 ml water at pH 2.2 (adjusted with HNO_3). Silver nitrate (0.66 g, 3.89 mmol) was added and the mixture was stirred at room temperature for 24 hours. After the mixture was filtered, 2-ethyl-3-hydroxy-pyran-4-one (0.18 g, 1.30 mmol) was added and then it was stirred at room temperature for 24 hours. A white precipitate was formed, filtered and dried at room temperature.

Yield: 0.400 g, 0.94 mmol, 72.0 %. IR (ATR) $v_{C=O}$ (cm^{-1}): 1858, 1919, 2018. ^{1}H NMR (300 MHz, MeOD) δ: 8.14 (d, J = 5.1 Hz, 1H), 6.77 (d, J = 5.1 Hz, 1H), 2.92 (q, J = 8.0 Hz, 2H), 1.27 (t, J = 7.6 Hz, 3H). ^{13}C NMR (300 MHz, MeOD) δ: 182.88, 160.68, 154.78, 154.39, 111.76, 29.28, 22.96, 21.18, 10.03.

3.6.14 *fac*-[Re(EM(naltol))(CO)₃(H₂O)]

ReAA (1.00 g, 1.30 mmol) was dissolved in 80 ml water at pH 2.2 (adjusted with HNO_3). Silver nitrate (0.66 g, 3.89 mmol) was added and the mixture was stirred at room temperature for 24 hours. After the mixture was filtered, 2-ethyl-3-hydroxy-1-methyl-4-pyridone (0.20 g, 1.30 mmol) was added and then it was stirred at room temperature for 24 hours. A white precipitate was formed, filtered and dried at room temperature.

Yield: 0.273 g, 0.62 mmol, 47.6 %. IR (ATR) $v_{C=O}$ (cm^{-1}): 1870, 1901, 2008. ^{1}H NMR (300 MHz, MeOD) δ: 7.52 (d, J = 6.8 Hz, 1H), 6.57 (d, J = 6.8 Hz, 1H), 3.93 (s, 3H), 3.00 (dd, J = 14.7, 7.3 Hz, 2H), 1.25 (t, J = 7.5 Hz, 3H). ^{13}C NMR (300 MHz, MeOD) δ: 173.42, 157.74, 141.43, 134.17, 109.76, 41.29, 18.81, 10.91.

3.6.15   *fac*-[Re(EE(naltol))(CO)$_3$(H$_2$O)]

ReAA (1.00 g, 1.30 mmol) was dissolved in 80 ml water at pH 2.2 (adjusted with HNO$_3$). Silver nitrate (0.66 g, 3.89 mmol) was added and the mixture was stirred at room temperature for 24 hours. After the mixture was filtered, 1,2-diethyl-3-hydroxy-4-pyridone (0.22 g, 1.30 mmol) was added and then it was stirred at room temperature for 24 hours. A white precipitate was formed, filtered and dried at room temperature.

Yield: 0.212 g, 0.47 mmol, 35.9 %. IR (ATR) v $_{C=O}$ (cm^{-1}): 1886, 2015. ^{1}H NMR (300 MHz, MeOD) δ: 7.58 (d, *J* = 6.9 Hz, 1H), 6.61 (d, *J* = 6.9 Hz, 1H), 4.23 (q, *J* = 7.2 Hz, 2H), 3.00 (q, 2H), 1.45 (t, *J* = 7.2 Hz, 3H), 1.26 (t, *J* = 7.5 Hz, 3H). ^{13}C NMR (300 MHz, MeOD) δ: 173.26, 157.91, 140.63, 132.80, 110.29, 49.33, 18.56, 15.81, 11.60.

3.6.16   *fac*-[Re(EI(naltol))(CO)$_3$(H$_2$O)]

ReAA (1.00 g, 1.30 mmol) was dissolved in 80 ml water at pH 2.2 (adjusted with HNO$_3$). Silver nitrate (0.66 g, 3.89 mmol) was added and the mixture was stirred at room temperature for 24 hours. After the mixture was filtered, 2-ethyl-3-hydroxy-1-isopropyl-4-pyridone (0.24 g, 1.30 mmol) was added and then it was stirred at room temperature for 24 hours. A white precipitate was formed, filtered and dried at room temperature.

Yield: 0.396 g, 0.85 mmol, 65.0 %. IR (ATR) v $_{C=O}$ (cm^{-1}): 1885, 2011. ^{1}H NMR (300 MHz, DMSO) δ: 7.75 (d, *J* = 7.0 Hz, 1H), 6.55 (d, *J* = 7.0 Hz, 1H), 4.68 (dt, *J* = 13.0, 6.5 Hz, 1H), 3.07 – 2.79 (m, 2H), 1.43 (d, *J* = 6.5 Hz, 6H), 1.12 (t, *J* = 7.4 Hz, 3H). ^{13}C NMR (300 MHz, DMSO) δ: 207.02, 173.78, 158.75, 139.24, 129.42, 110.48, 53.11, 31.15, 23.44, 18.46, 13.55.

3.6.17   *fac*-[Re(ME(naltol))(CO)$_3$(Pyr)]

Pyridine (1 ml of a 1.95 x 10^{-3} M methanol solution) and *fac*-[Re(ME(naltol))(CO)$_3$(H$_2$O)] (10 ml of a 1.95 x 10^{-4} M methanol solution) were stirred for 1 hour at room temperature. The reaction mixture was dried *in vacuo* to yield a yellow product. The crystals reported in Chapter 8 were grown from a DMSO solution of this product (Section 8.3). IR (ATR) v $_{C=O}$ (cm^{-1}): 1920, 2016.

3.6.18   *fac*-[Re(EM(naltol))(CO)$_3$(Pyr)]

Pyridine (1 ml of a 1.95 x 10^{-3} M methanol solution) and *fac*-[Re(EM(naltol))(CO)$_3$(H$_2$O)] (10 ml of a 1.95 x 10^{-4} M methanol solution) were stirred for 1 hour at room temperature. The reaction mixture was dried *in vacuo* to yield a yellow product. The crystals reported in Chapter 8 were grown from a DMSO solution of this product (Section 8.4). IR (ATR) v $_{C=O}$ (cm^{-1}): 1918, 2016.

3.6.19   *fac*-[Re(EE(naltol))(CO)$_3$(Pyr)]

Pyridine (1 ml of a 1.95 x 10^{-3} M methanol solution) and *fac*-[Re(EE(naltol))(CO)$_3$(H$_2$O)] (10 ml of a 1.95 x 10^{-4} M methanol solution) were stirred for 1 hour at room temperature. The reaction mixture was dried *in vacuo* to yield a yellow product. The crystals reported in Chapter 8 were grown from a DMSO solution of this product (Section 8.5). IR (ATR) v $_{C=O}$ (cm^{-1}): 1919, 2016.

3.7 *fac*-Tricarbonylbis(pyridinonato)rhenium(I) synthetic validation

To see if it was possible to isolate the bis-complex *fac*-[Re(EM(naltol))(EM(naltol)H)(CO)$_3$] from the aqua procedure (from *fac*-[Re(CO)$_3$(H$_2$O)$_3$]$^+$) by simply doubling the ligand quantity or by refluxing the mixture of ligand and the rhenium synthon *fac*-[Re(CO)$_3$(H$_2$O)$_3$]$^+$ the following two modified procedures were carried out. Only the aqua complex, *fac*-[Re(EM(naltol))(CO)$_3$(H$_2$O)] was obtained in the first attempt (Section 3.7.1) with slightly higher yields, the second attempt (Section 3.7.2) was unsuccessful. Therefore it could be confirmed that the bis-complexes can only be synthesized from the bromido starting synthon *fac*-[Re(CO)$_3$Br$_3$]$^{2-}$.

3.7.1 First attempted synthesis of *fac*-[Re(EM(naltol))(EM(naltol)H)(CO)$_3$]

ReAA (1.00 g, 1.30 mmol) was dissolved in 80 ml water at pH 2.2 (adjusted with HNO$_3$). Silver nitrate (0.66 g, 3.89 mmol) was added and the mixture was stirred at room temperature for 24 hours. After the mixture was filtered, 2-ethyl-3-hydroxy-1-methyl-4-pyridone (0.40 g, 2.60 mmol) was added and then it was stirred at room temperature for 24 hours. A white precipitate was formed, filtered and dried at room temperature.

Yield: 0.6530 g, 1.13 mmol, 87.2 %. IR (ATR) v $_{C=O}$ (cm^{-1}): 1870, 1901,2008. ^{1}H NMR (300 MHz, MeOD) δ: 7.52 (d, *J* = 6.8 Hz, 1H), 6.57 (d, *J* = 6.8 Hz, 1H), 3.93 (s, 3H), 3.00 (dd, *J* = 14.7, 7.3 Hz, 2H), 1.25 (t, *J* = 7.5 Hz, 3H). ^{13}C NMR (300 MHz, MeOD) δ: 173.42, 157.74, 141.43, 134.17, 109.76, 41.29, 18.81, 10.91.

3.7.2 Second attempted synthesis of *fac*-[Re(EM(naltol))(EM(naltol)H)(CO)$_3$]

ReAA (1.00 g, 1.30 mmol) was dissolved in 80 ml water at pH 2.2 (adjusted with HNO$_3$). Silver nitrate (0.66 g, 3.89 mmol) was added and the mixture was stirred at room temperature for 24 hours. After the mixture was filtered, 2-ethyl-3-hydroxy-1-methyl-4-pyridone (0.40 g, 2.60 mmol) was added and then refluxed overnight. The reaction mixture was dried *in vacuo*. A brown oil with various inseparable by-product was obtained. Therefore *fac*-[Re(EM(naltol))(EM(naltol)H)(CO)$_3$] could not be synthesized from the aqua starting synthon *fac*-[Re(CO)$_3$(H$_2$O)$_3$]$^+$.

3.8 Synthesis of rhodium complexes

In all the preceding rhodium synthetic procedures, the rhodium synthon used in the coordination of 3-hydroxypyran-4-one derivatives to rhodium(I) is the dinuclear complex, [Rh(μ-Cl)(CO)$_2$]$_2$ (Scheme 3.6). The [Rh(μ-Cl)(CO)$_2$]$_2$ complex is prepared *in situ* by refluxing RhCl$_3$.xH$_2$O in DMF until a colour change from red to yellow is observed. This colour change indicates the formation of the desired complex. The complex is not isolated from solution but directly used *in situ* for further reactions.
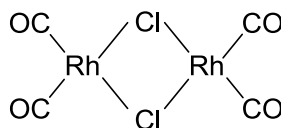
Scheme 3.6: A schematic representation of the [Rh(μ-Cl)(CO)$_2$]$_2$ complex formed *in situ* for the synthesis of rhodium(I) complexes.

3.8.1 [Rh(maltol)(CO)$_2$]

RhCl$_3$·3H$_2$O (0.100 g, 0.478 mmol) was refluxed in 2 ml of DMF until the red colour turned yellow (approx. 30 min). The solution was then cooled to room temperature before adding 3-hydroxy-2-methyl-pyran-4-one (0.066 g, 0.526 mmol) to the reaction mixture. This was followed by the addition of sodium acetate (0.043 g, 0.526 mmol). The dark green product was precipitated by the addition of ice-water and then collected by centrifugation. The dark green product was collected in acetone and upon drying turned yellow.

Yield: 0.0514 g, 0.18 mmol, 37.9 %. IR (ATR) v $_{C=O}$ (cm^{-1}): 1980, 2053. ^{1}H NMR (300 MHz, C$_3$D$_6$O) δ: 8.29 (d, J = 5.1 Hz, 1H), 6.88 (d, J = 5.1 Hz, 1H), 2.48 (s, 3H). ^{13}C NMR (300 MHz, C$_3$D$_6$O) δ: 185.53, 182.68, 156.41, 153.87, 111.25, 13.53.

3.8.2 [Rh(MM(naltol))(CO)$_2$]

RhCl$_3$·3H$_2$O (0.200 g, 0.956 mmol) was refluxed in 2 ml of DMF until the red colour turned yellow (approx. 30 min). The solution was then cooled to room temperature before adding 3-hydroxy-1,2-dimethyl-4-pyridone (0.146 g, 1.052 mmol) to the reaction mixture. This was followed by the addition of sodium acetate (0.086 g, 1.052 mmol). The yellow product was precipitated by the addition of ice-water and then collected by centrifugation.

Yield: 0.135 g, 0.45 mmol, 47.4 %. IR (ATR) v $_{C=O}$ (cm^{-1}): 1987, 2058. ^{1}H NMR (300 MHz, C$_3$D$_6$O) δ: 7.64 (d, J = 6.8 Hz, 1H), 6.56 (d, J = 6.8 Hz, 1H), 3.97 (s, 3H), 2.47 (s, 3H). ^{13}C NMR (300 MHz, C$_3$D$_6$O) δ: 186.93, 185.98, 174.00, 161.88, 158.94, 133.50, 109.30, 42.16, 35.25, 10.86.

3.8.3   [Rh(ME(naltol))(CO)₂]

RhCl$_3$·3H$_2$O (0.200 g, 0.956 mmol) was refluxed in 2 ml of DMF until the red colour turned yellow (approx. 30 min). The solution was then cooled to room temperature before adding 1-ethyl-3-hydroxy-2-methyl-4-pyridone (0.161 g, 1.052 mmol) to the reaction mixture. This was followed by the addition of sodium acetate (0.086 g, 1.052 mmol). The golden yellow product was precipitated by the addition of ice-water and then collected by centrifugation.

Yield: 0.123 g, 0.40 mmol, 41.4 %. IR (ATR) v $_{C=O}$ (cm^{-1}): 1980, 2046. ^{1}H NMR (300 MHz, C$_3$D$_6$O) δ: 7.68 (d, J = 6.9 Hz, 1H), 6.60 (d, J = 6.9 Hz, 1H), 4.31 (q, J = 7.2 Hz, 2H), 2.50 (s, 3H), 1.44 (t, J = 7.2 Hz, 3H). ^{13}C NMR (300 MHz, C$_3$D$_6$O) δ: 186.94, 186.00, 173.91, 159.15, 134.55, 132.31, 109.85, 49.84, 15.46, 10.38.

3.8.4   [Rh(MI(naltol))(CO)₂]

RhCl$_3$·3H$_2$O (0.200 g, 0.956 mmol) was refluxed in 2 ml of DMF until the red colour turned yellow (approx. 30 min). The solution was then cooled to room temperature before adding 3-hydroxy-2-methyl-1-isopropyl-4-pyridone (0.177 g, 1.052 mmol) to the reaction mixture. This was followed by the addition of sodium acetate (0.086 g, 1.052 mmol). The yellow crystalline product was formed from the ice-water mixture upon evaporation.

Yield: 0.270 g, 0.83 mmol, 86.3 %. IR (ATR) v $_{C=O}$ (cm^{-1}): 1978, 2051. ^{1}H NMR (300 MHz, C$_3$D$_6$O) δ: 7.77 (d, J = 7.1 Hz, 1H), 6.64 (d, J = 7.1 Hz, 1H), 4.88 (dt, J = 13.3, 6.7 Hz, 1H), 2.54 (s, 3H), 1.53 (d, J = 6.7 Hz, 6H). ^{13}C NMR (300 MHz, C$_3$D$_6$O) δ: 186.99, 186.05, 173.55, 158.74, 134.73, 128.05, 109.98, 53.66, 22.12, 10.32.

3.8.5 [Rh(E(maltol))(CO)$_2$]

RhCl$_3$·3H$_2$O (0.200 g, 0.956 mmol) was refluxed in 2 ml of DMF until the red colour turned yellow (approx. 30 min). The solution was then cooled to room temperature before adding 2-ethyl-3-hydroxy-pyran-4-one (0.147 g, 1.052 mmol) to the reaction mixture. This was followed by the addition of sodium acetate (0.086 g, 1.052 mmol). The dark yellow product was precipitated by the addition of ice-water and then collected by centrifugation.

Yield: 0.1540 g, 0.51 mmol, 53.9 %. IR (ATR) v $_{C=O}$ (cm^{-1}): 1997, 2070. ^{1}H NMR (300 MHz, C$_3$D$_6$O) δ: 8.31 (d, J = 5.1 Hz, 1H), 6.87 (d, J = 5.1 Hz, 1H), 2.90 (dd, J = 15.1, 7.6 Hz, 2H), 1.24 (t, J = 7.6 Hz, 3H). ^{13}C NMR (300 MHz, C$_3$D$_6$O) δ: 182.99, 160.42, 160.38, 156.01, 153.92, 111.22, 111.19, 21.17, 10.08.

3.8.6 [Rh(EM(naltol))(CO)$_2$]

RhCl$_3$·3H$_2$O (0.200 g, 0.956 mmol) was refluxed in 2 ml of DMF until the red colour turned yellow (approx. 30 min). The solution was then cooled to room temperature before adding 2-ethyl-3-hydroxy-1-methyl-4-pyridone (0.161 g, 1.052 mmol) to the reaction mixture. This was followed by the addition of sodium acetate (0.086 g, 1.052 mmol). The yellow product was precipitated by the addition of ice-water and then collected by centrifugation.

Yield: 0.121 g, 0.39 mmol, 37.9 %. IR (ATR) v $_{C=O}$ (cm^{-1}): 1983, 2059. ^{1}H NMR (300 MHz, C$_3$D$_6$O) δ: 7.60 (d, J = 6.8 Hz, 1H), 6.56 (d, J = 6.8 Hz, 1H), 4.02 (s, 3H), 3.04 − 2.95 (m, 2H), 1.19 (t, J = 7.5 Hz, 3H). ^{13}C NMR (300 MHz, C$_3$D$_6$O) δ: 185.99, 174.54, 158.81, 140.30, 133.71, 109.48, 109.45, 41.63, 18.73, 11.15.

3.8.7　[Rh(EE(naltol))(CO)$_2$]

RhCl$_3$·3H$_2$O (0.200 g, 0.956 mmol) was refluxed in 2 ml of DMF until the red colour turned yellow (approx. 30 min). The solution was then cooled to room temperature before adding 3-hydroxy-2-methyl-pyran-4-one (0.176 g, 1.052 mmol) to the reaction mixture. This was followed by the addition of sodium acetate (0.086 g, 1.052 mmol). The yellow product was precipitated by the addition of ice-water and then collected by centrifugation.

Yield: 0.240 g, 0.18 mmol, 77 %. IR (ATR) v $_{C=O}$ (cm^{-1}): 1981, 2051. ^{1}H NMR (300 MHz, C$_3$D$_6$O) δ: 7.68 (d, J = 6.9 Hz, 1H), 6.62 (d, J = 6.9 Hz, 1H), 4.32 (q, J = 7.2 Hz, 2H), 1.46 (t, J = 7.2 Hz, 3H), 1.20 (t, J = 7.5 Hz, 3H). ^{13}C NMR (300 MHz, C$_3$D$_6$O) δ: 185.93, 174.29, 162.01, 158.82, 132.43, 110.09, 49.35, 35.30, 18.50, 16.36, 11.82.

3.8.8　[Rh(EI(naltol))(CO)$_2$]

RhCl$_3$·3H$_2$O (0.200 g, 0.956 mmol) was refluxed in 2 ml of DMF until the red colour turned yellow (approx. 30 min). The solution was then cooled to room temperature before adding 2-ethyl-3-hydroxy-1-isopropyl-4-pyridone (0.176 g, 1.052 mmol) to the reaction mixture. This was followed by the addition of sodium acetate (0.086 g, 1.052 mmol). The yellow product barely precipitated and upon evacuation it had decomposed to a dark brown solid. Unsuccessful.

3.9　Synthesis of dicarbonylpyridinonatotriphenylphosphine-rhodium(I) complexes

The respective dicarbonyl [Rh^I(pyrone/pyridinonato)(CO)$_2$] complex (0.100 g, 0.352 mmol) in each case was dissolved in acetone to which triphenylphosphine (0.138 g, 0.526 mmol) was added, resulting in the immediate evolution of CO gas. The solution was filtered and dried, a yellow product was isolated (Vaska's complex, see Section 9.4) in each case. The synthesis of [Rh^I(O,O'-bid)PPh$_3$CO] complexes with these chelator systems was unsuccessful and it was not pursued any further.

3.10 Discussion

During the course of the synthesis part of this project, two novel chelators (3-hydroxy-2-methyl-1-isopropyl-4-pyridinone and 2-ethyl-3-hydroxy-1-isopropyl-4-pyridinone) were synthesized and four existing chelators (3-hydroxy-1,2-dimethyl-4-pyridone, 1-ethyl-3-hydroxy-2-methyl-4-pyridone, 2-ethyl-3-hydroxy-1-methyl-4-pyridone and 1,2-diethyl-3-hydroxy-4-pyridone) were re-synthesized and characterized.[1-3] The more significant focus area revolved around the respective complexes of these metal centres (Zr(V), Hf(V), Re(I) and Rh(I)). Eight complexes of Zr and eight complexes of Hf were successfully synthesized. [Zr(E(maltol))$_4$] and [Hf(maltol)$_4$] were completely insoluble in most deuterated solvents and were therefore not characterized by NMR spectroscopy. However the obtained samples were uniform in colour with no visible impurities in the samples. Other than these two complexes the Zr and Hf compounds were all soluble in water and dimethyl sulfoxide. The yields in this section were relatively high and ranging between approximately 60 % and 100 %.

With regards to the rhenium complexes 17 novel *fac*-[Re(CO)$_3$]$^+$ type compounds are reported. All of these compounds have the potential to serve as precursors to which biomolecules can be attached or serve directly as radiopharmaceuticals as pyrone and pyridinone ligands have known biological activity. Additionally five interesting bis-complexes were obtained and successfully validated by NMR and X-ray diffraction (see Chapter 5). The synthetic procedure of these complexes was also validated by modifying the aqua procedure (Section 3.6.9 – 3.6.16) by adjusting the Re: Ligand ratio to 1: 2 and refluxing (Section 3.7) to prove that this complex can only be obtained from the bromido synthetic procedure (Sections 3.6.1, 3.6.5 and 3.6.8). The results confirmed that these bis-complexes cannot be obtained from the aqua procedure and can only be obtained from the bromido procedure (Section 3.6.1 – 3.6.8). In the room temperature synthesis (Section 3.7.1) the aqua complex *fac*-[Re(EM(naltol))(CO)$_3$(H$_2$O)] was obtained instead of *fac*-[Re(EM(naltol))(EM(naltol)H)(CO)$_3$] but with higher yields (approximately double the yield). The refluxed reaction (Section 3.7.2) yielded a brown oil with various

[1] P. P. Molokoane, M. Schutte, G. Steyl, *Acta Crystallogr. E*, **2012**, *68*, o3235.

[2] G. J. Kontoghiorghes, L. Sheppard, *Inorg. Chim. Acta.*, **1987**, *136*, L11.

[3] L. Simpson, S. J. Rettig, J. Trotter, C. Orvig, *Can. J. Chem.*, **1991**, *69*, 893.

inseparable by-products. Pyridine substituted complexes are also reported, these were synthesized from the corresponding aqua complexes (Section 3.6.17 - 3.6.19) and their crystal structures are reported in Chapter 8. The tricarbonyl carbon atom peaks in most of the rhenium complexes were not observed on the ^{13}C NMR spectra, this is mainly due to economic reasons as these could only be detected over extended periods of time. A trend was observed for the IR stretching frequencies of the metal complexes, although the IR stretching frequencies of two of the complexes were not obtained. Between the rhenium complexes and the bromido complexes, and due to the high electronegativity of the Br, which will decrease the electron density on the rhenium atom and because all the other functionalities are constant in the corresponding aqua complexes (tricarbonyls and bidentate chelators) the stretching frequencies will resonate at much lower wavenumbers (bromido range [1841: 2004], aqua range [1858: 2018]). Because Rh is a d^8 centre and Re a d^5 centre it means Rh is much softer and hence more electron rich and the chelator system is still the same with only one less carbonyl functional group contributing to backbonding, they will typically resonate at higher stretching frequencies (range [1978: 2070]) (see Table 3.1). The yields in this section were fairly good and ranging between approximately 40 % and 90 %.

O,O'-bidentate ligands are hard metal chelaters and accordingly bind to hard metal ions which is consistent with the stable complexes obtained for Zr, Hf and Re and with ease (the aqua procedure was room temperature stirring). The soft metal centre Rh required assisted deprotonation of the ligands upon coordination and hence a mild base (sodium acetate was used). Furthermore the [Rh(EI(naltol))(CO)$_2$] complex decomposed upon drying and all the other complexes upon coordinating PPh$_3$ decomposed and only the Vaska's complex was isolated. The yields in this section were fairly modest and ranging between approximately 30 % and 80 %.

Table 3.1: Summary of the spectroscopic data for the synthesized rhenium(I) and rhodium(I) complexes.

Complex (Bromido)	$\nu_{C=O}$ (asym), (sym) (cm^{-1})	Complex (Aqua)	$\nu_{C=O}$ (asym), (sym) (cm^{-1})	Complex (Rh)	$\nu_{C=O}$ (asym), (sym) (cm^{-1})
fac-[NEt$_4$][Re(maltol)(CO)$_3$(Br)]	1847, 1996	*fac*-[Re(maltol)(CO)$_3$(H$_2$O)]	-	[Rh(maltol)(CO)$_2$]	1980, 2053
fac-[Re(MM(naltol))(MM(naltol)H)(CO)$_3$]	1848, 1997	*fac*-[Re(MM(naltol))(CO)$_3$(H$_2$O)]	1870, 2014	[Rh(MM(naltol))(CO)$_2$]	1987, 2058
fac-[NEt$_4$][Re(ME(naltol))(CO)$_3$(ME(naltol)H)]	1860, 1998	*fac*-[Re(ME(naltol))(CO)$_3$(H$_2$O)]	1882, 2015	[Rh(ME(naltol))(CO)$_2$]	1980, 2046
fac-[NEt$_4$][Re(MI(naltol))(CO)$_3$(MI(naltol)H)]	1843, 1996	*fac*-[Re(MI(naltol))(CO)$_3$(H$_2$O)]	1882, 2015	[Rh(MI(naltol))(CO)$_2$]	1978, 2051
fac-[NEt$_4$][Re(E(maltol))(CO)$_3$(Br)]	1847, 1996	*fac*-[Re(E(maltol))(CO)$_3$(H$_2$O)]	1858, 1919, 2018	[Rh(E(maltol))(CO)$_2$]	1997, 2070
fac-[Re(EM(naltol))(EM(naltol)H)(CO)$_3$]	1841, 1983, 2001	*fac*-[Re(EM(naltol))(CO)$_3$(H$_2$O)]	1870, 1901, 2008	[Rh(EM(naltol))(CO)$_2$]	1983, 2059
fac-[Re(EE(naltol))(EE(naltol)H)(CO)$_3$]	1843, 1867, 1997	*fac*-[Re(EE(naltol))(CO)$_3$(H$_2$O)]	1886, 2015	[Rh(EE(naltol))(CO)$_2$]	1981, 2051
fac-[NEt$_4$][Re(EI(naltol))(CO)$_3$(Br)]	1882, 2004	*fac*-[Re(EI(naltol))(CO)$_3$(H$_2$O)]	1885, 2011	[Rh(EI(naltol))(CO)$_2$]	-

4 Crystallographic Study of [Hf(E(maltol))₃Cl]·2CHCl₃

$$\text{4 Crystallographic Study of [Hf(E(maltol))}_3\text{Cl]·2CHCl}_3$$

4.1 Introduction

It was illustrated in Chapter 3 that six chelators were synthesized from two commercially available starting materials. In this chapter the crystal structure of chlorido-tris(2-ethyl-3-hydroxy-1-methyl-4-pyridonato)hafnium(IV) dichloroform solvate is reported. The significance of structural characterization of zirconium and hafnium complexes is in the divergence of chemical properties of the compounds of these two metals. Any anomalies between these compounds can potentially form the basis for separation of these metals from base ores. It is proposed that subtle mutations in the chelators can form the basis of this divergence in chemical properties as the electronic and steric demands are manipulated. Several methods and solvents were used in an attempt to grow crystals of the zirconium and hafnium complexes synthesized in this study for characterization with the XRD, however only one structure was obtained from a chloroform solution as illustrated in Scheme 4.1.
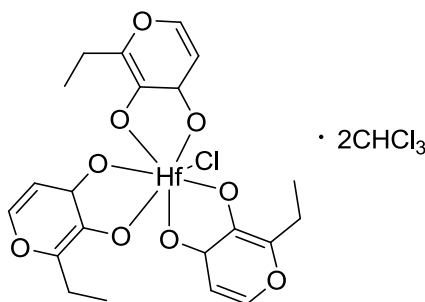
Scheme 4.1: Illustration of the crystal structure of [Hf(E(maltol))₃Cl]·2CHCl₃.

This chapter will focus on the structural data of [Hf(E(maltol))₃Cl]·2CHCl₃ and the general molecular geometry and intermolecular interactions that contribute to the stability of the crystal

packing. Geometric parameters such as the different bond distances and angles in the molecules will also be highlighted and discussed.

4.2 Experimental

The reflection data of [Hf(E(maltol))$_3$Cl]·2CHCl$_3$ (**1**) was collected on a Bruker X8 Apex II 4K Kappa CCD diffractometer using graphite monochromated Mo Kα radiation (λ= 0.70926 Å) with ω- and φ-scans at 100(2) K. The Apex II software package was utilized along with the optimum measurement method in collecting more than a hemisphere of reciprocal space as predicted by COSMO.[1,2] Frame integration and data reduction was performed using the SAINT-Plus and XPREP software packages and SADABS was used for multi-scan absorption correction.[3,4] The structure was solved using the direct methods package SIR97 and refined using the WinGX software incorporating SHELXL.[5-11] All atoms were refined anisotropically with the exception of hydrogen atoms. The hydrogen atoms were positioned geometrically and refined utilizing a riding model with fixed C-H distances of 0.95 Å (CH) [U_{iso}(H) = 1.2 U_{eq}] for aromatic hydrogens, 0.97 Å (CH) [U_{iso}(H) = 1.2 U_{eq}] for methylene H-atoms and 0.96 Å (CH) [U_{iso}(H) = 1.2 U_{eq}] for methyl H-atoms. Molecular diagrams were generated with DIAMOND with 50 % probability ellipsoids for all non-hydrogen atoms.[12] General crystal data and refinement parameters are represented in Table 4.1 with the complete list of atomic coordinates, equivalent isotropic parameters and hydrogen coordinates given in Appendix A.

[1] **Apex2**, Version 2012.10-0, Bruker AXS Inc.,Madison, Wisconsin, USA, **2012**.

[2] **COSMO**, Version 1.48, Bruker AXS Inc., Madison, Wisconsin, USA, **2003**.

[3] **SADABS**, Version 2012/1, BrukerAXS Inc, Madison, Wisconsin, USA, **2012**.

[4] **SAINT-Plus**, Version 8.27B including XPREP, Bruker AXS Inc., Madison, Wisconsin, USA, **2012**.

[5] A. Altomare, G. Cascarano, C. Giacovazzo, A. Guagliardi, M. C. Burla, G. Polidori, M. Camalli, *J. Appl. Cryst.*, **1994**, *27*, 435.

[6] A. Altomare, M. C. Burla, M. Camalli, G. L. Cascarano, C. Giacovazzo, A. Guagliardi, A. G. G. Moliterni, G. Polidori, R. Spagna, *J. Appl. Cryst.*, **1999**, *32*, 115.

[7] M. C. Burla, M. Camalli, B. Carrozzini, G. L. Cascarano, C. Giacovazzo, G. Polidori, R. Spagna, *J. Appl. Cryst.*, **2003**, *36*, 1103.

[8] P. T. Beurskens, G. Admiraal, G. Beurskens, W. P. Bosman, S. Garcia-Granda, R. O. Gould, J. M. M. Smits, C. Smykalla, Crystallography Laboratory, University of Nijmegen, Toernooiveld, The Netherlands.

[9] L. Palatinus, G. Chapuis, *J. Appl. Cryst.*, **2007**, *40*, 786.

[10] **WinGX**. L. J. Farrugia, *J. Appl. Cryst.*, **2012**, *45*, 849.

[11] G. M. Sheldrick, *Acta Cryst.*, **2008**, *A64*, 112.

[12] K. Brandenburg, H. Putz, DIAMOND, Release 3.0e, Crystal Impact GbR, Bonn, Germany, **2006**.

Table 4.1: General X-ray crystallographic data and refinement parameters for [Hf(E(maltol))$_3$Cl]·2CHCl$_3$ solvate.

Crystallographic data	(1)
Empirical formula	C$_{23}$H$_{22}$C$_{17}$Hf O$_9$
Formula weight (g.mol^{-1})	869.05
Temperature (K)	100(2)
Crystal system	Orthorhombic
Space group	*Pca*2$_1$
a (Å)	28.546(3)
b (Å)	9.623(1)
c (Å)	11.282(1)
α (°)	90
β (°)	90
γ (°)	90
Volume (Å^3)	3099.1(5)
Z	4
ρ $_{calc.}$ (g.cm^{-3})	1.863
Crystal colour	Colourless
Crystal morphology	Cuboid
Crystal size (mm^3)	0.377 x 0.272 x 0.128
μ (mm^{-1})	4.016
F(000)	1692.0
θ range (°)	4.150 to 27.993
Index ranges	-37 ≤ h ≤ 37
	-12 ≤ k ≤ 12
	-14 ≤ l ≤ 11
Reflections collected	81601
Unique reflections	7495
Reflections with I > 2σ(I)	9637
R$_{int}$	0.0578
Completeness to θ (°; %)	25.24, 99.3
Data/restraints/parameters	6982 / 31 / 383
GooF	1.054
R [I>2σ(I)]	R$_1$ = 0.0286
	wR$_2$ = 0.0672
R (all data)	R$_1$ = 0.0313
	wR$_2$ = 0.0682
ρ$_{max}$, ρ$_{min}$ (e.Å^{-3})	1.145 and -4.285

4.3 Crystal structure of [Hf(E(maltol))₃Cl]·2CHCl₃ solvate (1)

The complex, $[Hf(E(maltol))_3Cl]\cdot 2CHCl_3$ has been synthesized as described in Chapter 3 (Paragraph 3.4.5). The colourless crystals were obtained from a chloroform solution of the product. This neutral complex crystallized in the orthorhombic $Pca2_1$ space group with four independent molecules in the unit cell ($Z = 4$). The Flack parameter is 0.044(3) which indicates that the absolute configuration of the structure was correctly assigned. The large number of restraints is mainly due to the omission of outliers, as suggested by the cifcheck. In this structure the molecular geometry observed is distorted pentagonal bipyramidal, with the hafnium atom surrounded by six oxygen atoms and a chlorido ligand. A summary of the general crystal data of (**1**) is given in Table 4.1. Selected bond distances and angles are presented in Table 4.2 while the molecular diagram and numbering scheme of $[Hf(E(maltol))_3Cl]\cdot 2CHCl_3$ is shown in Figure 4.1.
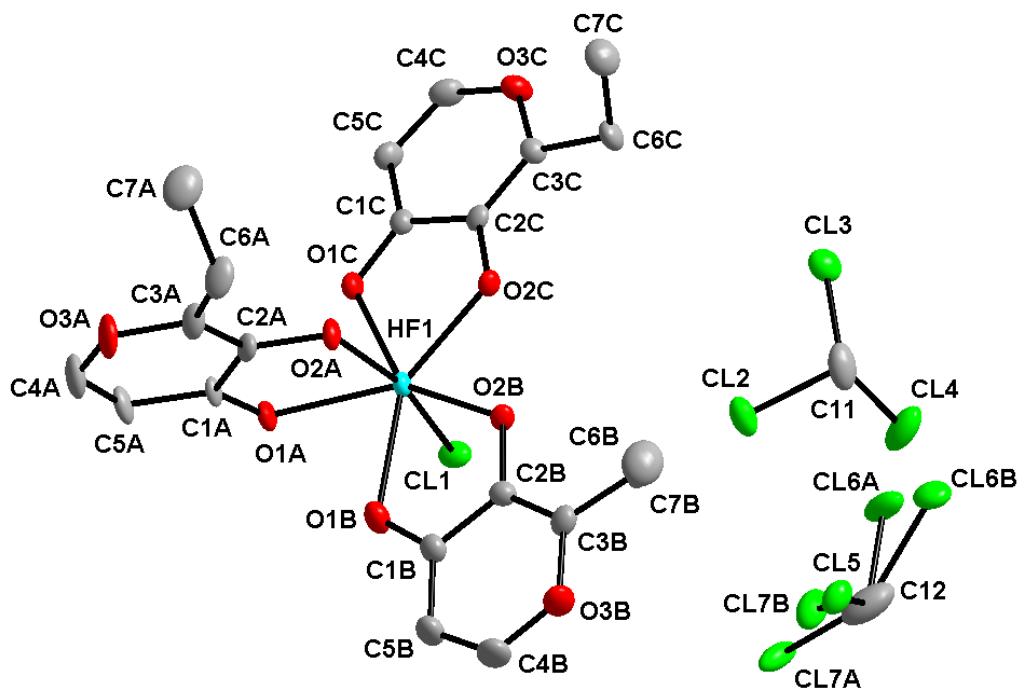
Figure 4.1: Molecular representation of [Hf(E(maltol))₃Cl]·2CHCl₃ (1) showing the atom numbering scheme. Displacement ellipsoids are drawn at 50 % probability level. Disorder on one CHCl₃ shown. Hydrogen atoms are omitted for clarity.

C11 (the carbon atom of the one chloroform molecule), was refined with the hydrogen riding on the C atom, however no additional electron density was observed in the vicinity of C12 of the

second chloroform molecule. The second chloroform molecule (C12, Cl5, Cl6, Cl7) has a positional disorder with the CL6A/ Cl7A and CL6B/ Cl7B atoms having an occupancy ratio of 0.69: 0.31. The refinement of this molecule is unstable with the placement of a riding hydrogen on C12. The hydrogen atom was therefore removed and the final data set was adequately refined as indicated by the refinement parameters of $wR_2 = 0.0682$, R = 0.0313 and GooF = 1.054. Somewhat high electron density is detected close to the hafnium atom. However this is assumed to be the fact that the high oxidation state of the Hf causes the crystallographic corrections not to accommodate 100 % this non-spherical diffraction correction profiles.

Table 4. 2: Selected bond distances (Å) and angles (°) for the crystal structure of (1).

Bond	Bond distance (Å)	Bond angle (atoms)	Bond angle (°)
Hf(1)-O(2A)	2.063(4)	O(2B)-Hf(1)-O(1B)	72.9(2)
Hf(1)-O(2C)	2.084(4)	O(2C)-Hf(1)-O(2B)	72.6(2)
Hf(1)-O(2B)	2.084(5)	O(2C)-Hf(1)-O(1C)	72.7(2)
Hf(1)-O(1A)	2.223(4)	O(2A)-Hf(1)-O(1A)	74.8(2)
Hf(1)-O(1B)	2.234(5)	O(2A)-Hf(1)-O(2B)	92.0(2)
Hf(1)-O(1C)	2.237(5)	O(2A)-Hf(1)-O(1C)	92.0(2)
Hf(1)-Cl(1)	2.463(2)	O(2A)-Hf(1)-Cl(1)	167.1(1)
		O(1C)-Hf(1)-Cl(1)	83.8 (1)
		O(1A)-Hf(1)-Cl(1)	92.3(1)
		O(1B)-Hf(1)-Cl(1)	84.7(1)

Some of the Hf−O bond distances are approximately 2.1 Å which is in good agreement with similar structures reported in literature (see section 4.4).[13-22] There is however a deviation from this in three bond distances: Hf(1)-O(1A), Hf(1)-O(1B) and Hf(1)-O(1C). These bond distances are ~ 2.2 Å which is indicative of a geometrical distortion in the structure as predefined by the

[13] M. C. Karunarathne, J. W. Baumann, M. J. Heeg, P. D. Martin, C. H. Winter, *J. Organomet. Chem.,* **2017**, *1*, 1.

[14] F. Hentschel, V. V. Vinogradov, A. V. Vinogradov, A. V. Agafonov, V. V. Guliants, I. Persson, G. A. Seisenbaeva, V. G. Kessler, *Polyhedron*, **2015**, *89*, 297.

[15] G. I. Spijksma, G. A. Seisenbaeva, H. J. M. Bouwmeester, D. H. A. Blank, V. G. Kessler, *Polyhedron*, **2013**, *53*, 150.

[16] N. B. Morozova, K. V. Zherikova, I. A. Baidina, S. V. Sysoev, P. P. Semyannikov, L. V. Yakovkina, T. P. Smirnova, N. V. Gelfond, I. K. Igumenov, G. Carta, G. Rossetto, *J. Phys. Chem. Solids.,* **2008**, *69*, 673.

[17] E. Y. Tshuva, S. Groysman, I. Goldberg, M. Kol, *Organometallics,* **2002,** *21,* 662.

[18] E. Hey-Hawkins, *Chem. Rev.,* **1994**, *94,* 1661.

[19] S. M. Draper, N. Kelly, *Coord. Chem. Rev.*, **1995**, *146*, 141.

[20] Z. A. Starikova, E. P. Turevskaya, N. I. Kozlova, N. Y. Turova, D. V. Berdyev, A. I. Yanovsky, *Polyhedron*, **1999**, *18*, 941.

[21] A. Tissier, J. Laugier, P. Boyer, *Acta Cryst.*, **1977**, *B33*, 392.

[22] A. R. Davis, F. W. B. Eistein, *Acta Cryst.*, **1978**, *B34*, 2110.

ligand thereon. The Hf−Cl bond distance is longer than the Hf−O bond distance by approximately 0.4 Å, but is in good agreement with some chlorido containing Hf and Zr structures reported in literature (see Section 4.4).[23,24]
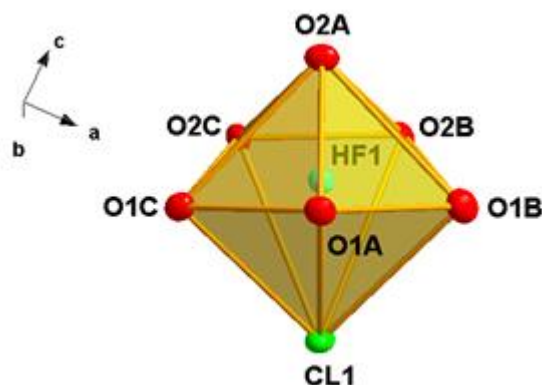
Figure 4.2: Illustration of the distorted pentagonal bipyramidal coordination polyhedron surrounding the Hf^IV atom.

The hafnium atom in this structure is situated at the centre of a distorted pentagonal bipyramidal coordination environment (Figure 4.2), with the deviating Hf−O bonds indicated above at the periphery of the pentagon. The longer bond distances of Hf(1)−O(1A), Hf(1)−O(1B) and Hf(1)−O(1C) (the respective oxygen atoms formerly carbonyls in the free ligand) indicate that they are more loosely coordinated which could be related to the richer electron density thereon compared to the other three oxygen atoms (O2A, O2B and O2C) which were hydroxyls in the free ligand. The bond angles O-Hf-O forming the vertices of the pentagon are ~ 72 ˚ which is in accordance with this particular ideal pentagonal molecular geometry and there are no significant deviations. The Cl-Hf-O bond angles perpendicular to the pentagon range from 83.8(1) ˚ to 92.3(1) ˚ indicating some significant distortions in the molecular geometry of the structure. The angle between the oxygen atom (O2A) at the one end of the bipyramidal vertex through the hafnium atom to the *trans*-chlorido ligand, O(2A)-Hf-Cl is 167.1(1) ˚ instead of the ideal 180 ˚ which might be due to steric demands around the hafnium atom as well as the inhibiting bite angle of the maltol, being only ca. 72 ˚.

---

[23] C. H. Saldarriaga-Molina, A. Clearfield, I. Bernal, *Inorg. Chem*., **1974**, *13*, 2880.
[24] M. F. Lappert, P. I. Riley, P. I. W. Yarrow, J. L. Atwood, W. E. Hunter, M. J. Zaworotko, *J. Chem. Soc., Dalton Trans*. **1981**,814.
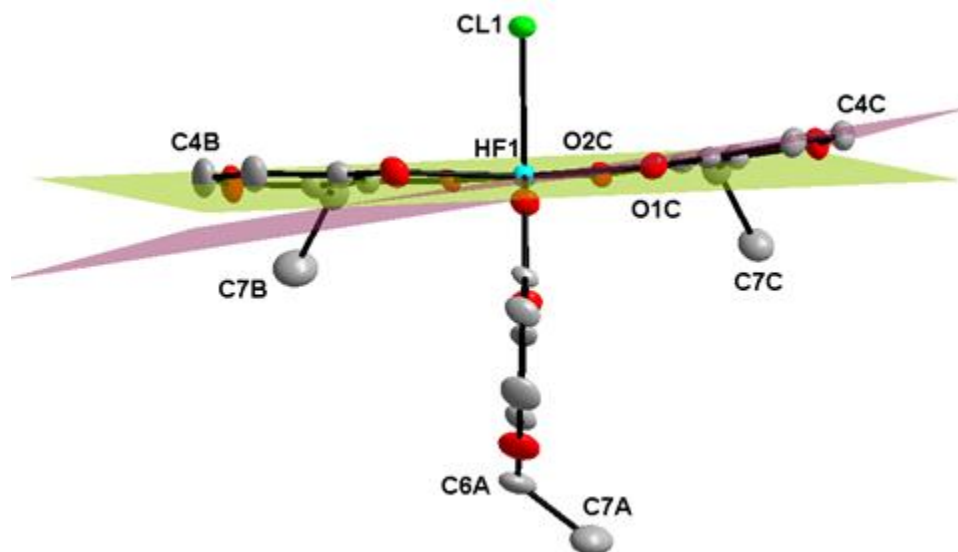
Figure 4.3: Illustration of the dihedral angle between the pentagonal plane (Hf1, O1B, O2B, O2C, O1C, O1A) and the plane through the coordinated heterocycle (C1C, C2C, C3C, O3C, C4C, C5C) of the ethyl maltol ligand (C).

The pentagonal bipyramidal geometry surrounding the hafnium atom is distorted as indicated above. The five oxygen atoms forming the approximate peripheral pentagon are non-planar and as a result the two in-plane bidentate ligands are bent out of the pentagonal plane (Hf1, O1B, O2B, O2C, O1C, O1A). The vertical axis of the bipyramid is also distorted and non-linear as a result. The ligand opposite to the chlorido ligand (labelled A) lies in a plane that is 86.540(6) ° to the pentagonal plane of the pentagonal bipyramid. The dihedral angles between the pentagonal plane and the plane through the heterocyclic rings C1B, C2B, C3B, O3B, C4B, C5B and C1C, C2C, C3C, O3C, C4C, C5C (Figure 4.3 above) are 7.903(9) ° and 9.354(9) ° respectively. This further indicates various distortions in the structure.
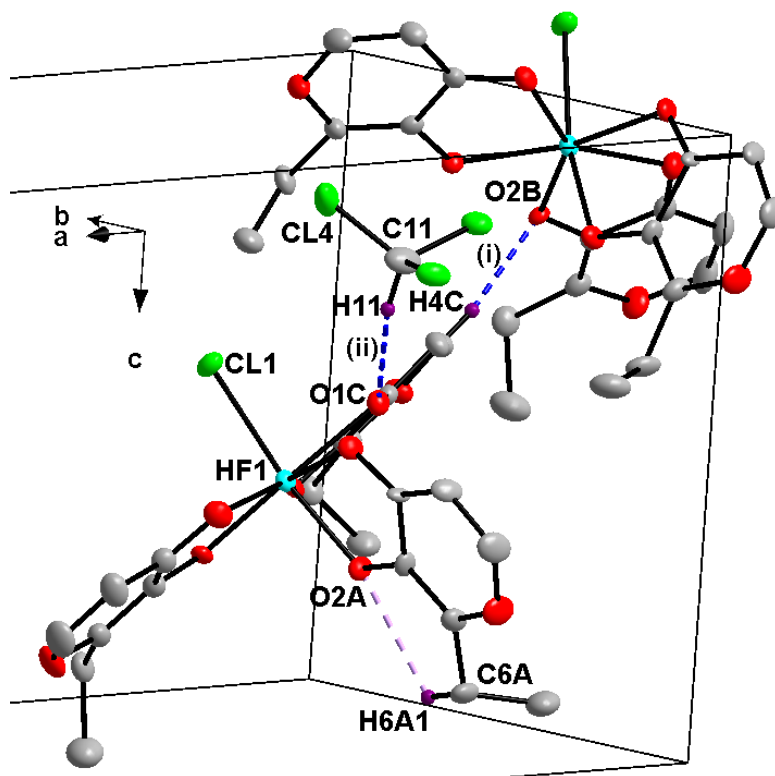
Figure 4.4: Hydrogen interactions observed in the structure of [Hf(E(maltol))₃Cl]·2CHCl₃ (1).

Only three hydrogen interactions are observed in this structure, see Figure 4.4: one intra-molecular (C-H…O, represented by light purple fragmented bonds) and two inter-molecular (all C-H…O interactions, represented by blue fragmented bonds) hydrogen interactions with one of them being a solvent interaction. The bond distances, bond angles and symmetry operators are given in Table 4.3.

Table 4.3: Summary of the hydrogen interactions (distance (Å) and angle (°)) observed in the structure of (1).

D-H…A	d(D-H) (Å)	d(H…A) (Å)	d(D…A) (Å)	∟ (D-H…A)(°)
C4C-H4C...O2B [(i)]	0.93	2.30	3.223	173
C6A-H6A1…O2A	0.97	2.58	2.980	105
C11-H11...O1C [(ii)]	0.98	2.30	3.228	157

Symmetry codes, transformations used to generate equivalent atoms: (i) 1/2-x, y, z-1/2; (ii) x, +1+y, +1+z;
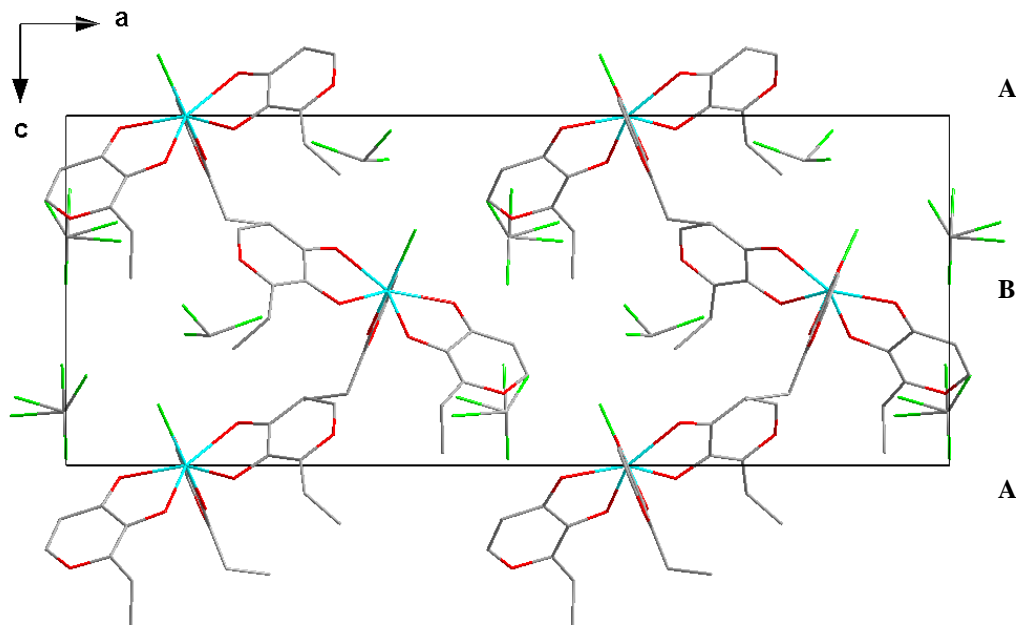
Figure 4.5: Crystal packing of (1) in the unit cell, viewed along the *b*-axis. Hydrogen atoms are omitted for clarity.

The molecules in the layer **A** pack in a parallel manner to the second layer **A** along the *ac*-plane with alternating orientations in between (layer **B**) (see Figure 4.5, **ABA**). This array is stabilized by inter-molecular C-H…O interactions with the solvent chloroform molecules.

4.4   Discussion

Two similar structures of hafnium and zirconium are compared to (**1**) to highlight some structural properties and to correlate some structural data between hafnium and zirconium complexes (see Figure 4.6 and Table 4.4).
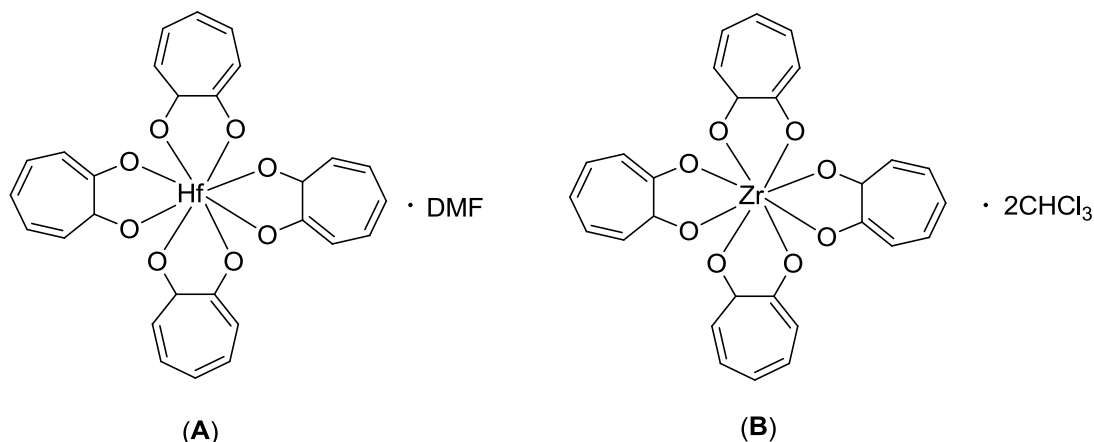
Figure 4.6: Illustration of the crystal structures of [Hf(C₇H₅O₂)₄]·DMF (A) and [Zr(C₇H₅O₂)₄]·2CHCl₃ (B).

Table 4.4: Selected bond distances and angles of hafnium(IV)- and zirconium(IV)- O,O'-bidentate complexes.

Complexes			
Formula	[Hf(C₇H₇O₃)₃Cl]·2CHCl₃ (**1**) [a]	[Hf(C₇H₅O₂)₄]·DMF (**A**) [b]	[Zr(C₇H₅O₂)₄]·2CHCl₃ (**B**) [c]
M−O (M = Hf/Zr) Å			
Hf−O	2.063(4)	2.175 (6)	2.188 (6)
Hf−O	2.084(4)	2.171 (7)	2.172 (6)
Hf−O	2.084(5)	2.168 (9)	2.161 (7)
Hf−O	2.223(4)	2.175 (9)	2.172 (8)
Hf−O	2.234(5)	2.183 (9)	2.197 (6)
Hf−O	2.237(5)	2.196 (8)	2.208 (14)
Hf−O	-	2.199 (10)	2.206 (7)
Hf−O	-	2.193 (10)	2.168 (8)
Hf−Cl	2.463(2)	-	-
O-M-O (M = Hf/Zr) °			
O-Hf-O	74.8(2)	70.4	69.4 (2)
O-Hf-O	72.9(2)	69.2	69.0 (3)
O-Hf-O	72.7(2)	69.5	71.5 (5)
O-Hf-O	-	69.4	68.8 (3)

[a] Current study, [b] A. Tissier *et al.* [21], [c] A. R. Davis *et al.* [22]

The two tropolone complexes with Hf and Zr, (**A**) and (**B**) are both tetrakis(tropolonato) modalities with square-antiprismatic coordination polyhedra around the Hf and Zr centres. Both structures crystalize out with solvents, dimethylformamide disolvate and dichloroform solvate for Hf and Zr respectively. These metal centres are both eight-coordinate while (**1**) is seven-coordinate and a chlorido-tris(2-ethyl-3-hydroxypyronato) with a pentagonal bipyramidal coordination polyhedron. The structure reported in this study (**1**), has two kinds of Hf−O bonds one approximately 2.1 Å (these were formerly hydroxyls in the free ligand) and the second

approximately 2.2 Å which were formerly carbonyls in the free ligand. The tropolonato ligand in (**A**)/ (**B**) on the other hand is symmetrical and upon coordination to Hf/ Zr the carbonyl and the hydroxyl functional groups become indistinguishable and all the M−O bonds distances (M = Hf/ Zr) are approximately 2.2 Å. In (**A**) the Hf−O bond distances range from 2.168(9) to 2.199(10) Å, and in (**B**) the Zr−O bond distances range from 2.161(7) Å to 2.208(14) Å. The range is significantly larger in (**B**) (0.047(16) Å) compared to 0.031(13) Å in (**A**). Despite the difference in Hf−O bond distances in (**1**), it is still comparable to the Hf−O and Zr−O bond distances in (**A**) and (**B**) respectively. In both (**A**) and (**B**) the O-Hf-O bite angles are approximately 70 ° while (**1**) has two kinds of O-Hf-O bite angles. The first kind is the two angles in the periphery of the pentagon of the pentagonal bipyramidal coordination polyhedron and they are approximately 73 °. The other one is at a right angle to the pentagon and is significantly larger at 74.8(2) °. In order to compare the M−Cl bond distances, the reported structures of $Cp_2Zr(C1)(CH_3)$ and $Cp_2(CH_2)_3HfCl_2$ reported by W. E. Hunter *et al.* and Saldarriaga-Molina *et al.* are referenced. These indicate that the Zr−Cl bond distance is 2.476(9) Å and the Hf−Cl bond distance is 2.42 Å respectively which are both in range of the Hf−Cl bond distance of 2.463(2) Å of (**1**).[23,24]

4.5 Conclusion

In order to effectively evaluate the structural data presented above and the significance of these pyronato/ pyridinonato hafnium and zirconium compounds, a comparison of certain structural aspects of the hafnium and zirconium complexes determined crystallographically, need to be taken into consideration. Unfortunately during this study only one hafnium structure was successfully obtained and in literature only the two tropolonato complexes of Zr and Hf are reported as similar chelating systems.[21,22] Specific aspects worth considering are summarized in the following general points with regards to hafnium and zirconium complexes with all the various chelators:[21-28]

➢ Coordination number (extent of coordination) which can translate to various physical properties which can be utilized for separation.

➢ Coordination mode and geometry around the metal centre which is directly influenced by the above wherein two possibilities appear to be prevalent throughout literature for

various bidentate donor chelator systems, *i.e.* square-antiprismatic or dodecahedral which can also translate into factors affecting selectivity or affinity between hafnium and zirconium or physical properties of the complexes.[25-28] The structure reported in this study had a pentagonal bipyramidal coordination geometry with only three bidentate ligands coordinated to the hafnium and one chlorido ligand. This has never been reported before as the coordination number of Hf(IV) is (always) eight.

➢ Nature of specific bond lengths and bite angles: this information can give insights with regards to stability or volatility which can be related to the structures of these complexes. With a variation in chelator donor systems this will eventually give a desired divergence in properties which can be related to chelator systems. In this study two kinds of Hf−O bond distances were noted, these were ~ 2.1 Å and 2.2 Å with two different bite angles for the same chelator which were ~ 73 ˚ and 75 ˚ respectively.

➢ Effective packing which may be influenced by the presence/absence of solvent molecules and may influence the stability of the compounds in the solid state, depending on the separation technique used; this may be a significant and important factor.

Although all the hafnium compounds synthesized in this project were soluble mainly in water or DMSO, only (**1**) was successfully obtained from a chloroform solution; none of the rest could be crystallized successfully. The corresponding zirconium compounds were also mainly soluble in water or DMSO however none of them could be crystallized in these solvents. A solvent mixture of 1:1 chloroform: DCM yielded suitable crystals of the corresponding zirconium compound, however the X-ray data was not good enough and the structure could not be solved successfully.

Nevertheless, although only one complex could be isolated, crystallographically evaluated and described in detail, as reported here, this is considered a success since it proves these ligand systems may stabilize Zr/ Hf and may be further explored on these hard metal centres in future.

Thus, in the next chapter, these ligand systems are explored for application in examples of the *middle* transition elements.

[25] M. Steyn, H. G. Visser, A. Roodt, *Z. Kristallogr. - New Cryst. Struct. 228,* **2013**, *3*, 413.
[26] M. Steyn, H. G. Visser, A. Roodt, *Z. Kristallogr. - New Cryst. Struct. 229*, **2014**, *1*, 67.
[27] M. Steyn, H. G. Visser, A. Roodt, *ActaCryst.* **2012**, *E68,* m1344.
[28] J. A. Viljoen, H. G. Visser, A. Roodt, M. Steyn, *Acta Cryst.* **2009**, *E65,* m1367.

5 Crystallographic Study of *fac*-Re(I)Bis(pyridinonato)tricarbonyl Complexes

5.1 Introduction

In an attempt to synthesize *fac*-[Re^I(O,O'-Bid)(CO)$_3$Br]^n (O,O′-Bid = pyridinone type ligands, n = -2) complexes based on the respective bidentate pyridinone ligands (Section 3.5.1 to 3.5.8) a unique combination of bonding modes was observed which was inherent to five of the ligands, *i.e*., MM(naltol)H, ME(naltol)H, MI(naltol)H, EM(naltol)H and EE(naltol)H (Sections 3.5.2, 3.5.3, 3.5.4, 3.5.6 and 3.5.7 respectively). *fac*-[Re^I(Bid)(CO)$_3$Br] (Bid = bidentate ligand) complexes are commonly used in catalysis, sensing devices and as building blocks in self-assembled metallomacrocycles.[1-5]

In the current work, the normal (accepted in literature) procedure for the synthesis of the bromido complex was followed.[6] However, instead of isolating the mono-bromido complex surprisingly instead the bis(O,O'-Bid)-complex was isolated with one bidentate coordinated ligand and a second bidentate ligand coordinated in a *monodentate* fashion (Scheme 5.1).

To enable better understanding of this interesting phenomenon observed, some additional background and different critical experimental results obtained, specifically with respect to solution behavior, are included here.

[1] M. L. Merlau, M. del Pilar Mejia, S. T. Nguyen, J. T. Hupp, *Angew. Chem. Int. Ed*., **2001**, *113*, 4239.
[2] A. Abou-Hamdan, A. Roodt, A. E. Merbach, *Inorg. Chem.*, **1998**, *37*, 1278.
[3] M. H. Keefe, J. L. O'Donnell, R. C. Bailey, S. T. Nguyen, J. T. Hupp, *Adv. Mater.*, **2003**, *15*, 1936.
[4] G. A. Mines, B.-C. Tzeng, K. G. Stevenson, J. Li, J. T. Hupp, *Angew. Chem. Int. Ed.*, **2002**, *114*, 154.
[5] S.-S. Sun, A. J. Lees, *Coord. Chem. Rev.*, **2002**, *230*, 171.
[6] T. Brasey, A. Buryak, R. Scopelliti, K. Severin, *Eur. J. Inorg. Chem.,* **2004**, 964.
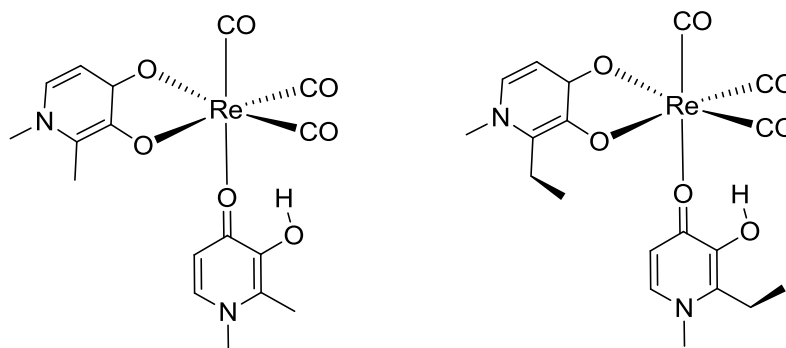
fac-[Re(MM(naltol))(CO)$_3$(MM(naltol)H)] (**2**)   *fac*-[Re(EM(naltol))(CO)$_3$(EM(naltol)H)] (**3**)

Scheme 5.1: Schematic representation of the two crystal structures reported in this chapter.

The infrared spectra of (**2**) and (**3**) are characteristic of a *fac*-[Re(CO)$_3$]$^+$ complex with strong bands in the carbonyl region ($\nu(\mathbf{2})_{CO}$ = 1997, 1848 cm^{-1} and $\nu(\mathbf{3})_{CO}$ = 2001, 1893, 1841). The NMR spectra of (**2**) and (**3**) in CD$_3$OD confirmed the presence of the two pyridinone ligands in each respective case (Figures 5.1 and 5.2). *fac*-[Re(MM(naltol))(CO)$_3$(MM(naltol)H)] (**2**) is stable in solution and does not undergo a methanol solvolysis to form the corresponding solvento species *fac*-[Re(MM(naltol))(CO)$_3$(CH$_3$OH)]. This is clear from the ^{1}H NMR spectra as illustrated in Figure 5.1. The free ligand peaks with chemical shifts denoted by *a-d* do not correspond with any of the chemical shifts in the ^{1}H NMR spectrum of the complex *fac*-[Re(MM(naltol))(CO)$_3$(MM(naltol)H)] indicating that there is no free ligand in solution and confirms that both ligands are coordinated, albeit differently. Since the rhenium metal centre forms two coordination bonds with the bidentate coordinated ligand the chemical shift peaks of this ligand will resonate downfield compared to those of the monodentate coordinated ligand, as this has a more deshielding effect on the respective chemical shifts. These chemical shifts that are more deshielded and denoted by *a'-d'* and those of the monodentate coordinated ligand are denoted by *a"-d"*. The respective integrals are denoted by the symbol ∫ with a number indicating the number of protons of the respective integral. The chemical shifts of the monodentate coordinated ligand are approximately one third of the actual expected value; the reason for this is not clear at this point.

fac-[Re(MM(naltol))(CO)₃(MM(naltol)H)] (2)
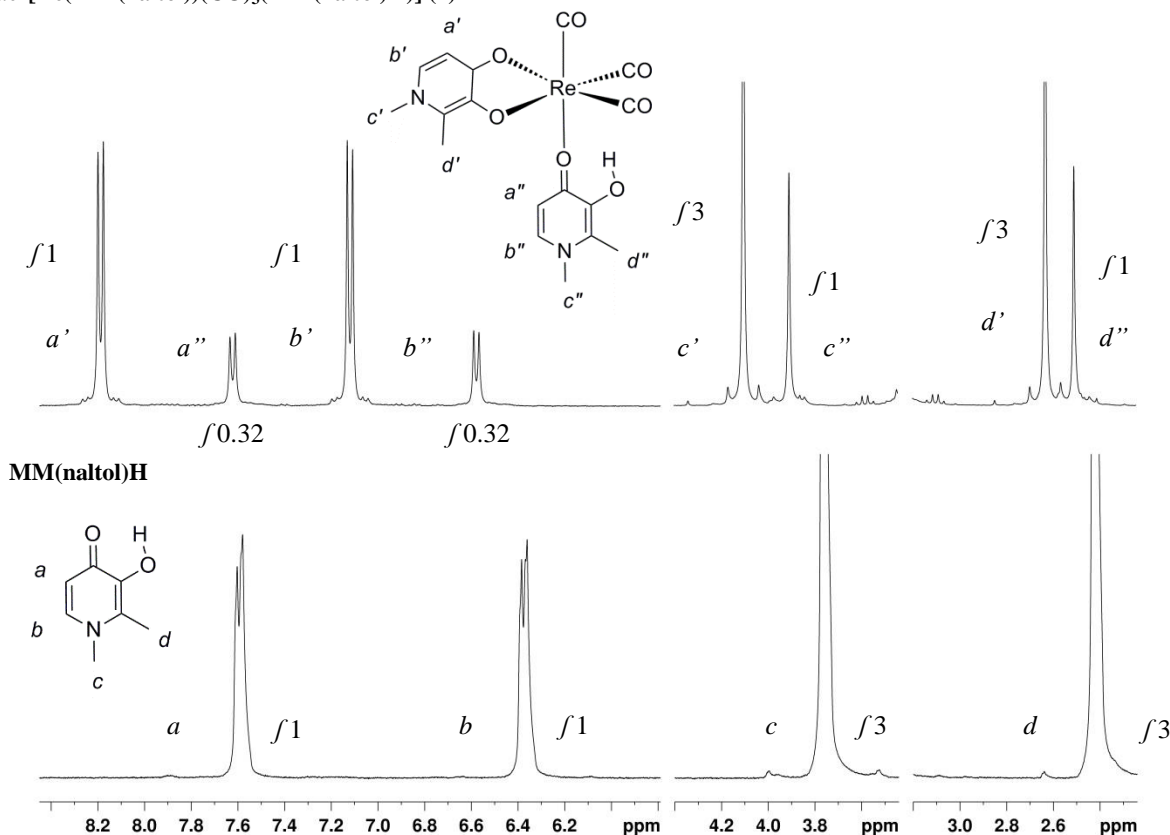
MM(naltol)H

Figure 5.1: ^{1}H NMR (300 MHz) spectra of *fac*-[Re(MM(naltol))(CO)₃(MM(naltol)H)] (2) and MM(naltol)H in CD₃OD respectively. The free ligand chemical shifts are indicated by *a-d*, the bidentate ligand chemical shifts are indicated by *a'-d'* and the mono coordinated bidentate ligand chemical shifts are indicated by *a"-d"*. The symbol ∫ indicates the respective integrals of the chemical shifts.

The ^{1}H NMR spectrum illustrated in Figure 5.2 shows that (**3**) undergoes a methanol solvolysis to give *fac*-[Re(EM(naltol))(CO)₃(CD₃OD)] and the free ligand EM(naltol)H. The free ligand chemical shifts denoted by *a-e* correspond with the chemical shifts in the ^{1}H NMR spectrum of complex (**3**), indicating two compounds in solution; the methanol substituted product and the free ligand. Thus the chemical shifts of the free ligand peaks *a-e* are also present in this spectrum; additionally because the bidentate ligand is still coordinated and more deshielded compared to the free ligand with peaks' and chemical shifts resonating downfield and corresponding with *a"-e"*. The respective integrals are denoted by the symbol ∫ with a number indicating the number of protons of the respective integral. There is however additional peaks in the spectrum that could not be assigned or explained and it appears that perhaps there is still the undissociated form of the complex (**3**) in solution at much lower concentrations that has not undergone a methanol solvolysis.

However, contrary to the solution behavior, the crystal structures clearly indicate that the monoanionic pyridinone derivatives are in a *bidentate* mode coordinated *via* the two oxygen donor atoms to the Re centre (Figure 5.3 and 5.10) and the protonated form is *mono*-coordinated *via* the carbonyl oxygen. This is different from what has been observed for Ru, Pb, Sn, Cu, Zn, Rh, Ir and Fe complexes with these types of ligands.[7-30] To the best of knowledge gathered to date, this is the first structurally characterized macrocyclic *fac*-[Re(CO)$_3$]$^+$ complex exhibiting this combination of coordination modes.

[7] W. Kandioller, C. G. Hartinger, A. A. Nazarov, J. Kasser, R. John, M. A. Jakupec, V. B. Arion, P. J. Dyson, B. K. Keppler, *J. Organomet. Chem.*, **2009**, *694*, 922.

[8] J. H. Kasser, W. Kandioller, C. G. Hartinger, A. A. Nazarov, V. B. Arion, P. J. Dyson, B. K. Keppler, *J. Organomet. Chem.*, **2010**, *695*, 875.

[9] M. Gras, B. Therrien, G. Suss-Fink, P. Štěpnička, A. K. Renfrew, P. J. Dyson, *J. Organomet. Chem.*, **2008**, *693*, 3419.

[10] A. Wu, D. C. Kennedy, B. O. Patrick, B. R. James, *Inorg. Chem.,* **2003**, *42*, 7579.

[11] R. Lang, K. Polborn, T. Severin, K. Severin, *Inorg. Chim. Acta.,* **1999**, *294*, 62.

[12] D. C. Kennedy, A. Wu, B. O. Patrick, B. R. James, *J. Inorg. Biochem.*, **2006**, *100*, 1974.

[13] D. C. Kennedy, A. Wu, B. O. Patrick, B. R. James, *Inorg. Chem.,* **2005**, *44*, 6529.

[14] M. A. Telpoukhovskaia, C. Rodríguez-Rodríguez, L. E. Scott, B. D. G. Page, B. O. Patrick, C. Orvig, *J. Inorg. Biochem.*, **2014**, *132*, 59.

[15] M. C. Barret, P. H. Bhatia, G. Kociok-Koöhn, K. C. Molloy, *Transition Met. Chem.*, **2015**, *40*, 241.

[16] L. E. Scott, B. D. G. Page, B. O. Patrick, C. Orvig, *J. Chem. Soc., Dalton Trans.*, **2008**, 6364.

[17] L. E. Scott, M. Telpoukhovskaia, C. Rodríguez-Rodríguez, M. Merkel, M. L. Bowen, B. D. G. Page, D. E. Green, T. Storr, F. Thomas, D. D. Allen, P. R. Lockman, B. O. Patrick, M. J. Adam, C. Orvig, *Chem. Sci.*, **2011**, *2*, 642.

[18] M. Rangel, A. Leite, A. M. N. Silva, T. Moniz, A. Nunes, M. J. Amorim, C. Queirós, L. Cunha-Silva, P. Gameiro, J. Burgess, *J. Chem. Soc., Dalton Trans.*, **2014**, *43*, 9722.

[19] A. El-Jammal, P. L. Howell, M. A. Turner, N. Li, D. M. Templeton, *J. Med. Chem.*, **1994**, *37*, 46.

[20] D. E. Green, M. L. Bowen, L. E. Scott, T. Storr, M. Merkel, K. Bohmerle, K. H. Thompson, B. O. Patrick, H. J. Schugar, C. Orvig, CCDC 746850: Experimental Crystal Structure Determination, 2014, DOI: 10.5517/cct24yy

[21] M. A. Telpoukhovskaia, C. Rodríguez-Rodríguez, J. F. Cawthray, L. E. Scott, B. D. G. Page, J. Alí-Torres, M. Sodupe, G. A. Bailey, B. O. Patrick, C. Orvig, *Metallomics*, **2014**, *6*, 249.

[22] E. T. Clarke, A. E. Martell, J. Reibenspies, *Inorg. Chim. Acta.,* **1992**, *196,* 177.

[23] T. F. Tam, R. Leung-Toung, Y. Wang, M. Spino, G. Williams, A. J. Lough, *Acta Cryst. Sect. E*, **2005**, *E61*, m2055.

[24] P. S. Dobbin, R. C. Hider, A. D. Hall, P. D. Taylor, P. Sarpong, J. B. Porter, G. Xiao, D. van der Helm, *J. Med. Chem.*, **1993**, *36*, 2448.

[25] G. Xiao, D. van der Helm, R. C. Hider, P. S. Dobbin, *J. Chem. Soc., Dalton Trans.*, **1992**, 3265.

[26] S. I. Ahmed, J. Burgess, J. Fawcett, S. A. Parsons, D. R. Russell, S. H. Laurie, *Polyhedron*, **2000**, *19*, 129.

[27] M. L. Merlau, M. del Pilar Mejia, S. T. Nguyen, J. T. Hupp, *Angew. Chem. Int. Ed.*, **2001**, *113*, 4239. A. Abou-Hamdan, A. Roodt, A. E. Merbach, *Inorg. Chem.*, **1998**, *37*, 1278.

[28] M. H. Keefe, J. L. O'Donnell, R. C. Bailey, S. T. Nguyen, J. T. Hupp, *Adv. Mater.*, **2003**, *15*, 1936.

[29] G. A. Mines, B.-C. Tzeng, K. G. Stevenson, J. Li, J. T. Hupp, *Angew. Chem. Int. Ed.*, **2002**, *114*, 154.

[30] S.-S. Sun, A. J. Lees, *Coord. Chem. Rev.*, **2002**, *230*, 171.

Figure 5.2: ^{1}H NMR (300 MHz) spectra of *fac*-[Re(EM(naltol))(CO)$_3$(EM(naltol)H)] (3) and EM(naltol)H in CD$_3$OD. The spectrum of (3) shows two compounds namely; *fac*-[Re(EM(naltol))(CO)$_3$(CD$_3$OD)] and EM(naltol)H respectively. The free ligand chemical shifts are indicated by *a-e*, the bidentate ligand chemical shifts are indicated by *a"-e"*. The symbol ∫ indicates the respective integrals of the chemical shifts.

Another research question that emanated from the isolation of these kinds of compounds was whether the same compounds could be synthesized from the corresponding aqua synthon *fac*-[Re(CO)$_3$(H$_2$O)$_3$]$^+$. To answer this, two similar reactions were carried out based on the aqua synthetic procedure (see Section 3.7). In both cases the rhenium: ligand ratios were changed to 1:2. One of the reactions was refluxed and one was stirred at room temperature. The refluxed sample yielded a variety of by products which could not be separated, while the room temperature sample yielded the aqua complex with slightly higher yields than normal. From this it was concluded that these compounds could not be synthesized from the aqua synthetic procedure (at least under the conditions utilized) and can only be successfully synthesized from the bromido starting complex *fac*-[NEt$_4$]$_2$[ReBr$_3$(CO)$_3$].

5.2 Experimental

The reflection data of (**2**) and (**3**) was collected on a Bruker X8 Apex II 4K Kappa CCD diffractometer using graphite monochromated Mo Kα radiation (λ= 0.70926 Å) with ω- and φ-scans at 100(2) K. The Apex II software package was utilized along with the optimum measurement method in collecting more than a hemisphere of reciprocal space as predicted by COSMO.[31,32] Frame integration and data reduction was performed using the SAINT-Plus and XPREP software packages and SADABS was used for multi-scan absorption correction.[33,34] The structures were solved using direct methods package SIR97 and refined using the WinGX software incorporating SHELXL.[35-41] All atoms were refined anisotropically with the exception of hydrogen atoms. The hydrogen atoms were positioned geometrically and refined utilizing a riding model with fixed C-H distances of 0.95 Å (CH) [$U_{iso}(H) = 1.2\ U_{eq}$] for aromatic hydrogens, 0.98 Å (CH) [$U_{iso}(H) = 1.2\ U_{eq}$] for methylene H-atoms and 0.96 Å (CH) [$U_{iso}(H) = 1.2\ U_{eq}$] for methyl H-atoms. Molecular diagrams were generated with DIAMOND with 50 % probability ellipsoids for all non-hydrogen atoms.[42] General crystal data and refinement parameters are represented in Table 5.1 with the complete list of atomic coordinates, equivalent isotropic parameters and hydrogen coordinates given in Appendix A.

[31] **Apex2**, Version 2012.10-0, Bruker AXS Inc.,Madison, Wisconsin, USA, **2012**.

[32] **COSMO**, Version 1.48, Bruker AXS Inc., Madison, Wisconsin, USA, **2003**.

[33] **SADABS**, Version 2012/1, BrukerAXS Inc, Madison, Wisconsin, USA, **2012**.

[34] **SAINT-Plus**, Version 8.27B including XPREP, Bruker AXS Inc., Madison, Wisconsin, USA, **2012**.

[35] A. Altomare, G. Cascarano, C. Giacovazzo, A. Guagliardi, M. C. Burla, G. Polidori, M. Camalli, *J. Appl. Cryst.*, **1994**, *27*, 435.

[36] A. Altomare, M. C. Burla, M. Camalli, G. L. Cascarano, C. Giacovazzo, A. Guagliardi, A. G. G. Moliterni, G. Polidori, R. Spagna, *J. Appl. Cryst.*, **1999**, *32*, 115.

[37] M. C. Burla, M. Camalli, B. Carrozzini, G. L. Cascarano, C. Giacovazzo, G. Polidori, R. Spagna, *J. Appl. Cryst.*, **2003**, *36*, 1103.

[38] P. T. Beurskens, G. Admiraal, G. Beurskens, W. P. Bosman, S. Garcia-Granda, R. O. Gould, J. M. M. Smits, C. Smykalla, Crystallography Laboratory, University of Nijmegen, Toernooiveld, The Netherlands.

[39] L. Palatinus, G. Chapuis, *J. Appl. Cryst.*, **2007**, *40*, 786.

[40] **WinGX**. L. J. Farrugia, *J. Appl. Cryst.*, **2012**, *45*, 849.

[41] G. M. Sheldrick, *Acta Cryst.*, **2008**, *A64*, 112.

[42] K. Brandenburg, H. Putz, DIAMOND, Release 3.0e, Crystal Impact GbR, Bonn, Germany, **2006**.

Table 5.1: General X-ray crystallographic data and refinement parameters for *fac*-[Re(MM(naltol))(CO)$_3$(MM(naltol)H)] (2) and *fac*-[Re(EM(naltol))(CO)$_3$(EM(naltol)H)] (3).

Crystallographic data	(**2**)	(**3**)
Empirical formula	C$_{17}$H$_{17}$N$_2$O$_7$Re	C$_{41}$H$_{42}$N$_4$O$_{15}$Re$_2$
Formula weight (g.mol^{-1})	547.54	1203.21
Temperature (K)	100(2)	100(2)
Crystal system	Monoclinic	Triclinic
Space group	$P2_1/c$	$P\bar{1}$
a (Å)	7.387(1)	9.845(1)
b (Å)	15.703(3)	10.546(1)
c (Å)	15.770(3)	10.979(1)
α (°)	90	87.670(3)
β (°)	98.920(6)	85.446(3)
γ (°)	90	68.572(3)
Volume (Å^3)	1807.2(5)	1057.7(2)
Z	4	2
$\rho_{calc.}$ (g.cm^{-3})	2.012	1.889
Crystal colour	Yellow	Yellow
Crystal morphology	Cuboid	Cuboid
Crystal size (mm^3)	0.277 x 0.12 x 0.104	0.396 x 0.19 x 0.146
μ (mm^{-1})	6.767	5.792
F(000)	1056.0	586.0
θ range (°)	4.169 to 27.998	4.951 to 28.000
Index ranges	-8 ≤ h ≤ 9	-13 ≤ h ≤ 13
	-20 ≤ k ≤ 20	-9 ≤ k ≤ 13
	-20 ≤ l ≤ 19	-14 ≤ l ≤ 14
Reflections collected	35608	19985
Unique reflections	4358	5104
Reflections with I > 2σ(I)	9620	9891
R$_{int}$	0.0521	0.0502
Completeness to θ (°; %)	25.24, 99.3	25.24, 98.9
Data/restraints/parameters	4336 / 0 / 249	5057 / 18 / 293
GooF	1.092	1.093
R [I>2σ(I)]	R$_1$ = 0.0193	R$_1$ = 0.0204
	wR$_2$ = 0.0420	wR$_2$ = 0.0515
R (all data)	R$_1$ = 0.0226	R$_1$ = 0.0213
	wR$_2$ = 0.0434	wR$_2$ = 0.0521
ρ_{max}, ρ_{min} (e.Å^{-3})	0.650 and -1.057	0.720 and -1.043

5.3 Crystal structure of *fac*-[Re(MM(naltol))(CO)₃(MM(naltol)H)] (2)

The complex, *fac*-[Re(MM(naltol))(CO)$_3$(MM(naltol)H)] (**2**) has been synthesized as described in the synthesis section (Paragraph 3.5.2). The yellow cuboidal crystals were obtained from a DMSO solution of the product. This complex crystallized in the monoclinic $P2_1/c$ space group with four independent molecules in the unit cell (Z = 4). In the structure of *fac*-[Re(MM(naltol))(CO)$_3$(MM(naltol)H)] (**2**) the Re atom is octahedrally surrounded by three facially orientated carbonyl ligands, one mono-anionic bidentate coordinated ligand and a second neutral bidentate ligand coordinated in a monodentate fashion. The bidentate coordinated ligand carries a mono-negative charge as it loses a proton, while the monodentate coordinated bidentate ligand is neutral and still has a hydroxyl functional group (crystallographically confirmed, see Figure 5.3 below). This was also confirmed in solution, see Paragraph 5.1. A summary of the general interatomic bond distances and angles are given in Table 5.2 while the numbering scheme of the neutral molecule is shown in Figure 5.3.
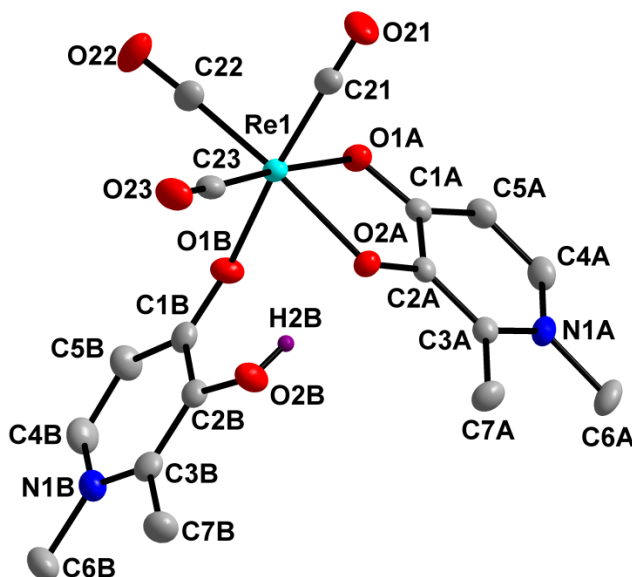
Figure 5.3: Molecular representation of *fac*-[Re(MM(naltol))(CO)₃(MM(naltol)H)] (2) showing the atom numbering scheme, displacement ellipsoids are drawn at 50 % probability level. Hydrogen atoms are omitted for clarity except for the hydroxyl hydrogen (H2B).

Table 5.2: Selected bond distances (Å) and angles (°) for the crystal structure of (2).

Bond	Bond distance (Å)	Bond angle (atoms)	Bond angle (°)
O(1A)-Re(1)	2.140(2)	O(2A)-Re(1)-O(1A)	77.56(7)
O(1B)-Re(1)	2.168(2)	C(22)-Re(1)-C(23)	86.36(12)
O(2A)-Re(1)	2.1316(19)	C(22)-Re(1)-O(1A)	99.18(10)
C(21)-Re(1)	1.901(3)	C(23)-Re(1)-O(2A)	97.05(10)
C(22)-Re(1)	1.905(3)	C(21)-Re(1)-O(1B)	172.49(2)
C(23)-Re(1)	1.901(3)	O(21)-C(21)-Re(1)	179.1(3)
C(1)-O(1)	1.143(4)	C(21)-Re(1)-C(23)	86.93(12)
C(2)-O(2)	1.153(4)	C(22)-Re(1)-C(21)	89.84(13)
C(3)-O(3)	1.157(4)	C(21)-Re(1)-O(2A)	97.24(11)
C(1A)-O(1A)	1.291(3)	C(21)-Re(1)-O(1A)	92.16(10)
C(1B)-O(1B)	1.277(3)	C(23)-Re(1)-O(1B)	100.38(10)
		O(1A)-Re(1)-C(23)	174.38(10)
		O(2A)-Re(1)-C(22)	172.28(11)

All the bond distances and angles are within normal ranges compared to similar structures.[43-56] The Re−C bond distances of the three facial carbonyl groups are ~ 1.9 Å. The Re−O bond distances are ~ 2.14 Å, the longest being Re(1)−O1B (2.168(2) Å) possibly because of the electron density on the double bond and the lone pair on the oxygen atom (O1B). However, there is seemingly no significant resultant *trans* influence due to this monodentate mode of coordination as all the Re−C bond distances are approximately equal. Furthermore, the Re(1)−O(1B) bond distance falls within the same range as the Re−O bond distances found in similar rhenium complexes which have undergone methanol solvation as well as aqua complexes (~ 2.2 Å).[43-57] The bidentate coordinated ligand has a bite angle O(1A)-Re(1)-O(2A) of 77.56(7)

[43] M. Sánchez-Lozano, E. M. Vázquez-López, J. M. Hermida-Ramón, C. M. Estévez, *Polyhedron*, **2011**, *30*, 953.
[44] J. Mukiza, E. C. Hosten, T. I. A. Gerber, *Polyhedron*, **2015**, *98*, 251.
[45] S. Mundwiler, M. Kündig, K. Ortner, R. Alberto, *J. Chem. Soc. Dalton Trans.*, **2004**, 1320.
[46] T. R. Hayes, B. B. Kasten, C. L. Barnes, P. D. Benny, *Dalton Trans.*, **2014**, *43*, 6998.
[47] M. Schutte, A. Roodt, H. G. Visser, *Inorg. Chem.*, **2012**, *51*, 11996.
[48] M. Schutte, G. Kemp, H. G. Visser, A. Roodt, *Inorg. Chem.*, **2011**, *50*, 12486.
[49] F. Ragone, G. T. Ruiz, O. E. Piro, G. A. Echeverría, F. M. Cabrerizo, G. Petroselli, R. Erra-Balsells, K. Hiraoka, F. S. García Einschlag, E. Wolcan, *Eur. J. Inorg. Chem.*, **2012**, 4801.
[50] M. Schutte, H. G. Visser, A. Roodt, *Acta Cryst. Sect. E*, **2008**, *E64*, m1610.
[51] K. O. Piletska, K. V. Domasevitch, A. V. Shtemenko, *Acta Cryst. Sect. E*, **2016**, *E72*, 590.
[52] A. Brink, H. G.Visser, A. Roodt, *J. Coord. Chem.*, **2011**, *64*, 122.
[53] A. Brink, H. G.Visser, A. Roodt, CCDC 801586: Experimental Crystal Structure Determination, **2014**, DOI: 10.5517/ccvx3mg
[54] A. Brink, H. G. Visser, A. Roodt, *Inorg. Chem.*, **2013**, *52*, 8950.
[55] B. Shankar, P. Elumalai, R. Shanmugam, V. Singh, D. T. Masram, M. Sathiyendiran, *Inorg. Chem.*, **2013**, *52*, 10217.
[56] A. Brink, H. G. Visser, A. Roodt, *Inorg. Chem.*, **2014**, *53*, 12480.
[57] M. Schutte, H. G. Visser, A. Roodt, Acta Cryst., **2008**, *E64*, m1610.

° which is larger than that of similar structures of tropolone and tribromotropolone (74.82(17) ° and 74.07(16) ° respectively).[47,50]

The octahedral polyhedron around the rhenium atom is distorted with angles ranging from 77.55(1) ° to 179.1(3) °. The three axes through the vertices of the distorted octahedron are nonlinear and range from 172.28(11) ° to 174.38(10) °. The C23-O23 axis lies in the plane deviating slightly upwards in contrast to the C22-O22 axis which is more distorted and lies below the equatorial plane hence further substantiating the distortions in the octahedron of the structure. The C(21)-Re(1)-O(1B) angle is 172.49(2) ° also indicating that there is a distortion in the structure from the vertical axis through the Re centre (see Figure 5.4). The neutral monodentate coordinated ligand is flat in contrast to the bidentate ligand which is slightly bent downwards out of the equatorial plane (see Figure 5.4).
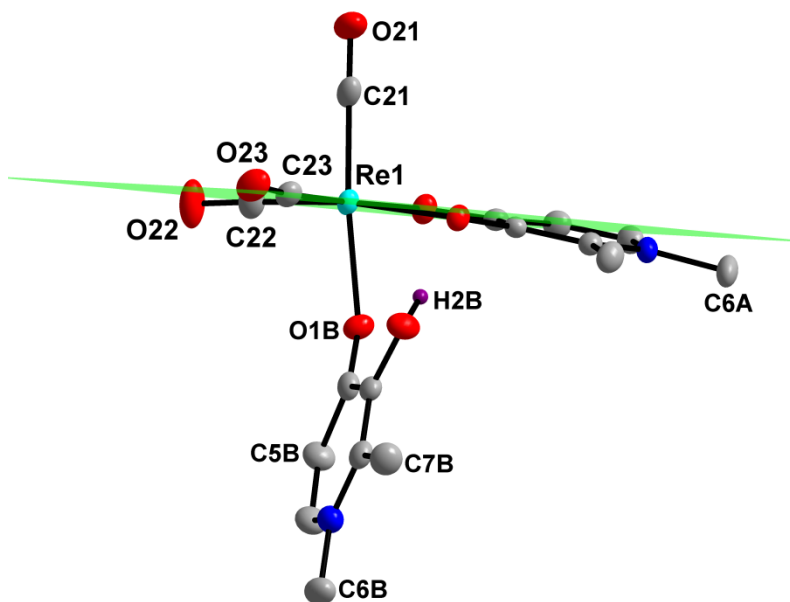
Figure 5.4: Illustration of the equatorial plane (C23 O2A O1A C22 Re1) showing the bidentate coordinated ligand bending out of the plane. Hydrogen atoms are omitted for clarity except for the hydroxyl hydrogen (H2B).

The dihedral angle between the equatorial plane (C23 O2A O1A C22 Re1) and the ring of the bidentate coordinated pyridinone ligand (C1A C2A C3A N1A C4A C5A) is only 7.58(1) ˚ (see Figure 5.5 below). The bending of the bidentate ligand results in the torsion angle of the coordination site O(1A)-C(1A)-C(2A)-O(2A) equal to 4.10(4) ˚.
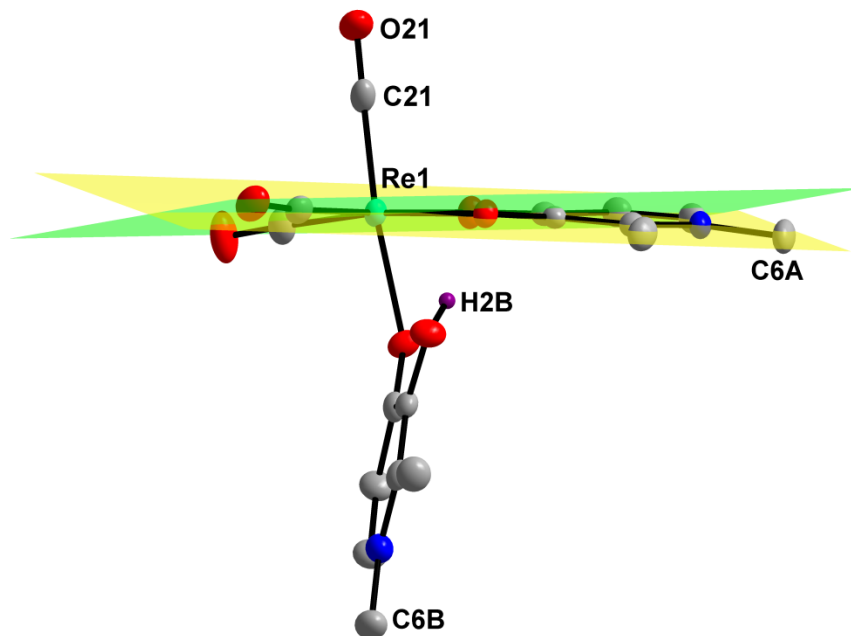
Figure 5.5: Illustration of the dihedral angle between the equatorial plane (C23 O2A O1A C22 Re1) and the plane through the heterocycle of the bidentate coordinated ligand (C1A C2A C3A N1A C4A C5A).

The monodentate coordinated ligand is close to planar and this is illustrated by the small deviations of all the atoms from the plane through the cyclic part of the pyridinone structure. The largest deviation is 0.0124(2) Å for C1B, in contrast to the bidentate coordinated ligand, where the largest is 0.0226(3) Å for C1A. The torsion angle of the bidentate coordination site O(1B)-C(1B)-C(2B)-O(2B) is only 1.08(4) ˚; with the numerical difference between the two torsion angles O(1)-C(1)-C(2)-O(2) on the two ligands being 3.02(6) ˚. The monodentate coordinated ligand lies in a plane that forms a dihedral angle of 77.899(8) ˚ with the equatorial plane, see Figure 5.6 below, also showing the planarity of the monodentate coordinated ligand and the distortion in the vertical axis of the structure.
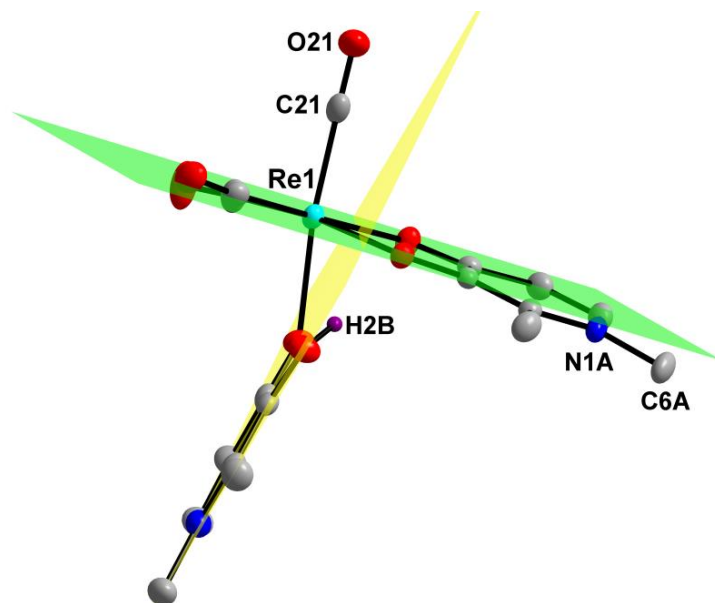
Figure 5.6: Illustration of the dihedral angle between the equatorial plane (C23 O2A O1A C22 Re1) and the plane through the heterocycle of the monodentate coordinated ligand (C1B C2B C3B N1B C4B C5B).

Seven hydrogen interactions are observed in this structure; four intra-molecular (two O-H…O and two C-H…O, represented by light purple fragmented bonds) with H2B a bifurcated O-H…O hydrogen interaction and three inter-molecular (all C-H…O interactions, represented by green fragmented bonds) hydrogen interactions. These hydrogen interactions are illustrated in Figure 5.7, while the distances, angles and symmetry operators are given in Table 5.3.
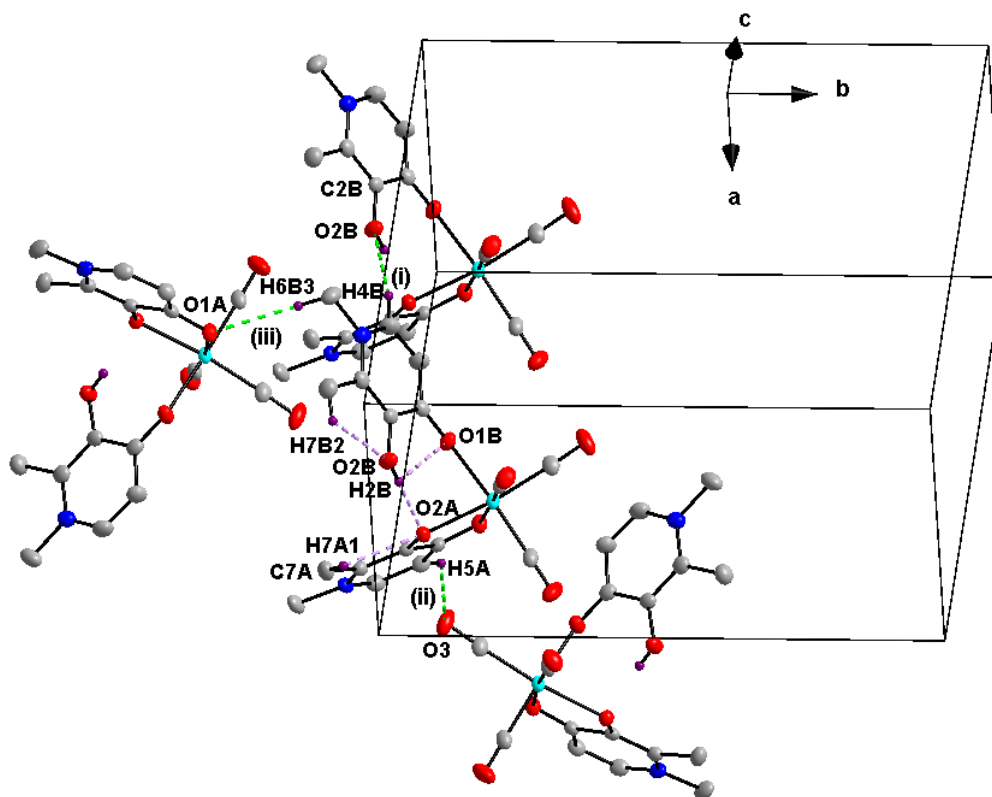
Figure 5.7: Hydrogen interactions observed in the structure of *fac*-[Re(MM(naltol))(CO)$_3$(MM(naltol)H)] (2).

Table 5.3 Summary of the hydrogen interactions, distances (Å) and angles (°) observed in (2).

D-H…A	d(D-H) (Å)	d(H…A) (Å)	d(D…A) (Å)	⊾ (D-H…A)(°)
O2B-H2B...O1B	0.82	2.46	2.8322	109
O2B-H2B...O2A	0.82	1.85	2.6579	170
C4B-H4B...O2B [(i)]	0.93	2.45	3.3505	163
C5A-H5A...O3 [(ii)]	0.93	2.56	3.2276	129
C6B-H6B3...O1A [(iii)]	0.96	2.54	3.4979	177
C7A-H7A1...O2A	0.96	2.45	2.8651	106
C7B-H7B2...O2B	0.96	2.36	2.8059	108

Symmetry codes, transformations used to generate equivalent atoms: (i) -x,1-y,1-z; (ii) x,-1+y,z; (iii) x, 1/2-y, z-1/2

The molecules in the layer **A** pack in a parallel manner to the second layer **A** along the *bc*-plane with a second alternating orientation in between (layer **B**), both layers have two units overlapping at the bidentate heterocycles (**ABA**). This packing array is stabilized by C-H…O inter-molecular interactions (Figure 5.8).
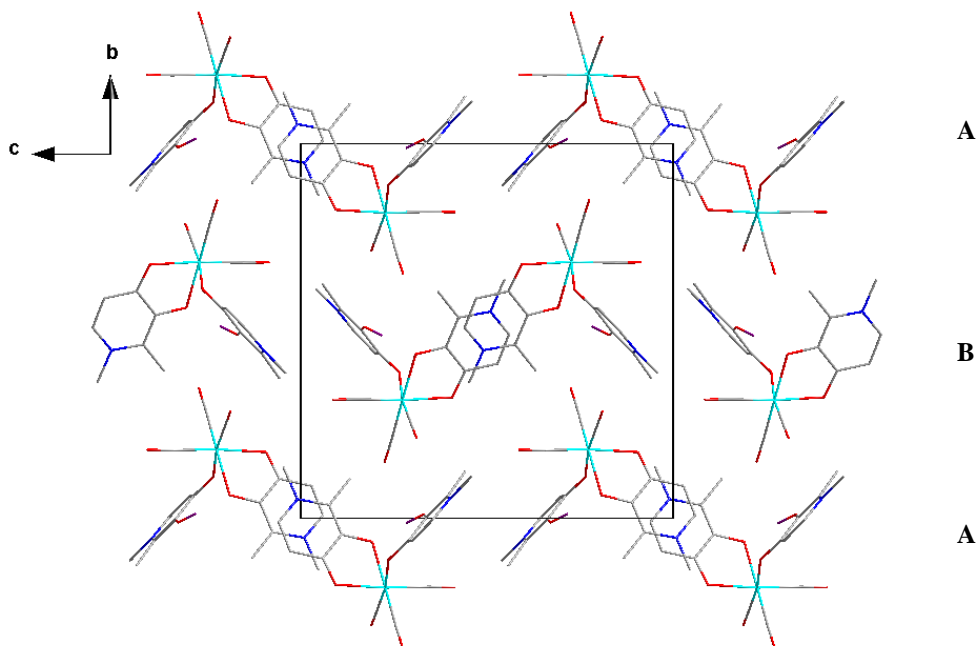
Figure 5.8: Crystal packing of (2) in the unit cell, viewed along the *a*-axis. Hydrogen atoms are omitted for clarity.

5.4 Crystal structure of *fac*-[Re(EM(naltol))(CO)₃(EM(naltol)H)] (3)

The complex, *fac*-[Re(EM(naltol))(CO)$_3$(EM(naltol)H)] (**3**) has been synthesized as described in the synthesis section (Paragraph 3.5.6). The yellow cuboidal crystals were obtained from a DMSO solution of the product. This complex crystallized in the triclinic $P\bar{1}$ space group with one independent molecule in the asymmetric unit (Z = 2). The Flack parameter is 0.004(3) which indicates that the absolute configuration of the structure was correctly assigned. The large number of restraints is mainly due to the omission of outliers, as suggested by the cifcheck. In the structure of *fac*-[Re(EM(naltol))(CO)$_3$(EM(naltol)H)] (**3**) the Re atom is octahedrally surrounded by three facially orientated carbonyl ligands, one mono-anionic bidentate coordinated ligand and a second bidentate neutral ligand, coordinated as in (**2**), in a *mono*dentate fashion. The bidentate coordinated ligand carries a mono negative charge as it loses a proton, while the monodentate coordinated bidentate ligand is neutral and still has a hydroxyl functional group (crystallographically confirmed, see Figure 5.9 below). This was also confirmed in

solution, see Paragraph 5.1. A summary of the general interatomic bond distances and angles are given in Table 5.4 while the numbering scheme of the neutral molecule is shown in Figure 5.9.
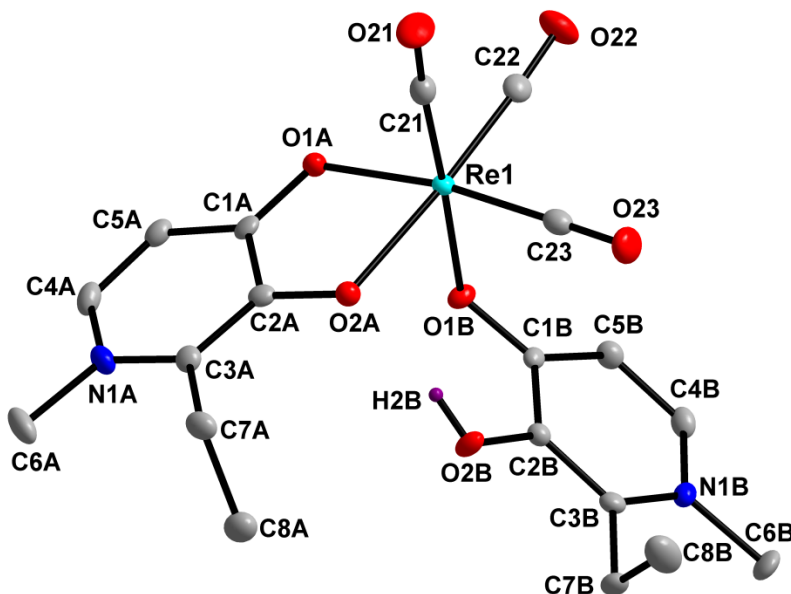
Figure 5.9: Molecular representation of *fac*-[Re(EM(naltol))(CO)₃(EM(naltol)H)] (3) showing the atom numbering scheme, displacement ellipsoids are drawn at 50 % probability level. Hydrogen atoms are omitted for clarity except for the hydroxyl hydrogen (H2B).

Table 5.4: Selected bond distances (Å) and angles (°) for the crystal structure of (3).

Bond	Bond distance (Å)	Bond angle (atoms)	Bond angle (°)
O(1A)-Re(1)	2.124(2)	O(2A)-Re(1)-O(1A)	77.45(7)
O(1B)-Re(1)	2.174(2)	C(22)-Re(1)-C(23)	89.25(12)
O(2A)-Re(1)	2.141(2)	C(22)-Re(1)-O(1A)	95.49(10)
C(21)-Re(1)	1.885(3)	C(23)-Re(1)-O(2A)	97.47(10)
C(22)-Re(1)	1.900(3)	C(21)-Re(1)-O(1B)	177.85(2)
C(233)-Re(1)	1.911(3)	O(21)-C(21)-Re(1)	176.4(3)
C(21)-O(21)	1.169(4)	C(21)-Re(1)-C(23)	87.26(12)
C(22)-O(22)	1.156(3)	C(22)-Re(1)-C(21)	86.22(13)
C(23)-O(23)	1.153(3)	C(21)-Re(1)-O(2A)	99.60(11)
C(1A)-O(1A)	1.295(3)	C(21)-Re(1)-O(1A)	97.44(11)
C(1B)-O(1B)	1.304(3)	C(23)-Re(1)-O(1B)	94.00(10)
		O(1A)-Re(1)-C(23)	171.88(9)
		O(2A)-Re(1)-C(22)	172.47(9)

All the bond distances and angles are within normal range compared to similar structures.[43-56] The Re−C bond distances of the three facial carbonyl groups are ~ 1.9 Å, with only the Re(1)−C(21) bond distance slightly shorter (1.885(3) Å) which might be due to the *trans* influence of the monodentate ligand. The Re−O bond distances are ~ 2.1 Å, the longest being Re(1)−O(1B) (2.1742(7) Å) possibly because of the electron density on the double bond and the lone pair on the oxygen atom (O1B). Furthermore, the Re(1)−O(1B) bond distance falls within the same range as the Re−O bond distances found in the methanol solvated rhenium complexes and the aqua complexes (~ 2.2 Å).[43-56] The bidentate coordinated ligand has a bite angle O(1A)-Re(1)-O(2A) of 77.45(2) ˚ which is larger than that of similar structures of tropolone and tribromotropolone (74.82(17) ˚ and 74.07(16) ˚ respectively).[47,50] However this bite angle is within esd's identical to the bite angle of (**2**).

The octahedral polyhedron around the rhenium atom is distorted with angles ranging from 77.45(2) ˚ to 177.85(2) ˚ which is slightly larger in terms of range compared to (**2**). The three axes through the vertices of the octahedral system are nonlinear and range from 171.88(9) ˚ to 176.4(3) ˚. The C22-O22 and the C23-O23 axis both lie in the plane deviating slightly in contrast to the same axis in (**2**), which is more distorted. The angle C(21)-Re(1)-O(1B) is 177.85(2) ˚ also indicating that there is a distortion in the structure from the vertical axis through the Re centre. The monodentate ligand is flat in contrast to the bidentate ligand which is slightly bent downwards out of the equatorial plane (Figure 5.10).
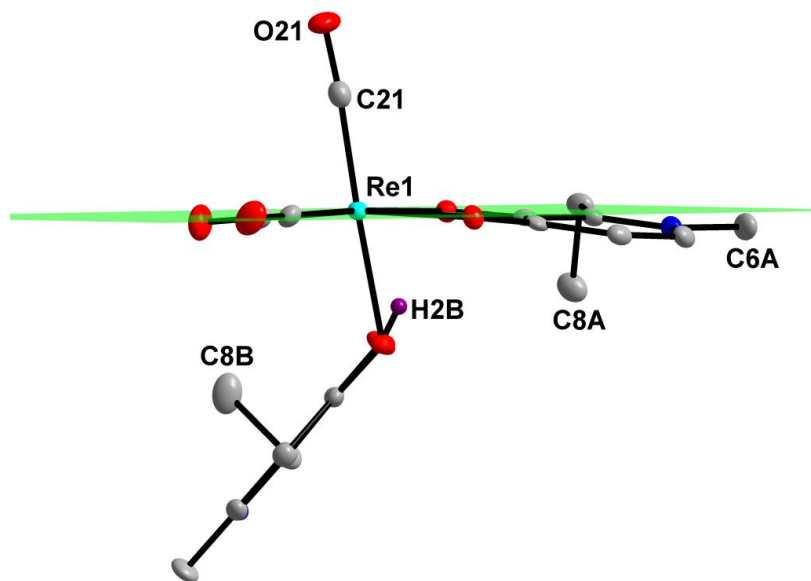
Figure 5.10: Illustration of the equatorial plane (C23 O2A O1A C22 Re1) showing the bidentate coordinated ligand bending out of the plane. Hydrogen atoms are omitted for clarity except for the hydroxyl hydrogen (H2B).

The dihedral angle between the equatorial plane (C23 O2A O1A C22 Re1) and the ring of the bidentate coordinated pyridinone ligand (C1A C2A C3A N1A C4A C5A) is 7.113(7) ˚ (Figure 5.11). The bending of the bidentate ligand results in the torsion angle of the coordination site O(1A)-C(1A)-C(2A)-O(2A) equal to 3.70(6) ˚ which is slightly smaller compared to (**2**).
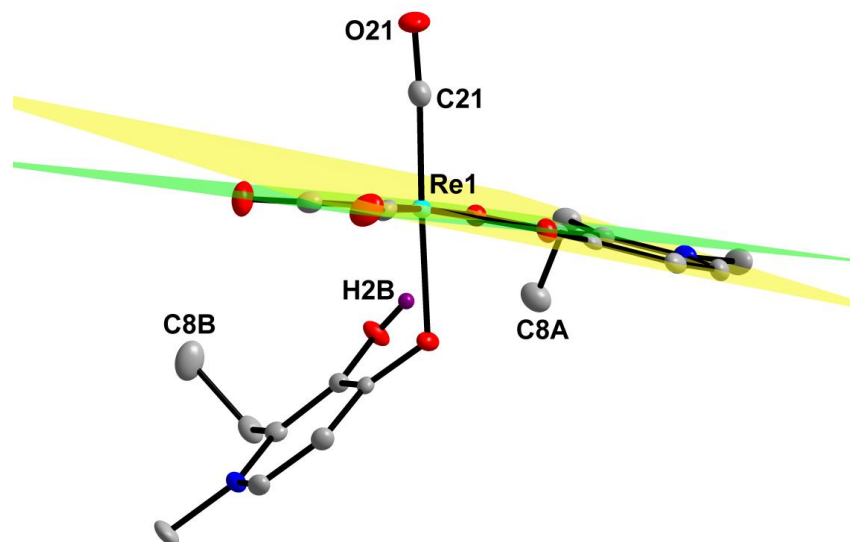
Figure 5.11: Illustration of the dihedral angle between the equatorial plane (C23 O2A O1A C22 Re1) and the plane through the heterocycle of the bidentate coordinated ligand (C1A C2A C3A N1A C4A C5A).

The planarity of the monodentate ligand is illustrated by the small deviations of all the atoms from the plane through the cyclic part of the pyridinone structure (C1B C2B C3B N1B C4B C5B). The largest deviation is 0.0124(4) Å for C2B, in contrast to the bidentate coordinated ligand where the largest deviation is 0.0257(4) Å for C2A. The torsion angle of the bidentate coordination site O(1B)-C(1B)-C(2B)-O(2B) is 1.36(6) ˚, while the numerical difference between the two torsion angles O(1)-C(1)-C(2)-O(2) on the two ligands is only 2.34(8) ˚. The monodentate coordinated ligand lies in a plane that forms a dihedral angle of 48.693(4) ˚ with the equatorial plane (Figure 5.12), with the planarity of the monodentate coordinated ligand and the distortion in the vertical axis of the structure also illustrated in Figure 5.12. Compared to (**2**) the monodentate coordinated ligand is less vertical by some 14.7 ˚; obtained by simply measuring the angle Re(1)-O(1B)-C(1B).
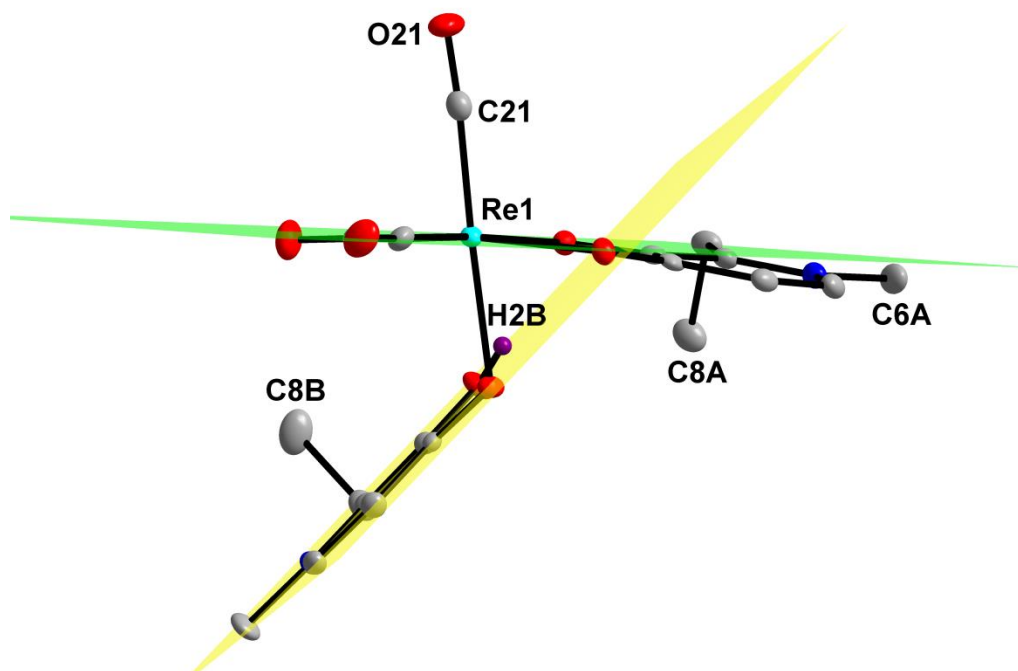
Figure 5.12: Illustration of the dihedral angle between the equatorial plane (C23 O2A O1A C22 Re1) and the plane through the heterocycle of the monodentate coordinated ligand (C1B C2B C3B N1B C4B C5B).

Eight hydrogen interactions are observed in this structure; four intra-molecular (two O-H…O and two C-H…O, represented by light purple fragmented bonds) with H2B a bifurcated O-H…O hydrogen interaction and four inter-molecular (all C-H…O interactions, represented by green fragmented bonds) hydrogen interactions. These hydrogen interactions are illustrated in Figure 5.13, while the distances, angles and symmetry operators are given in Table 5.5.
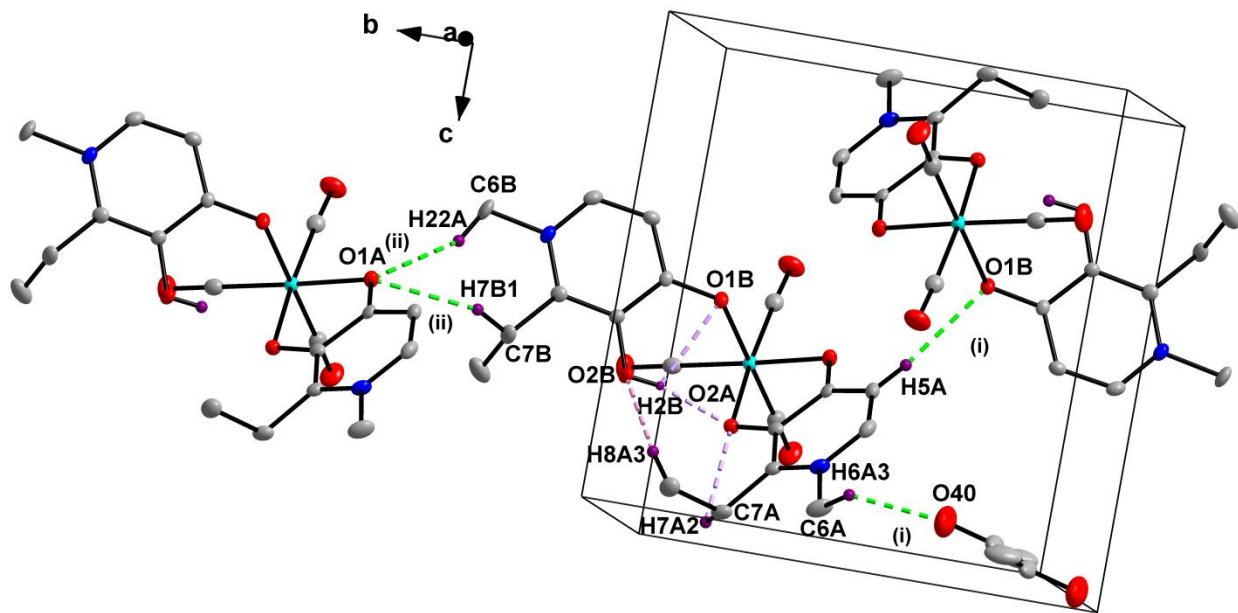
Figure 5.13: Hydrogen interactions observed in the structure of *fac*-[Re(EM(naltol))(CO)₃(EM(naltol)H)] (3).

Table 5.5: Summary of the hydrogen interaction, distances (Å) and angles (°) observed in (3).

D-H…A	d(D-H) (Å)	d(H…A) (Å)	d(D…A) (Å)	﹂ (D-H…A)(°)
O2B-H2B...O1B	0.82	2.38	2.788(3)	112
O2B-H2B...O2A	0.82	1.88	2.683(3)	167
C8A-H8A3...O2B	0.96	2.57	3.483(4)	159
C7A-H7A2...O2A	0.97	2.53	2.866(4)	101
C5A-H5A...O1B [(i)]	0.93	2.54	3.460(4)	173
C6A-H6A3...O40 [(i)]	0.96	2.20	2.871(6)	126
C7B-H7B1...O1A[(ii)]	0.97	2.51	3.413(4)	155
C6B-H22A...O1A[(ii)]	0.96	2.52	3.400(4)	153

Symmetry codes, transformations used to generate equivalent atoms: (i) -x, 1-y, 1-z; (ii) x, y-1, +z;

The molecules in the layer **A** pack in a parallel manner to the second layer **A** along the *ac*-plane with alternating orientations in between orientated at 180 ° (layer **B**), (**ABA**) stabilized by inter-molecular C-H…O interactions (Figure 5.14).
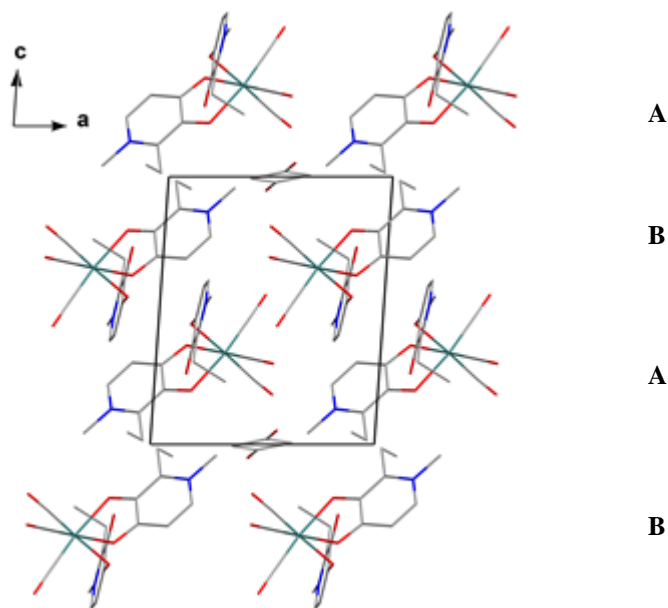
Figure 5.14: Crystal packing of (3) in the unit cell, viewed along the *a*-axis. Hydrogen atoms are omitted for clarity.

5.5 Discussion

Three similar rhenium structures with O,O'-bidentate ligands coordinated to the rhenium centre are compared here to (**2**) and (**3**) to highlight some structural properties and to correlate some structural data between the different complexes (see Figure 5.15 and Table 5.6).
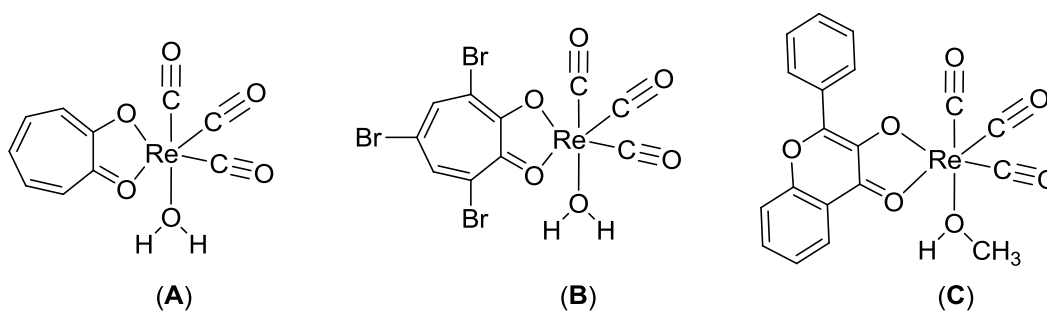
Figure 5.15: Illustration of the crystal structures of *fac*-[Re(Trop)(CO)$_3$(H$_2$O)] (A), *fac*-[Re(TropBr$_3$)(CO)$_3$(H$_2$O)] (B) and *fac*-[Re(Flav)(CO)$_3$(CH$_3$OH)] (C).

Table 5.6: Selected bond distances and angles of *fac*-[Re(O,O'-bidentate)(CO)₃(O,O'-monodentate)] complexes.

Complexes					
Formula	**(2)** [a]	**(3)** [a]	[Re(Trop)(H₂O)] (A) [b]	[Re(TropBr₃)(H₂O)] (B) [c]	[Re(Flav)(CH₃OH)] (C) [d]
Re−X (X = O/C) Å					
Re−O(1A)	2.140(2)	2.124(2)	2.121(5)	2.123 (5)	2.141(3)
Re−O(2A)	2.1316(19)	2.141(2)	2.108(4)	2.146 (4)	2.147(3)
Re−O(1B)	2.168(2)	2.174(2)	2.213(5)	2.170 (5)	2.204(4)
Re−C(21)	1.901(3)	1.885(3)	1.890(2)	1.882 (7)	1.905(5)
Re−C(22)	1.905(3)	1.900(3)	1.886(7)	1.897 (6)	1.906(5)
Re−C(23)	1.901(3)	1.911(3)	1.894(8)	1.899 (7)	1.893(5)
O-Re-X (X = O/C) ˚					
O(1A)-Re-O(2A)	77.56(7)	77.45(7)	74.82(17)	74.07 (16)	76.25
C(21)-Re-O(1B)	172.49(2)	177.85(2)	176.8(2)	174.33(3)	173.91

[a] Current study, [b] Schutte *et al.* [47], [c] Schutte *et al.* [57], [d] Schutte *et al.* [48]. [Re(Trop)(H₂O)] = *fac*-[NEt₄][Re(Trop)(CO)₃(H₂O)]·NO₃·H₂O with TropH = Tropolone, [Re(TropBr₃)(H₂O)] = *fac*-[Re(TropBr₃)(CO)₃(H₂O)] with TropBr₃H = tribromotropolone and [Re(Flav)(CH₃OH)] = *fac*-[Re(Flav)(CO)₃(CH₃OH)]·CH₃OH with FlavH = 3-hydroxyflavone.

In all the complexes mentioned above, the Re−O bond distances of the bidentate coordinated ligands are approximately 2.1 Å. The Re−O bond distance of the monodentate coordinated ligand (either MM(naltol)H, EM(naltol)H, H₂O or MeOH) is slightly longer and approximately 2.2 Å. The Re−C bond distances are approximately 1.9 Å with only (**A**) and (**B**) on average having slightly shorter bond distances. This might imply that MM(naltol)H, EM(naltol)H and flavone are more nucleophilic compared to tropolone and tribromotropolone, thus increasing the electron density on the rhenium centre, resulting in lesser backbonding to the rhenium centre by the carbonyl groups causing longer Re−C bond distances. The bite angles of the bidentate coordinated ligands are approximately 77 ˚ for (**2**) and (**3**) which is larger than (**C**) (76 ˚) followed by (**A**) and (**B**) in decreasing order at approximately 74 ˚ in both. The vertical axis through the structures C(21)-Re-O(1B) is nonlinear showing deviations from the ideal octahedral conformation (180 ˚). This could be due to steric demands in the structure. The most linear C(21)-Re-O(1B) bond angle is seen in (**3**) with an angle of 177.85(2) ˚.

5.6 Conclusion

Two compounds of the form *fac*-[Re(I)bis(pyridinonato)(CO)$_3$] were successfully synthesized and characterised by NMR and single crystal X-ray crystallography. Three more bis-complexes were also successfully characterized but no crystals were obtained (see Sections 3.5.3, 3.5.4 and 3.5.7). The results were reproducible in terms of both synthesis and characterization. Furthermore, the synthetic procedure to obtain these complexes was verified by a few additional experiments which indicated that these complexes can, with current knowledge in hand, only be synthesized from the bromido synthon *fac*-[NEt$_4$]$_2$[ReBr$_3$(CO)$_3$] (see Section 3.7). By increasing the ligand ratio to the rhenium in the normal aqua synthesis (Section 3.6.9 − 3.6.16), only increased yields were obtained and not the bis-complexes.

In both (**2**) and (**3**) the octahedral polyhedron is distorted with bite angles of the bidentate coordinated ligands approximately 77 ˚. The ligands are also bent out of the equatorial plane with dihedral angles between the equatorial plane and the plane through the hetero cyclic ring approximately 7 ˚ in both cases. The compounds (**2**) and (**3**) compare well with similar complexes with an O,O'-bidentate ligand, facial tricarbonyls and a monodentate oxo-coordinated ligand such as an aqua and methanol in an octahedral coordination geometry. A distinct feature of (**2**) and (**3**) is the larger bite angles (which can potentially activate the rhenium centre more towards nucleophilic substitution reactions) of the bidentate coordinated ligands and the unique combination of coordination modes. More work is however clearly required to evaluate if there are any significant desirable properties displayed by these unique compounds in terms of synthesis as precursors of drugs and as potential radiopharmaceuticals for imaging and therapy.

6 Crystallographic Study of *fac-*Re(I)-Tricarbonyl Pyridinonato Aqua Complexes

6.1 Introduction

The substitution reactions of *fac*-[Re(O,O'-Bid)(CO)$_3$(H$_2$O)]^n (O,O'-Bid = bidentate ligand, n = 0) complexes in methanol as solvent by a wide range of monodentate entering ligands indicate that the process is solvolytic in nature and hence the aqua complexes are typically solvated by methanol once dissolved therein, hence *methanol* will be the formal leaving group upon reaction with monodentate nucleophiles.[1-5] The [2 + 1] approach entails the coordination of a bidentate ligand of which the lipophilicity can be modulated and a monodentate bifunctional that can act as a potential linker to a biologically active molecule, which is the basis for much interest in these kinds of complexes.[6-8] This [2 + 1] approach thus in principle allows the labeling of bioactive molecules with selected radionuclides if they contain a monodentate or a bidentate donor site. The isolation and characterization of these aqua complexes reported herein is thus important in the process of systematically analysing and evaluating structural properties which are linked to the activation and reactivity of these kinds of compounds.

[1] A. Brink, H. G. Visser, A. Roodt, *Inorg. Chem.,***2014**, *53*, 12480.
[2] A. Brink, H. G. Visser, A. Roodt, *Inorg. Chem.,***2013**, *52*, 8950.
[3] M. Schutte, A. Roodt, H. G. Visser, *Inorg. Chem.,***2012**, *51*, 11996.
[4] M. Schutte, G. Kemp, H. G. Visser, A. Roodt, *Inorg. Chem.,* **2011**, *50*, 12486.
[5] M. Schutte, H. G. Visser, *Polyhedron,***2015**, *89*, 122.
[6] S. Mundwiler, M. Kundig, K. Ortner, R. Alberto, *J. Chem. Soc., Dalton Trans.*, **2004**, *9*, 1320.
[7] N. I. Gorshkov, R. Schibli, A. P. Schubiger, A. A. Lumpov, A. E. Miroslavov, D. N. Suglobov, *J. Organomet. Chem.*, **2004**, *689*, 4757.
[8] R. Alberto, *Top. Curr.Chem.*, **2005**, *252*, 1.

The four crystal structures reported here, *fac*-[Re(E(maltol))(CO)$_3$(H$_2$O)]·C$_2$H$_6$OS (**4**), *fac*-[Re(MM(naltol)(CO)$_3$(H$_2$O)]·C$_2$H$_6$OS (**5**), *fac*-[Re(MI(naltol)(CO)$_3$(H$_2$O)]·C$_2$H$_6$OS (**6**) and *fac*-[Re(MI(naltol)(CO)$_3$(H$_2$O)]·C$_3$H$_6$O (**7**) all contain subtle variations of the bidentate pyrone/pyridone ligand backbone and are excellent examples of the above-mentioned entities as presented in Scheme 6.1.

(4)   **(5)**

(6)   **(7)**
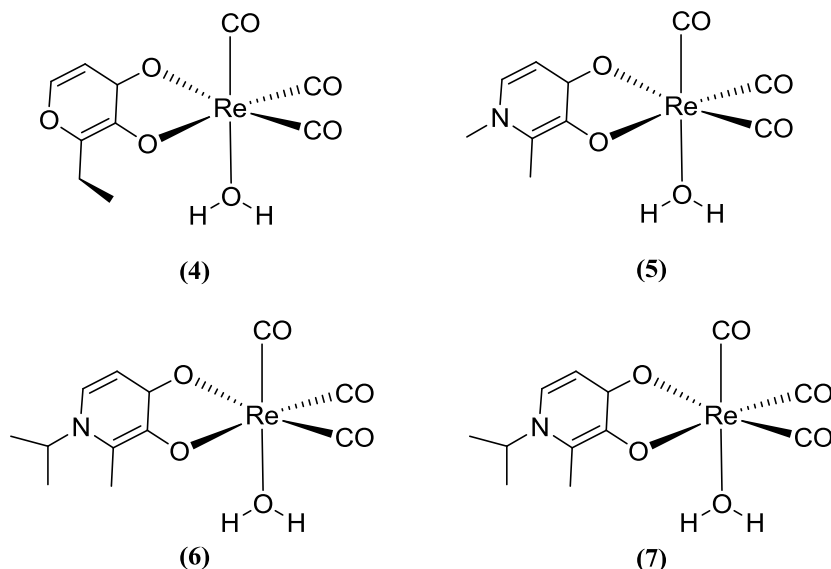
Scheme 6.1: Schematic representation of the four crystal structures reported in this chapter.

6.2 Experimental

The reflection data of (**4**)-(**7**) was collected on a Bruker X8 Apex II 4K Kappa CCD diffractometer using graphite monochromated Mo Kα radiation (λ= 0.70926 Å) with ω- and φ-scans at 100(2) K. The Apex II software package was utilized along with the optimum measurement method in collecting more than a hemisphere of reciprocal space as predicted by COSMO.[9,10] Frame integration and data reduction was performed using the SAINT-Plus and XPREP software packages and SADABS was used for multi-scan absorption correction.[11,12] The structures were solved using direct methods package SIR97 and refined using the WinGX

[9] **Apex2**, Version 2012.10-0, Bruker AXS Inc.,Madison, Wisconsin, USA, **2012**.

[10] **COSMO**, Version 1.48, Bruker AXS Inc., Madison, Wisconsin, USA, **2003**.

[11] **SADABS**, Version 2012/1, BrukerAXSInc, Madison, Wisconsin, USA, **2012**.

[12] **SAINT-Plus**, Version 8.27B including XPREP, Bruker AXS Inc., Madison, Wisconsin, USA, **2012**.

software incorporating SHELXL.[13-19] All atoms were refined anisotropically with the exception of hydrogen atoms. The hydrogen atoms were positioned geometrically and refined utilizing a riding model with fixed C-H distances of 0.95 Å (CH) [U_{iso}(H)= 1.2 U_{eq}] for aromatic hydrogens, 0.98 Å (CH) [U_{iso}(H)= 1.2 U_{eq}] for methine H-atoms, 0.97 Å (CH) [U_{iso}(H)= 1.2 U_{eq}] for methylene H-atoms and 0.96 Å (CH) [U_{iso}(H)= 1.2 U_{eq}] for methyl H-atoms. Molecular diagrams were generated with DIAMOND with 50 % probability ellipsoids for all non-hydrogen atoms.[20] General crystal data and refinement parameters are represented in Table 6.1 with the complete list of atomic coordinates, equivalent isotropic parameters and hydrogen coordinates given in Appendix A.

[13] A. Altomare, G. Cascarano, C. Giacovazzo, A. Guagliardi, M. C. Burla, G. Polidori, M. Camalli, *J. Appl.Cryst.*, **1994**, *27*, 435.

[14] A. Altomare, M. C. Burla, M. Camalli, G. L. Cascarano, C. Giacovazzo, A. Guagliardi, A. G. G. Moliterni, G. Polidori, R. Spagna, *J. Appl. Cryst.*, **1999**, *32*, 115.

[15] M. C. Burla, M. Camalli, B. Carrozzini, G. L. Cascarano, C. Giacovazzo, G. Polidori, R. Spagna, *J. Appl.Cryst.*, **2003**, *36*, 1103.

[16] P. T. Beurskens, G. Admiraal, G. Beurskens, W. P. Bosman, S. Garcia-Granda, R. O. Gould, J. M.M. Smits, C. Smykalla, Crystallography Laboratory, University of Nijmegen, Toernooiveld, The Netherlands.

[17] L. Palatinus, G. Chapuis, *J. Appl. Cryst.*, **2007**, *40*, 786.

[18] **WinGX**. L. J. Farrugia, *J. Appl. Cryst.*, **2012**, *45*, 849.

[19] G. M. Sheldrick, *ActaCryst.*, **2008**, *A64*, 112.

[20] K. Brandenburg, H. Putz, DIAMOND, Release 3.0e, Crystal Impact GbR, Bonn, Germany, **2006**.

Table 6.1: General X-ray crystallographic data and refinement parameters for *fac*-[Re(E(maltol))(CO)$_3$(H$_2$O)]·C$_2$H$_6$OS (4), *fac*-[Re(MM(naltol))(CO)$_3$(H$_2$O)]·C$_2$H$_6$OS (5), *fac*-[Re(MI(naltol))(CO)$_3$(H$_2$O)]·C$_2$H$_6$OS (6) and *fac*-[Re(MI(naltol))(CO)$_3$(H$_2$O)]·C$_3$H$_6$O (7).

Crystallographic data	(4)	(5)	(6)	(7)
Empirical formula	C$_{12}$H$_{13}$O$_8$ReS	C$_{12}$H$_{16}$NO$_7$ReS	C$_{14}$H$_{20}$NO$_7$ReS	C$_{15}$H$_{20}$NO$_7$Re
Formula weight (g.mol^{-1})	503.49	504.53	532.58	512.53
Temperature (K)	100(2)	100(2)	100(2)	100(2)
Crystal system	Triclinic	Triclinic	Triclinic	Triclinic
Space group	$P\bar{1}$	$P1$	$P\bar{1}$	$P\bar{1}$
a (Å)	9.406(1)	9.598(5)	10.283(1)	10.110 (2)
b (Å)	10.207(2)	9.753(5)	10.522(1)	10.129(2)
c (Å)	10.25(1)	10.761(6)	10.549(1)	10.493(2)
α (°)	61.111(4)	65.903(2)	102.825(3)	96.243(5)
β (°)	84.760(4)	64.213(2)	109.198(3)	103.646(5)
γ (°)	69.137(4)	65.897(2)	114.345(3)	119.445(4)
Volume (Å^3)	800.9(2)	794.7(7)	893.3(2)	876.6(3)
Z	2	2	2	2
ρ$_{calc.}$ (g.cm^{-3})	2.088	2.109	1.980	1.942
Crystal colour	Yellow	Colourless	Yellow	Yellow
Crystal morphology	Cuboid	Cuboid	Cuboid	Cuboid
Crystal size (mm^3)	0.524 x 0.153 x 0.122	0.345 x 0.143 x 0.104	0.258 x 0.142 x 0.104	0.307 x 0.132 x 0.125
μ (mm^{-1})	7.751	7.809	6.953	6.966
F(000)	480	484	516.0	496.0
θ range (°)	2.859 to 27.999	4.771 to 28.345	4.675 to 27.998	4.752 to 28.000
Index ranges	-12 ≤ h ≤ 12	-8 ≤ h ≤ 12	-13 ≤ h ≤ 9	-13 ≤ h ≤ 13
	-13 ≤ k ≤ 13	-11 ≤ k ≤ 13	-13 ≤ k ≤ 13	-10 ≤ k ≤ 13
	-11 ≤ l ≤ 13	-13 ≤ l ≤ 14	-13 ≤ l ≤ 13	-13 ≤ l ≤ 13
Reflections collected	14002	12630	26268	16690
Unique reflections	3873	7918	4304	4243
Reflections with I > 2σ(I)	9951	9949	9883	9905
R$_{int}$	0.0443	0.0234	0.0427	0.0479
Completeness to θ (°; %)	25.24, 98.3	25.24, 99.1	25.24, 99.1	25.24, 99.0
Data/restraints/parameters	3816 / 6 / 202	6251 / 7 / 418	4278 / 0 / 230	4207 / 0 / 226
GooF	1.292	1.051	1.108	1.169
R [I>2σ(I)]	R$_1$ = 0.0563	R$_1$ = 0.0159	R$_1$ = 0.0146	R$_1$ = 0.0201
	wR$_2$ = 0.1752	wR$_2$ = 0.0357	wR$_2$ = 0.0374	wR$_2$ = 0.0534
R (all data)	R$_1$ = 0.0568	R$_1$ = 0.0175	R$_1$ = 0.0151	R$_1$ = 0.0210
	wR$_2$ = 0.1755	wR$_2$ = 0.0364	wR$_2$ = 0.0376	wR$_2$ = 0.0539
ρ$_{max}$, ρ$_{min}$(e.Å^{-3})	7.694 and -5.879	0.608 and -0.791	0.874 and -1.308	0.873 and -1.349

6.3 Crystal structure of *fac*-[Re(E(maltol))(CO)$_3$(H$_2$O)]·C$_2$H$_6$OS (4)

The complex, *fac*-[Re(E(maltol))(CO)$_3$(H$_2$O)]·C$_2$H$_6$OS (**4**) has been synthesized as described in the synthesis section (Paragraph 3.5.13), where the yellow cuboidal crystals were obtained from a DMSO solution of the product. This complex crystallized in a triclinic crystal system in the $P\bar{1}$ space group with two independent molecules in the unit cell (Z = 2). In the structure of *fac*-[Re(E(maltol))(CO)$_3$(H$_2$O)]·C$_2$H$_6$OS (**4**) the Re atom is octahedrally surrounded by three facially orientated carbonyl ligands, one mono-anionic bidentate coordinated ligand and a neutral water molecule with a DMSO solvent molecule in the crystal system. The bidentate ligand carries a mono-negative charge as it loses a proton, while the water molecule is neutral, which results in a neutral molecular complex. A summary of the general crystal data of (**4**) is presented in Table 6.1, with the general interatomic bond distances and angles given in Table 6.2, while the numbering scheme of the neutral complex is shown in Figure 6.1.
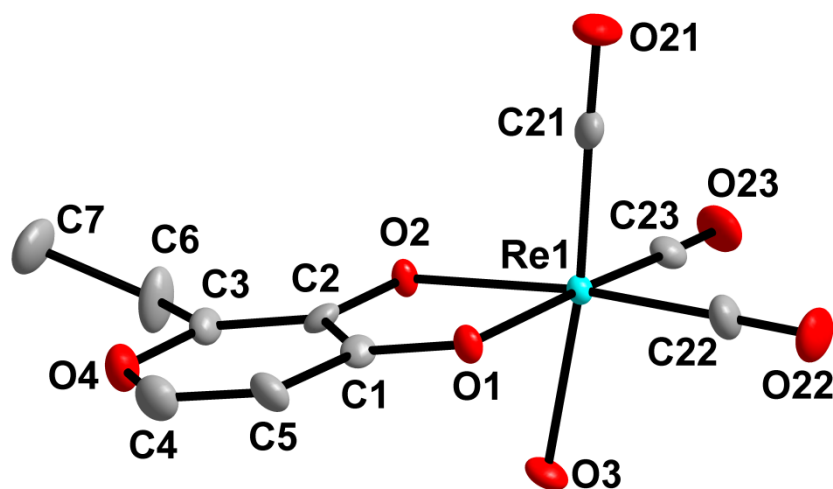
Figure 6.1: Molecular representation of *fac*-[Re(E(maltol))(CO)$_3$(H$_2$O)]·C$_2$H$_6$OS (4) showing the atom numbering scheme; displacement ellipsoids are drawn at 50 % probability level. Hydrogen atoms are omitted for clarity except the water hydrogen atoms which could not be refined as there was no additional electron density around O3.

Table 6.2: Selected bond distances (Å) and angles (°) for the crystal structure of (4).

Bond	Bond distance (Å)	Bond angle (atoms)	Bond angle (°)
O(1)-Re(1)	2.126(9)	O(1)-Re(1)-O(2)	77.245 (5)
O(2)-Re(1)	2.154(9)	C(22)-Re(1)-C(23)	88.5(6)
C(21)-Re(1)	1.869(2)	C(22)-Re(1)-O(1)	96.1(5)
C(22)-Re(1)	1.896(14)	C(23)-Re(1)-O(2)	97.7(5)
C(23)-Re(1)	1.908(14)	C(21)-Re(1)-O(1)	96.2(5)
C(21)-O(21)	1.185(17)	O(21)-C(21)-Re(1)	178.1(13)
C(22)-O(22)	1.172(18)	C(21)-Re(1)-C(23)	89.0(6)
C(23)-O(23)	1.155(17)	C(22)-Re(1)-C(21)	88.8(6)
O(3)-Re(1)	2.164(9)	C(21)-Re(1)-O(2)	95.9(5)
C(1)-O(1)	1.280(16)	C(23)-Re(1)-O(1)	173.1(5)
C(2)-O(2)	1.328(16)	C(22)-Re(1)-O(2)	172.2(5)
		C(21)-Re(1)-O(3)	173.1(5)

All the bond distances and angles are within normal ranges compared to similar structures.[21-35] The Re−C bond distances of the three facial carbonyl groups are ~ 1.9 Å, while the Re−O bond distances are ~ 2.1 Å, the longest being Re(1)−O(3) (2.164(9) Å) and Re(1)−O(2) (2.154(9) Å). The *trans* influence due to the coordinated water molecule is minimal, however the opposite bond distance Re(1)−C(21) is slightly shorter (1.869(2) Å). Furthermore, the Re(1)−O(3) bond distance (aqua ligand) falls within the same range as the Re−O bond distances found in other methanol solvated rhenium complexes and aqua complexes (~ 2.2 Å).[21-35] The bidentate coordinated ligand has a bite angle O(1)-Re(1)-O(2) of 77.245(5) ° which is larger than that of similar structures of tropolone and tribromotropolone (74.82(17) ° and 74.07(16) ° respectively) and slightly smaller compared to the bis-structures (**2**) and (**3**) reported in Chapter 5.[25,28]

[21] M. Sánchez-Lozano, E. M. Vázquez-López, J. M. Hermida-Ramón, C. M. Estévez, *Polyhedron*, **2011**, *30*, 953.

[22] J. Mukiza, E. C. Hosten, T. I. A. Gerber, *Polyhedron*, **2015**, *98*, 251.

[23] S. Mundwiler, M. Kündig, K. Ortner, R. Alberto, *J. Chem. Soc. Dalton Trans.*, **2004**, 1320.

[24] T. R. Hayes, B. B. Kasten, C. L. Barnes, P. D. Benny, *Dalton Trans.*, **2014**, *43*, 6998.

[25] M. Schutte, A. Roodt, H. G. Visser, *Inorg. Chem.*, **2012**, *51*, 11996.

[26] M. Schutte, G. Kemp, H. G. Visser, A. Roodt, *Inorg. Chem.*, **2011**, *50*, 12486.

[27] F. Ragone, G. T. Ruiz, O. E. Piro, G. A. Echeverría, F. M. Cabrerizo, G. Petroselli, R. Erra-Balsells, K. Hiraoka, F. S. GarcíaEinschlag, E. Wolcan, *Eur. J. Inorg. Chem.*, **2012**, 4801.

[28] M. Schutte, H. G. Visser, A. Roodt, *ActaCryst. Sect. E*, **2008**, *E64*, m1610.

[29] K. O. Piletska, K. V. Domasevitch, A. V. Shtemenko, *ActaCryst. Sect. E*, **2016**, *E72*, 590.

[30] A. Brink, H. G.Visser, A. Roodt, *J. Coord. Chem.*, **2011**, *64*, 122.

[31] A. Brink, H. G.Visser, A. Roodt, CCDC 801586: Experimental Crystal Structure Determination, **2014**, DOI: 10.5517/ccvx3mg

[32] A. Brink, H. G. Visser, A. Roodt, *Inorg. Chem.*, **2013**, *52*, 8950.

[33] B. Shankar, P. Elumalai, R. Shanmugam, V. Singh, D. T. Masram, M. Sathiyendiran, *Inorg. Chem.*, **2013**, *52*, 10217.

[34] A. Brink, H. G. Visser, A. Roodt, *Inorg. Chem.*, **2014**, *53*, 12480.

[35] M. Schutte, H. G. Visser, A. Roodt, Acta Cryst., **2008**, *E64*, m1610.

The octahedral system surrounding the rhenium atom is distorted with angles ranging from 77.245(5) ° to 178.1(13) ° which is very similar to the ranges of the bis-structures (**2**) and (**3**) reported in Chapter 5. The three axes through the vertices of the octahedral system are nonlinear and approximately 173 °. The C22-O22 and the C23-O23 axis both lie in the equatorial plane with minimal deviations in contrast to (**2**), which was more distorted. The angle C(21)-Re(1)-O(3) is 173.1(5) ° also indicating that there is a distortion in the structure from the vertical axis through the Re centre (Figure 6.2).

Figure 6.2: Illustration of the equatorial plane (C23 O2 O1 C22 Re1) showing the bidentate coordinated ligand bending out of the plane. Hydrogen atoms are omitted for clarity.

The bidentate coordinated pyrone ligand bends downwards out of the equatorial plane, away from the apical carbonyl, with the deviation such that the equatorial plane intersects C7 which would ideally lie above the equatorial plane (Figure 6.2).

Figure 6.3: Illustration of the dihedral angle between the equatorial plane (C23 O2 O1 C22 Re1) and the plane through the heterocycle of the bidentate coordinated ligand (C1 C2 C3 N1 C4 C5).

The dihedral angle between the equatorial plane (C23 O2 O1 C22 Re1) and ring of the bidentate coordinated pyrone ligand (C1 C2 C3 N1 C4 C5) is 7.59 ° which is very similar to (**2**) and (**3**) (Figure 6.3). This dihedral angle indicates the distortion in the planarity of the bidentate coordinated ligand. The influence of this bending results in a torsion angle of the bidentate coordination site O(1)-C(1)-C(2)-O(2) of 2.01(5) ° which is smaller than that of (**2**) and (**3**) (~ 4 °).
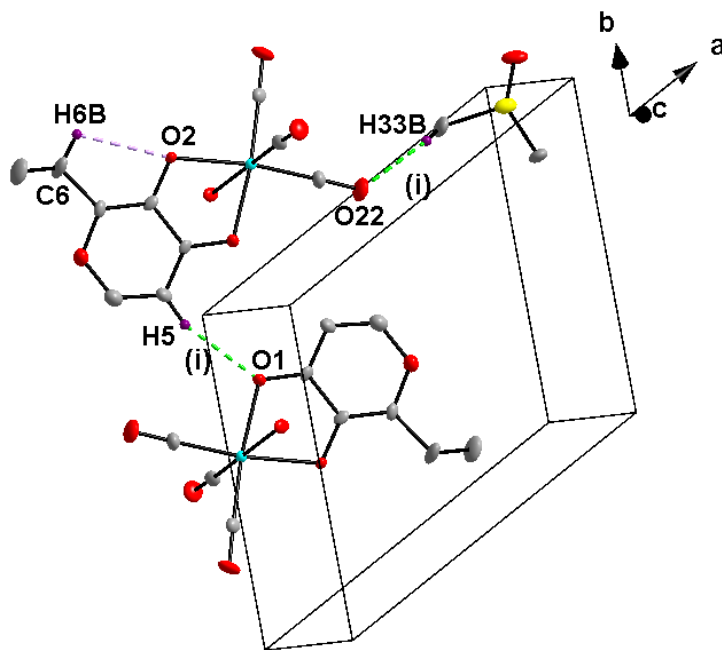
Figure 6.4: Hydrogen interactions observed in the structure of *fac*-[Re(E(maltol))(CO)$_3$(H$_2$O)]·C$_2$H$_6$OS (4).

108

Only three C-H…O hydrogen interactions are observed in this structure: one intramolecular (represented by light purple fragmented bonds) and two inter-molecular (represented by green fragmented bonds) hydrogen interactions, as illustrated in Figure 6.4, while the distances, angles and symmetry operators are given in Table 6.3.

Table 6.3: Summary of the hydrogen interactions, distances (Å) and angles (˚) observed in (4).

D-H…A	d(D-H) (Å)	d(H…A) (Å)	d(D…A) (Å)	∟ (D-H…A)(˚)
C(5)-H(5)...O(1) [(i)]	0.93	2.41	3.30(2)	160
C(6)-H(6B)...O(2)	0.97	2.60	2.95(2)	101
C(33)-H(33B)...O(23) [(i)]	0.96	2.48	3.37(2)	155

Symmetry codes, transformations used to generate equivalent atoms: (i) 2-x, -y,1-z

The molecules pack in an alternating fashion along the *bc*-plane facing in and out of the *bc*-plane stabilized by inter-molecular C-H…O interactions (Figure 6.5).
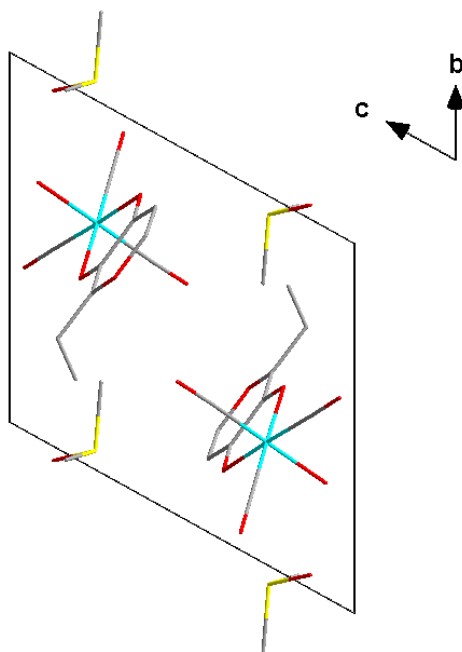
Figure 6.5: Crystal packing of (4) in the unit cell, viewed along the *a*-axis. Hydrogen atoms are omitted for clarity.

109

6.4   Crystal structure of *fac*-[Re(MM(naltol)(CO)$_3$(H$_2$O)]·C$_2$H$_6$OS (5)

The complex, *fac*-[Re(MM(naltol)(CO)$_3$(H$_2$O)]·C$_2$H$_6$OS (**5**) has been synthesized as described in the synthesis section (Paragraph 3.5.10), and the colourless cuboidal crystals were obtained by recrystallizing from a DMSO solution. This complex crystallized in the triclinic crystal system in the *P*1 space group with two independent molecules in the asymmetric unit (Z = 2). The Flack parameter is 0.493(17) which indicates that there is a racemic twin in the structure (see Figure 6.6).

In the structure of *fac*-[Re(MM(naltol)(CO)$_3$(H$_2$O)]·C$_2$H$_6$OS (**5**) the Re atom is octahedrally surrounded by three facially orientated carbonyl ligands, one mono-anionic bidentate coordinated ligand and a coordinated water molecule with, as in the case of (**4**), a DMSO solvent molecule in the crystal system. The bidentate ligand carries a mono-negative charge as it loses a proton, while the water molecule is neutral, which results in a neutral complex. A summary of the general crystal data of (**5**) is given in Table 6.1, while the general interatomic bond distances and angles are given in Table 6.4 with the numbering scheme of the neutral complex shown in Figure 6.6.

(I) Molecule A
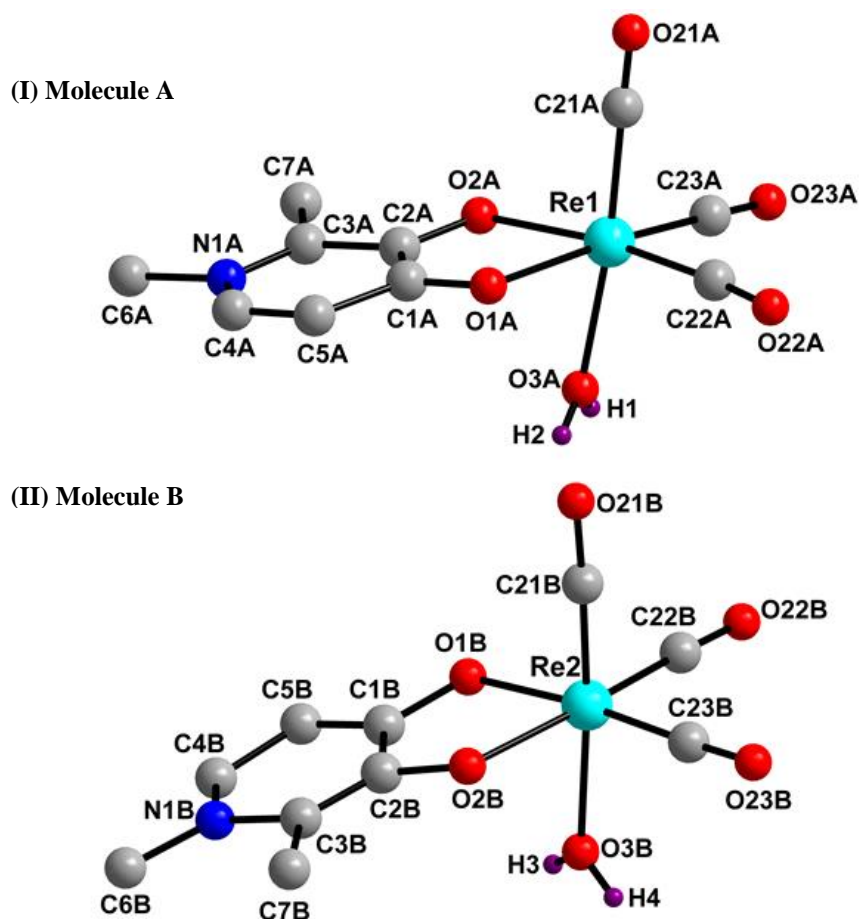
(II) Molecule B

Figure 6.6: Molecular representation of *fac*-[Re(MM(naltol)(CO)₃(H₂O)]·C₂H₆OS (5) showing the atom numbering scheme in molecule A and B. Hydrogen atoms are omitted for clarity except for the coordinated aqua ligand. Due to some atoms having non-positive definites the structure is not illustrated as thermal ellipsoids.

Table 6.4: Selected bond distances (Å) and angles (°) for the crystal structure of (5).

Bond	Bond distance (Å)		Bond angle (atoms)	Bond angle (°)	
	A	B		A	B
O(1)-Re	2.102(14)	2.146(14)	O(1)-Re-O(2)	76.20(2)	78.6(4)
O(2)-Re	2.215(12)	2.085(11)	C(22)-Re-C(23)	87.5(7)	90.6(8)
C(21)-Re	1.919(19)	1.873(13)	C(22)-Re-O(1)	98.4(6)	91.8(6)
C(22)-Re	1.929(12)	1.877(18)	C(23)-Re-O(2)	97.2(6)	98.7(7)
C(23)-Re	1.928(15)	1.88(2)	C(21)-Re-O(1)	99.4(7)	97.3(6)
C(21)-O(21)	1.105(2)	1.273(19)	O(21)-C(21)-Re	176.0(16)	177.8(13)
C(22)-O(22)	1.148(18)	1.17(2)	C(21)-Re-C(23)	88.7(7)	87.3(8)
C(23)-O(23)	1.16(2)	1.16(2)	C(22)-Re-C(21)	89.5(7)	89.8(7)
O(3)-Re	2.150(13)	2.190(12)	C(21)-Re-O(2)	96.1(6)	94.9(6)
C(1)-O(1)	1.25(2)	1.351(18)	C(23)-Re-O(1)	170.0(7)	174.8(8)
C(2)-O(2)	1.324(19)	1.374(18)	C(21)-Re-O(3)	174.5(7)	174.5(6)
			O(2)-Re-C(22)	172.8(6)	169.8(6)

All the bond distances and angles are within normal ranges compared to similar structures.[21-35] The Re−C bond distances of the three facial carbonyl groups are ~ 1.92 Å for molecule A and ~ 1.87 Å for molecule B. The Re−O bond distances are ~ 2.1 Å in both molecules. The is no observable *trans* influence due to the coordinated aqua molecules in both molecule A and B as the opposite bond distance are approximately equal (1.9 Å). Furthermore, the Re−O(3) bond distance falls within the same range as (**2**), (**3**), and (**4**) (~ 2.2 Å).[21-35] The bidentate coordinated ligand has a bite angle O(1)-Re-O(2) of 76.20(2) ˚ in molecule A and 78.6(4) ˚ in molecule B which is larger than that of similar structures of tropolone and tribromotropolone (74.82(17) ˚ and 74.07(16) ˚ respectively) but within range of (**2**), (**3**), and (**4**).[25,28]
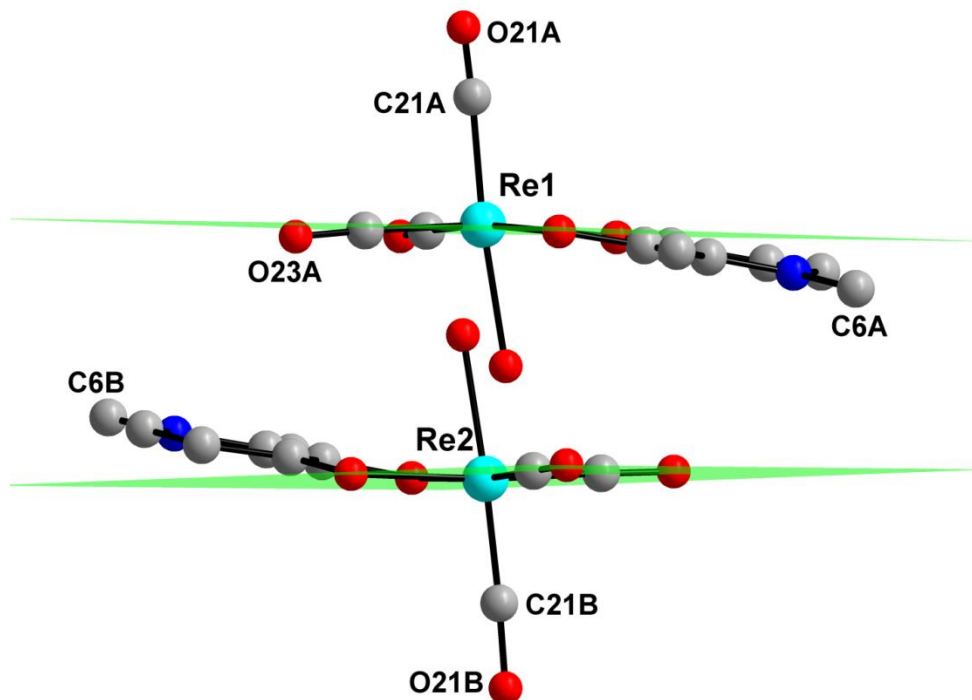
Figure 6.7: Illustration of the equatorial planes in molecules A and B (C23 O2 O1 C22 Re) showing the bidentate coordinated ligands bending out of the plane. Hydrogen atoms are omitted for clarity.

The octahedral system surrounding the rhenium atoms in both molecule A and B is distorted with angles ranging from 76.20(2) ˚ to 176.0(16) ˚ in molecule A and 78.6(4) ˚ to 177.8(13) ˚ in molecule B. These angles are still within range of previously discussed structures (**2**), (**3**), and (**4**). The three axes through the vertices of the octahedral system are nonlinear and range from 170 ˚ to 174 ˚ in molecule A and 169 ˚ to 174 ˚ in molecule B. The C22-O22 and the C23-O23

axis both lie in the plane with the C23-O23 axis in both molecules deviating slightly more out of plane (C23A deviation from the equatorial plane = 0.0457(40) Å compared to C22A = 0.0042(40) Å and C23B deviation from the equatorial plane = 0.0225(40) Å compared to C22B = 0.0099(40) Å). The angle C(21)-Re-O(3) is ~ 174 ° in both molecules also indicating that there is a distortion in the vertical axes of the molecules through the Re centres (Figure 6.7).
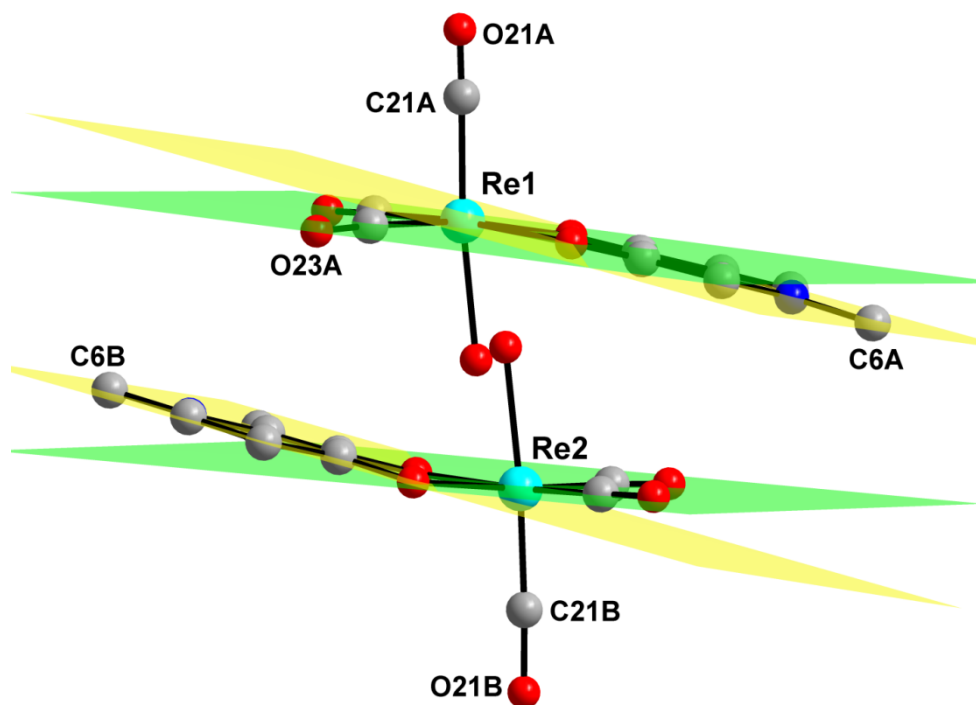
Figure 6.8: Illustration of the dihedral angle between the equatorial plane (C23 O2 O1 C22 Re) and the plane through the heterocycle of the bidentate coordinated ligand (C1 C2 C3 N1 C4 C5) in both molecule A and B.

The dihedral angle between the equatorial plane (C23 O2 O1 C22 Re) and ring of the bidentate coordinated pyridinone ligand (C1 C2 C3 N1 C4 C5) in molecule A is 8.40(1) ° and 11.19(1) ° in molecule B (numerical difference = 2.79(2) °) (Figure 6.8). This indicates the distortions in the planarity of the bidentate coordinated ligands in both molecules which is significantly larger compared to (**2**), (**3**), and (**4**) which was ~ 7.5 °. The ring bends out of the equatorial plane in both molecules towards the coordinated water molecule with the torsion angle of the bidentate coordination site O(1)-C(1)-C(2)-O(2) equal to 2.87(7) ° for molecule A and 2.94(6) °for molecule B (Figure 6.7 and 6.8).
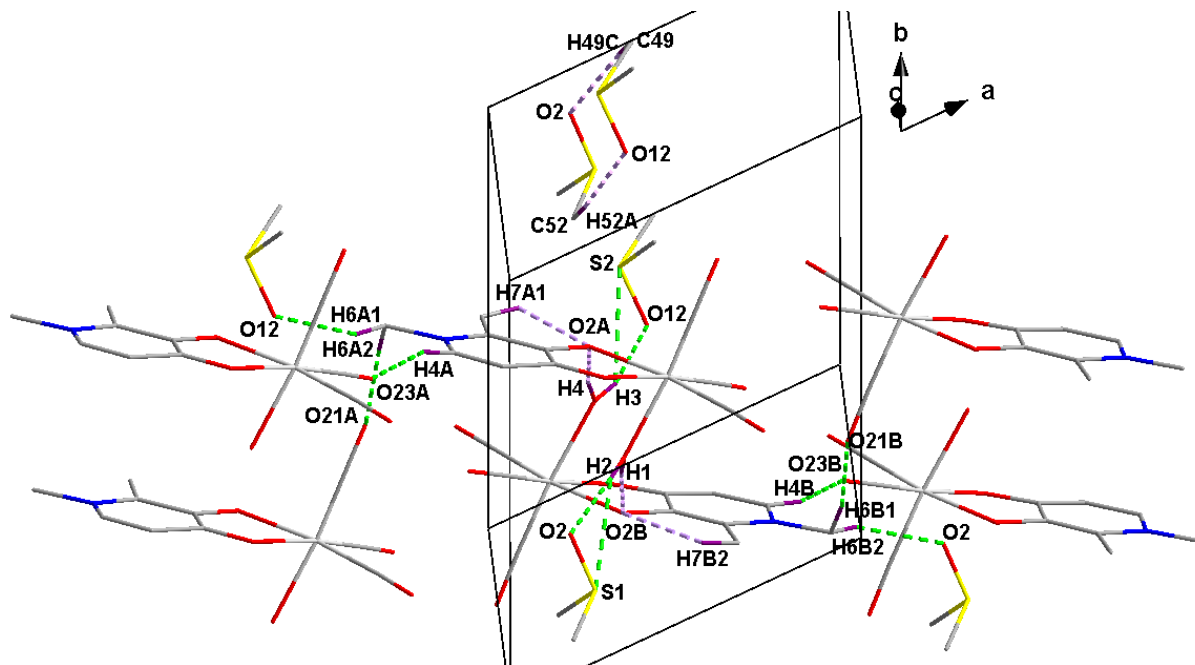
Figure 6.9: Hydrogen interactions observed in the structure of *fac*-**[Re(MM(naltol)(CO)$_3$(H$_2$O)]·C$_2$H$_6$OS (5).**

The structure displays 16 hydrogen interactions: ten of which are inter-molecular (a combination of O-H…O, O-H…S and C-H…O interactions, represented by green fragmented bonds) with H3 and H2 bifurcated O-H…O and O-H…S hydrogen interactions and six intra-molecular (a combination of O-H…O and C-H…O interactions, represented by light purple fragmented bonds). These hydrogen interactions are illustrated in Figure 6.9, while the distances, angles and symmetry operators are given in Table 6.5.

Table 6.5: Summary of the hydrogen interactions, distances (Å) and angles (°) observed in (5).

D-H…A	d(D-H) (Å)	d(H…A) (Å)	d(D…A) (Å)	� (D-H…A)(°)
O3A-H1...O2B	0.80(4)	1.94(5)	2.738(17)	173(6)
O3A-H2...S1 (i)	0.81(6)	2.69(6)	3.373(14)	143(5)
O3A-H2...O2 (i)	0.81(6)	1.86(6)	2.655(17)	167(8)
O3B-H3...S2 (ii)	0.81(6)	2.79(6)	3.380(13)	131(5)
O3B-H3...O12 (ii)	0.81(6)	1.87(6)	2.649(17)	163(6)
O3B-H4...O2A	0.81(5)	1.77(5)	2.565(18)	167(7)
C7B-H7B2...O2B	0.96	2.58	2.97(2)	105
C6A-H6A1...O12 (iii)	0.96	2.42	3.33(2)	157
C4A-H4A...O23A (iv)	0.93	2.39	3.26(2)	155
C4B-H4B...O23B (v)	0.93	2.47	3.30(2)	148
C6A-H6A2...O21A (iii)	0.96	2.51	3.46(3)	170
C6B-H6B1...O21B (vi)	0.95	2.50	3.43(3)	168
C6B-H6B2...O2 (vii)	0.96	2.36	3.24(2)	152
C7A-H7A1...O2A	0.96	2.31	2.77(2)	109
C49-H49C...O2	0.96	2.58	3.48(3)	156
C52-H52A...O12	0.96	2.47	3.39(3)	163

Symmetry codes, transformations used to generate equivalent atoms: (i) x, y, z-1; (ii) x, y-1, z; (iii) 1+x, y, z; (iv) x-1, y, 1+z; (v) x-1, y, z; (vi) 1+x, y, z-1; (vii) 1+x, y-1, z-1

The molecules pack in pairs orientated head to head along the *bc*-plane with solvent molecules on either side. These orientations are stabilized by inter-molecular O-H…O, O-H…S and C-H…O interactions (Figure 6.10).
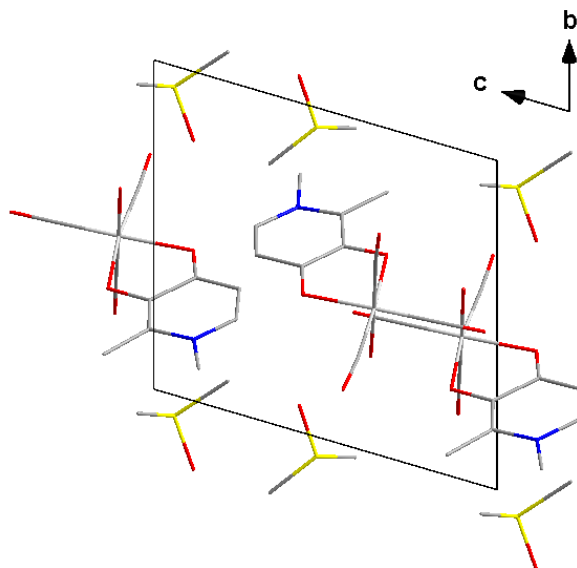
Figure 6.10: Crystal packing of (5) in the unit cell, viewed along the *a*-axis. Hydrogen atoms are omitted for clarity.

6.5 Crystal structure of *fac*-[Re(MI(naltol)(CO)₃(H₂O)]·C₂H₆OS (6)

The complex, *fac*-[Re(MI(naltol)(CO)₃(H₂O)]·C₃H₆OS (**6**) has been synthesized as described in the synthesis section (Paragraph 3.5.12). The yellow cuboidal crystals were obtained from a DMSO solution of the product. This complex crystallized in the triclinic crystal system in the $P\bar{1}$ space group with two independent molecules in the unit cell (Z = 2). In the structure of *fac*-[Re(MI(naltol)(CO)₃(H₂O)]·C₃H₆OS (**6**) the Re atom is octahedrally surrounded by three facially orientated carbonyl ligands, one mono-anionic bidentate coordinated ligand and a neutral water molecule with a DMSO solvent molecule. The bidentate ligand carries a mono-negative charge as it loses a proton, while the water molecule is neutral, which results in a neutral complex. A summary of the general crystal data of (**6**) is given in Table 6.1. A summary of the general interatomic bond distances and angles are given in Table 6.6 while the numbering scheme of the neutral complex is shown in Figure 6.11.
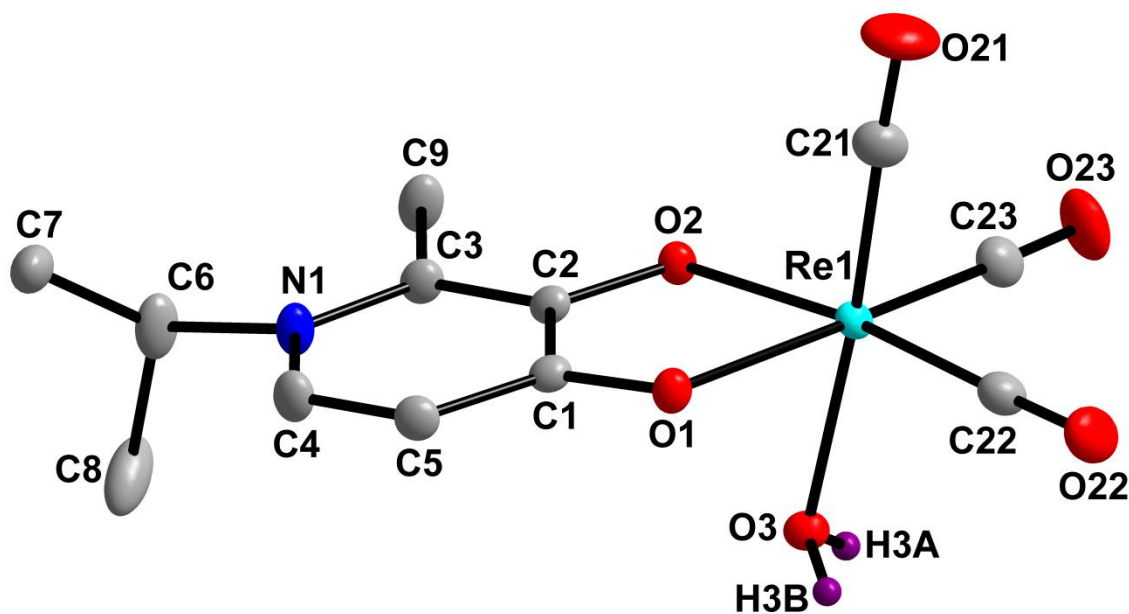
Figure 6.11: Molecular representation of *fac*-[Re(MI(naltol)(CO)₃(H₂O)]·C₂H₆OS (6) showing the atom numbering scheme; displacement ellipsoids are drawn at 50 % probability level. Hydrogen atoms are omitted for clarity except for the coordinated aqua ligand.

Table 6.6: Selected bond distances (Å) and angles (°) for the crystal structure of (6).

Bond	Bond distance (Å)	Bond angle (atoms)	Bond angle (°)
O(1)-Re(1)	2.1316(17)	O(1)-Re(1)-O(2)	77.413(15)
O(2)-Re(1)	2.1318(15)	C(22)-Re(1)-C(23)	89.00(10)
C(21)-Re(1)	1.879(3)	C(22)-Re(1)-O(1)	98.05(8)
C(22)-Re(1)	1.907(2)	C(23)-Re(1)-O(2)	95.15(8)
C(23)-Re(1)	1.908(3)	C(21)-Re(1)-O(1)	96.35(9)
C(21)-O(21)	1.171(3)	O(21)-C(21)-Re(1)	177.4(2)
C(22)-O(22)	1.155(3)	C(21)-Re(1)-C(23)	88.64(10)
C(23)-O(23)	1.158(3)	C(22)-Re(1)-C(21)	85.84(11)
O(3)-Re(1)	2.190(2)	C(21)-Re(1)-O(2)	99.66(9)
C(1)-O(1)	1.298(2)	C(23)-Re(1)-O(1)	171.62(7)
C(2)-O(2)	1.332(2)	C(21)-Re(1)-O(3)	174.16(8)
		C(22)-Re(1)-O(2)	173.17(7)

All the bond distances and angles are within normal ranges compared to similar structures.[21-35] The Re−C bond distances of the three facial carbonyl groups are ~ 1.9 Å. The Re−O bond distances are ~ 2.1 Å, the longest being Re(1)−O(3) (2.190(2) Å). The *trans* influence due to the coordinated water molecule is minimal, however the opposite bond distance Re(1)−C(21) is slightly shorter (1.879(3) Å). Furthermore, the Re(1)−O(3) bond distance falls within the same range as the Re−O bond distances found in the methanol solvated and the aqua rhenium complexes (~ 2.2 Å).[21-35] The bidentate coordinated ligand has a bite angle O(1)-Re(1)-O(2) of 77.413(15) ° which is larger than that of similar structures of tropolone and tribromotropolone (74.82(17) ° and 74.07(16) ° respectively) and is within range compared to (**2**), (**3**), (**4**), and (**5**).[25,28] The octahedral system surrounding the rhenium atom is distorted with angles ranging from 77.413(15) ° to 177.4(2) ° which is approximately equal to (**2**), (**3**), (**4**), and (**5**). The three axes through the vertices of the octahedral system are nonlinear and range between 171 ° and 174 °. The C22-O22 and the C23-O23 axis both lie in the plane with minimal deviations in contrast to (**2**) which was more distorted. The angle C(21)-Re(1)-O(3) is 174.16(8) ° also indicating that there is a distortion in the structure from the vertical axis through the Re centre (Figure 6.12).
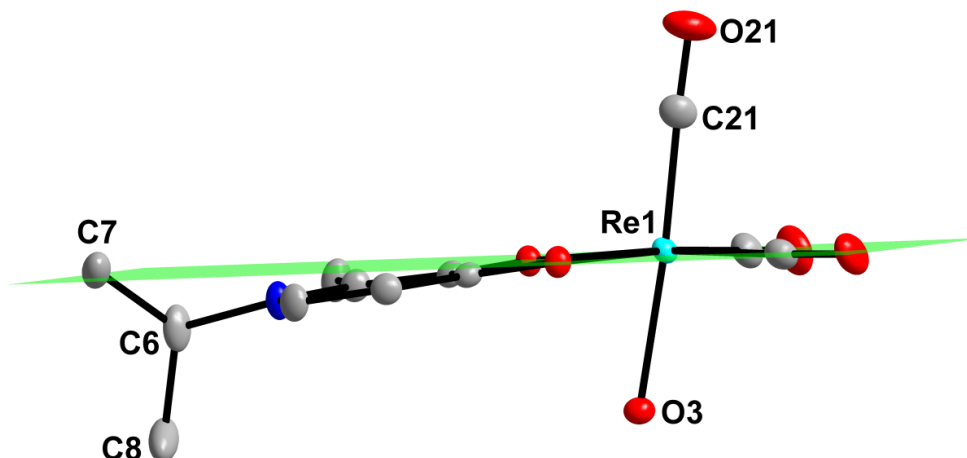
Figure 6.12: Illustration of the equatorial plane (C23 O2 O1 C22 Re1) showing the bidentate coordinated ligand bending out of the plane. Hydrogen atoms are omitted for clarity.

The bidentate coordinated pyridinone ligand bends downwards out of the equatorial plane with the deviation such that the equatorial plane intersects C7 which would ideally lie above the plane (Figure 6.12).
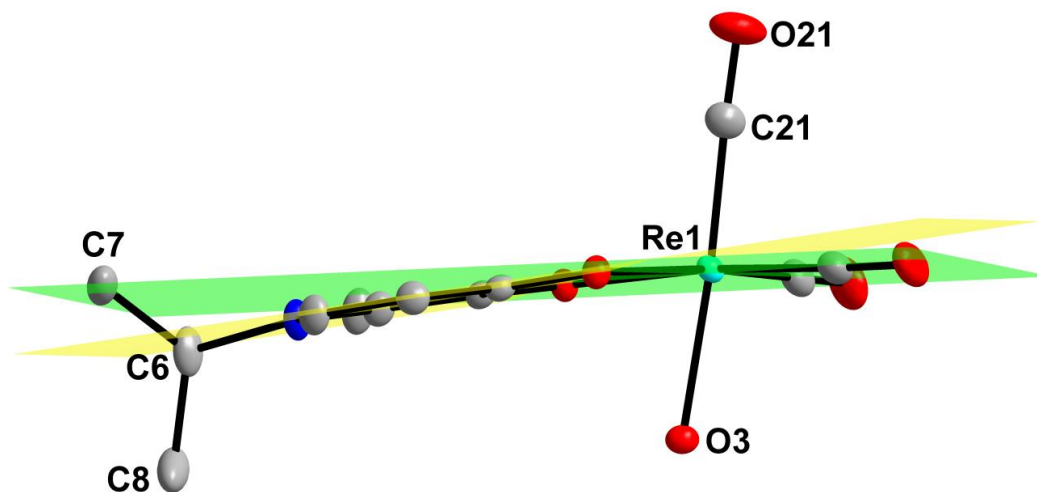
Figure 6.13: Illustration of the dihedral angle between the equatorial plane (C23 O2 O1 C22 Re1) and the plane through the heterocycle of the bidentate coordinated ligand (C1 C2 C3 N1 C4 C5).

The dihedral angle between the equatorial plane and ring of the bidentate coordinated pyridinone ligand is 6.399(9) ° which is smaller compared to (**2**), (**3**), (**4**), and (**5**) (Figure 6.13). This indicates that the distortion in the planarity of the bidentate coordinated ligand is less. The influence of this bending results in a torsion angle of the bidentate coordination site O(1)-C(1)-

C(2)-O(2) of 0.700(44) ° which is even smaller compared to the pyrone aqua complex (**4**), both the bis-structures (**2**) and (**3**) and the pyridinone aqua complex (**5**).
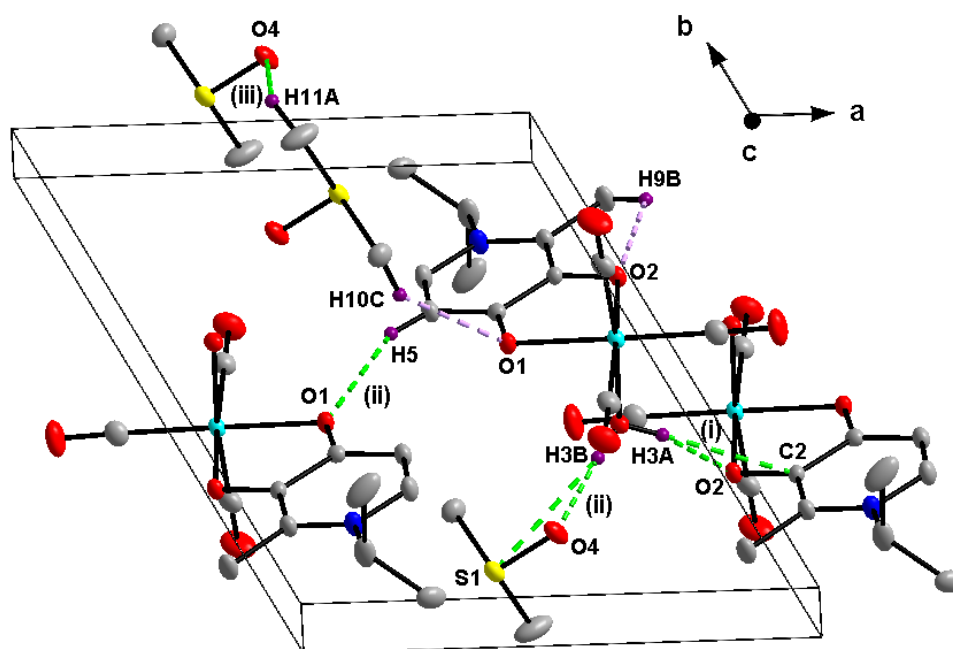
Figure 6.14: Hydrogen interactions observed in the structure of *fac*-[Re(MI(naltol)(CO)$_3$(H$_2$O)]·C$_2$H$_6$OS (6).

Only six hydrogen interactions are observed in this structure: two intramolecular (C-H…O interactions, represented by light purple fragmented bonds) and four inter-molecular (a combination of two O-H…O and two C-H…O interactions, represented by green fragmented bonds) with H3A and H3B bifurcated O-H…O, C-H…O and O-H…S hydrogen interaction. These hydrogen interactions are illustrated in Figure 6.14, while the distances, angles and symmetry operators are given in Table 6.7.

Table 6.7: Summary of the hydrogen interactions, distances (Å) and angles (°) observed in (6).

D-H…A	d(D-H) (Å)	d(H…A) (Å)	d(D…A) (Å)	⌞ (D-H…A)(°)
O3-H3A...O2 [(i)]	0.88(5)	1.81(4)	2.656(3)	162(3)
O3-H3B...O4 [(ii)]	0.81(5)	1.81(5)	2.621(3)	174(5)
C5-H5...O1 [(ii)]	0.93	2.56	3.436(3)	156
C9-H9B...O2	0.96	2.42	2.865(4)	108
C10-H10C...O1	0.96	2.48	3.318(4)	146
C11-H11A…O4 [(iii)]	0.96	2.60	3.326(4)	133

Symmetry codes, transformations used to generate equivalent atoms: (i) -x, 1-y, 1-z; (ii) 1-x, 1-y, 1-z; (iii) 1-x, -y, -1-z;

The molecules pack in alternating layers along the *bc*-plane with the molecules in the layer **A** parallel to the second layer **A**. The **A** layer consist of a pair of molecules arranged tail to tail, in between these **A** layers is a combination of pairs lying in a staggered conformation (layer **B**) (**ABA**). This packing is stabilized by inter-molecular O-H…O and C-H…O interactions (Figure 6.15).
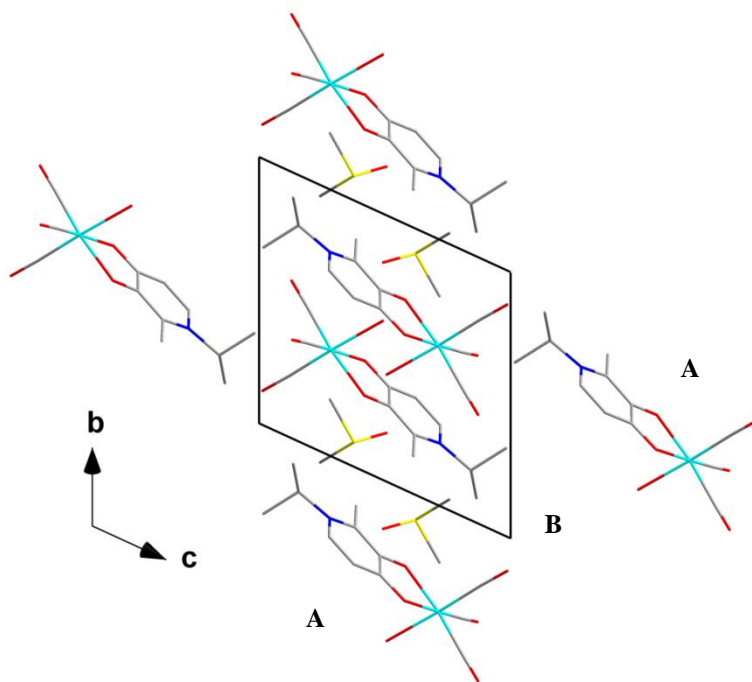
Figure 6.15: Crystal packing of (6) in the unit cell, viewed along the *a*-axis. Hydrogen atoms are omitted for clarity.

6.6   Crystal structure of *fac*-[Re(MI(naltol)(CO)₃(H₂O)]·C₃H₆O (7)

The complex, *fac*-[Re(MI(naltol)(CO)$_3$(H$_2$O)]·C$_3$H$_6$O (**7**) has been synthesized as described in the synthesis section (Paragraph 3.5.12). The yellow cuboidal crystals were obtained from an acetone solution of the product. This complex crystallized in the triclinic crystal system in the $P\bar{1}$ space group with two independent molecules in the unit cell (Z = 2). In the structure of *fac*-[Re(MI(naltol)(CO)$_3$(H$_2$O)]·C$_3$H$_6$O (**7**) the Re atom is octahedrally surrounded by three facially orientated carbonyl ligands, one mono-anionic bidentate coordinated ligand and a neutral water molecule with an acetone solvent molecule in the crystal system. The bidentate ligand has a mono-negative charge, while the water molecule is neutral, which overall results in a neutral complex. A summary of the general crystal data of (**7**) is given in Table 6.1. A summary of the general interatomic bond distances and angles are given in Table 6.8 while the numbering scheme of the neutral complex is shown in Figure 6.16.
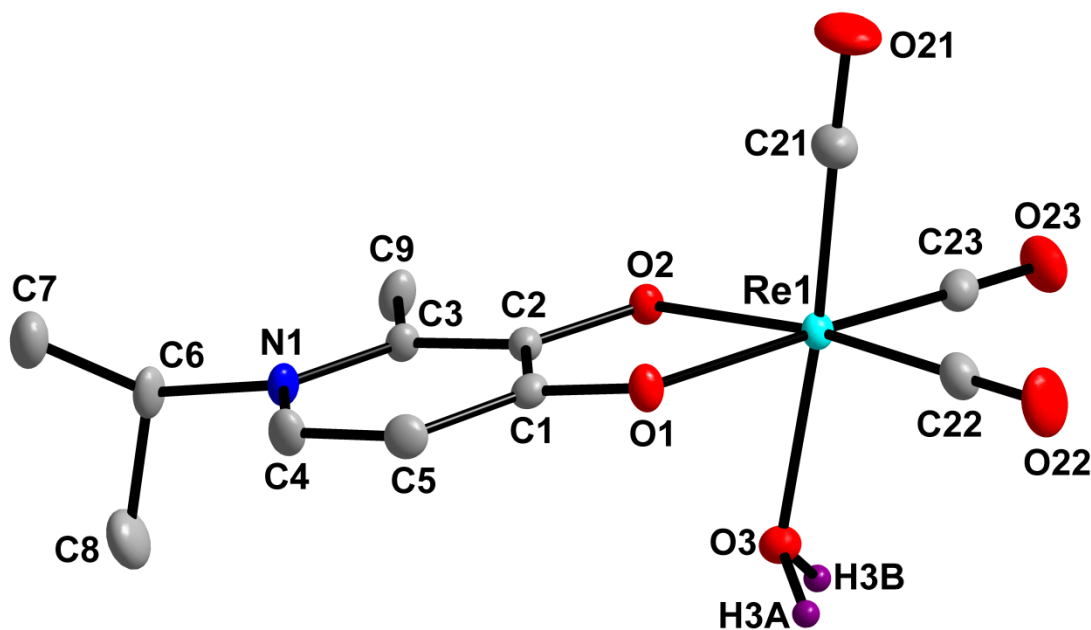
Figure 6.16: Molecular representation of *fac*-[Re(MI(naltol)(CO)₃(H₂O)]·C₃H₆O (8) showing the atom numbering scheme; displacement ellipsoids are drawn at 50 % probability level. Hydrogen atoms are omitted for clarity except for the coordinated aqua ligand.

Table 6.8: Summary of the hydrogen bond distances (Å) and angles (°) observed in (8).

Bond	Bond distance (Å)	Bond angle (atoms)	Bond angle (°)
O(1)-Re(1)	2.124(2)	O(1)-Re(1)-O(2)	77.147(6)
O(2)-Re(1)	2.142(2)	C(22)-Re(1)-C(23)	87.99(15)
C(21)-Re(1)	1.888(4)	C(22)-Re(1)-O(1)	97.73(13)
C(22)-Re(1)	1.908(4)	C(23)-Re(1)-O(2)	96.71(12)
C(23)-Re(1)	1.912(4)	C(21)-Re(1)-O(1)	97.92(13)
C(21)-O(21)	1.160(4)	O(21)-C(21)-Re(1)	178.3(3)
C(22)-O(22)	1.152(4)	C(21)-Re(1)-C(23)	87.17(15)
C(23)-O(23)	1.155(4)	C(22)-Re(1)-C(21)	87.23(16)
O(3)-Re(1)	2.191(2)	C(21)-Re(1)-O(2)	98.41(13)
C(1)-O(1)	1.302(4)	C(23)-Re(1)-O(1)	172.50(12)
C(2)-O(2)	1.348(4)	C(21)-Re(1)-O(3)	175.16(13)
		C(22)-Re(1)-O(2)	172.81(12)

All the bond distances and angles are within normal ranges compared to similar structures.[21-35] The Re−C bond distances of the three facial carbonyl groups are ~ 1.9 Å. The Re−O bond distances are ~ 2.1 Å, the longest being Re(1)−O(3) (2.191(2) Å). The *trans* influence due to the coordinated water molecule is minimal, however the opposite bond distance Re(1)−C(21) is slightly shorter (1.888(4) Å). Furthermore, the Re(1)−O(3) bond distance falls within the same range as the Re−O bond distances found in the methanol solvated and the aqua rhenium complexes (~ 2.2 Å).[21-35] The bidentate coordinated ligand has a bite angle O(1)-Re(1)-O(2) of 77.147(6) ° which is larger than that of similar structures of tropolone and tribromotropolone (74.82(17) ° and 74.07(16) ° respectively) and is within range compared to (**2**), (**3**), (**4**), (**5**) and (**6**).[25,28] The octahedral system surrounding the rhenium atom is distorted with angles ranging from 77.147(6) ° to 178.3(3) ° which is approximately equal to (**2**), (**3**), (**4**), (**5**) and (**6**). The three axes through the vertices of the octahedral system are nonlinear and range between 172 ° and 175 °. The C22-O22 and the C23-O23 axes both lie in the plane with minimal deviations in contrast to (**2**), which is more distorted. The angle between C(21)-Re(1)-O(3) is 175.16(13) ° also indicating that there is a distortion in the structure from the vertical axis through the Re centre (Figure 6.17).
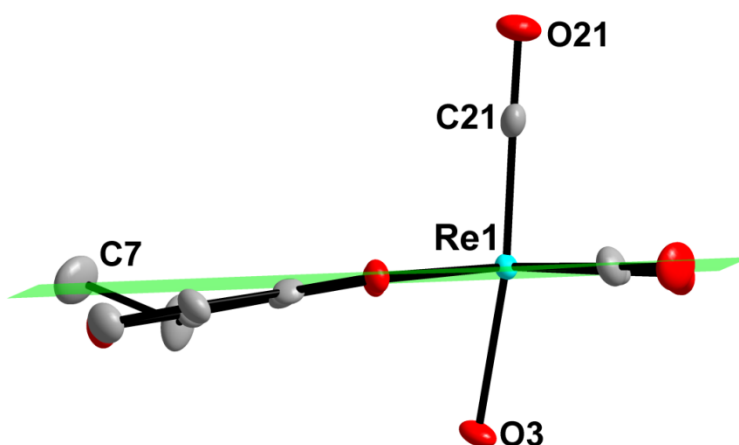
Figure 6.17: Illustration of the equatorial plane (C23 O2 O1 C22 Re1) showing the bidentate coordinated ligand bending out of the plane. Hydrogen atoms are omitted for clarity.

The bidentate coordinated pyridinone ligand bends downwards out of the equatorial plane with the deviation such that the equatorial plane intersects C7 which would ideally lie above the plane (Figure 6.17).
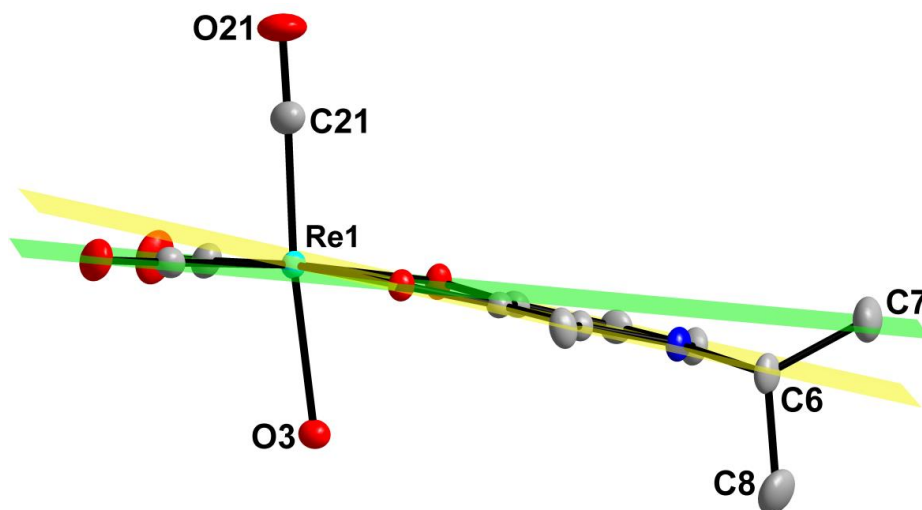
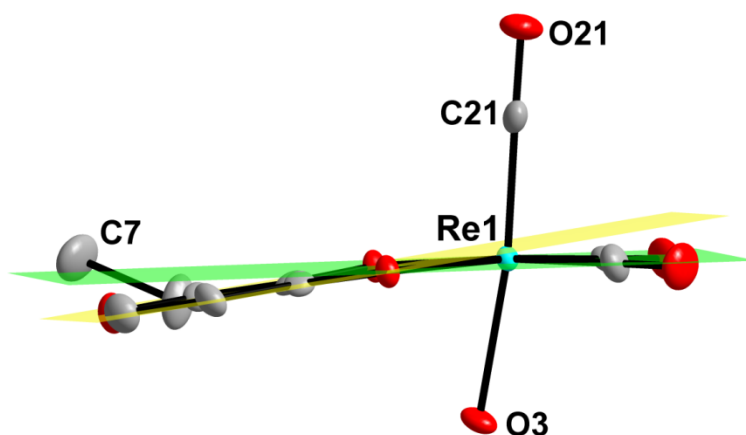**Figure 6.18: Illustration of the dihedral angle between the equatorial plane (C23 O2 O1 C22 Re1) and the plane through the heterocycle of the bidentate coordinated ligand (C1 C2 C3 N1 C4 C5).**

The dihedral angle between the equatorial plane and ring of the bidentate coordinated pyridinone ligand is 7.376 ° which is approximately equal to (**2**), (**3**), (**4**) and (**5**) but bigger than (**6**) (Figure 6.18). This indicates the distortion in the planarity of the bidentate coordinated ligand. The

123

influence of this bending results in a torsion angle of the bidentate coordination site O(1)-C(1)-C(2)-O(2) of 2.273(19) ˚ which is larger compared to (**6**) by 1.573 ˚ and approximately half of (**2**) and (**3**) and within range of (**4**) and (**5**).

Figure 6.19: Hydrogen interactions observed in the structure of *fac*-[Re(MI(naltol)(CO)$_3$(H$_2$O)]·C$_3$H$_6$O (8).

Only seven hydrogen interactions are observed in this structure: two intra-molecular (a combination of one O-H…O interaction and one C-H…O interaction, represented by light purple fragmented bonds) with H3A a bifurcated hydrogen interaction and five inter-molecular (a combination of one O-H…O and four C-H…O interactions, represented by green fragmented bonds). Some of these hydrogen interactions are bi-(H50C, H3A) and tri-furcated (H3B). These hydrogen interactions are illustrated in Figure 6.19, while the distances, angles and symmetry operators are given in Table 6.9.

Table 6.9: Summary of the hydrogen interactions, distances (Å) and angles (˚) observed in (7).

D-H…A	d(D-H) (Å)	d(H…A) (Å)	d(D…A) (Å)	∟ (D-H…A)(˚)
O3-H3A...O11	0.96(6)	1.78(6)	2.727(4)	171(4)
O3-H3B...O2 [(i)]	0.99(6)	1.60(6)	2.595(4)	178(8)
C5-H5...O1 [(ii)]	0.93	2.31	3.199(4)	159
C9-H9B...O2	0.96	2.45	2.897(5)	108
C9-H9C...O21[(iii)]	0.96	2.51	3.316(6)	141
C50-H50C…O1[(iv)]	0.96	2.45	3.387(7)	165
C52-H52C…O2[(v)]	0.96	2.53	3.401(6)	151

Symmetry codes, transformations used to generate equivalent atoms: (i) -x+2, -y+2, -z+1; (ii) –x+1, -y+1, -z+1; (iii) –x+1, -y+2, -z+1; (iv) x, y, z; (v) –x+1, -y+2, -z+1;

The molecules pack along the *ab*-plane in pairs orientated head to head with only one layer (**AA**), this packing order is stabilized by inter-molecular O-H…O and C-H…O interactions (Figure 6.20).
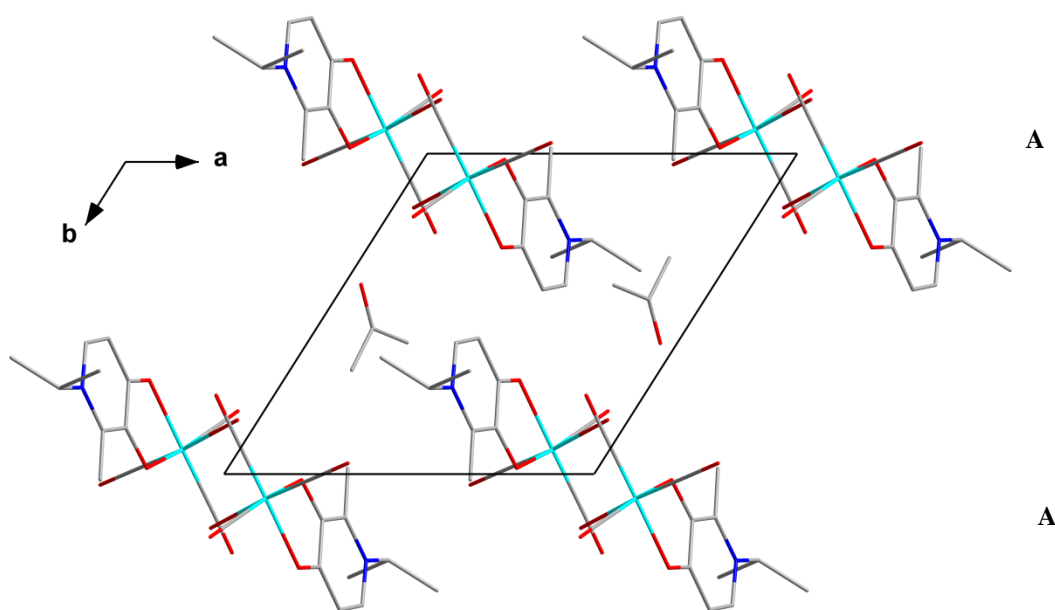
Figure 6.20: Crystal packing of (7) in the unit cell, viewed along the *a*-axis. Hydrogen atoms are omitted for clarity.

6.7 Discussion

Three similar rhenium structures with O,O'-bidentate ligands coordinated to the rhenium center are compared here to (**4**), (**5**), (**6**) and (**7**) to highlight some structural properties and to correlate some structural data between the different complexes (see Figure 6.21 and Table 6.10).

(D)   **(E)**   **(F)**
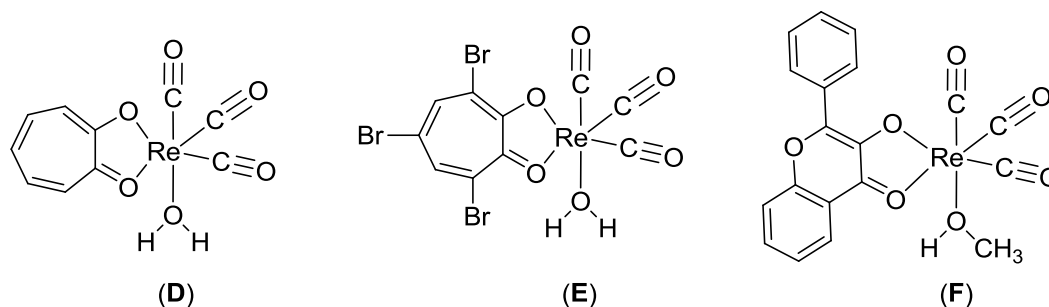
Figure 6.21: Illustration of the crystal structures of *fac*-[Re(Trop)(CO)$_3$(H$_2$O)] (D), *fac*-[Re(TropBr$_3$)(CO)$_3$(H$_2$O)] (E) and *fac*-[Re(Flav)(CO)$_3$(CH$_3$OH)] (F).

Table 6.10: Selected bond distances and angles of *fac*-[Re(O,O'-bidentate)(CO)$_3$(O,O'-monodentate)] complexes.

Formula	(4) [a]	(5) [a] A	(5) [a] B	(6) [a]	(7) [a]	(D) [b]	(E) [c]	(F) [d]
Complexes								
Re−X (X = O/C) Å								
Re−O(1)	2.126(9)	2.102(14)	2.146(14)	2.1316(17)	2.124(2)	2.121(5)	2.123 (5)	2.141(3)
Re−O(2)	2.154(9)	2.215(12)	2.085(11)	2.1318(15)	2.142(2)	2.108(4)	2.146 (4)	2.147(3)
Re−O(3)	2.164(9)	2.150(13)	2.190(12)	2.190(2)	2.191(2)	2.213(5)	2.170 (5)	2.204(4)
Re−C(21)	1.869(2)	1.919(19)	1.873(13)	1.879(3)	1.888(4)	1.890(2)	1.882 (7)	1.905(5)
Re−C(22)	1.896(14)	1.929(12)	1.877(18)	1.907(2)	1.908(4)	1.886(7)	1.897 (6)	1.906(5)
Re−C(23)	1.908(14)	1.928(15)	1.88(2)	1.908(3)	1.912(4)	1.894(8)	1.899 (7)	1.893(5)
O-Re-X (X = O/C) °								
O(1)-Re-O(2)	77.245 (5)	76.20(2)	78.6(4)	77.413(15)	77.147(6)	74.82(17)	74.07 (16)	76.25
C(21)-Re-O(3)	173.1(5)	174.5(7)	174.5(6)	174.16(8)	175.16(13)	176.8(2)	174.33(3)	173.91

[a] Current study, [b] Schutte *et al.* [25], [c] Schutte *et al.* [35], [d] Schutte *et al.* [26]. [Re(Trop)(H$_2$O)] = *fac*-[NEt$_4$][Re(Trop)(CO)$_3$(H$_2$O)]·NO$_3$·H$_2$O with TropH = Tropolone, [Re(TropBr$_3$)(H$_2$O)] = *fac*-[Re(TropBr$_3$)(CO)$_3$(H$_2$O)] with TropBr$_3$H = tribromotropolone and [Re(Flav)(CH$_3$OH)] = *fac*-[Re(Flav)(CO)$_3$(CH$_3$OH)]·CH$_3$OH with FlavH = 3-hydroxyflavone.

In all the complexes mentioned above, Re−O bond distances of the bidentate coordinated ligands are approximately 2.1 Å with only one outlier (**5**) molecule **A** which has a Re−O bond distance of 2.215(12) Å. The Re−O bond distance of the monodentate coordinated ligand (either H$_2$O or MeOH) is slightly longer at ~ 2.2 Å in all the complexes. The Re−C bond distances are approximately 1.9 Å. The bite angles of the bidentate coordinated ligands are somewhat larger than those of (**D**), (**E**) and (**F**), with (**F**) being in range molecule **A** of (**5**) (~ 76 °). The largest bite angle is in molecule **B** (**5**) (78.6(4) °) with (**4**), (**6**) and (**7**) having bite angles of ~ 77 °

followed by (**D**) and (**E**) at approximately 74 ° in both. The vertical axis through the structures C(21)-Re-O(1B) is nonlinear showing deviations from the ideal octahedral conformation (180 °). This could be due to steric demands in the respective structures. The most linear C(21)-Re-O(1B) bond angle is seen in (**D**) with an angle of 176.8(2) °.

6.8   Conclusion

Four crystal structures of the form *fac*-[Re(I)(pyridinonato)(CO)$_3$(H$_2$O)] were successfully obtained and reported in detail in this chapter. Of the four structures, two were close to being *iso-structural i.e.* (**6**) and (**7**) although they crystallized with different solvents namely dimethyl sulfoxide and acetone, respectively. Both (**6**) and (**7**) crystallized in the triclinic space group $P\bar{1}$ with the following crystal parameters; (**6**): a = 10.283(1) Å, b = 10.522(1) Å, c = 10.549(1) Å, α = 102.825(3) °, β = 109.198(3) °, γ = 109.198(3) ° and (**7**): a = 10.110(2) Å, b = 10.129(2) Å, c = 10.493(2) Å, α = 96.243(5) °, β = 103.646(5) °, γ = 119.445(4) °.

In all the structures (**4**) - (**7**) the octahedral systems are distorted with bite angles of the bidentate coordinated ligand ranging from 76 ° to 78 °. These ligands are also bent out of the equatorial plane with dihedral angles between the equatorial plane and the plane through the hetero cyclic ring ranging from 6.4 ° to 11.2 ° in all cases. The structures reported in this chapter show some similarities in their molecular packing and intermolecular interactions. Their structural properties, including bond angles and bond distances are very similar with just a few exceptions. With regards to similar structures in literature one noteworthy point is the larger bite angles of (**4**) **-** (**7**) which could potentially result in better activation of the rhenium centre for synthetic purposes with these compounds as precursors to radiopharmaceuticals. This crystallographic study will add to the existing data in the Crystallographic Cambridge Structural Data base, as little to no structures have been reported on Re(I) tricarbonyl complexes with pyrone and pyridinones as ligand systems.

7 Crystallographic Study of *fac*-[Re(EI(naltol))(CO)$_3$(Y)]

7.1 Introduction

The methanol substitution reactions by a wide range of entering ligands from complexes of the type *fac*-[Re(L,L′-Bid)(CO)$_3$(MeOH)]^n (where L,L′-Bid = N,N′- N,O'-, and O,O′- donor bidentate ligands, n = -1, 0, +1) in methanol as solvent have been reported to validate the [2 + 1] approach adopted by Alberto.[1-5] The [2 + 1] approach entails the coordination of a bidentate ligand of which the lipophilicity can be modulated and a monodentate bifunctional that can act as a potential linker to a biologically active molecule.[6-8] This [2 + 1] approach allows the labeling of bioactive molecules containing a monodentate or a bidentate donor site. This is a versatile synthetic pathway where one can optimize the properties of radionuclides. By varying the bidentate ligand from N,N′-Bid (1,10-phenanthroline, 2,2′-bipyridine) to N,O'-Bid (2-picolinate, 2-quinolate) and O,O′-Bid (tribromotropolonate, hydroxyflavonate) the activation for methanol substitution can be increased.[3] The isolation of both the aqua and methanol coordinated complexes supports the hypothesis made in the latter solution studies that the complexes under investigation undergo a substitution to form the methanol solvated product of the corresponding aqua complex which in turn undergoes a similar substitution to form the final product (e.g. substituted by pyridine as entering nucleophile). This will be further substantiated in the kinetic studies (Chapter 10). The crystal structures of *fac*-[Re(EI(naltol)(CO)$_3$(H$_2$O)] (**8**) and *fac*-

[1] A. Brink, H. G. Visser, A. Roodt, *Inorg. Chem.,* **2014**, *53*, 12480.
[2] A. Brink, H. G. Visser, A. Roodt, *Inorg. Chem.,* **2013**, *52*, 8950.
[3] M. Schutte, A. Roodt, H. G. Visser, *Inorg. Chem.,* **2012**, *51*, 11996.
[4] M. Schutte, G. Kemp, H. G. Visser, A. Roodt, *Inorg. Chem.,* **2011**, *50*, 12486.
[5] M. Schutte, H. G. Visser, *Polyhedron,* **2015**, *89*, 122.
[6] S. Mundwiler, M. Kundig, K. Ortner, R. Alberto, *J. Chem. Soc., Dalton Trans.*, **2004**, *9*, 1320.
[7] N. I. Gorshkov, R. Schibli, A. P. Schubiger, A. A. Lumpov, A. E. Miroslavov, D. N. Suglobov, *J. Organomet. Chem.*, **2004**, *689*, 4757.
[8] R. Alberto, *Top. Curr. Chem.*, **2005**, *252*, 1.

[Re(EI(naltol)(CO)$_3$(MeOH)] (**9**) are reported in this chapter, with a schematic representation of both shown in Scheme 7.1 below.

fac-[Re(EI(naltol))(CO)$_3$(H$_2$O)] (**8**)   *fac*-[Re(EI(naltol))(CO)$_3$(CH$_3$OH)] (**9**)
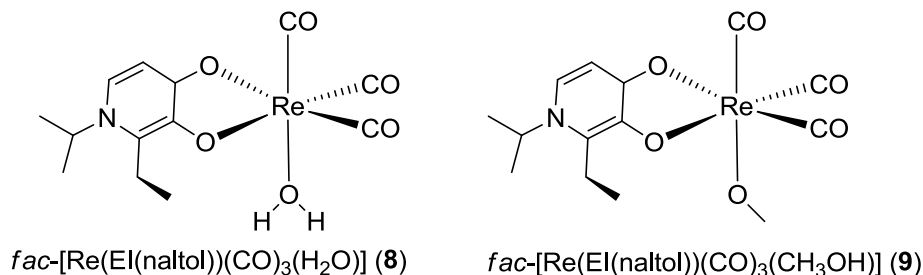
Scheme 7.1: Schematic representation of *fac*-[Re(EI(naltol)(CO)$_3$(H$_2$O)] (8) and *fac*-[Re(EI(naltol)(CO)$_3$(CH$_3$OH)] (9).

7.2   Experimental

The reflection data of (**8**) and (**9**) was collected on a Bruker X8 Apex II 4K Kappa CCD diffractometer using graphite monochromated Mo Kα radiation (λ = 0.70926 Å) with ω- and φ-scans at 100(2) K. The Apex II software package was utilized along with the optimum measurement method in collecting more than a hemisphere of reciprocal space as predicted by COSMO.[9,10] Frame integration and data reduction was performed using the SAINT-Plus and XPREP software packages and SADABS was used for multi-scan absorption correction.[11,12] The structures were solved using direct methods package SIR97 and refined using the WinGX software incorporating SHELXL.[13-19] All atoms were refined anisotropically with the exception of hydrogen atoms. The hydrogen atoms were positioned geometrically and refined utilizing a

[9] **Apex2**, Version 2012.10-0, Bruker AXS Inc.,Madison, Wisconsin, USA, **2012**.

[10] **COSMO**, Version 1.48, Bruker AXS Inc., Madison, Wisconsin, USA, **2003**.

[11] **SADABS**, Version 2012/1, BrukerAXS Inc, Madison, Wisconsin, USA, **2012**.

[12] **SAINT-Plus**, Version 8.27B including XPREP, Bruker AXS Inc., Madison, Wisconsin, USA, **2012**.

[13] A. Altomare, G. Cascarano, C. Giacovazzo, A. Guagliardi, M. C. Burla, G. Polidori, M. Camalli, *J. Appl. Cryst.*, **1994**, *27*, 435.

[14] A. Altomare, M. C. Burla, M. Camalli, G. L. Cascarano, C. Giacovazzo, A. Guagliardi, A. G. G. Moliterni, G. Polidori, R. Spagna, *J. Appl. Cryst.*, **1999**, *32*, 115.

[15] M. C. Burla, M. Camalli, B. Carrozzini, G. L. Cascarano, C. Giacovazzo, G. Polidori, R. Spagna, *J. Appl. Cryst.*, **2003**, *36*, 1103.

[16] P. T. Beurskens, G. Admiraal, G. Beurskens, W. P. Bosman, S. Garcia-Granda, R. O. Gould, J. M. M. Smits, C. Smykalla, Crystallography Laboratory, University of Nijmegen, Toernooiveld, The Netherlands.

[17] L. Palatinus, G. Chapuis, *J. Appl. Cryst.*, **2007**, *40*, 786.

[18] **WinGX**. L. J. Farrugia, *J. Appl. Cryst.*, **2012**, *45*, 849.

[19] G. M. Sheldrick, *Acta Cryst.*, **2008**, *A64*, 112.

riding model with fixed C-H distances of 0.95 Å (CH) [$U_{iso}(H)$ = 1.2 U_{eq}] for aromatic hydrogens, 0.98 Å (CH) [$U_{iso}(H)$ = 1.2 U_{eq}] for methine H-atoms, 0.97 Å (CH) [$U_{iso}(H)$ = 1.2 U_{eq}] for methylene H-atoms and 0.96 Å (CH) [$U_{iso}(H)$ = 1.2 U_{eq}] for methyl H-atoms. Molecular diagrams were generated with DIAMOND with 50 % probability ellipsoids for all non-hydrogen atoms.[20] General crystal data and refinement parameters are represented in Table 7.1 with the complete list of atomic coordinates, equivalent isotropic parameters and hydrogen coordinates given in Appendix A.

---

[20] K. Brandenburg, H. Putz, DIAMOND, Release 3.0e, Crystal Impact GbR, Bonn, Germany, **2006**.

Table 7.1: General X-ray crystallographic data and refinement parameters for *fac*-
[Re(EI(naltol))(CO)$_3$(H$_2$O)]·C$_2$H$_6$OS (8) and *fac*-**[Re(EI(naltol)(CO)$_3$(CH$_3$OH)] (9).**

Crystallographic data	(**8**)	(**9**)
Empirical formula	C$_{15}$H$_{22}$NO$_7$ReS	C$_{14}$H$_{18}$NO$_6$Re
Formula weight (g.mol^{-1})	546.61	482.50
Temperature (K)	100(2)	100(2)
Crystal system	Monoclinic	Triclinic
Space group	$P2_1/n$	$P\bar{1}$
a (Å)	9.569(2)	9.312(2)
b (Å)	18.969(3)	9.833(2)
c (Å)	10.233(2)	10.258(2)
α (°)	90	96.496(6)
β (°)	96.523(6)	112.807(5)
γ (°)	90	110.674(5)
Volume (Å^3)	1845.4(6)	775.3(3)
Z	4	2
ρ $_{calc.}$ (g.cm^{-3})	1.967	2.067
Crystal colour	Colourless	Colourless
Crystal morphology	Cuboid	Plate
Crystal size (mm^3)	0.496 x 0.362 x 0.134	0.285 x 0.284 x 0.083
μ (mm^{-1})	6.734	7.865
F(000)	1064.0	464.0
θ range (°)	3.500 to 28.000	4.038 to 27.997
Index ranges	-9 ≤ h ≤ 12	-12 ≤ h ≤ 8
	-25 ≤ k ≤ 24	-12 ≤ k ≤ 12
	-13 ≤ l ≤ 13	-11 ≤ l ≤ 13
Reflections collected	49762	16203
Unique reflections	4454	3746
Reflections with I > 2σ(I)	9319	9620
R$_{int}$	0.0493	0.0343
Completeness to θ (°; %)	25.24, 99.6	25.24, 99.4
Data/restraints/parameters	4443 / 0 / 239	3728 / 0 / 204
GooF	1.435	1.047
R [I>2σ(I)]	R$_1$ = 0.0229	R$_1$ = 0.0176
	wR$_2$ = 0.0762	wR$_2$ = 0.0410
R (all data)	R$_1$ = 0.0258	R$_1$ = 0.0201
	wR$_2$ = 0.0956	wR$_2$ = 0.0420
ρ$_{max}$, ρ$_{min}$ (e.Å^{-3})	1.164 and -3.342	1.136 and -1.080

7.3   Crystal structure of *fac*-[Re(EI(naltol)(CO)$_3$(H$_2$O)]·C$_3$H$_6$OS (8)

The complex, *fac*-[Re(EI(naltol)(CO)$_3$(H$_2$O)]·C$_3$H$_6$OS (**8**) has been synthesized as described in the synthesis section (Paragraph 3.5.16). The colourless cuboidal crystals were obtained from a DMSO solution of the product. This complex crystallized in a monoclinic crystal system in the *P* 2$_1$/*n* space group with four independent molecules in the unit cell (Z = 4). In the structure of *fac*-[Re(EI(naltol)(CO)$_3$(H$_2$O)]·C$_3$H$_6$OS (**8**) the Re atom is octahedrally surrounded by three facially orientated carbonyl ligands, one mono-anionic bidentate coordinated ligand and a neutral water molecule with a DMSO solvent molecule in the crystal system. The bidentate ligand carries a mono-negative charge as it loses a proton, while the water molecule is neutral, which results in a neutral complex. A summary of the general crystal data of (**8**) is given in Table 7.1. A summary of the general interatomic bond distances and angles are given in Table 7.2 while the numbering scheme of the neutral complex is shown in Figure 7.1.
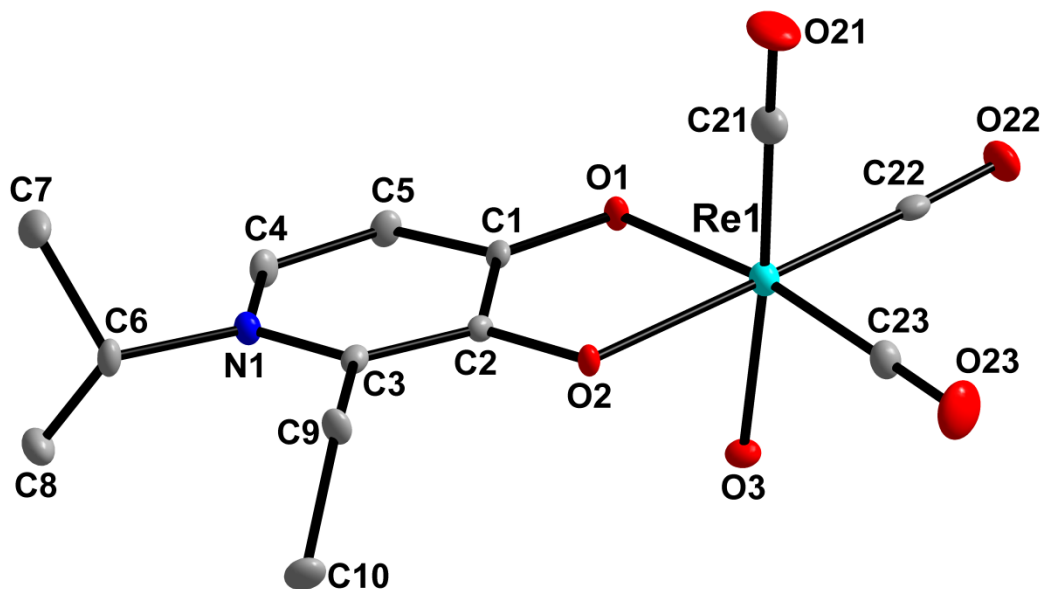
Figure 7.1: Molecular representation of *fac*-[Re(EI(naltol)(CO)$_3$(H$_2$O)]·C$_2$H$_6$OS (8) showing the atom numbering scheme, displacement ellipsoids are drawn at 50 % probability level. Hydrogen atoms are omitted for clarity.

Table 7.2: Selected bond distances (Å) and angles (°) for the crystal structure of (8).

| Bond	Bond distance (Å)	Bond angle (atoms)	Bond angle (°)
O(1)-Re(1)	2.131(3)	O(1)-Re(1)-O(2)	78.07(10)
O(2)-Re(1)	2.139(3)	C(22)-Re(1)-C(23)	87.72(17)
C(21)-Re(1)	1.895(5)	C(22)-Re(1)-O(1)	97.36(14)
C(22)-Re(1)	1.909(4)	C(23)-Re(1)-O(2)	96.55(14)
C(23)-Re(1)	1.909(4)	C(21)-Re(1)-O(1)	97.50(16)
C(21)-O(21)	1.158(6)	O(21)-C(21)-Re(1)	179.5(4)
C(22)-O(22)	1.150(5)	C(21)-Re(1)-C(23)	88.46(19)
C(23)-O(23)	1.160(6)	C(22)-Re(1)-C(21)	86.76(18)
O(3)-Re(1)	2.203(3)	C(21)-Re(1)-O(2)	96.48(16)
C(1)-O(1)	1.308(5)	C(23)-Re(1)-O(1)	172.35(14)
C(2)-O(2)	1.342(5)	C(21)-Re(1)-O(3)	175.78(16)
		C(22)-Re(1)-O(2)	174.69(14)

All the bond distances and angles are within normal ranges compared to similar structures.[21-35] The Re−C bond distances of the three facial carbonyl groups are ~ 1.9 Å. The Re−O bond distances are ~ 2.1 Å, the longest being Re(1)−O(3) (2.203(3) Å). The *trans* influence due to the coordinated water molecule is minimal, however the opposite bond distance Re(1)−C(21) is slightly shorter (1.895(5) Å). Furthermore, the Re(1)−O(3) bond distance falls within the same range as the Re−O bond distances found in the S_N1 methanol substituted rhenium complexes and the aqua complexes (~ 2.2 Å).[21-35] The bidentate coordinated ligand has a bite angle O(1)-Re(1)-O(2) of 78.073(14) ° which is larger than that of similar structures of tropolone and tribromotropolone (74.82(17) ° and 74.07(16) ° respectively) and is within range compared to (**2**), (**3**), (**4**), (**5**), (**6**) and (**7**).[25,28] The octahedral system surrounding the rhenium atom is distorted

[21] M. Sánchez-Lozano, E. M. Vázquez-López, J. M. Hermida-Ramón, C. M. Estévez, *Polyhedron*, **2011**, *30*, 953.

[22] J. Mukiza, E. C. Hosten, T. I. A. Gerber, *Polyhedron*, **2015**, *98*, 251.

[23] S. Mundwiler, M. Kündig, K. Ortner, R. Alberto, *J. Chem. Soc. Dalton Trans.*, **2004**, 1320.

[24] T. R. Hayes, B. B. Kasten, C. L. Barnes, P. D. Benny, *Dalton Trans.*, **2014**, *43*, 6998.

[25] M. Schutte, A. Roodt, H. G. Visser, *Inorg. Chem.*, **2012**, *51*, 11996.

[26] M. Schutte, G. Kemp, H. G. Visser, A. Roodt, *Inorg. Chem.*, **2011**, *50*, 12486.

[27] F. Ragone, G. T. Ruiz, O. E. Piro, G. A. Echeverría, F. M. Cabrerizo, G. Petroselli, R. Erra-Balsells, K. Hiraoka, F. S. GarcíaEinschlag, E. Wolcan, *Eur. J. Inorg. Chem.*, **2012**, 4801.

[28] M. Schutte, H. G. Visser, A. Roodt, *ActaCryst. Sect. E*, **2008**, *E64*, m1610.

[29] K. O. Piletska, K. V. Domasevitch, A. V. Shtemenko, *ActaCryst. Sect. E*, **2016**, *E72*, 590.

[30] A. Brink, H. G.Visser, A. Roodt, *J. Coord. Chem.*, **2011**, *64*, 122.

[31] A. Brink, H. G.Visser, A. Roodt, CCDC 801586: Experimental Crystal Structure Determination, **2014**, DOI: 10.5517/ccvx3mg

[32] A. Brink, H. G. Visser, A. Roodt, *Inorg. Chem.*, **2013**, *52*, 8950.

[33] B. Shankar, P. Elumalai, R. Shanmugam, V. Singh, D. T. Masram, M. Sathiyendiran, *Inorg. Chem.*, **2013**, *52*, 10217.

[34] A. Brink, H. G. Visser, A. Roodt, *Inorg. Chem.*, **2014**, *53*, 12480.

[35] M. Schutte, H. G. Visser, A. Roodt, Acta Cryst., **2008**, *E64*, m1610.

with angles ranging from 78.07(10) ˚ to 179.5(4) ˚ which is approximately equal to (**2**), (**3**), (**4**), (**5**), (**6**) and (**7**). The three axes through the vertices of the octahedral system are nonlinear and range between 172 ˚ and 175 ˚. The C22-O22 and the C23-O23 axes both lie in the plane with minimal deviations in contrast to (**2**), which are more distorted. The angle between C(21)-Re(1)-O(3) is 175.78(16) ˚ also indicating that there is a distortion in the structure from the vertical axis through the Re centre.

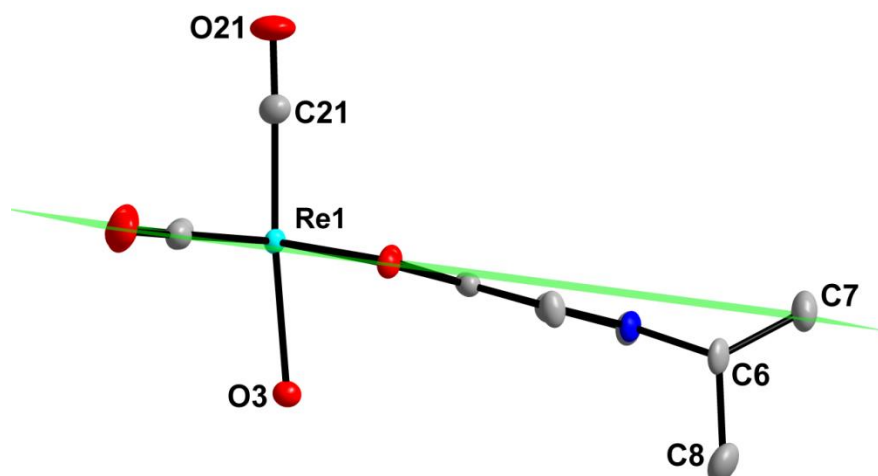**Figure 7.2: Illustration of the equatorial plane (C23 O2 O1 C22 Re1) showing the bidentate coordinated ligand bending out of the plane. Hydrogen atoms are omitted for clarity.**

The bidentate coordinated pyridinone ligand bends downwards out of the equatorial plane, however the equatorial plane intersects C6 instead of C7 as in (**2**) and (**6**), which indicates a lesser distortion in this structure (Figure 7.2).
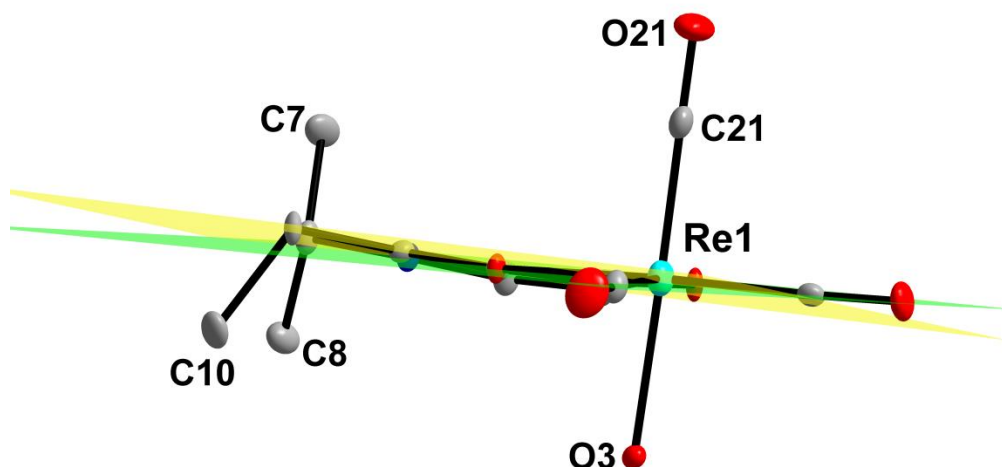
Figure 7.3: Illustration of the dihedral angle between the equatorial plane (C23 O2 O1 C22 Re1) and the plane through the heterocycle of the bidentate coordinated ligand (C1 C2 C3 N1 C4 C5).

The dihedral angle between the equatorial plane and ring of the bidentate coordinated pyridinone ligand is 6.048(15) ° which is smaller by a factor ~ 0.351 ° compared to (**6**) (Figure 7.3). This indicates that the distortion in the planarity of the bidentate coordinated ligand is less compared to (**2**), (**3**), (**4**), (**5**), (**6**) and (**7**). The influence of this bending results in a torsion angle of the bidentate coordination site O(1)-C(1)-C(2)-O(2) of 4.670(54) ° which is bigger compared to (**4**), (**5**), (**6**) and (**7**) but similar to (**2**) and (**3**).
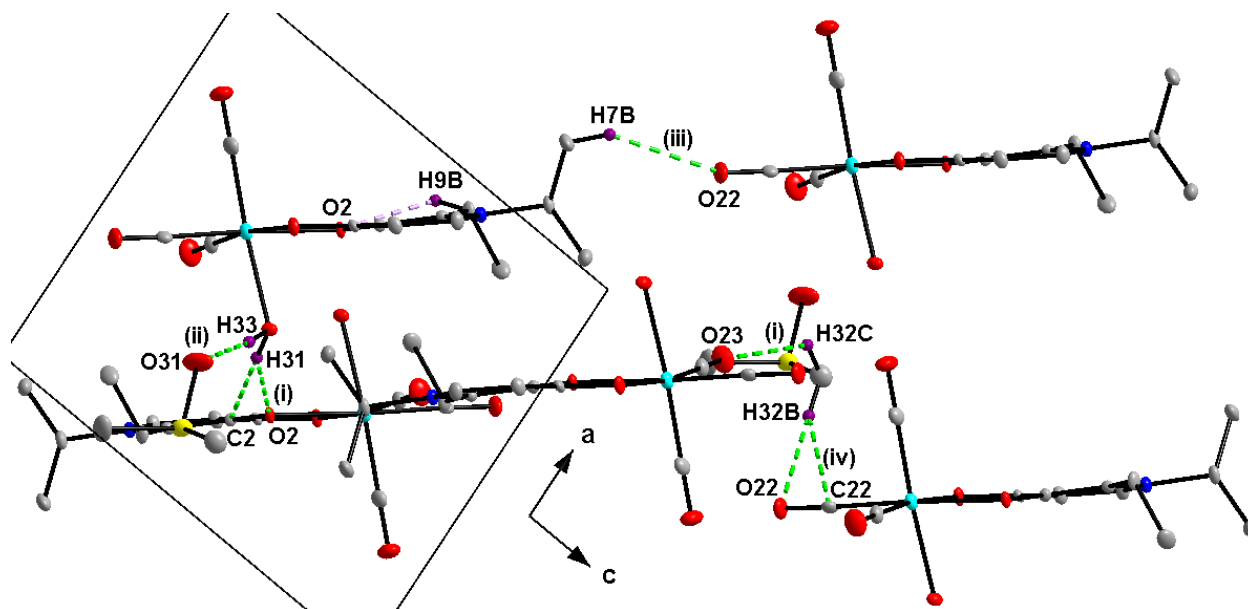
Figure 7.4: Hydrogen interactions observed in the structure of *fac*-[Re(MI(naltol)(CO)₃(H₂O)]·C₂H₆OS (8).

Six hydrogen interactions are observed in this structure, one intramolecular (C-H…O interactions, represented by light purple fragmented bonds) and five inter-molecular (a combination of two O-H…O and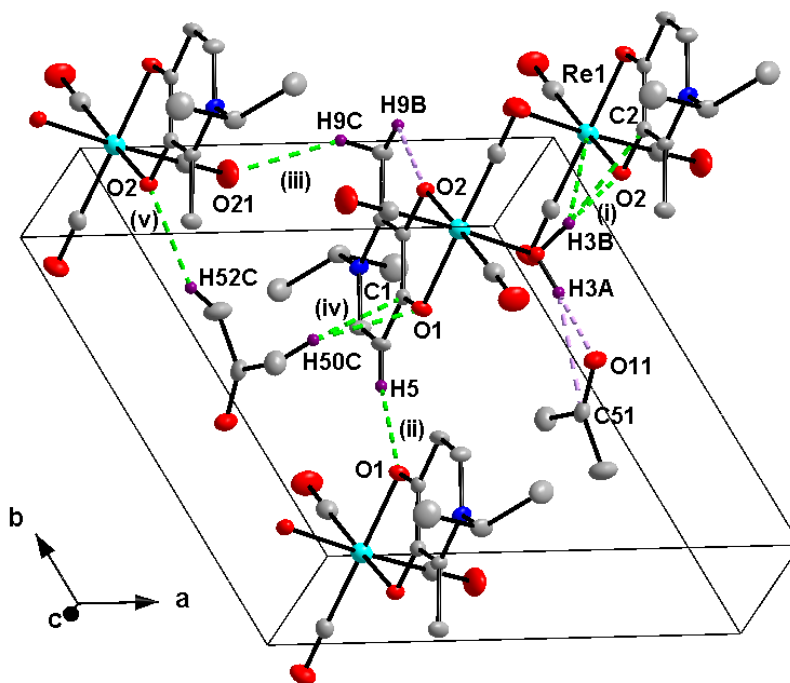 three C-H…O interactions, represented by green fragmented bonds) with H31 and H32B bifurcated O-H…O, C-H…O and C-H…C hydrogen interactions. These hydrogen interactions are illustrated in Figure 7.4, while the distances, angles and symmetry operators are given in Table 7.3.

Table 7.3: Summary of the hydrogen interactions, distances (Å) and angles (°) observed in (8).

D-H…A	d(D-H) (Å)	d(H…A) (Å)	d(D…A) (Å)	∟ (D-H…A)(°)
O3-H31...O2 (i)	1.01(8)	1.75(8)	2.696(4)	154(7)
O3-H33...O31(ii)	0.70(6)	1.97(6)	2.659(5)	168(7)
C7-H7B...O22 (iii)	0.96	2.59	3.461(5)	151
C9-H9B...O2	0.97	2.43	2.853(5)	106
C32-H32B...O22(iv)	0.96	2.55	3.488(6)	164
C32-H32C...O23(i)	0.96	2.55	3.203(7)	125

Symmetry codes, transformations used to generate equivalent atoms: (i) -x,1-y,-z; (ii) -1/2+x,1/2-y,-1/2+z; (iii) 1+x,y,1+z; (iv) x,y,1+z;

The molecules pack in alternating layers along the *bc*-plane with each layer constituted by a pair of molecules orientated in a staggered conformation (**ABA**) (Figure 7.5). This packing order is stabilized by inter-molecular O-H…O and C-H…O interactions.
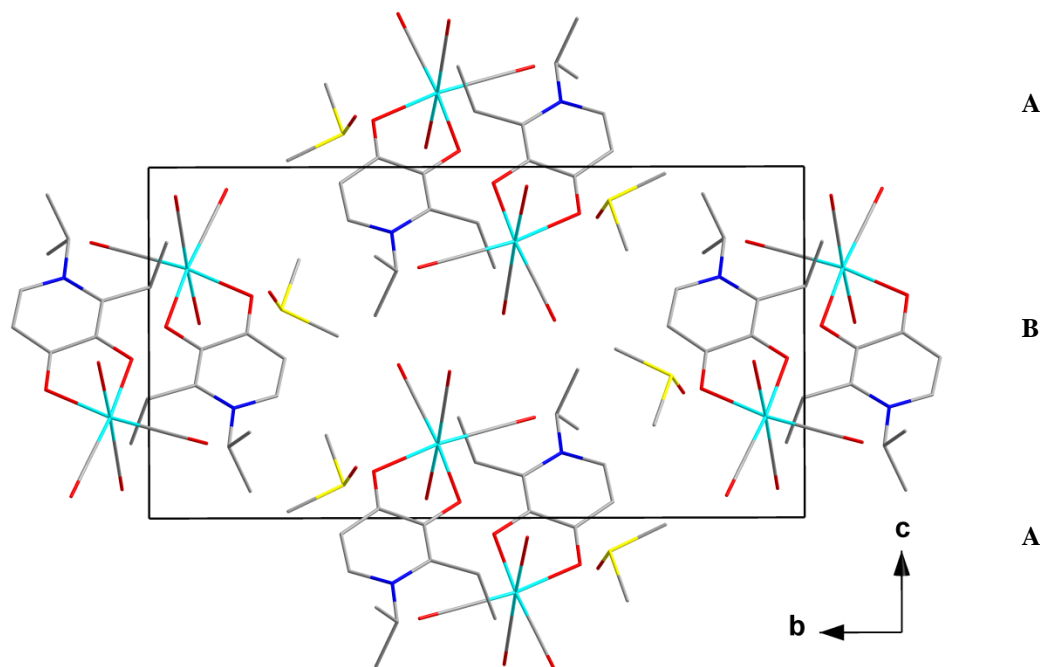
Figure 7.5: Crystal packing of (8) in the unit cell, viewed along the *a*-axis. Hydrogen atoms are omitted for clarity.

7.4   Crystal structure of *fac*-[Re(EI(naltol)(CO)₃(CH₃OH)] (9)

Colourless plates of the complex *fac*-[Re(EI(naltol)(CO)$_3$(CH$_3$OH)] (**9**) were obtained from a methanol solution of the corresponding aqua complex *fac*-[Re(EI(naltol)(CO)$_3$(H$_2$O)] (Paragraph 3.5.16). This complex crystallized in the triclinic $P\bar{1}$ space group with two independent molecules in the unit cell (Z = 2). In the structure of *fac*-[Re(EI(naltol)(CO)$_3$(CH$_3$OH)] (**9**) the Re atom is octahedrally surrounded by three facially orientated carbonyl ligands, one mono-anionic bidentate coordinated ligand and a neutral methanol ligand. The bidentate coordinated ligand carries a mono-negative charge as it loses a proton and the coordinated methanol is neutral. A summary of the general interatomic bond distances and angles are given in Table 7.4 while the numbering scheme of the neutral molecule is shown in Figure 7.6.

137
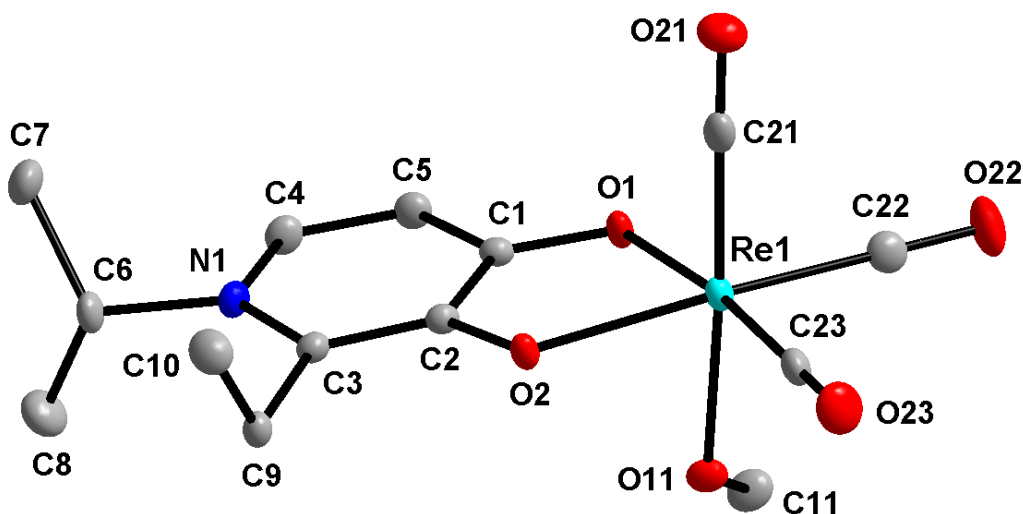
Figure 7.6: Molecular representation of *fac*-**[Re(EI(naltol)(CO)₃(CH₃OH)] (9) showing the atom numbering scheme, displacement ellipsoids are drawn at 50 % probability level. Hydrogen atoms are omitted for clarity.**

Table 7.4: Selected bond distances (Å) and angles (°) for the crystal structure of (9).

Bond	Bond distance (Å)	Bond angle (atoms)	Bond angle (°)
O(1)-Re(1)	2.1141(19)	O(1)-Re(1)-O(2)	77.57(2)
O(2)-Re(1)	2.148(2)	C(22)-Re(1)-C(23)	88.93(13)
C(21)-Re(1)	1.895(3)	C(22)-Re(1)-O(1)	96.20(11)
C(22)-Re(1)	1.902(3)	C(23)-Re(1)-O(2)	96.95(11)
C(23)-Re(1)	1.922(3)	C(21)-Re(1)-O(1)	95.76(10)
C(21)-O(21)	1.158(3)	O(21)-C(21)-Re(1)	178.4(3)
C(22)-O(22)	1.156(4)	C(21)-Re(1)-C(23)	88.06(12)
C(23)-O(23)	1.153(4)	C(22)-Re(1)-C(21)	87.16(12)
O(11)-Re(1)	2.200(2)	C(21)-Re(1)-O(2)	99.11(10)
C(1)-O(1)	1.300(3)	C(23)-Re(1)-O(1)	173.74(9)
C(2)-O(2)	1.354(3)	C(21)-Re(1)-O(11)	175.62(2)
		C(22)-Re(1)-O(2)	171.51(9)

All the bond distances and angles are within normal ranges compared to similar structures.[21-35] The Re−C bond distances of the three facial carbonyl groups are ~ 1.9 Å. The Re−O bond distances are ~ 2.14 Å, the longest being Re(1)−O(11) (2.200(2) Å), possibly due to the nucleophilic properties of the methanol ligand and the lone pair on the oxygen atom (O11). The *trans* influence due to the coordinated methanol is minimal, however the opposite bond distance Re(1)−C(21) is slightly shorter (1.895(3) Å). Furthermore, the Re(1)−O(11) bond distance falls within the same range as the Re−O bond distances found in the S$_N$1 methanol substituted rhenium complexes and the aqua complexes (~ 2.2 Å).[21-35] The bidentate coordinated ligand has

a bite angle O(1)-Re(1)-O(2) of 77.57(2) ° which is larger than that of similar structures of tropolone and tribromotropolone (74.82(17) ° and 74.07(16) ° respectively) but equal to (**2**), (**3**), (**4**), (**5**), (**6**), (**7**) and (**8**).[25,28]

The octahedral system surrounding the rhenium atom is distorted with angles ranging from 77.57(2) ° to 178.4(3) ° which is approximately equal to (**2**), (**3**), (**4**), (**5**), (**6**), (**7**) and (**8**). The three axes through the vertices of the octahedral system are nonlinear and range between 171 ° and 175 °. The C22-O22 and the C23-O23 axes both lie in the plane with minimal deviations in contrast to (**2**), which was more distorted. The angle between C(21)-Re(1)-O(11) is 175.62(2) ° also indicating that there is a distortion in the structure from the vertical axis through the Re centre.
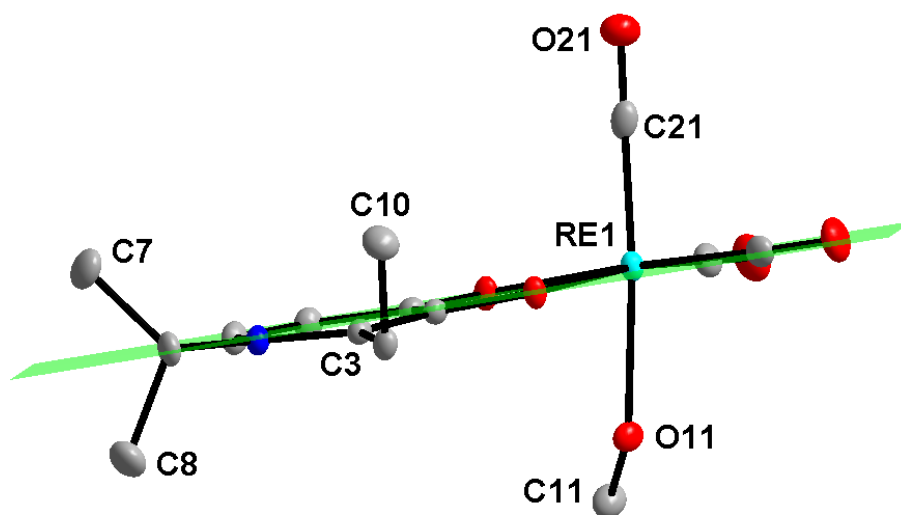
Figure 7.7: Illustration of the equatorial plane (C23 O2 O1 C22 Re1) showing the bidentate coordinated ligand bending out of the plane. Hydrogen atoms are omitted for clarity.

The dihedral angle between the equatorial plane (C23 O2 O1 C22 Re1) and the ring of the bidentate coordinated pyridinone ligand (C1 C2 C3 N1 C4 C5) is 3.001(9) ° which is approximately half compared to that of (**6**) and (**8**) and a lot smaller compared to (**2**), (**3**), (**4**), (**5**) and (**7**). This indicates the planarity of the bidentate coordinated ligand. The ring bends out of the equatorial plane with the torsion angle of the bidentate coordination site O(1)-C(1)-C(2)-O(2)

equal to 2.42(5) ° which is approximately equal to (**4**), (**5**) and (**7**), bigger than (**6**) but a lot smaller compared to (**2**), (**3**) and (**8**) (Figure 7.7).
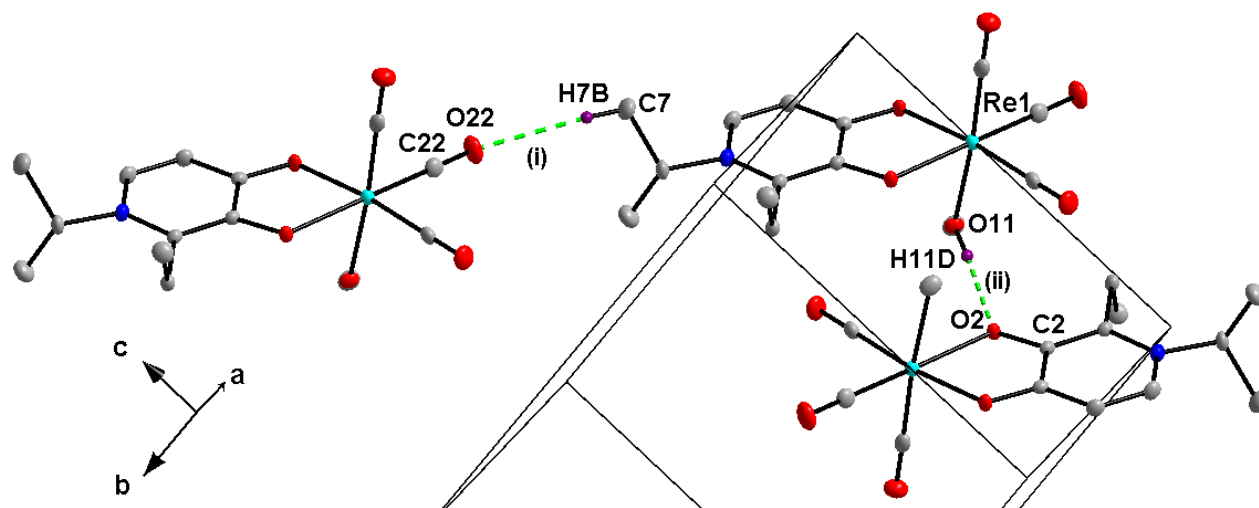
Figure 7.8: Hydrogen interactions observed in the structure of *fac*-[Re(EI(naltol)(CO)$_3$(CH$_3$OH)] (9).

Only two hydrogen interactions are observed in this structure and they are both inter-molecular hydrogen interactions (O-H…O and C-H…O, both represented by green fragmented bonds). These hydrogen interactions are illustrated in Figure 7.8, while the distances, angles and symmetry operators are given in Table 7.5.

Table 7.5: Summary of the hydrogen interactions, distances (Å) and angles (°) observed in (9).

D-H…A	d(D-H) (Å)	d(H…A) (Å)	d(D…A) (Å)	∠ (D-H…A)(°)
O11-H11D...O2 [(i)]	0.77(4)	1.80(4)	2.571(3)	173(5)
C7-H7B...O22 [(ii)]	0.96	2.53	3.438(5)	158

Symmetry codes, transformations used to generate equivalent atoms: (i) -x+1, -y+2, -z+1; (ii) x, +1+y, +1+z;

The molecules pack in two alternating layers (**AB**) along the *bc*-plane with molecules in the layer **B** orientated at ~ 180 ° to molecules in layer **A** and stabilized by inter-molecular O-H…O and C-H…O hydrogen interactions (Figure 7.9).
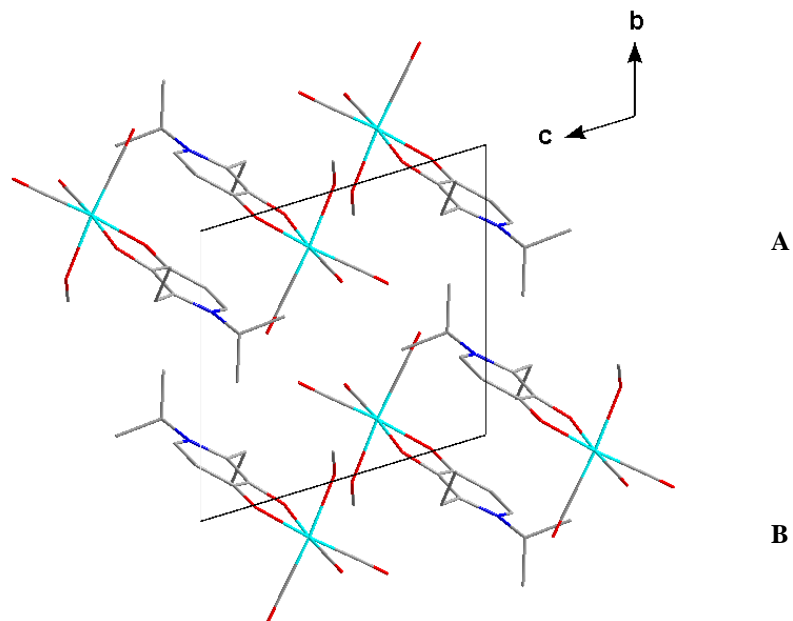
Figure 7.9: Crystal packing of (9) in the unit cell, viewed along the *a*-axis. Hydrogen atoms are omitted for clarity.

7.5 Discussion

Three similar rhenium structures with O,O'-bidentate ligands coordinated to the rhenium center are compared here to (**8**) and (**9**) to highlight some structural properties and to correlate some structural data between the different complexes (see Figure 7.10 and Table 7.6).
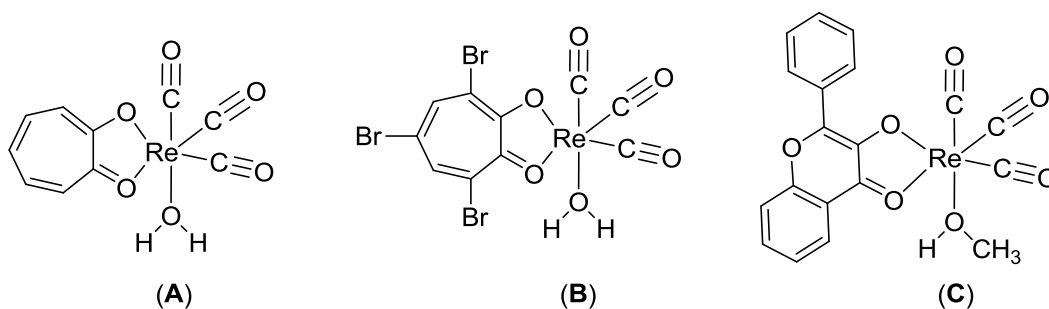
Figure 7.10: Illustration of the crystal structures of *fac*-[Re(Trop)(CO)$_3$(H$_2$O)] (A), *fac*-[Re(TropBr$_3$)(CO)$_3$(H$_2$O)] (B) and *fac*-[Re(Flav)(CO)$_3$(CH$_3$OH)] (C).

141

Table 7.6: Selected bond distances and angles of *fac*-[Re(O,O'-bidentate)(CO)$_3$(Y)] complexes (Y = aqua or MeOH).

Formula	(8) [a]	(9) [a]	[Re(Trop)(H$_2$O)] [b]	[Re(TropBr$_3$)(H$_2$O)] [c]	[Re(Flav)(CH$_3$OH)] [d]
			Complexes		
			Re−X (X = O/C) Å		
Re−O(1)	2.131(3)	2.1141(19)	2.121(5)	2.123 (5)	2.141(3)
Re−O(2)	2.139(3)	2.148(2)	2.108(4)	2.146 (4)	2.147(3)
Re−O(3)/ O(11)	2.203(3)	2.200(2)	2.213(5)	2.170 (5)	2.204(4)
Re−C(21)	1.895(5)	1.895(3)	1.890(2)	1.882 (7)	1.905(5)
Re−C(22)	1.909(4)	1.902(3)	1.886(7)	1.897 (6)	1.906(5)
Re−C(23)	1.909(4)	1.922(3)	1.894(8)	1.899 (7)	1.893(5)
			O-Re-X (X = O/C) °		
O(1A)-Re-O(2A)	78.07(10)	77.57(2)	74.82(17)	74.07 (16)	76.25
C(21)-Re-O(1B)	175.78(16)	175.62(2)	176.8(2)	174.33(3)	173.91

[a] Current study, [b] Schutte *et al.* [25], [c] Schutte *et al.* [35], [d] Schutte *et al.* [26]. [Re(Trop)(H$_2$O)] = *fac*-[NEt$_4$][Re(Trop)(CO)$_3$(H$_2$O)]·NO$_3$·H$_2$O with TropH = Tropolone, [Re(TropBr$_3$)(H$_2$O)] = *fac*-[Re(TropBr$_3$)(CO)$_3$(H$_2$O)] with TropBr$_3$H = tribromotropolone and [Re(Flav)(CH$_3$OH)] = *fac*-[Re(Flav)(CO)$_3$(CH$_3$OH)]·CH$_3$OH with FlavH = 3-hydroxyflavone.

In all the complexes mentioned above, the Re−O bond distances of the bidentate coordinated ligands are approximately 2.1 Å. The Re−O bond distance of the monodentate coordinated ligand (either H$_2$O or MeOH) is slightly longer ~ 2.2 Å in all the complexes. The Re−C bond distances are approximately 1.9 Å. The bite angles of the bidentate coordinated ligands in (**8**) and (**9**) are a little larger than those of (**A**), (**B**) and (**C**), with both (**8**) and (**9**) having bite angles ~ 78 ° followed by (**C**) with 76 ° and (**A**) and (**B**) at approximately 74 ° in both. The vertical axis through the structures C(21)-Re(1)-O(3/11) is nonlinear showing deviations from the ideal octahedral conformation (180 °). This could be due to the steric demands in the structures, with the most linear one being (**A**).

7.6 Conclusion

fac-[Re(EI(naltol))(CO)$_3$(H$_2$O)] (**8**) was dissolved in methanol to do preliminary investigations of the methanol substitution reactions of all the respective aqua complexes synthesized in this study (Section 3.6.9 - 3.6.16). Suitable crystals of (**9**) were obtained for X-ray crystallography characterization. However, in this case, the structure of (**9**) confirmed the formation of the methanol solvated product of (**8**) which is *fac*-[Re(EI(naltol))(CO)$_3$(CH$_3$OH)] (**9**). This then serves as proof and a reasonable basis to construct the solution experiments in Chapter 10, and

confirms that the aqua complexes rapidly convert to the methanol species (in methanol as solvent) for all the compounds/structures described in the previous chapters too.

In both (**8**) and (**9**) the octahedral system is distorted with bite angles of the bidentate coordinated ligands approximately 78 °, these ligands are also bent out of the equatorial plane with dihedral angles between the equatorial plane and the plane through the hetero-cyclic ring ranging between 3 ° and 7 ° in both cases. The compounds (**8**) and (**9**) however compare well with similar complexes with an O,O'-bidentate ligand, three facial carbonyl ligands and a monodentate O-donor coordinating ligand such as an aqua or methanol in an octahedral coordination geometry. A distinct feature of (**8**) and (**9**) is the larger bite angles (which can potentially activate the rhenium center more for synthetic purposes as precursors for metallodrugs) of the coordinated ligands.

Although only one methanol coordinated structure was obtained in this study, this structure (**9**) and work done by Roodt *et al.* serves as substantial proof that the methanol solvation does occur.[32-34] This forms the basis for the kinetic studies in Chapter 10, wherein more definite evidence will be reported from the solution kinetic studies, and complete reaction mechanisms, as supporting arguments.

8 Crystallographic Study of *fac*-Re(I)(CO)₃ Kinetic Substitution Products

8.1 Introduction

Different *fac*-[Re(O,O′-Bid)(CO)$_3$(H$_2$O)] (O,O′-BidH = pyridinone type ligands) complexes have been successfully synthesized as described in Chapter 3, and the pyridine substitution reactions were investigated in methanol, see following chapters. The crystal structures of the kinetic substitution products *fac*-[Re(ME(naltol))(CO)$_3$(4-MPyr)] (**10**) (4-MPyr = 4-Methylpyridine), *fac*-[Re(EM(naltol))(CO)$_3$(Pyr)] (**11**) and *fac*-[Re(EE(naltol))(CO)$_3$(Pyr)] (**12**) (Pyr = pyridine) are reported here to confirm the substitution mode as to be discussed later.

Some receptors are abundantly found in some organs or are overexpressed in tumor cells, making them appropriate target molecules for tumor imaging or organ imaging agents. For theranostic applications, antibodies or biomolecules can be attached either on the bifunctional bidentate ligand or on the monodentate ligand that are selective for appropriate receptors. Additionally, some receptors can in principle be targeted directly by exploiting their ability towards nucleophilic attack at the Re center as some receptors are good electron donors and therefore mimic different ligand systems (e.g. glutamine a tumor nutrient with a nucleophilic *N*-functional group). In this context the reaction rates of such processes are then very important. A schematic representation of example crystal structures of three kinetic substitution products reported in this chapter is given in Scheme 8.1 below.
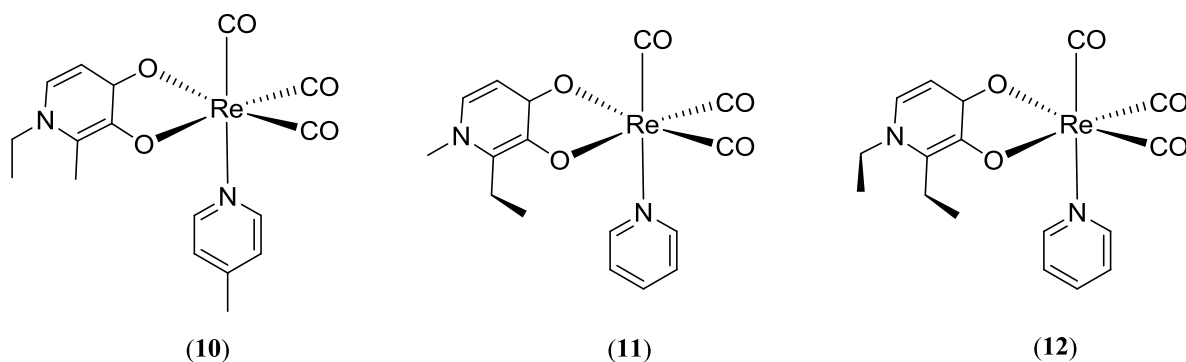
Scheme 8.1: Schematic representation of the three crystal structures, the final products in the substitution reactions described later, as reported in this chapter.

8.2 Experimental

The reflection data of (**10**), (**11**) and (**12**) was collected on a Bruker X8 Apex II 4K Kappa CCD diffractometer using graphite monochromated Mo Kα radiation (λ= 0.70926 Å) with ω- and φ-scans at 100(2) K. The Apex II software package was utilized along with the optimum measurement method in collecting more than a hemisphere of reciprocal space as predicted by COSMO.[1,2] Frame integration and data reduction was performed using the SAINT-Plus and XPREP software packages and SADABS was used for multi-scan absorption correction.[3,4] The structures were solved using direct methods package SIR97 and refined using the WinGX software incorporating SHELXL.[5-11] All atoms were refined anisotropically with the exception of hydrogen atoms. The hydrogen atoms were positioned geometrically and refined utilizing a riding model with fixed C-H distances of 0.95 Å (CH) [$U_{iso}(H) = 1.2\ U_{eq}$] for aromatic

[1] **Apex2**, Version 2012.10-0, Bruker AXS Inc.,Madison, Wisconsin, USA, **2012**.

[2] **COSMO**, Version 1.48, Bruker AXS Inc., Madison, Wisconsin, USA, **2003**.

[3] **SADABS**, Version 2012/1, BrukerAXS Inc, Madison, Wisconsin, USA, **2012**.

[4] **SAINT-Plus**, Version 8.27B including XPREP, Bruker AXS Inc., Madison, Wisconsin, USA, **2012**.

[5] A. Altomare, G. Cascarano, C. Giacovazzo, A. Guagliardi, M. C. Burla, G. Polidori, M. Camalli, *J. Appl. Cryst.*, **1994**, *27*, 435.

[6] A. Altomare, M. C. Burla, M. Camalli, G. L. Cascarano, C. Giacovazzo, A. Guagliardi, A. G. G. Moliterni, G. Polidori, R. Spagna, *J. Appl. Cryst.*, **1999**, *32*, 115.

[7] M. C. Burla, M. Camalli, B. Carrozzini, G. L. Cascarano, C. Giacovazzo, G. Polidori, R. Spagna, *J. Appl. Cryst.*, **2003**, *36*, 1103.

[8] P. T. Beurskens, G. Admiraal, G. Beurskens, W. P. Bosman, S. Garcia-Granda, R. O. Gould, J. M. M. Smits, C. Smykalla, Crystallography Laboratory, University of Nijmegen, Toernooiveld, The Netherlands.

[9] L. Palatinus, G. Chapuis, *J. Appl. Cryst.*, **2007**, *40*, 786.

[10] **WinGX**. L. J. Farrugia, *J. Appl. Cryst.*, **2012**, *45*, 849.

[11] G. M. Sheldrick, *Acta Cryst.*, **2008**, *A64*, 112.

hydrogens, 0.97 Å (CH) [U_{iso}(H) = 1.2 U_{eq}] for methylene H-atoms and 0.96 Å (CH) [U_{iso}(H) = 1.2 U_{eq}] for methyl H-atoms. Molecular diagrams were generated with DIAMOND with 50 % probability ellipsoids for all non-hydrogen atoms.[12] General crystal data and refinement parameters are represented in Table 5.1 with the complete list of atomic coordinates, equivalent isotropic parameters and hydrogen coordinates given in Appendix A.

---

[12] K. Brandenburg, H. Putz, DIAMOND, Release 3.0e, Crystal Impact GbR, Bonn, Germany, **2006**.

Table 8.1: General X-ray crystallographic data and refinement parameters for *fac*-[Re(ME(naltol))(CO)$_3$(4-MPyr)] (10), *fac*-[Re(EM(naltol))(CO)$_3$(Pyr)] (11) and *fac*-[Re(EE(naltol))(CO)$_3$(Pyr)] (12).

Crystallographic data	(10)	(11)	(12)
Empirical formula	C$_{17}$H$_{17}$N$_2$O$_5$Re	C$_{16}$H$_{17}$N$_2$O$_6$Re	C$_{17}$H$_{19}$N$_2$O$_6$Re
Formula weight (g.mol^{-1})	515.54	519.53	533.55
Temperature (K)	100(2)	100(2)	100(2)
Crystal system	Monoclinic	Monoclinic	Monoclinic
Space group	*P*2$_1$/*n*	*P*2$_1$/*c*	*P*2$_1$/*c*
a (Å)	8.112(1)	15.942(2)	16.658(2)
b (Å)	13.106(1)	8.328(3)	8.1684(7)
c (Å)	16.238(2)	13.357(4)	13.265(1)
α (°)	90	90	90
β (°)	93.140(3)	103.865(8)	96.300(3)
γ (°)	90	90	90
Volume (Å^3)	1723.8(3)	1721.7(8)	1794.0(3)
Z	4	4	4
ρ $_{calc.}$ (g.cm^{-3})	1.987	2.004	1.975
Crystal colour	Yellow	Yellow	Yellow
Crystal morphology	Cuboid	Cuboid	Cuboid
Crystal size (mm^3)	0.416 x 0.337 x 0.211	0.563 x 0.464 x 0.296	0.496 x 0.362 x 0.134
μ (mm^{-1})	7.079	7.093	6.810
F(000)	992.0	1000.0	1032.0
θ range (°)	2.512 to 27.999	5.070 to 27.999	4.849 to 27.999
Index ranges	$-10 \leq h \leq 10$	$-21 \leq h \leq 17$	$-22 \leq h \leq 22$
	$-17 \leq k \leq 14$	$-11 \leq k \leq 11$	$-7 \leq k \leq 10$
	$-21 \leq l \leq 18$	$-14 \leq l \leq 17$	$-17 \leq l \leq 15$
Reflections collected	30153	27709	31274
Unique reflections	4174	4144	4338
Reflections with I > 2σ(I)	9948	9703	9840
R$_{int}$	0.0480	0.0455	0.0468
Completeness to θ (°; %)	25.24, 99.3	25.24, 96.4	25.24, 98.8
Data/restraints/parameters	4151 / 0 / 230	4016 / 0 / 236	4302 / 0 / 245
GooF	1.271	1.190	1.064
R [I>2σ(I)]	R$_1$ = 0.0307	R$_1$ = 0.0359	R$_1$ = 0.0187
	wR$_2$ = 0.0627	wR$_2$ = 0.0852	wR$_2$ = 0.0505
R (all data)	R$_1$ = 0.0315	R$_1$ = 0.0391	R$_1$ = 0.0199
	wR$_2$ = 0.0631	wR$_2$ = 0.0873	wR$_2$ = 0.0514
ρ$_{max}$, ρ$_{min}$ (e.Å^{-3})	1.912 and -1.239	2.405 and -2.653	1.366 and -1.209

8.3   Crystal structure of *fac*-[Re(ME(naltol))(CO)₃(4-MPyr)] (10)

The complex, *fac*-[Re(ME(naltol))(CO)$_3$(4-MPyr)] (4-MPyr = 4-methyl pyridine/ γ-picoline) (**10**) has been synthesized as described in the synthesis section (Paragraph 3.5.17). The yellow cuboidal crystals were obtained from a DMSO solution of the product. This complex crystallized in the monoclinic crystal system in the *P*2$_1$/*n* space group with four independent molecules in the unit cell (Z = 4). In the structure of *fac*-[Re(ME(naltol))(CO)$_3$(4-MPyr)] (**10**) the Re atom is octahedrally surrounded by three facially orientated carbonyl ligands, one mono-anionic bidentate coordinated ligand and a neutral pyridine-type molecule. The bidentate ligand carries a mono-negative charge while the pyridine ligand is neutral, thus yielding a neutral complex. A summary of the general crystal data of (**10**) is given in Table 8.1, while the general interatomic bond distances and angles are given in Table 8.2 and the numbering scheme of the neutral complex is shown in Figure 8.1.
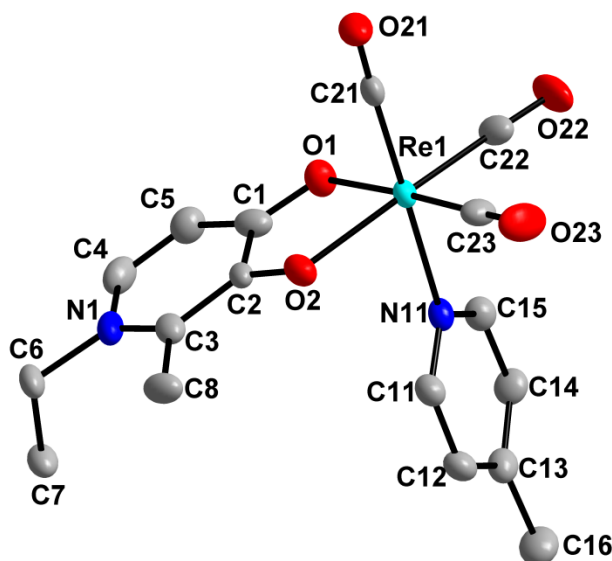
Figure 8.1: Molecular representation of *fac*-[Re(ME(naltol))(CO)₃(4-MPyr)] (10) showing the atom numbering scheme, displacement ellipsoids are drawn at 50 % probability level. Hydrogen atoms are omitted for clarity.

148

Table 8.2: Selected bond distances (Å) and angles (°) for the crystal structure of (10).

Bond	Bond distance (Å)	Bond angle (atoms)	Bond angle (°)
O(1)-Re(1)	2.121(4)	O(1)-Re(1)-O(2)	78.222(11)
O(2)-Re(1)	2.116(3)	C(22)-Re(1)-C(23)	86.6(2)
C(21)-Re(1)	1.915(5)	C(22)-Re(1)-O(1)	95.5(2)
C(22)-Re(1)	1.908(5)	C(23)-Re(1)-O(2)	99.61(19)
C(23)-Re(1)	1.894(5)	C(21)-Re(1)-O(1)	95.68(18)
C(21)-O(21)	1.142(6)	O(21)-C(21)-Re(1)	177.5(4)
C(22)-O(22)	1.156(6)	C(21)-Re(1)-C(23)	85.9(2)
C(23)-O(23)	1.160(6)	C(22)-Re(1)-C(21)	87.2(2)
N(11)-Re(1)	2.235(4)	C(21)-Re(1)-O(2)	98.15(16)
C(1)-O(1)	1.272(6)	C(23)-Re(1)-O(1)	177.47(18)
C(2)-O(2)	1.364(6)	C(21)-Re(1)-N(11)	179.32(17)
		C(22)-Re(1)-O(2)	172.1(2)

All the bond distances and angles are within normal ranges compared to similar structures.[13-27] The Re−C bond distances of the three facial carbonyl groups are ~ 1.9 Å, while the Re−O ones are ~ 2.1 Å and the Re−N bond distance is = 2.235(4) Å, which is slightly longer than the conventional Re−O bond distance.[13-27] There is no apparent *trans* influence due to the coordinated 4-methylpyridine as all the Re−C bond distances are very similar. Furthermore, the Re−N bond distance falls within range of the Re−N bond distances found in the pyridine-type nucleophiles coordinated in a number of rhenium complexes.[17,24,26-29] The bidentate coordinated ligand has a bite angle O(1)-Re(1)-O(2) of 78.222(11) ° which is larger than that of similar structures of tropolone and tribromotropolone (74.82(17) ° and 74.07(16) ° respectively).[20,17]

[13] M. Sánchez-Lozano, E. M. Vázquez-López, J. M. Hermida-Ramón, C. M. Estévez, *Polyhedron*, **2011**, *30*, 953.

[14] J. Mukiza, E. C. Hosten, T. I. A. Gerber, *Polyhedron*, **2015**, *98*, 251.

[15] S. Mundwiler, M. Kündig, K. Ortner, R. Alberto, *J. Chem. Soc. Dalton Trans.*, **2004**, 1320.

[16] T. R. Hayes, B. B. Kasten, C. L. Barnes, P. D. Benny, *Dalton Trans.*, **2014**, *43*, 6998.

[17] M. Schutte, A. Roodt, H. G. Visser, *Inorg. Chem.*, **2012**, *51*, 11996.

[18] M. Schutte, G. Kemp, H. G. Visser, A. Roodt, *Inorg. Chem.*, **2011**, *50*, 12486.

[19] F. Ragone, G. T. Ruiz, O. E. Piro, G. A. Echeverría, F. M. Cabrerizo, G. Petroselli, R. Erra-Balsells, K. Hiraoka, F. S. García Einschlag, E. Wolcan, *Eur. J. Inorg. Chem.*, **2012**, 4801.

[20] M. Schutte, H. G. Visser, A. Roodt, *Acta Cryst. Sect. E*, **2008**, *E64*, m1610.

[21] K. O. Piletska, K. V. Domasevitch, A. V. Shtemenko, *Acta Cryst. Sect. E*, **2016**, *E72*, 590.

[22] A. Brink, H. G.Visser, A. Roodt, *J. Coord. Chem.*, **2011**, *64*, 122.

[23] A. Brink, H. G.Visser, A. Roodt, CCDC 801586: Experimental Crystal Structure Determination, **2014**, DOI: 10.5517/ccvx3mg

[24] A. Brink, H. G. Visser, A. Roodt, *Inorg. Chem.*, **2013**, *52*, 8950.

[25] B. Shankar, P. Elumalai, R. Shanmugam, V. Singh, D. T. Masram, M. Sathiyendiran, *Inorg. Chem.*, **2013**, *52*, 10217.

[26] A. Brink, H. G. Visser, A. Roodt, *Inorg. Chem.*, **2014**, *53*, 12480.

[27] M. Schutte, PhD Thesis, University of the Free State, **2011**.

[28] A. Manicum, M. Schutte-Smith , G. Kemp, H.G. Visser, *Polyhedron,* **2015**, *85*, 190.

[29] P. D. Benny, G. A. Fugate, A. O. Barden, J. E. Morley, E. Silva-Lopez, B. Twamley, *Inorg. Chem.*, **2008**, *47*, 2240.
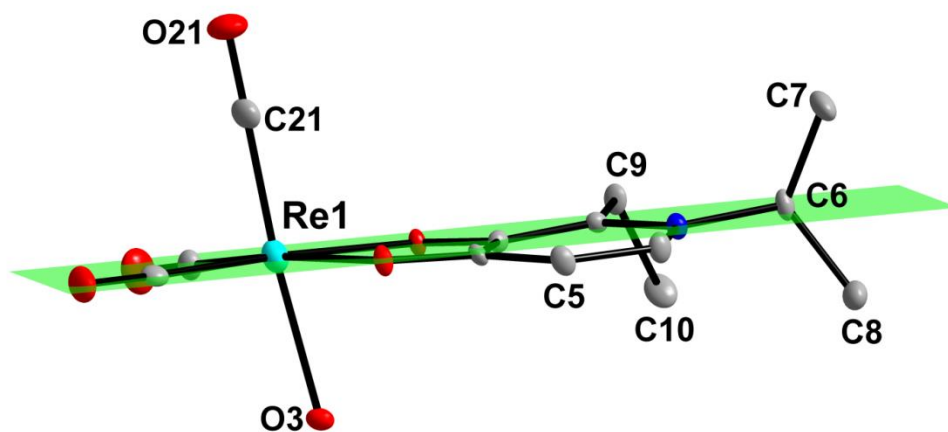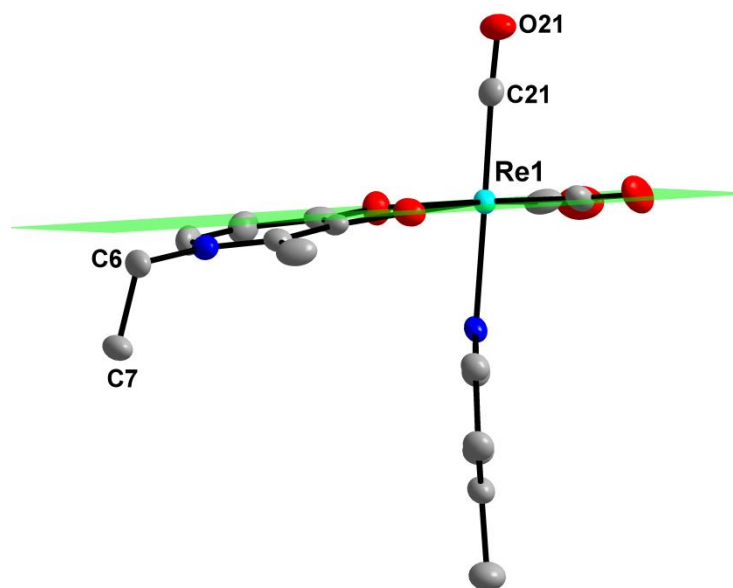
Figure 8.2: Illustration of the equatorial plane (C23 O2 O1 C22 Re1) showing the bidentate coordinated ligand bending out of the plane. Hydrogen atoms are omitted for clarity.

The octahedral system surrounding the rhenium(I) metal centre is distorted with angles ranging from 78.222(11) ˚ to 179.32(17) ˚. The bidentate coordinated ligand is slightly bent downwards out of the equatorial plane (Figure 8.2). The three axes through the vertices of the octahedral system are nonlinear and range between 172 ˚ and 179 ˚. The C23-O23 and C22-O22 axes lie in the equatorial plane with minimal deviations compared to (**2**) which was more distorted. The angle between C(21)-Re(1)-N(11) is 179.32(17) ˚ indicating minimal distortion in the vertical axis through the Re centre.
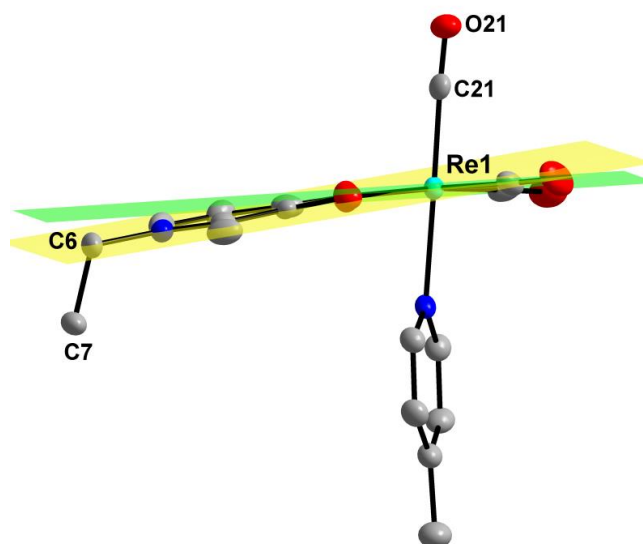
Figure 8.3: Illustration of the dihedral angle between the equatorial plane (C23 O2 O1 C22 Re1) and the plane through the heterocycle of the bidentate coordinated ligand (C1 C2 C3 N1 C4 C5).

The dihedral angle between the equatorial plane (C23 O2 O1 C22 Re1) and the ring of the bidentate coordinated pyridinone ligand (C1 C2 C3 N1 C4 C5) is 7.248(8) ° (Figure 8.3) which is approximately equal to that of (**2**), (**3**), (**4**) and (**8**). The ring bends out of the equatorial plane with the torsion angle of the bidentate coordination site O(1)-C(1)-C(2)-O(2) equal to 5.02(4) ° which is the largest so far compared to the previously discussed structures.
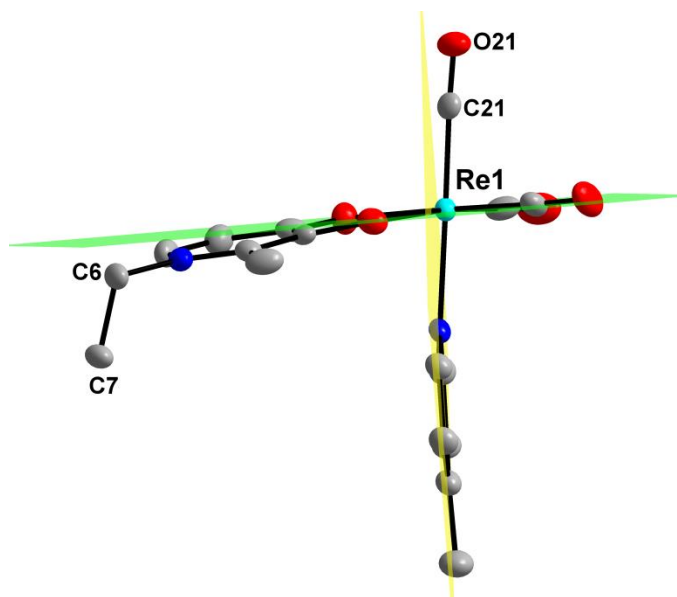
Figure 8.4: Illustration of the dihedral angle between the equatorial plane (C23 O2 O1 C22 Re1) and the plane through the heterocycle of the monodentate coordinated ligand (C11 C12 C13 N11 C14 C15).

The planarity of the monodentate coordinated ligand is illustrated by the small deviations of all the atoms from the plane through the pyridine heterocycle, with the largest deviation being 0.0169(2) Å for N11. The coordinated bidentate ligand is more planar with the largest deviation only 0.0122(3) Å for C2. The monodentate 4-methylpyridine lies in a plane that forms a dihedral angle of 88.658(7) ˚ with the equatorial plane (Figure 8.4) also showing the planarity of the monodentate coordinated ligand and the distortion in the vertical axis of the structure which is minimal.

Six C-H…O hydrogen interactions are observed in this structure; two intra-molecular (represented by light purple fragmented bonds) and four inter-molecular (represented by green fragmented bonds) hydrogen interactions. These hydrogen interactions are illustrated in Figure 8.5, while the distances, angles and symmetry operators are given in Table 8.3.
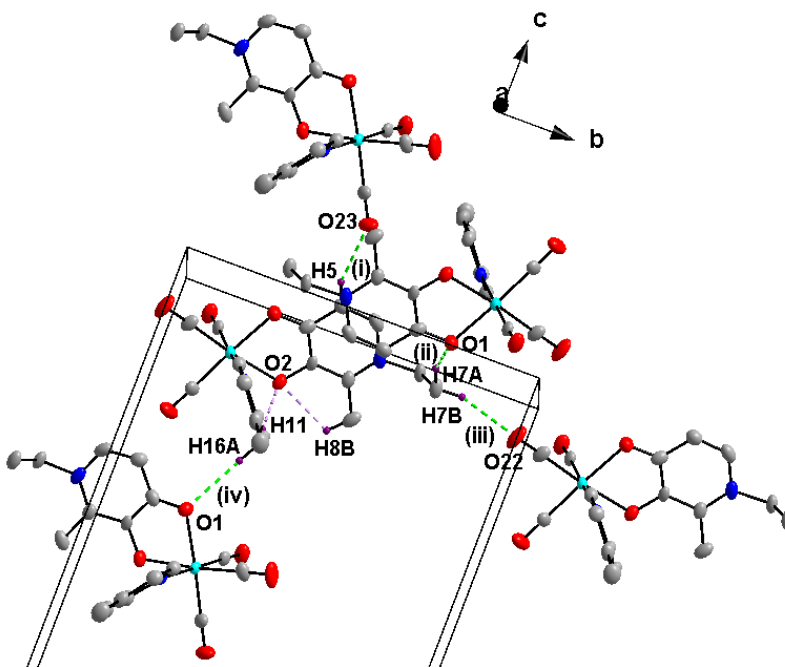
Figure 8.5: Hydrogen interactions observed in the structure of *fac*-[Re(ME(naltol))(CO)₃(4-MPyr)] (10).

Table 8.3: Summary of the hydrogen interactions, distances (Å) and angles (˚) observed in (10).

D-H…A	d(D-H) (Å)	d(H…A) (Å)	d(D…A) (Å)	∟ (D-H…A)(˚)
C(5)-H(5)...O(23) (i)	0.93	2.41	3.265(7)	153
C(7)-H(7A)...O(1) (ii)	0.96	2.56	3.435(7)	152
C(7)-H(7B)...O(22) (iii)	0.96	2.57	3.393(7)	144
C(8)-H(8B)...O(2)	0.96	2.39	2.850(7)	109
C(11)-H(11)...O(2)	0.93	2.49	2.964(6)	112
C(16)-H(16A)...O(1) (iv)	0.96	2.54	3.497(8)	178

Symmetry codes, transformations used to generate equivalent atoms: (i) 2-x,-y,1-z; (ii) 1/2+x,1/2-y,1/2+z; (iii) x,-1+y,z; (iv) 1/2+x,1/2-y,-1/2+z

The molecules pack in alternating patterns along the *bc*-plane with two units overlapping by the bidentate heterocycles and forming two distinct layers **A** and **B** (**ABA**). This packing order is stabilized by inter-molecular C-H…O interactions (Figure 8.6).
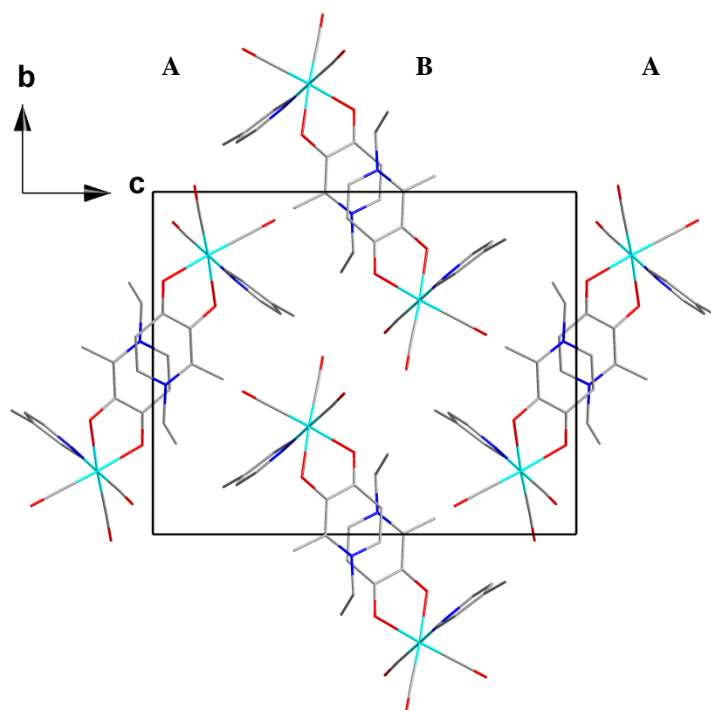
Figure 8.6: Crystal packing of (10) in the unit cell, viewed along the *a*-axis. Hydrogen atoms are omitted for clarity.

8.4 Crystal structure of *fac*-[Re(EM(naltol))(CO)$_3$(Pyr)] (11)

The complex, *fac*-[Re(EM(naltol))(CO)$_3$(Pyr)] (Pyr = pyridine) (**11**) has been synthesized as described in the synthesis section (Paragraph 3.5.18). The yellow cuboidal crystals were obtained from a DMSO solution of the product. This complex crystallized in the monoclinic *P*2$_1$/*c* space group with four independent molecule in the unit cell (Z = 4). In the structure of *fac*-[Re(EM(naltol))(CO)$_3$(Pyr)] (**11**) the Re atom is octahedrally surrounded by three facially orientated carbonyl ligands, one mono-anionic bidentate coordinated ligand and a neutral pyridine ligand. The bidentate ligand carries a mono-negative charge as it loses a proton, while the pyridine ligand is neutral, which results in a neutral complex. A summary of the general interatomic bond distances and angles are given in Table 8.4 while the numbering scheme of the neutral molecule is shown in Figure 8.7.
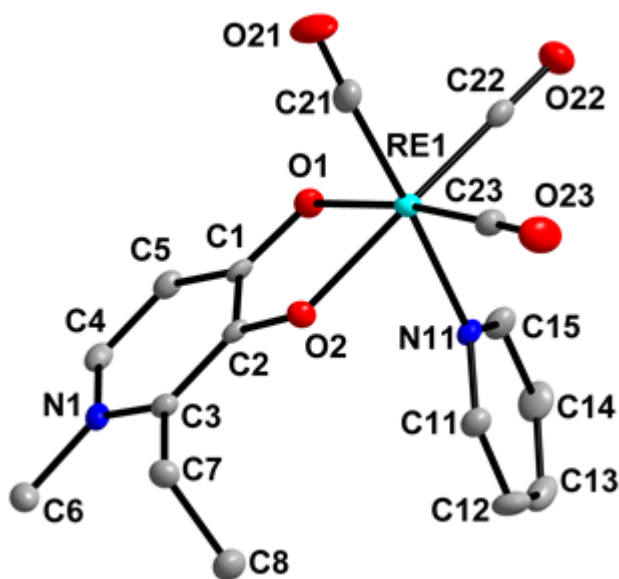
Figure 8.7: Molecular representation of *fac*-[Re(EM(naltol))(CO)$_3$(Pyr)] (11) showing the atom numbering scheme, displacement ellipsoids are drawn at 50 % probability level. Hydrogen atoms are omitted for clarity.

Table 8.4: Selected bond distances (Å) and angles (°) for the crystal structure of (11).

Bond	Bond distance (Å)	Bond angle (atoms)	Bond angle (°)
O(1)-Re(1)	2.142(4)	O(1)-Re(1)-O(2)	77.283(11)
O(2)-Re(1)	2.129(4)	C(22)-Re(1)-C(23)	89.6(2)
C(21)-Re(1)	1.926(6)	C(22)-Re(1)-O(1)	96.3(2)
C(22)-Re(1)	1.903(6)	C(23)-Re(1)-O(2)	96.6(2)
C(23)-Re(1)	1.905(6)	C(21)-Re(1)-O(1)	95.5(2)
C(21)-O(21)	1.145(8)	O(21)-C(21)-Re(1)	176.939(20)
C(22)-O(22)	1.160(7)	C(21)-Re(1)-C(23)	87.9(3)
C(23)-O(23)	1.159(7)	C(22)-Re(1)-C(21)	87.4(3)
N(11)-Re(1)	2.207(5)	C(21)-Re(1)-O(2)	97.4(2)
C(1)-O(1)	1.314(7)	C(23)-Re(1)-O(1)	173.3(2)
C(2)-O(2)	1.338(6)	C(21)-Re(1)-N(11)	176.9(2)
		C(22)-Re(1)-O(2)	172.3(2)

All the bond distances and angles are within normal ranges compared to similar structures.[13-27] The Re−C bond distances of the three facial carbonyl groups are ~ 1.9 Å. The Re−O bond distances are ~ 2.1 Å and the Re−N bond distance is = 2.207(5) Å which is slightly longer than the conventional Re−O bond distance.[13-27] There Re(1)−C(21) bond distance is slightly longer by ~ 0.0256(8) Å which could be due to the *trans* influence of the coordinated pyridine. Furthermore, the Re−N bond distance falls within range of the Re−N bond distances found in the pyridine-type nucleophiles coordinated in a number of rhenium complexes.[17,24,26-29] The bidentate coordinated ligand has a bite angle O(1)-Re(1)-O(2) of 77.283(11) ° which is larger than that of similar structures of tropolone and tribromotropolone (74.82(17) ° and 74.07(16) ° respectively).[17,20]
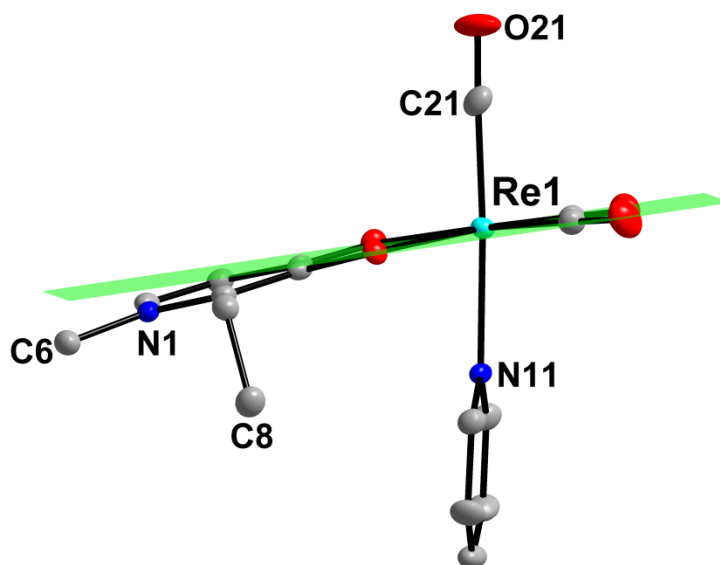
Figure 8.8: Illustration of the equatorial plane (C23 O2 O1 C22 Re1) showing the bidentate coordinated ligand bending out of the plane. Hydrogen atoms are omitted for clarity.

The octahedral polyhedron around the rhenium atom is distorted with angles ranging from 77.283(11) ˚ to 176.9(2) ˚. The bidentate coordinated ligand is slightly bent downwards out of the equatorial plane (Figure 8.8). The three axes through the vertices of the octahedral system are nonlinear and range between 172 ˚ and 176 ˚. The C23-O23 and C22-O22 axes lie in the equatorial plane with minimal deviations compared to previous structures which were more distorted e.g. (**2**). The angle C(21)-Re-N(11) is 176.9(2) ˚ indicating the distortion in the vertical axis through the Re centre.
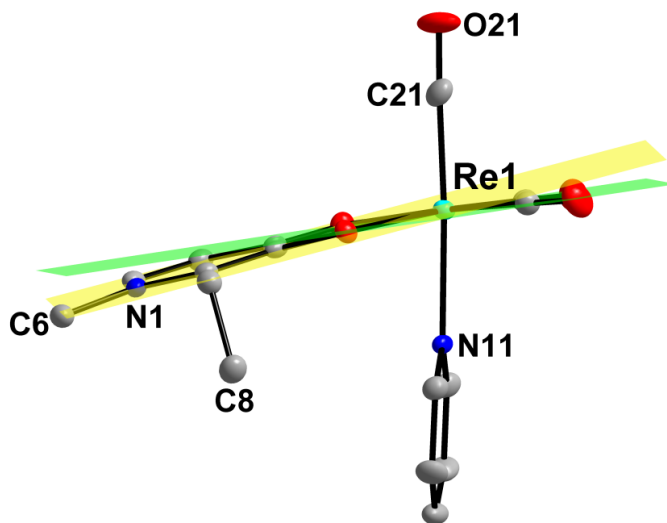
Figure 8.9: Illustration of the dihedral angle between the equatorial plane (C23 O2 O1 C22 Re1) and the plane through the heterocycle of the bidentate coordinated ligand (C1 C2 C3 N1 C4 C5).

The dihedral angle between the equatorial plane (C23 O2 O1 C22 Re1) and the ring of the bidentate coordinated pyridinone ligand (C11 C12 C13 N11 C14 C15) is 6.693(3) ˚ (Figure 8.9) which is approximately equal to (**6**) and (**7**). The ring bends out of the equatorial plane with a very small resultant torsion angle of the bidentate coordination site O(1)-C(1)-C(2)-O(2) of only 1.73(4) ˚.
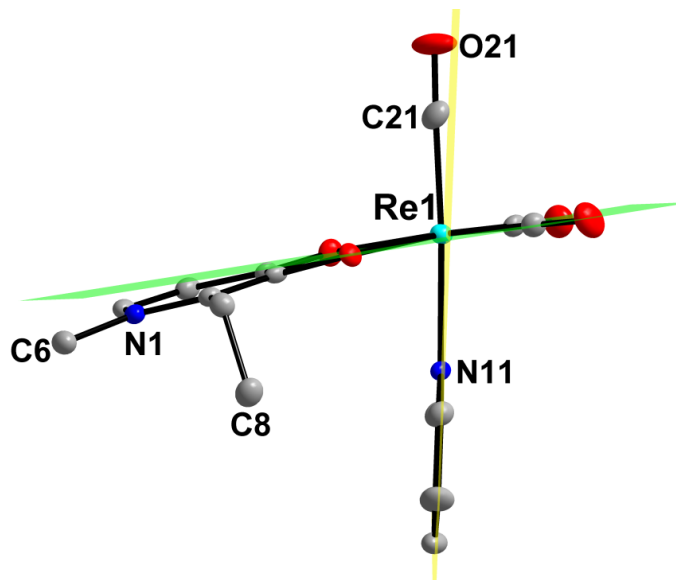
Figure 8.10: Illustration of the dihedral angle between the equatorial plane (C23 O2 O1 C22 Re1) and the plane through the heterocycle of the monodentate coordinated ligand (C11 C12 C13 N11 C14 C15).

The monodentate pyridine ligand is planar and as illustrated by the small deviations of all the atoms from the plane through the pyridine heterocycle. The largest deviation is only 0.0072(3) Å for C13. In contrast to this is the largest deviation in the bidentate coordinated ligand twice as large at 0.0150(3) Å for C1. The pyridine ligand lies in a plane that forms a dihedral angle of 79.192(3) ˚ with the equatorial plane (Figure 8.10) also indicating the planarity of the monodentate coordinated ligand and the distortion in the vertical axis of the complex.

Five hydrogen interactions are observed in this structure; two intra-molecular (a combination of one O-H…O and one C-H…O interactions, represented by light purple fragmented bonds) and three inter-molecular (a combination of one O-H…O and two C-H…O interactions, represented by green fragmented bonds) hydrogen interactions with H25B a trifurcated intermolecular interaction. These hydrogen interactions are illustrated in Figure 8.11, while the distances, angles and symmetry operators are given in Table 8.5.
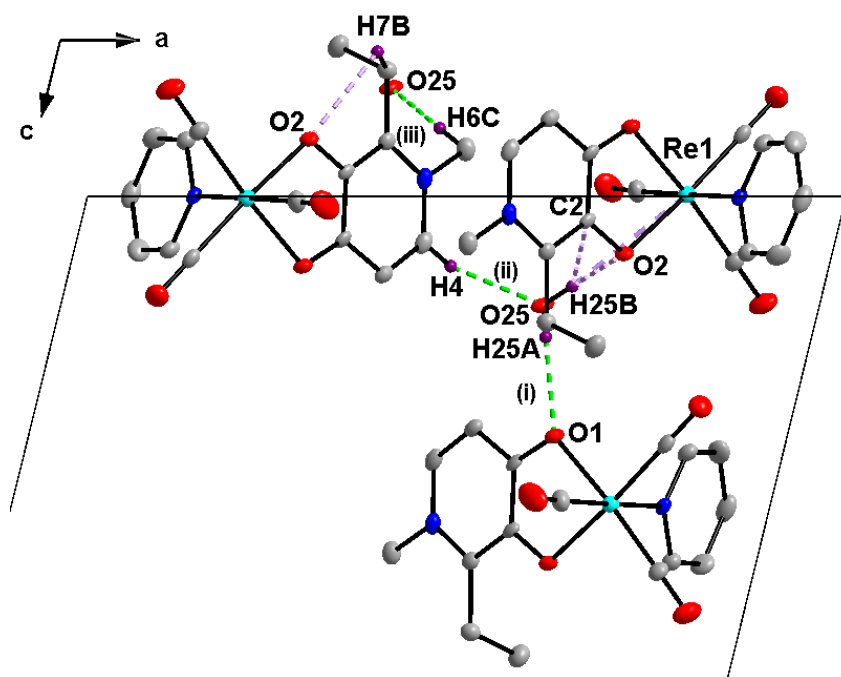
Figure 8.11: Hydrogen interactions observed in the structure of *fac*-[Re(EM(naltol))(CO)₃(Pyr)] (11).

Table 8.5: Summary of the hydrogen interactions, distances (Å) and angles (°) observed in (11).

D-H…A	d(D-H) (Å)	d(H…A) (Å)	d(D…A) (Å)	∟ (D-H…A)(°)
O25-H25A...O1 [(i)]	0.67(8)	2.09(8)	2.755(7)	172(10)
O25-H25B...O2	0.96(10)	1.83(10)	2.789(6)	175(10)
C4-H4...O25 [(ii)]	0.93	2.34	3.235(8)	162
C6-H6C...O25[(iii)]	0.96	2.56	3.491(8)	165
C7-H7B...O2	0.97	2.53	2.864(7)	100

Symmetry codes, transformations used to generate equivalent atoms: (i) -x+1, +y-1/2, -z+1/2; (ii) x, y, z; (iii) −x+1, -y-1, -z;

The molecules pack along the *ac*-plane with a tail to tail conformation by the bidentate heterocycles (**AA**) stabilized by inter-molecular O-H…O and C-H…O interactions (Figure 8.12).
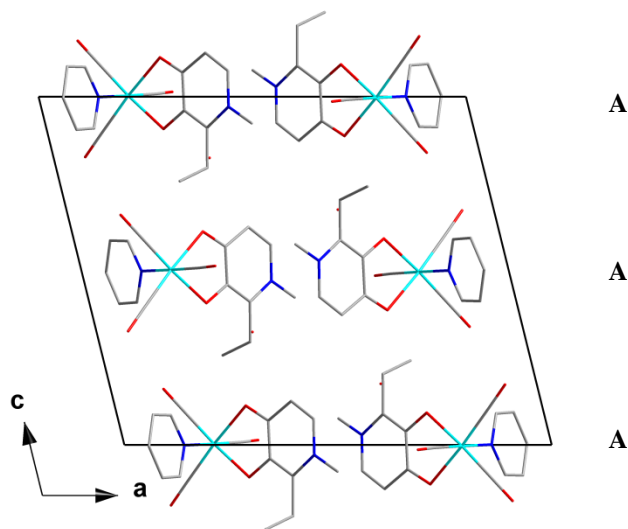
Figure 8.12: Crystal packing of (11) in the unit cell, viewed along the *b*-axis. Hydrogen atoms are omitted for clarity.

8.5   Crystal structure of *fac*-[Re(EE(naltol))(CO)₃(Pyr)] (12)

The complex, *fac*-[Re(EE(naltol))(CO)$_3$(Pyr)] (Pyr = pyridine) (**12**) has been synthesized as described in the synthesis section (Paragraph 3.5.19). The yellow cuboidal crystals were obtained from a DMSO solution of the product. This complex crystallizes in the monoclinic *P*2$_1$/*c* space group with four independent molecules in the unit cell (Z = 4). In the structure of *fac*-[Re(EE(naltol))(CO)$_3$(Pyr)] (**12**) the Re atom is octahedrally surrounded by three facially orientated carbonyl ligands, one mono-anionic bidentate coordinated ligand and a neutral pyridine ligand. The bidentate ligand carries a mono-negative charge as it loses a proton, while the pyridine molecule is neutral, which results in a neutral complex. A summary of the general interatomic bond distances and angles are given in Table 8.6 while the numbering scheme of the neutral molecule is shown in Figure 8.13.
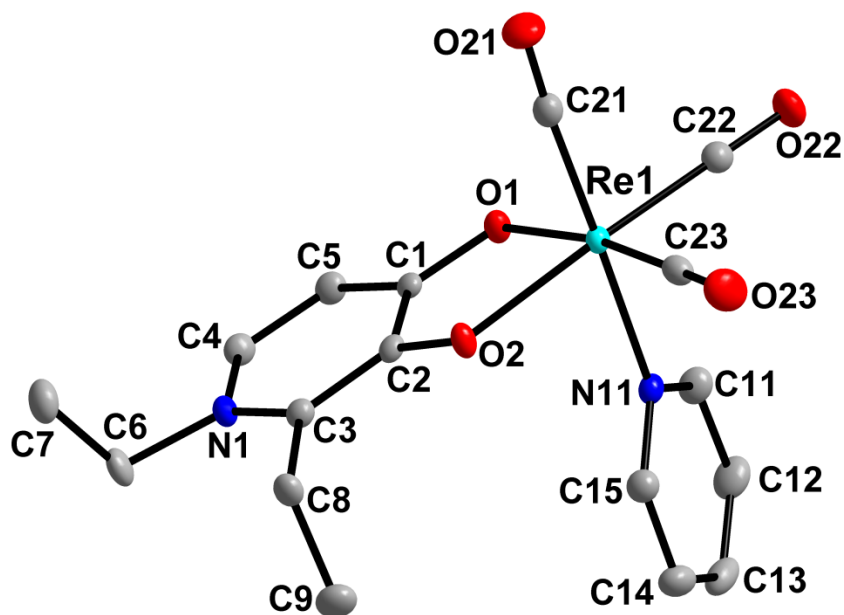
Figure 8.13: Molecular representation of *fac*-[Re(EE(naltol))(CO)₃(Pyr)] (12) showing the atom numbering scheme, displacement ellipsoids are drawn at 50 % probability level. Hydrogen atoms are omitted for clarity.

Table 8.6: Selected bond distances (Å) and angles (°) for the crystal structure of (12).

Bond	Bond distance (Å)	Bond angle (atoms)	Bond angle (°)
O(1)-Re(1)	2.1448(17)	O(1)-Re(1)-O(2)	77.092(2)
O(2)-Re(1)	2.1260(16)	C(22)-Re(1)-C(23)	89.25(11)
C(21)-Re(1)	1.923(3)	C(22)-Re(1)-O(1)	97.37(9)
C(22)-Re(1)	1.909(2)	C(23)-Re(1)-O(2)	95.95(8)
C(23)-Re(1)	1.896(3)	C(21)-Re(1)-O(1)	96.85(9)
C(21)-O(21)	1.152(3)	O(21)-C(21)-Re(1)	176.495(5)
C(22)-O(22)	1.154(3)	C(21)-Re(1)-C(23)	87.55(11)
C(23)-O(23)	1.162(3)	C(22)-Re(1)-C(21)	87.62(11)
N(11)-Re(1)	2.206(2)	C(21)-Re(1)-O(2)	97.77(9)
C(1)-O(1)	1.310(3)	C(23)-Re(1)-O(1)	172.18(9)
C(2)-O(2)	1.326(3)	C(21)-Re(1)-N(11)	178.64(9)
		C(22)-Re(1)-O(2)	172.65(9)

All the bond distances and angles are within normal ranges compared to similar structures.[13-27] The Re−C bond distances of the three facial carbonyl groups are ~ 1.9 Å. The Re−O bond distances are ~ 2.1 Å, the Re−N bond distance is = 2.2061(2) Å which is slightly longer than the conventional Re−O bond distance.[13-27] There Re(1)−C(21) bond distance is slightly longer by ~ 0.0230(1) Å which is due to the *trans* influence of the coordinated pyridine. Furthermore, the Re−N bond distance falls within range of the Re−N bond distances found in the pyridine type substituted rhenium complexes.[17,24,26-29] The bidentate coordinated ligand has a bite angle O(1)-Re(1)-O(2) of 77.092(2) ° which is larger than that of similar structures of tropolone and tribromotropolone (74.82(17) ° and 74.07(16) ° respectively).[17,20]
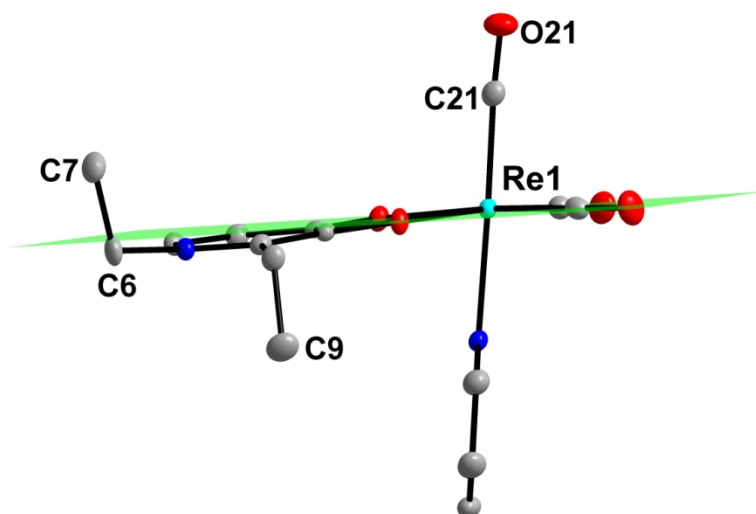
Figure 8.14: Illustration of the equatorial plane (C23 O2 O1 C22 Re1) showing the bidentate coordinated ligand bending below the plane. Hydrogen atoms are omitted for clarity.

The coordination octahedron around the rhenium atom is distorted with angles ranging from 77.092(2) ° to 176.495(5) °. The bidentate coordinated ligand is slightly bent downwards out of the equatorial plane (Figure 8.14). The three axes through the vertices of the octahedral system are nonlinear and range between 172 ° and 178 °. The C23-O23 and C22-O22 axes lie in the equatorial plane with minimal deviations compared to previous structures which were more distorted e.g. (**2**). The angle C(21)-Re(1)-N(11) is 178.64(9) ° indicating minimal distortion in the vertical axis through the Re centre.
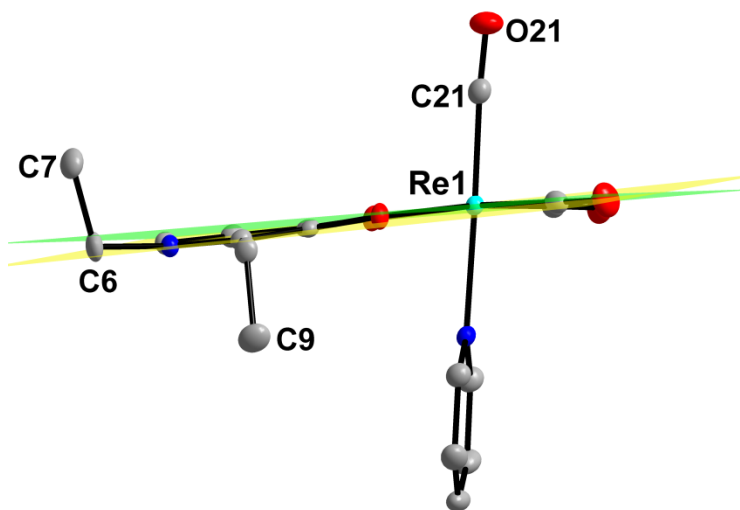
Figure 8.15: Illustration of the dihedral angle between the equatorial plane (C23 O2 O1 C22 Re1) and the plane through the heterocycle of the bidentate coordinated ligand (C1 C2 C3 N1 C4 C5).

The dihedral angle between the equatorial plane (C23 O2 O1 C22 Re1) and the ring of the bidentate coordinated pyridinone ligand (C1 C2 C3 N1 C4 C5) is 3.368 ˚ (Figure 8.15) which is within range of (**9**). The ring bends out of the equatorial plane with a resultant torsion angle of the bidentate coordination site O(1)-C(1)-C(2)-O(2) equal to 2.181(7) ˚.
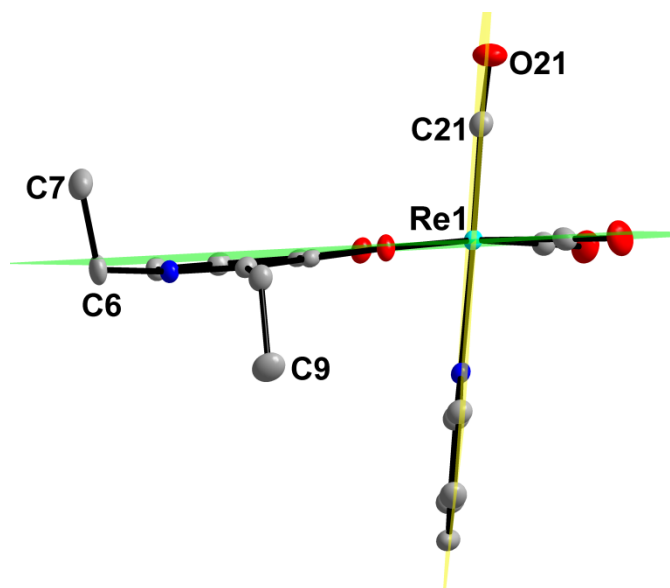
Figure 8.16: Illustration of the dihedral angle between the equatorial plane (C23 O2 O1 C22 Re1) and the plane through the heterocycle of the monodentate coordinated ligand (C11 C12 C13 N11 C14 C15).

The monodentate coordinated ligand is planar and this is illustrated by the small deviations of all the atoms from the plane through the pyridine heterocycle; the largest deviation being 0.0040(0) Å for C13, compared to the bidentate coordinated ligand where the largest deviation is 0.0193(0) Å for C2. The monodentate coordinated ligand lies in a plane that forms a dihedral angle of 83.044 ˚ with the equatorial plane (Figure 8.16) also showing the planarity of the monodentate coordinated ligand and the distortion in the vertical axis of the structure.

Five hydrogen interactions are observed in this structure; two intra-molecular (a combination of one O-H…O and one C-H…O interactions, represented by light purple fragmented bonds) and three inter-molecular (a combination of one O-H…O and two C-H…O interactions, represented by green fragmented bonds) hydrogen interactions with H25A and H25B bifurcated intermolecular and intramolecular interactions respectively. These hydrogen interactions are illustrated in Figure 8.17, while the distances, angles and symmetry operators are given in Table 8.7.
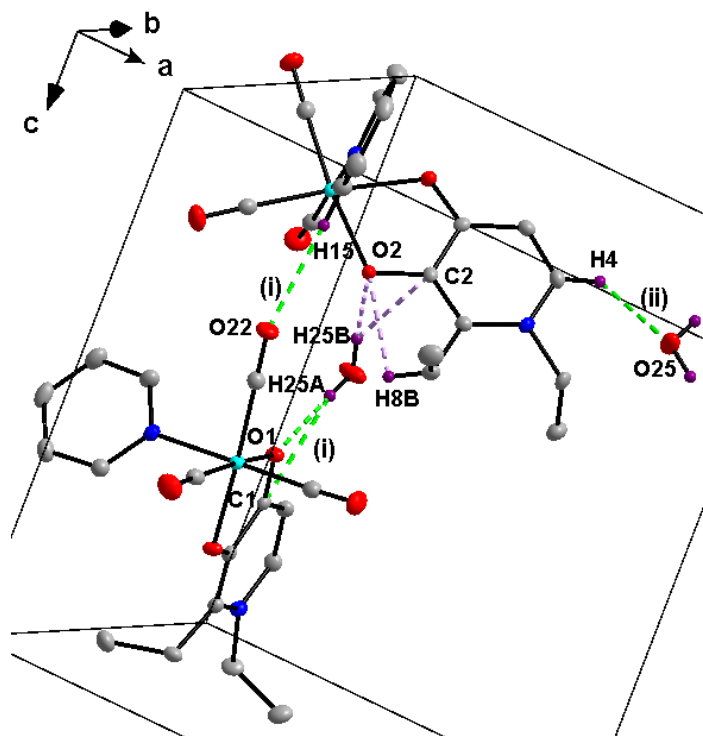
Figure 8.17: Hydrogen interactions observed in the structure of *fac*-[Re(EE(naltol))(CO)₃(Pyr)] (12).

The molecules pack along the *ac*-plane with a tail to tail conformation by the bidentate heterocycles (**AA**) stabilized by inter-molecular O-H…O and C-H…O interactions (Figure 8.18).

Table 8.7: Summary of the hydrogen bond distances (Å) and angles (°) observed in (12).

D-H…A	d(D-H) (Å)	d(H…A) (Å)	d(D…A) (Å)	∟ (D-H…A)(°)
O25-H25A...O1 [(i)]	0.82(4)	1.96(4)	2.775(3)	173(4)
O25-H25B...O2	0.87(5)	1.99(5)	2.843(3)	167(5)
C4-H4...O25 [(ii)]	0.93	2.56	3.272(3)	134
C8-H8B...O2	0.97	2.50	2.859(3)	102
C15-H15...O22 [(i)]	0.93	2.58	3.502(3)	169

Symmetry codes, transformations used to generate equivalent atoms: (i) 1-x,1/2+y,1/2-z; (ii) x,1/2-y,1/2+z;
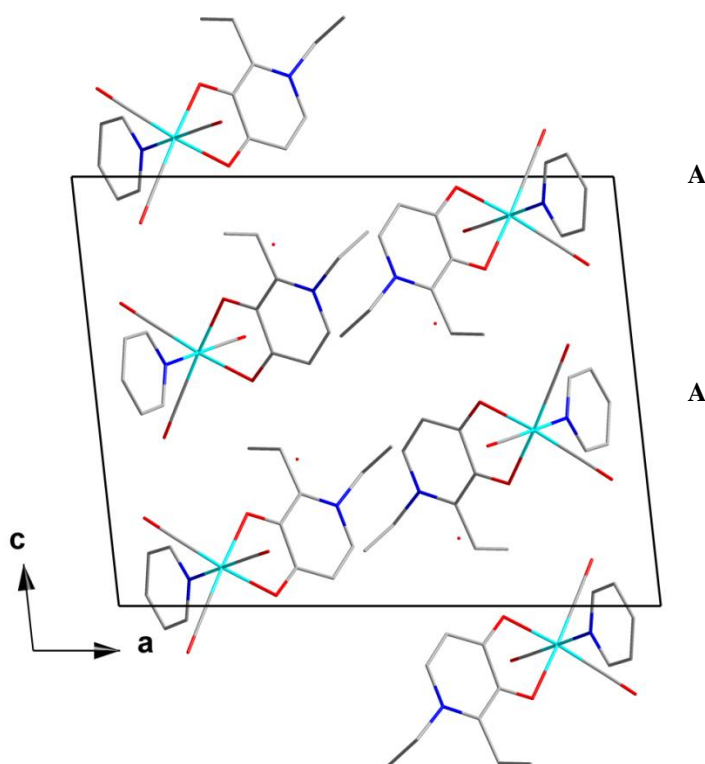
Figure 8.18: Crystal packing of (12) in the unit cell, viewed along the *b*-axis. Hydrogen atoms are omitted for clarity.

8.6 Discussion

Two similar rhenium structures with both a tropolone O,O'-bidentate ligand coordinated to the rhenium center, as well as a coordinated pyridine type ligand in the sixth position, are compared here to (**10**), (**11**) and (**12**) to highlight some structural properties and correlate some structural data between the different complexes (see Figure 8.19 and Table 8.8).
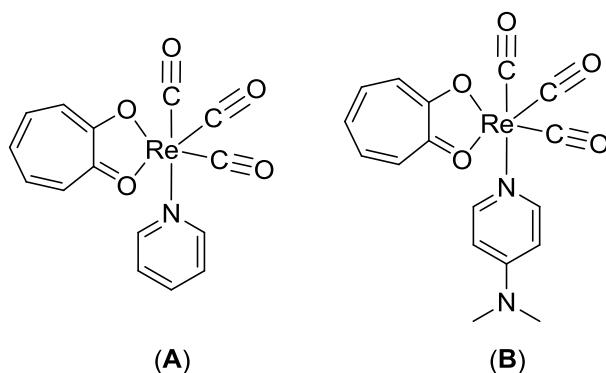
Figure 8.19: Illustration of the crystal structures of *fac*-[Re(Trop)(CO)₃(Pyr)] (A) and *fac*-[Re(Trop)(CO)₃(DMAP)] (B) (DMAP = 4-dimethylaminopyridine).

Table 8.8: Selected bond distances and angles in *fac*-[Re(O,O'-bidentate)(CO)₃(PY)] (PY = Pyridine type ligands) complexes.

	Complexes				
Formula	**(10)** [a]	**(11)** [a]	**(12)** [a]	[Re(Trop)(Pyr)] [b]	[Re(Trop)(DMAP)] [c]
Re−X (X = O/C) Å					
Re−O(1)	2.121(4)	2.142(4)	2.1448(17)	2.121(4)	2.129(4)
Re−O(2)	2.116(3)	2.129(4)	2.1260(16)	2.136(3)	2.121(4)
Re−N(11)	2.235(4)	2.207(5)	2.206(2)	2.208(4)	2.205(4)
Re−C(21)	1.915(5)	1.926(6)	1.923(3)	1.930(6)	1.916(6)
Re−C(22)	1.908(5)	1.903(6)	1.909(2)	1.898(5)	1.893(6)
Re−C(23)	1.894(5)	1.905(6)	1.896(3)	1.909(6)	1.915(7)
O-Re-X (X = O/C) ˚					
O(1)-Re-O(2)	78.222(11)	77.283(11)	77.092(2)	74.68(14)	74.90(18)
C(21)-Re-N(11)	179.32(17)	176.9(2)	178.64(9)	177.55(18)	176.6(2)

[a] Current study, [b] Schutte *et al*.[17], [c] Schutte *et al*.[27]. [Re(Trop)(Pyr)] = *fac*-[Re(Trop)(CO)₃(Pyr)] with TropH = tropolone, [Re(Trop)(DMAP)] = *fac*-[Re(Trop)(CO)₃(DMAP)] with DMAP = 4-dimethylaminopyridine.

In all five complexes mentioned above Re−O bond distances of the bidentate coordinated ligands are approximately 2.1 Å. The Re−N bond distance of the pyridine type ligand (4-methylpyridine, pyridine or 4-dimethylaminopyridine) is slightly longer at ~ 2.2 Å in all the complexes. However, the Re−N bond distance in (**10**) is significantly longer and since the functional groups on the bidentate ligands in (**10**) and (**11**) are similar this is assumed to be linked to the methyl group on the pyridine ligand *i.e.* the 4-methylpyridine is more electron donating than the unsubstituted pyridine in (**11**) and (**12**). Because the Re−N bond distances of (**11**), (**12**) and (**A**) are approximately equal with the monodentate ligand in all three ligands the same, it suggests that the three ligands EM(naltol)H, EE(naltol)H and tropolone have similar nucleophilic

properties. Additionally using the same logic it appears 4-dimethylaminopyridine and pyridine have similar nucleophilic properties due to the almost equal Re−N bond distances in (**11**), (**12**), (**A**) and (**B**). However, it is quite possible that these observed bond distances are primarily due to packing effects within the structure.

The Re−C bond distances are approximately 1.9 Å, while the metal bite angles of the bidentate coordinated ligands in (**10**), (**11**) and (**12**) are larger than those in (**A**) and (**B**), with (**10**) having a bite angle of 78 °, followed by both (**11**) and (**12**) bite angles of ~ 77 °, and (**A**) and (**B**) both bite angles of approximately 74 °. The vertical axis through the structures C(21)-Re(1)-N(11), except for (**10**) is nonlinear showing deviations from the ideal octahedral conformation (180 °). This is possibly due to steric demands in the structures. The most linear angle is reported for the structure of (**10**) with an angle very close to the ideal 180 °, *i.e.*, of 179.32(17) °.

8.7 Conclusion

Three structures of product complexes of the form *fac*-[Re^I(O,O'-Bid)(CO)$_3$(Pyr)] have been crystallographically studied and were reported in this chapter. These complexes are representative of the various substitution products obtained from the substitution kinetic work to be reported in Chapter 10.

In all three structures (**10**) to (**12**) the octahedral polyhedron is distorted with small metal bite angles of the bidentate coordinated ligands in a narrow range from 77 ° - 78 °. These ligands are also bent out of the equatorial plane with small dihedral angles between the equatorial plane and the plane through the hetero cyclic ring ranging between 3.4 ° and 7.2 °. It appears that EM(naltol)H, EE(naltol)H and tropolone exhibit similar solid state nucleophilic properties and those of 4-dimethylaminopyridine and pyridine are also comparable. A distinct feature of pyrones and pyridinones as chelating systems to rhenium as opposed to tropolone is the larger bite angles of the coordinated ligands which can potentially activate the rhenium centre more *via* increased orbital overlap and make these precursors more desirable in synthetic processes.

Additionally this could potentially alter the stability of the respective *fac*-[Re^I(O,O'-Bid)(CO)$_3$(Pyr)] precursors where biomolecules could possibly be attached to.

The structures reported in this chapter show reasonable similarities in their molecular packing and intermolecular interactions. Their general structural properties, including bond angles and bond distances are also very similar with just a few exceptions. This crystallographic study will add to the existing data in the Crystallographic Cambridge Structural Data base, as little to no structures have been reported on Re(I) tricarbonyl system with pyrone and pyridinones as ligand systems.

Moreover, this study clearly illustrated and confirmed the character, structural properties and solid-state stability of these reaction products and the ability of these versatile pyrone/pyridinone types of bidentate ligands in Re(I) chemistry, which is very important when proceeding with the mechanistic study associated with future *in vivo* applications, as presented hereafter.

9 Crystallographic Study of [Rh(EE(naltol))(CO)₂] and Associated Work

9.1 Introduction

The methanol carbonylation to produce acetic acid is an important homogeneously catalysed industrial process, and the original catalyst is the anion cis-[Rh(CO)$_2$I$_2$]$^-$. The process produces acetyl iodide which is subsequently hydrolysed to acetic acid,[1] wherein the d^8 square-planar character of this anion and similar compounds undergo oxidative addition reactions with different substrates.[2-7] The conditions used in this process (30-60 bar pressure and 150-200 °C) have led to the search and development of new catalysts that might operate under milder conditions. One route that is favoured is to increase the activity of the catalyst cis-[Rh(CO)$_2$I$_2$]$^-$ by introducing electron-donating ligands.[8-14] The resultant complexes are however unstable under harsh reaction conditions as required by the 'organic sub-cycle' in the overall process. The corresponding iridium complexes are however generally more stable which led to the

[1] D. Forster, M. Singleton, *J. Mol. Catal.*, **1982**, *17*, 299.
[2] H. A. Zahalka, H. Alper, *Organometallics*, **1986**, *5*, 2597.
[3] P. M. Maitlis, A. Haynes, G. J. Sunley, M. J. Howard, *J. Chem. Soc., Dalton Trans.*, **1996**, 2187.
[4] L. Cavallo, M. Sola, *J. Am. Chem. Soc.*, **2001**, *123*, 12294.
[5] A. Haynes, P. M. Maitlis, G. E. Morris, G. J. Sunley, H. Adams, P. W. Badger, C. M. Bowers, D. B. Cook, P. I. P. Elliott, T. Ghaffer, H. Green, T. R. Griffin, M. Payne, J. M. Pearson, M. J. Taylor, P. W. Vickers, R. J. Watt, *J. Am. Chem. Soc.*, **2004**, *126*, 2847.
[6] J. H. Jones, *Platinum Met. Rev.*, **2000**, *44*, 94.
[7] A. Roodt, G. J. J. Steyn, *Recent Res. Devel. Inorganic Chem.*, **2000**, *2*, 1.
[8] X. F. Wu, H. Neumann, *ChemCatChem,* **2012,** *4*, 447.
[9] D. K. Dutta, B. Deb, G. Hua, J. D. Woollins, *J. Mol. Catal.*, **2012**, A 353-354, 7.
[10] R. J. Adcock, D. H. Nguyen, S. Ladeira, C. Le Berre, P. Serp, P. Kalck, *Inorg. Chem.*, **2012**, 51, 8670.
[11] G. L. Williams, C. M. Parks, C. R. Smith, H. Adams, A. Haynes, A. J. H. M. Meijer, G. J. Sunley, S. Gaemers, *Organometallics*, **2011**, *30*, 6166.
[12] J. Rankin, A. C. Benyei, A. D. Poole, D. J. Cole-Hamilton, *J. Chem. Soc. Dalton Trans.*, **1999**, 3771.
[13] L. Gonsalvi, H. Adams, G. J. Sunley, E. Ditzel, A. Haynes, *J. Am. Chem. Soc.*, **2002**, *124*, 13597.
[14] L. Gonsalvi, J. A. Gaunt, H. Adams, A. Castro, G. J. Sunley, A. Haynes, *Organometallics*, **2003**, *22*, 1047.

development of the Cativa process based on *cis*-[Ir(CO)$_2$I$_2$]$^-$ which is currently the most efficient industrial process for the manufacturing of acetic acid.[15-22]

Nevertheless, highly active and stable rhodium complexes have been reported based on phosphorous, arsine and stibine containing ligand systems in order to improve the catalytic activity of the rhodium catalyst.[23,24] By increasing the electron density on the rhodium centre and introducing larger donor elements like arsines and stibines, the steric crowding within the rhodium(I) catalyst molecule is reduced by a subtle increase in strategic bond lengths. This results not only in a larger cavity for the entering moieties in reactions such as substitution and oxidative addition but makes the rhodium centre more electron rich increasing electron density on the elements from P to Sb.

The main objective of this part of the study was to investigate and potentially apply pyridinones to the design of a new phosphine based Rh(I) complex in an attempt to expand the knowledge base and improve the propensity of the catalyst for the fundamental oxidative addition reaction. The rhodium dicarbonyl complexes were successfully synthesized, but only the crystal structure of [Rh(EE(naltol)(CO)$_2$] (**13**) was successfully obtained. Attempts to isolate the corresponding phosphine complexes were all unsuccessful. In an attempt to isolate a phosphine complex a rhodium(I) Vaska type complex (**14**) and free PPh$_3$ (**15**) were isolated which are accordingly reported in this chapter.[23] For this reason the iodomethane oxidative addition was not evaluated. Thus, only preliminary results of the expansion of the PhD study to these rhodium(I) complexes are reported herein. Nevertheless, it illustrates that there is definitely potential of these pyridinones to further explore in future.

[15] F. Paulik, J. E. Roth, *J. Chem. Soc. Chem. Commun.*, **1968**, 1578.
[16] K. K. Robinson, A. Hershman, J. H. Craddock, J. F. Roth, *J. Catal.*, **1972**, *27*, 389.
[17] A. Hershman, W. R. Knox, F. E. Paulik, J. E. Roth, Monsanto Company, US Patent, **1973**, 3769329.
[18] T. W. Dekleva, D. Forster, *Adv. Catal.*, **1986**, *34*, 81.
[19] D. Brodzki, B. Denise, G. Pannetier, *J. Mol. Catal.*, **1977**, *2*, 149.
[20] T. Matsumoto, K. Mori, A. Ozaki, *J. Catal.*, **1978**, *51*, 96.
[21] T. Mizoroki, T. Matsumoto, A. Ozaki, *Bull. Chem. Soc. Jpn*, **1979**, 52, 479.
[22] D. Forster, *Adv. Organometal. Chem.*, **1979**, 17, 255.
[23] A. Roodt, S. Otto, G. Steyl, *Coord. Chem. Rev.*, **2003**, *245*, 121.
[24] A. Brink, A. Roodt, G. Steyl, H. G. Visser, *Dalton Trans.*, **2010**, *39*, 5572.

(13)   **(14)**   **(15)**
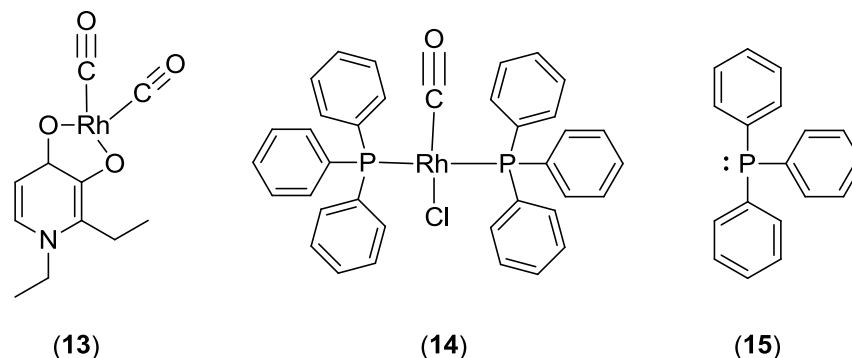
Scheme 9.1: Schematic representation of the three crystal structures reported in this chapter.

9.2 Experimental

The reflection data of (**13**), (**14**) and (**15**) were collected on a Bruker X8 Apex II 4K Kappa CCD diffractometer using graphite monochromated Mo Kα radiation (λ= 0.70926 Å) with ω- and φ-scans at 100(2) K. The Apex II software package was utilized along with the optimum measurement method in collecting more than a hemisphere of reciprocal space as predicted by COSMO.[25,26] Frame integration and data reduction was performed using the SAINT-Plus and XPREP software packages and SADABS was used for multi-scan absorption correction.[27,28] The structure was solved using direct methods package SIR97 and refined using the WinGX software incorporating SHELXL.[29-35] All atoms were refined anisotropically with the exception of hydrogen atoms. The hydrogen atoms were positioned geometrically and refined utilizing a riding model with fixed C-H distances of 0.95 Å (CH) [$U_{iso}(H) = 1.2\ U_{eq}$] for aromatic hydrogens, 0.97 Å (CH) [$U_{iso}(H) = 1.2\ U_{eq}$] for methylene H-atoms and 0.96 Å (CH) [$U_{iso}(H) =$

[25] **Apex2**, Version 2012.10-0, Bruker AXS Inc.,Madison, Wisconsin, USA, **2012**.

[26] **COSMO**, Version 1.48, Bruker AXS Inc., Madison, Wisconsin, USA, **2003**.

[27] **SADABS**, Version 2012/1, BrukerAXS Inc, Madison, Wisconsin, USA, **2012**.

[28] **SAINT-Plus**, Version 8.27B including XPREP, Bruker AXS Inc., Madison, Wisconsin, USA, **2012**.

[29] A. Altomare, G. Cascarano, C. Giacovazzo, A. Guagliardi, M. C. Burla, G. Polidori, M. Camalli, *J. Appl. Cryst.*, **1994**, *27*, 435.

[30] A. Altomare, M. C. Burla, M. Camalli, G. L. Cascarano, C. Giacovazzo, A. Guagliardi, A. G. G. Moliterni, G. Polidori, R. Spagna, *J. Appl. Cryst.*, **1999**, *32*, 115.

[31] M. C. Burla, M. Camalli, B. Carrozzini, G. L. Cascarano, C. Giacovazzo, G. Polidori, R. Spagna, *J. Appl. Cryst.*, **2003**, *36*, 1103.

[32] P. T. Beurskens, G. Admiraal, G. Beurskens, W. P. Bosman, S. Garcia-Granda, R. O. Gould, J. M. M. Smits, C. Smykalla, Crystallography Laboratory, University of Nijmegen, Toernooiveld, The Netherlands.

[33] L. Palatinus, G. Chapuis, *J. Appl. Cryst.*, **2007**, *40*, 786.

[34] **WinGX**. L. J. Farrugia, *J. Appl. Cryst.*, **2012**, *45*, 849.

[35] G. M. Sheldrick, *Acta Cryst.*, **2008**, *A64*, 112.

1.2 U_{eq}] for methyl H-atoms. Molecular diagrams were generated with DIAMOND with 50 % probability ellipsoids for all non-hydrogen atoms.[36] General crystal data and refinement parameters are represented in Table 9.1 with the complete list of atomic coordinates, equivalent isotropic parameters and hydrogen coordinates given in Appendix A.

Table 9.1: General X-ray crystallographic data and refinement parameters for [Rh(EE(naltol))(CO)$_2$] (13), *trans*-[RhCO(PPh$_3$)$_2$Cl] (14) and PPh$_3$ (15).

Crystallographic data	(13)	(14)	(15)
Empirical formula	$C_{11}H_{12}NO_4Rh$	$C_{37}H_{30}ClOP_2Rh$	$C_{18}H_{15}P$
Formula weight (g.mol^{-1})	325.13	690.91	262.27
Temperature (K)	100(2)	100(2)	100(2)
Crystal system	Monoclinic	Monoclinic	Monoclinic
Space group	$P2_1/n$	$P2_1/n$	$P2_1/c$
a (Å)	9.719(1)	11.823(2)	8.416(1)
b (Å)	12.111(1)	23.893(4)	14.854(2)
c (Å)	9.779(1)	12.113(2)	11.276(1)
α (°)	90	90	90
β (°)	90.383(3)	113.024(5)	91.927(4)
γ (°)	90	90	90
Volume (Å^3)	1151.0(2)	3149(2)	1408.8(3)
Z	4	4	4
ρ $_{calc.}$ (g.cm^{-3})	1.876	1.457	1.237
Crystal colour	Yellow	Yellow	Yellow
Crystal morphology	Cuboid	Cuboid	Cuboid
Crystal size (mm^3)	0.542 x 0.353 x 0.307	0.27 x 0.167 x 0.085	0.41 x 0.264 x 0.118
μ (mm^{-1})	1.485	0.758	0.178
F(000)	648	1408	552.0
θ range (°)	4.473 to 27.999	2.499 to 28.000	4.421 to 27.996
Index ranges	$-12 \le h \le 12$	$-15 \le h \le 15$	$-11 \le h \le 7$
	$-16 \le k \le 12$	$-26 \le k \le 31$	$-19 \le k \le 19$
	$-11 \le l \le 12$	$-16 \le l \le 14$	$-14 \le l \le 14$
Reflections collected	18207	85042	25767
Unique reflections	2774	7599	3402
Reflections with I > 2σ(I)	9962	9879	9931
R$_{int}$	0.0523	0.0475	0.0497
Completeness to θ (°; %)	25.24, 99.1	25.24, 99.5	25.24, 99.5
Data/restraints/parameters	2760 / 0 / 156	7573 / 0 / 379	3389 / 0 / 172
GooF	1.098	1.073	1.027
R [I>2σ(I)]	$R_1 = 0.0194$	$R_1 = 0.0285$	$R_1 = 0.0345$
	$wR_2 = 0.0504$	$wR_2 = 0.0573$	$wR_2 = 0.0836$
R (all data)	$R_1 = 0.0199$	$R_1 = 0.0429$	$R_1 = 0.0431$
	$wR_2 = 0.0508$	$wR_2 = 0.0644$	$wR_2 = 0.0903$
ρ$_{max}$, ρ$_{min}$ (e.Å^{-3})	0.374 and -0.714	0.567 and -0.556	0.320 and -0.256

---

[36] K. Brandenburg, H. Putz, DIAMOND, Release 3.0e, Crystal Impact GbR, Bonn, Germany, **2006**.

9.3 Crystal structure of [Rh(EE(naltol))(CO)₂] (13)

The complex, [Rh(EE(naltol))(CO)$_2$] (**13**) has been synthesized as described in the synthesis section (Paragraph 3.6.7). The yellow crystals were obtained from a 50:50 methanol:DMSO solution of the product. The compound (**13**) crystallized in the monoclinic $P2_1/n$ space group with four independent molecules in the unit cell (Z = 4). In the structure of (**13**) the Rh atom is in a square planar geometry coordinated by two *cis* orientated carbonyl functional groups and one mono-anionic bidentate ligand. The bidentate coordinated ligand carries a mono-negative charge as it loses a proton, while the carbonyls are neutral. A summary of the general interatomic bond distances and angles are given in Table 9.2 while the numbering scheme of the neutral molecule is shown in Figure 9.1.
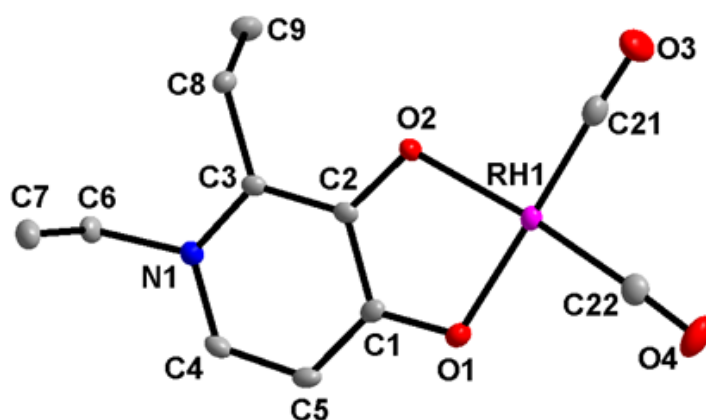
Figure 9.1: Molecular representation of [Rh(EE(naltol))(CO)₂] showing the atom numbering scheme. Displacement ellipsoids are drawn at 50 % probability level. Hydrogen atoms are omitted for clarity.

Table 9.2: Selected bond distances (Å) and angles (°) for the crystal structure of (13).

Bond	Bond distance (Å)	Bond angle (atoms)	Bond angle (°)
Rh(1)-C(22)	1.841(2)	O(2)-Rh(1)-O(1)	82.23(5)
Rh(1)-C(21)	1.843(2)	C(22)-Rh(1)-C(21)	88.20(8)
Rh(1)-O(2)	2.033(1)	C(21)-Rh(1)-O(2)	96.48(7)
Rh(1)-O(1)	2.037(2)	C(22)-Rh(1)-O(1)	93.09(7)
C(3)-C(2)	1.389(2)	O(4)-C(22)-Rh(1)	177.1(2)
C(8)-C(9)	1.531(2)	O(3)-C(21)-Rh(1)	178.2(2)
O(4)-C(22)	1.137(2)	C(21)-Rh(1)-O(1)	178.70(6)
O(3)-C(21)	1.137(2)	C(22)-Rh(1)-O(2)	175.20(6)
N(1)-C(4)	1.357(2)		
N(1)-C(6)	1.485(2)		

A geometric search on the crystallographic database MOGUL for the Rh—C bond distance indicated that the bonds (~ 1.84 Å) were well in the range for carbonyl bond distances with a reported average Rh—C bond distance of 1.848 Å in the CSD.[37,38] The C=O bond distances were determined as 1.137(3) Å and 1.137(4) Å and were similarly in good agreement with the average bond distance of ~ 1.137 Å reported.[38] The Rh—O bond distances were longer (~ 2.03 Å) compared to the Rh—C and C=O bond distances but were well within range of similar reported structures, with an O-Rh-O bite angle of 82.23(1) °.[39-44] The square planar system surrounding the rhodium atom is distorted with none of the angles equal to 90 ° and range from 82.23(1) ° to 96.48(2) °. The dihedral angle between the equatorial plane (O1 O2 C21 C22 Rh1) and the ring of the bidentate coordinated ligand (C1 C2 C3 N1 C4 C5) is 7.081(12) ° (Figure 9.2 below). This geometry (square planar) is favoured by Rh(I) complexes as well as other complexes containing transition metals with a d^8 electron configuration.[45]
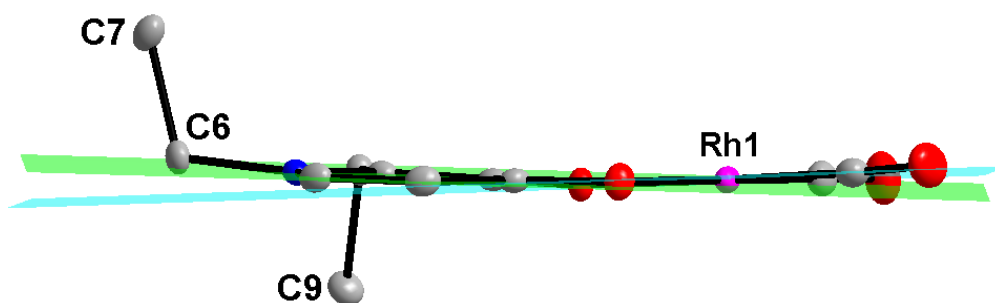
Figure 9.2: Illustration of the dihedral angle between the equatorial plane and the plane through the heterocycle of the bidentate coordinated ligand.

[37] **MOGUL**: Retrieval of Crystallographically-Derived Molecular Geometry Information, I. J. Bruno, J. C. Cole, M. Kessler, J. Luo, W. D. S. Motherwell, L. H. Purkis, B. R. Smith, R. Taylor, R. I. Cooper, S. E. Harris, A. G. Orpen, *J. Chem. Inf. Comput. Sci.*, **2004**, *44*, 2133.

[38] **Cambridge Structural Database** (CSD), Version 5.35, November 2013 update, F. H. Allen, *Acta Cryst.*, **2002**, *B58*, 380.

[39] R. Lang, A. Schörwerth, K. Polborn, W. Ponikwar, W. Beck, T. Severin, K. Severin, *Z. Anorg. Allg. Chem.*, **1999**, *625*, 1384.

[40] G. Steyl, G. J. Kruger, A. Roodt, *Acta Cryst.*, **2004**, *C60*, m473.

[41] T. N. Hill, G. Steyl, *Acta Cryst.*, **2008**, *E64*, m1580.

[42] G. Steyl, *Polyhedron*, **2007**, *26*, 5324.

[43] G. Steyl, A. Roodt, *Acta Cryst.*, **2004**, *C60*, m324.

[44] G. Steyl, *Acta Cryst.*, **2007**, *E63*, m23.

[45] R. Janes, E. Moore, *Metal-Ligand Bonding*, The Open University, Bath Press, Bath, United Kingdom, **2004**, 31.

The C2=C3 and C4=C5 bond distances are ~ 1.38 Å and are slightly longer than a normal aliphatic C=C bond distance (aliphatic C=C bond distance = 1.337(6) Å).[46] These bond distances (C(2)—C(3) = 1.389(5) Å and C(4)—C(5) = 1.374(5) Å) confirm double bond character in the structure (aromatic C=C bond distance ~ 1.4 Å).[46] Furthermore this also indicates that although there are double bonds in the structure, they are not conjugated and as a result there is a minimum electron delocalization in the structure.[46] The rest of the bond distances indicate single bond character with the cyclic N—C bond distances being shorter than the acyclic N(1)—C(6) bond distance. The two cyclic C—C bond distances *i.e.* C(1)—C(2) and C(1)—C(5) are shorter than the acyclic C−C bond distances.
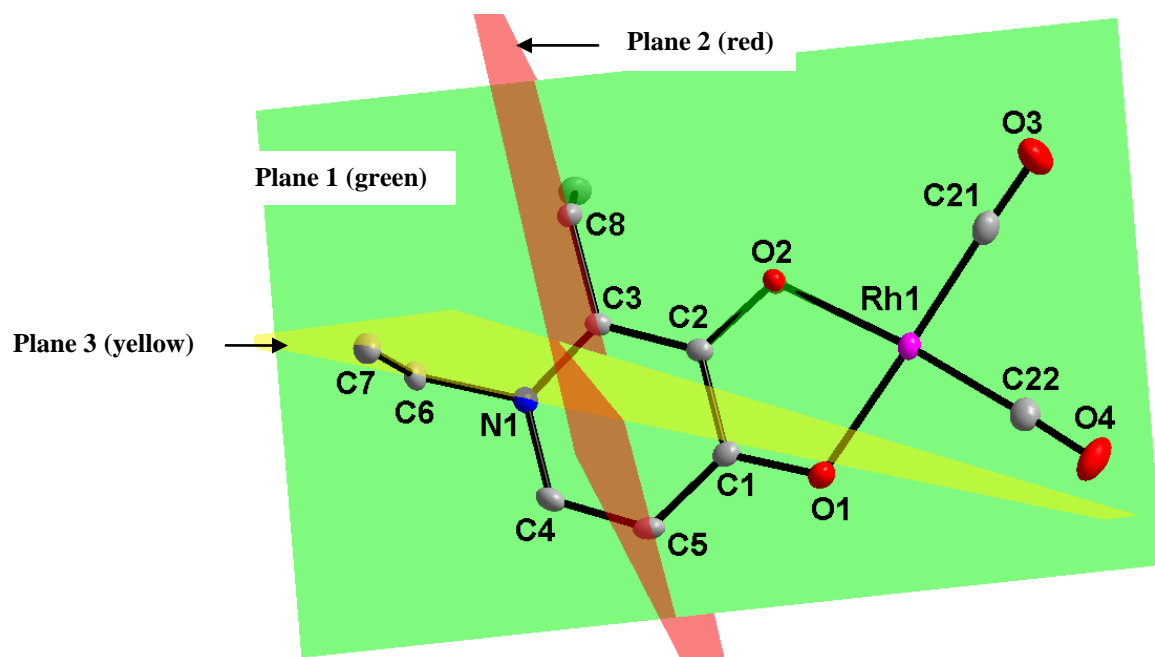
Figure 9.3: Molecular representation of [Rh(EE(naltol))(CO)$_2$] (13) showing the different planes through the molecule. Hydrogen atoms are omitted for clarity. Displacement ellipsoids are drawn at 50 % probability level.

The dihedral angle between plane 1 (C21 O2 O1 C22 Rh1) and plane 2 (C3 C8 C9) is 89.13(1) ˚ (Figure 9.3). The dihedral angles between plane 1 (C21 O2 O1 C22 Rh1) and plane 3 (N1 C6 C7) and between plane 2 (C3 C8 C9) and plane 3 (N1 C6 C7) are 87.662(8) ˚ and 62.27(1) ˚ respectively, showing that C7 is almost at right angles to the plane formed by the heterocyclic part of the molecule (Figure 9.3).

---

[46] R. C. Weast, M. J. Astle, *CRC Handbook of Chemistry and Physics*, 60th ed. CRC Press: Boca Raton, **1980**.
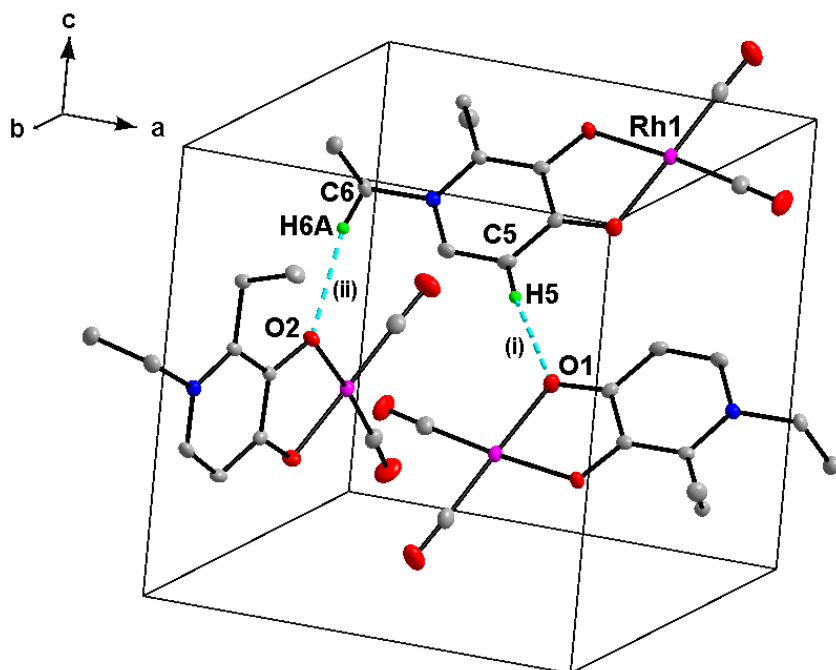
Figure 9.4: Hydrogen interactions observed in the structure of [Rh(EE(naltol))(CO)$_2$] (13).

Only two hydrogen interactions are observed in this structure and both are C-H…O inter-molecular (represented by turquoise fragmented bonds) hydrogen interactions. These hydrogen interactions are illustrated in Figure 9.4, while the distances, angles and symmetry operators are given in Table 9.3.

Table 9.3 Summary of the hydrogen interactions (distance (Å) and angle (°)) observed in the structure of (13).

D-H…A	d(D-H) (Å)	d(H…A) (Å)	d(D…A) (Å)	∟ (D-H…A)(°)
C5-H5...O1 [(i)]	0.93	2.56	3.481(3)	171
C6-H6A...O2 [(ii)]	0.97	2.45	3.392(2)	163

Symmetry codes, transformations used to generate equivalent atoms: (i) 1-x, -y, 1-z; (ii) x-1/2, ½-y, z-1/2;

The molecules pack in an alternating fashion along the *ab*-plane when viewed along the *c*-axis, the molecules forming layer **B** are orientated at ~ 90 ° to the molecules forming layer **A** (Figure 9.5). The third layer **C** is then orientated at ~ 180 ° to layer **B**, layer **D** is orientated at ~ 90 ° to layer **C** after which the series starts again (**ABCD**). It is often the case that metallophillic interactions (dz^2 interactions) between two pairs of Rh(I) molecules occur in these types of complexes.[47]

---

[47] M. M. Conradie, P. H. van Rooyen, C. Pretorius, A. Roodt, J. Conradie, *J. Mol. Struct.*, **2017**, *1144*, 280.

It is therefore interesting to note that no metallophilic interactions were observed in this structure. The reasons(s) for this is certainly not clear but will also be explored in future investigations.
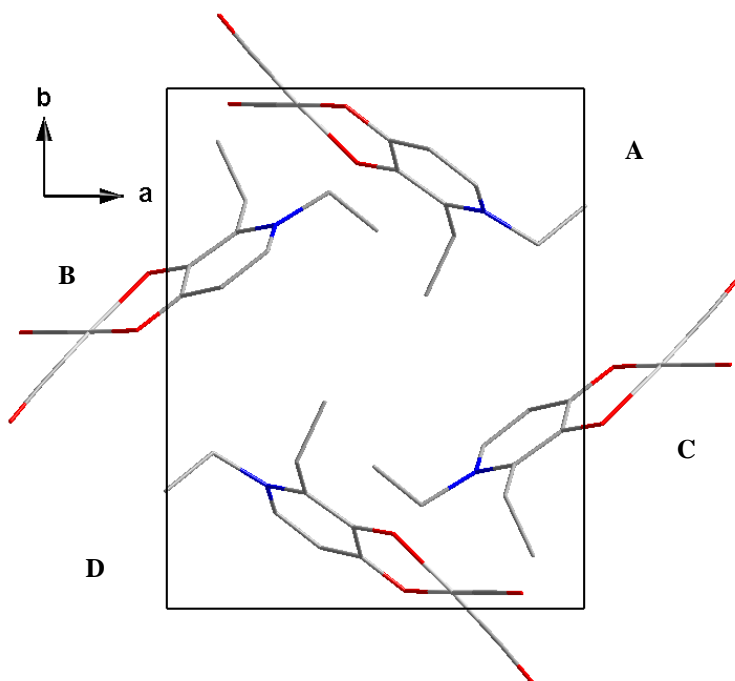
Figure 9.5: Crystal packing of (13) in the unit cell, viewed along the *c*-axis. Hydrogen atoms are omitted for clarity.

9.4 Crystal structure of *trans*-[RhCO(PPh$_3$)$_2$Cl] (14)

The complex *trans*-[RhCO(PPh$_3$)$_2$Cl] was first prepared by Angoletta and later correctly formulated by Vaska in 1961.[48,49] In an attempt to synthesize [Rh(O,O-Bid)(CO)PPh$_3$] the reaction exclusively yielded quantitative amounts of *trans*-[RhCO(PPh$_3$)$_2$Cl] as product. Yellow crystals were obtained from the acetone solution of the reaction. This complex crystallized in the monoclinic *P*2$_1$/*n* space group with four independent molecules in the unit cell (Z = 4). In the structure of (**14**) the Rh atom is in a square planar geometric configuration surrounded by two *trans* orientated triphenylphosphine functional groups, a carbonyl and a chlorido ligand. The chlorido ligand carries a mono-negative charge, while the carbonyl and phosphine ligands are

---

[48] M. Angoletta, *Gazz. Chim. Ital.*, **1959**, *89*, 2359.
[49] L. Vaska, J. W. Di Luzio, *J. Am. Chem. Soc.*, **1961**, *83*, 2784.

neutral resulting in a neutral complex. A summary of the general interatomic bond distances and angles are given in Table 9.4 while the numbering scheme of the neutral molecule is shown in Figure 9.6.
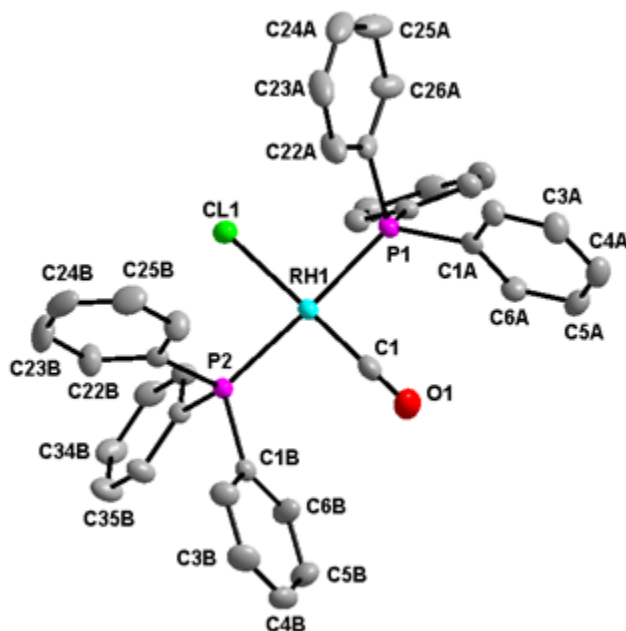
Figure 9.6: Molecular representation of *trans*-[RhCO(PPh$_3$)$_2$Cl] (14) showing the atom numbering scheme. Displacement ellipsoids are drawn at 50 % probability level. Hydrogen atoms are omitted for clarity.

Table 9.4: Selected bond distances (Å) and angles (°) for the crystal structure of (14).

Bond	Bond distance (Å)	Bond angle (atoms)	Bond angle (°)
Rh(1)-C(1)	1.819(2)	C(1)-Rh(1)-P(2)	91.85(7)
Rh(1)-P(2)	2.3179(11)	C(1)-Rh(1)-P(1)	91.74(7)
Rh(1)-P(1)	2.3225(11)	P(2)-Rh(1)-P(1)	176.16(2)
Rh(1)-Cl(1)	2.3654(7)	C(1)-Rh(1)-Cl(1)	175.45(7)
O(1)-C(1)	1.138(3)	P(2)-Rh(1)-Cl(1)	87.28(2)
		P(1)-Rh(1)-Cl(1)	89.25(2)
		O(1)-C(1)-Rh(1)	177.0(2)

The structure of *trans*-[RhCO(PPh$_3$)$_2$Cl] has already been reported in different studies *i.e.* Roodt *et al.*, Dunbar *et al.*, Del Pra *et al.*, Rheingold *et al.* and Churchill *et al.* reported the Iridium analogue (see Table 9.6).[50-54] The crystalline form obtained in this study is exactly the same as

[50] G. Kemp, A. Roodt, W. Purcell, *Rhodium Express*, **1995**, *12*, 21.

[51] K. R. Dunbar, S. C. Haefner, *Inorg. Chem.*, **1992**, *31*, 3676.

[52] A. L. Del Pra, G. Zanotti, P. Segala, *Cryst. Struct. Commun.*, **1979**, *8*, 959.

that reported by Rheingold *et al*. The CO stretching frequency of 1980 cm^{-1} and 1946 cm^{-1} is comparable to the 1983 cm^{-1} reported by Rheingold *et al*., in both cases the compound crystallized without solvent. The origin of the Vaska complex in the synthetic protocols followed as described herein, is normally a result of unreacted [Rh(CO)$_2$Cl)]$_2$ after addition of the bidentate ligand (refer to Chapter 3). However, in this case the Vaska compound was not a by-product and the yields were quantitative. Furthermore, the dicarbonyl products in each case were thoroughly washed with cold water, dried and characterized before addition of the phosphine. The resultant product was then quantitative amounts of the Vaska's complex.

A possible reason for the lack of coordination to the soft Rh(I) centre may be due to the fact that pyridinones are hard ligands with proven affinity for hard metals consistent with the results obtained from the Zr and Hf work (refer to Chapters 3 & 4) and the Cu and Fe work reported in literature.[55-58] Thus the ligands are concluded to be weakly bound to soft metals and hence easily substituted by the stronger (soft) nucleophile triphenylphosphine.

[53] A. L. Rheingold, S. J. Geib, *Acta Cryst. Sect. C*, **1987**, *43*, 784.

[54] M. R. Churchill, J. C. Fettinger, L. A. Buttrey, L. A. Barkan, J. S. Thomson, *J. Organomet. Chem.*, **1988**, *340*, 257.

[55] D. E. Green, M. L. Bowen, L. E. Scott, T. Storr, M. Merkel, K. Bohmerle, K. H. Thompson, B. O. Patrick, H. J. Schugar, C. Orvig, CCDC 746850: Experimental Crystal Structure Determination, 2014, DOI: 10.5517/cct24yy

[56] M. A. Telpoukhovskaia, C. Rodríguez-Rodríguez, J. F. Cawthray, L. E. Scott, B. D. G. Page, J. Alí-Torres, M. Sodupe, G. A. Bailey, B. O. Patrick, C. Orvig, *Metallomics*, **2014**, *6*, 249.

[57] E. T. Clarke, A. E. Martell, J. Reibenspies, *Inorg. Chim. Acta.*, **1992**, *196*, 177.

[58] T. F. Tam, R. Leung-Toung, Y. Wang, M. Spino, G. Williams, A. J. Lough, *Acta Cryst. Sect. E*, **2005**, *E61*, m2055.
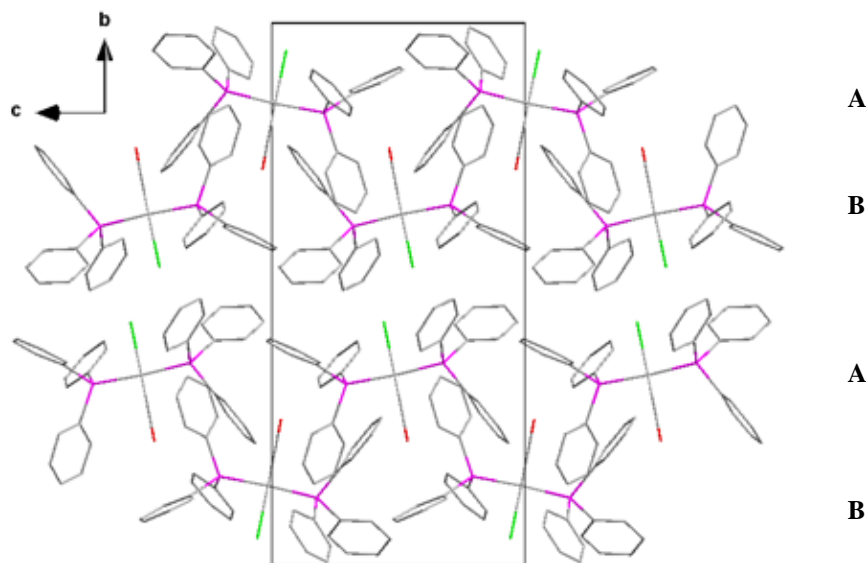
Figure 9.7: Crystal packing of (14) in the unit cell, viewed along the c-axis. Hydrogen atoms are omitted for clarity.

When viewed along the *a*-axis the molecules pack in an alternating fashion with the first layer having the chlorine atoms pointing upwards and the second layer pointing downwards (**ABA**) (Figure 9.7).

9.5   Crystal structure of Triphenylphosphine (15)

Yellow cuboidal crystals (0.41 x 0.264 x 0.118 mm^3) of $C_{18}H_{15}P$ (**15**) were obtained from an acetone solution. This compound crystallized in the monoclinic $P2_1/c$ space group with four independent molecules in the unit cell (Z = 4). In the structure of (**15**) the phosphorous atom is in a tetrahedral geometric configuration surrounded by three phenyl groups at the vertices of the tetrahedron. The fourth vertex is occupied by a lone pair of electrons. There are slight distortions in the structure with angles deviating from the expected value of 109 ° to ~ 103 °. The numbering scheme of the neutral molecule is shown in Figure 9.8.
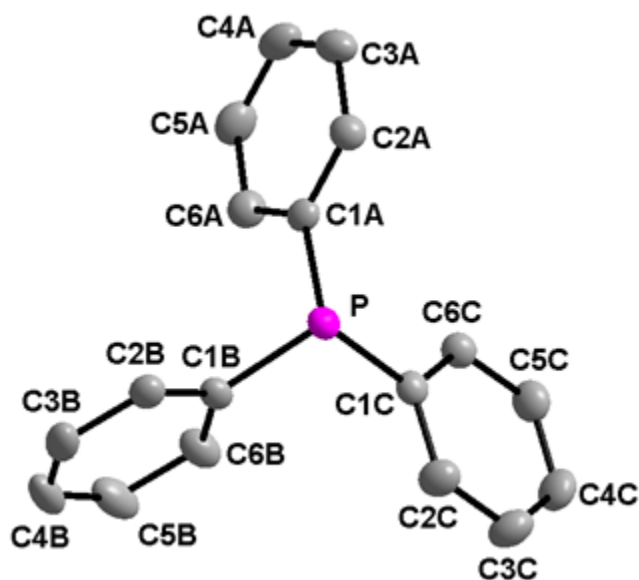
Figure 9.8: Molecular representation of PPh$_3$ (15) showing the atom numbering scheme. Displacement ellipsoids are drawn at 50 % probability level. Hydrogen atoms are omitted for clarity.
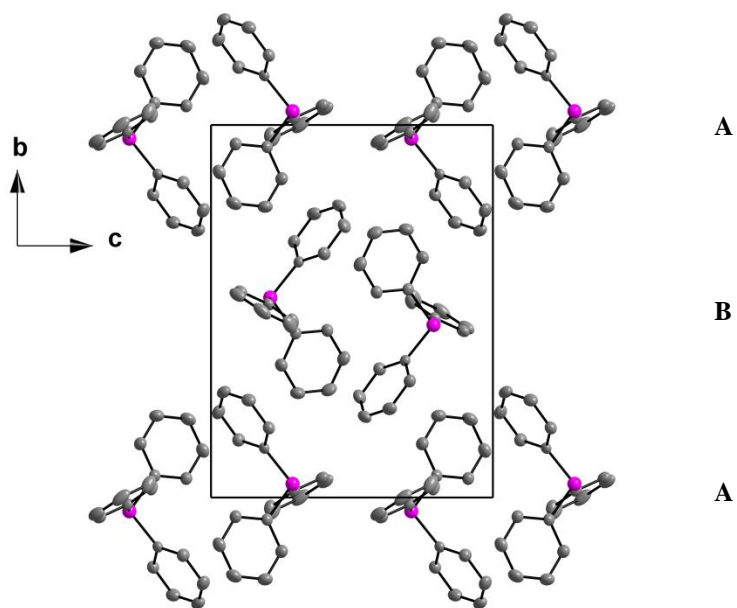
Figure 9.9: Crystal packing of (15) in the unit cell, viewed along the *a*-axis. Hydrogen atoms are omitted for clarity.

The molecules pack in pairs arranged in a staggered conformation with two layers alternating (**AB**), there are no hydrogen interactions observed in this structure (Figure 9.9).

9.6 Discussion

Six similar rhodium structures with O,O'-bidentate ligands coordinated to the rhodium centre are compared here to (**13**) (see Figure 9.10 and Table 9.5) and five Vaska type complexes are separately compared to (**14**) (Table 9.6) in both cases to highlight some structural properties and to correlate some structural data between the different complexes.
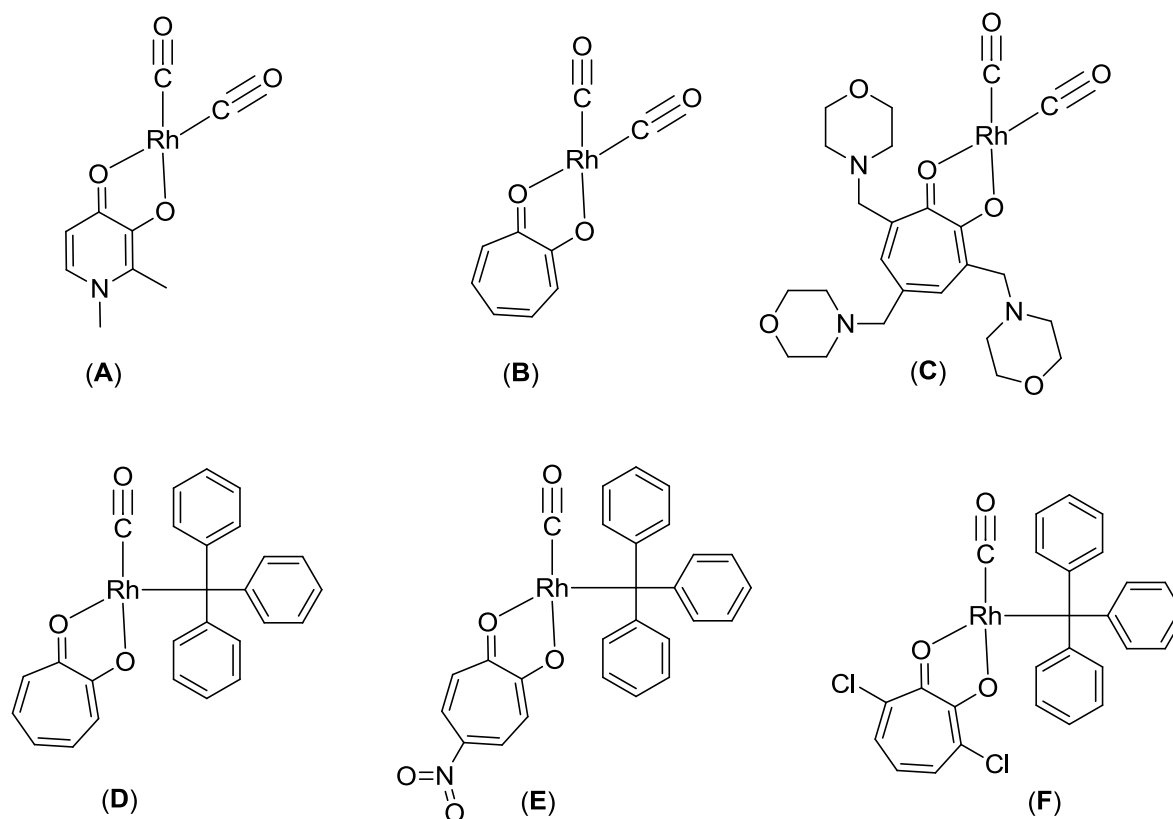
Figure 9.10: Illustration of the crystal structures of [Rh(MM(naltol))(CO)$_2$] (A), [Rh(Trop)(CO)$_2$] (B), [Rh(C$_{22}$H$_{32}$N$_3$O$_5$)(CO)$_2$] (C), [Rh(Trop)CO(PPh$_3$)] (D), [Rh(5-NO$_2$Trop)(CO)PPh$_3$] (E) and [Rh(TropCl$_2$)CO(PPh$_3$)] (F) .

Table 9.5: Selected bond distances and angles of [Rh(O,O'-bidentate)(CO)$_2$] and [Rh(O,O'-bidentate)(CO)(PPh$_3$)] complexes.

Formula	(13) [a]	(A) [b]	(B) [c]	(C) [d]	(D) [e]	(E) [f]	(F) [g]
Complexes							
Re−X (X = O/C/P) Å							
Rh−O(1)	2.033(1)	2.026(3)	2.021 (5)	2.0209 (16)	2.045(2)	2.068 (4)	2.0563 (16)
Rh−O(2)	2.037(2)	2.041(3)	2.032 (5)	2.0212 (15)	2.083(2)	2.072 (4)	2.0860 (16)
Rh−C(21)	1.841(2)	1.825(4)	1.825 (10)	1.835 (3)	1.805(3)	1.775 (7)	1.809 (2)
Rh−C(22)	1.843(2)	1.835(4)	1.826 (9)	1.840 (2)	-	-	-
Rh−P	-	-	-	-	2.223(1)	2.2397 (17)	2.2377 (8)
O-Re-X (X = O/P) °							
O(1)-Rh-O(2)	82.23(5)	82.29(11)	79.4 (2)	79.18 (6)	77.90(9)	77.09 (16)	76.60 (6)
C(21)-Rh-C(22)/P	88.20(8)	89.25(18)	88.3 (4)	91.18 (11)	87.19(11)	89.3 (2)	87.00 (7)

[a] Current study, [b] R. Lang *et al.* [39], [c] G. Steyl *et al.* [40], [d] T. N. Hill *et al.* [41], [e] G. Steyl *et al.* [42], [f] G. Steyl *et al.* [43], [g] G. Steyl *et al.* [44].

All the rhodium complexes (**A**) to (**F**) compared here with (**13**) are square planar in coordination geometry. In all the complexes the Rh−O bond distances of the bidentate coordinated ligands are approximately 2.0 Å with the exception of (**E**) and (**F**) with both Rh−O bond distances approximately 2.1 Å. The Rh−C bond distances of the coordinated carbonyls are shorter than the Rh−O bond distance, at ~ 1.8 Å in all the complexes showing strong back bonding by the carbonyls. The Rh−P bond distances are approximately 2.2 Å making them slightly longer than the Rh−O bond distances which could be due to the steric demands of the PPh$_3$. The bite angles of the bidentate coordinated ligands in (**13**) and (**A**) are approximately 82 ° which are larger than all the other complexes which range between 76 ° to 79 °. The 'bite' angle C(21)-Rh-C(22)/P (between the two carbonyl carbons in dicarbonyl complexes or between the carbonyl carbon and the phosphorus atom in phosphine complexes) ranges between 87 ° and 89 ° in all the complexes except the dicarbonyl compound (**C**) which is ~ 91 °. This is unexpected as phosphines ligands, because of their bulkiness, would typically be more sterically demanding with the resultant larger bite angles. However, the longer Rh−P bond distances possibly allow for a smaller steric demand from the phosphine substituent.

Table 9.6: Comparison of crystal parameters for different Vaska type complexes reported in literature.

	Current study	Roodt et al.[50]	Dunbar et al.[51]	Del Pra et al.[52]	Rheingold et al.[53]	Churchill et al.[54]
Formula	$RhCO(PPh_3)_2Cl$	$RhCO(PPh_3)_2Cl$	$RhCO(PPh_3)_2Cl$	$RhCO(PPh_3)_2Cl$	$RhCO(PPh_3)_2Cl$	$IrCO(PPh_3)_2Cl$
v_{CO} **(cm^{-1})**	1980, 1947	1965	1965	(a)	1983	(a)
Crystal system	Monoclinic	Triclinic	Orthorhombic	Triclinic	Monoclinic	Triclinic
Space group	$P2_1/n$	$P\bar{1}$	$Pbca$	$P1$	$P2_1/n$	$P\bar{1}$
a (Å)	11.823(2)	9.176(2)	20.527(4)	10.420(7)	11.968(3)	9.2076(10)
b (Å)	23.893(4)	9.648(2)	8.054(4)	9.688(7)	24.505(7)	9.6458(16)
c (Å)	12.113(2)	20.085(4)	23.343(4)	9.187(7)	12.191(4)	10.4601(11)
α (°)	90	80.34(3)	90	110.6(1)	90	72.290(11)
β (°)	113.024(5)	80.66(3)	90	89.69(1)	113.27(2)	89.597(10)
γ (°)	90	69.50(3)	90	107.6(1)	90	69.568(11)
Rh-P(1)	2.3225(9)	2.313(7)	2.322(1)	2.363(2)	2.333(1)	2.330(1)
Rh-P(2)	2.3179	2.349(7)		2.304(2)	2.327(1)	2.330(1)
Rh-Cl(1)	2.3654(5)	2.380(11)	2.382(1)	2.405(4)	2.395(1)	2.382(3)
Rh-C(1)	1.8186(4)	1.74(3)	1.77(1)	1.99(1)	1.821(5)	1.791(13)
C(1)-O(1)	1.1380(2)	1.20(5)	1.14(2)	0.74(1)	1.141(6)	1.161(18)
P(1)-Rh-Cl(1)	89.248(11)	97.3(4)	93.6(1)	89.2(1)	89.1(1)	87.75(8)
P(1)-Rh-P(2)	176.161(21)	171.7(6)	180.0(1)	178.7(1)	176.1(1)	180.0(-)
O(1)-C(1)-Rh	177.040(16)	164(4)	169(2)	176(1)	177.2(4)	175.1(12)
Solvent	Acetone	Acetone	Dichloromethane	Acetone	(a)	(a)

(a) Not reported

Churchill unambiguously reported that the Ir complex crystallized in the triclinic $P\bar{1}$ space group (Z = 1) and that it was *iso*-structural to the Rh(I) complex reported by Del Pra *et al.* (Table 9.6) although the latter structure (Del Pra *et al.*) crystallized in the non-centrosymmetric triclinic $P1$ space group (Z = 1). In the study by Roodt *et al.* the space group was determined as triclinic, $P\bar{1}$, Z = 2 and the cell parameters were similar to the structure of Del Pra and they also reported disorders in the Cl-Rh-CO axis similar to Del Pra. The more common mode of crystallization for *trans*-[RhCO(PPh$_3$)$_2$Cl] is that reported by Rheingold having a CO stretching frequency of 1983 cm^{-1} which crystallizes without any solvent and is the same as (**14**) exhibiting a primary CO stretching frequency at 1980 cm^{-1}.

9.7 Conclusion

In total seven rhodium(I) dicarbonyl complexes were successfully synthesized and characterized (see Chapter 3). Another dicarbonyl complex (based on 2-ethyl-3-hydroxy-1-isopropyl-4-pyridone) was water soluble and did not precipitate after the addition of cold water as the typical synthesis protocol suggests. This complex was therefore not characterized fully as upon evaporation of the DMF and water mixture it had decomposed (the colour changed from yellow to dark brown and black). The corresponding phosphine complexes could not be isolated and for this reason the iodomethane oxidative addition was not evaluated. This certainly a pity since it would be very interesting to compare the activation, if any, induced by these pyrone/ pyridinone types of ligands to the Rh(I) centre.

From the synthesized dicarbonyl complexes only one structure is reported here as an additional characterization method and proof-of-concept for the attainment of these pyridinonato based Rh(I) dicarbonyls and to indicate the affinity of these chelators for both hard and soft metals. Finally and perhaps an important observation to make is that it would appear that the limits of these hard metal chelators for soft metals is around the platinum group metals as addition of a phosphine group indicated total instability with a subsequent formation of the Vaska's complex, *trans*-[RhCO(PPh$_3$)$_2$Cl]. This crystallographic study will add to the existing data in the Crystallographic Cambridge Structural Data base, as only one structure by R. Lang *et al.* is available in terms of pyrone and pyridinones as ligand systems.

10 Evaluation of Monodentate Substitution Reactions in Re(I) Tricarbonyl Complexes

10.1 Introduction

Tricarbonyl complexes of group 7 transition metals (Mn, Tc and Re) have received notable attention because of their capacity to accept a variety of bifunctional chelators containing different donor atoms.[1-4] This property and the high kinetic stability of the carbonyl ligands in the low-spin d^6 *fac*-[M(CO)$_3$]$^+$ core has allowed for the development of potential Re- and Tc-based radiopharmaceuticals in complexes with a low valent central metal core.[5-11] For diagnostic nuclear medicine the radionuclides ^{99m}Tc, ^{18}F, ^{123}I and ^{68}Ga, are very important, with ^{99m}Tc representing approximately 80 % of all current clinically administered radiopharmaceuticals.[2,11] Kinetic data of *fac*-[M(CO)$_3$(H$_2$O)$_3$]$^+$ (M = Mn, Re and ^{99m}Tc) on water exchange and water substitution reactions indicate that ligand substitution in these types of complexes depends on the

[1] R. Alberto, R. Schibli, R. Waibel, U. Abram, A. P. Schubiger, *Coord. Chem. Rev*., **1999**, *192*, 901.

[2] S. Sulieman, D. Can, J. Mertens, H. W. P. N'Dongo, Y. Liu, P. Schmutz, M. Bauwens, B. Spingler, R. Alberto, *Organometallics*, **2012**, *31*, 6880.

[3] A. Frei, D. Sidler, P. Mokolokolo, H. Braband, T. Fox, B. Spingler, A. Roodt, R. Alberto, *Inorg. Chem*., **2016**, *55*, 9352.

[4] M. B. Ismail, I. N. Booysen, M. P. Akerman, C. Grimmer, *J. Organomet. Chem.,* **2017**, *833*, 18.

[5] R. Alberto, R. Schibli, A. Egli, A. P. Schubiger, W. A. Herrmann, G. Artus, U. Abram, T. A. Kaden, *J. Organomet. Chem*., **1995**, *493*, 119.

[6] A. Egli, R. Alberto, L. Tannahill, R. Schibli, U. Abram, A. Shaffland, R. Waibel, D. Tourvé, L. Jeannin, K. Iterbeke, A. P. Schubiger, *J. Nucl. Med.,* **1999**, *40*, 1913.

[7] R. Alberto, R. Schibli, A. P. Schubiger, U. Abram, H. J. Pietzsch, B. Johannsen, *J. Am. Chem. Soc.,* **1999**, *121*, 6076.

[8] C. Xavier, P. Jae-Kyoung, I. Santos, R. Alberto, *J. Organomet. Chem.,* **2007**, *692*, 1332.

[9] S. Wirth, A. U. Wallek, A. Zernickel, F. Feil, M. Sztiller-Sikorska, K. Lesiak-Mieczkowska, C. Bräuchle, I. P. Lorenz, M. Czyz, *J. Inorg. Biochem.,* **2010**, *104*, 774.

[10] T. W. Spradau, W. B. Edwards, C. J. Anderson, M. J. Welch, J. A. Katzenellenbogen, *Nucl. Med. Biol.,* **1999**, *26*, 1.

[11] F. Rösch, *Appl. Radiat. Isot.,* **2013**, *76*, 24.

nature of the incoming ligand.[12-14] A mechanistic transition occurs from interchange dissociative (I_d) for hard chelators to interchange associative (I_a) for soft chelators.

The fac-$[M(CO)_3(H_2O)_3]^+$ synthon is tailored via the [2+1] mixed ligand approach.[15] In this approach a bidentate ligand effectively occupies two of the three reactive aqua sites leaving one site available for substitution.[16] The lipophilicity can then be mildly modulated by coordinating a biologically active molecule either on the third aqua site or on the backbone of the bidentate ligand. The theoretically countless possibilities with regards to the different combinations of bidentate (O'O, N'O, S'O etc.) and monodentate (N, P, S, O etc.) ligands allows for the optimization of the properties and reactivity of the model compounds, in this chapter O,O'-bidentate activation and kinetics is explored.

Of predominant interest to this study is the fact that rhenium can be used as a non-radioactive model for technetium as well as a potential radiotherapeutic agent with its β^- emitting isotopes ^{186}Re and ^{188}Re.[17-19] Accordingly and of critical importance is the kinetic behaviour of fac-$[Re(O,O'\text{-Bid})(CO)_3(H_2O)]^n$ (O,O'-Bid = bidentate ligand, n = 0) complexes. These studies can give some insights with regards to the following clinical aspects: patient administration, uptake, reactivity and clearance of the radiopharmaceutical agent.

To add to the current knowledge of these tricarbonyl complexes the type of reaction mechanism is critical to its application and therefore has to be determined. One way of accomplishing this is by considering the coordination of a broad variety of chelators to this synthon (fac-$[Re(CO)_3(H_2O)_3]^+$) and also incorporating a variety of substitution reactions on this metal core. For this reason, in this chapter the kinetic behaviour of two of the complexes synthesized in this study is investigated namely fac-$[Re(EM(naltol))(CO)_3(H_2O)]$ (**16**) and fac-$[Re(EM(naltol))(CO)_3(EM(naltol)H)]$ (**3**) (Scheme 10.1) with EM(naltol)H = 2-ethyl-3-hydroxy-

[12] B. Salignac, P. V. Grundler, S. Cayemittes, U. Frey, R. Scopelliti, A. E. Merbach, *Inorg. Chem.,* **2003**, *42*, 3516.

[13] P. V. Grundler, B. Salignac, S. Cayemittes, R. Alberto, A. E. Merbach, *Inorg. Chem.,* **2004**, *43*, 865.

[14] P. V. Grundler, L. Helm, R. Alberto, A. E. Merbach, *Inorg. Chem.,* **2006**, *45*, 10378.

[15] S. Mundwiler, M. Kündig, K. Ortner, R. Alberto, *Dalton Trans.*, **2004**, 1320.

[16] S. Mundwiler, M. Kündig, K. Ortner, R. Alberto, *Dalton Trans.,* **2004**, 1320.

[17] R. Alberto, *Eur. J. Nucl. Med. Mol. Imaging*, **2003**, *30*, 1299.

[18] J. R. Ballinger, M. S. Cooper, S. J. Mather, *Eur. J. Nucl. Med. Mol. Imaging*, **2004**, *31*, 304.

[19] S. Liu, *Chem. Soc. Rev.*, **2004**, *33*, 445.

1-methyl-4-pyridone. Of specific significance is the fact that the bidentate ligand (EM(naltol)H), can as proved by this study, act as both a bidentate and a monodentate ligand (see Chapter 5). Up until now it has always been assumed that solvolysis precedes the monodentate substitution on the sixth position in these types of complexes (*fac*-[Re(O,O'-Bid)(CO)$_3$(H$_2$O)]).[20-24] With the unique set of complexes obtained in this study this assumption from the results of these kinetic experiments can now be validated.

fac-[Re(EM(naltol))(CO)$_3$(H$_2$O)] (**16**)   *fac*-[Re(EM(naltol))(CO)$_3$(EM(naltol)H)] (**3**)

fac-[Re(EM(naltol))(CO)$_3$(CH$_3$OH)] (**16a**)   *fac*-[Re(EM(naltol))(CO)$_3$(Pyr)] (**11**)
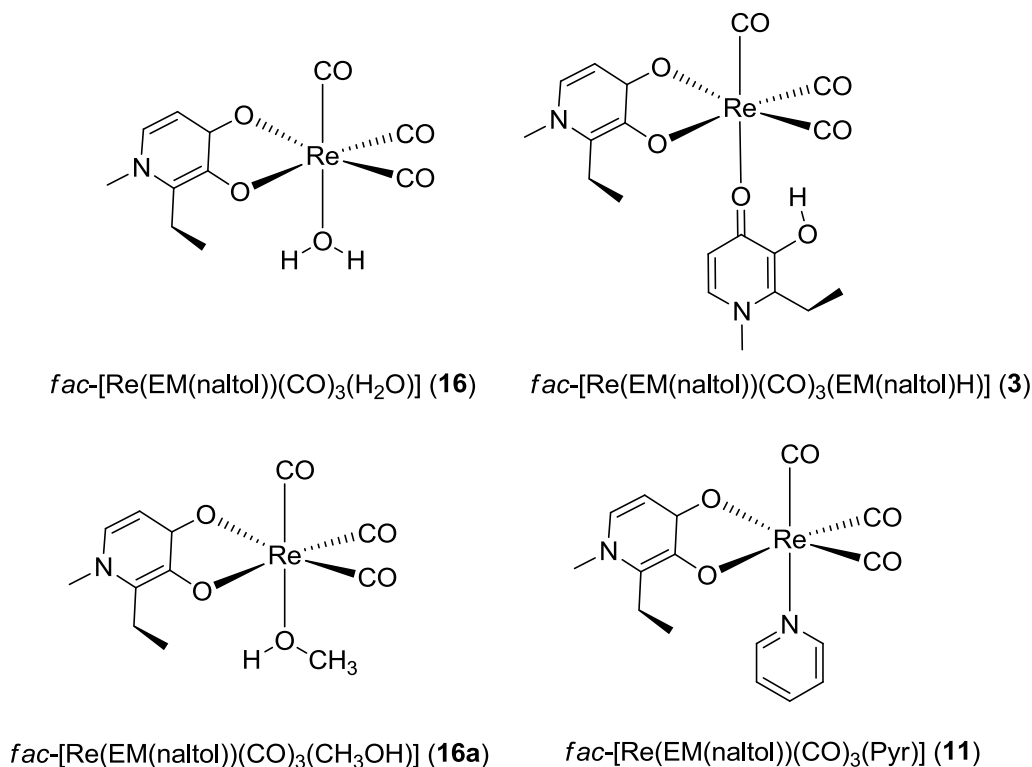
Scheme 10.1: Schematic representation of the two complexes dissolved in methanol and used as reactants in this kinetic substitution study (16 and 3; with 16a representing the MeOH solvated compound) giving the substitution product (11).

[20] A. Brink, H. G. Visser, A. Roodt, *Inorg. Chem.,* **2014**, *53*, 12480.
[21] A. Brink, H. G. Visser, A. Roodt, *Inorg. Chem.,* **2013**, *52*, 8950.
[22] M. Schutte, A. Roodt, H. G. Visser, *Inorg. Chem.,* **2012**, *51*, 11996.
[23] M. Schutte, G. Kemp, H. G. Visser, A. Roodt, *Inorg. Chem.,* **2011**, *50*, 12486.
[24] M. Schutte, H. G. Visser, *Polyhedron,* **2015**, *89*, 122.

10.2 Background on characterization of reactants and products

If the assertion that solvolysis precedes the monodentate substitution is true then the formation rate constants for (**16**) and (**3**) should be very similar under similar kinetic conditions, because upon solvolysis in methanol they should essentially proceed *via* the same substitution compound *fac*-[Re(EM(naltol))(CO)$_3$(CH$_3$OH)]. ^{1}H and ^{13}C NMR solution studies in Chapter 3 and 5 indicated that S$_N$1 solvolysis is not always 100 % prevalent as (**2**) remained only to a small extent intact in solution (see Figure 5.1). However (**3**) and (**16**) indicated formation of the methanol substituted product (see Figure 10.1). Once (**16**) is dissolved in methanol it immediately exchanges the water molecule for MeOH.[20-24] Figure 10.1 illustrates the formation of *fac*-[Re(EM(naltol))(CO)$_3$(CH$_3$OH)] in solution from (**16**) and (**3**), which also indicates the free ligand EM(naltol)H in solution upon methanol substitution of the latter. Additionally the are smaller peaks in the spectrum of (**3**) which could not be assigned, however these are believed to be due to small amounts of (**3**) which are still non-dissociated in solution. The integrals of these peaks are ~ 60 % smaller than those of the coordinated and free ligands.

To further verify this, the rate constants of the substitution reactions from both (**16**) and (**3**) will be determined. Thus, in this chapter the methanol substitution of *fac*-[Re(EM(naltol))(CO)$_3$(CH$_3$OH)] from (**3**) and (**16**) will be evaluated to see if the rate constants are similar as expected (based on NMR results) or whether the free neutral ligand (H$_2$O or EM(naltol)H) in solution that was substituted by methanol has an influence in the kinetics (equimolar amounts of the free neutral ligand is present). Although single crystal X-ray diffraction data confirmed the formation of this MeOH product from *fac*-[Re(EI(naltol))(CO)$_3$(H$_2$O)] (see Chapter 7 for (**8**)) as crystals, the same product could not be isolated from a methanol solution of *fac*-[Re(EM(naltol))(CO)$_3$(EM(naltol)H)] (**3**) but can be seen to a small extent in solution state. For this reason (**3**) was chosen to verify this assertion unequivocally due to the observed modes of coordination in the structure. It will thus also be kinetically investigated as to whether (**3**) is directly substituted or the process is solvolytic in nature by comparing the respective reaction rates of (**3**) with the corresponding aqua complex *fac*-[Re(EM(naltol))(CO)$_3$(H$_2$O)] (**16**). Aqua complexes are known to undergo methanol

substitution.[19-24] If the rates are similar then this would unequivocally mean that the process is solvolytic in nature.
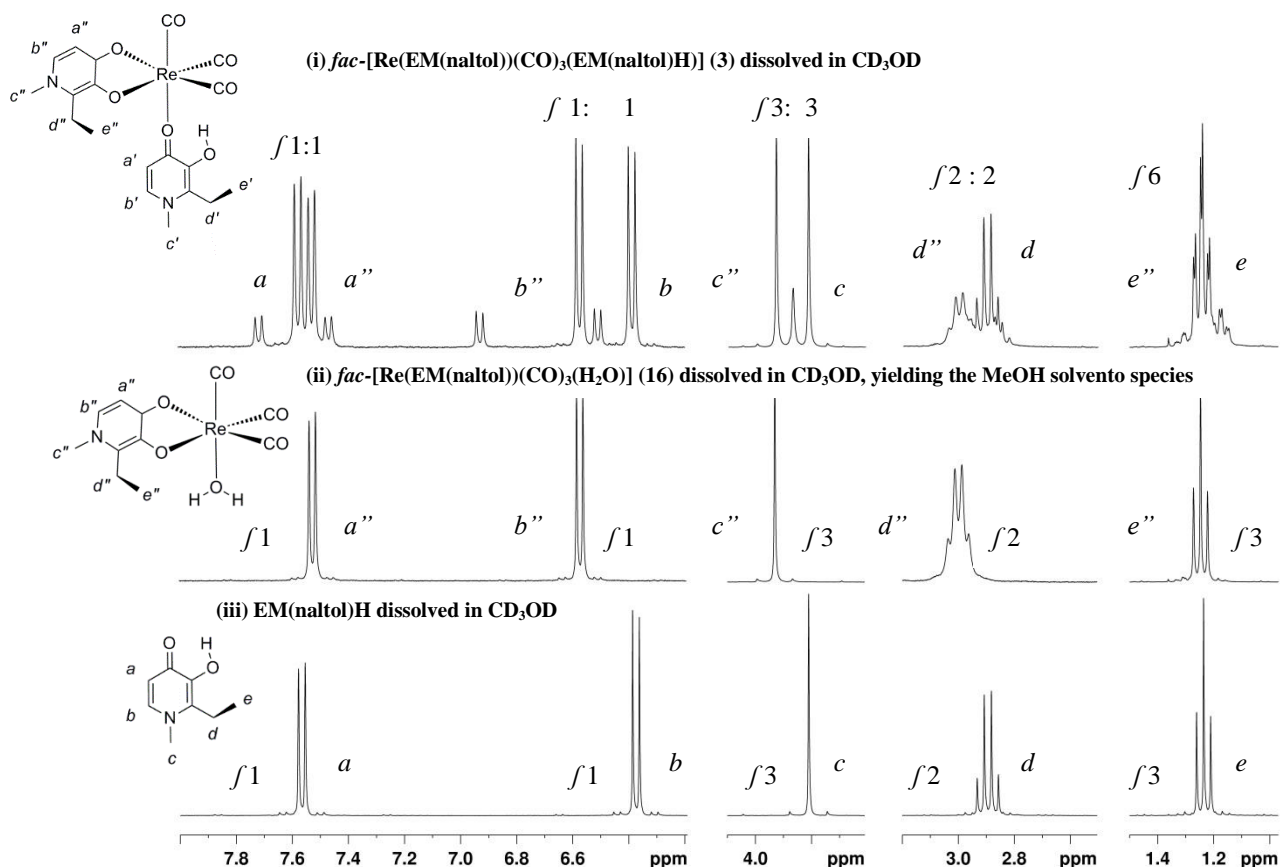
Figure 10.1: ^{1}H NMR (300 MHz) spectra of (i) *fac*-[Re(EM(naltol))(CO)$_3$(EM(naltol)H)] (3), (ii) *fac*-[Re(EM(naltol))(CO)$_3$(H$_2$O)] (16) and (iii) EM(naltol)H dissolved in CD$_3$OD. Chemical shifts δ: (i) free ligand; *a-e*, coordinated bidentate ligand; *a"-e"* (ii) coordinated bidentate ligand; *a"-e"* (iii) free ligand; *a-e*. The symbol ∫ indicates the respective integrals of the chemical shifts.

It is clear that *fac*-[Re(EI(naltol))(CO)$_3$(H$_2$O)] did undergo the methanol substitution to yield the corresponding solvento product (**4**) (refer to Chapter 7) and therefore the resultant kinetic evaluation on this particular complex would be the methanol substitution process. It's also clear from the NMR data above that both (**3**) and (**16**) dissociate when dissolved in methanol. But based on some of the results obtained it is not always the case and what is clear is that solvolysis in these types of complexes depends on the nature of the activating bidentate ligand on the rhenium(I) core as (**2**) showed no such activation (see Figure 5.1). Preliminary substitution experiments on these complexes with 3-hydroxypyridinones as a ligand system indicated that the reactions are very fast and the equilibrium constant is ≫ 1000 M^{-1}. This presented a unique

challenge in that if the observed rate constants are fairly large, the reverse rate constants (intercepts) are quite small and might be difficult to determine within experimental error.

In this chapter the substitution reaction(s) under evaluation is the replacement of neutral ligands (CH_3OH or EM(naltol)H) by neutral monodentate ligands. No change in the oxidation state of the metal occurs during the reaction or as a result of the substitution. The enticing objective of this study is that it will indicate whether the substitution is solvolytic or not and provide a chelator system as basis for two specific desirable dynamics depending on the desired objective in rhenium therapeutic applications. The mechanism for the reaction can either be associative, interchange or dissociative in nature. In an associative mechanism (A) a seven coordinate transition state which is the rate determining step is formed followed by a fast dissociation of the leaving group.[25,26] In an interchange mechanism a rapid pre-equilibrium is formed where there is an interchange of ligands within the outer-sphere complex subsequent to a slower rate determining step which can be either associative (I_a) or dissociative (I_d) in nature.[26] In a dissociative mechanism (D) a five coordinate transition state is formed upon dissociation which is the rate determining step and is then succeeded by the fast substitution.[27-29] Insights on the stability and reactivity of these new complexes in a controlled chemical environment might provide knowledge or at the very least informed estimates with regards to potential behavioural patterns *in vivo*, with the ultimate objective always being the enhancement of the targeting capacity and the optimization of the labeling process and its efficacy.

The substitution reactions between (**3**) and (**16**) and various entering ligands were studied (Scheme 10.2), with pyridine (Py), imidazole (Im), 4-dimethylaminopyridine (DMAP) and 3-chloropyridine (3-ClPy) used as entering ligands. These complexes are also soluble in acetonitrile and for this reason we considered a liquid IR study to further validate the reproducible data obtained but were limited by the available equipment.

---

[25] T. W. Swaddle, *Adv. Inorg. Bioinorg. Mech.,* **1983**, *2*, 95.

[26] R. G. Wilkins, *Kinetics and Mechanism of reactions of Transition Metal Complexes*, 2nd Ed., VCH Publishers, Inc., New York, 2002.

[27] G. Alibrandi, G. Bruno, S. Lanza, D. Minniti, R. Romeo, M. L. Tobe, *Inorg. Chem.*, **1987**, *26*, 185.

[28] G. Alibrandi, D. Minniti, L. M. Scolaro, R. Romeo, *Inorg. Chem.*, **1989**, *28*, 1939.

[29] R. Romeo, A. Grassi, L. M. Scolaro, *Inorg. Chem.*, **1992**, *31*, 4383.

$$fac\text{-}[Re(O,O'\text{-}Bid)(CO)_3(CH_3OH)] \quad + \quad X \quad \underset{k_{-1}}{\overset{k_1, K_1}{\rightleftharpoons}} \quad [Re(O,O'\text{-}Bid)(CO)_3(X)] \quad + \quad CH_3OH$$
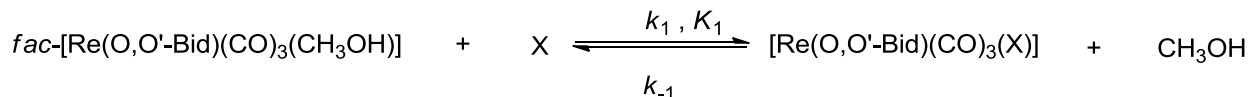
X = Py, DMAP, Im and 3-ClPy

Scheme 10.2: Schematic representation of simple substitution reactions between *fac*-[Re(EM(naltol))(CO)₃(CH₃OH)] and various entering ligands.

10.3 Experimental

All reagents and chemicals were of analytical grade. Anhydrous methanol and the pyridine reagents were obtained from Sigma Aldrich South Africa and were used as received. Preliminary kinetic measurements were done on a Varian Cary 50 Conc UV-Visible Spectrophotometer equipped with a Julabo F12-mV temperature cell regulator (accurate within 0.1 °C) in a $1.00 \pm$ cm quartz cuvette cell. Some of the reactions were too fast to study on the Cary and as a result all the successive work was done on a Hi-Tech SF-61DX2 Stopped-flow instrument equipped with a Julabo F12-mV temperature cell regulator. The dead time of the mixing unit is estimated to be less than 2.0 ms. The Stopped-flow system is a multiple wavelength instrument with a diode-array mode which can be used to scan within a defined wavelength range to determine the wavelength of optimum absorbance change. After the specific wavelength was selected, the Stopped-flow system was changed to the more sensitive photo-multiplier setup in order to more accurately study the kinetic reactions. The Hi-Tech Stopped-flow instrument is Microsoft Windows operated with Kinet Asyst Stopped-flow Kinetic Studio software for the acquisition and analysis of kinetic data.[30] All kinetic measurements were performed under *pseudo* first-order conditions in which the ligand concentration is at least ten times greater than the total rhenium complex concentration. The data was fitted to selected functions using the Scientist MicroMath, version 2.01 program (See paragraph 10.4).[31] The solid lines in the figures represent computer least-squares fits of data, while experimental values are represented as individual points, denoted by selected symbols. Note: From here onwards in the text (**3**) and (**16**) dissolved in methanol indicate the methanol complex formed from (**3**) and (**16**) indicates the methanol complex formed from the aqua complex, respectively.

---

[30] TgK Scientific Kinetic Studio, Version 1.0.8.32278, Copyright © TgK Scientific, 2008.
[31] Micromath Scientist for Windows, Version 2.01, Copyright ©1986-1995, MicroMath, Inc.

10.4 Data analysis

All the reactions monitored in this study were performed under *pseudo* first-order conditions with [L]>>[Re]. The observed *pseudo* first-order rate constants for these substitution reactions were obtained from fitting experimentally obtained data as a function of time:

$$A_{obs} = A_\infty - (A_\infty - A_0)e^{-k_{obs}t}$$ \hfill 10.1

where A_{obs} = observed absorbance, A_∞ = final absorbance, A_0 = initial absorbance, k_{obs} = *pseudo* first-order rate constant and t = time (s). In order to determine the *pseudo* first-order rate constant (k_{obs}), a least-squares fit of the absorbance *vs* time data was done. If not documented in the text, the individual observed rate constants are calculated for all the reactions studied and given in the supplementary material.

The activation parameters were calculated for a selection of the reactions to obtain more evidence of the type of mechanism for these reactions. Values for the standard activation enthalpy change ($\Delta H^{\neq}$) and the standard activation entropy change ($\Delta S^{\neq}$) were determined by using the logarithmic form of the Eyring equation (Equation 10.2).

$$\ln\frac{k}{T} = \frac{-\Delta H^{\neq}}{RT} + \ln\frac{k_B}{h} + \frac{\Delta S^{\neq}}{R}$$ \hfill 10.2

A plot of $\left(\ln\frac{k}{T}\right)$ *vs* $\left(\frac{1}{T}\right)$ would give a linear relation with a slope of $\left(\frac{-\Delta H^{\neq}}{R}\right)$ and intercept of

$\left(\ln\frac{k_B}{h} + \frac{\Delta S^{\neq}}{R}\right)$.

In Equation 10.2, k represents the experimentally determined rate constants at each temperature T. k_B is the Boltzmann constant (1.381×10^{-23} m^2.kg.s^{-2}.K^{-1}), R is the universal gas constant (8.314 J.K^{-1}.mol^{-1}) and h is Planck's constant (6.626×10^{-34} m^2.kg.s^{-1}). Accordingly the only unknown variables from this equation remain the enthalpy of activation ($\Delta H^{\neq}$) and the entropy of activation ($\Delta S^{\neq}$), which is calculated from the experimental data.

10.5 Results and discussion

The substitution kinetics of *fac*-[Re(EM(naltol))(CO)$_3$(H$_2$O)] (**16**) and *fac*-[Re(EM(naltol))(CO)$_3$(EM(naltol)H)] (**3**) dissolved in methanol were investigated and evaluated with different entering ligands and the results are reported below. The selected complexes were chosen because of the unique coordination observed in (**3**) and its corresponding methanol coordinated complex. These compounds allow the capacity to validate whether the mechanism of this substitution is *via* the solvent pathway or not. This is in addition to the suggestions in the preceding chapters that (**3**) cannot be formed from (**16**) (see Chapter 3). Due to the biological applications of these chelators and the fact that these coordination modes have not been reported before, this study is quite significant and unique as rhenium chemistry parallels technetium chemistry. This interesting coordination mode coupled with the biological activity of these bidentate ligands might be the basis for newly developed radiotherapeutic, radio-imaging and non radiotherapeutic clinical applications.

For this reason, in addition to the validation of the mechanism, the substitution process needed to be evaluated to determine the rate constants which would give some insights with regards to the reactivity of these compounds with certain nucleophiles (these can be viewed as specific receptors for targeting). The entering monodentate ligands selected for the substitution reactions in this study are the neutral amine ligands pyridine (Py), imidazole (Im), 4-dimethylaminopyridine (DMAP) and 3-chloropyridine (3-ClPy). These ligands were chosen to monitor and evaluate primarily the electronic effects induced by the substituents on the nitrogen atom of the entering ligand, on the second order reaction rate constants. Under *pseudo* first-order conditions, with [X] >> [*fac*-[Re(O,O'-Bid)(CO)$_3$(X)]] (O,O'-Bid = bidentate ligand system, X = monodentate entering ligand), only one reaction was observed for all of the reactions studied and the rates of these reactions increased systematically as the entering ligand concentration was increased. Accordingly from the reaction mechanism in Scheme 10.2 the rate of the reaction is given in Equation 10.3 below.

Rate = k_1[*fac*-[Re(O,O'-Bid)(CO)$_3$(CH$_3$OH)]][X] – k_{-1}[*fac*-[Re(O,O'-Bid)(CO)$_3$(X)]]   10.3

where k_1 and k_{-1} represents the rate constants for the forward and reverse reactions respectively. [fac-[Re(O,O'-Bid)(CO)$_3$(CH$_3$OH)]] is the concentration of the rhenium starting complex, [fac-[Re(O,O'-Bid)(CO)$_3$X]] is the concentration of the kinetic product and [X] is the concentration of the entering ligand. By employing $pseudo$ first-order conditions the concentration of the entering ligand is in excess ([X] $\gg$[fac-[Re(O,O'-Bid)(CO)$_3$(CH$_3$OH)]], [fac-[Re(O,O'-Bid)(CO)$_3$X]]), and the expression for the $pseudo$ first-order rate constant k_{obs} in Eq. 10.4 follows from Eq. 10.3:

$$k_{obs} = k_1[X] + k_{-1} \qquad \qquad 10.4$$

This expression enables one to determine the second-order rate constant by first obtaining k_{obs} at different ligand concentrations. Equation 10.4 also holds for equilibrium reactions and the equilibrium constant K_1 is given by:

$$K_1 = \frac{k_1}{k_{-1}} \qquad \qquad 10.5$$

k_1 and k_{-1} are obtained from a graph of k_{obs} vs [X] that yields a straight line with k_{-1} as the intercept and k_1 as the slope. The equilibrium constant K_1, can be determined by means of Equation 10.5. However, due to the large K_1 and k_1 values obtained in this study the corresponding k_{-1} values were very small and difficult to determine kinetically and accurately. For this reason the prime focus of this study was to determine the k_1 values and to determine these values by fixing the k_{-1} values and assigning them a value of zero in the mathematical model. Although some k_{-1} values were (small) negative they were still acceptable within the statistical margin of error.

The equilibrium constant K_1 was also obtained thermodynamically from a non-linear least-squares fit to Equation 10.6, using the established relationship based on UV/Vis data.[32,33] This is

[32] H. J. van der Westhuizen, R. Meijboom, A. Roodt, M. Schutte, *Inorg. Chem.,* **2010**, *49*, 9599.

[33] A. Roodt, J. G. Leipoldt, E. A. Deutsch, J. C. Sullivan, *Inorg. Chem.,* **1992**, *31*, 1080.

due to, as mentioned earlier, the reverse rate constants being extremely low and therefore difficult to determine accurately.

$$A_{obs} = (A_M + A_{ML}K_1[L])/(1 + K_1[L]) \hspace{4cm} 10.6$$

In Equation 10.6, A_M and A_{ML} are the observed absorbances of the starting complex and the kinetic product respectively, A_{obs} is the observed absorbance and $[L]$ is the concentration of the entering ligands.

10.6 Stopped-flow kinetic study of the methanol substitution in *fac*-[Re(EM(naltol))(CO)$_3$(CH$_3$OH)] by monodentate pyridine type ligands

The synthesis of the aqua complex *fac*-[Re(EM(naltol))(CO)$_3$(H$_2$O)] (**16**), from the pentacarbonyl starting synthon has been described in Chapter 3. As explained earlier (**16**) immediately exchanges the aqua molecule for methanol thus in solution (**16**) forms *fac*-[Re(EM(naltol))(CO)$_3$(CH$_3$OH)]. Upon monitoring the solutions of the complex as well as the entering ligands in methanol on a UV/Vis spectrophotometer, preliminary studies indicated that the compounds were stable for several days. The ligation reaction between *fac*-[Re(EM(naltol))(CO)$_3$(CH$_3$OH)] and pyridine was studied at various temperatures ranging from 14.4 °C to 46.8 °C while the reactions with DMAP, imidazole and 3-chloropyridine were only studied at 25 °C. The standard enthalpy of activation ($\Delta H^{\neq}$) and the standard entropy of activation ($\Delta S^{\neq}$) were determined for the reactions with pyridine from Eyring plots (Equation 10.2).

10.6.1 Substitution reaction between *fac-*[Re(EM(naltol))(CO)₃(CH₃OH)] and pyridine

The spectral change for the methanol substitution reaction between *fac-*[Re(EM(naltol))(CO)$_3$(CH$_3$OH)] and pyridine in methanol as solvent is illustrated in Figure 10.2. The concentration of pyridine as entering ligand was varied between 2 x 10^{-3} and 1 x 10^{-1} M while the metal complex was kept constant at [Re] = 7.49 x 10^{-4} M. The reaction was monitored at 365 nm and the k_{obs} *vs* [Py] data were obtained at 14.4 °C, 25.7 °C, 35.3 °C and 46.8 °C and the k_{obs} *vs* [Py] data were fitted to Eq. 10.4. The graph of k_{obs} *vs* [Py] at four temperatures are presented in Figure 10.3. The thermodynamic equilibrium constant (K_1) was determined by fitting the data to Eq. 10.3 and the plot of A_{obs} *vs* [Py] at 46.8 °C is depicted in Figure 10.4. The respective rate constants, Eyring plot and activation parameters are reported in Table 10.1, Figure 10.5 and Table 10.2 respectively.
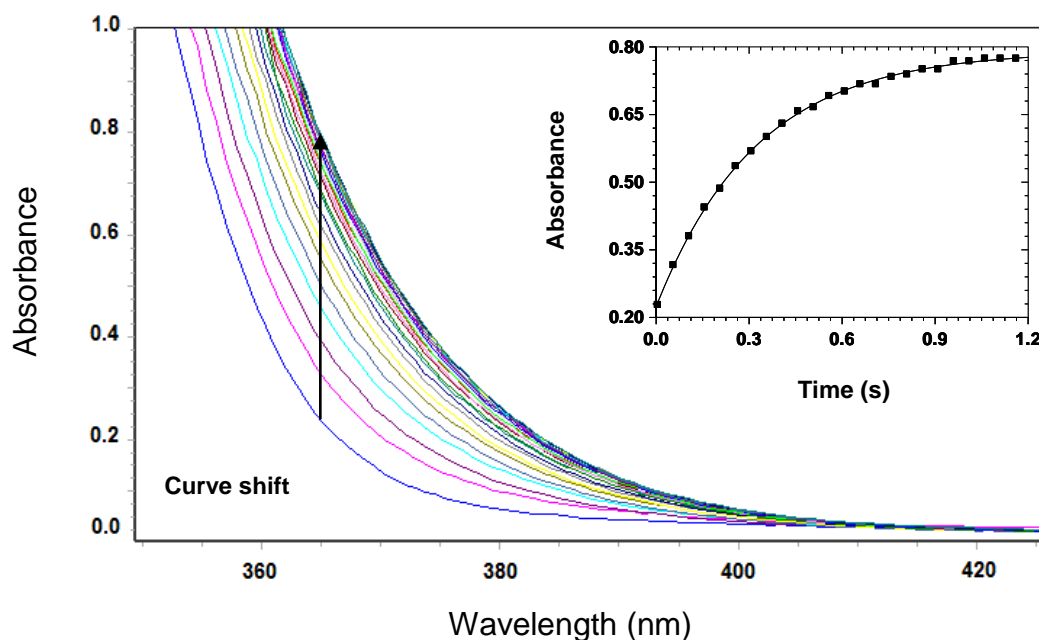
Figure 10.2: Characteristic UV/Vis spectra for the methanol substitution reaction between *fac-*[Re(EM(naltol))(CO)$_3$(CH$_3$OH)] and Py in methanol as solvent at 25.7 °C; [Re] = 7.49 x 10^{-4} M, [Py] = 1.0 x 10^{-1} M. The insert indicates the absorbance change *vs* time data at λ = 365 nm, Δt = 5.0 x 10^{-2} s. The line shows the least-squares fit to Equation 10.1 (k_{obs} = 3.12(4) s^{-1}).
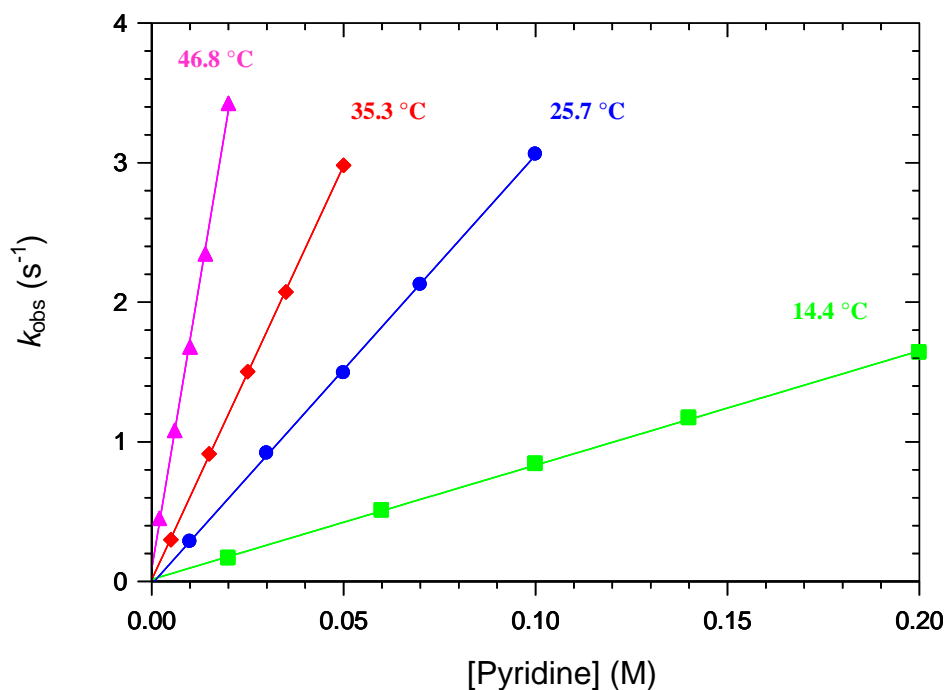
Figure 10.3: Plot of k_{obs} vs [Py] for the reaction between *fac*-[Re(EM(naltol))(CO)$_3$(CH$_3$OH)] and Py in methanol as solvent at various temperatures; [Re] = 7.49 x 10^{-4} M and [Py] = 2.0 x 10^{-3} – 2.0 x 10^{-1} M, λ = 365 nm.
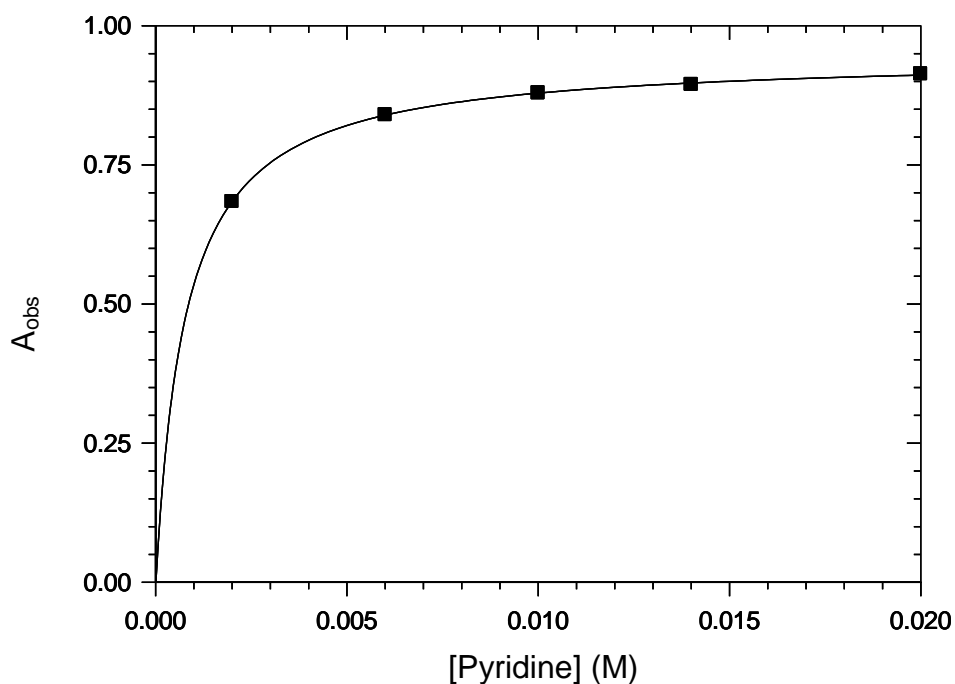
Figure 10.4: Thermodynamic determination of the equilibrium constant (K_1), for the methanol substitution reaction between *fac*-[Re(EM(naltol))(CO)$_3$(CH$_3$OH)] and Py in methanol as solvent from the UV/Vis spectral change data *vs* [Py] at 365 nm, 46.8 °C; [Re] = 7.49 x 10^{-4} M, [Py] = 2.0 x 10^{-3} – 2.0 x 10^{-1} M.
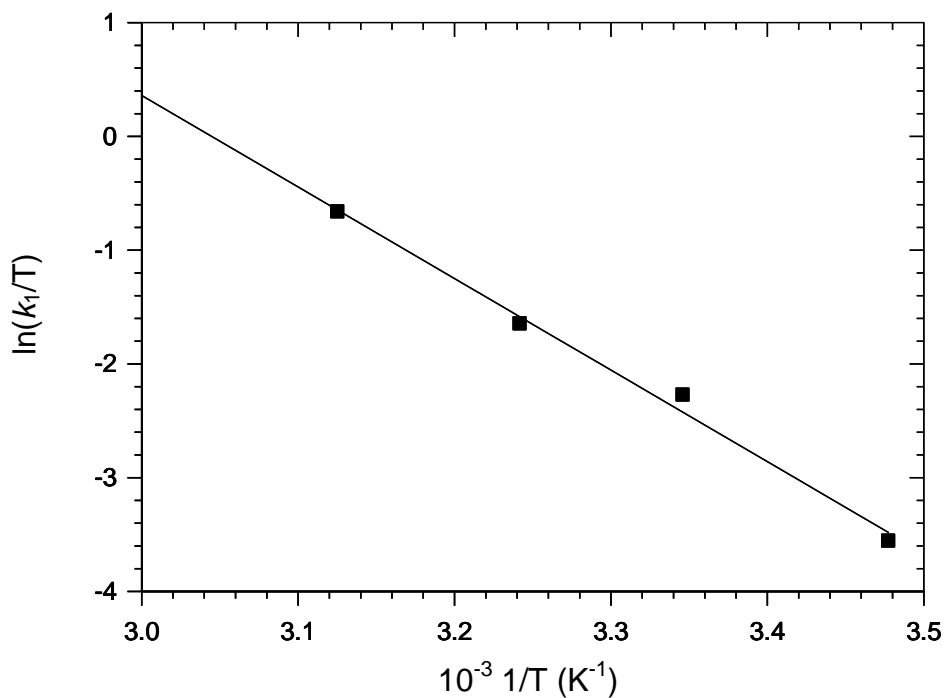
Figure 10.5: Eyring plot of $\ln(k_1/T)$ *vs* $1/T$ for the reaction between *fac*-[Re(EM(naltol))(CO)$_3$(CH$_3$OH)] and pyridine in methanol as solvent for the temperature range 14.4 °C to 46.8 °C, $\lambda = 365$ nm.

Table 10.1: Summary of the observed rate constants for the reaction between *fac*-[Re(EM(naltol))(CO)$_3$(CH$_3$OH)] and pyridine in methanol at different temperatures and concentration ranges. [Re] = 7.49 x 10^{-4} M, $\lambda = 365$ nm.

Observed rate constants							
[Py] (M) 14.4 °C	k_{obs} (s^{-1}) (average)	[Py] (M) 25.7 °C	k_{obs} (s^{-1}) (average)	[Py] (M) 35.3 °C	k_{obs} (s^{-1}) (average)	[Py] (M) 46.8 °C	k_{obs} (s^{-1}) (average)
0.002	0.167(1)	0.01	0.287(3)	0.005	0.299(3)	0.002	0.452(5)
0.006	0.509(4)	0.03	0.92(2)	0.015	0.91(1)	0.006	1.08(1)
0.010	0.842(9)	0.05	1.49(4)	0.025	1.50(1)	0.010	1.68(3)
0.014	1.17(2)	0.07	2.13(5)	0.035	2.07(2)	0.014	2.35(4)
0.020	1.64(1)	0.10	3.06(7)	0.050	2.98(3)	0.020	3.42(5)

Table 10.2: Kinetic data for the reactions between *fac*-[Re(EM(naltol))(CO)$_3$(CH$_3$OH)] and pyridine in methanol as solvent at different temperatures and concentration ranges. [Re] = 7.49 x 10^{-4} M, λ = 365 nm.

Rate constants/activation parameters	14.4 °C	25.7 °C	35.3 °C	46.8 °C
k_1 (M^{-1}s^{-1})	8.19(9)	30.7(1)	59.3(4)	164(4)
k_1 (M^{-1}s^{-1})^a	8.29(5)	30.5(1)	59.7(2)	171(2)
k_{-1} (s^{-1})	1.4(1.1) x 10^{-2}	*ca.* 0	1.2(1.1) x 10^{-2}	8.7(4.5) x 10^{-2}
K_1 (M^{-1})^b	569(426)	>1000	4901(4582)	1895(991)
K_1 (M^{-1})^c	>1000	>1000	>1000	1329(349)
ΔH$^{\neq}$ (kJ mol^{-1})		67(4)		
ΔS$^{\neq}$ (JK^{-1} mol^{-1})		6(13)		

^{a}Second order rate constant determined by fixing the intercept at the origin. ^{b} $K_1 = k_1/k_{-1}$ Eq. 10.5, ^{c} Thermodynamically estimated using Eq. 10.6.

For every [pyridine] the k_{obs} was determined from an average of five or six traces. The equilibrium constant was determined in two ways *i.e.* using Eq. 10.5 and Eq. 10.6. The reverse rate constants were of the order 10^{-2} s^{-1} except for the reaction at 25.7 °C which was even smaller and thus difficult to determine accurately.

10.6.2   Substitution reaction between *fac*-[Re(EM(naltol))(CO)$_3$(CH$_3$OH)] and DMAP

The spectral change for the methanol substitution reaction between *fac*-[Re(EM(naltol))(CO)$_3$(CH$_3$OH)] and DMAP in methanol as solvent is illustrated in Figure 10.6. The DMAP concentrations as entering ligand were varied between 1.0 x 10^{-2} and 1.0 x 10^{-1} M while the metal complex was kept constant at [Re] = 7.58 x 10^{-4} M. The reaction was monitored at 365 nm and 25.1 °C, the k_{obs} *vs* [DMAP] data were fitted to Eq. 10.3. The graph of k_{obs} *vs* [DMAP] at 25.1 °C is depicted in Figure 10.7. The thermodynamic equilibrium constant (K_1) was determined by fitting the data to Eq. 10.6 and the plot of A_{obs} *vs* [DMAP] at 25.1 °C is depicted in Figure 10.8. The rate constants were obtained from least-squares fits of the k_{obs} *vs* [DMAP] data and are reported in Table 10.3.
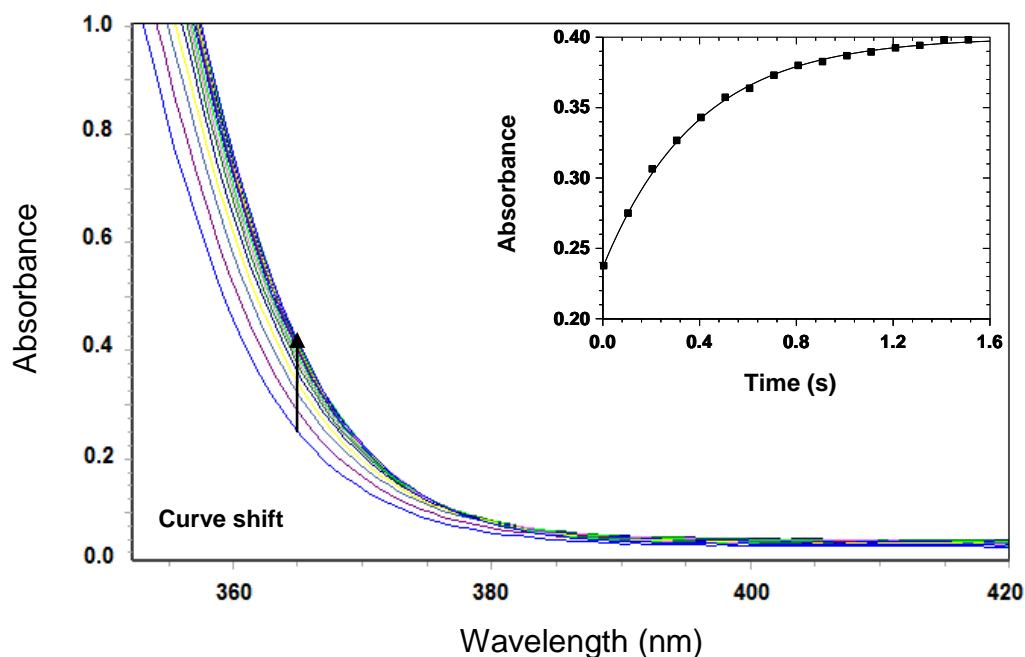
Figure 10.6: Characteristic UV/Vis spectra for the methanol substitution reaction between *fac*-
[Re(EM(naltol))(CO)$_3$(CH$_3$OH)] and DMAP in methanol as solvent at 25.1 °C; [Re] = 7.58 x 10^{-4} M, [DMAP]
= 1.0 x 10^{-1} M. The insert indicates the absorbance change *vs* **time data at λ = 365 nm, Δt = 1.0 x 10^{-1} s. The**
line shows the least-squares fit to Equation 10.1 (k_{obs} = 2.55(2) s^{-1}).
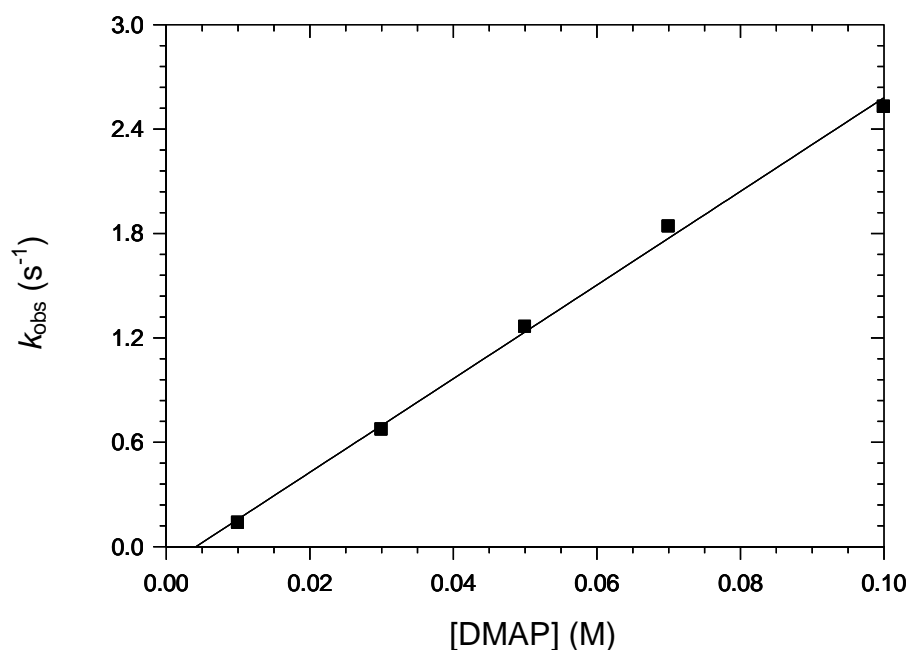
Figure 10.7: Plot of k_{obs} *vs* **[DMAP] for the reaction between** *fac*-**[Re(EM(naltol))(CO)$_3$(CH$_3$OH)] and DMAP**
in methanol as solvent at 25.1 °C; [Re] = 7.58 x 10^{-4} M and [DMAP] = 1.0 x 10^{-2} − 1.0 x 10^{-1} M, λ = 365 nm.
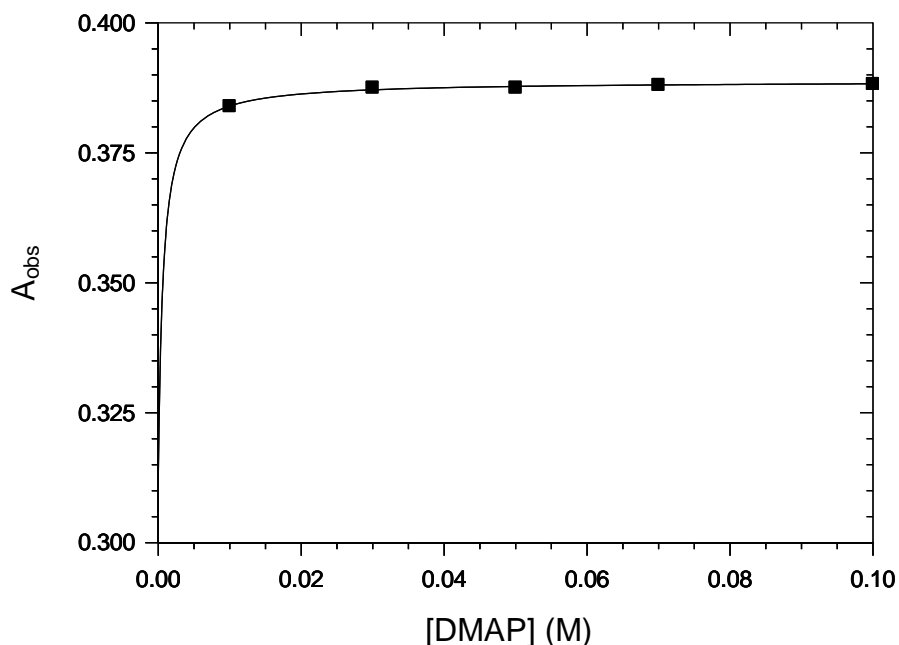
Figure 10.8: Thermodynamic determination of the equilibrium constant (K_1), for the methanol substitution reaction between *fac*-[Re(EM(naltol))(CO)$_3$(CH$_3$OH)] and DMAP in methanol as solvent from the UV/Vis spectral change data *vs* [DMAP] at 365 nm, 25.1 °C; [Re] = 7.58 x 10^{-4} M, [DMAP] = 1.0 x 10^{-2} − 1.0 x 10^{-1} M.

Table 10.3: Kinetic data for the reaction between *fac*-[Re(EM(naltol))(CO)$_3$(CH$_3$OH)] and DMAP in methanol as solvent at 25.1 °C; [Re] = 7.58 x 10^{-4} M and [DMAP] = 1.0 x 10^{-2} − 1.0 x 10^{-1} M, λ = 365 nm.

[DMAP] (M)	k_{obs} (s^{-1}) (average)	Rate/ Equilibrium constants	
0.01	0.137(3)	k_1 (M^{-1}s^{-1})	26.9(8)
0.03	0.67(2)	k_1 (M^{-1}s^{-1})^a	25.3(6)
0.05	1.26(3)	k_{-1} (s^{-1})	*ca.* 0
0.07	1.84(4)	K_1 (M^{-1})^b	>1000
0.10	2.53(5)	K_1 (M^{-1})^c	>1000

^{a}Second order rate constant determined by fixing the intercept at the origin. ^{b} $K_1 = k_1/k_{-1}$ Eq. 10.5, ^{c} Thermodynamically determined using Eq. 10.6.

10.6.3 Substitution reaction between *fac*-[Re(EM(naltol))(CO)₃(CH₃OH)] and imidazole

The spectral change for the methanol substitution reaction between *fac*-[Re(EM(naltol))(CO)$_3$(CH$_3$OH)] and imidazole in methanol as solvent is illustrated in Figure 10.9. The imidazole concentrations as entering ligand were varied between 1.0×10^{-2} and 1.0×10^{-1} M while the metal complex was kept constant at [Re] = 7.49×10^{-4} M. The reaction was monitored at 365 nm and 25.1 °C, while the k_{obs} *vs* [imidazole] data were fitted to Eq. 10.3. The graph of k_{obs} *vs* [imidazole] at 25.1 °C is depicted in Figure 10.10. The thermodynamic equilibrium constant (K_1) was determined by fitting the data to Eq. 10.6 and the plot of A_{obs} *vs* [imidazole] at 25.1 °C is shown in Figure 10.11. The rate constants were obtained from least-squares fits of the k_{obs} *vs* [imidazole] data and are reported in Table 10.4.
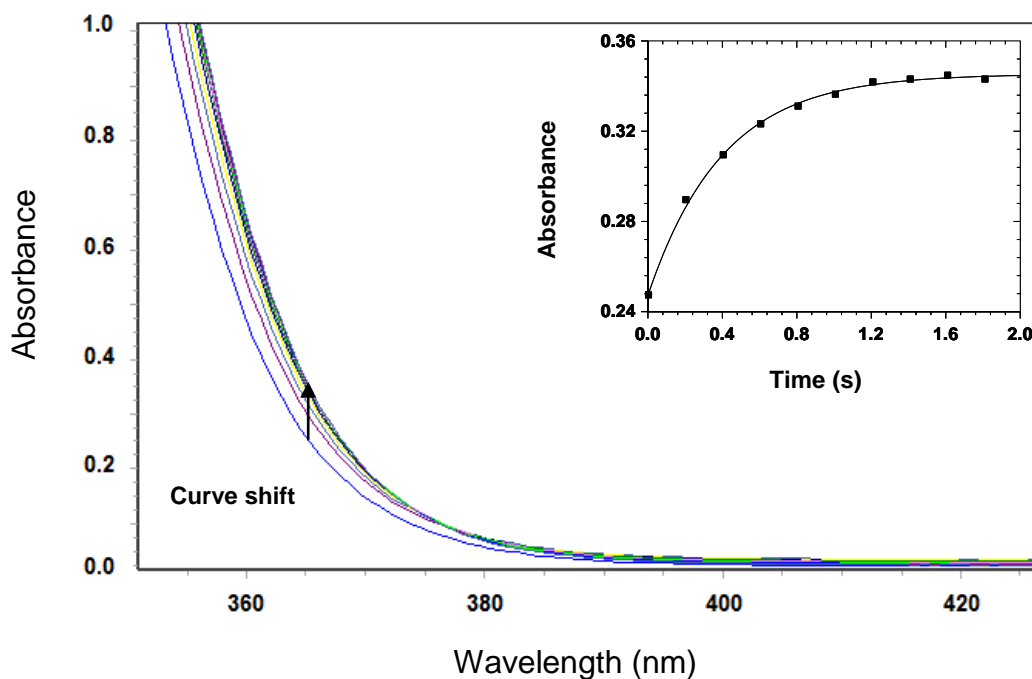
Figure 10.9: Characteristic UV/Vis spectra for the methanol substitution reaction between *fac*-[Re(EM(naltol))(CO)$_3$(CH$_3$OH)] and imidazole in methanol as solvent at 25.1 °C; [Re] = 7.49 x 10^{-4} M, [imidazole] = 1.0 x 10^{-1} M. The insert indicates the absorbance change *vs* time data at λ = 365 nm, Δt = 2.0 x 10^{-1} s. The line shows the least-squares fit to Equation 10.1 (k_{obs} = 2.11(4) s^{-1}).
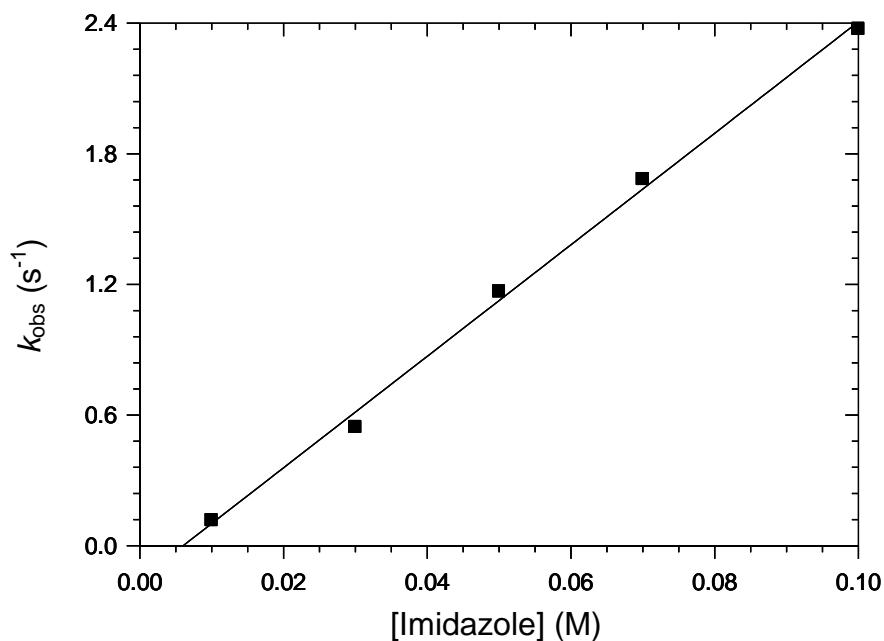
Figure 10.10: Plot of k_{obs} *vs* [imidazole] for the reaction between *fac*-[Re(EM(naltol))(CO)$_3$(CH$_3$OH)] and imidazole in methanol as solvent at 25.1 °C; [Re] = 7.49 x 10^{-4} M and [imidazole] = 1.0 x 10^{-2} − 1.0 x 10^{-1} M, λ = 365 nm.
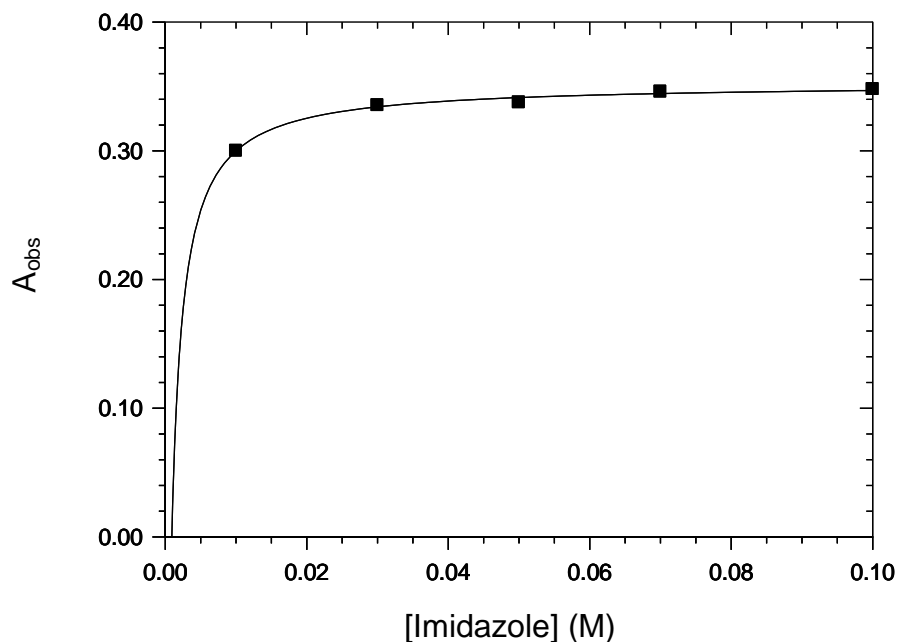
Figure 10.11: Thermodynamic determination of the equilibrium constant (K_1), for the methanol substitution reaction between *fac*-[Re(EM(naltol))(CO)$_3$(CH$_3$OH)] and imidazole in methanol as solvent from the UV/Vis spectral change data *vs* [imidazole] at 365 nm, 25.1 °C; [Re] = 7.49 x 10^{-4} M, [imidazole] = 1.0 x 10^{-2} − 1.0 x 10^{-1} M.

Table 10.4: Kinetic data for the reaction between *fac*-[Re(EM(naltol))(CO)$_3$(CH$_3$OH)] and imidazole in methanol as solvent at 25.1 °C; [Re] = 7.49 x 10^{-4} M and [imidazole] = 1.0 x 10^{-2} − 1.0 x 10^{-1} M, λ = 365 nm.

[Imidazole] (M)	k_{obs} (s^{-1}) (average)	Rate/ Equilibrium constants	
0.01	0.117(6)	k_1 (M^{-1}s^{-1})	25.6(8)
0.03	0.55(4)	k_1 (M^{-1}s^{-1})^a	23.4(8)
0.05	1.17(6)	k_{-1} (s^{-1})	*ca.* 0
0.07	1.68(6)	K_1 (M^{-1})^b	>1000
0.10	2.4(1)	K_1 (M^{-1})^c	>1000

^{a}Second order rate constant determined by fixing the intercept at the origin. ^{b} K_1 = k_1/k_{-1} Eq. 10.5, ^{c} Thermodynamically determined using Eq. 10.6.

10.6.4 Substitution reaction between *fac*-[Re(EM(naltol))(CO)$_3$(CH$_3$OH)] and 3-chloropyridine

The spectral change for the methanol substitution reaction between *fac*-[Re(EM(naltol))(CO)$_3$(CH$_3$OH)] and 3-chloropyridine in methanol as solvent is illustrated in Figure 10.12. The 3-chloropyridine concentrations as entering ligand were varied between 1.0 x 10^{-2} and 1.0 x 10^{-1} M while the metal complex was kept constant at [Re] = 7.58 x 10^{-4} M. The reaction was monitored at 380 nm and 25.2 °C and the k_{obs} *vs* [3-chloropyridine] data were fitted to Eq. 10.3. The graph of k_{obs} *vs* [3-chloropyridine] at 25.2 °C is depicted in Figure 10.13. The thermodynamic equilibrium constant (K_1) was determined by fitting the data to Eq. 10.6 and the plot of A_{obs} *vs* [3-chloropyridine] at 25.2 °C is shown in Figure 10.14. The rate constants were obtained from least-squares fits of the k_{obs} *vs* [3-chloropyridine] data and are reported in Table 10.5.
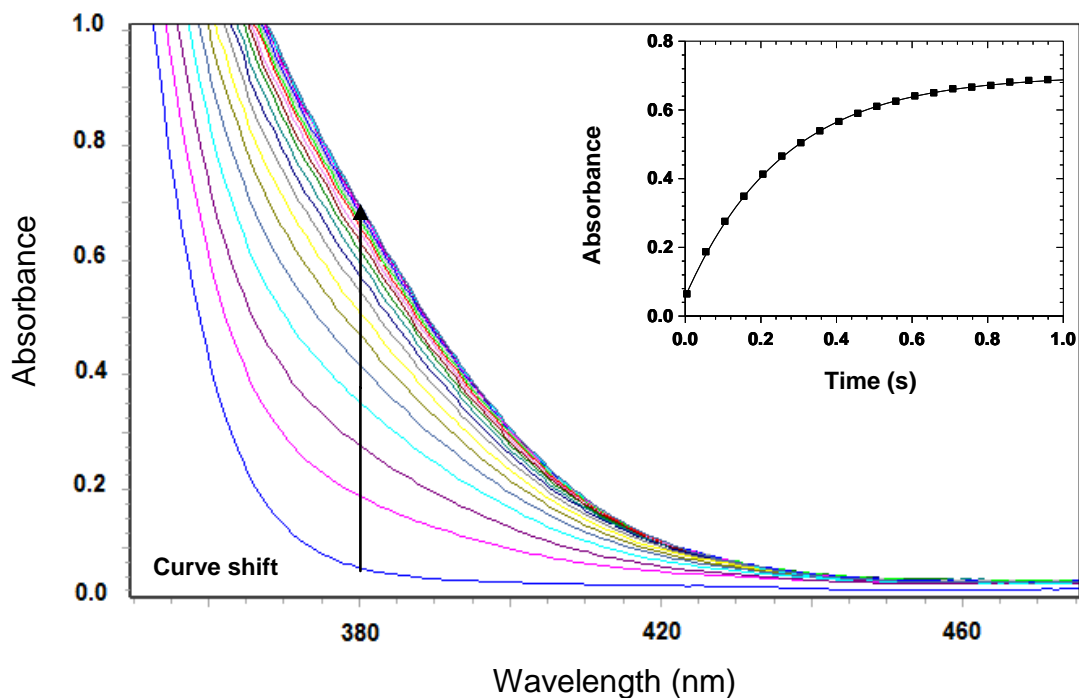
Figure 10.12: Characteristic UV/Vis spectra for the methanol substitution reaction between *fac*-
[Re(EM(naltol))(CO)$_3$(CH$_3$OH)] and 3-chloropyridine in methanol as solvent at 25.2 °C; [Re] = 7.58 x 10^{-4} M,
[3-chloropyridine] = 1.0 x 10^{-1} M. The insert indicates the absorbance change *vs* **time data at λ = 380 nm, Δt =**
5.0 x 10^{-2} s. The line shows the least-squares fit to Equation 10.1 (k_{obs} = 3.85(1) s^{-1}).
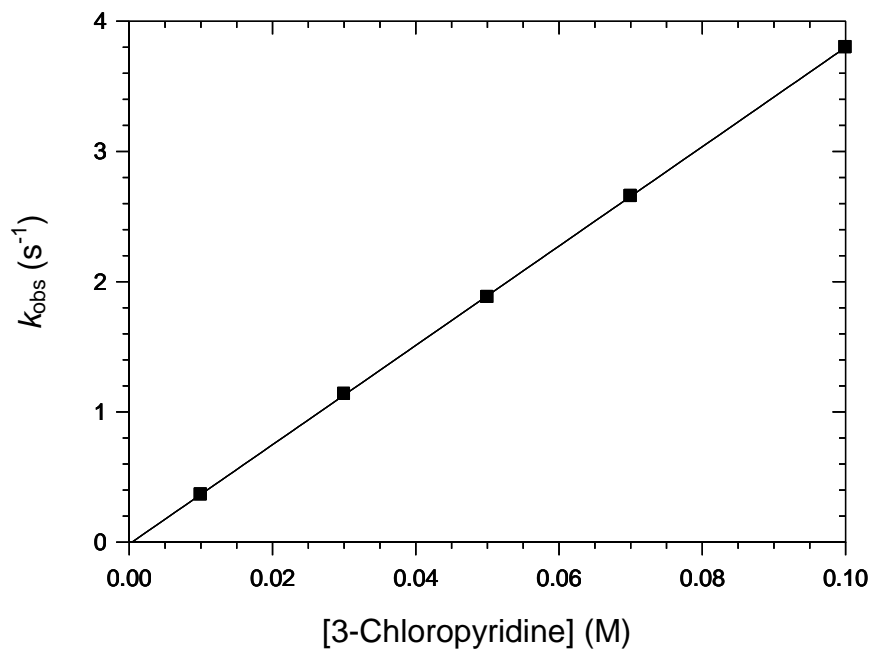
Figure 10.13 Plot of k_{obs} *vs* [3-chloropyridine] for the reaction between *fac*-**[Re(EM(naltol))(CO)$_3$(CH$_3$OH)]**
and 3-chloropyridine in methanol as solvent at 25.2 °C; [Re] = 7.58 x 10^{-4} M and [3-chloropyridine] = 1.0 x 10^{-2} − 1.0 x 10^{-1} M, λ = 380 nm.

206
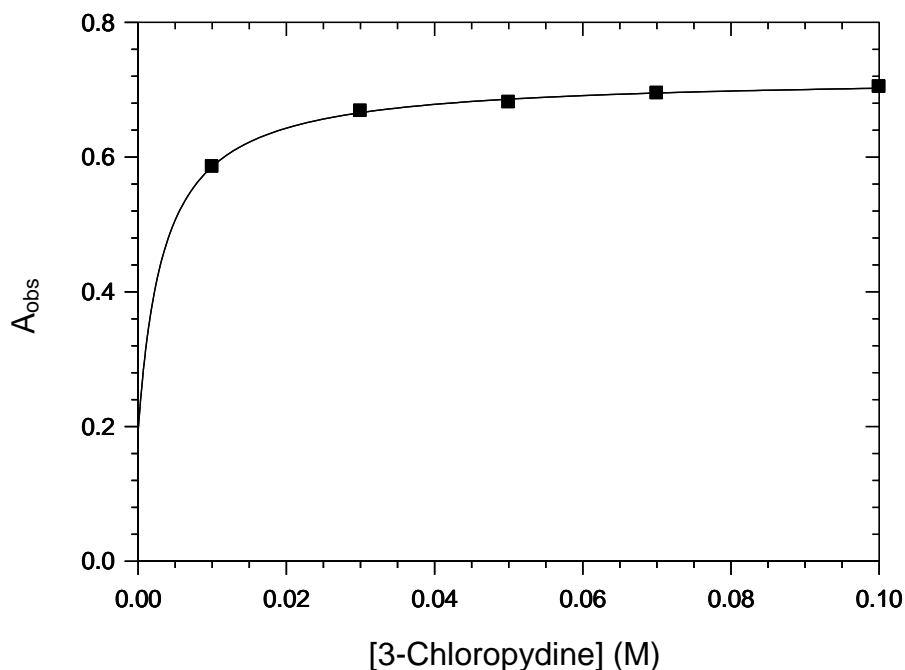
Figure 10.14: Thermodynamic determination of the equilibrium constant (K_1), for the methanol substitution reaction between fac-[Re(EM(naltol))(CO)$_3$(CH$_3$OH)] and 3-chloropyridine in methanol as solvent from the UV/Vis spectral change vs [3-chloropyridine] at 380 nm, 25.2 °C; [Re] = 7.58 x 10^{-4} M, [3-chloropyridine] = 1.0 x 10^{-2} − 1.0 x 10^{-1} M.

Table 10.5: Kinetic data for the reaction between fac-[Re(EM(naltol))(CO)$_3$(CH$_3$OH)] and 3-chloropyridine in methanol as solvent at 25.2 °C; [Re] = 7.58 x 10^{-4} M and [3-chloropyridine] = 1.0 x 10^{-2} − 1.0 x 10^{-1} M, λ = 380 nm.

[3-Chloropyridine] (M)	k_{obs} (s^{-1}) (average)	Rate/ Equilibrium constants	
0.01	0.366(4)	k_1 (M^{-1}s^{-1})	38.1(1)
0.03	1.14(1)	k_1 (M^{-1}s^{-1})^a	37.94(8)
0.05	1.88(1)	k_{-1} (s^{-1})	$ca.$ 0
0.07	2.66(2)	K_1 (M^{-1})^b	>1000
0.10	3.80(3)	K_1 (M^{-1})^c	>1000

^{a}Second order rate constant determined by fixing the intercept at the origin. ^{b} $K_1 = k_1/k_{-1}$ Eq. 10.5, ^{c} Thermodynamically determined using Eq. 10.6.

10.7 Substitution reaction between (3) dissolved in methanol and Pyridine

The spectral change for the methanol substitution reaction between *fac-*[Re(EM(naltol))(CO)$_3$(EM(naltol)H)] (**3**) dissolved in methanol and pyridine in methanol as solvent is illustrated in Figure 10.15. The pyridine concentrations as entering ligand were varied between 1.0 x 10^{-2} and 1.0 x 10^{-1} M while the metal complex was kept constant at [Re] = 7.82 x 10^{-4} M. The reaction was monitored at 365 nm and 25 °C, the k_{obs} *vs* [pyridine] data was fitted to Eq. 10.3. The graph of k_{obs} *vs* [pyridine] at 25 °C is depicted in Figure 10.16. The thermodynamic equilibrium constant (K_1) was determined by fitting the data to Eq. 10.6 and the plot of A_{obs} *vs* [pyridine] at 25 °C is shown in Figure 10.17. The rate constants were obtained from least-squares fits of the k_{obs} *vs* [pyridine] data and are reported in Table 10.6.
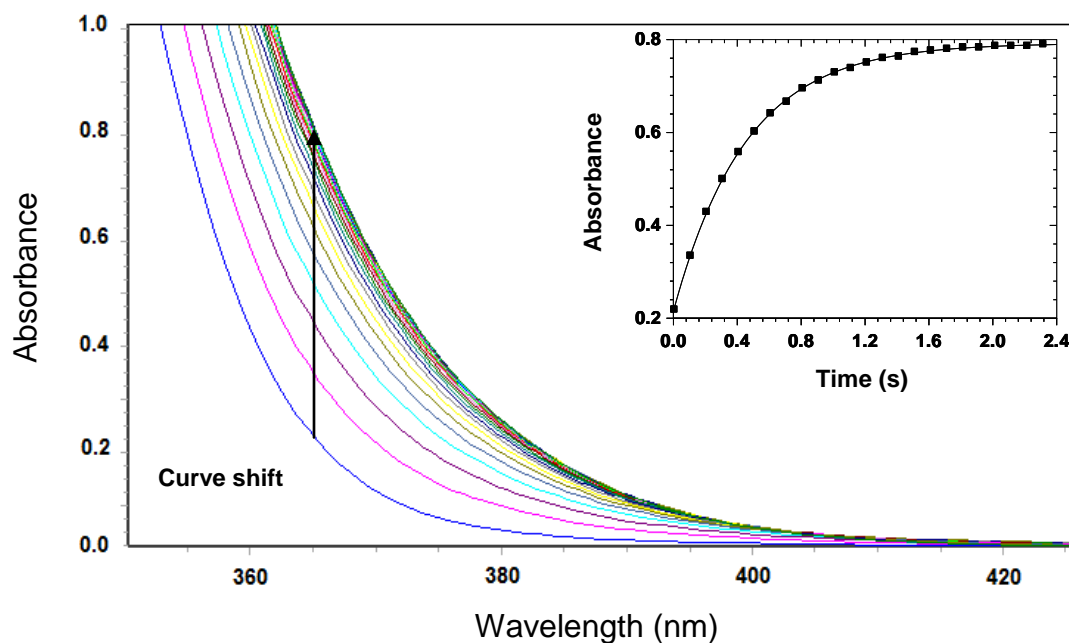
Figure 10.15: Characteristic UV/Vis spectra change for the methanol substitution reaction between *fac-*[Re(EM(naltol))(CO)$_3$(EM(naltol)H)] (3) dissolved in methanol and pyridine in methanol as solvent at 25 °C; [Re] = 7.82 x 10^{-4} M, [Py] = 1.0 x 10^{-1} M. The insert indicates the absorbance change *vs* time data at λ = 365 nm, Δt = 1.0 x 10^{-1} s. The line shows the least-squares fit to Equation 10.1 (k_{obs} = 2.18(1) s^{-1}).
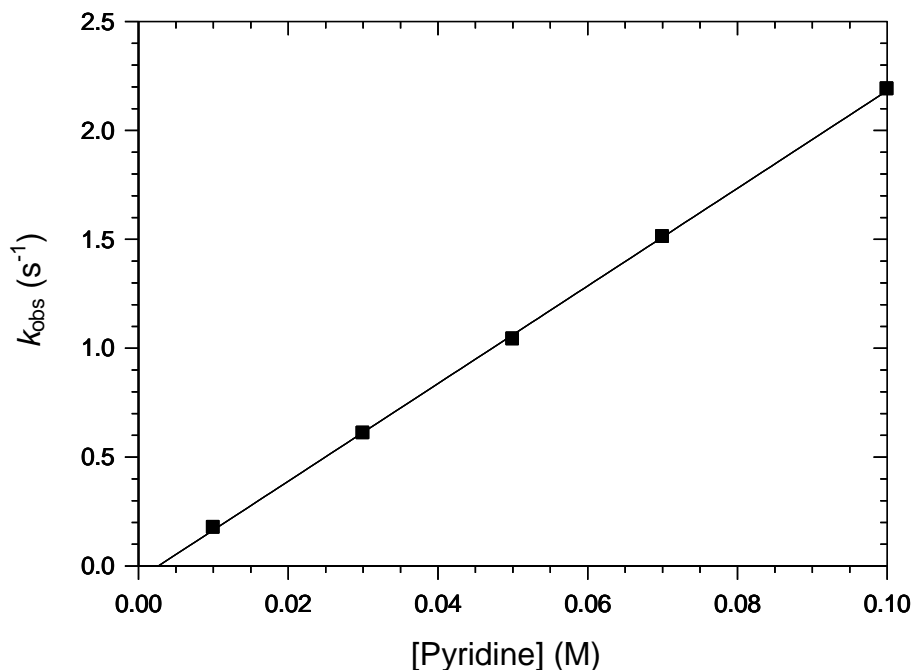
Figure 10.16: Plot of k_{obs} vs [Py] for the reaction between *fac*-**[Re(EM(naltol))(CO)$_3$(EM(naltol)H)] (3) dissolved in methanol and pyridine in methanol as solvent at 25 °C; [Re] = 7.82 x 10^{-4} M and [Py] = 1.0 x 10^{-2} − 1.0 x 10^{-1} M, λ = 365 nm.**
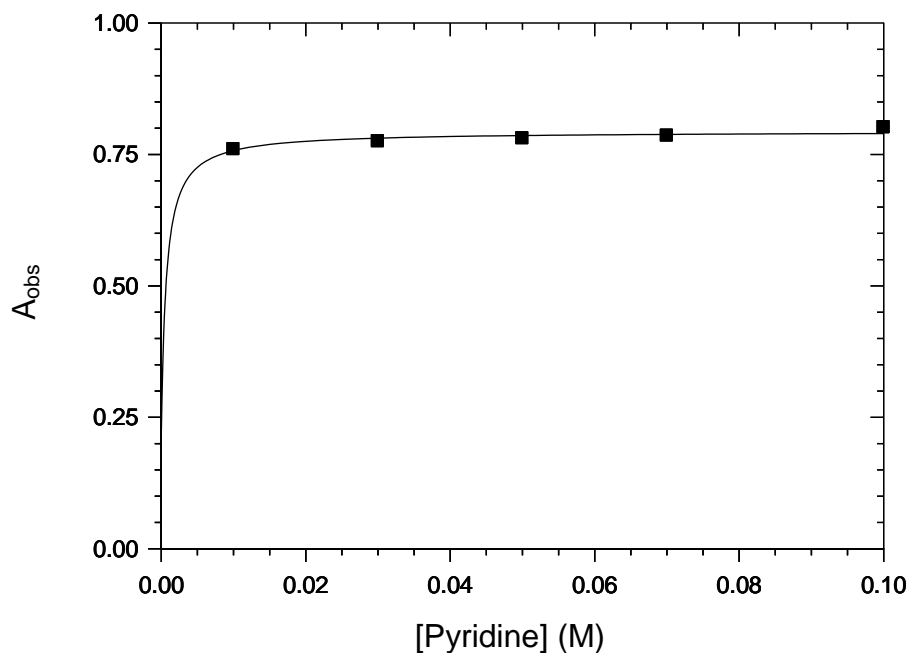
Figure 10.17: Thermodynamic determination of the equilibrium constant (K_1), for the methanol substitution reaction between *fac*-**[Re(EM(naltol))(CO)$_3$(EM(naltol)H)] (3) dissolved in methanol and pyridine in methanol as solvent from the UV/Vis spectral change** *vs* **[Py] data at 365 nm, 25 °C; [Re] = 7.82 x 10^{-4} M, [Py] = 1.0 x 10^{-2} − 1.0 x 10^{-1} M.**

Table 10.6: Kinetic data for the reaction between *fac*-[Re(EM(naltol))(CO)$_3$(EM(naltol)H)] (3) dissolved in methanol and pyridine in methanol as solvent at 25 °C; [Re] = 7.82 x 10^{-4} M and [Py] = 1.0 x 10^{-2} − 1.0 x 10^{-1} M, λ = 365 nm.

[Pyridine] (M)	k_{obs} (s^{-1}) (average)	Rate/ Equilibrium constants	
0.01	0.177(2)	k_1 (M^{-1}s^{-1})	22.4(2)
0.03	0.611(9)	k_1 (M^{-1}s^{-1})^a	21.6(3)
0.05	1.04(1)	k_{-1} (s^{-1})	*ca.* 0
0.07	1.51(2)	K_1 (M^{-1})^b	>1000
0.10	2.19(2)	K_1 (M^{-1})^c	>1000

^{a}Second order rate constant determined by fixing the intercept at the origin. ^{b} K_1 = k_1/k_{-1} Eq. 10.5, ^{c} Thermodynamically determined using Eq. 10.6.

Table 10.7: Summary of the kinetic data for the substitution reactions between *fac*-[Re(EM(naltol))(CO)$_3$(CH$_3$OH)] and various entering ligands in methanol as solvent at ~ 25 °C.

Monodentate Ligand	k_1 (M^{-1}s^{-1})	k_1 (M^{-1}s^{-1})^a	k_{-1} (s^{-1})	K (M^{-1})^c
3-Chloropyridine	38.1(1)	37.94(8)	−	>1000
Pyridine	30.7(1)	30.5(1)	−	>1000
DMAP	26.9(8)	25.3(6)	−	>1000
Imidazole	25.6(8)	23.4(8)	−	>1000

^{a}Second order rate constant determined by fixing the intercept at the origin. ^{c} Thermodynamically determined using Eq. 10.6.

10.8 Discussion

Two neutral rhenium(I) tricarbonyl complexes were selected for the substitution study: *fac*-[Re(EM(naltol))(CO)$_3$(CH$_3$OH)] and *fac*-[Re(EM(naltol))(CO)$_3$(EM(naltol)H)] (**3**). The methanol and the neutral mono-coordinated bidentate ligand EM(naltol)H coordinated in the axial position are both susceptible to substitution by monodentate ligands. An unanswered question is whether this substitution process occurs *via* a solvent pathway or direct substitution by the monodentate ligand, or both.

The solid state structure of the kinetic substitution product *fac*-[Re(EM(naltol))(CO)$_3$(Py)] is reported in Chapter 8 with various monodentate substitution products. These solid state structures (kinetic products) validate the formation of the substitution products. What still needs to be verified is whether the process is solvolytic in nature. This can be determined by comparing the kinetic substitution data of *fac*-[Re(EM(naltol))(CO)$_3$(CH$_3$OH)] and pyridine with that of *fac*-[Re(EM(naltol))(CO)$_3$(EM(naltol)H)] (**3**) dissolved in methanol and pyridine. The analysed data and the respective rate constants for the substitution reactions with different monodentate ligands are summarized in Table 10.7 and graphically illustrated in Figure 10.18.
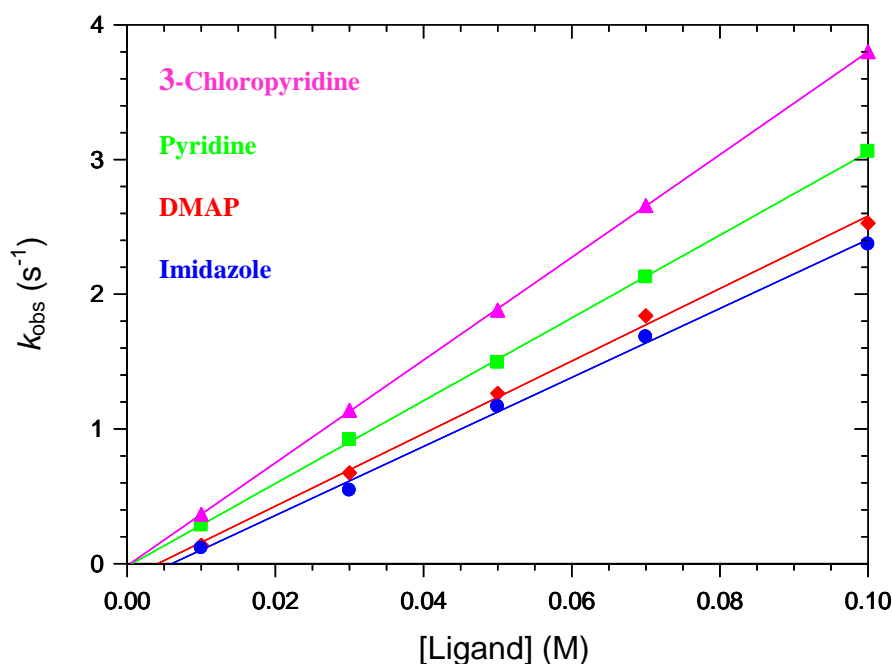
Figure 10.18: Plot of k_{obs} *vs* [ligand] for the reactions between *fac*-[Re(EM(naltol))(CO)$_3$(CH$_3$OH)] and various entering ligands at ~ 25 °C.

A comparison of the second order rate constants, k_1, in Table 10.7, of *fac*-[Re(EM(naltol))(CO)$_3$(CH$_3$OH)] with various monodentate nitrogen donor ligands indicates that the reaction rates increase in the following order: 3-chloropyridine > pyridine > DMAP > imidazole. Electron withdrawing groups on the pyridine ring make the pyridine ligand more acidic and less nucleophilic while electron donating groups will make the pyridine ligand more basic and more nucleophilic. One would then typically expect that the order of reactivity will be; DMAP > imidazole > pyridine > 3-chloropyridine based on their respective pK$_a$ values (9.8, 6.9,

5.23, 2.81). Based on the obtained results this is however not the case and appears to suggest that steric hindrance might be more prevalent.

An almost 30 % increase in k_1 is seen from pyridine (30.7(1) $M^{-1}s^{-1}$) to the chloro-substituted derivative (3-chloropyridine = 38.1(1) $M^{-1}s^{-1}$). The decrease in k_1 from pyridine to the dimethyl amino substituted pyridine (DMAP = 26.9(8) $M^{-1}s^{-1}$) is approximately 12 %. The second order rate constant also decreases from the reaction with pyridine compared to the reaction with imidazole (25.6(8) $M^{-1}s^{-1}$) by approximately 17 %. In spite of this change observed in the four entering ligands' data, the relatively small variation in second order rate constants is indicative of a D-activation since it is virtually *independent* of the entering ligand. This, in spite of the fact that the electron donating ability of the four ligands, as manifested in the pK_a values given above, is about *six orders-of-magnitude*.

The reverse rate constants were extremely small and difficult to obtain accurately and were roughly of the same order of magnitude. The equilibrium constants were very large in all the respective reactions and the numerical values were all above $> 1000\ M^{-1}$ in the cases were the determinations were successfully done. The small reverse rate constants and the large equilibrium values are both indicative of a favoured kinetic product and high stability of the resultant nitrogen substituted kinetic product. A reasonable agreement exists between the equilibrium constant (K_1) determined kinetically (1895(991) M^{-1}) and thermodynamically (1329(349) M^{-1}) with the slight difference accounted for within the relative error of measurement. The enthalpy of activation $\Delta H^{\ddagger} = 67(4)$ kJ mol^{-1} and the entropy of activation $\Delta S^{\ddagger} = 6(13)$ J K^{-1} mol^{-1} based on the pyridine temperature studies are indicative of a relatively high ordered system in the transition state of the substitution reaction. The small value of $\Delta S^{\ddagger}$ and the linear relationship between k_{obs} *vs* [pyridine] is, superficially considered, potentially indicative of an interchange mechanism. However, the virtual independence on entering ligand in spite of a very large variation in the Brønsted basicity [> 6 orders-of-magnitude] clearly points to a D-activation. These findings should be further investigated with high-pressure kinetics to unequivocally determine the reaction mechanism.

Similar work done by Brink with *fac*-[Re^I(N,O'-Bid)(CO)$_3$(CH$_3$OH)] (N,O'-Bid = N,O' bidentate ligand) with 3-chloropyridine, pyridine and DMAP typically showed the same order of succession which is; 3-chloropyridine, pyridine and DMAP.[20,34] The divergence in the monodentate k_{obs} *vs* [ligand] data between 3-chloropyridine and DMAP at approximately 0.8 M was 1.2240 s^{-1} in the study by Brink and 1.2659 s^{-1} at 0.1 M in this study but however the actual rate constant were a lot smaller in the study by Brink.[20,34]

A comparison of the methanol and EM(naltol)H substitution rates between *fac*-[Re(EM(naltol))(CO)$_3$(CH$_3$OH)] and *fac*-[Re(EM(naltol))(CO)$_3$(EM(naltol)H)] (**3**) respectively with pyridine as entering ligand is given in Table 10.8 and graphically illustrated in Figure 10.19.
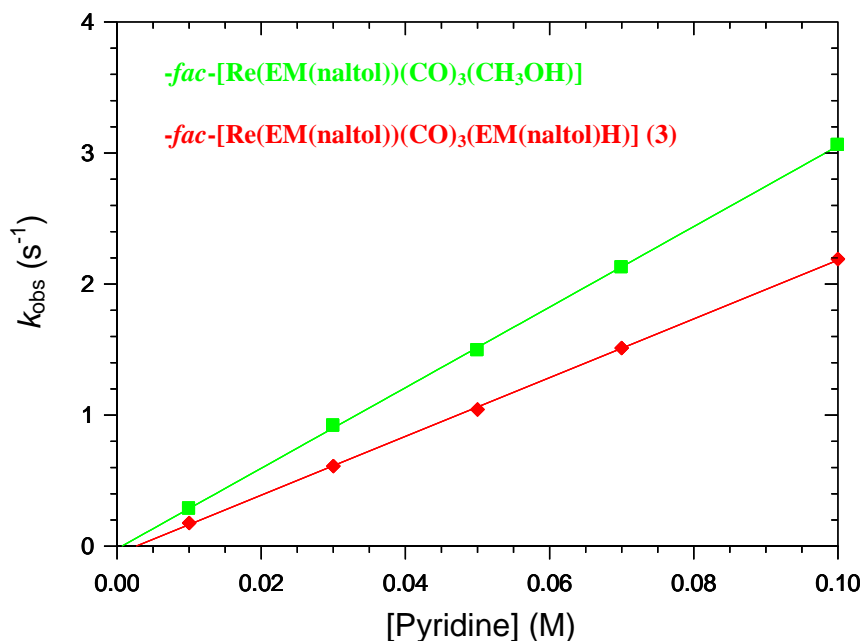
Figure 10.19: Plot of k_{obs} *vs* [Py] for the reactions between *fac*-[Re(EM(naltol))(CO)$_3$(CH$_3$OH)] and *fac*-[Re(EM(naltol))(CO)$_3$(EM(naltol)H)] dissolved in methanol with pyridine in methanol as solvent at ~ 25 °C.

---

[34] A. Brink, PhD Thesis, University of the Free State, **2011**.

Table 10.8: Summary of the rate constants for the substitution reactions of the two Re(I) tricarbonyl complexes dissolved in methanol and pyridine in methanol as solvent at ~ 25 °C.

Complexes	k_1 (M^{-1}s^{-1})	k_1 (M^{-1}s^{-1})^a	k_{-1} (s^{-1})	K_1 (M^{-1})^c
fac-[Re(EM(naltol))(CO)$_3$(CH$_3$OH)]	30.7(1)	30.5(1)	−	>1000
fac-[Re(EM(naltol))(CO)$_3$(EM(naltol)H)] (**3**)	22.4(2)	21.6(3)	−	>1000

^{a}Second order rate constant determined by fixing the intercept at the origin. ^{c} Thermodynamically determined using Eq. 10.6.

By comparing the second order rate constants (k_1) of these reactions at ~ 25 °C the *fac*-[Re(EM(naltol))(CO)$_3$(CH$_3$OH)] reacts faster compared to the *fac*-[Re(EM(naltol))(CO)$_3$(EM(naltol)H)] (**3**) complex. The second order rate constant for the reaction with the methanol coordinated complex is ~ 1.4 times larger than the reaction with *fac*-[Re(EM(naltol))(CO)$_3$(EM(naltol)H)] (**3**). This could be due to several reasons, from the ^{1}H and ^{13}C NMR solution studies carried out in CD$_3$OD in Chapter 3, Chapter 5 and Figure 10.1 it appears that (**3**) dissociates the monodentate coordinated ligand EM(naltol)H in solution. The concentration of (**3**) was kept constant at [Re] = 7.82 x 10^{-4} M meaning in solution the concentration of the dissociated EM(naltol)H is approximately 7.82 x 10^{-4} M. It is quite possible that perhaps the EM(naltol)H ligand is more competitive than the methanol molecule is (more nucleophilic) and interferes with the substitution reaction and hence slows this process by ~ 27 % as it is clear from NMR studies that the free ligand is present in solution. The fact that these rate constants are approximately the same strongly suggests that both the substitution reactions proceed by the same intermediate *fac*-[Re(EM(naltol))(CO)$_3$(CH$_3$OH)]. In the case of the EM(naltol)H complex, the decrease in rate compared to the methanol complex roughly approximates the change of the equilibrium, see Fig. 10.1, 10.19 and Table 10.8 . This means that the process is solvolytic in nature and it is thus a methanol substitution process in both cases. The relative decrease in rate between (**16**) and (**3**) is thus assumed to be due to the trapping of the metal centre by the EM(naltol)H, and the slow solvolysis thereof decreases the rate of substitution by the entering pyridine nucleophile by some 10-20 %.

The slightly smaller rate constants observed in (**3**) might be due to some steric hindrance in (**3**), and that *fac*-[Re(EM(naltol))(CO)$_3$(EM(naltol)H)] is actually more stable and the monodentate coordinated bidentate ligand is a better nucleophile compared to the coordinated methanol ligand, which can be seen as more labile. However, there is not enough evidence to support this argument and both the NMR and kinetic results support the solvolytic methanol substitution process which proceeds by *fac*-[Re(EM(naltol))(CO)$_3$(CH$_3$OH)].

The k_1 values for these reactions are generally significantly larger than the k_{-1} values which indicates that the products are thermodynamically favoured and stable (see Table 10.8). The equilibrium constants of the two complexes were similar and > 1000 M^{-1} indicating favourable product formation consistent with the small reverse rate constant values. Similar studies with O,O'-bidentate ligands coordinated to the rhenium(I) centre with pyridine as entering ligand have also been reported (see Table 10.9).

Table 10.9: Summary of the kinetic data of similar substitution studies done on the methanol substitution reactions between Re(I) tricarbonyl O,O'-bidentate complexes with pyridine at ~ 25 °C.

Equilibrium /rate constants	[Re(Trop)][a]	[Re(Isa)][b]	[Re(TropBr$_3$)][c]	[Re(Flav)][c]	[Re(EM)][d]	[Re(EM)(EMH)][e]
	Py	**Py**	**Py**	**Py**		
k_1 (M^{-1}s^{-1})	0.2632(1)	0.0177(2)	0.0203(7)	1.38(8)	30.7(1)	22.4(2)
k_{-1} (s^{-1})	7(1) x 10^{-5}	2.44(5) x 10^{-3}	1.6(2) x 10^{-3}	0.3(1) x 10^{-3}	–	–
K (M^{-1})	3760(537)	7.3(2)	12(2)	4.6(1)x10^3	>1000	>1000

[a] Schutte *et al.*[22] [b] Schutte.[35] [c] Schutte *et al.*[23] [d] *fac*-[Re(EM(naltol))(CO)$_3$(CH$_3$OH)]. [e] *fac*-[Re(EM(naltol))(CO)$_3$(EM(naltol)H)] (**2**). [Re(Trop)] = *fac*-[Re(Trop)(CO)$_3$(MeOH)] where TropH = Tropolone, [Re(Isa)] = *fac*-[Re(Isa)(CO)$_3$(MeOH)] where IsaH = Isatin, [Re(TropBr$_3$)] = *fac*-[Re(TropBr$_3$)(CO)$_3$(MeOH)] where TropBr$_3$H = tribromotropolone and [Re(Flav)] = *fac*-[Re(Flav)(CO)$_3$(MeOH)] where FlavH = 3-hydroxyflavone.

[35] M. Schutte, PhD Thesis, University of the Free State, **2011**.

A comparison between the studies listed in Table 10.9 indicates that the reactions reported in this study are much faster than those reactions carried out with the Re(I) tricarbonyl complexes with tropolone, isatin, tribromotropolone and flavone as bidentate ligand systems. The reactions with *fac*-[Re(EM(naltol))(CO)$_3$(CH$_3$OH)] are ~ 29 times faster than the *fac*-[Re(Flav)(CO)$_3$(MeOH)] reactions reported by Schutte.[35]

In fact, the ligands reported here are the most activating of all bidentate ligands studied by our group to date, which is an interesting observation and it would not have been anticipated at the beginning of this study. It will be further explored in future.

10.9 Conclusion

The kinetic data of the substitution reactions of the two complexes *fac*-[Re(EM(naltol))(CO)$_3$(H$_2$O)] (**16**) and *fac*-[Re(EM(naltol))(CO)$_3$(EM(naltol)H)] (**3**) dissolved in methanol with various entering ligands in methanol as solvent were reported and discussed in this chapter. The results obtained from NMR and kinetic studies indicate that there is a probable D-activated methanol substitution which is operative. The reported second order rate constants (k_1) show a virtual independence on the steric and electronic influences from the entering ligands. The calculated entropy of activation ($\Delta S^{\ddagger}$) value might point towards an *I*-type mechanism. However, the overall six order-of-magnitude difference in the electron donating ability (as manifested by the pK$_a$ values of the entering ligands) indicates a virtual independence on the electron donating ability of the entering ligand, and thus a *D*-activation.

Further studies will be conducted in future, also including High-Pressure work, in an attempt to more accurately elucidate the mechanism. However, with the evidence in hand it is, and indicated above, concluded that the substitution in the rhenium complexes reported herein proceeds *via* a highly activated mode, and a *D*-activation.

These results also indicate that these 3-hydroxypyridinone chelators generally have a stronger activation effect on the rhenium metal centre compared to the O,O'-Bid complexes reported by Schutte *et al*. and the reaction rates are significantly larger.[23,24,**Error! Bookmark not defined.**] The nature of this contribution is quite unique and will contribute significantly to future kinetic investigations of Re(I) tricarbonyl complexes as it substantiates the notion of a D-activation.

11 Crystallographic Evaluation of the Solid State Properties of the Different complexes

11.1 Introduction

A range of O,O'-bidentate ligands with a small steric influence (five membered metallocycle; based on pyrones and pyridinone analogues) were systematically synthesized by imparting different electronic properties to the basic ligand backbone. These ligands were then coordinated to an array of metals to form the corresponding complexes. These ligands were explored in three broad metal types: *(i)* Early Transition Metals; for the potential beneficiation of hafnium and zirconium, *(ii)* Middle Transition Metals; for the modelling of potential radiopharmaceuticals from the non-radioactive rhenium metal for possible theranostic applications based on the radioactive isotopes ^{99m}Tc, $^{186/188}$Re and ^{105}Rh modalities with the radioactive ^{89}Zr compounds also having potential PET applications; *(iii)* Platinum Group Metals; for the evaluation of rhodium(I) phosphine complexes of these ligand systems in homogeneous catalysis.

The functionalization of the bidentate ligands was such that different steric and electronic properties could be introduced to the metal centre to study their effects in the solid- as well as in the solution state. The systemic divergence in steric and electronic properties was envisaged to have influences that could be exploited in the three respective domains of this research. In this chapter, the information obtained from the solid state results is presented and correlations, if any, will be discussed. The structures of the different complexes studied are illustrated in Figure 11.1.
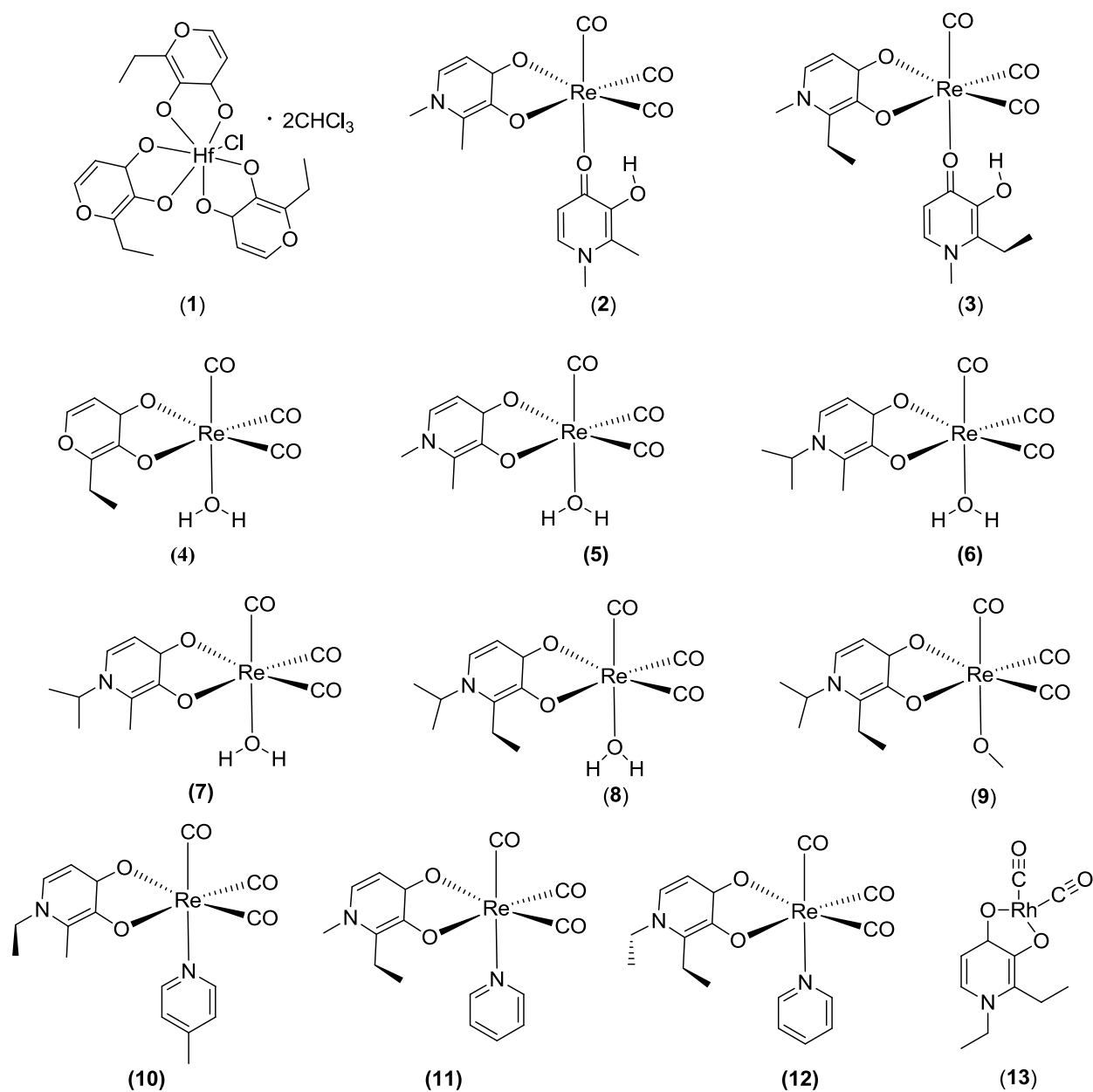
Figure 11.1: An illustration of the thirteen crystal structures compared in this chapter with different metal centers and chelating systems.

11.2 Discussion

In this section the crystal structures (**1**) to (**13**) will serve as representative structures in all the domains researched in this thesis e.g. as models for beneficiation, radiopharmaceuticals and homogeneous catalysis. This discussion is therefore to briefly evaluate and correlate the solid state influence of these ligand systems in the different domains. The hafnium structure (**1**) will serve as a representative 'snap-shot' structure for all the synthetic work done on Hf and Zr, as will the rhodium structure (**13**) represent a similar brief result on the synthetic work done on rhodium. The rhenium structures (**2**) to (**12**) which encompasses the bulk of the efforts in this PhD study, will represent all the synthetic work done on rhenium. Selected bond distances and bond angles of (**1**) to (**13**) are summarized Table 11.1 and Table 11.2.

Table 11.1: Selected bond distances and angles of complexes (1) – (7).

					Complexes			
No.	**(1)**	**(2)**	**(3)**	**(4)**	**(5)** A	B	**(6)**	**(7)**
M−O (M = Hf/ Zr /Re /Rh) Å								
M−O	2.063(4)	2.140(2)	2.124(2)	2.126(9)	2.102(14)	2.146(14)	2.1316(17)	2.124(2)
M−O	2.084(4)	2.1316(19)	2.141(2)	2.154(9)	2.215(12)	2.085(11)	2.1318(15)	2.142(2)
M−O	2.084(5)	2.168(2)	2.174(2)	2.164(9)	2.150(13)	2.190(12)	2.190(2)	2.191(2)
M−O	2.223(4)	-	-	-	-	-	-	-
M−O	2.234(5)	-	-	-	-	-	-	-
M−O	2.237(5)	-	-	-	-	-	-	-
M−C	-	1.901(3)	1.885(3)	1.869(2)	1.919(19)	1.873(13)	1.879(3)	1.888(4)
M−C	-	1.905(3)	1.900(3)	1.896(14)	1.929(12)	1.877(18)	1.907(2)	1.908(4)
M−C	-	1.901(3)	1.911(3)	1.908(14)	1.928(15)	1.88(2)	1.908(3)	1.912(4)
M−N	-	-	-	-	-	-	-	-
M−Cl	2.463(2)	-	-	-	-	-	-	-
O-M-O (M = Hf/ Zr/ Re/ Rh) ˚								
O-M-O	74.8(2)	77.56(7)	77.45(7)	77.245 (5)	76.20(2)	78.6(4)	77.413(15)	77.147(6)
O-M-O	72.9(2)	-	-	-	-	-	-	-
O-M-O	72.7(2)	-	-	-	-	-	-	-
O-M-O	-	-	-	-	-	-	-	-
C(21)-M-O(1B)/N(11)	-	172.49(2)	177.85(2)	173.1(5)	174.5(7)	174.5(6)	174.16(8)	175.16(13)
O(2A)-M-Cl	167.1(1)	-	-	-	-	-	-	-

Table 11.2: Selected bond distances and angles of complexes (8) – (13).

No.	(8)	(9)	(10)	(11)	(12)	(13)
	Complexes					
	(8)	(9)	(10)	(11)	(12)	(13)
M−O (M = Hf/ Zr /Re /Rh) Å						
M−O	2.131(3)	2.1141(19)	2.121(4)	2.142(4)	2.1448(17)	2.033(1)
M−O	2.139(3)	2.148(2)	2.116(3)	2.129(4)	2.1260(16)	2.037(2)
M−O	2.203(3)	2.200(2)	2.235(4)	2.207(5)	2.206(2)	-
M−O	-	-	-	-	-	-
M−O	-	-	-	-	-	-
M−O	-	-	-	-	-	-
M−C	1.895(5)	1.895(3)	1.915(5)	1.926(6)	1.923(3)	1.841(2)
M−C	1.909(4)	1.902(3)	1.908(5)	1.903(6)	1.909(2)	1.843(2)
M−C	1.909(4)	1.922(3)	1.894(5)	1.905(6)	1.896(3)	-
M−N	-	-	-	-	-	-
M−Cl	-	-	-	-	-	-
O-M-O (M = Hf/ Zr/ Re/ Rh) °						
O-M-O	78.07(10)	77.57(2)	78.222(11)	77.283(11)	77.092(2)	82.23(5)
O-M-O	-	-	-	-	-	-
O-M-O	-	-	-	-	-	-
O-M-O	-	-	-	-	-	-
C(21)-M-O(1B)/N(11)	175.62(2)	175.62(2)	179.32(17)	176.9(2)	178.64(9)	-
O(2A)-M-Cl	-	-	-	-	-	-

The Hf(IV) and Zr(IV) metal centres are both d^0 metal centres which can form eight coordination bonds with chelators. The preferred geometry of these compounds appears to either be square-antiprismatic or dodecahedral coordination which is normally *tetrakis* in nature.[1-8] However (**1**) is seven-coordinate exhibiting a distorted pentagonal bipyramidal coordination geometry and is a chlorido tris-(pyrone) structure.

[1] A. Tissier, J. Laugier, P. Boyer, *Acta Cryst*., **1977**, *B33*, 392.

[2] A. R. Davis, F. W. B. Eistein, *Acta Cryst*., **1978**, *B34*, 2110.

[3] C. H. Saldarriaga-Molina, A. Clearfield, I. Bernal, *Inorg. Chem*., **1974**, *13*, 2880.

[4] M. F. Lappert, P. I. Riley, P. I. W. Yarrow, J. L. Atwood, W. E. Hunter, M. J. Zaworotko, *J. Chem. Soc., Dalton Trans.* **1981**,814.

[5] M. Steyn, H. G. Visser, A. Roodt, *Z. Kristallogr. - New Cryst. Struct. 228,* **2013**, *3*, 413.

[6] M. Steyn, H. G. Visser, A. Roodt, *Z. Kristallogr. - New Cryst. Struct. 229*, **2014**, *1*, 67.

[7] M. Steyn, H. G. Visser, A. Roodt, *ActaCryst.* **2012**, *E68,* m1344.

[8] J. A. Viljoen, H. G. Visser, A. Roodt, M. Steyn, *Acta Cryst.* **2009**, *E65,* m1367.

The rhenium(I) metal centre, on the other hand, is a d^6 species which can form six coordination bonds with chelators. The preferred geometry of these tricarbonyl compounds is distorted octahedral coordination geometry, which is consistent with all the rhenium structures reported in this thesis (**2**) to (**12**).[9-11]

Finally, the rhodium(I) metal centre is a d^8 species which can form four coordination bonds with chelators. The preferred geometry in these compounds is square planar coordination geometry, which is consistent with the rhodium structure reported in this thesis (**13**).[12-18]

There are two types of M−O bond distances in the hafnium structure (**1**), both from the bidentate coordinated ligand: one approximately 2.1 Å and the second ~ 2.2 Å. The rhenium complexes on the other hand have three types of M−O bond distances two from the bidentate coordinated ligand and one from the monodentate oxygen coordinated ligand (H_2O or CH_3OH), the former approximately 2.1 Å and the latter slightly longer and approximately 2.2 Å. The rhodium complex has two types of M−O bond distances both from the bidentate coordinated ligand and are approximately 2.0 Å. They are shorter than both types of M−O bond distances found in the hafnium (**1**) and rhenium structures (**1**) – (**12**).

The hafnium structure does not have any M−C bonds while the rhenium complexes all have three facial M−C (carbonyl) bonds and all these M−C bond distances are approximately 1.9 Å. The Re−C(21) bond distances are slightly shorter in some cases depending on the *trans* influence of the monodentate coordinated ligand. The rhodium structure has only one type of M−C bond,

[9] M. Schutte, A. Roodt, H. G. Visser, *Inorg. Chem.*, **2012**, *51*, 11996.
[10] M. Schutte, G. Kemp, H. G. Visser, A. Roodt, *Inorg. Chem.*, **2011**, *50*, 12486.
[11] M. Schutte, H. G. Visser, A. Roodt, Acta Cryst., **2008**, *E64*, m1610.
[12] R. Lang, A. Schörwerth, K. Polborn, W. Ponikwar, W. Beck, T. Severin, K. Severin, *Z. Anorg. Allg. Chem.*, **1999**,
[13] G. Steyl, G. J. Kruger, A. Roodt, *Acta Cryst.*, **2004**, *C60*, m473.
[14] T. N. Hill, G. Steyl, *Acta Cryst.*, **2008**, *E64*, m1580.
[15] G. Steyl, *Polyhedron*, **2007**, *26*, 5324.
[16] G. Steyl, *Acta Cryst.*, **2007**, *E63*, m23.
[17] Janes, E. Moore, *Metal-Ligand Bonding*, The Open University, Bath Press, Bath, United Kingdom, **2004**, 31.
[18] G. Steyl, A. Roodt, *Acta Cryst.*, **2004**, *C60*, m324.

the carbonyl bonds and they are both approximately 1.8 Å which is slightly shorter compared to the Re−C (carbonyl) bond distances in structures (**2**) – (**12**). This indicates stronger back bonding by the carbonyl groups to the rhodium metal centre in these rhodium complexes. This is consistent with the stretching frequencies which resonate at higher wavenumbers (see Table 3.1) compared to those of the corresponding rhenium complexes.

There are three different O-M-O bite angles in the hafnium structure; one approximately 75 ° and two approximately 73 °. There is only one O-M-O bite angle in all the rhenium structures which ranges between 77 ° and 78 ° which is significantly larger than all the O-M-O bite angles found in the hafnium structure. There is only one O-M-O bite angle in the rhodium structure which is 82 ° which is the largest in the series between the three sets of metal groups investigated. Since the same ligand (EE(naltol)) is coordinated in (**12**) with an octahedral coordination geometry and the bite angle there is 77 °, it is clear that coordination geometry influences the bite angle. The vertical axis through the pentagonal bipyramid O(2A)-M-Cl in the hafnium structure (**1**) and C(21)-M-O(1B)/N(11) in the octahedral rhenium structures (**2**) – (**12**) is distorted from the ideal 180 °, with (**10**) being the most linear at 179 ° and (**1**) the least linear at 167 °.

11.3 Conclusion

The M−O bond distances in the hafnium (**1**) structure and the rhenium structures (**2**) – (**12**) range between 2.1 Å and 2.2 Å while the rhodium structure is approximately 2.0 Å. The rhodium structure has M−C bond distances of approximately 1.8 Å while the rhenium structures have M−C bond distances of approximately 1.9 Å which shows that the back bonding to the metal centre is significantly stronger in the rhodium complex (**13**) compared to the rhenium structures (**2**) – (**12**). The O-M-O bite angle is larger in the rhodium structure (**13**) at 82 °, followed by the rhenium structures (**2**) – (**12**) ranging at 77 ° and 78 ° and the hafnium structure at ~ 72 ° and ~ 74 °. This is possibly due to steric demands in the different coordination geometries and the different coordination numbers of the different metal centres *i.e.* four, six and seven respectively.

The vertical axis through the coordination polyhedra are all distorted with (**10**) being the most linear and (**1**) the least linear.

The overarching conclusion form this summary of solid-state structures is that these pyrone/ pyridinone ligands are very good ligand systems for the middle transition metal, Re(I), when available and utilised as the *fac*-[Re^I(CO)$_3$]$^+$ synthon. They can also be explored for early and late transition metals, but some modifications to the ligands themselves, or in the synthetic procedures and related techniques employed, will have to be considered.

12 Evaluation of Study

12.1 Introduction

The main objective of this study was to successfully synthesize and characterize 3-hydroxypyridinones from the two commercially available 3-hydroxypyrones (maltol and ethyl maltol) and apply them as ligand systems across three groups of transition metals. In total six 3-hydroxypyridinones were successfully synthesized and characterized and the yields were all relatively good and above 70 % except for EI(naltol)H which was approximately 40 %. In total two 3-hydroxypyrone ligands and six 3-hydroxypyridinones ligands were used as two distinct but similar chelator systems in this study (thus eight ligands).

The second step was to evaluate the coordination of these eight chelators on early, middle and platinum group metals and to evaluate the corresponding complexes in the respective fields of the metal centres and in the context of the outlined specific objectives. The synthesis and characterization was a success with 16 novel complexes obtained from the zirconium and hafnium work. Only [Zr(E(matlol))$_4$] and [Hf(matlol)$_4$] were insoluble and could not be characterized by NMR however the samples were uniform in composition indicating high purity. The yields of these complexes were quite high, ranging between approximately 60 % and 100 %. All these complexes were very stable but difficult to crystallize in many solvents (almost all crystallization processes resulted in the precipitation of the compounds). Only one crystal structure was obtained in this domain, which was [Hf(E(maltol))$_3$Cl]·2CHCl$_3$ (**1**) the remaining data collections were either of poor quality or could not be solved.

The rhenium work was also a success with 17 novel *fac*-[Re^I(O,O'-bid)(CO)$_3$(Y)] complexes reported in this thesis (O,O'-bid = O,O'-bidentate ligand and Y = monodentate ligand). Only *fac*-[Re(maltol)(CO)$_3$(H$_2$O)] was not successfully isolated and characterized, upon solvent removal

in vacuo a black mass which could not be purified was obtained indicating instability of this particular aqua complex. However the corresponding bromido complex was successfully obtained and characterized. Although three bromido complexes are reported in this section no crystal structures were obtained for these. However, two very novel and unexpected crystal structures of the bis-complexes are reported in Chapter 5. These bis-complexes were obtained from the attempted synthesis of the corresponding bromido complexes in each case (five of these complexes are reported in Chapter 3). In total 11 crystal structures of the form *fac*-[Re^I(O,O'-bid)(CO)$_3$(Y)] are reported in this thesis (**2**)-(**12**). The remaining data collections were either of poor quality or could not be solved (Chapters 5 to 8). The yields in this section were also fairly good and ranged between approximately 40 % and 90 %. All these complexes were relatively stable with no decomposition noted.

The rhodium work was also a success with 6 novel [Rh^I(O,O'-bid)(CO)$_2$] complexes reported in this thesis (O,O'-bid = O,O'-bidentate ligand). Only [Rh^I(EI(naltol))(CO)$_2$] was not successfully isolated and characterized as this complex was water soluble and barely precipitated. Upon solvent removal *in vacuo* this compound had decomposed to a dark brown crystalline material. The reflections were not good enough for X-ray diffraction, which indicated the instability of this specific dicarbonyl complex. The attempted synthesis of the respective monocarbonyl phosphines were all unsuccessful, in most cases resulting in the formation of the Vaska's complex (*trans*-[RhCO(PPh$_3$)$_2$Cl]). However, one crystal structure of [Rh^I(EE(naltol))(CO)$_2$] was indeed obtained and reported in Chapter 9. Although these dicarbonyl complexes are fairly soluble in most solvents the crystal quality isolated therefrom was not good enough as obtained from most solvents and hence most structures cannot be successfully reported at this point in time. The yields in this section were fairly modest and ranged between approximately 30 % and 80 %. All these complexes were relatively stable with no decomposition noted besides that of [Rh^I(EI(naltol))(CO)$_2$].

12.2 Crystallographic Analysis

Three-dimensional structural characterization of 13 novel complexes of hafnium(IV), rhenium(I) and rhodium(I) pyrone and pyridinone based complexes have been reported and discussed in detail in Chapters 4 to 9.

The hafnium structure which was representative of the work done on hafnium and zirconium revealed that these complexes could possibly all have a pentagonal bipyramidal coordination geometry instead of the popular square antiprismatic coordination geometry.[1-4] The rhenium and rhodium work showed octahedral and square planar coordination geometries respectively, which is consistent with similar work in literature on these metal centres.[5-15]

Significant insights into crystal lattice packing and stabilization, bond lengths, coordination modes and ligand bite angles between early, middle and late transition metals were evaluated and reported on these ligand systems. This was a remarkable feets, to be able to display the above mentioned with two ligand systems as ideally hard chelators coordinate hard metals only and the same is true for soft chelators and soft metals.

A few milestones in the rhenium work include:

[1] M. Steyn, H. G. Visser, A. Roodt, *Z. Kristallogr. - New Cryst. Struct. 228,* **2013**, *3*, 413.
[2] M. Steyn, H. G. Visser, A. Roodt, *Z. Kristallogr. - New Cryst. Struct. 229*, **2014**, *1*, 67.
[3] M. Steyn, H. G. Visser, A. Roodt, *ActaCryst.* **2012**, *E68,* m1344.
[4] J. A. Viljoen, H. G. Visser, A. Roodt, M. Steyn, *Acta Cryst.* **2009**, *E65,* m1367.
[5] M. Schutte, A. Roodt, H. G. Visser, *Inorg. Chem.*, **2012**, *51*, 11996.
[6] M. Schutte, G. Kemp, H. G. Visser, A. Roodt, *Inorg. Chem.*, **2011**, *50*, 12486.
[7] M. Schutte, H. G. Visser, A. Roodt, Acta Cryst., **2008**, *E64*, m1610.
[8] M. Schutte, A. Roodt, H. G. Visser, *Inorg. Chem.*, **2012**, *51*, 11996.
[9] M. Schutte, PhD Thesis, University of the Free State, **2011**.
[10] 10 R. Lang, A. Schörwerth, K. Polborn, W. Ponikwar, W. Beck, T. Severin, K. Severin, *Z. Anorg. Allg. Chem.*, **1999**, *625*, 1384.
[11] G. Steyl, G. J. Kruger, A. Roodt, *Acta Cryst.*, **2004**, *C60*, m473.
[12] T. N. Hill, G. Steyl, *Acta Cryst.*, **2008**, *E64*, m1580.
[13] G. Steyl, *Polyhedron*, **2007**, *26*, 5324.
[14] G. Steyl, A. Roodt, *Acta Cryst.*, **2004**, *C60*, m324.
[15] G. Steyl, *Acta Cryst.*, **2007**, *E63*, m23.

(i) crystallographic characterization of the starting material for the kinetic studies (**3**) and the kinetic substituted product (**11**) in Chapters 5 and 8 respectively;

(ii) iso-structural study of *fac*-[Re(MI(naltol)(CO)$_3$(H$_2$O)] in Chapter 6;

(iii) crystallographic evidence of solvolysis of aqua complexes, the transition from *fac*-[Re(EI(naltol)(CO)$_3$(H$_2$O)] (**8**) to *fac*-[Re(EI(naltol)(CO)$_3$(MeOH)] (**9**) (both structures reported in Chapter 7);

(iv) crystallographic characterization of a unique combination of coordination modes by the same chelator (**2**) and (**3**) in Chapter 5;

(v) extended crystallographical evidence presented which show that the coordination geometry does have an influence on the bite angle of the bidentate coordinated ligands in these chelator systems, the O-M-O bite angle increases from the range of 72 ˚ to 74 ˚ in the pentagonal bipyramidal coordination geometry, to the range of 77 ˚ to 78 ˚ in an octahedral coordination geometry and 82 ˚ in a square planar coordination geometry (Chapter 11).

12.3 Kinetic Studies

The *in situ* kinetic evaluations were a success in many fronts. Firstly the kinetic study was structured in such a way that it would primarily address two things; *(i)* whether the process is solvolytic in nature and proceeds by an intermediate solvent precursor *in situ i.e. fac*-[Re(EM(naltol)(CO)$_3$(MeOH)] *(ii)* which one of these complexes is more reactive, *fac*-[Re(EM(naltol))(CO)$_3$(H$_2$O)] or *fac*-[Re(EM(naltol))(CO)$_3$(EM(naltol)H)]. Not only did these studies show that the process is solvolytic in nature and proceeds by a dissociative type mechanism, it was also shown that the bis-complexes can be regarded as a lesser reactive or less potent alternative of the aqua complexes implying that the rates can be tailor made and modulated depending on the desired outcomes. This has broad and significant implications in models for potential radiopharmaceutical industry. Furthermore the study was also able to give insights into the thermodynamic parameters, equilibrium constants and second order rate constants of the process. This data and NMR experiments were in agreement and indicated a D-

activated methanol substitution mechanism. Additionally, these ligand systems were by far the most activating chelators on the *fac*-[Re^I(CO)$_3$]$^+$ core investigated to date.[16-20]

12.4 Future Work

While this project was a success in many fronts at the time of this thesis submission, many results were not yet available to be included as chapters and in particular biological tests which include cytotoxicity, pharmacokinetics and anti-cancer activity. More work still has to be done to obtain better quality crystals in the Zr, Hf and Rh work to do a full evaluation of the solid state character of these compounds and to report it. The illusive [Rh^I(O,O'-Bid)(CO)PPh$_3$] still has to be isolated with these ligand systems and subsequent characterization, for the catalytic evaluation of these complexes and the evaluation of the respective electronic and steric parameters of the chelator systems with regards to iodomethane oxidative addition.

Additionally, some points to be pursued in future are also summarized below:

➢ Mechanistic studies on the formation of the Zr and Hf complexes might provide significant insights which could potentially serve as a basis for beneficiation. From these determinations the manipulation of formation influences, the suppression of certain intermediate products could be induced.

➢ Solubility studies on the Zr and Hf complexes as preliminary evaluations have already indicated different affinities for different solvents. If there is any anomalies in solution behaviour for either zirconium or hafnium counterparts of these complexes, simple compound separation can be achieved *in principle*.

➢ The work on the development of theranostic drugs was at a slightly more advanced stage compared to the other domains of research, for this reason the next step would be the labeling with radioactive metals ^{99m}Tc, $^{186/188}$Re, ^{105}Rh and ^{89}Zr to evaluate the stability of

[16] A. Brink, H. G. Visser, A. Roodt, *Inorg. Chem.,* **2014**, *53*, 12480.

[17] A. Brink, H. G. Visser, A. Roodt, *Inorg. Chem.,* **2013**, *52*, 8950.

[18] M. Schutte, A. Roodt, H. G. Visser, *Inorg. Chem.,* **2012**, *51*, 11996.

[19] M. Schutte, G. Kemp, H. G. Visser, A. Roodt, *Inorg. Chem.,* **2011**, *50*, 12486.

[20] M. Schutte, H. G. Visser, *Polyhedron,* **2015**, *89*, 122.

these radioactive drugs and to hopefully do some preclinical evaluations based on these stability tests and accordingly proceed in adherence with all the necessary regulations pending the results of these evaluations.

APPENDIX A

Table A.1: Atomic coordinates (x 10^4) and equivalent isotropic displacement parameters (Å^2x 10^3) for [Hf(E(maltol))$_3$Cl]·2CHCl$_3$ solvate (1). U(eq) is defined as one third of the trace of the orthogonalized U^{ij} tensor.

	x	y	z	U(eq)
Hf(1)	3642(1)	186(1)	5002(1)	14(1)
Cl(1)	3953(1)	1442(2)	3271(2)	23(1)
O(2B)	3876(2)	1530(5)	6323(4)	15(1)
O(1A)	3785(2)	-1870(4)	4180(4)	19(1)
O(1C)	3049(2)	-328(4)	3780(4)	19(1)
O(1B)	4391(2)	-342(5)	5356(4)	24(1)
O(2C)	3098(1)	1563(4)	5375(4)	16(1)
C(4B)	5222(2)	1079(8)	7408(8)	33(2)
C(3C)	2344(2)	2447(6)	4844(7)	18(1)
C(5B)	5064(2)	234(7)	6538(7)	28(2)
C(2C)	2710(2)	1542(6)	4716(5)	15(1)
C(5C)	2301(2)	463(7)	3066(6)	22(1)
O(2A)	3421(2)	-1257(4)	6234(4)	19(1)
C(1B)	4593(2)	391(6)	6161(6)	21(1)
C(1C)	2696(2)	494(6)	3821(6)	16(1)
C(3B)	4496(2)	2224(7)	7608(6)	21(1)
C(2A)	3484(2)	-2603(6)	5978(6)	18(1)
C(6B)	4253(2)	3317(7)	8298(7)	26(1)
C(7B)	4263(3)	3077(10)	9623(7)	45(2)
C(2B)	4314(2)	1423(7)	6738(6)	19(1)
C(4C)	1959(2)	1405(8)	3243(6)	26(1)
C(1A)	3680(2)	-2893(6)	4807(6)	13(1)
O(3A)	3446(2)	-4999(5)	6407(5)	31(1)
C(5A)	3745(3)	-4328(7)	4537(6)	23(1)

231

C(4A)	3623(3)	-5297(7)	5333(7)	32(2)
C(6A)	3184(3)	-3499(7)	7956(6)	29(2)
C(3A)	3375(2)	-3655(6)	6740(6)	23(1)
O(3C)	1969(2)	2358(5)	4109(4)	23(1)
O(3B)	4953(2)	2047(5)	7940(5)	29(1)
Cl(2)	3648(1)	6695(2)	1249(2)	45(1)
Cl(3)	2792(1)	8192(2)	763(2)	43(1)
Cl(4)	3674(1)	9530(3)	430(3)	69(1)
C(11)	3371(3)	8333(8)	1285(7)	35(2)
C(12)	4982(3)	7042(12)	8466(9)	56(3)
C(6C)	2297(2)	3524(7)	5795(6)	24(1)
C(7C)	1903(3)	3193(8)	6661(7)	31(2)
C(7A)	2699(3)	-4120(9)	8113(7)	40(2)
Cl(5)	5003(1)	6220(3)	9808(3)	61(1)
Cl(6A)	4427(2)	7427(7)	8050(8)	88(2)
Cl(7A)	5232(2)	5767(7)	7440(4)	72(2)
Cl(7B)	4957(6)	6428(13)	7115(10)	78(4)
Cl(6B)	4386(4)	8106(16)	8586(11)	70(3)

Table A.2: Bond distances (Å) and angles (°) for [Hf(E(maltol))$_3$Cl]·2CHCl$_3$ solvate (1).

_____

Hf(1)-O(2A)	2.063(4)
Hf(1)-O(2C)	2.084(4)
Hf(1)-O(2B)	2.084(5)
Hf(1)-O(1A)	2.223(4)
Hf(1)-O(1B)	2.234(5)
Hf(1)-O(1C)	2.237(5)
Hf(1)-Cl(1)	2.4626(19)
O(2B)-C(2B)	1.337(7)
O(1A)-C(1A)	1.249(7)
O(1C)-C(1C)	1.282(7)
O(1B)-C(1B)	1.286(8)
O(2C)-C(2C)	1.334(7)
C(4B)-O(3B)	1.348(9)

C(4B)-C(5B)	1.352(11)
C(4B)-H(4B)	0.9300
C(3C)-O(3C)	1.356(8)
C(3C)-C(2C)	1.368(8)
C(3C)-C(6C)	1.498(9)
C(5B)-C(1B)	1.416(9)
C(5B)-H(5B)	0.9300
C(2C)-C(1C)	1.428(8)
C(5C)-C(4C)	1.348(9)
C(5C)-C(1C)	1.414(9)
C(5C)-H(5C)	0.9300
O(2A)-C(2A)	1.338(7)
C(1B)-C(2B)	1.431(9)
C(3B)-C(2B)	1.352(9)
C(3B)-O(3B)	1.367(8)
C(3B)-C(6B)	1.482(9)
C(2A)-C(3A)	1.364(9)
C(2A)-C(1A)	1.462(9)
C(6B)-C(7B)	1.513(11)
C(6B)-H(6B1)	0.9700
C(6B)-H(6B2)	0.9700
C(7B)-H(7B1)	0.9600
C(7B)-H(7B2)	0.9600
C(7B)-H(7B3)	0.9600
C(4C)-O(3C)	1.341(8)
C(4C)-H(4C)	0.9300
C(1A)-C(5A)	1.426(8)
O(3A)-C(4A)	1.343(10)
O(3A)-C(3A)	1.361(8)
C(5A)-C(4A)	1.341(11)
C(5A)-H(5A)	0.9300
C(4A)-H(4A)	0.9300
C(6A)-C(3A)	1.483(10)
C(6A)-C(7A)	1.520(11)
C(6A)-H(6A1)	0.9700

C(6A)-H(6A2)	0.9700
Cl(2)-C(11)	1.765(8)
Cl(3)-C(11)	1.759(9)
Cl(4)-C(11)	1.735(9)
C(11)-H(11)	0.9800
C(12)-Cl(7B)	1.636(15)
C(12)-Cl(6A)	1.693(11)
C(12)-Cl(5)	1.710(11)
C(12)-Cl(7A)	1.831(13)
C(12)-Cl(6B)	1.991(17)
C(6C)-C(7C)	1.523(10)
C(6C)-H(6C1)	0.9700
C(6C)-H(6C2)	0.9700
C(7C)-H(7C1)	0.9600
C(7C)-H(7C2)	0.9600
C(7C)-H(7C3)	0.9600
C(7A)-H(7A1)	0.9600
C(7A)-H(7A2)	0.9600
C(7A)-H(7A3)	0.9600
Cl(6A)-Cl(6B)	0.899(12)
Cl(6A)-Cl(7B)	2.079(15)
Cl(7A)-Cl(7B)	1.075(15)
O(2A)-Hf(1)-O(2C)	93.71(17)
O(2A)-Hf(1)-O(2B)	91.96(18)
O(2C)-Hf(1)-O(2B)	72.59(16)
O(2A)-Hf(1)-O(1A)	74.80(17)
O(2C)-Hf(1)-O(1A)	141.91(16)
O(2B)-Hf(1)-O(1A)	142.32(17)
O(2A)-Hf(1)-O(1B)	91.07(17)
O(2C)-Hf(1)-O(1B)	145.27(16)
O(2B)-Hf(1)-O(1B)	72.88(17)
O(1A)-Hf(1)-O(1B)	72.29(16)
O(2A)-Hf(1)-O(1C)	92.03(17)
O(2C)-Hf(1)-O(1C)	72.65(15)

O(2B)-Hf(1)-O(1C)	145.19(16)
O(1A)-Hf(1)-O(1C)	71.66(16)
O(1B)-Hf(1)-O(1C)	141.57(16)
O(2A)-Hf(1)-Cl(1)	167.07(12)
O(2C)-Hf(1)-Cl(1)	96.70(12)
O(2B)-Hf(1)-Cl(1)	98.44(13)
O(1A)-Hf(1)-Cl(1)	92.27(13)
O(1B)-Hf(1)-Cl(1)	84.73(13)
O(1C)-Hf(1)-Cl(1)	83.81(13)
C(2B)-O(2B)-Hf(1)	120.2(4)
C(1A)-O(1A)-Hf(1)	114.9(4)
C(1C)-O(1C)-Hf(1)	115.8(4)
C(1B)-O(1B)-Hf(1)	115.6(4)
C(2C)-O(2C)-Hf(1)	119.8(3)
O(3B)-C(4B)-C(5B)	123.3(6)
O(3B)-C(4B)-H(4B)	118.4
C(5B)-C(4B)-H(4B)	118.4
O(3C)-C(3C)-C(2C)	119.9(6)
O(3C)-C(3C)-C(6C)	114.3(5)
C(2C)-C(3C)-C(6C)	125.7(6)
C(4B)-C(5B)-C(1B)	118.1(7)
C(4B)-C(5B)-H(5B)	121.0
C(1B)-C(5B)-H(5B)	121.0
O(2C)-C(2C)-C(3C)	124.5(5)
O(2C)-C(2C)-C(1C)	115.3(5)
C(3C)-C(2C)-C(1C)	120.3(6)
C(4C)-C(5C)-C(1C)	118.3(6)
C(4C)-C(5C)-H(5C)	120.8
C(1C)-C(5C)-H(5C)	120.8
C(2A)-O(2A)-Hf(1)	117.7(4)
O(1B)-C(1B)-C(5B)	125.4(6)
O(1B)-C(1B)-C(2B)	116.8(6)
C(5B)-C(1B)-C(2B)	117.7(6)
O(1C)-C(1C)-C(5C)	126.3(6)
O(1C)-C(1C)-C(2C)	116.1(5)

C(5C)-C(1C)-C(2C)	117.6(6)
C(2B)-C(3B)-O(3B)	119.7(6)
C(2B)-C(3B)-C(6B)	127.3(6)
O(3B)-C(3B)-C(6B)	113.0(6)
O(2A)-C(2A)-C(3A)	123.5(6)
O(2A)-C(2A)-C(1A)	115.5(5)
C(3A)-C(2A)-C(1A)	121.0(5)
C(3B)-C(6B)-C(7B)	113.7(6)
C(3B)-C(6B)-H(6B1)	108.8
C(7B)-C(6B)-H(6B1)	108.8
C(3B)-C(6B)-H(6B2)	108.8
C(7B)-C(6B)-H(6B2)	108.8
H(6B1)-C(6B)-H(6B2)	107.7
C(6B)-C(7B)-H(7B1)	109.5
C(6B)-C(7B)-H(7B2)	109.5
H(7B1)-C(7B)-H(7B2)	109.5
C(6B)-C(7B)-H(7B3)	109.5
H(7B1)-C(7B)-H(7B3)	109.5
H(7B2)-C(7B)-H(7B3)	109.5
O(2B)-C(2B)-C(3B)	124.7(6)
O(2B)-C(2B)-C(1B)	114.5(6)
C(3B)-C(2B)-C(1B)	120.7(6)
O(3C)-C(4C)-C(5C)	123.5(6)
O(3C)-C(4C)-H(4C)	118.2
C(5C)-C(4C)-H(4C)	118.2
O(1A)-C(1A)-C(5A)	127.6(6)
O(1A)-C(1A)-C(2A)	116.9(5)
C(5A)-C(1A)-C(2A)	115.4(5)
C(4A)-O(3A)-C(3A)	120.5(6)
C(4A)-C(5A)-C(1A)	119.7(6)
C(4A)-C(5A)-H(5A)	120.1
C(1A)-C(5A)-H(5A)	120.1
C(5A)-C(4A)-O(3A)	123.6(6)
C(5A)-C(4A)-H(4A)	118.2
O(3A)-C(4A)-H(4A)	118.2

C(3A)-C(6A)-C(7A)	113.8(6)
C(3A)-C(6A)-H(6A1)	108.8
C(7A)-C(6A)-H(6A1)	108.8
C(3A)-C(6A)-H(6A2)	108.8
C(7A)-C(6A)-H(6A2)	108.8
H(6A1)-C(6A)-H(6A2)	107.7
O(3A)-C(3A)-C(2A)	119.8(6)
O(3A)-C(3A)-C(6A)	114.0(6)
C(2A)-C(3A)-C(6A)	126.2(6)
C(4C)-O(3C)-C(3C)	120.4(5)
C(4B)-O(3B)-C(3B)	120.5(6)
Cl(4)-C(11)-Cl(3)	109.5(4)
Cl(4)-C(11)-Cl(2)	110.9(5)
Cl(3)-C(11)-Cl(2)	110.2(4)
Cl(4)-C(11)-H(11)	108.8
Cl(3)-C(11)-H(11)	108.8
Cl(2)-C(11)-H(11)	108.8
Cl(7B)-C(12)-Cl(6A)	77.3(8)
Cl(7B)-C(12)-Cl(5)	131.3(9)
Cl(6A)-C(12)-Cl(5)	112.3(6)
Cl(7B)-C(12)-Cl(7A)	35.6(6)
Cl(6A)-C(12)-Cl(7A)	109.6(6)
Cl(5)-C(12)-Cl(7A)	103.6(6)
Cl(7B)-C(12)-Cl(6B)	102.2(9)
Cl(6A)-C(12)-Cl(6B)	26.7(4)
Cl(5)-C(12)-Cl(6B)	102.0(6)
Cl(7A)-C(12)-Cl(6B)	136.1(7)
C(3C)-C(6C)-C(7C)	112.4(6)
C(3C)-C(6C)-H(6C1)	109.1
C(7C)-C(6C)-H(6C1)	109.1
C(3C)-C(6C)-H(6C2)	109.1
C(7C)-C(6C)-H(6C2)	109.1
H(6C1)-C(6C)-H(6C2)	107.9
C(6C)-C(7C)-H(7C1)	109.5
C(6C)-C(7C)-H(7C2)	109.5

H(7C1)-C(7C)-H(7C2)	109.5	
C(6C)-C(7C)-H(7C3)	109.5	
H(7C1)-C(7C)-H(7C3)	109.5	
H(7C2)-C(7C)-H(7C3)	109.5	
C(6A)-C(7A)-H(7A1)	109.5	
C(6A)-C(7A)-H(7A2)	109.5	
H(7A1)-C(7A)-H(7A2)	109.5	
C(6A)-C(7A)-H(7A3)	109.5	
H(7A1)-C(7A)-H(7A3)	109.5	
H(7A2)-C(7A)-H(7A3)	109.5	
Cl(6B)-Cl(6A)-C(12)	95.4(10)	
Cl(6B)-Cl(6A)-Cl(7B)	140.6(10)	
C(12)-Cl(6A)-Cl(7B)	50.1(6)	
Cl(7B)-Cl(7A)-C(12)	62.3(7)	
Cl(7A)-Cl(7B)-C(12)	82.2(10)	
Cl(7A)-Cl(7B)-Cl(6A)	129.2(9)	
C(12)-Cl(7B)-Cl(6A)	52.6(5)	
Cl(6A)-Cl(6B)-C(12)	57.9(9)	

Table A.3. Anisotropic displacement parameters ($Å^2$ x 10^3) for [Hf(E(maltol))$_3$Cl]·2CHCl$_3$ solvate (1). The anisotropic displacement factor exponent takes the form: $-2\pi^2[\,h^2a^{*2}U^{11} + ... + 2\,h\,k\,a^*\,b^*\,U^{12}\,]$

	U^{11}	U^{22}	U^{33}	U^{23}	U^{13}	U^{12}
Hf(1)	17(1)	10(1)	16(1)	-3(1)	0(1)	1(1)
Cl(1)	20(1)	26(1)	23(1)	9(1)	2(1)	-1(1)
O(2B)	18(2)	15(2)	12(2)	1(2)	-5(2)	1(2)
O(1A)	25(2)	12(2)	19(2)	-4(2)	1(2)	4(2)
O(1C)	21(2)	15(2)	21(2)	-4(2)	2(2)	0(2)
O(1B)	28(2)	19(2)	26(3)	-2(2)	-3(2)	6(2)
O(2C)	18(2)	14(2)	15(2)	-3(1)	-4(2)	-1(2)
C(4B)	20(4)	31(4)	48(5)	1(3)	-11(3)	5(3)
C(3C)	19(2)	20(2)	16(4)	-1(3)	2(3)	2(2)
C(5B)	22(3)	22(3)	40(4)	-2(3)	-6(3)	6(3)
C(2C)	18(3)	13(2)	14(4)	2(2)	0(2)	-4(2)

238

C(5C)	21(3)	25(3)	19(3)	-5(3)	-1(3)	-3(2)
O(2A)	28(2)	10(2)	19(2)	-3(2)	4(2)	0(2)
C(1B)	22(3)	18(3)	23(3)	2(3)	-1(3)	3(2)
C(1C)	18(3)	16(3)	15(3)	0(2)	3(2)	-2(2)
C(3B)	25(3)	17(3)	21(3)	2(2)	-4(3)	-2(2)
C(2A)	22(3)	8(3)	22(3)	3(2)	-1(3)	0(2)
C(6B)	30(3)	17(3)	31(4)	-5(3)	-3(3)	-4(3)
C(7B)	57(5)	49(5)	30(5)	-6(3)	8(4)	-5(4)
C(2B)	17(3)	19(3)	20(3)	1(2)	0(2)	0(2)
C(4C)	20(3)	35(4)	21(4)	0(3)	-3(3)	-2(3)
C(1A)	24(3)	9(2)	7(4)	-3(2)	-1(2)	4(2)
O(3A)	53(3)	9(2)	30(3)	2(2)	1(3)	2(2)
C(5A)	39(4)	14(3)	17(3)	-6(2)	0(3)	9(3)
C(4A)	52(5)	12(3)	32(5)	-3(2)	-3(3)	7(3)
C(6A)	49(4)	21(3)	17(3)	5(3)	-2(3)	-7(3)
C(3A)	35(4)	14(3)	20(3)	2(2)	-5(3)	-1(3)
O(3C)	19(2)	29(2)	20(2)	-3(2)	-2(2)	5(2)
O(3B)	23(2)	28(3)	35(3)	-5(2)	-13(2)	0(2)
Cl(2)	67(1)	35(1)	34(1)	-2(1)	-6(1)	18(1)
Cl(3)	48(1)	51(1)	31(1)	-3(1)	1(1)	7(1)
Cl(4)	82(2)	50(1)	76(2)	22(1)	-33(1)	-31(1)
C(11)	60(5)	23(4)	23(4)	-6(3)	-2(4)	6(3)
C(12)	47(5)	74(7)	46(6)	10(5)	-5(4)	-32(5)
C(6C)	25(3)	19(3)	29(4)	-8(3)	1(3)	5(2)
C(7C)	38(4)	35(4)	22(4)	-5(3)	3(3)	3(3)
C(7A)	56(5)	43(5)	21(4)	1(4)	5(4)	-9(4)
Cl(5)	74(2)	60(1)	48(2)	-3(1)	-7(1)	-20(1)
Cl(6A)	51(2)	78(4)	134(5)	46(3)	-32(3)	-19(2)
Cl(7A)	65(3)	104(4)	47(2)	-30(2)	22(2)	-44(3)
Cl(7B)	108(7)	71(5)	55(5)	-12(4)	26(5)	-27(5)
Cl(6B)	53(4)	87(6)	72(6)	14(5)	13(4)	-13(4)

Table A.4: Hydrogen coordinates (x 10^4) and isotropic displacement parameters (Å^{2}x 10^3)

[Hf(E(maltol))$_3$Cl]·2CHCl$_3$ solvate (1).

	x	y	z	U(eq)
H(4B)	5531	988	7652	40
H(5B)	5258	-431	6198	34
H(5C)	2278	-191	2462	26
H(6B1)	3929	3366	8040	31
H(6B2)	4398	4207	8128	31
H(7B1)	4102	2229	9807	68
H(7B2)	4113	3839	10018	68
H(7B3)	4582	3010	9886	68
H(4C)	1702	1394	2736	31
H(5A)	3872	-4590	3812	28
H(4A)	3663	-6226	5131	39
H(6A1)	3172	-2518	8151	35
H(6A2)	3397	-3941	8510	35
H(11)	3363	8664	2107	43
H(6C1)	2238	4420	5432	29
H(6C2)	2590	3588	6227	29
H(7C1)	1609	3210	6250	47
H(7C2)	1900	3872	7283	47
H(7C3)	1952	2286	6994	47
H(7A1)	2495	-3781	7500	60
H(7A2)	2576	-3857	8873	60
H(7A3)	2718	-5114	8066	60

Table A.5: Torsion angles [°] for [Hf(E(maltol))₃Cl]·2CHCl₃ solvate (1)

_____

O(3B)-C(4B)-C(5B)-C(1B)	0.8(12)
Hf(1)-O(2C)-C(2C)-C(3C)	-176.3(5)
Hf(1)-O(2C)-C(2C)-C(1C)	2.9(6)
O(3C)-C(3C)-C(2C)-O(2C)	178.5(5)
C(6C)-C(3C)-C(2C)-O(2C)	-5.5(10)
O(3C)-C(3C)-C(2C)-C(1C)	-0.7(9)
C(6C)-C(3C)-C(2C)-C(1C)	175.4(6)
Hf(1)-O(1B)-C(1B)-C(5B)	179.4(6)
Hf(1)-O(1B)-C(1B)-C(2B)	1.1(7)
C(4B)-C(5B)-C(1B)-O(1B)	-179.1(7)
C(4B)-C(5B)-C(1B)-C(2B)	-0.9(10)
Hf(1)-O(1C)-C(1C)-C(5C)	173.8(5)
Hf(1)-O(1C)-C(1C)-C(2C)	-5.8(7)
C(4C)-C(5C)-C(1C)-O(1C)	179.5(6)
C(4C)-C(5C)-C(1C)-C(2C)	-0.9(9)
O(2C)-C(2C)-C(1C)-O(1C)	2.2(8)
C(3C)-C(2C)-C(1C)-O(1C)	-178.6(6)
O(2C)-C(2C)-C(1C)-C(5C)	-177.4(5)
C(3C)-C(2C)-C(1C)-C(5C)	1.7(9)
Hf(1)-O(2A)-C(2A)-C(3A)	176.6(5)
Hf(1)-O(2A)-C(2A)-C(1A)	-3.5(7)
C(2B)-C(3B)-C(6B)-C(7B)	122.8(8)
O(3B)-C(3B)-C(6B)-C(7B)	-56.5(8)
Hf(1)-O(2B)-C(2B)-C(3B)	-178.6(5)
Hf(1)-O(2B)-C(2B)-C(1B)	3.0(7)
O(3B)-C(3B)-C(2B)-O(2B)	-178.3(6)
C(6B)-C(3B)-C(2B)-O(2B)	2.6(11)
O(3B)-C(3B)-C(2B)-C(1B)	0.0(10)
C(6B)-C(3B)-C(2B)-C(1B)	-179.1(6)
O(1B)-C(1B)-C(2B)-O(2B)	-2.6(9)
C(5B)-C(1B)-C(2B)-O(2B)	178.9(6)
O(1B)-C(1B)-C(2B)-C(3B)	178.9(6)
C(5B)-C(1B)-C(2B)-C(3B)	0.5(10)

C(1C)-C(5C)-C(4C)-O(3C)	-1.1(10)
Hf(1)-O(1A)-C(1A)-C(5A)	-177.8(5)
Hf(1)-O(1A)-C(1A)-C(2A)	-0.4(7)
O(2A)-C(2A)-C(1A)-O(1A)	2.5(8)
C(3A)-C(2A)-C(1A)-O(1A)	-177.6(6)
O(2A)-C(2A)-C(1A)-C(5A)	-179.8(6)
C(3A)-C(2A)-C(1A)-C(5A)	0.1(9)
O(1A)-C(1A)-C(5A)-C(4A)	178.2(7)
C(2A)-C(1A)-C(5A)-C(4A)	0.8(10)
C(1A)-C(5A)-C(4A)-O(3A)	-1.3(12)
C(3A)-O(3A)-C(4A)-C(5A)	0.9(12)
C(4A)-O(3A)-C(3A)-C(2A)	0.1(10)
C(4A)-O(3A)-C(3A)-C(6A)	-179.2(6)
O(2A)-C(2A)-C(3A)-O(3A)	179.4(6)
C(1A)-C(2A)-C(3A)-O(3A)	-0.5(10)
O(2A)-C(2A)-C(3A)-C(6A)	-1.4(11)
C(1A)-C(2A)-C(3A)-C(6A)	178.7(6)
C(7A)-C(6A)-C(3A)-O(3A)	-63.8(9)
C(7A)-C(6A)-C(3A)-C(2A)	117.0(8)
C(5C)-C(4C)-O(3C)-C(3C)	2.3(10)
C(2C)-C(3C)-O(3C)-C(4C)	-1.3(9)
C(6C)-C(3C)-O(3C)-C(4C)	-177.8(6)
C(5B)-C(4B)-O(3B)-C(3B)	-0.3(12)
C(2B)-C(3B)-O(3B)-C(4B)	-0.1(10)
C(6B)-C(3B)-O(3B)-C(4B)	179.2(6)
O(3C)-C(3C)-C(6C)-C(7C)	64.7(8)
C(2C)-C(3C)-C(6C)-C(7C)	-111.6(7)
Cl(7B)-C(12)-Cl(6A)-Cl(6B)	-158.8(11)
Cl(5)-C(12)-Cl(6A)-Cl(6B)	71.6(11)
Cl(7A)-C(12)-Cl(6A)-Cl(6B)	-173.8(10)
Cl(5)-C(12)-Cl(6A)-Cl(7B)	-129.6(9)
Cl(7A)-C(12)-Cl(6A)-Cl(7B)	-15.0(5)
Cl(6B)-C(12)-Cl(6A)-Cl(7B)	158.8(11)
Cl(6A)-C(12)-Cl(7A)-Cl(7B)	25.7(8)
Cl(5)-C(12)-Cl(7A)-Cl(7B)	145.8(9)

Cl(6B)-C(12)-Cl(7A)-Cl(7B)	21.7(12)
C(12)-Cl(7A)-Cl(7B)-Cl(6A)	-25.4(8)
Cl(6A)-C(12)-Cl(7B)-Cl(7A)	-155.2(8)
Cl(5)-C(12)-Cl(7B)-Cl(7A)	-46.5(13)
Cl(6B)-C(12)-Cl(7B)-Cl(7A)	-164.8(8)
Cl(5)-C(12)-Cl(7B)-Cl(6A)	108.7(10)
Cl(7A)-C(12)-Cl(7B)-Cl(6A)	155.2(8)
Cl(6B)-C(12)-Cl(7B)-Cl(6A)	-9.6(5)
Cl(7B)-Cl(6A)-Cl(6B)-C(12)	-26.0(14)

Table A. 6: Hydrogen bonds for [Hf(E(maltol))$_3$Cl]·2CHCl$_3$ solvate (1) [Å and °].

D-H…A	d(D-H) (Å)	d(H…A) (Å)	d(D…A) (Å)	∟ (D-H…A)(°)
C4C-H4C...O2B [(i)]	0.93	2.30	3.223	173
C6A-H6A1…O2A	0.97	2.58	2.980	105
C11-H11...O1C [(ii)]	0.98	2.30	3.228	157

Symmetry codes, transformations used to generate equivalent atoms: (i) 1/2-x, y, z-1/2; (ii) x, +1+y, +1+z;

Table A. 7: Atomic coordinates (x 10^4) and equivalent isotropic displacement parameters (Å^2 x 10^3) for *fac*-[Re(MM(naltol))(CO)$_3$(MM(naltol)H)] (2). U(eq) is defined as one third of the trace of the orthogonalized U^{ij} tensor.

	x	y	z	U(eq)
C(21)	9790(4)	2477(2)	2038(2)	26(1)
C(1A)	6983(4)	1061(2)	584(2)	19(1)
C(1B)	4716(4)	599(2)	2891(2)	22(1)
C(23)	8876(4)	1821(2)	3438(2)	23(1)
C(2A)	8008(3)	425(2)	1097(2)	17(1)
C(2B)	5846(4)	-28(2)	3377(2)	20(1)
C(22)	6593(4)	2870(2)	2552(2)	26(1)
C(3A)	8328(4)	-361(2)	761(2)	19(1)
C(3B)	5156(4)	-578(2)	3933(2)	24(1)
C(4A)	6800(4)	91(2)	-598(2)	26(1)
C(4B)	2215(4)	32(2)	3543(2)	31(1)
C(5A)	6434(4)	870(2)	-290(2)	24(1)
C(5B)	2848(4)	593(2)	2996(2)	28(1)
C(6A)	7949(4)	-1363(2)	-468(2)	31(1)
C(6B)	2561(5)	-1117(2)	4588(2)	34(1)
C(7A)	9291(4)	-1050(2)	1310(2)	27(1)
C(7B)	6306(4)	-1252(2)	4418(2)	32(1)
O(21)	11041(4)	2848(2)	1896(2)	42(1)
O(1A)	6611(3)	1769(1)	936(1)	23(1)
O(1B)	5288(3)	1102(1)	2354(1)	24(1)
O(23)	9649(3)	1829(1)	4132(1)	33(1)
O(2A)	8636(2)	624(1)	1919(1)	19(1)
O(2B)	7637(3)	-108(1)	3295(1)	26(1)
O(22)	5880(4)	3481(2)	2745(1)	41(1)
Re(1)	7728(1)	1844(1)	2270(1)	18(1)
N(1A)	7704(3)	-515(2)	-95(1)	22(1)
N(1B)	3344(3)	-529(2)	4006(2)	26(1)

Table A. 8:   Bond lengths [Å] and angles [°] for *fac*-[Re(MM(naltol))(CO)$_3$(MM(naltol)H)] (2).

_____

C(21)-O(21)	1.143(4)
C(21)-Re(1)	1.901(3)
C(1A)-O(1A)	1.291(3)
C(1A)-C(5A)	1.408(4)
C(1A)-C(2A)	1.426(4)
C(1B)-O(1B)	1.277(3)
C(1B)-C(5B)	1.416(4)
C(1B)-C(2B)	1.433(4)
C(23)-O(23)	1.153(4)
C(23)-Re(1)	1.905(3)
C(2A)-O(2A)	1.345(3)
C(2A)-C(3A)	1.378(4)
C(2B)-O(2B)	1.355(3)
C(2B)-C(3B)	1.384(4)
C(22)-O(22)	1.157(4)
C(22)-Re(1)	1.901(3)
C(3A)-N(1A)	1.378(3)
C(3A)-C(7A)	1.494(4)
C(3B)-N(1B)	1.363(4)
C(3B)-C(7B)	1.492(4)
C(4A)-N(1A)	1.347(4)
C(4A)-C(5A)	1.358(4)
C(4A)-H(4A)	0.9300
C(4B)-N(1B)	1.348(4)
C(4B)-C(5B)	1.365(4)
C(4B)-H(4B)	0.9300
C(5A)-H(5A)	0.9300
C(5B)-H(5B)	0.9300
C(6A)-N(1A)	1.479(4)
C(6A)-H(6A1)	0.9600
C(6A)-H(6A2)	0.9600
C(6A)-H(6A3)	0.9600
C(6B)-N(1B)	1.481(4)

C(6B)-H(6B1)	0.9600
C(6B)-H(6B2)	0.9600
C(6B)-H(6B3)	0.9600
C(7A)-H(7A1)	0.9600
C(7A)-H(7A2)	0.9600
C(7A)-H(7A3)	0.9600
C(7B)-H(7B1)	0.9600
C(7B)-H(7B2)	0.9600
C(7B)-H(7B3)	0.9600
O(1A)-Re(1)	2.140(2)
O(1B)-Re(1)	2.168(2)
O(2A)-Re(1)	2.1316(19)
O(2B)-H(2B)	0.8200
O(21)-C(21)-Re(1)	179.1(3)
O(1A)-C(1A)-C(5A)	123.8(2)
O(1A)-C(1A)-C(2A)	119.3(2)
C(5A)-C(1A)-C(2A)	116.9(2)
O(1B)-C(1B)-C(5B)	120.7(3)
O(1B)-C(1B)-C(2B)	123.6(3)
C(5B)-C(1B)-C(2B)	115.5(3)
O(23)-C(23)-Re(1)	176.4(3)
O(2A)-C(2A)-C(3A)	121.6(2)
O(2A)-C(2A)-C(1A)	117.2(2)
C(3A)-C(2A)-C(1A)	121.2(2)
O(2B)-C(2B)-C(3B)	117.6(2)
O(2B)-C(2B)-C(1B)	120.6(2)
C(3B)-C(2B)-C(1B)	121.8(3)
O(22)-C(22)-Re(1)	177.7(3)
C(2A)-C(3A)-N(1A)	118.7(2)
C(2A)-C(3A)-C(7A)	121.4(2)
N(1A)-C(3A)-C(7A)	119.8(2)
N(1B)-C(3B)-C(2B)	118.8(3)
N(1B)-C(3B)-C(7B)	119.0(3)
C(2B)-C(3B)-C(7B)	122.1(3)

N(1A)-C(4A)-C(5A)	122.2(3)
N(1A)-C(4A)-H(4A)	118.9
C(5A)-C(4A)-H(4A)	118.9
N(1B)-C(4B)-C(5B)	121.3(3)
N(1B)-C(4B)-H(4B)	119.3
C(5B)-C(4B)-H(4B)	119.3
C(4A)-C(5A)-C(1A)	120.0(3)
C(4A)-C(5A)-H(5A)	120.0
C(1A)-C(5A)-H(5A)	120.0
C(4B)-C(5B)-C(1B)	121.0(3)
C(4B)-C(5B)-H(5B)	119.5
C(1B)-C(5B)-H(5B)	119.5
N(1A)-C(6A)-H(6A1)	109.5
N(1A)-C(6A)-H(6A2)	109.5
H(6A1)-C(6A)-H(6A2)	109.5
N(1A)-C(6A)-H(6A3)	109.5
H(6A1)-C(6A)-H(6A3)	109.5
H(6A2)-C(6A)-H(6A3)	109.5
N(1B)-C(6B)-H(6B1)	109.5
N(1B)-C(6B)-H(6B2)	109.5
H(6B1)-C(6B)-H(6B2)	109.5
N(1B)-C(6B)-H(6B3)	109.5
H(6B1)-C(6B)-H(6B3)	109.5
H(6B2)-C(6B)-H(6B3)	109.5
C(3A)-C(7A)-H(7A1)	109.5
C(3A)-C(7A)-H(7A2)	109.5
H(7A1)-C(7A)-H(7A2)	109.5
C(3A)-C(7A)-H(7A3)	109.5
H(7A1)-C(7A)-H(7A3)	109.5
H(7A2)-C(7A)-H(7A3)	109.5
C(3B)-C(7B)-H(7B1)	109.5
C(3B)-C(7B)-H(7B2)	109.5
H(7B1)-C(7B)-H(7B2)	109.5
C(3B)-C(7B)-H(7B3)	109.5
H(7B1)-C(7B)-H(7B3)	109.5

H(7B2)-C(7B)-H(7B3)	109.5
C(1A)-O(1A)-Re(1)	113.20(16)
C(1B)-O(1B)-Re(1)	137.47(17)
C(2A)-O(2A)-Re(1)	112.55(15)
C(2B)-O(2B)-H(2B)	109.5
C(22)-Re(1)-C(21)	89.84(13)
C(22)-Re(1)-C(23)	86.36(12)
C(21)-Re(1)-C(23)	86.93(12)
C(22)-Re(1)-O(2A)	172.28(11)
C(21)-Re(1)-O(2A)	97.24(11)
C(23)-Re(1)-O(2A)	97.05(10)
C(22)-Re(1)-O(1A)	99.18(10)
C(21)-Re(1)-O(1A)	92.16(10)
C(23)-Re(1)-O(1A)	174.38(10)
O(2A)-Re(1)-O(1A)	77.56(7)
C(22)-Re(1)-O(1B)	92.33(12)
C(21)-Re(1)-O(1B)	172.49(10)
C(23)-Re(1)-O(1B)	100.38(10)
O(2A)-Re(1)-O(1B)	80.27(8)
O(1A)-Re(1)-O(1B)	80.40(8)
C(4A)-N(1A)-C(3A)	120.9(2)
C(4A)-N(1A)-C(6A)	118.8(2)
C(3A)-N(1A)-C(6A)	120.3(2)
C(4B)-N(1B)-C(3B)	121.6(3)
C(4B)-N(1B)-C(6B)	118.3(3)
C(3B)-N(1B)-C(6B)	120.0(3)

Table A. 9: Anisotropic displacement parameters ($Å^2$ x 10^3) for *fac*-[Re(MM(naltol))(CO)$_3$(MM(naltol)H)] (2). The anisotropic displacement factor exponent takes the form: $-2p^2[h^2a^{*2}U^{11} + ... + 2 h k a^* b^* U^{12}]$

	U^{11}	U^{22}	U^{33}	U^{23}	U^{13}	U^{12}
C(21)	40(2)	20(1)	18(1)	-1(1)	6(1)	-3(1)
C(1A)	20(1)	19(1)	17(1)	2(1)	4(1)	-3(1)
C(1B)	24(1)	24(1)	19(1)	-6(1)	1(1)	0(1)
C(23)	29(2)	17(1)	23(1)	1(1)	5(1)	-4(1)
C(2A)	17(1)	19(1)	15(1)	-1(1)	4(1)	-3(1)
C(2B)	21(1)	21(1)	19(1)	-6(1)	2(1)	-3(1)
C(22)	38(2)	24(2)	16(1)	2(1)	2(1)	3(1)
C(3A)	19(1)	21(1)	18(1)	-2(1)	3(1)	-3(1)
C(3B)	26(1)	22(1)	23(1)	-7(1)	1(1)	-2(1)
C(4A)	25(1)	33(2)	17(1)	-4(1)	1(1)	-4(1)
C(4B)	21(1)	38(2)	34(2)	-2(1)	5(1)	-1(1)
C(5A)	26(1)	27(2)	16(1)	3(1)	0(1)	-2(1)
C(5B)	21(1)	36(2)	28(2)	2(1)	2(1)	2(1)
C(6A)	31(2)	29(2)	33(2)	-16(1)	7(1)	-1(1)
C(6B)	40(2)	37(2)	28(2)	-3(1)	12(1)	-13(2)
C(7A)	28(2)	22(1)	31(2)	-2(1)	1(1)	4(1)
C(7B)	37(2)	29(2)	28(2)	5(1)	4(1)	1(1)
O(21)	53(2)	39(1)	37(1)	-7(1)	20(1)	-21(1)
O(1A)	31(1)	20(1)	17(1)	1(1)	1(1)	1(1)
O(1B)	23(1)	22(1)	24(1)	5(1)	-1(1)	-3(1)
O(23)	43(1)	34(1)	20(1)	4(1)	-1(1)	-8(1)
O(2A)	21(1)	18(1)	18(1)	-1(1)	1(1)	2(1)
O(2B)	21(1)	27(1)	29(1)	9(1)	3(1)	3(1)
O(22)	69(2)	28(1)	25(1)	-2(1)	3(1)	21(1)
Re(1)	25(1)	15(1)	14(1)	0(1)	2(1)	-1(1)
N(1A)	23(1)	23(1)	20(1)	-7(1)	5(1)	-3(1)
N(1B)	28(1)	28(1)	23(1)	-4(1)	7(1)	-4(1)

Table A. 10: Hydrogen bonds for *fac*-[Re(MM(naltol))(CO)$_3$(MM(naltol)H)] (2).

D-H...A	d(D-H) (Å)	d(H...A) (Å)	d(D...A) (Å)	Ь (D-H...A)(°)
O2B-H2B...O1B	0.82	2.46	2.8322	109
O2B-H2B...O2A	0.82	1.85	2.6579	170
C4B-H4B...O2B [(i)]	0.93	2.45	3.3505	163
C5A-H5A...O3 [(ii)]	0.93	2.56	3.2276	129
C6B-H6B3...O1A [(iii)]	0.96	2.54	3.4979	177
C7A-H7A1...O2A	0.96	2.45	2.8651	106
C7B-H7B2...O2B	0.96	2.36	2.8059	108

Symmetry codes, transformations used to generate equivalent atoms: (i) -x,1-y,1-z; (ii) x,-1+y,z; (iii) x, 1/2-y, z-1/2

Table A. 11: Atomic coordinates (x 10^4) and equivalent isotropic displacement parameters (Å^2 x 10^3) for *fac*-[Re(EM(naltol))(CO)$_3$(EM(naltol)H)] (3). U(eq) is defined as one third of the trace of the orthogonalized U^{ij} tensor.

	x	y	z	U(eq)
Re(1)	6934(1)	7357(1)	6589(1)	11(1)
O(2A)	8338(2)	7323(2)	7992(2)	13(1)
O(1B)	8531(2)	7994(2)	5514(2)	14(1)
O(1A)	8679(2)	5458(2)	6308(2)	14(1)
O(2B)	8606(2)	9708(2)	7353(2)	16(1)
O(22)	5304(2)	7072(2)	4423(2)	26(1)
O(23)	4763(2)	10276(2)	6987(2)	27(1)
O(21)	4722(2)	6460(2)	8137(2)	28(1)
N(1A)	11844(2)	4822(2)	8683(2)	16(1)
C(22)	5907(3)	7214(3)	5238(3)	16(1)
C(21)	5605(3)	6769(3)	7560(3)	18(1)
C(23)	5574(3)	9176(3)	6835(2)	16(1)
C(1A)	9726(3)	5240(2)	7025(2)	12(1)
C(1B)	8323(3)	9269(2)	5268(2)	11(1)
C(5B)	8071(3)	9844(3)	4090(2)	14(1)
C(2A)	9549(3)	6207(2)	7961(2)	12(1)
C(2B)	8372(3)	10158(2)	6192(2)	12(1)
C(3A)	10587(3)	5964(3)	8808(2)	14(1)
N(1B)	7967(2)	11986(2)	4766(2)	14(1)

C(5A)	11040(3)	4103(3)	6944(2)	15(1)
C(4B)	7888(3)	11182(3)	3877(2)	15(1)
C(4A)	12058(3)	3925(3)	7774(3)	18(1)
C(3B)	8222(3)	11490(3)	5935(2)	13(1)
C(8A)	11015(3)	8030(3)	9562(3)	23(1)
C(7A)	10352(3)	6927(3)	9846(2)	18(1)
C(6A)	12975(3)	4515(3)	9575(3)	24(1)
C(6B)	7751(3)	13425(3)	4473(3)	21(1)
C(7B)	8317(3)	12393(3)	6917(2)	18(1)
C(8B)	6855(3)	13064(3)	7652(3)	29(1)
C(31)	14804(9)	424(6)	9800(6)	37(2)
O(40)	14398(9)	1606(5)	9491(6)	71(2)
C(32)	13697(7)	-1(9)	9937(5)	99(2)

Table A. 12: Bond lengths [Å] and angles [°] for *fac*-[Re(EM(naltol))(CO)₃(EM(naltol)H)] (3).

Re(1)-C(21)	1.885(3)
Re(1)-C(22)	1.900(3)
Re(1)-C(23)	1.911(3)
Re(1)-O(1A)	2.124(2)
Re(1)-O(2A)	2.141(2)
Re(1)-O(1B)	2.174(2)
O(2A)-C(2A)	1.335(3)
O(1B)-C(1B)	1.304(3)
O(1A)-C(1A)	1.295(3)
O(2B)-C(2B)	1.350(3)
O(22)-C(22)	1.156(3)
O(23)-C(23)	1.153(3)
O(21)-C(21)	1.169(4)
N(1A)-C(4A)	1.354(4)
N(1A)-C(3A)	1.378(3)
N(1A)-C(6A)	1.479(3)
C(1A)-C(5A)	1.405(4)
C(1A)-C(2A)	1.432(3)
C(1B)-C(5B)	1.407(4)

C(1B)-C(2B)	1.425(3)
C(5B)-C(4B)	1.368(4)
C(2A)-C(3A)	1.384(4)
C(2B)-C(3B)	1.377(3)
C(3A)-C(7A)	1.504(4)
N(1B)-C(4B)	1.343(3)
N(1B)-C(3B)	1.373(3)
N(1B)-C(6B)	1.479(3)
C(5A)-C(4A)	1.365(4)
C(3B)-C(7B)	1.498(3)
C(8A)-C(7A)	1.539(4)
C(7B)-C(8B)	1.530(4)
C(31)-C(31)#1	0.940(12)
C(31)-O(40)	1.206(8)
C(31)-C(32)	1.318(11)
C(31)-C(32)#1	1.426(11)
C(32)-C(31)#1	1.427(11)
C(21)-Re(1)-C(22)	86.22(13)
C(21)-Re(1)-C(23)	87.26(12)
C(22)-Re(1)-C(23)	89.25(12)
C(21)-Re(1)-O(1A)	99.60(11)
C(22)-Re(1)-O(1A)	95.49(10)
C(23)-Re(1)-O(1A)	171.88(9)
C(21)-Re(1)-O(2A)	97.44(11)
C(22)-Re(1)-O(2A)	172.47(9)
C(23)-Re(1)-O(2A)	97.47(10)
O(1A)-Re(1)-O(2A)	77.45(7)
C(21)-Re(1)-O(1B)	177.85(9)
C(22)-Re(1)-O(1B)	95.54(10)
C(23)-Re(1)-O(1B)	94.00(10)
O(1A)-Re(1)-O(1B)	79.01(8)
O(2A)-Re(1)-O(1B)	80.67(8)
C(2A)-O(2A)-Re(1)	112.56(15)
C(1B)-O(1B)-Re(1)	122.77(16)

C(1A)-O(1A)-Re(1)	113.81(16)
C(4A)-N(1A)-C(3A)	121.3(2)
C(4A)-N(1A)-C(6A)	118.1(2)
C(3A)-N(1A)-C(6A)	120.5(2)
O(22)-C(22)-Re(1)	177.3(2)
O(21)-C(21)-Re(1)	176.4(3)
O(23)-C(23)-Re(1)	179.4(3)
O(1A)-C(1A)-C(5A)	123.9(2)
O(1A)-C(1A)-C(2A)	118.7(2)
C(5A)-C(1A)-C(2A)	117.5(2)
O(1B)-C(1B)-C(5B)	122.9(2)
O(1B)-C(1B)-C(2B)	121.0(2)
C(5B)-C(1B)-C(2B)	116.0(2)
C(4B)-C(5B)-C(1B)	120.5(2)
O(2A)-C(2A)-C(3A)	122.0(2)
O(2A)-C(2A)-C(1A)	117.3(2)
C(3A)-C(2A)-C(1A)	120.7(2)
O(2B)-C(2B)-C(3B)	117.6(2)
O(2B)-C(2B)-C(1B)	120.7(2)
C(3B)-C(2B)-C(1B)	121.7(2)
N(1A)-C(3A)-C(2A)	118.7(2)
N(1A)-C(3A)-C(7A)	120.5(2)
C(2A)-C(3A)-C(7A)	120.8(2)
C(4B)-N(1B)-C(3B)	120.7(2)
C(4B)-N(1B)-C(6B)	119.1(2)
C(3B)-N(1B)-C(6B)	120.2(2)
C(4A)-C(5A)-C(1A)	119.8(2)
N(1B)-C(4B)-C(5B)	121.9(2)
N(1A)-C(4A)-C(5A)	121.8(2)
N(1B)-C(3B)-C(2B)	119.1(2)
N(1B)-C(3B)-C(7B)	120.3(2)
C(2B)-C(3B)-C(7B)	120.7(2)
C(3A)-C(7A)-C(8A)	113.5(2)
C(3B)-C(7B)-C(8B)	112.5(2)
C(31)#1-C(31)-O(40)	166.4(14)

C(31)#1-C(31)-C(32)	76.4(11)
O(40)-C(31)-C(32)	110.9(9)
C(31)#1-C(31)-C(32)#1	63.8(10)
O(40)-C(31)-C(32)#1	108.1(8)
C(32)-C(31)-C(32)#1	140.2(5)
C(31)-C(32)-C(31)#1	39.8(5)

Symmetry transformations used to generate equivalent atoms:

#1 -x+3,-y,-z+2

**Table A. 13: Anisotropic displacement parameters ($Å^2$ x 10^3) for *fac-*
[Re(EM(naltol))(CO)$_3$(EM(naltol)H)] (3). The anisotropic displacement factor exponent takes the
form: $-2p^2[h^2a^{*2}U^{11} + ... + 2 h k a^* b^* U^{12}]$**

	U^{11}	U^{22}	U^{33}	U^{23}	U^{13}	U^{12}
Re(1)	11(1)	12(1)	12(1)	1(1)	-2(1)	-5(1)
O(2A)	14(1)	13(1)	12(1)	-1(1)	-2(1)	-5(1)
O(1B)	16(1)	12(1)	15(1)	0(1)	2(1)	-7(1)
O(1A)	15(1)	12(1)	15(1)	0(1)	-4(1)	-5(1)
O(2B)	28(1)	13(1)	12(1)	2(1)	-5(1)	-11(1)
O(22)	22(1)	39(1)	21(1)	-5(1)	-7(1)	-12(1)
O(23)	21(1)	17(1)	38(1)	-2(1)	-5(1)	0(1)
O(21)	22(1)	29(1)	35(1)	6(1)	7(1)	-13(1)
N(1A)	14(1)	21(1)	13(1)	5(1)	-5(1)	-7(1)
C(22)	12(1)	18(1)	19(1)	0(1)	2(1)	-5(1)
C(21)	18(1)	16(1)	20(1)	2(1)	-5(1)	-5(1)
C(23)	15(1)	21(1)	15(1)	1(1)	-2(1)	-9(1)
C(1A)	16(1)	10(1)	12(1)	3(1)	1(1)	-7(1)
C(1B)	7(1)	10(1)	14(1)	1(1)	0(1)	-3(1)
C(5B)	15(1)	17(1)	11(1)	-1(1)	-1(1)	-5(1)
C(2A)	15(1)	14(1)	11(1)	1(1)	1(1)	-9(1)
C(2B)	11(1)	13(1)	12(1)	1(1)	-2(1)	-5(1)
C(3A)	15(1)	15(1)	11(1)	3(1)	0(1)	-7(1)
N(1B)	13(1)	12(1)	17(1)	4(1)	-2(1)	-6(1)
C(5A)	18(1)	11(1)	16(1)	0(1)	2(1)	-6(1)

C(4B)	14(1)	18(1)	13(1)	4(1)	-1(1)	-4(1)
C(4A)	16(1)	14(1)	20(1)	5(1)	1(1)	-2(1)
C(3B)	11(1)	16(1)	14(1)	0(1)	-2(1)	-7(1)
C(8A)	29(2)	23(1)	20(1)	2(1)	-8(1)	-13(1)
C(7A)	21(1)	24(1)	12(1)	3(1)	-4(1)	-12(1)
C(6A)	16(1)	34(2)	20(1)	10(1)	-8(1)	-9(1)
C(6B)	26(2)	13(1)	25(2)	8(1)	-5(1)	-10(1)
C(7B)	23(1)	14(1)	19(1)	1(1)	-8(1)	-10(1)
C(8B)	28(2)	27(2)	29(2)	-12(1)	-7(1)	-4(1)
C(31)	61(5)	17(3)	20(3)	-3(2)	12(3)	-1(3)
O(40)	115(5)	22(3)	56(4)	2(2)	7(4)	-5(3)
C(32)	73(4)	177(6)	46(3)	-7(4)	15(3)	-49(4)

Table A. 14: Hydrogen coordinates (x 10^4) and isotropic displacement parameters (Å^2 x 10^3) for *fac*-[Re(EM(naltol))(CO)$_3$(EM(naltol)H)] (3).

	x	y	z	U(eq)
H(2B)	8522	8963	7436	24
H(5B)	8028	9311	3451	17
H(5A)	11215	3474	6326	18
H(4B)	7704	11545	3095	19
H(4A)	12921	3167	7714	21
H(8A1)	12046	7604	9354	34
H(8A2)	10859	8589	10266	34
H(8A3)	10554	8585	8887	34
H(7A1)	10781	6407	10559	22
H(7A2)	9310	7367	10045	22
H(6A1)	12634	4205	10330	35
H(6A2)	13170	5323	9716	35
H(6A3)	13857	3817	9258	35
H(22A)	7837	13867	5195	31
H(22B)	6796	13879	4183	31
H(22C)	8479	13464	3853	31

H(22D)	7571	13606	3625	31
H(22E)	8613	13594	4638	31
H(22F)	6929	14009	4967	31
H(7B1)	8637	13097	6547	21
H(7B2)	9045	11859	7466	21
H(8B1)	6156	13667	7128	43
H(8B2)	6987	13571	8309	43
H(8B3)	6504	12373	7979	43

Table A. 15: Hydrogen bonds for *fac*-[Re(EM(naltol))(CO)$_3$(EM(naltol)H)] (3).

D-H…A	d(D-H) (Å)	d(H…A) (Å)	d(D…A) (Å)	ᶀ (D-H…A)(˚)
O2B-H2B...O1B	0.82	2.38	2.788(3)	112
O2B-H2B...O2A	0.82	1.88	2.683(3)	167
C8A-H8A3...O2B	0.96	2.57	3.483(4)	159
C7A-H7A2...O2A	0.97	2.53	2.866(4)	101
C5A-H5A...O1B [(i)]	0.93	2.54	3.460(4)	173
C6A-H6A3...O40 [(i)]	0.96	2.20	2.871(6)	126
C7B-H7B1...O1A[(ii)]	0.97	2.51	3.413(4)	155
C6B-H22A...O1A[(ii)]	0.96	2.52	3.400(4)	153

Symmetry codes, transformations used to generate equivalent atoms: (i) -x, 1-y, 1-z; (ii) x, y-1, +z;

Table A. 16: Atomic coordinates (x 10^4) and equivalent isotropic displacement parameters (Å^2 x 10^3) for *fac*-[Re(E(maltol))(CO)$_3$(H$_2$O)]·C$_2$H$_6$OS (4). U(eq) is defined as one third of the trace of the orthogonalized U^{ij} tensor.

	x	y	z	U(eq)
Re(1)	1658(1)	13310(1)	2549(1)	10(1)
S(1)	9821(5)	9499(4)	2487(4)	23(1)
O(2)	-617(10)	15069(10)	2052(10)	13(2)
O(1)	322(10)	11893(11)	3800(10)	14(2)
O(4)	-4218(12)	14512(13)	3055(12)	23(2)
O(21)	2632(13)	13611(14)	5125(12)	27(2)
O(22)	3244(13)	15602(14)	441(13)	28(2)
O(23)	4676(13)	10480(14)	3301(14)	31(3)
C(22)	2665(15)	14717(16)	1235(15)	16(3)
C(2)	-1660(15)	14401(15)	2642(14)	14(2)
C(23)	3530(16)	11570(18)	3008(17)	22(3)
C(4)	-3703(18)	12921(19)	3947(18)	26(3)
C(1)	-1116(15)	12688(15)	3600(14)	14(2)
C(5)	-2217(16)	11988(18)	4240(16)	20(3)
C(3)	-3183(15)	15265(16)	2403(15)	16(3)
C(21)	2238(15)	13522(17)	4113(16)	17(3)
C(6)	-3905(18)	17025(18)	1400(20)	31(4)
O(3)	721(11)	13092(11)	841(10)	18(2)
O(11)	10709(15)	10377(14)	1286(13)	29(3)
C(20)	10487(19)	7551(18)	2650(20)	32(4)
C(33)	7956(19)	10170(20)	1650(20)	41(5)
C(7)	-5320(20)	17850(20)	1920(20)	36(4)

Table A. 17: Bond lengths [Å] and angles [°] for *fac*-[Re(E(maltol))(CO)$_3$(H$_2$O)]·C$_2$H$_6$OS (4).

_____

Re(1)-C(21)	1.869(14)
Re(1)-C(23)	1.896(14)
Re(1)-C(22)	1.908(14)
Re(1)-O(1)	2.126(9)
Re(1)-O(2)	2.154(9)
Re(1)-O(3)	2.164(9)
S(1)-O(11)	1.516(11)
S(1)-C(33)	1.770(19)
S(1)-C(20)	1.782(16)
O(2)-C(2)	1.328(16)
O(1)-C(1)	1.280(16)
O(4)-C(4)	1.339(19)
O(4)-C(3)	1.380(17)
O(21)-C(21)	1.185(17)
O(22)-C(22)	1.155(17)
O(23)-C(23)	1.172(18)
C(2)-C(3)	1.358(18)
C(2)-C(1)	1.442(17)
C(4)-C(5)	1.34(2)
C(1)-C(5)	1.401(19)
C(3)-C(6)	1.490(19)
C(6)-C(7)	1.51(2)
C(21)-Re(1)-C(23)	88.8(6)
C(21)-Re(1)-C(22)	89.0(6)
C(23)-Re(1)-C(22)	88.5(6)
C(21)-Re(1)-O(1)	96.2(5)
C(23)-Re(1)-O(1)	96.1(5)
C(22)-Re(1)-O(1)	173.1(5)
C(21)-Re(1)-O(2)	95.9(5)
C(23)-Re(1)-O(2)	172.2(5)
C(22)-Re(1)-O(2)	97.7(5)
O(1)-Re(1)-O(2)	77.2(3)

C(21)-Re(1)-O(3)	173.1(5)
C(23)-Re(1)-O(3)	96.0(5)
C(22)-Re(1)-O(3)	96.1(5)
O(1)-Re(1)-O(3)	78.4(4)
O(2)-Re(1)-O(3)	78.8(4)
O(11)-S(1)-C(33)	107.3(9)
O(11)-S(1)-C(20)	104.2(7)
C(33)-S(1)-C(20)	97.5(9)
C(2)-O(2)-Re(1)	112.1(7)
C(1)-O(1)-Re(1)	114.0(8)
C(4)-O(4)-C(3)	119.2(12)
O(22)-C(22)-Re(1)	178.2(13)
O(2)-C(2)-C(3)	122.7(12)
O(2)-C(2)-C(1)	117.3(11)
C(3)-C(2)-C(1)	119.9(12)
O(23)-C(23)-Re(1)	179.0(14)
O(4)-C(4)-C(5)	123.8(14)
O(1)-C(1)-C(5)	123.8(12)
O(1)-C(1)-C(2)	119.0(12)
C(5)-C(1)-C(2)	117.2(12)
C(4)-C(5)-C(1)	119.4(14)
C(2)-C(3)-O(4)	120.4(12)
C(2)-C(3)-C(6)	125.6(13)
O(4)-C(3)-C(6)	113.9(12)
O(21)-C(21)-Re(1)	178.1(13)
C(3)-C(6)-C(7)	115.1(14)

Table A. 18: Anisotropic displacement parameters ($\mathring{A}^2$ x 10^3) for *fac*-[Re(E(maltol))(CO)$_3$(H$_2$O)]·C$_2$H$_6$OS (4). The anisotropic displacement factor exponent takes the form: -2p^2[h^{2}a*^{2}U^{11} + ... + 2 h k a* b* U^{12}]

	U^{11}	U^{22}	U^{33}	U^{23}	U^{13}	U^{12}
Re(1)	9(1)	10(1)	11(1)	-4(1)	1(1)	-4(1)
S(1)	36(2)	20(2)	19(2)	-10(1)	7(1)	-14(2)
O(2)	9(4)	9(4)	14(4)	-2(3)	1(3)	-2(3)
O(1)	11(4)	13(4)	14(4)	-3(4)	1(3)	-5(3)
O(4)	16(5)	22(5)	26(5)	-8(4)	2(4)	-6(4)
O(21)	31(6)	32(6)	23(5)	-17(5)	-5(4)	-10(5)
O(22)	28(6)	33(6)	33(6)	-15(5)	10(5)	-24(5)
O(23)	21(5)	24(6)	39(7)	-16(5)	1(5)	4(4)
C(22)	17(6)	18(6)	14(6)	-6(5)	-3(5)	-6(5)
C(2)	19(6)	10(6)	10(5)	-6(5)	3(5)	-2(5)
C(23)	13(6)	21(7)	26(7)	-9(6)	-1(5)	-4(5)
C(4)	24(5)	26(5)	27(5)	-10(4)	2(4)	-13(4)
C(1)	17(6)	12(6)	7(5)	-1(5)	-2(4)	-3(5)
C(5)	18(6)	22(7)	21(7)	-7(6)	-1(5)	-11(6)
C(3)	14(6)	16(6)	13(6)	-5(5)	-3(5)	0(5)
C(21)	14(6)	19(6)	20(6)	-11(5)	6(5)	-6(5)
C(6)	20(7)	17(7)	31(8)	0(6)	5(6)	4(6)
O(3)	21(5)	17(5)	12(4)	-2(4)	-6(4)	-8(4)
O(11)	46(7)	24(5)	29(6)	-15(5)	16(5)	-23(5)
C(20)	27(8)	12(6)	43(10)	-2(7)	3(7)	-7(6)
C(33)	20(8)	18(8)	59(12)	-6(8)	-2(8)	3(6)
C(7)	28(8)	28(8)	40(10)	-20(8)	2(7)	7(7)

Table A. 19: Hydrogen coordinates (x 10^4) and isotropic displacement parameters ($Å^2$ x 10^3) for *fac*-[Re(E(maltol))(CO)$_3$(H$_2$O)]·C$_2$H$_6$OS (4).

	x	y	z	U(eq)
H(4)	-4415	12435	4389	31
H(5)	-1922	10887	4862	24
H(6A)	-4172	17211	416	38
H(6B)	-3156	17514	1292	38
H(20A)	10547	7645	1674	48
H(20B)	9791	7016	3176	48
H(20C)	11482	6944	3202	48
H(33A)	7730	11217	790	61
H(33B)	7228	10225	2358	61
H(33C)	7899	9440	1339	61
H(7A)	-6167	17632	1739	54
H(7B)	-5539	18989	1387	54
H(7C)	-5147	17467	2976	54

Table A. 20: Hydrogen bonds for *fac*-[Re(E(maltol))(CO)$_3$(H$_2$O)]·C$_2$H$_6$OS (4).

D-H…A	d(D-H) (Å)	d(H…A) (Å)	d(D…A) (Å)	∠ (D-H…A)(˚)
C(5)-H(5)...O(1) [(i)]	0.93	2.41	3.30(2)	160
C(6)-H(6B)...O(2)	0.97	2.60	2.95(2)	101
C(33)-H(33B)...O(23) [(i)]	0.96	2.48	3.37(2)	155

Symmetry codes, transformations used to generate equivalent atoms: (i) 2-x, -y,1-z

Table A. 21: Atomic coordinates (x 10^4) and equivalent isotropic displacement parameters ($Å^2$ x 10^3) for *fac*-[Re(MM(naltol)(CO)$_3$(H$_2$O)]·C$_2$H$_6$OS (5). U(eq) is defined as one third of the trace of the orthogonalized U^{ij} tensor.

	x	y	z	U(eq)
Re(1)	4713(1)	4412(1)	3582(1)	11(1)
Re(2)	1199(1)	4343(1)	1027(1)	11(1)

S(2)	3094(4)	9371(5)	9407(4)	17(1)
C(7B)	6574(15)	619(16)	1455(11)	14(3)
S(1)	2754(5)	9410(6)	5256(5)	36(1)
C(22A)	6507(16)	2721(17)	4070(16)	10(3)
O(3A)	3484(15)	2938(15)	3682(11)	20(3)
O(1A)	3012(17)	4202(18)	5657(15)	18(3)
O(12)	3845(14)	7917(13)	8849(12)	31(3)
C(21A)	5610(20)	5871(19)	3537(17)	23(4)
O(23B)	-891(18)	4113(18)	4154(15)	24(3)
O(2B)	3308(13)	2644(14)	1334(10)	7(2)
O(21A)	6111(17)	6702(18)	3437(16)	23(2)
N(1A)	-1492(16)	6804(19)	5802(16)	18(3)
N(1B)	7427(17)	1870(17)	-1163(16)	15(3)
C(23A)	5994(17)	4577(19)	1591(17)	8(3)
C(2A)	1291(18)	6030(18)	4468(18)	10(3)
C(4B)	7180(17)	2860(20)	-2397(17)	23(4)
C(5B)	5580(20)	3810(20)	-2485(19)	20(3)
C(1A)	1619(19)	5053(19)	5684(16)	21(3)
O(23A)	6697(17)	4686(17)	384(14)	21(3)
O(2A)	2462(14)	6153(16)	3216(13)	18(2)
O(22B)	-1518(18)	7079(18)	118(17)	29(3)
C(49)	3950(30)	10900(20)	7850(20)	46(5)
C(50)	1630(20)	9722(19)	4133(16)	36(4)
C(52)	2220(30)	7890(20)	6620(20)	36(3)
C(3B)	6119(18)	1784(18)	139(15)	18(4)
C(3A)	-327(16)	6980(14)	4525(16)	12(3)
C(6A)	-3195(18)	7820(20)	5735(18)	23(3)
O(21B)	-308(17)	1958(17)	1135(16)	23(2)
O(22A)	7478(16)	1679(18)	4484(16)	27(3)
O(3B)	2479(14)	5785(13)	981(12)	19(3)
O(1B)	2795(16)	4561(16)	-1148(15)	12(2)
C(23B)	-70(20)	4190(20)	2970(20)	24(5)
C(2B)	4650(20)	2670(20)	127(17)	16(4)
C(1B)	4344(18)	3758(16)	-1223(15)	12(3)
C(5A)	240(20)	4990(20)	7016(16)	20(4)

C(21B)	269(16)	2941(19)	1106(17)	12(3)
C(4A)	-1160(20)	5847(19)	7033(15)	22(4)
C(22B)	-450(20)	6030(20)	432(19)	25(4)
C(6B)	9060(20)	1040(20)	-1300(20)	28(4)
O(2)	2076(14)	10801(13)	5764(10)	27(3)
C(90)	4138(19)	9124(18)	10453(14)	33(4)
C(7A)	-604(19)	8065(17)	3204(16)	32(4)

Table A. 22: Bond lengths [Å] and angles [°] for *fac*-[Re(MM(naltol)(CO)$_3$(H$_2$O)]·C$_2$H$_6$OS (5).

_____

Re(1)-C(21A)	1.919(19)
Re(1)-C(23A)	1.928(15)
Re(1)-C(22A)	1.929(12)
Re(1)-O(1A)	2.102(14)
Re(1)-O(3A)	2.150(13)
Re(1)-O(2A)	2.215(12)
Re(2)-C(21B)	1.873(13)
Re(2)-C(22B)	1.877(18)
Re(2)-C(23B)	1.88(2)
Re(2)-O(2B)	2.085(11)
Re(2)-O(1B)	2.146(14)
Re(2)-O(3B)	2.190(12)
S(2)-O(12)	1.541(12)
S(2)-C(90)	1.701(16)
S(2)-C(49)	1.860(19)
C(7B)-C(3B)	1.519(17)
S(1)-O(2)	1.462(12)
S(1)-C(52)	1.68(2)
S(1)-C(50)	1.809(14)
C(22A)-O(22A)	1.148(18)
O(1A)-C(1A)	1.25(2)
C(21A)-O(21A)	1.05(2)
O(23B)-C(23B)	1.16(2)
O(2B)-C(2B)	1.374(18)
N(1A)-C(3A)	1.34(2)

N(1A)-C(4A)	1.36(2)
N(1A)-C(6A)	1.54(2)
N(1B)-C(4B)	1.34(2)
N(1B)-C(6B)	1.41(2)
N(1B)-C(3B)	1.42(2)
C(23A)-O(23A)	1.16(2)
C(2A)-O(2A)	1.324(19)
C(2A)-C(1A)	1.35(2)
C(2A)-C(3A)	1.435(18)
C(4B)-C(5B)	1.45(2)
C(5B)-C(1B)	1.36(2)
C(1A)-C(5A)	1.47(2)
O(22B)-C(22B)	1.17(2)
C(3B)-C(2B)	1.32(2)
C(3A)-C(7A)	1.44(2)
O(21B)-C(21B)	1.273(19)
O(1B)-C(1B)	1.351(18)
C(2B)-C(1B)	1.48(2)
C(5A)-C(4A)	1.26(2)
C(21A)-Re(1)-C(23A)	88.7(7)
C(21A)-Re(1)-C(22A)	89.5(7)
C(23A)-Re(1)-C(22A)	87.5(7)
C(21A)-Re(1)-O(1A)	99.4(7)
C(23A)-Re(1)-O(1A)	170.0(7)
C(22A)-Re(1)-O(1A)	98.4(6)
C(21A)-Re(1)-O(3A)	174.5(7)
C(23A)-Re(1)-O(3A)	94.0(6)
C(22A)-Re(1)-O(3A)	95.4(6)
O(1A)-Re(1)-O(3A)	77.5(5)
C(21A)-Re(1)-O(2A)	96.1(6)
C(23A)-Re(1)-O(2A)	97.2(6)
C(22A)-Re(1)-O(2A)	172.8(6)
O(1A)-Re(1)-O(2A)	76.2(5)
O(3A)-Re(1)-O(2A)	78.8(5)

264

C(21B)-Re(2)-C(22B)	89.8(7)
C(21B)-Re(2)-C(23B)	87.3(8)
C(22B)-Re(2)-C(23B)	90.6(8)
C(21B)-Re(2)-O(2B)	94.9(6)
C(22B)-Re(2)-O(2B)	169.8(6)
C(23B)-Re(2)-O(2B)	98.7(7)
C(21B)-Re(2)-O(1B)	97.3(6)
C(22B)-Re(2)-O(1B)	91.8(6)
C(23B)-Re(2)-O(1B)	174.8(8)
O(2B)-Re(2)-O(1B)	78.6(4)
C(21B)-Re(2)-O(3B)	174.5(6)
C(22B)-Re(2)-O(3B)	95.7(6)
C(23B)-Re(2)-O(3B)	93.1(7)
O(2B)-Re(2)-O(3B)	79.5(5)
O(1B)-Re(2)-O(3B)	82.0(5)
O(12)-S(2)-C(90)	107.0(8)
O(12)-S(2)-C(49)	103.8(8)
C(90)-S(2)-C(49)	96.8(8)
O(2)-S(1)-C(52)	109.6(8)
O(2)-S(1)-C(50)	106.3(8)
C(52)-S(1)-C(50)	101.0(9)
O(22A)-C(22A)-Re(1)	173.7(15)
C(1A)-O(1A)-Re(1)	114.1(11)
O(21A)-C(21A)-Re(1)	176.0(16)
C(2B)-O(2B)-Re(2)	115.0(10)
C(3A)-N(1A)-C(4A)	121.8(14)
C(3A)-N(1A)-C(6A)	113.9(14)
C(4A)-N(1A)-C(6A)	124.2(14)
C(4B)-N(1B)-C(6B)	114.0(14)
C(4B)-N(1B)-C(3B)	120.1(14)
C(6B)-N(1B)-C(3B)	125.8(15)
O(23A)-C(23A)-Re(1)	176.8(15)
O(2A)-C(2A)-C(1A)	120.4(15)
O(2A)-C(2A)-C(3A)	119.4(15)
C(1A)-C(2A)-C(3A)	120.2(16)

N(1B)-C(4B)-C(5B)	122.5(14)
C(1B)-C(5B)-C(4B)	116.8(14)
O(1A)-C(1A)-C(2A)	121.2(15)
O(1A)-C(1A)-C(5A)	122.4(15)
C(2A)-C(1A)-C(5A)	116.3(15)
C(2A)-O(2A)-Re(1)	107.9(10)
C(2B)-C(3B)-N(1B)	119.7(15)
C(2B)-C(3B)-C(7B)	125.8(14)
N(1B)-C(3B)-C(7B)	114.5(13)
N(1A)-C(3A)-C(2A)	118.0(14)
N(1A)-C(3A)-C(7A)	123.8(13)
C(2A)-C(3A)-C(7A)	118.1(14)
C(1B)-O(1B)-Re(2)	112.6(10)
O(23B)-C(23B)-Re(2)	177.7(18)
C(3B)-C(2B)-O(2B)	123.7(15)
C(3B)-C(2B)-C(1B)	121.1(15)
O(2B)-C(2B)-C(1B)	115.2(15)
O(1B)-C(1B)-C(5B)	123.0(13)
O(1B)-C(1B)-C(2B)	117.2(14)
C(5B)-C(1B)-C(2B)	119.5(14)
C(4A)-C(5A)-C(1A)	121.9(15)
O(21B)-C(21B)-Re(2)	177.8(13)
C(5A)-C(4A)-N(1A)	121.5(14)
O(22B)-C(22B)-Re(2)	177.2(17)

Table A. 23: Anisotropic displacement parameters (Å^2 x 10^3) for *fac*-[Re(MM(naltol)(CO)$_3$(H$_2$O)]·C$_2$H$_6$OS (5). The anisotropic displacement factor exponent takes the form: $-2p^2[\,h^2a^{*2}U^{11} + ... + 2\,h\,k\,a^*\,b^*\,U^{12}\,]$

	U^{11}	U^{22}	U^{33}	U^{23}	U^{13}	U^{12}
Re(1)	12(1)	11(1)	12(1)	-2(1)	-4(1)	-5(1)
Re(2)	12(1)	12(1)	11(1)	-3(1)	-4(1)	-5(1)
S(2)	9(1)	15(2)	25(2)	-14(1)	4(1)	-2(1)
C(7B)	12(5)	19(6)	3(4)	6(4)	-6(4)	-3(4)

S(1)	55(2)	26(2)	43(2)	0(2)	-31(2)	-21(2)
C(22A)	4(4)	11(5)	10(5)	1(4)	-6(3)	3(3)
O(3A)	37(6)	27(6)	2(4)	7(4)	-10(4)	-22(5)
O(1A)	23(5)	28(5)	9(4)	-6(3)	-3(3)	-13(4)
O(12)	41(7)	26(6)	36(6)	-14(5)	3(5)	-31(5)
C(21A)	31(8)	10(7)	11(7)	0(5)	-8(6)	10(5)
O(23B)	26(5)	32(6)	20(5)	-12(4)	-7(4)	-7(4)
O(2B)	7(3)	12(4)	-1(3)	2(2)	0(2)	-5(3)
O(21A)	26(4)	24(5)	35(5)	-14(4)	-8(4)	-19(4)
N(1A)	8(6)	29(7)	16(7)	-9(5)	5(5)	-13(5)
N(1B)	20(6)	10(5)	16(7)	-9(5)	-6(5)	2(4)
C(23A)	4(6)	8(7)	5(5)	4(5)	2(4)	-5(5)
C(2A)	8(6)	5(6)	21(8)	-9(5)	-5(5)	2(5)
C(4B)	4(5)	37(8)	28(8)	-21(6)	7(4)	-8(5)
C(5B)	22(6)	21(7)	19(6)	0(5)	-18(5)	-2(5)
C(1A)	20(6)	30(7)	17(5)	-17(5)	12(4)	-21(5)
O(23A)	22(4)	29(6)	11(4)	0(4)	0(3)	-16(4)
O(2A)	12(4)	19(4)	29(5)	-10(4)	-12(3)	0(3)
O(22B)	33(7)	18(7)	37(8)	1(6)	-22(6)	-6(5)
C(49)	108(13)	19(6)	36(7)	27(5)	-52(8)	-43(7)
C(50)	71(8)	18(6)	39(7)	-3(5)	-52(7)	0(5)
C(52)	59(6)	30(8)	32(6)	-7(6)	-17(5)	-24(5)
C(3B)	20(6)	33(8)	3(5)	-4(5)	6(4)	-21(5)
C(3A)	11(5)	3(5)	30(7)	-10(5)	-13(5)	5(4)
C(6A)	10(5)	35(7)	17(4)	-16(4)	-2(3)	5(4)
O(21B)	25(4)	22(5)	34(5)	-12(4)	-11(4)	-12(3)
O(22A)	17(6)	22(8)	31(8)	-9(6)	-9(5)	6(5)
O(3B)	22(5)	18(5)	26(6)	-13(4)	0(4)	-16(4)
O(1B)	11(3)	13(4)	11(4)	0(3)	-9(3)	-1(3)
C(23B)	31(10)	19(9)	35(10)	-11(7)	-21(8)	-5(7)
C(2B)	21(8)	26(8)	5(6)	-3(6)	2(6)	-17(6)
C(1B)	21(6)	7(5)	10(4)	4(3)	-15(4)	-3(4)
C(5A)	29(8)	22(7)	6(5)	-5(5)	6(5)	-18(6)
C(21B)	5(5)	21(8)	19(7)	-10(6)	-5(5)	-6(5)
C(4A)	42(9)	21(7)	4(6)	6(5)	-7(5)	-21(6)

C(22B)	37(8)	26(7)	18(6)	-9(5)	2(5)	-25(6)
C(6B)	22(6)	36(7)	30(6)	-5(5)	-8(5)	-14(5)
O(2)	48(7)	19(5)	8(5)	-2(4)	-8(4)	-7(5)
C(90)	52(7)	28(7)	19(6)	0(5)	2(5)	-31(6)
C(7A)	24(7)	31(8)	53(9)	-33(6)	-6(6)	-3(6)

Table A. 24: Hydrogen coordinates (x 10^4) and isotropic displacement parameters (Å^{2}x 10^3) for *fac*-[Re(MM(naltol)(CO)$_3$(H$_2$O)]·C$_2$H$_6$OS (5).

	x	y	z	U(eq)
H(7B1)	7028	-413	1331	21
H(7B2)	5630	640	2291	21
H(7B3)	7353	893	1575	21
H(4B)	8064	2941	-3230	28
H(5B)	5416	4416	-3362	24
H(49A)	5105	10527	7553	70
H(49B)	3597	11834	8126	70
H(49C)	3588	11112	7069	70
H(50A)	507	9892	4680	54
H(50B)	2007	8817	3802	54
H(50C)	1791	10621	3323	54
H(52A)	2597	7709	7378	53
H(52B)	2679	6974	6288	53
H(52C)	1062	8117	6972	53
H(6A1)	-3979	7539	6656	34
H(6A2)	-3402	7648	5022	34
H(6A3)	-3262	8904	5485	34
H(5A)	402	4285	7872	24
H(4A)	-1988	5828	7908	26
H(6B1)	9402	1286	-729	43
H(6B2)	9705	1318	-2293	43
H(6B3)	9170	-68	-984	43
H(90A)	3912	8291	11316	50

H(90B)	3820	10074	10699	50
H(90C)	5272	8867	9935	50
H(7A1)	409	8178	2480	49
H(7A2)	-1277	9063	3364	49
H(7A3)	-1127	7675	2889	49
H(3)	3020(70)	6280(60)	260(60)	49
H(2)	3140(80)	2280(50)	4390(60)	49
H(1)	3350(60)	2920(70)	3000(30)	49
H(4)	2330(80)	5980(60)	1700(30)	49

Table A. 25: Hydrogen bonds for *fac*-[Re(MM(naltol)(CO)$_3$(H$_2$O)]·C$_2$H$_6$OS (5).

D-H…A	d(D-H) (Å)	d(H…A) (Å)	d(D…A) (Å)	⊾ (D-H…A)(˚)
O3A-H1...O2B	0.80(4)	1.94(5)	2.738(17)	173(6)
O3A-H2...S1 [i]	0.81(6)	2.69(6)	3.373(14)	143(5)
O3A-H2...O2 [i]	0.81(6)	1.86(6)	2.655(17)	167(8)
O3B-H3...S2 [ii]	0.81(6)	2.79(6)	3.380(13)	131(5)
O3B-H3...O12 [ii]	0.81(6)	1.87(6)	2.649(17)	163(6)
O3B-H4...O2A	0.81(5)	1.77(5)	2.565(18)	167(7)
C7B-H7B2...O2B	0.96	2.58	2.97(2)	105
C6A-H6A1...O12 [iii]	0.96	2.42	3.33(2)	157
C4A-H4A...O23A [iv]	0.93	2.39	3.26(2)	155
C4B-H4B...O23B [v]	0.93	2.47	3.30(2)	148
C6A-H6A2...O21A [iii]	0.96	2.51	3.46(3)	170
C6B-H6B1...O21B [vi]	0.95	2.50	3.43(3)	168
C6B-H6B2...O2 [vii]	0.96	2.36	3.24(2)	152
C7A-H7A1...O2A	0.96	2.31	2.77(2)	109
C49-H49C...O2	0.96	2.58	3.48(3)	156
C52-H52A...O12	0.96	2.47	3.39(3)	163

Symmetry codes, transformations used to generate equivalent atoms: (i) x, y, z-1; (ii) x, y-1, z; (iii) 1+x, y, z; (iv) x-1, y, 1+z; (v) x-1, y, z; (vi) 1+x, y, z-1; (vii) 1+x, y-1, z-1

Table A. 26: Atomic coordinates (x 10^4) and equivalent isotropic displacement parameters (Å^2 x 10^3) for *fac*-[Re(MI(naltol)(CO)$_3$(H$_2$O)]·C$_3$H$_6$OS (6). U(eq) is defined as one third of the trace of the orthogonalized U^{ij} tensor.

	x	y	z	U(eq)
C(21)	10092(3)	7700(3)	8800(3)	22(1)
C(1)	7325(2)	6393(2)	4816(2)	14(1)
C(23)	11427(3)	6165(3)	8103(3)	21(1)
C(2)	8846(2)	7108(2)	4815(2)	13(1)
C(22)	8580(3)	4790(3)	8095(3)	20(1)
C(3)	9019(2)	7751(2)	3824(2)	16(1)
C(4)	6244(3)	6958(2)	2787(2)	19(1)
C(10)	5889(3)	7882(3)	7173(3)	22(1)
C(5)	6021(2)	6345(2)	3770(2)	16(1)
C(11)	5760(4)	10415(3)	7570(3)	39(1)
C(6)	7756(3)	8115(3)	1571(3)	24(1)
C(8)	6992(4)	6690(3)	181(3)	37(1)
C(7)	7013(3)	9068(3)	1358(3)	26(1)
C(9)	10633(3)	8563(3)	3864(3)	22(1)
N(1)	7695(2)	7648(2)	2810(2)	18(1)
O(21)	10494(2)	8717(2)	9863(2)	36(1)
O(1)	7222(2)	5836(2)	5785(2)	15(1)
O(23)	12674(2)	6292(2)	8676(2)	32(1)
O(2)	10077(2)	7146(2)	5812(2)	14(1)
O(22)	8088(2)	4087(2)	8705(2)	29(1)
O(3)	8374(2)	4030(2)	5082(2)	15(1)
O(4)	4081(2)	8175(2)	4939(2)	23(1)
Re(1)	9403(1)	6004(1)	7131(1)	12(1)
S(1)	5766(1)	9069(1)	6224(1)	17(1)

Table A. 27: Bond lengths [Å] and angles [°] for *fac*-[Re(MI(naltol)(CO)$_3$(H$_2$O)]·C$_3$H$_6$OS (6).

C(21)-O(21)	1.171(3)
C(21)-Re(1)	1.879(3)

C(1)-O(1)	1.298(2)
C(1)-C(5)	1.403(3)
C(1)-C(2)	1.429(3)
C(23)-O(23)	1.158(3)
C(23)-Re(1)	1.908(3)
C(2)-O(2)	1.332(2)
C(2)-C(3)	1.386(3)
C(22)-O(22)	1.155(3)
C(22)-Re(1)	1.907(2)
C(3)-N(1)	1.370(3)
C(3)-C(9)	1.501(3)
C(4)-N(1)	1.353(3)
C(4)-C(5)	1.370(3)
C(4)-H(4)	0.9300
C(10)-S(1)	1.783(2)
C(10)-H(10A)	0.9600
C(10)-H(10B)	0.9600
C(10)-H(10C)	0.9600
C(5)-H(5)	0.9300
C(11)-S(1)	1.773(3)
C(11)-H(11A)	0.9600
C(11)-H(11B)	0.9600
C(11)-H(11C)	0.9600
C(6)-C(7)	1.503(3)
C(6)-N(1)	1.506(3)
C(6)-C(8)	1.520(4)
C(6)-H(6)	0.9800
C(8)-H(8A)	0.9600
C(8)-H(8B)	0.9600
C(8)-H(8C)	0.9600
C(7)-H(7A)	0.9600
C(7)-H(7B)	0.9600
C(7)-H(7C)	0.9600
C(9)-H(9A)	0.9600
C(9)-H(9B)	0.9600

C(9)-H(9C)	0.9600
O(1)-Re(1)	2.1316(17)
O(2)-Re(1)	2.1318(15)
O(3)-Re(1)	2.1902(17)
O(3)-H(3B)	0.82(4)
O(3)-H(3A)	0.88(4)
O(4)-S(1)	1.5068(17)
O(21)-C(21)-Re(1)	177.4(2)
O(1)-C(1)-C(5)	123.39(18)
O(1)-C(1)-C(2)	118.83(18)
C(5)-C(1)-C(2)	117.78(18)
O(23)-C(23)-Re(1)	178.0(2)
O(2)-C(2)-C(3)	122.05(18)
O(2)-C(2)-C(1)	117.28(17)
C(3)-C(2)-C(1)	120.66(18)
O(22)-C(22)-Re(1)	178.3(2)
N(1)-C(3)-C(2)	118.98(18)
N(1)-C(3)-C(9)	120.30(18)
C(2)-C(3)-C(9)	120.72(18)
N(1)-C(4)-C(5)	122.32(19)
N(1)-C(4)-H(4)	118.8
C(5)-C(4)-H(4)	118.8
S(1)-C(10)-H(10A)	109.5
S(1)-C(10)-H(10B)	109.5
H(10A)-C(10)-H(10B)	109.5
S(1)-C(10)-H(10C)	109.5
H(10A)-C(10)-H(10C)	109.5
H(10B)-C(10)-H(10C)	109.5
C(4)-C(5)-C(1)	119.23(19)
C(4)-C(5)-H(5)	120.4
C(1)-C(5)-H(5)	120.4
S(1)-C(11)-H(11A)	109.5
S(1)-C(11)-H(11B)	109.5
H(11A)-C(11)-H(11B)	109.5

S(1)-C(11)-H(11C)	109.5
H(11A)-C(11)-H(11C)	109.5
H(11B)-C(11)-H(11C)	109.5
C(7)-C(6)-N(1)	112.31(19)
C(7)-C(6)-C(8)	113.1(2)
N(1)-C(6)-C(8)	109.01(19)
C(7)-C(6)-H(6)	107.4
N(1)-C(6)-H(6)	107.4
C(8)-C(6)-H(6)	107.4
C(6)-C(8)-H(8A)	109.5
C(6)-C(8)-H(8B)	109.5
H(8A)-C(8)-H(8B)	109.5
C(6)-C(8)-H(8C)	109.5
H(8A)-C(8)-H(8C)	109.5
H(8B)-C(8)-H(8C)	109.5
C(6)-C(7)-H(7A)	109.5
C(6)-C(7)-H(7B)	109.5
H(7A)-C(7)-H(7B)	109.5
C(6)-C(7)-H(7C)	109.5
H(7A)-C(7)-H(7C)	109.5
H(7B)-C(7)-H(7C)	109.5
C(3)-C(9)-H(9A)	109.5
C(3)-C(9)-H(9B)	109.5
H(9A)-C(9)-H(9B)	109.5
C(3)-C(9)-H(9C)	109.5
H(9A)-C(9)-H(9C)	109.5
H(9B)-C(9)-H(9C)	109.5
C(4)-N(1)-C(3)	120.99(17)
C(4)-N(1)-C(6)	117.68(18)
C(3)-N(1)-C(6)	120.88(17)
C(1)-O(1)-Re(1)	113.38(12)
C(2)-O(2)-Re(1)	112.93(12)
Re(1)-O(3)-H(3B)	106(2)
Re(1)-O(3)-H(3A)	116(2)
H(3B)-O(3)-H(3A)	114(3)

C(21)-Re(1)-C(22)	85.84(11)
C(21)-Re(1)-C(23)	88.64(10)
C(22)-Re(1)-C(23)	89.00(10)
C(21)-Re(1)-O(1)	96.35(9)
C(22)-Re(1)-O(1)	98.05(8)
C(23)-Re(1)-O(1)	171.62(7)
C(21)-Re(1)-O(2)	99.66(9)
C(22)-Re(1)-O(2)	173.17(7)
C(23)-Re(1)-O(2)	95.15(8)
O(1)-Re(1)-O(2)	77.41(6)
C(21)-Re(1)-O(3)	174.16(8)
C(22)-Re(1)-O(3)	94.43(9)
C(23)-Re(1)-O(3)	97.20(9)
O(1)-Re(1)-O(3)	77.83(6)
O(2)-Re(1)-O(3)	79.68(7)
O(4)-S(1)-C(11)	105.37(13)
O(4)-S(1)-C(10)	106.97(11)
C(11)-S(1)-C(10)	97.33(12)

Table A. 28: Anisotropic displacement parameters ($Å^2$ x 10^3) for *fac*-[Re(MI(naltol)(CO)$_3$(H$_2$O)]·C$_3$H$_6$OS (6). The anisotropic displacement factor exponent takes the form: $-2p^2[\, h^2a^{*2}U^{11} + ... + 2\, h\, k\, a^*\, b^*\, U^{12}\,]$

	U^{11}	U^{22}	U^{33}	U^{23}	U^{13}	U^{12}
C(21)	17(1)	22(1)	23(1)	8(1)	11(1)	6(1)
C(1)	14(1)	13(1)	16(1)	6(1)	9(1)	7(1)
C(23)	20(1)	26(1)	18(1)	10(1)	11(1)	10(1)
C(2)	11(1)	13(1)	17(1)	6(1)	7(1)	7(1)
C(22)	18(1)	20(1)	17(1)	6(1)	8(1)	7(1)
C(3)	12(1)	18(1)	21(1)	10(1)	9(1)	7(1)
C(4)	13(1)	24(1)	22(1)	13(1)	8(1)	11(1)
C(10)	25(1)	23(1)	20(1)	11(1)	10(1)	14(1)
C(5)	12(1)	19(1)	20(1)	8(1)	9(1)	8(1)
C(11)	66(2)	28(1)	28(1)	11(1)	19(1)	32(1)

C(6)	20(1)	36(1)	32(1)	26(1)	18(1)	16(1)
C(8)	67(2)	49(2)	37(2)	33(1)	40(2)	46(2)
C(7)	31(1)	20(1)	24(1)	12(1)	9(1)	11(1)
C(9)	14(1)	28(1)	31(1)	20(1)	14(1)	11(1)
N(1)	14(1)	24(1)	21(1)	15(1)	10(1)	10(1)
O(21)	36(1)	27(1)	28(1)	-3(1)	17(1)	7(1)
O(1)	13(1)	18(1)	18(1)	10(1)	9(1)	9(1)
O(23)	19(1)	51(1)	28(1)	21(1)	9(1)	21(1)
O(2)	11(1)	17(1)	16(1)	9(1)	8(1)	7(1)
O(22)	31(1)	31(1)	22(1)	15(1)	15(1)	9(1)
O(3)	14(1)	15(1)	17(1)	5(1)	9(1)	7(1)
O(4)	14(1)	22(1)	23(1)	11(1)	4(1)	4(1)
Re(1)	11(1)	14(1)	11(1)	5(1)	6(1)	6(1)
S(1)	13(1)	17(1)	19(1)	9(1)	8(1)	5(1)

Table A. 29: Hydrogen coordinates (x 10^4) and isotropic displacement parameters (Å^2 x 10^3) for *fac*-[Re(MI(naltol)(CO)$_3$(H$_2$O)]·C$_3$H$_6$OS (6).

	x	y	z	U(eq)
H(4)	5366	6897	2078	23
H(10A)	5037	7574	7441	32
H(10B)	6919	8444	8047	32
H(10C)	5776	6989	6541	32
H(5)	5016	5903	3745	20
H(11A)	5630	11141	7212	58
H(11B)	6767	10945	8465	58
H(11C)	4881	9888	7761	58
H(6)	8901	8750	1839	29
H(8A)	7429	6071	407	55
H(8B)	7223	6987	-553	55
H(8C)	5840	6111	-187	55
H(7A)	5867	8447	1000	39

H(7B)	7209	9455	655	39
H(7C)	7490	9911	2283	39
H(9A)	10569	8018	2964	33
H(9B)	11440	8605	4686	33
H(9C)	10921	9587	3969	33
H(3B)	7570(50)	3340(40)	5020(40)	52(10)
H(3A)	9050(40)	3760(40)	4980(40)	51(10)

Table A. 30: Hydrogen bonds for *fac*-[Re(MI(naltol)(CO)$_3$(H$_2$O)]·C$_3$H$_6$OS (6).

D-H…A	d(D-H) (Å)	d(H…A) (Å)	d(D…A) (Å)	Ь (D-H…A)(˚)
O3-H3A...O2 [(i)]	0.88(5)	1.81(4)	2.656(3)	162(3)
O3-H3B...O4 [(ii)]	0.81(5)	1.81(5)	2.621(3)	174(5)
C5-H5...O1 [(ii)]	0.93	2.56	3.436(3)	156
C9-H9B...O2	0.96	2.42	2.865(4)	108
C10-H10C...O1	0.96	2.48	3.318(4)	146
C11-H11A…O4[(iii)]	0.96	2.60	3.326(4)	133

Symmetry codes, transformations used to generate equivalent atoms: (i) -x, 1-y, 1-z; (ii) 1-x, 1-y, 1-z; (iii) 1-x, -y, -1-z;

Table A. 31: Atomic coordinates (x 10^4) and equivalent isotropic displacement parameters (Å^2 x 10^3) for *fac*-[Re(MI(naltol)(CO)$_3$(H$_2$O)]·C$_3$H$_6$O (7). U(eq) is defined as one third of the trace of the orthogonalized U^{ij} tensor.

	x	y	z	U(eq)
C(1)	5831(4)	7099(4)	4179(3)	13(1)
C(2)	6553(4)	8558(4)	3828(3)	13(1)
C(3)	5985(4)	8649(4)	2525(3)	13(1)
C(4)	4019(4)	5904(4)	1891(4)	18(1)
C(5)	4547(4)	5759(4)	3162(4)	16(1)
C(6)	4086(4)	7318(4)	123(3)	19(1)
C(7)	2256(5)	6367(5)	-452(4)	28(1)
C(8)	4860(6)	6779(5)	-710(4)	32(1)
C(9)	6748(4)	10172(4)	2139(4)	19(1)
C(21)	7442(4)	9920(4)	7635(4)	21(1)
C(23)	10399(4)	11237(4)	7599(3)	17(1)
C(22)	8991(4)	8495(4)	8195(4)	20(1)
C(50)	2694(5)	5895(5)	5661(4)	27(1)

C(51)	1515(4)	5450(4)	4280(4)	20(1)
C(52)	1667(5)	6748(5)	3640(5)	32(1)
N(1)	4681(3)	7298(3)	1574(3)	15(1)
O(1)	6373(3)	7070(3)	5424(2)	16(1)
O(2)	7806(3)	9814(3)	4823(2)	14(1)
O(3)	9435(3)	8313(3)	5441(2)	15(1)
O(11)	454(3)	4084(3)	3694(3)	24(1)
O(21)	6839(4)	10338(4)	8251(3)	35(1)
O(23)	11561(3)	12454(3)	8150(3)	26(1)
O(22)	9291(4)	8036(3)	9111(3)	33(1)
Re(1)	8457(1)	9239(1)	6681(1)	12(1)

Table A. 32: Bond lengths [Å] and angles [°] for *fac*-[Re(MI(naltol)(CO)$_3$(H$_2$O)]·C$_3$H$_6$O (7).

_____

C(1)-O(1)#1	1.302(4)
C(1)-O(1)	1.302(4)
C(1)-C(5)	1.402(5)
C(1)-C(2)	1.427(4)
C(2)-O(2)	1.348(4)
C(2)-C(3)	1.384(4)
C(3)-N(1)	1.383(4)
C(3)-C(9)	1.501(4)
C(4)-N(1)	1.353(4)
C(4)-C(5)	1.368(5)
C(4)-H(4)	0.9300
C(5)-H(5)	0.9300
C(6)-N(1)	1.505(4)
C(6)-C(7)	1.520(5)
C(6)-C(8)	1.521(5)
C(6)-H(6)	0.9800
C(7)-H(7A)	0.9600
C(7)-H(7B)	0.9600
C(7)-H(7C)	0.9600
C(8)-H(8A)	0.9600
C(8)-H(8B)	0.9600

C(8)-H(8C)	0.9600
C(9)-H(9A)	0.9600
C(9)-H(9B)	0.9600
C(9)-H(9C)	0.9600
C(21)-O(21)	1.160(4)
C(21)-Re(1)	1.888(4)
C(23)-O(23)	1.155(4)
C(23)-Re(1)	1.912(4)
C(22)-O(22)	1.152(4)
C(22)-Re(1)	1.908(4)
C(50)-C(51)	1.496(5)
C(50)-H(50A)	0.9600
C(50)-H(50B)	0.9600
C(50)-H(50C)	0.9600
C(51)-O(11)	1.220(4)
C(51)-C(52)	1.498(5)
C(52)-H(52A)	0.9600
C(52)-H(52B)	0.9600
C(52)-H(52C)	0.9600
O(1)-O(1)#1	0.000(9)
O(1)-Re(1)	2.124(2)
O(2)-Re(1)	2.142(2)
O(3)-Re(1)	2.191(2)
O(3)-H(3A)	0.97(5)
O(3)-H(3B)	1.00(5)
Re(1)-O(1)#1	2.124(2)
O(1)#1-C(1)-O(1)	0.0(2)
O(1)#1-C(1)-C(5)	122.9(3)
O(1)-C(1)-C(5)	122.9(3)
O(1)#1-C(1)-C(2)	119.0(3)
O(1)-C(1)-C(2)	119.0(3)
C(5)-C(1)-C(2)	118.1(3)
O(2)-C(2)-C(3)	122.7(3)
O(2)-C(2)-C(1)	116.4(3)

C(3)-C(2)-C(1)	120.9(3)
N(1)-C(3)-C(2)	118.6(3)
N(1)-C(3)-C(9)	120.1(3)
C(2)-C(3)-C(9)	121.3(3)
N(1)-C(4)-C(5)	122.5(3)
N(1)-C(4)-H(4)	118.7
C(5)-C(4)-H(4)	118.7
C(4)-C(5)-C(1)	119.1(3)
C(4)-C(5)-H(5)	120.5
C(1)-C(5)-H(5)	120.5
N(1)-C(6)-C(7)	111.5(3)
N(1)-C(6)-C(8)	109.1(3)
C(7)-C(6)-C(8)	113.3(3)
N(1)-C(6)-H(6)	107.6
C(7)-C(6)-H(6)	107.6
C(8)-C(6)-H(6)	107.6
C(6)-C(7)-H(7A)	109.5
C(6)-C(7)-H(7B)	109.5
H(7A)-C(7)-H(7B)	109.5
C(6)-C(7)-H(7C)	109.5
H(7A)-C(7)-H(7C)	109.5
H(7B)-C(7)-H(7C)	109.5
C(6)-C(8)-H(8A)	109.5
C(6)-C(8)-H(8B)	109.5
H(8A)-C(8)-H(8B)	109.5
C(6)-C(8)-H(8C)	109.5
H(8A)-C(8)-H(8C)	109.5
H(8B)-C(8)-H(8C)	109.5
C(3)-C(9)-H(9A)	109.5
C(3)-C(9)-H(9B)	109.5
H(9A)-C(9)-H(9B)	109.5
C(3)-C(9)-H(9C)	109.5
H(9A)-C(9)-H(9C)	109.5
H(9B)-C(9)-H(9C)	109.5
O(21)-C(21)-Re(1)	178.3(3)

O(23)-C(23)-Re(1)	179.0(3)
O(22)-C(22)-Re(1)	179.0(3)
C(51)-C(50)-H(50A)	109.5
C(51)-C(50)-H(50B)	109.5
H(50A)-C(50)-H(50B)	109.5
C(51)-C(50)-H(50C)	109.5
H(50A)-C(50)-H(50C)	109.5
H(50B)-C(50)-H(50C)	109.5
O(11)-C(51)-C(50)	121.6(3)
O(11)-C(51)-C(52)	120.8(3)
C(50)-C(51)-C(52)	117.6(3)
C(51)-C(52)-H(52A)	109.5
C(51)-C(52)-H(52B)	109.5
H(52A)-C(52)-H(52B)	109.5
C(51)-C(52)-H(52C)	109.5
H(52A)-C(52)-H(52C)	109.5
H(52B)-C(52)-H(52C)	109.5
C(4)-N(1)-C(3)	120.8(3)
C(4)-N(1)-C(6)	118.5(3)
C(3)-N(1)-C(6)	120.4(3)
O(1)#1-O(1)-C(1)	0(10)
O(1)#1-O(1)-Re(1)	0(2)
C(1)-O(1)-Re(1)	114.0(2)
C(2)-O(2)-Re(1)	113.06(19)
Re(1)-O(3)-H(3A)	115(3)
Re(1)-O(3)-H(3B)	120(3)
H(3A)-O(3)-H(3B)	105(4)
C(21)-Re(1)-C(22)	87.23(16)
C(21)-Re(1)-C(23)	87.17(15)
C(22)-Re(1)-C(23)	87.99(15)
C(21)-Re(1)-O(1)#1	97.92(13)
C(22)-Re(1)-O(1)#1	97.73(13)
C(23)-Re(1)-O(1)#1	172.50(12)
C(21)-Re(1)-O(1)	97.92(13)
C(22)-Re(1)-O(1)	97.73(13)

C(23)-Re(1)-O(1)	172.50(12)
O(1)#1-Re(1)-O(1)	0.0(2)
C(21)-Re(1)-O(2)	98.41(13)
C(22)-Re(1)-O(2)	172.81(12)
C(23)-Re(1)-O(2)	96.71(12)
O(1)#1-Re(1)-O(2)	77.15(9)
O(1)-Re(1)-O(2)	77.15(9)
C(21)-Re(1)-O(3)	175.16(13)
C(22)-Re(1)-O(3)	94.96(13)
C(23)-Re(1)-O(3)	97.21(12)
O(1)#1-Re(1)-O(3)	77.53(9)
O(1)-Re(1)-O(3)	77.53(9)
O(2)-Re(1)-O(3)	79.08(9)

_____

Symmetry transformations used to generate equivalent atoms:

#1 x,y,z

Table A. 33: Anisotropic displacement parameters ($Å^2$ x 10^3) for *fac*-[Re(MI(naltol)(CO)$_3$(H$_2$O)]·C$_3$H$_6$O (7). The anisotropic displacement factor exponent takes the form: -2p^2[h^{2}a*^{2}U^{11} + ... + 2 h k a* b* U^{12}]

_____

	U^{11}	U^{22}	U^{33}	U^{23}	U^{13}	U^{12}
C(1)	13(1)	14(1)	14(2)	5(1)	5(1)	8(1)
C(2)	13(1)	13(1)	12(2)	3(1)	4(1)	7(1)
C(3)	14(2)	11(1)	13(2)	4(1)	3(1)	6(1)
C(4)	19(2)	11(1)	16(2)	2(1)	1(1)	6(1)
C(5)	16(2)	11(1)	20(2)	7(1)	7(1)	5(1)
C(6)	21(2)	18(2)	13(2)	7(1)	-1(1)	9(1)
C(7)	26(2)	27(2)	22(2)	2(2)	-3(2)	13(2)
C(8)	39(2)	39(2)	14(2)	5(2)	4(2)	21(2)
C(9)	17(2)	16(2)	19(2)	8(1)	1(1)	7(1)
C(21)	21(2)	20(2)	21(2)	5(1)	8(1)	10(2)
C(23)	17(2)	20(2)	16(2)	6(1)	6(1)	10(1)
C(22)	21(2)	19(2)	16(2)	3(1)	5(1)	9(1)

C(50)	25(2)	29(2)	23(2)	1(2)	4(2)	15(2)
C(51)	20(2)	22(2)	22(2)	5(1)	7(1)	15(2)
C(52)	38(2)	18(2)	36(2)	8(2)	9(2)	13(2)
N(1)	18(1)	14(1)	11(1)	4(1)	0(1)	9(1)
O(1)	16(1)	14(1)	13(1)	6(1)	3(1)	5(1)
O(2)	15(1)	12(1)	13(1)	5(1)	3(1)	7(1)
O(3)	16(1)	14(1)	17(1)	7(1)	7(1)	9(1)
O(11)	25(1)	17(1)	26(1)	6(1)	3(1)	11(1)
O(21)	35(2)	39(2)	40(2)	4(1)	22(1)	23(1)
O(23)	22(1)	19(1)	24(1)	0(1)	4(1)	4(1)
O(22)	44(2)	33(2)	18(1)	14(1)	4(1)	19(1)
Re(1)	12(1)	12(1)	10(1)	4(1)	4(1)	6(1)

Table A. 34: Hydrogen coordinates (x 10^4) and isotropic displacement parameters (Å^{2}x 10^3) for *fac*-[Re(MI(naltol)(CO)$_3$(H$_2$O)]·C$_3$H$_6$O (7).

_____

	x	y	z	U(eq)
H(4)	3172	5010	1218	21
H(5)	4061	4785	3350	20
H(6)	4457	8411	119	22
H(7A)	1840	6766	111	42
H(7B)	1857	5284	-474	42
H(7C)	1915	6451	-1359	42
H(8A)	6011	7425	-301	48
H(8B)	4551	6867	-1620	48
H(8C)	4505	5703	-736	48
H(9A)	7182	10073	1439	28
H(9B)	7599	10995	2921	28
H(9C)	5952	10424	1810	28
H(50A)	2466	4965	5957	40
H(50B)	2604	6584	6290	40
H(50C)	3767	6422	5621	40
H(52A)	846	6311	2763	48

H(52B)	2709	7306	3539	48
H(52C)	1543	7459	4209	48
H(3A)	9480(60)	7430(60)	5660(50)	39(13)
H(3B)	10500(60)	9040(50)	5350(50)	27(11)

Table A. 35: Hydrogen bonds for *fac*-[Re(MI(naltol)(CO)$_3$(H$_2$O)]·C$_3$H$_6$O (7).

D-H…A	d(D-H) (Å)	d(H…A) (Å)	d(D…A) (Å)	⊾ (D-H…A)(˚)
O3-H3A...O11	0.96(6)	1.78(6)	2.727(4)	171(4)
O3-H3B...O2 (i)	0.99(6)	1.60(6)	2.595(4)	178(8)
C5-H5...O1 (ii)	0.93	2.31	3.199(4)	159
C9-H9B...O2	0.96	2.45	2.897(5)	108
C9-H9C...O21 (iii)	0.96	2.51	3.316(6)	141
C50-H50C…O1 (iv)	0.96	2.45	3.387(7)	165
C52-H52C…O2 (v)	0.96	2.53	3.401(6)	151

Symmetry codes, transformations used to generate equivalent atoms: (i) -x+2, -y+2, -z+1; (ii) –x+1, -y+1, -z+1; (iii) –x+1, -y+2, -z+1; (iv) x, y, z; (v) –x+1, -y+2, -z+1;

Table A. 36: Atomic coordinates (x 10^4) and equivalent isotropic displacement parameters (Å^2 x 10^3) for *fac*-[Re(El(naltol)(CO)$_3$(H$_2$O)]·C$_3$H$_6$OS (8). U(eq) is defined as one third of the trace of the orthogonalized U^{ij} tensor.

	x	y	z	U(eq)
Re(01)	5725(1)	591(1)	2883(1)	7(1)
S(1)	11357(1)	2027(1)	14048(1)	18(1)
O(3)	4358(3)	769(2)	4444(3)	11(1)
C(34)	10183(6)	2294(3)	12642(5)	32(1)
O(1)	6508(3)	1572(1)	3671(3)	10(1)
O(2)	7137(3)	260(1)	4541(3)	9(1)
O(23)	4540(4)	-877(2)	2139(4)	27(1)
O(22)	3691(3)	1189(2)	635(3)	20(1)
C(3)	8858(4)	708(2)	6203(4)	9(1)
O(21)	7776(4)	412(2)	829(4)	27(1)
N(1)	9446(4)	1293(2)	6858(4)	10(1)
C(7)	11965(4)	1536(3)	7544(4)	20(1)
C(22)	4435(4)	963(2)	1495(4)	11(1)
C(23)	4993(4)	-322(2)	2414(4)	13(1)
C(5)	8009(4)	2072(2)	5455(4)	12(1)

C(21)	7003(5)	479(2)	1613(5)	16(1)
C(6)	10617(4)	1219(2)	7956(4)	12(1)
C(9)	9344(4)	-20(2)	6592(4)	12(1)
C(8)	10223(5)	1543(2)	9222(4)	18(1)
C(4)	9001(4)	1948(2)	6510(4)	12(1)
C(1)	7399(4)	1498(2)	4730(4)	9(1)
C(10)	8788(5)	-274(2)	7859(4)	18(1)
C(2)	7792(4)	805(2)	5184(4)	8(1)
C(32)	11601(5)	2875(3)	14804(5)	24(1)
O(31)	12738(4)	1845(2)	13558(4)	30(1)

Table A. 37: Bond lengths [Å] and angles [°] for *fac*-[Re(El(naltol)(CO)$_3$(H$_2$O)]·C$_3$H$_6$OS (8).

_____

Re(01)-C(21)	1.895(5)
Re(01)-C(22)	1.909(4)
Re(01)-C(23)	1.909(4)
Re(01)-O(1)	2.131(3)
Re(01)-O(2)	2.139(3)
Re(01)-O(3)	2.203(3)
S(1)-O(31)	1.506(4)
S(1)-C(32)	1.789(5)
S(1)-C(34)	1.794(5)
O(3)-H(33)	0.71(6)
O(3)-H(31)	1.02(8)
C(34)-H(34A)	0.9600
C(34)-H(34B)	0.9600
C(34)-H(34C)	0.9600
O(1)-C(1)	1.308(5)
O(2)-C(2)	1.342(5)
O(23)-C(23)	1.160(6)
O(22)-C(22)	1.150(5)
C(3)-N(1)	1.381(5)
C(3)-C(2)	1.386(5)
C(3)-C(9)	1.498(5)
O(21)-C(21)	1.158(6)

N(1)-C(4)	1.348(5)
N(1)-C(6)	1.501(5)
C(7)-C(6)	1.525(6)
C(7)-H(7A)	0.9600
C(7)-H(7B)	0.9600
C(7)-H(7C)	0.9600
C(5)-C(4)	1.375(5)
C(5)-C(1)	1.406(5)
C(5)-H(5)	0.9300
C(6)-C(8)	1.520(6)
C(6)-H(6)	0.9800
C(9)-C(10)	1.533(6)
C(9)-H(9A)	0.9700
C(9)-H(9B)	0.9700
C(8)-H(8A)	0.9600
C(8)-H(8B)	0.9600
C(8)-H(8C)	0.9600
C(4)-H(4)	0.9300
C(1)-C(2)	1.431(5)
C(10)-H(10A)	0.9600
C(10)-H(10B)	0.9600
C(10)-H(10C)	0.9600
C(32)-H(32A)	0.9600
C(32)-H(32B)	0.9600
C(32)-H(32C)	0.9600
C(21)-Re(01)-C(22)	86.76(18)
C(21)-Re(01)-C(23)	88.46(19)
C(22)-Re(01)-C(23)	87.72(17)
C(21)-Re(01)-O(1)	97.50(16)
C(22)-Re(01)-O(1)	97.36(14)
C(23)-Re(01)-O(1)	172.35(14)
C(21)-Re(01)-O(2)	96.48(16)
C(22)-Re(01)-O(2)	174.69(14)
C(23)-Re(01)-O(2)	96.55(14)

O(1)-Re(01)-O(2)	78.07(10)
C(21)-Re(01)-O(3)	175.78(16)
C(22)-Re(01)-O(3)	95.49(15)
C(23)-Re(01)-O(3)	95.19(15)
O(1)-Re(01)-O(3)	78.69(12)
O(2)-Re(01)-O(3)	81.02(12)
O(31)-S(1)-C(32)	105.9(2)
O(31)-S(1)-C(34)	106.9(2)
C(32)-S(1)-C(34)	97.6(3)
Re(01)-O(3)-H(33)	109(5)
Re(01)-O(3)-H(31)	114(5)
H(33)-O(3)-H(31)	96(7)
S(1)-C(34)-H(34A)	109.5
S(1)-C(34)-H(34B)	109.5
H(34A)-C(34)-H(34B)	109.5
S(1)-C(34)-H(34C)	109.5
H(34A)-C(34)-H(34C)	109.5
H(34B)-C(34)-H(34C)	109.5
C(1)-O(1)-Re(01)	112.8(2)
C(2)-O(2)-Re(01)	112.4(2)
N(1)-C(3)-C(2)	118.9(4)
N(1)-C(3)-C(9)	121.0(4)
C(2)-C(3)-C(9)	120.1(4)
C(4)-N(1)-C(3)	120.8(3)
C(4)-N(1)-C(6)	118.1(3)
C(3)-N(1)-C(6)	121.1(3)
C(6)-C(7)-H(7A)	109.5
C(6)-C(7)-H(7B)	109.5
H(7A)-C(7)-H(7B)	109.5
C(6)-C(7)-H(7C)	109.5
H(7A)-C(7)-H(7C)	109.5
H(7B)-C(7)-H(7C)	109.5
O(22)-C(22)-Re(01)	177.9(3)
O(23)-C(23)-Re(01)	179.3(4)
C(4)-C(5)-C(1)	119.3(4)

C(4)-C(5)-H(5)	120.3
C(1)-C(5)-H(5)	120.3
O(21)-C(21)-Re(01)	179.5(4)
N(1)-C(6)-C(8)	111.3(3)
N(1)-C(6)-C(7)	109.8(3)
C(8)-C(6)-C(7)	112.0(4)
N(1)-C(6)-H(6)	107.8
C(8)-C(6)-H(6)	107.8
C(7)-C(6)-H(6)	107.8
C(3)-C(9)-C(10)	112.8(4)
C(3)-C(9)-H(9A)	109.0
C(10)-C(9)-H(9A)	109.0
C(3)-C(9)-H(9B)	109.0
C(10)-C(9)-H(9B)	109.0
H(9A)-C(9)-H(9B)	107.8
C(6)-C(8)-H(8A)	109.5
C(6)-C(8)-H(8B)	109.5
H(8A)-C(8)-H(8B)	109.5
C(6)-C(8)-H(8C)	109.5
H(8A)-C(8)-H(8C)	109.5
H(8B)-C(8)-H(8C)	109.5
N(1)-C(4)-C(5)	122.3(4)
N(1)-C(4)-H(4)	118.8
C(5)-C(4)-H(4)	118.8
O(1)-C(1)-C(5)	123.1(4)
O(1)-C(1)-C(2)	119.3(3)
C(5)-C(1)-C(2)	117.5(3)
C(9)-C(10)-H(10A)	109.5
C(9)-C(10)-H(10B)	109.5
H(10A)-C(10)-H(10B)	109.5
C(9)-C(10)-H(10C)	109.5
H(10A)-C(10)-H(10C)	109.5
H(10B)-C(10)-H(10C)	109.5
O(2)-C(2)-C(3)	122.0(4)
O(2)-C(2)-C(1)	117.3(3)

C(3)-C(2)-C(1)	120.6(4)
S(1)-C(32)-H(32A)	109.5
S(1)-C(32)-H(32B)	109.5
H(32A)-C(32)-H(32B)	109.5
S(1)-C(32)-H(32C)	109.5
H(32A)-C(32)-H(32C)	109.5
H(32B)-C(32)-H(32C)	109.5

Table A. 38: Anisotropic displacement parameters (Å^{2}x 10^3) for *fac*-[Re(El(naltol)(CO)$_3$(H$_2$O)]·C$_3$H$_6$OS (8). The anisotropic displacement factor exponent takes the form: -2p^2[h^{2}a*^{2}U^{11} + ... + 2 h k a* b* U^{12}]

	U^{11}	U^{22}	U^{33}	U^{23}	U^{13}	U^{12}
Re(01)	7(1)	7(1)	7(1)	1(1)	-1(1)	0(1)
S(1)	20(1)	16(1)	19(1)	3(1)	5(1)	7(1)
O(3)	10(1)	10(1)	13(1)	3(1)	3(1)	2(1)
C(34)	30(3)	38(3)	25(3)	-2(2)	-6(2)	19(2)
O(1)	11(1)	7(1)	11(1)	3(1)	-5(1)	-1(1)
O(2)	9(1)	8(1)	9(1)	2(1)	-4(1)	-1(1)
O(23)	29(2)	16(2)	35(2)	-7(1)	-4(2)	-4(1)
O(22)	18(2)	25(2)	15(2)	8(1)	-5(1)	2(1)
C(3)	8(2)	9(2)	10(2)	-1(1)	1(1)	0(1)
O(21)	22(2)	40(2)	19(2)	4(2)	11(1)	6(2)
N(1)	10(2)	11(2)	10(1)	1(1)	-2(1)	1(1)
C(7)	10(2)	34(2)	17(2)	4(2)	-2(2)	-3(2)
C(22)	10(2)	12(2)	13(2)	2(1)	4(1)	-2(1)
C(23)	14(2)	12(2)	14(2)	0(2)	-2(1)	1(2)
C(5)	12(2)	7(2)	16(2)	2(1)	-2(1)	1(1)
C(21)	13(2)	16(2)	17(2)	5(2)	-1(2)	3(2)
C(6)	11(2)	10(2)	13(2)	1(1)	-5(2)	-1(1)
C(9)	14(2)	8(2)	11(2)	3(1)	-3(1)	2(1)
C(8)	15(2)	26(2)	11(2)	1(2)	-1(2)	-1(2)
C(4)	14(2)	9(2)	13(2)	-1(1)	-3(2)	-1(1)
C(1)	5(2)	12(2)	10(2)	1(1)	-1(1)	0(1)

C(10)	17(2)	15(2)	21(2)	9(2)	1(2)	-3(2)
C(2)	9(2)	7(2)	8(2)	0(1)	1(1)	-1(1)
C(32)	24(2)	19(2)	29(3)	0(2)	1(2)	2(2)
O(31)	30(2)	23(2)	41(2)	13(2)	18(2)	17(2)

Table A. 39: Hydrogen coordinates (x 10^4) and isotropic displacement parameters (Å^2 x 10^3) for *fac*-[Re(El(naltol)(CO)$_3$(H$_2$O)]·C$_3$H$_6$OS (8).

_____

	x	y	z	U(eq)
H(34A)	10629	2647	12162	48
H(34B)	9338	2483	12928	48
H(34C)	9953	1893	12085	48
H(7A)	12159	1330	6727	30
H(7B)	12733	1441	8210	30
H(7C)	11852	2036	7437	30
H(5)	7744	2531	5223	14
H(6)	10781	714	8113	14
H(9A)	10364	-28	6714	14
H(9B)	9032	-344	5884	14
H(8A)	10140	2045	9119	26
H(8B)	10940	1438	9930	26
H(8C)	9342	1352	9418	26
H(4)	9379	2329	7002	15
H(10A)	9187	9	8585	27
H(10B)	9048	-758	8015	27
H(10C)	7782	-232	7769	27
H(32A)	12271	2839	15574	37
H(32B)	10720	3041	15050	37
H(32C)	11943	3199	14195	37
H(33)	3840(60)	1020(30)	4230(60)	19(15)
H(31)	3680(90)	370(40)	4550(80)	50(20)

Table A. 40: Torsion angles [°] for *fac*-[Re(El(naltol)(CO)$_3$(H$_2$O)]·C$_3$H$_6$OS (8).

C(2)-C(3)-N(1)-C(4)	-0.5(6)
C(9)-C(3)-N(1)-C(4)	-179.7(4)
C(2)-C(3)-N(1)-C(6)	-179.1(4)
C(9)-C(3)-N(1)-C(6)	1.7(6)
C(4)-N(1)-C(6)-C(8)	59.2(5)
C(3)-N(1)-C(6)-C(8)	-122.1(4)
C(4)-N(1)-C(6)-C(7)	-65.5(5)
C(3)-N(1)-C(6)-C(7)	113.2(4)
N(1)-C(3)-C(9)-C(10)	75.6(5)
C(2)-C(3)-C(9)-C(10)	-103.6(4)
C(3)-N(1)-C(4)-C(5)	-3.6(6)
C(6)-N(1)-C(4)-C(5)	175.0(4)
C(1)-C(5)-C(4)-N(1)	2.0(6)
Re(01)-O(1)-C(1)-C(5)	-177.2(3)
Re(01)-O(1)-C(1)-C(2)	3.2(4)
C(4)-C(5)-C(1)-O(1)	-176.1(4)
C(4)-C(5)-C(1)-C(2)	3.6(6)
Re(01)-O(2)-C(2)-C(3)	-173.1(3)
Re(01)-O(2)-C(2)-C(1)	3.5(4)
N(1)-C(3)-C(2)-O(2)	-177.3(3)
C(9)-C(3)-C(2)-O(2)	1.9(6)
N(1)-C(3)-C(2)-C(1)	6.1(6)
C(9)-C(3)-C(2)-C(1)	-174.7(4)
O(1)-C(1)-C(2)-O(2)	-4.7(5)
C(5)-C(1)-C(2)-O(2)	175.7(3)
O(1)-C(1)-C(2)-C(3)	172.0(3)
C(5)-C(1)-C(2)-C(3)	-7.6(5)

Table A. 41: Hydrogen bonds for *fac*-[Re(El(naltol)(CO)$_3$(H$_2$O)]·C$_3$H$_6$OS (8) [Å and °].

D-H...A	d(D-H)	d(H...A)	d(D...A)	<(DHA)
C(7)-H(7B)...O(22)#1	0.96	2.59	3.461(5)	150.8
C(9)-H(9B)...O(2)	0.97	2.43	2.853(5)	105.7

Symmetry transformations used to generate equivalent atoms:

#1 x+1,y,z+1

Table A. 42: Atomic coordinates (x 10^4) and equivalent isotropic displacement parameters (Å^2 x 10^3) for *fac*-[Re(El(naltol)(CO)$_3$(CH$_3$OH)] (9). U(eq) is defined as one third of the trace of the orthogonalized U^{ij} tensor.

	x	y	z	U(eq)
C(1)	8314(3)	890(3)	8830(3)	13(1)
C(2)	6630(3)	842(3)	8310(3)	12(1)
C(3)	6333(3)	1885(3)	9053(3)	12(1)
C(4)	9272(3)	2956(3)	10903(3)	16(1)
C(5)	9634(3)	1989(3)	10157(3)	16(1)
C(6)	7397(4)	3945(3)	11360(3)	16(1)
C(7)	8074(4)	3818(4)	12930(3)	25(1)
C(8)	8179(4)	5558(3)	11294(4)	27(1)
C(9)	4605(3)	1934(3)	8434(3)	14(1)
C(10)	3355(4)	945(3)	8935(3)	21(1)
C(11)	8635(4)	1013(3)	5359(3)	20(1)
C(21)	5815(4)	-3236(3)	7109(3)	17(1)
C(22)	7399(4)	-2646(3)	5476(3)	18(1)
C(23)	4146(4)	-2963(3)	4465(3)	16(1)
N(1)	7670(3)	2903(2)	10395(2)	14(1)
O(1)	8560(2)	-85(2)	8079(2)	14(1)
O(2)	5363(2)	-283(2)	7067(2)	13(1)
O(11)	6978(3)	248(2)	5298(2)	15(1)
O(21)	5548(3)	-4197(2)	7663(2)	24(1)

O(22)	8112(3)	-3200(2)	5064(2)	28(1)
O(23)	2834(3)	-3744(2)	3458(2)	26(1)
Re(1)	6294(1)	-1681(1)	6193(1)	12(1)

Table A. 43: Bond lengths [Å] and angles [°] for *fac*-[Re(El(naltol)(CO)$_3$(CH$_3$OH)] (9).

_____

C(1)-O(1)	1.300(3)
C(1)-C(5)	1.401(4)
C(1)-C(2)	1.427(4)
C(2)-O(2)	1.354(3)
C(2)-C(3)	1.377(4)
C(3)-N(1)	1.388(3)
C(3)-C(9)	1.505(4)
C(4)-N(1)	1.355(4)
C(4)-C(5)	1.366(4)
C(4)-H(4)	0.9300
C(5)-H(5)	0.9300
C(6)-N(1)	1.499(4)
C(6)-C(8)	1.516(4)
C(6)-C(7)	1.524(4)
C(6)-H(6)	0.9800
C(7)-H(7A)	0.9600
C(7)-H(7B)	0.9600
C(7)-H(7C)	0.9600
C(8)-H(8A)	0.9600
C(8)-H(8B)	0.9600
C(8)-H(8C)	0.9600
C(9)-C(10)	1.531(4)
C(9)-H(9A)	0.9700
C(9)-H(9B)	0.9700
C(10)-H(10A)	0.9600
C(10)-H(10B)	0.9600
C(10)-H(10C)	0.9600
C(11)-O(11)	1.430(3)
C(11)-H(11A)	0.9600

C(11)-H(11B)	0.9600
C(11)-H(11C)	0.9600
C(21)-O(21)	1.158(3)
C(21)-Re(1)	1.895(3)
C(22)-O(22)	1.156(4)
C(22)-Re(1)	1.902(3)
C(23)-O(23)	1.153(4)
C(23)-Re(1)	1.922(3)
O(1)-Re(1)	2.1141(19)
O(2)-Re(1)	2.148(2)
O(11)-Re(1)	2.200(2)
O(11)-H(11D)	0.76(4)
O(1)-C(1)-C(5)	122.8(2)
O(1)-C(1)-C(2)	119.5(2)
C(5)-C(1)-C(2)	117.8(2)
O(2)-C(2)-C(3)	122.6(2)
O(2)-C(2)-C(1)	116.4(2)
C(3)-C(2)-C(1)	121.0(2)
C(2)-C(3)-N(1)	118.5(2)
C(2)-C(3)-C(9)	121.3(2)
N(1)-C(3)-C(9)	120.2(2)
N(1)-C(4)-C(5)	122.1(3)
N(1)-C(4)-H(4)	118.9
C(5)-C(4)-H(4)	118.9
C(4)-C(5)-C(1)	119.6(3)
C(4)-C(5)-H(5)	120.2
C(1)-C(5)-H(5)	120.2
N(1)-C(6)-C(8)	110.5(2)
N(1)-C(6)-C(7)	110.8(2)
C(8)-C(6)-C(7)	112.8(2)
N(1)-C(6)-H(6)	107.5
C(8)-C(6)-H(6)	107.5
C(7)-C(6)-H(6)	107.5
C(6)-C(7)-H(7A)	109.5

C(6)-C(7)-H(7B)	109.5
H(7A)-C(7)-H(7B)	109.5
C(6)-C(7)-H(7C)	109.5
H(7A)-C(7)-H(7C)	109.5
H(7B)-C(7)-H(7C)	109.5
C(6)-C(8)-H(8A)	109.5
C(6)-C(8)-H(8B)	109.5
H(8A)-C(8)-H(8B)	109.5
C(6)-C(8)-H(8C)	109.5
H(8A)-C(8)-H(8C)	109.5
H(8B)-C(8)-H(8C)	109.5
C(3)-C(9)-C(10)	113.7(2)
C(3)-C(9)-H(9A)	108.8
C(10)-C(9)-H(9A)	108.8
C(3)-C(9)-H(9B)	108.8
C(10)-C(9)-H(9B)	108.8
H(9A)-C(9)-H(9B)	107.7
C(9)-C(10)-H(10A)	109.5
C(9)-C(10)-H(10B)	109.5
H(10A)-C(10)-H(10B)	109.5
C(9)-C(10)-H(10C)	109.5
H(10A)-C(10)-H(10C)	109.5
H(10B)-C(10)-H(10C)	109.5
O(11)-C(11)-H(11A)	109.5
O(11)-C(11)-H(11B)	109.5
H(11A)-C(11)-H(11B)	109.5
O(11)-C(11)-H(11C)	109.5
H(11A)-C(11)-H(11C)	109.5
H(11B)-C(11)-H(11C)	109.5
O(21)-C(21)-Re(1)	178.4(3)
O(22)-C(22)-Re(1)	178.2(2)
O(23)-C(23)-Re(1)	177.8(3)
C(4)-N(1)-C(3)	120.8(2)
C(4)-N(1)-C(6)	117.3(2)
C(3)-N(1)-C(6)	121.8(2)

C(1)-O(1)-Re(1)	114.04(17)
C(2)-O(2)-Re(1)	112.51(16)
C(11)-O(11)-Re(1)	123.74(17)
C(11)-O(11)-H(11D)	113(3)
Re(1)-O(11)-H(11D)	114(3)
C(21)-Re(1)-C(22)	87.16(12)
C(21)-Re(1)-C(23)	88.06(12)
C(22)-Re(1)-C(23)	88.93(13)
C(21)-Re(1)-O(1)	95.76(10)
C(22)-Re(1)-O(1)	96.20(11)
C(23)-Re(1)-O(1)	173.74(9)
C(21)-Re(1)-O(2)	99.11(10)
C(22)-Re(1)-O(2)	171.51(9)
C(23)-Re(1)-O(2)	96.95(11)
O(1)-Re(1)-O(2)	77.57(8)
C(21)-Re(1)-O(11)	175.62(9)
C(22)-Re(1)-O(11)	94.64(10)
C(23)-Re(1)-O(11)	95.96(10)
O(1)-Re(1)-O(11)	80.09(8)
O(2)-Re(1)-O(11)	78.71(8)

Table A. 44: Anisotropic displacement parameters ($Å^2$x 10^3) for *fac*-[Re(El(naltol)(CO)$_3$(CH$_3$OH)]
(9). The anisotropic displacement factor exponent takes the form: $-2p^2[h^2a^{*2}U^{11} + ... + 2 h k a^* b^* U^{12}]$

	U^{11}	U^{22}	U^{33}	U^{23}	U^{13}	U^{12}
C(1)	13(1)	13(1)	12(1)	5(1)	5(1)	6(1)
C(2)	12(1)	12(1)	10(1)	3(1)	3(1)	4(1)
C(3)	12(1)	13(1)	10(1)	3(1)	4(1)	5(1)
C(4)	11(1)	18(1)	13(1)	1(1)	2(1)	4(1)
C(5)	12(1)	19(1)	15(1)	4(1)	4(1)	7(1)
C(6)	18(1)	14(1)	14(1)	-1(1)	6(1)	8(1)
C(7)	34(2)	29(2)	16(1)	4(1)	13(1)	18(1)
C(8)	34(2)	16(1)	29(2)	5(1)	13(1)	11(1)

C(9)	16(1)	16(1)	12(1)	2(1)	6(1)	9(1)
C(10)	17(1)	20(1)	26(2)	7(1)	11(1)	7(1)
C(11)	12(1)	25(2)	19(1)	6(1)	6(1)	5(1)
C(21)	16(1)	22(1)	14(1)	1(1)	4(1)	12(1)
C(22)	13(1)	16(1)	17(1)	1(1)	4(1)	4(1)
C(23)	20(1)	15(1)	17(1)	3(1)	10(1)	11(1)
N(1)	14(1)	14(1)	11(1)	1(1)	5(1)	5(1)
O(1)	13(1)	16(1)	12(1)	0(1)	4(1)	9(1)
O(2)	10(1)	14(1)	12(1)	0(1)	2(1)	7(1)
O(11)	9(1)	19(1)	14(1)	6(1)	3(1)	6(1)
O(21)	25(1)	23(1)	27(1)	12(1)	11(1)	11(1)
O(22)	25(1)	25(1)	36(1)	0(1)	16(1)	14(1)
O(23)	18(1)	23(1)	21(1)	-4(1)	0(1)	5(1)
Re(1)	11(1)	13(1)	11(1)	1(1)	3(1)	6(1)

Table A. 45: Hydrogen coordinates (x 10^4) and isotropic displacement parameters (Å^{2}x 10^3) for *fac*-[Re(EI(naltol)(CO)$_3$(CH$_3$OH)] (9).

_____

	x	y	z	U(eq)

_____

	x	y	z	U(eq)
H(4)	10153	3675	11788	19
H(5)	10749	2059	10527	19
H(6)	6147	3614	10963	19
H(7A)	7538	2779	12909	38
H(7B)	7808	4434	13510	38
H(7C)	9304	4162	13360	38
H(8A)	7704	5576	10285	41
H(8B)	9410	5924	11696	41
H(8C)	7919	6197	11858	41
H(9A)	4078	1603	7364	17
H(9B)	4784	2977	8731	17
H(10A)	2282	1025	8500	32
H(10B)	3850	1283	9993	32
H(10C)	3149	-94	8628	32

H(11A)	9516	1046	6266	30
H(11B)	8831	2029	5315	30
H(11C)	8669	476	4538	30
H(11D)	6240(50)	200(40)	4590(40)	34(11)

Table A. 46: Hydrogen bonds for *fac*-[Re(EI(naltol)(CO)$_3$(CH$_3$OH)] (9) [Å and °].

D-H…A	d(D-H) (Å)	d(H…A) (Å)	d(D…A) (Å)	⊾(D-H…A)(˚)
O11-H11D...O2 [(i)]	0.77(4)	1.80(4)	2.571(3)	173(5)
C7-H7B...O22 [(ii)]	0.96	2.53	3.438(5)	158

Symmetry codes, transformations used to generate equivalent atoms: (i) -x+1, -y+2, -z+1; (ii) x, +1+y, +1+z;

Table A. 47: Atomic coordinates (x 10^4) and equivalent isotropic displacement parameters (Å^2 x 10^3) for *fac*-[Re(ME(naltol))(CO)$_3$(4-MPyr)] (10). U(eq) is defined as one third of the trace of the orthogonalized U^{ij} tensor.

	x	y	z	U(eq)
C(2)	1627(6)	3981(3)	9113(3)	23(1)
C(11)	3800(6)	3190(4)	7444(3)	27(1)
C(12)	5052(7)	3555(4)	6982(3)	31(1)
C(13)	6680(6)	3264(4)	7175(3)	31(1)
C(14)	6948(6)	2622(4)	7858(3)	30(1)
C(15)	5638(6)	2281(4)	8284(3)	27(1)
C(16)	8071(7)	3616(5)	6671(4)	44(1)
C(21)	111(6)	1258(3)	9226(3)	25(1)
C(22)	3071(6)	588(4)	8904(3)	33(1)
C(23)	1024(7)	1218(4)	7719(3)	29(1)
N(11)	4056(5)	2545(3)	8076(2)	22(1)
O(21)	-986(5)	886(3)	9519(3)	39(1)
O(22)	3767(5)	-174(3)	9013(3)	51(1)
O(23)	431(6)	831(3)	7133(2)	48(1)
Re(1)	1935(1)	1843(1)	8692(1)	19(1)
O(1)	2959(5)	2605(3)	9754(2)	32(1)
O(2)	976(4)	3335(3)	8522(2)	28(1)

C(1)	2605(6)	3551(4)	9759(3)	30(1)
C(3)	1274(6)	5024(4)	9076(3)	28(1)
C(4)	2801(7)	5223(4)	10361(3)	37(1)
C(5)	3188(7)	4232(4)	10402(3)	34(1)
N(1)	1849(5)	5633(3)	9695(3)	32(1)
C(8)	347(7)	5465(4)	8346(3)	36(1)
C(6)	1568(6)	6751(4)	9738(3)	31(1)
C(7)	3030(7)	7341(4)	9450(4)	34(1)

Table A. 48: Bond lengths [Å] and angles [°] for *fac*-[Re(ME(naltol))(CO)₃(4-MPyr)] (10).

_____

C(2)-O(2)	1.364(6)
C(2)-C(3)	1.397(6)
C(2)-C(1)	1.400(7)
C(11)-N(11)	1.337(6)
C(11)-C(12)	1.382(7)
C(11)-H(11)	0.9300
C(12)-C(13)	1.393(7)
C(12)-H(12)	0.9300
C(13)-C(14)	1.399(7)
C(13)-C(16)	1.502(7)
C(14)-C(15)	1.374(7)
C(14)-H(14)	0.9300
C(15)-N(11)	1.354(6)
C(15)-H(15)	0.9300
C(16)-H(16A)	0.9600
C(16)-H(16B)	0.9600
C(16)-H(16C)	0.9600
C(21)-O(21)	1.142(6)
C(21)-Re(1)	1.915(5)
C(22)-O(22)	1.156(6)
C(22)-Re(1)	1.908(5)
C(23)-O(23)	1.160(6)
C(23)-Re(1)	1.894(5)

N(11)-Re(1)	2.235(4)
Re(1)-O(2)	2.116(3)
Re(1)-O(1)	2.121(4)
O(1)-C(1)	1.272(6)
C(1)-C(5)	1.434(7)
C(3)-N(1)	1.346(7)
C(3)-C(8)	1.486(7)
C(4)-C(5)	1.337(8)
C(4)-N(1)	1.401(7)
C(4)-H(4)	0.9300
C(5)-H(5)	0.9300
N(1)-C(6)	1.485(6)
C(8)-H(8A)	0.9600
C(8)-H(8B)	0.9600
C(8)-H(8C)	0.9600
C(6)-C(7)	1.511(7)
C(6)-H(6A)	0.9700
C(6)-H(6B)	0.9700
C(7)-H(7A)	0.9600
C(7)-H(7B)	0.9600
C(7)-H(7C)	0.9600
O(2)-C(2)-C(3)	120.5(4)
O(2)-C(2)-C(1)	117.3(4)
C(3)-C(2)-C(1)	122.2(5)
N(11)-C(11)-C(12)	123.2(5)
N(11)-C(11)-H(11)	118.4
C(12)-C(11)-H(11)	118.4
C(11)-C(12)-C(13)	119.9(5)
C(11)-C(12)-H(12)	120.0
C(13)-C(12)-H(12)	120.0
C(12)-C(13)-C(14)	116.6(5)
C(12)-C(13)-C(16)	121.6(5)
C(14)-C(13)-C(16)	121.8(5)
C(15)-C(14)-C(13)	120.3(5)

C(15)-C(14)-H(14)	119.9
C(13)-C(14)-H(14)	119.9
N(11)-C(15)-C(14)	122.7(5)
N(11)-C(15)-H(15)	118.7
C(14)-C(15)-H(15)	118.7
C(13)-C(16)-H(16A)	109.5
C(13)-C(16)-H(16B)	109.5
H(16A)-C(16)-H(16B)	109.5
C(13)-C(16)-H(16C)	109.5
H(16A)-C(16)-H(16C)	109.5
H(16B)-C(16)-H(16C)	109.5
O(21)-C(21)-Re(1)	177.5(4)
O(22)-C(22)-Re(1)	178.4(5)
O(23)-C(23)-Re(1)	178.3(5)
C(11)-N(11)-C(15)	117.3(4)
C(11)-N(11)-Re(1)	120.8(3)
C(15)-N(11)-Re(1)	121.7(3)
C(23)-Re(1)-C(22)	86.6(2)
C(23)-Re(1)-C(21)	85.9(2)
C(22)-Re(1)-C(21)	87.2(2)
C(23)-Re(1)-O(2)	99.61(19)
C(22)-Re(1)-O(2)	172.1(2)
C(21)-Re(1)-O(2)	98.15(16)
C(23)-Re(1)-O(1)	177.47(18)
C(22)-Re(1)-O(1)	95.5(2)
C(21)-Re(1)-O(1)	95.68(18)
O(2)-Re(1)-O(1)	78.22(14)
C(23)-Re(1)-N(11)	94.53(18)
C(22)-Re(1)-N(11)	93.40(18)
C(21)-Re(1)-N(11)	179.32(17)
O(2)-Re(1)-N(11)	81.26(14)
O(1)-Re(1)-N(11)	83.88(14)
C(1)-O(1)-Re(1)	112.7(3)
C(2)-O(2)-Re(1)	110.9(3)
O(1)-C(1)-C(2)	120.4(5)

O(1)-C(1)-C(5)	123.1(5)
C(2)-C(1)-C(5)	116.5(5)
N(1)-C(3)-C(2)	119.1(5)
N(1)-C(3)-C(8)	120.3(5)
C(2)-C(3)-C(8)	120.5(5)
C(5)-C(4)-N(1)	121.9(5)
C(5)-C(4)-H(4)	119.0
N(1)-C(4)-H(4)	119.0
C(4)-C(5)-C(1)	120.1(5)
C(4)-C(5)-H(5)	119.9
C(1)-C(5)-H(5)	119.9
C(3)-N(1)-C(4)	120.2(4)
C(3)-N(1)-C(6)	124.9(5)
C(4)-N(1)-C(6)	114.9(4)
C(3)-C(8)-H(8A)	109.5
C(3)-C(8)-H(8B)	109.5
H(8A)-C(8)-H(8B)	109.5
C(3)-C(8)-H(8C)	109.5
H(8A)-C(8)-H(8C)	109.5
H(8B)-C(8)-H(8C)	109.5
N(1)-C(6)-C(7)	111.4(4)
N(1)-C(6)-H(6A)	109.3
C(7)-C(6)-H(6A)	109.3
N(1)-C(6)-H(6B)	109.3
C(7)-C(6)-H(6B)	109.3
H(6A)-C(6)-H(6B)	108.0
C(6)-C(7)-H(7A)	109.5
C(6)-C(7)-H(7B)	109.5
H(7A)-C(7)-H(7B)	109.5
C(6)-C(7)-H(7C)	109.5
H(7A)-C(7)-H(7C)	109.5
H(7B)-C(7)-H(7C)	109.5

Table A. 49: Anisotropic displacement parameters (Å^{2}x 10^3) for *fac*-[Re(ME(naltol))(CO)$_3$(4-MPyr)] (10). The anisotropic displacement factor exponent takes the form: -2p^2[h^{2}a*^{2}U^{11} + ... + 2 h k a* b* U^{12}]

	U^{11}	U^{22}	U^{33}	U^{23}	U^{13}	U^{12}
C(2)	24(2)	16(2)	30(2)	-1(2)	13(2)	0(2)
C(11)	24(2)	22(2)	35(2)	0(2)	3(2)	0(2)
C(12)	34(3)	23(2)	35(3)	4(2)	5(2)	-1(2)
C(13)	27(2)	26(2)	40(3)	-6(2)	9(2)	-5(2)
C(14)	20(2)	35(3)	35(3)	-2(2)	2(2)	0(2)
C(15)	24(2)	28(2)	30(2)	-2(2)	-1(2)	1(2)
C(16)	35(3)	43(3)	54(4)	-3(3)	15(3)	-6(3)
C(21)	27(2)	17(2)	30(2)	-1(2)	5(2)	6(2)
C(22)	26(2)	34(3)	40(3)	11(2)	13(2)	8(2)
C(23)	34(3)	26(2)	27(2)	2(2)	5(2)	-10(2)
N(11)	18(2)	19(2)	30(2)	-6(2)	1(2)	-1(2)
O(21)	35(2)	30(2)	54(2)	3(2)	21(2)	0(2)
O(22)	40(2)	31(2)	84(3)	20(2)	21(2)	18(2)
O(23)	63(3)	51(3)	30(2)	-6(2)	-4(2)	-25(2)
Re(1)	18(1)	15(1)	23(1)	-1(1)	1(1)	2(1)
O(1)	33(2)	28(2)	32(2)	-4(2)	-2(2)	2(2)
O(2)	23(2)	24(2)	39(2)	5(2)	3(1)	4(1)
C(1)	22(2)	33(3)	34(3)	10(2)	4(2)	-1(2)
C(3)	23(2)	24(2)	38(3)	-1(2)	10(2)	-2(2)
C(4)	39(3)	38(3)	33(3)	-13(2)	9(2)	-12(2)
C(5)	35(3)	38(3)	30(3)	-3(2)	2(2)	0(2)
N(1)	31(2)	23(2)	42(2)	-8(2)	17(2)	-4(2)
C(8)	29(3)	37(3)	44(3)	15(2)	10(2)	8(2)
C(6)	32(3)	18(2)	44(3)	-6(2)	13(2)	-1(2)
C(7)	31(3)	23(2)	50(3)	-4(2)	16(2)	-5(2)

Table A. 50. Hydrogen coordinates (x 10^4) and isotropic displacement parameters (Å^{2}x 10^3) for *fac*-[Re(ME(naltol))(CO)$_3$(4-MPyr)] (10).

	x	y	z	U(eq)
H(11)	2725	3404	7310	32
H(12)	4810	3995	6543	37
H(14)	8016	2425	8024	36
H(15)	5847	1852	8734	33
H(16A)	8016	3267	6151	66
H(16B)	9106	3467	6962	66
H(16C)	7981	4338	6580	66
H(4)	3174	5653	10787	44
H(5)	3836	3985	10848	41
H(8A)	-684	5737	8510	54
H(8B)	138	4942	7940	54
H(8C)	986	6000	8117	54
H(6A)	1375	6941	10302	37
H(6B)	591	6928	9397	37
H(7A)	3994	7177	9794	51
H(7B)	2811	8060	9485	51
H(7C)	3213	7163	8889	51

Table A. 51: Torsion angles [°] for *fac*-[Re(ME(naltol))(CO)$_3$(4-MPyr)] (10).

N(11)-C(11)-C(12)-C(13)	-1.0(8)
C(11)-C(12)-C(13)-C(14)	-1.6(7)
C(11)-C(12)-C(13)-C(16)	178.0(5)
C(12)-C(13)-C(14)-C(15)	2.3(7)
C(16)-C(13)-C(14)-C(15)	-177.3(5)
C(13)-C(14)-C(15)-N(11)	-0.4(8)
C(12)-C(11)-N(11)-C(15)	2.9(7)
C(12)-C(11)-N(11)-Re(1)	-172.5(4)
C(14)-C(15)-N(11)-C(11)	-2.2(7)

C(14)-C(15)-N(11)-Re(1)	173.1(4)
C(3)-C(2)-O(2)-Re(1)	174.4(3)
C(1)-C(2)-O(2)-Re(1)	-7.5(5)
Re(1)-O(1)-C(1)-C(2)	0.4(6)
Re(1)-O(1)-C(1)-C(5)	-178.5(4)
O(2)-C(2)-C(1)-O(1)	5.0(7)
C(3)-C(2)-C(1)-O(1)	-177.0(5)
O(2)-C(2)-C(1)-C(5)	-176.0(4)
C(3)-C(2)-C(1)-C(5)	2.0(7)
O(2)-C(2)-C(3)-N(1)	175.9(4)
C(1)-C(2)-C(3)-N(1)	-2.1(7)
O(2)-C(2)-C(3)-C(8)	-7.1(7)
C(1)-C(2)-C(3)-C(8)	174.9(5)
N(1)-C(4)-C(5)-C(1)	-1.0(8)
O(1)-C(1)-C(5)-C(4)	178.5(5)
C(2)-C(1)-C(5)-C(4)	-0.4(8)
C(2)-C(3)-N(1)-C(4)	0.6(7)
C(8)-C(3)-N(1)-C(4)	-176.5(5)
C(2)-C(3)-N(1)-C(6)	-179.9(4)
C(8)-C(3)-N(1)-C(6)	3.1(7)
C(5)-C(4)-N(1)-C(3)	1.0(8)
C(5)-C(4)-N(1)-C(6)	-178.6(5)
C(3)-N(1)-C(6)-C(7)	-98.2(6)
C(4)-N(1)-C(6)-C(7)	81.3(6)

Table A. 52: Hydrogen bonds for *fac*-[Re(ME(naltol))(CO)₃(4-MPyr)] (10) [Å and °].

D-H…A	d(D-H) (Å)	d(H…A) (Å)	d(D…A) (Å)	ㄴ (D-H…A)(°)
C(5)-H(5)...O(23) (i)	0.93	2.41	3.265(7)	153
C(7)-H(7A)...O(1) (ii)	0.96	2.56	3.435(7)	152
C(7)-H(7B)...O(22) (iii)	0.96	2.57	3.393(7)	144
C(8)-H(8B)...O(2)	0.96	2.39	2.850(7)	109
C(11)-H(11)...O(2)	0.93	2.49	2.964(6)	112
C(16)-H(16A)...O(1) (iv)	0.96	2.54	3.497(8)	178

Symmetry codes, transformations used to generate equivalent atoms: (i) 2-x,-y,1-z; (ii) 1/2+x,1/2-y,1/2+z; (iii) x,-1+y,z; (iv) 1/2+x,1/2-y,-1/2+z

Table A. 53: Atomic coordinates (x 10^4) and equivalent isotropic displacement parameters (Å^2 x 10^3) for *fac*-[Re(EM(naltol))(CO)$_3$(Pyr)] (11). U(eq) is defined as one third of the trace of the orthogonalized U^{ij} tensor.

	x	y	z	U(eq)
C(1)	3509(3)	334(6)	699(4)	14(1)
C(2)	3332(3)	272(6)	-393(4)	12(1)
C(3)	3767(4)	-811(6)	-888(4)	14(1)
C(4)	4579(4)	-1691(7)	749(5)	18(1)
C(5)	4158(4)	-667(7)	1260(4)	16(1)
C(6)	4833(4)	-3010(7)	-759(5)	20(1)
C(7)	3539(4)	-949(7)	-2038(4)	17(1)
C(8)	2821(4)	-2180(8)	-2425(5)	24(1)
C(11)	1118(4)	-465(7)	-904(5)	18(1)
C(12)	701(4)	-1922(7)	-944(5)	23(1)
C(13)	568(4)	-2595(7)	-42(6)	24(1)
C(14)	848(4)	-1757(8)	869(5)	24(1)
C(15)	1260(4)	-303(7)	857(5)	19(1)
C(21)	2775(4)	4575(8)	83(5)	23(1)
C(22)	1568(4)	3609(7)	1005(4)	16(1)
C(23)	1259(4)	3594(7)	-1059(5)	18(1)
N(1)	4386(3)	-1782(6)	-288(4)	16(1)
N(11)	1404(3)	346(5)	-9(4)	13(1)
O(1)	3067(3)	1344(5)	1128(3)	17(1)
O(2)	2738(3)	1283(4)	-926(3)	14(1)
O(21)	3155(4)	5752(6)	139(4)	35(1)
O(22)	1240(3)	4187(6)	1604(4)	26(1)
O(23)	745(3)	4153(6)	-1733(4)	29(1)
O(25)	6352(3)	-3584(6)	1757(4)	22(1)
Re(1)	2106(1)	2638(1)	29(1)	13(1)

Table A. 54: Bond lengths [Å] and angles [°] for *fac*-[Re(EM(naltol))(CO)₃(Pyr)] (11).

C(1)-O(1)	1.314(7)
C(1)-C(5)	1.399(8)
C(1)-C(2)	1.419(8)
C(2)-O(2)	1.338(6)
C(2)-C(3)	1.396(8)
C(3)-N(1)	1.375(7)
C(3)-C(7)	1.497(8)
C(4)-N(1)	1.347(8)
C(4)-C(5)	1.365(8)
C(4)-H(4)	0.9300
C(5)-H(5)	0.9300
C(6)-N(1)	1.472(7)
C(6)-H(6A)	0.9600
C(6)-H(6B)	0.9600
C(6)-H(6C)	0.9600
C(7)-C(8)	1.532(8)
C(7)-H(7A)	0.9700
C(7)-H(7B)	0.9700
C(8)-H(8A)	0.9600
C(8)-H(8B)	0.9600
C(8)-H(8C)	0.9600
C(11)-N(11)	1.354(7)
C(11)-C(12)	1.379(8)
C(11)-H(11)	0.9300
C(12)-C(13)	1.391(10)
C(12)-H(12)	0.9300
C(13)-C(14)	1.382(10)
C(13)-H(13)	0.9300
C(14)-C(15)	1.379(8)
C(14)-H(14)	0.9300
C(15)-N(11)	1.345(7)
C(15)-H(15)	0.9300
C(21)-O(21)	1.145(8)

C(21)-Re(1)	1.926(6)
C(22)-O(22)	1.160(7)
C(22)-Re(1)	1.903(6)
C(23)-O(23)	1.159(7)
C(23)-Re(1)	1.905(6)
N(11)-Re(1)	2.207(5)
O(1)-Re(1)	2.142(4)
O(2)-Re(1)	2.129(4)
O(25)-O(25)#1	0.000(14)
O(25)-H(25B)	0.96(10)
O(25)-H(25A)	0.67(8)
O(1)-C(1)-C(5)	123.6(5)
O(1)-C(1)-C(2)	118.5(5)
C(5)-C(1)-C(2)	117.9(5)
O(2)-C(2)-C(3)	121.6(5)
O(2)-C(2)-C(1)	117.7(5)
C(3)-C(2)-C(1)	120.7(5)
N(1)-C(3)-C(2)	118.2(5)
N(1)-C(3)-C(7)	121.1(5)
C(2)-C(3)-C(7)	120.6(5)
N(1)-C(4)-C(5)	122.1(5)
N(1)-C(4)-H(4)	119.0
C(5)-C(4)-H(4)	119.0
C(4)-C(5)-C(1)	119.6(5)
C(4)-C(5)-H(5)	120.2
C(1)-C(5)-H(5)	120.2
N(1)-C(6)-H(6A)	109.5
N(1)-C(6)-H(6B)	109.5
H(6A)-C(6)-H(6B)	109.5
N(1)-C(6)-H(6C)	109.5
H(6A)-C(6)-H(6C)	109.5
H(6B)-C(6)-H(6C)	109.5
C(3)-C(7)-C(8)	112.1(5)
C(3)-C(7)-H(7A)	109.2

C(8)-C(7)-H(7A)	109.2
C(3)-C(7)-H(7B)	109.2
C(8)-C(7)-H(7B)	109.2
H(7A)-C(7)-H(7B)	107.9
C(7)-C(8)-H(8A)	109.5
C(7)-C(8)-H(8B)	109.5
H(8A)-C(8)-H(8B)	109.5
C(7)-C(8)-H(8C)	109.5
H(8A)-C(8)-H(8C)	109.5
H(8B)-C(8)-H(8C)	109.5
N(11)-C(11)-C(12)	122.0(6)
N(11)-C(11)-H(11)	119.0
C(12)-C(11)-H(11)	119.0
C(11)-C(12)-C(13)	119.6(6)
C(11)-C(12)-H(12)	120.2
C(13)-C(12)-H(12)	120.2
C(14)-C(13)-C(12)	118.4(6)
C(14)-C(13)-H(13)	120.8
C(12)-C(13)-H(13)	120.8
C(15)-C(14)-C(13)	119.1(6)
C(15)-C(14)-H(14)	120.4
C(13)-C(14)-H(14)	120.4
N(11)-C(15)-C(14)	122.9(6)
N(11)-C(15)-H(15)	118.5
C(14)-C(15)-H(15)	118.5
O(21)-C(21)-Re(1)	177.4(6)
O(22)-C(22)-Re(1)	179.3(5)
O(23)-C(23)-Re(1)	178.8(5)
C(4)-N(1)-C(3)	121.4(5)
C(4)-N(1)-C(6)	117.7(5)
C(3)-N(1)-C(6)	120.8(5)
C(15)-N(11)-C(11)	117.9(5)
C(15)-N(11)-Re(1)	121.2(4)
C(11)-N(11)-Re(1)	120.9(4)
C(1)-O(1)-Re(1)	113.2(3)

C(2)-O(2)-Re(1)	113.1(3)	
O(25)#1-O(25)-H(25B)	0(10)	
O(25)#1-O(25)-H(25A)	0(10)	
H(25B)-O(25)-H(25A)	107(8)	
C(22)-Re(1)-C(23)	89.6(2)	
C(22)-Re(1)-C(21)	87.4(3)	
C(23)-Re(1)-C(21)	87.9(3)	
C(22)-Re(1)-O(2)	172.3(2)	
C(23)-Re(1)-O(2)	96.6(2)	
C(21)-Re(1)-O(2)	97.4(2)	
C(22)-Re(1)-O(1)	96.3(2)	
C(23)-Re(1)-O(1)	173.3(2)	
C(21)-Re(1)-O(1)	95.5(2)	
O(2)-Re(1)-O(1)	77.28(15)	
C(22)-Re(1)-N(11)	94.3(2)	
C(23)-Re(1)-N(11)	94.7(2)	
C(21)-Re(1)-N(11)	176.9(2)	
O(2)-Re(1)-N(11)	80.66(16)	
O(1)-Re(1)-N(11)	81.74(16)	

Table A. 55: Anisotropic displacement parameters ($Å^2 x\ 10^3$) for *fac*-[Re(EM(naltol))(CO)$_3$(Pyr)] (11). The anisotropic displacement factor exponent takes the form: $-2p^2[\ h^2a^{*2}U^{11} + ... + 2\ h\ k\ a^*\ b^*\ U^{12}\ ]$

	U^{11}	U^{22}	U^{33}	U^{23}	U^{13}	U^{12}
C(1)	11(2)	14(2)	14(3)	-2(2)	-3(2)	-3(2)
C(2)	11(2)	12(2)	12(2)	1(2)	-2(2)	-4(2)
C(3)	14(3)	13(2)	15(3)	-1(2)	2(2)	-3(2)
C(4)	14(3)	13(2)	24(3)	2(2)	0(2)	-2(2)
C(5)	15(3)	17(3)	15(3)	1(2)	-1(2)	-3(2)
C(6)	18(3)	16(3)	27(3)	-1(2)	6(2)	-1(2)
C(7)	19(3)	17(3)	16(3)	-1(2)	4(2)	0(2)
C(8)	20(3)	25(3)	25(3)	-5(2)	1(2)	-1(2)
C(11)	17(3)	19(3)	16(3)	-1(2)	2(2)	-2(2)

C(12)	27(3)	19(3)	22(3)	-7(2)	1(2)	-6(2)
C(13)	17(3)	16(3)	37(4)	5(2)	0(3)	-3(2)
C(14)	24(3)	24(3)	26(3)	11(2)	7(3)	-4(2)
C(15)	17(3)	23(3)	16(3)	2(2)	-1(2)	-3(2)
C(21)	17(3)	28(3)	24(3)	-4(2)	7(2)	-3(2)
C(22)	12(3)	17(3)	18(3)	0(2)	-2(2)	-2(2)
C(23)	17(3)	17(3)	17(3)	-2(2)	1(2)	-1(2)
N(1)	11(2)	12(2)	23(3)	0(2)	4(2)	-1(2)
N(11)	11(2)	12(2)	14(2)	2(2)	0(2)	-1(2)
O(1)	17(2)	21(2)	11(2)	0(2)	0(2)	1(2)
O(2)	17(2)	13(2)	10(2)	2(1)	1(2)	2(1)
O(21)	45(3)	26(2)	40(3)	-12(2)	19(2)	-21(2)
O(22)	27(2)	28(2)	24(2)	-6(2)	7(2)	2(2)
O(23)	34(3)	27(2)	22(2)	2(2)	-4(2)	7(2)
O(25)	24(2)	26(2)	11(2)	4(2)	-2(2)	-5(2)
Re(1)	14(1)	12(1)	13(1)	-1(1)	2(1)	-1(1)

Table A. 56: Hydrogen coordinates (x 10^4) and isotropic displacement parameters (Å^{2}x 10^3) for _fac_-[Re(EM(naltol))(CO)$_3$(Pyr)] (11).

_____

	x	y	z	U(eq)

_____

H(4)	5013	-2346	1129	21
H(5)	4302	-635	1977	20
H(6A)	5269	-3520	-233	30
H(6B)	5099	-2512	-1254	30
H(6C)	4424	-3799	-1099	30
H(7A)	4049	-1263	-2267	21
H(7B)	3353	91	-2337	21
H(8A)	3009	-3218	-2147	36
H(8B)	2690	-2226	-3164	36
H(8C)	2313	-1869	-2206	36
H(11)	1206	-25	-1511	22
H(12)	511	-2452	-1571	28

H(13)	297	-3586	-52	29
H(14)	760	-2167	1484	29
H(15)	1446	253	1474	23
H(25B)	6680(60)	-2840(120)	1450(80)	50(30)
H(25A)	6490(50)	-3520(90)	2270(60)	12(19)

Table A. 57:Torsion angles [°] for *fac*-[Re(EM(naltol))(CO)₃(Pyr)] (11).

_____

O(1)-C(1)-C(2)-O(2)	1.7(7)
C(5)-C(1)-C(2)-O(2)	-177.0(5)
O(1)-C(1)-C(2)-C(3)	-178.3(5)
C(5)-C(1)-C(2)-C(3)	3.0(8)
O(2)-C(2)-C(3)-N(1)	178.3(5)
C(1)-C(2)-C(3)-N(1)	-1.7(8)
O(2)-C(2)-C(3)-C(7)	-4.0(8)
C(1)-C(2)-C(3)-C(7)	176.0(5)
N(1)-C(4)-C(5)-C(1)	-0.5(8)
O(1)-C(1)-C(5)-C(4)	179.4(5)
C(2)-C(1)-C(5)-C(4)	-1.9(8)
N(1)-C(3)-C(7)-C(8)	88.8(6)
C(2)-C(3)-C(7)-C(8)	-88.9(6)
N(11)-C(11)-C(12)-C(13)	-0.1(10)
C(11)-C(12)-C(13)-C(14)	1.1(10)
C(12)-C(13)-C(14)-C(15)	-1.0(10)
C(13)-C(14)-C(15)-N(11)	0.0(10)
C(5)-C(4)-N(1)-C(3)	1.8(8)
C(5)-C(4)-N(1)-C(6)	-175.5(5)
C(2)-C(3)-N(1)-C(4)	-0.7(8)
C(7)-C(3)-N(1)-C(4)	-178.4(5)
C(2)-C(3)-N(1)-C(6)	176.6(5)
C(7)-C(3)-N(1)-C(6)	-1.1(8)
C(14)-C(15)-N(11)-C(11)	1.0(9)
C(14)-C(15)-N(11)-Re(1)	-177.9(5)
C(12)-C(11)-N(11)-C(15)	-0.9(9)
C(12)-C(11)-N(11)-Re(1)	178.0(5)

C(5)-C(1)-O(1)-Re(1)	-178.6(4)
C(2)-C(1)-O(1)-Re(1)	2.7(6)
C(3)-C(2)-O(2)-Re(1)	174.8(4)
C(1)-C(2)-O(2)-Re(1)	-5.2(6)

Table A. 58: Hydrogen bonds for *fac*-[Re(EM(naltol))(CO)$_3$(Pyr)] (11) [Å and °].

D-H...A	d(D-H)	d(H...A)	d(D...A)	<(DHA)
O(25)-H(25A)...O(1)#2	0.67(8)	2.09(8)	2.755(6)	172(8)
C(4)-H(4)...O(25)#1	0.93	2.34	3.234(7)	161.8
C(6)-H(6C)...O(25)#3	0.96	2.55	3.490(8)	164.7
C(7)-H(7B)...O(2)	0.97	2.53	2.865(7)	100.3

Symmetry transformations used to generate equivalent atoms: #1 x,y,z   #2 -x+1,y-1/2,-z+1/2   #3 -x+1,-y-1,-z

Table A. 58: Atomic coordinates (x 10^4) and equivalent isotropic displacement parameters (Å^2 x 10^3) for *fac*-[Re(EE(naltol))(CO)$_3$(Pyr)] (12). U(eq) is defined as one third of the trace of the orthogonalized U^{ij} tensor.

	x	y	z	U(eq)
O(2)	2557(1)	3597(2)	2151(1)	14(1)
O(1)	2923(1)	3546(2)	248(1)	15(1)
O(21)	2866(1)	-1023(2)	1271(2)	29(1)
C(21)	2556(2)	232(3)	1148(2)	18(1)
O(22)	1181(1)	757(3)	-1076(1)	24(1)
C(22)	1480(2)	1309(3)	-326(2)	17(1)
O(23)	652(1)	825(3)	2048(2)	28(1)
C(23)	1153(2)	1363(3)	1602(2)	16(1)
N(11)	1351(1)	4618(3)	616(2)	14(1)
C(15)	1068(2)	5447(3)	1379(2)	18(1)
C(13)	531(2)	7553(3)	261(3)	23(1)
C(14)	658(2)	6913(4)	1228(2)	23(1)

C(11)	1220(2)	5248(3)	-323(2)	20(1)
C(12)	811(2)	6709(4)	-524(2)	24(1)
O(25)	3589(1)	1500(3)	3420(2)	28(1)
C(3)	3580(1)	5564(3)	2620(2)	14(1)
C(2)	3150(1)	4557(3)	1914(2)	12(1)
C(4)	4438(2)	6348(3)	1385(2)	16(1)
C(1)	3352(1)	4499(3)	894(2)	12(1)
C(5)	4009(2)	5428(3)	649(2)	16(1)
N(1)	4226(1)	6430(3)	2339(2)	14(1)
C(8)	3302(2)	5785(3)	3655(2)	17(1)
C(6)	4767(2)	7336(3)	3106(2)	19(1)
C(9)	2721(2)	7229(4)	3672(2)	26(1)
C(7)	5349(2)	6179(4)	3711(2)	24(1)
Re(1)	1982(1)	2261(1)	899(1)	11(1)

Table A. 59: Bond lengths [Å] and angles [°] for *fac*-[Re(EE(naltol))(CO)₃(Pyr)] (12).

_____

O(2)-C(2)	1.326(3)
O(2)-Re(1)	2.1260(16)
O(1)-C(1)	1.310(3)
O(1)-Re(1)	2.1448(17)
O(21)-C(21)	1.152(3)
C(21)-Re(1)	1.923(3)
O(22)-C(22)	1.154(3)
C(22)-Re(1)	1.909(2)
O(23)-C(23)	1.162(3)
C(23)-Re(1)	1.896(3)
N(11)-C(11)	1.343(3)
N(11)-C(15)	1.346(3)
N(11)-Re(1)	2.206(2)
C(15)-C(14)	1.382(4)
C(15)-H(15)	0.9300
C(13)-C(12)	1.373(4)
C(13)-C(14)	1.380(4)
C(13)-H(13)	0.9300

C(14)-H(14)	0.9300
C(11)-C(12)	1.386(4)
C(11)-H(11)	0.9300
C(12)-H(12)	0.9300
O(25)-H(25A)	0.82(4)
O(25)-H(25B)	0.86(6)
C(3)-N(1)	1.374(3)
C(3)-C(2)	1.385(3)
C(3)-C(8)	1.506(3)
C(2)-C(1)	1.431(3)
C(4)-N(1)	1.352(3)
C(4)-C(5)	1.369(3)
C(4)-H(4)	0.9300
C(1)-C(5)	1.398(3)
C(5)-H(5)	0.9300
N(1)-C(6)	1.482(3)
C(8)-C(9)	1.527(4)
C(8)-H(8A)	0.9700
C(8)-H(8B)	0.9700
C(6)-C(7)	1.518(4)
C(6)-H(6A)	0.9700
C(6)-H(6B)	0.9700
C(9)-H(9A)	0.9600
C(9)-H(9B)	0.9600
C(9)-H(9C)	0.9600
C(7)-H(7A)	0.9600
C(7)-H(7B)	0.9600
C(7)-H(7C)	0.9600
C(2)-O(2)-Re(1)	113.71(14)
C(1)-O(1)-Re(1)	113.50(14)
O(21)-C(21)-Re(1)	176.5(2)
O(22)-C(22)-Re(1)	178.8(2)
O(23)-C(23)-Re(1)	178.8(2)
C(11)-N(11)-C(15)	118.0(2)

314

C(11)-N(11)-Re(1)	121.16(17)
C(15)-N(11)-Re(1)	120.79(16)
N(11)-C(15)-C(14)	122.4(2)
N(11)-C(15)-H(15)	118.8
C(14)-C(15)-H(15)	118.8
C(12)-C(13)-C(14)	119.1(3)
C(12)-C(13)-H(13)	120.5
C(14)-C(13)-H(13)	120.5
C(13)-C(14)-C(15)	119.0(3)
C(13)-C(14)-H(14)	120.5
C(15)-C(14)-H(14)	120.5
N(11)-C(11)-C(12)	122.3(2)
N(11)-C(11)-H(11)	118.8
C(12)-C(11)-H(11)	118.8
C(13)-C(12)-C(11)	119.1(3)
C(13)-C(12)-H(12)	120.4
C(11)-C(12)-H(12)	120.4
H(25A)-O(25)-H(25B)	106(4)
N(1)-C(3)-C(2)	118.9(2)
N(1)-C(3)-C(8)	120.9(2)
C(2)-C(3)-C(8)	120.0(2)
O(2)-C(2)-C(3)	122.3(2)
O(2)-C(2)-C(1)	117.6(2)
C(3)-C(2)-C(1)	120.1(2)
N(1)-C(4)-C(5)	121.7(2)
N(1)-C(4)-H(4)	119.2
C(5)-C(4)-H(4)	119.2
O(1)-C(1)-C(5)	123.7(2)
O(1)-C(1)-C(2)	118.0(2)
C(5)-C(1)-C(2)	118.2(2)
C(4)-C(5)-C(1)	119.5(2)
C(4)-C(5)-H(5)	120.2
C(1)-C(5)-H(5)	120.2
C(4)-N(1)-C(3)	121.5(2)
C(4)-N(1)-C(6)	117.8(2)

C(3)-N(1)-C(6)	120.4(2)
C(3)-C(8)-C(9)	111.4(2)
C(3)-C(8)-H(8A)	109.4
C(9)-C(8)-H(8A)	109.4
C(3)-C(8)-H(8B)	109.4
C(9)-C(8)-H(8B)	109.4
H(8A)-C(8)-H(8B)	108.0
N(1)-C(6)-C(7)	110.9(2)
N(1)-C(6)-H(6A)	109.5
C(7)-C(6)-H(6A)	109.5
N(1)-C(6)-H(6B)	109.5
C(7)-C(6)-H(6B)	109.5
H(6A)-C(6)-H(6B)	108.0
C(8)-C(9)-H(9A)	109.5
C(8)-C(9)-H(9B)	109.5
H(9A)-C(9)-H(9B)	109.5
C(8)-C(9)-H(9C)	109.5
H(9A)-C(9)-H(9C)	109.5
H(9B)-C(9)-H(9C)	109.5
C(6)-C(7)-H(7A)	109.5
C(6)-C(7)-H(7B)	109.5
H(7A)-C(7)-H(7B)	109.5
C(6)-C(7)-H(7C)	109.5
H(7A)-C(7)-H(7C)	109.5
H(7B)-C(7)-H(7C)	109.5
C(23)-Re(1)-C(22)	89.25(11)
C(23)-Re(1)-C(21)	87.55(11)
C(22)-Re(1)-C(21)	87.62(11)
C(23)-Re(1)-O(2)	95.95(8)
C(22)-Re(1)-O(2)	172.65(9)
C(21)-Re(1)-O(2)	97.77(9)
C(23)-Re(1)-O(1)	172.18(9)
C(22)-Re(1)-O(1)	97.37(9)
C(21)-Re(1)-O(1)	96.85(9)
O(2)-Re(1)-O(1)	77.09(6)

C(23)-Re(1)-N(11)	93.56(9)
C(22)-Re(1)-N(11)	93.17(9)
C(21)-Re(1)-N(11)	178.64(9)
O(2)-Re(1)-N(11)	81.35(7)
O(1)-Re(1)-N(11)	81.95(7)

Table A. 60: Anisotropic displacement parameters ($Å^2$x 10^3) for *fac*-[Re(EE(naltol))(CO)$_3$(Pyr)] (12). The anisotropic displacement factor exponent takes the form: -2p^2[h^{2}a*^{2}U^{11} + ... + 2 h k a* b* U^{12}]

	U^{11}	U^{22}	U^{33}	U^{23}	U^{13}	U^{12}
O(2)	14(1)	18(1)	11(1)	1(1)	1(1)	-6(1)
O(1)	13(1)	20(1)	12(1)	-1(1)	1(1)	-2(1)
O(21)	31(1)	22(1)	33(1)	2(1)	-1(1)	9(1)
C(21)	16(1)	21(1)	17(1)	-1(1)	1(1)	-1(1)
O(22)	24(1)	30(1)	18(1)	-8(1)	-1(1)	-3(1)
C(22)	17(1)	17(1)	18(1)	0(1)	2(1)	0(1)
O(23)	27(1)	29(1)	29(1)	0(1)	13(1)	-8(1)
C(23)	20(1)	15(1)	14(1)	-1(1)	0(1)	0(1)
N(11)	11(1)	15(1)	16(1)	1(1)	0(1)	0(1)
C(15)	18(1)	20(1)	17(1)	0(1)	1(1)	1(1)
C(13)	14(1)	17(1)	37(2)	6(1)	2(1)	2(1)
C(14)	20(1)	21(1)	28(1)	-4(1)	6(1)	2(1)
C(11)	19(1)	24(1)	16(1)	3(1)	2(1)	1(1)
C(12)	21(1)	26(1)	25(1)	9(1)	0(1)	2(1)
O(25)	28(1)	41(1)	18(1)	9(1)	8(1)	14(1)
C(3)	13(1)	15(1)	13(1)	1(1)	1(1)	1(1)
C(2)	10(1)	13(1)	14(1)	2(1)	1(1)	1(1)
C(4)	15(1)	16(1)	17(1)	2(1)	4(1)	-2(1)
C(1)	11(1)	12(1)	13(1)	0(1)	-1(1)	3(1)
C(5)	16(1)	18(1)	13(1)	2(1)	2(1)	1(1)
N(1)	13(1)	14(1)	15(1)	-1(1)	-1(1)	-2(1)
C(8)	17(1)	21(1)	12(1)	-3(1)	1(1)	-2(1)
C(6)	18(1)	20(1)	19(1)	-3(1)	0(1)	-9(1)

C(9)	26(2)	30(2)	22(1)	-6(1)	5(1)	6(1)
C(7)	21(1)	28(1)	22(1)	1(1)	-5(1)	-5(1)
Re(1)	10(1)	13(1)	11(1)	0(1)	0(1)	-1(1)

Table A. 61: Hydrogen coordinates (x 10^4) and isotropic displacement parameters (Å^{2}x 10^3) for *fac*-[Re(EE(naltol))(CO)$_3$(Pyr)] (12).

	x	y	z	U(eq)
H(15)	1150	5018	2032	22
H(13)	260	8542	143	28
H(14)	470	7461	1771	27
H(11)	1411	4683	-857	23
H(12)	726	7113	-1183	29
H(4)	4886	6931	1224	19
H(5)	4153	5422	-9	19
H(8A)	3767	5968	4149	20
H(8B)	3035	4794	3844	20
H(6A)	4446	7908	3562	23
H(6B)	5071	8146	2770	23
H(9A)	2985	8211	3485	39
H(9B)	2562	7350	4342	39
H(9C)	2252	7034	3199	39
H(7A)	5049	5342	4013	36
H(7B)	5667	6779	4233	36
H(7C)	5698	5683	3268	36
H(25A)	3370(20)	1550(50)	3940(30)	40(10)
H(25B)	3280(30)	2020(60)	2960(40)	64(15)

Table A. 62: Torsion angles [°] for *fac*-[Re(EE(naltol))(CO)$_3$(Pyr)] (12).

C(11)-N(11)-C(15)-C(14)	-0.6(4)
Re(1)-N(11)-C(15)-C(14)	-178.9(2)
C(12)-C(13)-C(14)-C(15)	0.5(4)

318

N(11)-C(15)-C(14)-C(13)	0.2(4)
C(15)-N(11)-C(11)-C(12)	0.4(4)
Re(1)-N(11)-C(11)-C(12)	178.6(2)
C(14)-C(13)-C(12)-C(11)	-0.7(4)
N(11)-C(11)-C(12)-C(13)	0.3(4)
Re(1)-O(2)-C(2)-C(3)	177.85(18)
Re(1)-O(2)-C(2)-C(1)	-3.5(3)
N(1)-C(3)-C(2)-O(2)	175.1(2)
C(8)-C(3)-C(2)-O(2)	-9.1(4)
N(1)-C(3)-C(2)-C(1)	-3.5(3)
C(8)-C(3)-C(2)-C(1)	172.3(2)
Re(1)-O(1)-C(1)-C(5)	178.50(18)
Re(1)-O(1)-C(1)-C(2)	0.3(3)
O(2)-C(2)-C(1)-O(1)	2.2(3)
C(3)-C(2)-C(1)-O(1)	-179.1(2)
O(2)-C(2)-C(1)-C(5)	-176.1(2)
C(3)-C(2)-C(1)-C(5)	2.6(3)
N(1)-C(4)-C(5)-C(1)	-2.4(4)
O(1)-C(1)-C(5)-C(4)	-177.8(2)
C(2)-C(1)-C(5)-C(4)	0.4(3)
C(5)-C(4)-N(1)-C(3)	1.5(4)
C(5)-C(4)-N(1)-C(6)	174.7(2)
C(2)-C(3)-N(1)-C(4)	1.5(3)
C(8)-C(3)-N(1)-C(4)	-174.2(2)
C(2)-C(3)-N(1)-C(6)	-171.5(2)
C(8)-C(3)-N(1)-C(6)	12.7(3)
N(1)-C(3)-C(8)-C(9)	85.3(3)
C(2)-C(3)-C(8)-C(9)	-90.4(3)
C(4)-N(1)-C(6)-C(7)	-95.6(3)
C(3)-N(1)-C(6)-C(7)	77.7(3)

Table A. 63: Hydrogen bonds for *fac*-[Re(EE(naltol))(CO)$_3$(Pyr)] (12) [Å and °].

D-H...A	d(D-H)	d(H...A)	d(D...A)	<(DHA)
O(25)-H(25A)...O(1)#1	0.82(4)	1.96(4)	2.775(3)	173(4)
O(25)-H(25B)...O(2)	0.86(6)	2.00(6)	2.843(3)	167(5)
C(4)-H(4)...O(25)#2	0.93	2.56	3.272(3)	134.0
C(8)-H(8B)...O(2)	0.97	2.50	2.859(3)	101.8

Symmetry transformations used to generate equivalent atoms: #1 x,-y+1/2,z+1/2   #2 -x+1,y+1/2,-z+1/2

Table A. 64: Atomic coordinates (x 10^4) and equivalent isotropic displacement parameters (Å^2 x 10^3) for [Rh(EE(naltol))(CO)$_2$] (13). U(eq) is defined as one third of the trace of the orthogonalized U^{ij} tensor.

	x	y	z	U(eq)
Rh(1)	6854(1)	321(1)	8699(1)	12(1)
O(2)	5427(1)	1446(1)	9298(1)	13(1)
O(1)	5717(1)	349(1)	6941(1)	16(1)
O(4)	8743(2)	-1393(1)	7601(2)	29(1)
N(1)	2400(1)	2370(1)	7460(1)	12(1)
O(3)	8503(2)	306(1)	11278(2)	29(1)
C(8)	3110(2)	2826(1)	9854(2)	12(1)
C(3)	3318(2)	2234(1)	8522(2)	11(1)
C(21)	7858(2)	321(1)	10305(2)	18(1)
C(5)	3692(2)	1179(1)	6013(2)	14(1)
C(6)	1104(2)	3001(1)	7635(2)	14(1)
C(7)	-24(2)	2272(2)	8223(2)	18(1)
C(9)	3781(2)	3970(1)	9862(2)	17(1)
C(22)	8050(2)	-725(1)	8035(2)	17(1)
C(4)	2591(2)	1865(1)	6237(2)	14(1)
C(1)	4652(2)	1006(1)	7066(2)	12(1)
C(2)	4471(2)	1576(1)	8327(2)	11(1)

Table A. 65: Bond lengths [Å] and angles [°] for [Rh(EE(naltol))(CO)₂] (13).

_____

Rh(1)-C(22)	1.8406(18)
Rh(1)-C(21)	1.843(2)
Rh(1)-O(2)	2.0333(12)
Rh(1)-O(1)	2.0372(15)
O(2)-C(2)	1.3328(19)
O(1)-C(1)	1.313(2)
O(4)-C(22)	1.137(2)
N(1)-C(4)	1.357(2)
N(1)-C(3)	1.374(2)
N(1)-C(6)	1.485(2)
O(3)-C(21)	1.137(2)
C(8)-C(3)	1.502(2)
C(8)-C(9)	1.531(2)
C(8)-H(8A)	0.9700
C(8)-H(8B)	0.9700
C(3)-C(2)	1.389(2)
C(5)-C(4)	1.374(2)
C(5)-C(1)	1.401(2)
C(5)-H(5)	0.9300
C(6)-C(7)	1.523(2)
C(6)-H(6A)	0.9700
C(6)-H(6B)	0.9700
C(7)-H(7A)	0.9600
C(7)-H(7B)	0.9600
C(7)-H(7C)	0.9600
C(9)-H(9A)	0.9600
C(9)-H(9B)	0.9600
C(9)-H(9C)	0.9600
C(4)-H(4)	0.9300
C(1)-C(2)	1.425(2)
C(22)-Rh(1)-C(21)	88.20(8)
C(22)-Rh(1)-O(2)	175.20(6)

C(21)-Rh(1)-O(2)	96.48(7)
C(22)-Rh(1)-O(1)	93.09(7)
C(21)-Rh(1)-O(1)	178.70(6)
O(2)-Rh(1)-O(1)	82.23(5)
C(2)-O(2)-Rh(1)	110.35(9)
C(1)-O(1)-Rh(1)	110.79(10)
C(4)-N(1)-C(3)	121.35(14)
C(4)-N(1)-C(6)	117.09(13)
C(3)-N(1)-C(6)	121.39(13)
C(3)-C(8)-C(9)	112.13(13)
C(3)-C(8)-H(8A)	109.2
C(9)-C(8)-H(8A)	109.2
C(3)-C(8)-H(8B)	109.2
C(9)-C(8)-H(8B)	109.2
H(8A)-C(8)-H(8B)	107.9
N(1)-C(3)-C(2)	119.02(14)
N(1)-C(3)-C(8)	120.54(13)
C(2)-C(3)-C(8)	120.39(13)
O(3)-C(21)-Rh(1)	178.21(17)
C(4)-C(5)-C(1)	119.25(14)
C(4)-C(5)-H(5)	120.4
C(1)-C(5)-H(5)	120.4
N(1)-C(6)-C(7)	110.97(13)
N(1)-C(6)-H(6A)	109.4
C(7)-C(6)-H(6A)	109.4
N(1)-C(6)-H(6B)	109.4
C(7)-C(6)-H(6B)	109.4
H(6A)-C(6)-H(6B)	108.0
C(6)-C(7)-H(7A)	109.5
C(6)-C(7)-H(7B)	109.5
H(7A)-C(7)-H(7B)	109.5
C(6)-C(7)-H(7C)	109.5
H(7A)-C(7)-H(7C)	109.5
H(7B)-C(7)-H(7C)	109.5
C(8)-C(9)-H(9A)	109.5

C(8)-C(9)-H(9B)	109.5
H(9A)-C(9)-H(9B)	109.5
C(8)-C(9)-H(9C)	109.5
H(9A)-C(9)-H(9C)	109.5
H(9B)-C(9)-H(9C)	109.5
O(4)-C(22)-Rh(1)	177.12(16)
N(1)-C(4)-C(5)	121.63(14)
N(1)-C(4)-H(4)	119.2
C(5)-C(4)-H(4)	119.2
O(1)-C(1)-C(5)	122.94(14)
O(1)-C(1)-C(2)	118.46(14)
C(5)-C(1)-C(2)	118.59(14)
O(2)-C(2)-C(3)	121.98(14)
O(2)-C(2)-C(1)	117.98(14)
C(3)-C(2)-C(1)	120.04(14)

Table A. 66: Anisotropic displacement parameters ($Å^2$ x 10^3) for [Rh(EE(naltol))(CO)₂] (13). The anisotropic displacement factor exponent takes the form: $-2p^2[h^2a^{*2}U^{11} + ... + 2 h k a^* b^* U^{12}]$

	U^{11}	U^{22}	U^{33}	U^{23}	U^{13}	U^{12}
Rh(1)	10(1)	11(1)	14(1)	0(1)	1(1)	1(1)
O(2)	12(1)	14(1)	13(1)	-2(1)	-3(1)	2(1)
O(1)	16(1)	17(1)	15(1)	-4(1)	0(1)	3(1)
O(4)	28(1)	23(1)	36(1)	-1(1)	12(1)	10(1)
N(1)	12(1)	10(1)	13(1)	1(1)	-1(1)	0(1)
O(3)	29(1)	32(1)	26(1)	-4(1)	-11(1)	8(1)
C(8)	13(1)	12(1)	11(1)	-1(1)	0(1)	2(1)
C(3)	13(1)	9(1)	10(1)	0(1)	0(1)	-2(1)
C(21)	16(1)	15(1)	22(1)	-1(1)	2(1)	4(1)
C(5)	18(1)	15(1)	10(1)	-3(1)	1(1)	-3(1)
C(6)	13(1)	15(1)	16(1)	0(1)	-2(1)	4(1)
C(7)	13(1)	24(1)	17(1)	1(1)	1(1)	0(1)
C(9)	22(1)	12(1)	18(1)	-4(1)	-1(1)	0(1)
C(22)	16(1)	16(1)	19(1)	3(1)	2(1)	-1(1)

C(4)	14(1)	16(1)	11(1)	0(1)	-3(1)	-3(1)
C(1)	12(1)	11(1)	13(1)	-1(1)	3(1)	-2(1)
C(2)	12(1)	10(1)	10(1)	0(1)	0(1)	-3(1)

Table A. 67: Hydrogen coordinates (x 10^4) and isotropic displacement parameters ($Å^2$x 10^3) for [Rh(EE(naltol))(CO)$_2$] (13).

	x	y	z	U(eq)
H(8A)	3498	2387	10591	15
H(8B)	2132	2905	10019	15
H(5)	3799	833	5171	17
H(6A)	806	3292	6758	17
H(6B)	1269	3620	8244	17
H(7A)	-118	1619	7674	27
H(7B)	-878	2670	8222	27
H(7C)	215	2068	9143	27
H(9A)	4755	3894	9739	26
H(9B)	3606	4326	10720	26
H(9C)	3402	4406	9132	26
H(4)	1961	1986	5533	16

Table A. 68: Torsion angles [°] for [Rh(EE(naltol))(CO)$_2$] (13).

C(4)-N(1)-C(3)-C(2)	0.8(2)
C(6)-N(1)-C(3)-C(2)	175.90(13)
C(4)-N(1)-C(3)-C(8)	178.19(14)
C(6)-N(1)-C(3)-C(8)	-6.7(2)
C(9)-C(8)-C(3)-N(1)	-88.48(17)
C(9)-C(8)-C(3)-C(2)	88.92(17)
C(4)-N(1)-C(6)-C(7)	90.78(16)
C(3)-N(1)-C(6)-C(7)	-84.56(17)
C(3)-N(1)-C(4)-C(5)	1.4(2)
C(6)-N(1)-C(4)-C(5)	-173.97(14)

C(1)-C(5)-C(4)-N(1)	-0.8(2)
Rh(1)-O(1)-C(1)-C(5)	-179.80(12)
Rh(1)-O(1)-C(1)-C(2)	0.69(17)
C(4)-C(5)-C(1)-O(1)	178.75(14)
C(4)-C(5)-C(1)-C(2)	-1.7(2)
Rh(1)-O(2)-C(2)-C(3)	174.82(11)
Rh(1)-O(2)-C(2)-C(1)	-4.52(16)
N(1)-C(3)-C(2)-O(2)	177.34(13)
C(8)-C(3)-C(2)-O(2)	-0.1(2)
N(1)-C(3)-C(2)-C(1)	-3.3(2)
C(8)-C(3)-C(2)-C(1)	179.22(13)
O(1)-C(1)-C(2)-O(2)	2.7(2)
C(5)-C(1)-C(2)-O(2)	-176.82(13)
O(1)-C(1)-C(2)-C(3)	-176.64(13)
C(5)-C(1)-C(2)-C(3)	3.8(2)

Table A. 69: Hydrogen bonds for [Rh(EE(naltol))(CO)$_2$] (13) [Å and °].

D-H…A	d(D-H) (Å)	d(H…A) (Å)	d(D…A) (Å)	∟ (D-H…A)(°)
C5-H5...O1 [(i)]	0.93	2.56	3.481(3)	171
C6-H6A...O2 [(ii)]	0.97	2.45	3.392(2)	163

Symmetry codes, transformations used to generate equivalent atoms: (i) 1-x, -y, 1-z; (ii) x-1/2, ½-y, z-1/2;

Table A. 70: Atomic coordinates (x 10^4) and equivalent isotropic displacement parameters (Å^2 x 10^3) for *trans*-[RhCO(PPh$_3$)$_2$Cl]. U(eq) is defined as one third of the trace of the orthogonalized U^{ij} tensor.

	x	y	z	U(eq)
Rh(1)	6808(1)	1483(1)	10138(1)	19(1)
P(2)	6666(1)	1258(1)	8227(1)	17(1)
P(1)	6902(1)	1649(1)	12061(1)	20(1)
Cl(1)	7019(1)	514(1)	10567(1)	27(1)
C(32B)	4625(2)	551(1)	7761(2)	24(1)
C(36A)	4769(2)	1018(1)	11527(2)	26(1)

C(6A)	6157(2)	2752(1)	12138(2)	29(1)
O(1)	6805(2)	2694(1)	9639(2)	45(1)
C(36B)	5038(2)	818(1)	6046(2)	29(1)
C(21B)	8007(2)	852(1)	8320(2)	19(1)
C(31B)	5341(2)	845(1)	7277(2)	20(1)
C(2A)	8263(2)	2566(1)	13398(2)	25(1)
C(4A)	7433(2)	3488(1)	13325(2)	33(1)
C(2B)	7522(2)	1974(1)	6844(2)	29(1)
C(24B)	10125(2)	256(1)	8597(2)	38(1)
C(5B)	5388(2)	2605(1)	6038(2)	37(1)
C(1B)	6593(2)	1840(1)	7224(2)	21(1)
C(3B)	7379(2)	2422(1)	6062(2)	35(1)
C(31A)	5494(2)	1441(1)	12247(2)	23(1)
C(26A)	8077(2)	1103(1)	14274(2)	34(1)
C(1A)	7129(2)	2374(1)	12586(2)	22(1)
C(3A)	8409(2)	3124(1)	13751(2)	32(1)
C(34B)	3350(2)	212(1)	5804(2)	34(1)
C(25B)	10203(2)	733(1)	9252(2)	39(1)
C(35A)	3677(2)	860(1)	11618(2)	32(1)
C(35B)	4052(2)	501(1)	5316(2)	36(1)
C(22A)	9286(2)	1247(1)	13102(2)	41(1)
C(26B)	9147(2)	1028(1)	9123(2)	32(1)
C(33B)	3630(2)	235(1)	7019(2)	31(1)
C(34A)	3298(2)	1134(1)	12419(2)	35(1)
C(32A)	5118(2)	1703(1)	13079(2)	30(1)
C(6B)	5525(2)	2164(1)	6818(2)	32(1)
C(1)	6774(2)	2229(1)	9825(2)	28(1)
C(33A)	4016(2)	1549(1)	13153(2)	35(1)
C(25A)	9093(3)	862(1)	15181(2)	47(1)
C(4B)	6318(2)	2733(1)	5658(2)	34(1)
C(5A)	6302(2)	3302(1)	12517(2)	32(1)
C(21A)	8165(2)	1289(1)	13232(2)	26(1)
C(24A)	10199(3)	820(1)	15047(3)	49(1)
C(23B)	8996(3)	76(1)	7814(3)	45(1)
C(23A)	10307(3)	1023(1)	14022(3)	49(1)

C(22B)	7935(2)	371(1)	7671(2)	33(1)

Table A. 71: Bond lengths [Å] and angles [°] for *trans*-[RhCO(PPh₃)₂Cl].

_____

Rh(1)-C(1)	1.819(2)
Rh(1)-P(2)	2.3179(11)
Rh(1)-P(1)	2.3225(11)
Rh(1)-Cl(1)	2.3654(7)
P(2)-C(21B)	1.824(2)
P(2)-C(1B)	1.827(2)
P(2)-C(31B)	1.828(2)
P(1)-C(21A)	1.823(2)
P(1)-C(1A)	1.829(2)
P(1)-C(31A)	1.833(2)
C(32B)-C(33B)	1.391(3)
C(32B)-C(31B)	1.393(3)
C(32B)-H(32B)	0.9300
C(36A)-C(35A)	1.390(3)
C(36A)-C(31A)	1.391(3)
C(36A)-H(36A)	0.9300
C(6A)-C(5A)	1.381(3)
C(6A)-C(1A)	1.394(3)
C(6A)-H(6A)	0.9300
O(1)-C(1)	1.138(3)
C(36B)-C(35B)	1.382(3)
C(36B)-C(31B)	1.393(3)
C(36B)-H(36B)	0.9300
C(21B)-C(22B)	1.375(3)
C(21B)-C(26B)	1.383(3)
C(2A)-C(3A)	1.390(3)
C(2A)-C(1A)	1.394(3)
C(2A)-H(2A)	0.9300
C(4A)-C(3A)	1.375(3)
C(4A)-C(5A)	1.386(3)
C(4A)-H(4A)	0.9300

C(2B)-C(1B)	1.384(3)
C(2B)-C(3B)	1.395(3)
C(2B)-H(2B)	0.9300
C(24B)-C(23B)	1.370(4)
C(24B)-C(25B)	1.370(4)
C(24B)-H(24B)	0.9300
C(5B)-C(6B)	1.381(3)
C(5B)-C(4B)	1.382(4)
C(5B)-H(5B)	0.9300
C(1B)-C(6B)	1.395(3)
C(3B)-C(4B)	1.374(4)
C(3B)-H(3B)	0.9300
C(31A)-C(32A)	1.399(3)
C(26A)-C(21A)	1.380(3)
C(26A)-C(25A)	1.396(3)
C(26A)-H(26A)	0.9300
C(3A)-H(3A)	0.9300
C(34B)-C(35B)	1.378(3)
C(34B)-C(33B)	1.378(4)
C(34B)-H(34B)	0.9300
C(25B)-C(26B)	1.389(3)
C(25B)-H(25B)	0.9300
C(35A)-C(34A)	1.382(3)
C(35A)-H(35A)	0.9300
C(35B)-H(35B)	0.9300
C(22A)-C(23A)	1.391(4)
C(22A)-C(21A)	1.398(3)
C(22A)-H(22A)	0.9300
C(26B)-H(26B)	0.9300
C(33B)-H(33B)	0.9300
C(34A)-C(33A)	1.379(4)
C(34A)-H(34A)	0.9300
C(32A)-C(33A)	1.390(3)
C(32A)-H(32A)	0.9300
C(6B)-H(6B)	0.9300

C(33A)-H(33A)	0.9300
C(25A)-C(24A)	1.383(4)
C(25A)-H(25A)	0.9300
C(4B)-H(4B)	0.9300
C(5A)-H(5A)	0.9300
C(24A)-C(23A)	1.384(4)
C(24A)-H(24A)	0.9300
C(23B)-C(22B)	1.390(3)
C(23B)-H(23B)	0.9300
C(23A)-H(23A)	0.9300
C(22B)-H(22B)	0.9300
C(1)-Rh(1)-P(2)	91.85(7)
C(1)-Rh(1)-P(1)	91.74(7)
P(2)-Rh(1)-P(1)	176.16(2)
C(1)-Rh(1)-Cl(1)	175.45(7)
P(2)-Rh(1)-Cl(1)	87.28(2)
P(1)-Rh(1)-Cl(1)	89.25(2)
C(21B)-P(2)-C(1B)	105.09(9)
C(21B)-P(2)-C(31B)	105.22(10)
C(1B)-P(2)-C(31B)	100.77(10)
C(21B)-P(2)-Rh(1)	109.87(7)
C(1B)-P(2)-Rh(1)	116.95(7)
C(31B)-P(2)-Rh(1)	117.57(7)
C(21A)-P(1)-C(1A)	102.21(10)
C(21A)-P(1)-C(31A)	106.49(11)
C(1A)-P(1)-C(31A)	103.32(10)
C(21A)-P(1)-Rh(1)	113.80(8)
C(1A)-P(1)-Rh(1)	116.96(7)
C(31A)-P(1)-Rh(1)	112.79(7)
C(33B)-C(32B)-C(31B)	120.1(2)
C(33B)-C(32B)-H(32B)	120.0
C(31B)-C(32B)-H(32B)	120.0
C(35A)-C(36A)-C(31A)	120.8(2)
C(35A)-C(36A)-H(36A)	119.6

C(31A)-C(36A)-H(36A)	119.6
C(5A)-C(6A)-C(1A)	120.7(2)
C(5A)-C(6A)-H(6A)	119.7
C(1A)-C(6A)-H(6A)	119.7
C(35B)-C(36B)-C(31B)	120.6(2)
C(35B)-C(36B)-H(36B)	119.7
C(31B)-C(36B)-H(36B)	119.7
C(22B)-C(21B)-C(26B)	118.8(2)
C(22B)-C(21B)-P(2)	123.38(16)
C(26B)-C(21B)-P(2)	117.73(16)
C(36B)-C(31B)-C(32B)	118.91(19)
C(36B)-C(31B)-P(2)	119.77(16)
C(32B)-C(31B)-P(2)	121.32(16)
C(3A)-C(2A)-C(1A)	120.1(2)
C(3A)-C(2A)-H(2A)	119.9
C(1A)-C(2A)-H(2A)	119.9
C(3A)-C(4A)-C(5A)	119.9(2)
C(3A)-C(4A)-H(4A)	120.1
C(5A)-C(4A)-H(4A)	120.1
C(1B)-C(2B)-C(3B)	120.1(2)
C(1B)-C(2B)-H(2B)	120.0
C(3B)-C(2B)-H(2B)	120.0
C(23B)-C(24B)-C(25B)	119.3(2)
C(23B)-C(24B)-H(24B)	120.3
C(25B)-C(24B)-H(24B)	120.3
C(6B)-C(5B)-C(4B)	120.1(2)
C(6B)-C(5B)-H(5B)	120.0
C(4B)-C(5B)-H(5B)	120.0
C(2B)-C(1B)-C(6B)	118.8(2)
C(2B)-C(1B)-P(2)	123.99(17)
C(6B)-C(1B)-P(2)	117.21(16)
C(4B)-C(3B)-C(2B)	120.6(2)
C(4B)-C(3B)-H(3B)	119.7
C(2B)-C(3B)-H(3B)	119.7
C(36A)-C(31A)-C(32A)	119.0(2)

C(36A)-C(31A)-P(1)	119.15(16)
C(32A)-C(31A)-P(1)	121.86(17)
C(21A)-C(26A)-C(25A)	120.2(3)
C(21A)-C(26A)-H(26A)	119.9
C(25A)-C(26A)-H(26A)	119.9
C(6A)-C(1A)-C(2A)	118.8(2)
C(6A)-C(1A)-P(1)	119.41(17)
C(2A)-C(1A)-P(1)	121.80(16)
C(4A)-C(3A)-C(2A)	120.4(2)
C(4A)-C(3A)-H(3A)	119.8
C(2A)-C(3A)-H(3A)	119.8
C(35B)-C(34B)-C(33B)	120.3(2)
C(35B)-C(34B)-H(34B)	119.8
C(33B)-C(34B)-H(34B)	119.8
C(24B)-C(25B)-C(26B)	120.2(2)
C(24B)-C(25B)-H(25B)	119.9
C(26B)-C(25B)-H(25B)	119.9
C(34A)-C(35A)-C(36A)	119.5(2)
C(34A)-C(35A)-H(35A)	120.2
C(36A)-C(35A)-H(35A)	120.2
C(34B)-C(35B)-C(36B)	119.9(2)
C(34B)-C(35B)-H(35B)	120.0
C(36B)-C(35B)-H(35B)	120.0
C(23A)-C(22A)-C(21A)	120.1(3)
C(23A)-C(22A)-H(22A)	120.0
C(21A)-C(22A)-H(22A)	119.9
C(21B)-C(26B)-C(25B)	120.6(2)
C(21B)-C(26B)-H(26B)	119.7
C(25B)-C(26B)-H(26B)	119.7
C(34B)-C(33B)-C(32B)	120.1(2)
C(34B)-C(33B)-H(33B)	120.0
C(32B)-C(33B)-H(33B)	120.0
C(33A)-C(34A)-C(35A)	120.4(2)
C(33A)-C(34A)-H(34A)	119.8
C(35A)-C(34A)-H(34A)	119.8

C(33A)-C(32A)-C(31A)	119.9(2)
C(33A)-C(32A)-H(32A)	120.1
C(31A)-C(32A)-H(32A)	120.1
C(5B)-C(6B)-C(1B)	120.8(2)
C(5B)-C(6B)-H(6B)	119.6
C(1B)-C(6B)-H(6B)	119.6
O(1)-C(1)-Rh(1)	177.0(2)
C(34A)-C(33A)-C(32A)	120.3(2)
C(34A)-C(33A)-H(33A)	119.8
C(32A)-C(33A)-H(33A)	119.8
C(24A)-C(25A)-C(26A)	120.0(3)
C(24A)-C(25A)-H(25A)	120.0
C(26A)-C(25A)-H(25A)	120.0
C(3B)-C(4B)-C(5B)	119.7(2)
C(3B)-C(4B)-H(4B)	120.2
C(5B)-C(4B)-H(4B)	120.2
C(6A)-C(5A)-C(4A)	120.1(2)
C(6A)-C(5A)-H(5A)	120.0
C(4A)-C(5A)-H(5A)	120.0
C(26A)-C(21A)-C(22A)	119.6(2)
C(26A)-C(21A)-P(1)	122.11(18)
C(22A)-C(21A)-P(1)	118.07(19)
C(25A)-C(24A)-C(23A)	120.2(2)
C(25A)-C(24A)-H(24A)	119.9
C(23A)-C(24A)-H(24A)	119.9
C(24B)-C(23B)-C(22B)	120.9(2)
C(24B)-C(23B)-H(23B)	119.5
C(22B)-C(23B)-H(23B)	119.5
C(24A)-C(23A)-C(22A)	119.9(3)
C(24A)-C(23A)-H(23A)	120.1
C(22A)-C(23A)-H(23A)	120.1
C(21B)-C(22B)-C(23B)	120.1(2)
C(21B)-C(22B)-H(22B)	120.0
C(23B)-C(22B)-H(22B)	120.0

Table A. 72: Anisotropic displacement parameters ($Å^2$ x 10^3) for *trans*-[RhCO(PPh$_3$)$_2$Cl]. The anisotropic displacement factor exponent takes the form: -2p^2[h^{2}a*^{2}U^{11} + ... + 2 h k a* b* U^{12}]

	U^{11}	U^{22}	U^{33}	U^{23}	U^{13}	U^{12}
Rh(1)	18(1)	21(1)	17(1)	-1(1)	7(1)	2(1)
P(2)	16(1)	19(1)	18(1)	0(1)	7(1)	1(1)
P(1)	19(1)	24(1)	17(1)	-2(1)	6(1)	2(1)
Cl(1)	30(1)	28(1)	26(1)	4(1)	12(1)	7(1)
C(32B)	21(1)	27(1)	24(1)	4(1)	8(1)	1(1)
C(36A)	24(1)	30(1)	23(1)	2(1)	7(1)	2(1)
C(6A)	24(1)	32(1)	26(1)	0(1)	7(1)	2(1)
O(1)	71(1)	26(1)	44(1)	0(1)	29(1)	-1(1)
C(36B)	29(1)	35(1)	22(1)	0(1)	8(1)	-9(1)
C(21B)	17(1)	22(1)	20(1)	3(1)	9(1)	1(1)
C(31B)	16(1)	22(1)	20(1)	0(1)	5(1)	1(1)
C(2A)	20(1)	29(1)	28(1)	-3(1)	11(1)	0(1)
C(4A)	39(1)	24(1)	42(1)	-3(1)	24(1)	-5(1)
C(2B)	24(1)	35(1)	28(1)	3(1)	10(1)	-3(1)
C(24B)	32(1)	40(1)	52(2)	20(1)	27(1)	18(1)
C(5B)	42(1)	32(1)	37(1)	10(1)	16(1)	12(1)
C(1B)	24(1)	20(1)	19(1)	-2(1)	9(1)	-2(1)
C(3B)	35(1)	40(1)	34(1)	6(1)	17(1)	-10(1)
C(31A)	21(1)	27(1)	19(1)	3(1)	7(1)	2(1)
C(26A)	28(1)	35(1)	30(1)	5(1)	0(1)	-7(1)
C(1A)	23(1)	25(1)	20(1)	-1(1)	12(1)	1(1)
C(3A)	26(1)	33(1)	38(1)	-7(1)	15(1)	-7(1)
C(34B)	26(1)	30(1)	34(1)	2(1)	-2(1)	-8(1)
C(25B)	18(1)	48(2)	46(2)	9(1)	9(1)	5(1)
C(35A)	26(1)	37(1)	30(1)	4(1)	7(1)	-3(1)
C(35B)	38(1)	39(1)	21(1)	0(1)	2(1)	-10(1)
C(22A)	32(1)	56(2)	31(1)	-8(1)	8(1)	15(1)
C(26B)	21(1)	34(1)	37(1)	-7(1)	8(1)	1(1)
C(33B)	22(1)	32(1)	38(1)	7(1)	10(1)	-5(1)
C(34A)	25(1)	46(2)	38(1)	12(1)	16(1)	1(1)

C(32A)	33(1)	32(1)	26(1)	1(1)	14(1)	0(1)
C(6B)	34(1)	33(1)	36(1)	9(1)	22(1)	9(1)
C(1)	31(1)	34(1)	20(1)	-4(1)	11(1)	-1(1)
C(33A)	39(1)	41(1)	35(1)	4(1)	24(1)	7(1)
C(25A)	47(2)	43(2)	30(1)	9(1)	-7(1)	-11(1)
C(4B)	47(2)	27(1)	27(1)	5(1)	11(1)	-4(1)
C(5A)	34(1)	26(1)	38(1)	5(1)	17(1)	7(1)
C(21A)	26(1)	22(1)	23(1)	-6(1)	3(1)	4(1)
C(24A)	43(2)	41(2)	39(2)	-9(1)	-12(1)	16(1)
C(23B)	45(2)	36(1)	60(2)	-9(1)	28(1)	11(1)
C(23A)	33(1)	62(2)	42(2)	-19(1)	4(1)	18(1)
C(22B)	27(1)	34(1)	39(1)	-9(1)	13(1)	1(1)

Table A. 73: Hydrogen coordinates (x 10^4) and isotropic displacement parameters (Å^{2}x 10^3) for *trans*-[RhCO(PPh$_3$)$_2$Cl].

_____

	x	y	z	U(eq)
H(32B)	4813	566	8581	29
H(36A)	5017	838	10978	32
H(6A)	5402	2632	11578	34
H(36B)	5503	1016	5711	34
H(2A)	8923	2320	13705	30
H(4A)	7531	3859	13578	39
H(2B)	8243	1765	7110	35
H(24B)	10830	57	8683	46
H(5B)	4669	2815	5769	44
H(3B)	8007	2510	5812	42
H(26A)	7338	1138	14373	41
H(3A)	9173	3252	14278	38
H(34B)	2684	0	5311	41
H(25B)	10966	859	9786	46
H(35A)	3206	571	11144	38
H(35B)	3863	481	4496	43

H(22A)	9349	1368	12399	49
H(26B)	9206	1348	9580	38
H(33B)	3153	39	7344	37
H(34A)	2555	1038	12463	42
H(32A)	5604	1979	13583	35
H(6B)	4899	2081	7075	38
H(33A)	3761	1726	13699	42
H(25A)	9026	730	15875	57
H(4B)	6225	3030	5132	41
H(5A)	5640	3547	12231	38
H(24A)	10872	655	15647	59
H(23B)	8939	-249	7372	54
H(23A)	11062	1010	13950	59
H(22B)	7175	244	7135	40

Table A. 74: Torsion angles [°] for *trans*-[RhCO(PPh$_3$)$_2$Cl].

_____

C(1B)-P(2)-C(21B)-C(22B)	-99.8(2)
C(31B)-P(2)-C(21B)-C(22B)	6.1(2)
Rh(1)-P(2)-C(21B)-C(22B)	133.62(18)
C(1B)-P(2)-C(21B)-C(26B)	82.85(19)
C(31B)-P(2)-C(21B)-C(26B)	-171.25(17)
Rh(1)-P(2)-C(21B)-C(26B)	-43.78(19)
C(35B)-C(36B)-C(31B)-C(32B)	-0.7(3)
C(35B)-C(36B)-C(31B)-P(2)	178.87(19)
C(33B)-C(32B)-C(31B)-C(36B)	0.3(3)
C(33B)-C(32B)-C(31B)-P(2)	-179.30(17)
C(21B)-P(2)-C(31B)-C(36B)	-73.72(19)
C(1B)-P(2)-C(31B)-C(36B)	35.3(2)
Rh(1)-P(2)-C(31B)-C(36B)	163.64(15)
C(21B)-P(2)-C(31B)-C(32B)	105.89(18)
C(1B)-P(2)-C(31B)-C(32B)	-145.05(17)
Rh(1)-P(2)-C(31B)-C(32B)	-16.7(2)
C(3B)-C(2B)-C(1B)-C(6B)	-0.5(3)
C(3B)-C(2B)-C(1B)-P(2)	179.03(18)

C(21B)-P(2)-C(1B)-C(2B)	-10.9(2)
C(31B)-P(2)-C(1B)-C(2B)	-120.02(19)
Rh(1)-P(2)-C(1B)-C(2B)	111.28(18)
C(21B)-P(2)-C(1B)-C(6B)	168.66(17)
C(31B)-P(2)-C(1B)-C(6B)	59.51(19)
Rh(1)-P(2)-C(1B)-C(6B)	-69.19(19)
C(1B)-C(2B)-C(3B)-C(4B)	-0.2(4)
C(35A)-C(36A)-C(31A)-C(32A)	0.8(3)
C(35A)-C(36A)-C(31A)-P(1)	-178.19(17)
C(21A)-P(1)-C(31A)-C(36A)	-98.48(18)
C(1A)-P(1)-C(31A)-C(36A)	154.25(17)
Rh(1)-P(1)-C(31A)-C(36A)	27.03(19)
C(21A)-P(1)-C(31A)-C(32A)	82.6(2)
C(1A)-P(1)-C(31A)-C(32A)	-24.7(2)
Rh(1)-P(1)-C(31A)-C(32A)	-151.93(16)
C(5A)-C(6A)-C(1A)-C(2A)	-1.9(3)
C(5A)-C(6A)-C(1A)-P(1)	-179.93(17)
C(3A)-C(2A)-C(1A)-C(6A)	0.2(3)
C(3A)-C(2A)-C(1A)-P(1)	178.18(17)
C(21A)-P(1)-C(1A)-C(6A)	-160.83(18)
C(31A)-P(1)-C(1A)-C(6A)	-50.36(19)
Rh(1)-P(1)-C(1A)-C(6A)	74.18(18)
C(21A)-P(1)-C(1A)-C(2A)	21.2(2)
C(31A)-P(1)-C(1A)-C(2A)	131.66(18)
Rh(1)-P(1)-C(1A)-C(2A)	-103.80(17)
C(5A)-C(4A)-C(3A)-C(2A)	-1.5(4)
C(1A)-C(2A)-C(3A)-C(4A)	1.5(3)
C(23B)-C(24B)-C(25B)-C(26B)	0.1(4)
C(31A)-C(36A)-C(35A)-C(34A)	1.2(3)
C(33B)-C(34B)-C(35B)-C(36B)	-0.4(4)
C(31B)-C(36B)-C(35B)-C(34B)	0.8(4)
C(22B)-C(21B)-C(26B)-C(25B)	1.4(4)
P(2)-C(21B)-C(26B)-C(25B)	178.91(19)
C(24B)-C(25B)-C(26B)-C(21B)	-1.0(4)
C(35B)-C(34B)-C(33B)-C(32B)	0.0(4)

C(31B)-C(32B)-C(33B)-C(34B)	0.1(3)
C(36A)-C(35A)-C(34A)-C(33A)	-2.2(4)
C(36A)-C(31A)-C(32A)-C(33A)	-1.8(3)
P(1)-C(31A)-C(32A)-C(33A)	177.15(18)
C(4B)-C(5B)-C(6B)-C(1B)	-0.5(4)
C(2B)-C(1B)-C(6B)-C(5B)	0.8(4)
P(2)-C(1B)-C(6B)-C(5B)	-178.7(2)
C(35A)-C(34A)-C(33A)-C(32A)	1.2(4)
C(31A)-C(32A)-C(33A)-C(34A)	0.8(4)
C(21A)-C(26A)-C(25A)-C(24A)	1.3(4)
C(2B)-C(3B)-C(4B)-C(5B)	0.5(4)
C(6B)-C(5B)-C(4B)-C(3B)	-0.2(4)
C(1A)-C(6A)-C(5A)-C(4A)	1.9(4)
C(3A)-C(4A)-C(5A)-C(6A)	-0.2(4)
C(25A)-C(26A)-C(21A)-C(22A)	-1.4(4)
C(25A)-C(26A)-C(21A)-P(1)	-175.84(19)
C(23A)-C(22A)-C(21A)-C(26A)	-0.6(4)
C(23A)-C(22A)-C(21A)-P(1)	174.0(2)
C(1A)-P(1)-C(21A)-C(26A)	85.0(2)
C(31A)-P(1)-C(21A)-C(26A)	-23.0(2)
Rh(1)-P(1)-C(21A)-C(26A)	-147.93(17)
C(1A)-P(1)-C(21A)-C(22A)	-89.5(2)
C(31A)-P(1)-C(21A)-C(22A)	162.49(19)
Rh(1)-P(1)-C(21A)-C(22A)	37.6(2)
C(26A)-C(25A)-C(24A)-C(23A)	0.8(4)
C(25B)-C(24B)-C(23B)-C(22B)	0.4(4)
C(25A)-C(24A)-C(23A)-C(22A)	-2.9(4)
C(21A)-C(22A)-C(23A)-C(24A)	2.8(4)
C(26B)-C(21B)-C(22B)-C(23B)	-0.9(4)
P(2)-C(21B)-C(22B)-C(23B)	-178.2(2)
C(24B)-C(23B)-C(22B)-C(21B)	0.0(4)

Table A. 75: Atomic coordinates (x 10^4) and equivalent isotropic displacement parameters (Å^2 x 10^3) for Triphenylphosphine (15). U(eq) is defined as one third of the trace of the orthogonalized Uij tensor.

	x	y	z	U(eq)
P(1)	3541(1)	4633(1)	7895(1)	21(1)
C(1A)	3288(2)	3676(1)	6886(1)	22(1)
C(1C)	2854(2)	5590(1)	6991(1)	23(1)
C(1B)	5693(2)	4811(1)	7955(1)	23(1)
C(2B)	6523(2)	4469(1)	8943(1)	28(1)
C(6C)	2107(2)	5512(1)	5875(1)	26(1)
C(2A)	1965(2)	3129(1)	7053(1)	27(1)
C(4C)	1624(2)	7105(1)	5814(1)	37(1)
C(2C)	2975(2)	6445(1)	7504(1)	33(1)
C(6A)	4311(2)	3452(1)	5982(1)	30(1)
C(5C)	1493(2)	6266(1)	5293(1)	33(1)
C(5A)	4011(2)	2706(1)	5271(1)	36(1)
C(6B)	6528(2)	5268(1)	7096(1)	32(1)
C(3A)	1671(2)	2384(1)	6339(1)	34(1)
C(3C)	2373(2)	7195(1)	6925(2)	39(1)
C(5B)	8170(2)	5357(1)	7211(2)	40(1)
C(4A)	2695(2)	2170(1)	5454(1)	36(1)
C(3B)	8168(2)	4562(1)	9055(2)	37(1)
C(4B)	8981(2)	4999(1)	8184(2)	40(1)

Table A. 76: Bond lengths [Å] and angles [°] for Triphenylphosphine (15).

P(1)-C(1A)	1.8282(14)
P(1)-C(1B)	1.8295(17)
P(1)-C(1C)	1.8311(14)
C(1A)-C(2A)	1.3954(19)
C(1A)-C(6A)	1.3964(19)
C(1C)-C(6C)	1.3930(19)
C(1C)-C(2C)	1.397(2)

C(1B)-C(2B)	1.3912(19)
C(1B)-C(6B)	1.3919(19)
C(2B)-C(3B)	1.393(2)
C(2B)-H(2B)	0.9300
C(6C)-C(5C)	1.389(2)
C(6C)-H(6C)	0.9300
C(2A)-C(3A)	1.385(2)
C(2A)-H(2A)	0.9300
C(4C)-C(5C)	1.380(2)
C(4C)-C(3C)	1.390(2)
C(4C)-H(4C)	0.9300
C(2C)-C(3C)	1.380(2)
C(2C)-H(2C)	0.9300
C(6A)-C(5A)	1.386(2)
C(6A)-H(6A)	0.9300
C(5C)-H(5C)	0.9300
C(5A)-C(4A)	1.385(2)
C(5A)-H(5A)	0.9300
C(6B)-C(5B)	1.390(2)
C(6B)-H(6B)	0.9300
C(3A)-C(4A)	1.378(2)
C(3A)-H(3A)	0.9300
C(3C)-H(3C)	0.9300
C(5B)-C(4B)	1.379(3)
C(5B)-H(5B)	0.9300
C(4A)-H(4A)	0.9300
C(3B)-C(4B)	1.378(3)
C(3B)-H(3B)	0.9300
C(4B)-H(4B)	0.9300
C(1A)-P(1)-C(1B)	103.32(6)
C(1A)-P(1)-C(1C)	103.28(7)
C(1B)-P(1)-C(1C)	101.64(6)
C(2A)-C(1A)-C(6A)	118.26(13)
C(2A)-C(1A)-P(1)	116.46(10)

C(6A)-C(1A)-P(1)	125.28(11)
C(6C)-C(1C)-C(2C)	118.31(13)
C(6C)-C(1C)-P(1)	124.23(11)
C(2C)-C(1C)-P(1)	117.24(10)
C(2B)-C(1B)-C(6B)	118.89(13)
C(2B)-C(1B)-P(1)	116.56(10)
C(6B)-C(1B)-P(1)	124.54(11)
C(1B)-C(2B)-C(3B)	120.50(14)
C(1B)-C(2B)-H(2B)	119.7
C(3B)-C(2B)-H(2B)	119.7
C(5C)-C(6C)-C(1C)	120.61(13)
C(5C)-C(6C)-H(6C)	119.7
C(1C)-C(6C)-H(6C)	119.7
C(3A)-C(2A)-C(1A)	120.97(13)
C(3A)-C(2A)-H(2A)	119.5
C(1A)-C(2A)-H(2A)	119.5
C(5C)-C(4C)-C(3C)	119.89(14)
C(5C)-C(4C)-H(4C)	120.1
C(3C)-C(4C)-H(4C)	120.1
C(3C)-C(2C)-C(1C)	121.16(14)
C(3C)-C(2C)-H(2C)	119.4
C(1C)-C(2C)-H(2C)	119.4
C(5A)-C(6A)-C(1A)	120.55(14)
C(5A)-C(6A)-H(6A)	119.7
C(1A)-C(6A)-H(6A)	119.7
C(4C)-C(5C)-C(6C)	120.25(14)
C(4C)-C(5C)-H(5C)	119.9
C(6C)-C(5C)-H(5C)	119.9
C(4A)-C(5A)-C(6A)	120.29(14)
C(4A)-C(5A)-H(5A)	119.9
C(6A)-C(5A)-H(5A)	119.9
C(5B)-C(6B)-C(1B)	120.35(14)
C(5B)-C(6B)-H(6B)	119.8
C(1B)-C(6B)-H(6B)	119.8
C(4A)-C(3A)-C(2A)	120.09(14)

C(4A)-C(3A)-H(3A)	120.0
C(2A)-C(3A)-H(3A)	120.0
C(2C)-C(3C)-C(4C)	119.78(14)
C(2C)-C(3C)-H(3C)	120.1
C(4C)-C(3C)-H(3C)	120.1
C(4B)-C(5B)-C(6B)	120.09(15)
C(4B)-C(5B)-H(5B)	120.0
C(6B)-C(5B)-H(5B)	120.0
C(3A)-C(4A)-C(5A)	119.83(14)
C(3A)-C(4A)-H(4A)	120.1
C(5A)-C(4A)-H(4A)	120.1
C(4B)-C(3B)-C(2B)	119.85(15)
C(4B)-C(3B)-H(3B)	120.1
C(2B)-C(3B)-H(3B)	120.1
C(3B)-C(4B)-C(5B)	120.29(14)
C(3B)-C(4B)-H(4B)	119.9
C(5B)-C(4B)-H(4B)	119.9

Table A. 77: Anisotropic displacement parameters ($Å^2$x 10^3) for Triphenylphosphine (15). The anisotropic displacement factor exponent takes the form: $-2p^2[h^2a^{*2}U^{11} + ... + 2hka^*b^*U^{12}]$

	U^{11}	U^{22}	U^{33}	U^{23}	U^{13}	U^{12}
P(1)	21(1)	25(1)	18(1)	0(1)	2(1)	-1(1)
C(1A)	26(1)	22(1)	19(1)	2(1)	-3(1)	1(1)
C(1C)	21(1)	26(1)	22(1)	1(1)	3(1)	-1(1)
C(1B)	22(1)	25(1)	22(1)	-6(1)	0(1)	-1(1)
C(2B)	31(1)	25(1)	29(1)	-5(1)	-5(1)	1(1)
C(6C)	26(1)	28(1)	25(1)	-1(1)	0(1)	0(1)
C(2A)	28(1)	29(1)	26(1)	2(1)	0(1)	-1(1)
C(4C)	39(1)	30(1)	42(1)	9(1)	-2(1)	6(1)
C(2C)	41(1)	30(1)	28(1)	-2(1)	-4(1)	-1(1)
C(6A)	32(1)	31(1)	28(1)	-1(1)	4(1)	0(1)
C(5C)	33(1)	37(1)	30(1)	6(1)	-4(1)	1(1)
C(5A)	44(1)	35(1)	29(1)	-6(1)	4(1)	7(1)

341

C(6B)	28(1)	42(1)	25(1)	-5(1)	3(1)	-7(1)
C(3A)	37(1)	28(1)	36(1)	1(1)	-8(1)	-6(1)
C(3C)	51(1)	25(1)	40(1)	-1(1)	-1(1)	2(1)
C(5B)	30(1)	54(1)	37(1)	-15(1)	11(1)	-12(1)
C(4A)	49(1)	26(1)	33(1)	-6(1)	-10(1)	4(1)
C(3B)	31(1)	33(1)	45(1)	-13(1)	-14(1)	7(1)
C(4B)	20(1)	47(1)	54(1)	-26(1)	-2(1)	-1(1)

Table A. 78: Hydrogen coordinates (x 10^4) and isotropic displacement parameters (Å^{2}x 10^3) for Triphenylphosphine (15).

_____

	x	y	z	U(eq)
H(2B)	5976	4176	9533	34
H(6C)	2019	4950	5515	32
H(2A)	1272	3267	7651	33
H(4C)	1211	7608	5422	44
H(2C)	3469	6509	8250	39
H(6A)	5201	3806	5857	36
H(5C)	993	6206	4549	40
H(5A)	4696	2565	4668	43
H(6B)	5985	5514	6441	38
H(3A)	781	2029	6458	41
H(3C)	2468	7760	7276	46
H(5B)	8722	5659	6632	48
H(4A)	2503	1666	4980	43
H(3B)	8717	4330	9716	44
H(4B)	10081	5052	8252	48

Table A. 79: Torsion angles [°] for Triphenylphosphine (15).

_____

C(1B)-P(1)-C(1A)-C(2A)	152.06(10)
C(1C)-P(1)-C(1A)-C(2A)	-102.34(11)
C(1B)-P(1)-C(1A)-C(6A)	-27.40(13)

C(1C)-P(1)-C(1A)-C(6A)	78.20(13)
C(1A)-P(1)-C(1C)-C(6C)	8.60(13)
C(1B)-P(1)-C(1C)-C(6C)	115.47(12)
C(1A)-P(1)-C(1C)-C(2C)	-176.89(11)
C(1B)-P(1)-C(1C)-C(2C)	-70.02(12)
C(1A)-P(1)-C(1B)-C(2B)	-100.32(11)
C(1C)-P(1)-C(1B)-C(2B)	152.84(10)
C(1A)-P(1)-C(1B)-C(6B)	80.38(13)
C(1C)-P(1)-C(1B)-C(6B)	-26.47(13)
C(6B)-C(1B)-C(2B)-C(3B)	-1.6(2)
P(1)-C(1B)-C(2B)-C(3B)	179.05(10)
C(2C)-C(1C)-C(6C)-C(5C)	-0.3(2)
P(1)-C(1C)-C(6C)-C(5C)	174.14(11)
C(6A)-C(1A)-C(2A)-C(3A)	-0.2(2)
P(1)-C(1A)-C(2A)-C(3A)	-179.66(11)
C(6C)-C(1C)-C(2C)-C(3C)	0.0(2)
P(1)-C(1C)-C(2C)-C(3C)	-174.87(12)
C(2A)-C(1A)-C(6A)-C(5A)	0.2(2)
P(1)-C(1A)-C(6A)-C(5A)	179.61(11)
C(3C)-C(4C)-C(5C)-C(6C)	0.0(2)
C(1C)-C(6C)-C(5C)-C(4C)	0.3(2)
C(1A)-C(6A)-C(5A)-C(4A)	-0.4(2)
C(2B)-C(1B)-C(6B)-C(5B)	1.7(2)
P(1)-C(1B)-C(6B)-C(5B)	-179.01(11)
C(1A)-C(2A)-C(3A)-C(4A)	0.4(2)
C(1C)-C(2C)-C(3C)-C(4C)	0.4(2)
C(5C)-C(4C)-C(3C)-C(2C)	-0.4(2)
C(1B)-C(6B)-C(5B)-C(4B)	-0.4(2)
C(2A)-C(3A)-C(4A)-C(5A)	-0.6(2)
C(6A)-C(5A)-C(4A)-C(3A)	0.7(2)
C(1B)-C(2B)-C(3B)-C(4B)	0.2(2)
C(2B)-C(3B)-C(4B)-C(5B)	1.1(2)
C(6B)-C(5B)-C(4B)-C(3B)	-1.0(2)

APPENDIX B

The methanol substitution reactions of *fac*-[Re(EM(naltol))(CO)$_3$(H$_2$O)] (**16**) and *fac*-[Re(EM(naltol))(CO)$_3$(EM(naltol)H)] (**3**) with different entering monodentate ligands pyridine (Py), imidazole (Im), 4-dimethylaminopyridine (DMAP) and 3-chloropyridine (3-ClPy) were studied. The respective reactions were performed at different temperatures and the rhenium concentration was kept constant at ~ 7.49 x 10^{-4} M.

Table B.1: Temperature and [Py] dependence of the *pseudo* first-order reaction between *fac*-[Re(EM(naltol))(CO)$_3$(H$_2$O)] (16) and pyridine in dry MeOH.

[Py] (M)	\[Re] = 7.4925 x 10^{-4} M/ 0.0660 g in 100 ml (14.4 °C) + Pyridine 365 nm													
	Observed rate constants													
	DP1	SD1	DP2	SD2	DP3	SD3	DP4	SD4	DP5	SD5	DP6	SD6	A$_v$	Varience
0.02	0.16675	0.00049	0.16808	0.00068	0.16578	0.00059							0.16687	1.05 E-06
0.06	0.51376	0.000132	0.51319	0.00142	0.51314	0.0022	0.51138	0.0022	0.49494	0.00256			0.509282	1.83 E-05
0.1	0.84101	0.0028	0.84028	0.00286	0.84364	0.0037	0.83677	0.00422	0.84723	0.00531			0.841786	7.57 E-05
0.14	1.15231	0.00539	1.16739	0.00567	1.18883	0.00502	1.16492	0.00631	1.18213	0.0084	1.16974	0.01038	1.170887	0.000305
0.2	1.63772	0.00447	1.65379	0.00564	1.62355	0.00821	1.61787	0.00685	1.66674	0.00722			1.639934	0.000218

Table B.2: Temperature and [Py] dependence of the *pseudo* first-order reaction between *fac*-[Re(EM(naltol))(CO)$_3$(H$_2$O)] (16) and pyridine in dry MeOH.

| [Py] (M) | [Re] = 7.4925 x 10^{-4} M/ 0.0660 g in 100 ml (25.7 °C) + Pyridine 365 nm |

[Py] (M)	DP1	SD1	DP2	SD2	DP3	SD3	DP4	SD4	DP5	SD5	DP6	SD6	A$_v$	Varience
0.01	0.28499	0.00001	0.28697	0.00121	0.28655	0.00176	0.28885	0.00153	0.28569	0.00173			0.28661	1.09E-05
0.03	0.90989	0.00627	0.93102	0.00487	0.9176	0.00667	0.93391	0.00565	0.90885	0.0066	0.9187	0.01065	0.919995	0.000296
0.05	1.49305	0.0129	1.51047	0.02358	1.51636	0.01654	1.49511	0.01471	1.49323	0.01902	1.4602	0.01859	1.494737	0.00192
0.07	2.1595	0.02019	2.02571	0.02603	2.13787	0.02099	2.18269	0.02171	2.13373	0.0221	2.13135	0.0093	2.128475	0.002572
0.1	3.11663	0.03829	3.1339	0.04152	3.0419	0.03214	2.97401	0.02234	3.05237	0.02021	3.04983	0.01765	3.06144	0.005442

Table B.3: Temperature and [Py] dependence of the *pseudo* first-order reaction between *fac*-[Re(EM(naltol))(CO)$_3$(H$_2$O)] (16) and pyridine in dry MeOH.

| [Py] (M) | [Re] = 7.4925 x 10^{-4} M/ 0.0660 g in 100 ml (35.3 °C) + Pyridine 365 nm |

[Py] (M)	DP1	SD1	DP2	SD2	DP3	SD3	DP4	SD4	DP5	SD5	DP6	SD6	A$_v$	Varience
0.005	0.3062	0.00113	0.3007	0.00125	0.29725	0.00131	0.29139	0.00124	0.29974	0.00117	0.30124	0.0012	0.29942	8.9E-06
0.015	0.91102	0.00296	0.92368	0.00365	0.91902	0.00401	0.92866	0.00364	0.92076	0.0036	0.88201	0.00541	0.914192	9.36E-05
0.025	1.51929	0.00532	1.51504	0.00531	1.51663	0.00555	1.51699	0.00586	1.50719	0.00532	1.44243	0.00784	1.502928	0.000211
0.035	2.11489	0.00799	2.12498	0.00794	2.13834	0.0077	2.09189	0.00789	2.09943	0.00812	1.87504	0.00902	2.074095	0.000396
0.05	2.98958	0.01078	2.99407	0.01077	3.04465	0.01099	3.01589	0.01104	2.96782	0.01079	2.87475	0.0172	2.981127	0.000887

Table B.4: Temperature and [Py] dependence of the *pseudo* first-order reaction between *fac*-[Re(EM(naltol))(CO)$_3$(H$_2$O)] (16) and pyridine in dry MeOH.

[Py] (M)														
	[Re] = 7.4925 x 10^{-4} M/ 0.0660 g in 100 ml (46.8 °C) + Pyridine 365 nm												

[Py] (M)	DP1	SD1	DP2	SD2	DP3	SD3	DP4	SD4	DP5	SD5	DP6	SD6	A$_v$	Variance
0.002	0.44656	0.00164	0.44908	0.00184	0.45522	0.0019	0.45454	0.002	0.45317	0.00189	0.45185	0.00251	0.451737	2.36 E-05
0.006	1.09101	0.00499	1.07697	0.00503	1.08749	0.00472	1.07801	0.0047	1.08726	0.00501	1.06905	0.00655	1.081632	0.000163
0.01	1.69019	0.00914	1.68858	0.00686	1.6733	0.00956	1.67392	0.00957	1.6854	0.01058	1.67103	0.02498	1.680403	0.00105
0.014	2.27761	0.01366	2.32488	0.01587	2.35733	0.01409	2.36956	0.01482	2.37739	0.01519	2.37251	0.01498	2.346547	0.001312
0.02	3.36687	0.02067	3.40229	0.01998	3.43767	0.01807	3.41879	0.01685	3.44977	0.01955	3.47386	0.01817	3.424875	0.002149

Table B.5: Temperature and [Im] dependence of the *pseudo* first-order reaction between *fac*-[Re(EM(naltol))(CO)$_3$(H$_2$O)] (16) and imidazole in dry MeOH.

Observed rate constants — [Re] = 7.4925 x 10^{-4} M/ 0.0660 g in 100 ml (25 °C) + Imidazole 365 nm

[Im] (M)	DP1	SD1	DP2	SD2	DP3	SD3	DP4	SD4	DP5	SD5	DP6	SD6	A$_v$	Variance
0.01	0.10729	0.00144	0.13172	0.00218	0.11755	0.00302	0.11212	0.00243	0.11629	0.00235	0.11853	0.00195	0.11725	3.12 E-05
0.03	0.56148	0.01737	0.54717	0.01509	0.55651	0.01192	0.55021	0.01212	0.55513	0.01147	0.50008	0.01873	0.545097	0.001301
0.05	1.38457	0.03569	1.12682	0.02944	1.12368	0.02522	1.12278	0.01999	1.07968	0.02348			1.167506	0.003727
0.07	1.75557	0.03369	1.66513	0.0223	1.58976	0.02428	1.55463	0.023	1.85398	0.03452			1.683814	0.003942
0.1	2.43302	0.04726	2.51574	0.04062	2.53653	0.04066	2.34107	0.04281	2.30766	0.03933	2.10593	0.0364	2.373325	0.010241

Table B.6: Temperature and [DMAP] dependence of the *pseudo* first-order reaction between *fac*-[Re(EM(naltol))(CO)$_3$(H$_2$O)] (16) and DMAP in dry MeOH.

[Re] = 7.5833 x 10^{-4} M/ 0.0668 g in 100 ml (25.1 °C) + DMAP 365 nm													
	Observed rate constants												
[DMAP] (M)	DP1	SD1	DP2	SD2	DP3	SD3	DP4	SD4	DP5	SD5	DP6	SD6	A$_v$	Varience
0.01	0.15649	0.00121	0.17145	0.00133	0.017173	0.00128	0.16016	0.00163	0.15593	0.00151	0.16339	0.00134	0.137432167	0.000011604
0.03	0.67919	0.00826	0.66389	0.00749	0.67959	0.0067	0.67387	0.00651	0.67387	0.00611	0.6712	0.01538	0.673601667	0.000485474
0.05	1.26021	0.01262	1.29495	0.01029	1.25301	0.01143	1.24672	0.00945	1.26789	0.01178	1.26021	0.01262	1.263831667	0.000783129
0.07	1.81485	0.0013	1.92215	0.02116	1.86536	0.01699	1.81641	0.01971	1.80734	0.01815	1.81658	0.01334	1.840448333	0.001801268
0.1	2.66605	0.02217	2.55049	0.02039	2.55005	0.01905	2.55894	0.02111	2.48106	0.01935	2.36206	0.02074	2.528108333	0.002520366

Table B.7: Temperature and [3-ClPy] dependence of the *pseudo* first-order reaction between *fac*-[Re(EM(naltol))(CO)$_3$(H$_2$O)] (16) and 3-Cl-pyridine in dry MeOH.

[Re] = 7.5833 x 10^{-4} M/ 0.0668 g in 100 ml (25.2 °C) + 3-Chloropyridine 380 nm													
[3-ClPy] (M)	Observed rate constants												
	DP1	SD1	DP2	SD2	DP3	SD3	DP4	SD4	DP5	SD5	DP6	SD6	Average	Varience
0.01	0.3575	0.00177	0.36122	0.00183	0.37035	0.00219	0.36662	0.00175	0.3697	0.00165	0.37025	0.00152	0.36594	1.94 E-05
0.03	1.06494	0.00752	1.13182	0.00529	1.15096	0.00548	1.14723	0.00503	1.1592	0.00517	1.17162	0.00516	1.137628	0.000193
0.05	1.85872	0.00597	1.87792	0.00569	1.87592	0.00509	1.89279	0.00559	1.89083	0.00542	1.89347	0.00591	1.881608	0.000189
0.07	2.64521	0.00747	2.68734	0.00831	2.62863	0.00887	2.66907	0.00938	2.6609	0.00928	2.65961	0.00884	2.65846	0.000456
0.1	3.75031	0.00885	3.84659	0.00993	3.81849	0.01095	3.81405	0.01166	3.77398	0.00968	3.80018	0.01186	3.8006	0.000667

Table B.8: Temperature and [Py] dependence of the *pseudo* first-order reaction between *fac*-[Re(EM(naltol))(CO)$_3$(EM(naltol)H)] (3) and Py in dry MeOH.

[Py] (M)	[Re] = 7.8178 x 10^{-4} M/ 0.0450 g in 50 ml (25 °C) + Pyridine 365 nm													
	Observed rate constants													
	DP1	SD1	DP2	SD2	DP3	SD3	DP4	SD4	DP5	SD5	DP6	SD6	A$_v$	Varie nce
0.01	0.16 169	0.00 067	0.17 825	0.00 058	0.18 207	0.00 062	0.18 313	0.00 065	0.18 389	0.00 064	0.17 529	0.00 08	0.177 387	2.64 E-06
0.03	0.59 059	0.00 301	0.62 281	0.00 315	0.62 476	0.00 318	0.62 097	0.00 348	0.60 255	0.00 421	0.60 391	0.00 413	0.610 932	7.6E- 05
0.05	1.04 936	0.00 388	1.04 933	0.00 639	1.04 211	0.00 612	1.04 061	0.00 583	1.04 153	0.00 544	1.03 32	0.00 495	1.042 69	0.000 181
0.07	1.47 88	0.00 541	1.53 487	0.00 704	1.53 664	0.00 744	1.53 492	0.00 693	1.49 823	0.00 699	1.48 645	0.00 657	1.511 652	0.000 274
0.1	2.14 635	0.00 746	2.18 029	0.00 792	2.19 964	0.00 903	2.19 858	0.00 784	2.19 106	0.00 933	2.22 91	0.01 317	2.190 837	0.000 522